

Efluateak deskontaminatzeko oxidazio-teknologia aurreratuen areagotzea

Egilea:

Cristian Ferreiro Santiso

Zuzendariak:

José Ignacio Lombraña Alonso irakasle jauna

María José Rivero Martínez irakasle andrea

Leioa 2021

Ingeniaritza Kimikoko doktorego-programa (99/2011 ED)

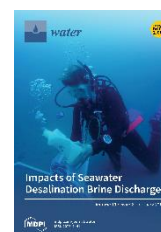
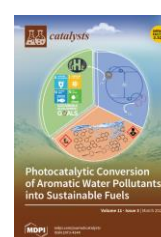
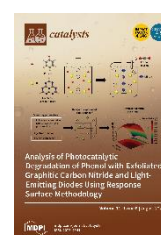
Euskal Herriko Unibertsitateko (EHU/UPV) Ingeniaritza Kimikoa Saileko Ingeniaritza Kimikoa Energian eta Ingurumenean izeneko ikerketa-taldean egin da doktore-tesi honetan deskribatutako ikerketa.

Ikerketa hau Eusko Jaurlaritzak finantzatu du Euskal Unibertsitate Sistemari onartutako taldeak finantzatzeko IT1080-16 laguntzari esker eta Euskal Herriko Unibertsitateak (EHU/UPV) onartutako ikerketa taldeen finantzaziorako PPGA19/63, PPGA20/33 eta GIU20/56 laguntzen bidez.

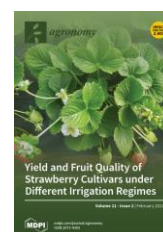
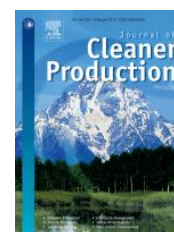
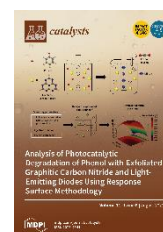
Euskal Herriko Unibertsitatearen Ikerketa Arloko Errektoreordetzak emandako doktoratu aurreko beka bat (PIF16/367) jaso du egileak.

Doktor-tesi hau bata bestearekin erlazionatutako ikerketa zientifiko batzuen bilduma gisa egin da, zuzendari zientifikoei aurkeztu eta haiek onartutako azken ikerketa-planari jarraituz. Tesi-modalitate honetan jasotzen diren artikuluko zientifikoak *Journal Citation Reports* (JCR) zerrendan indexatutako nazioarteko aldizkarietan argitaratuta daude:

1. C. Ferreiro, J. Sanz, N. Villota, A. de Luis, J.I. Lombraña. Kinetic modelling for concentration and toxicity changes during the oxidation of 4-chlorophenol by UV/H₂O₂. *Scientific Reports*, 11, 1, 15726, 2021. DOI: 10.1038/s41598-021-95083-7. Q1, IF (2020): 4.379. Multidisciplinary Sciences (17/73).
2. N. Villota, C. Ferreiro, H.A. Qulatein, J.M. Lomas, J.I. Lombraña. Turbidity changes during carbamazepine oxidation by photo-Fenton. *Catalysts*, 11, 8, 894, 2021. DOI: 10.3390/catal11080894. Q2, IF (2020): 4.146. Chemistry, Physical (67/162).
3. N. Villota, C. Ferreiro, H.A. Qulatein, J.M. Lomas, L.M. Camarero, J.I. Lombraña. Colour changes during the carbamazepine oxidation by photo-Fenton. *Catalysts*, 11, 3, 386, 2021. DOI: 10.3390/catal11030386. Q2, IF (2020): 4.146. Chemistry, Physical (67/162).
4. C. Ferreiro, N. Villota, J.I. Lombraña, M.J. Rivero, V. Zúñiga, J.M. Rituerto. Analysis of a hybrid suspended-supported photocatalytic reactor for the treatment of wastewater containing benzothiazole and aniline. *Water*, 11, 2, 337, 2019. DOI: 10.3390/w11020337. Q2, IF (2019): 2.544. Water Resources (31/94).
5. C. Ferreiro, N. Villota, J.I. Lombraña, M.J. Rivero, V. Zúñiga, J.M. Rituerto. Removal of aniline and benzothiazole wastewaters using an efficient MnO₂/GAC catalyst in a photocatalytic fluidised bed reactor. *Materials*, 14, 18, 5207, 2021. DOI: 10.3390/ma14185207. Q1, IF (2020): 3.623. Metallurgy & Metallurgical Engineering (17/80).
6. C. Ferreiro, N. Villota, A. de Luis, J.I. Lombraña. Analysis of the effect of the operational conditions in a combined adsorption-ozonation process with granular activated carbon for the treatment of phenol wastewater. *Reaction Chemistry & Engineering*, 5, 4, 760-778, 2020. DOI: 10.1039/c9re00424f. Q2, IF (2020): 4.239. Chemical Engineering (40/143).



7. C. Ferreiro, A. de Luis, N. Villota, J.M. Lomas, J.I. Lombrana, L.M. Camarero. Application of a combined adsorption–ozonation process for phenolic wastewater treatment in a continuous fixed–bed reactor. *Catalysts*, 11, 8, 1014, 2021. DOI: 10.3390/catal11081014.
Q2, IF (2020): 4.146. Chemistry, Physical (67/162).
8. C. Ferreiro, N. Villota, J.I. Lombrana, M.J. Rivero. An efficient catalytic process for the treatment of genotoxic aniline wastewater using a new granular activated carbon-supported titanium dioxide composite. *Journal of Cleaner Production*, 228 1282–1295, 2019. DOI: 10.1016/j.jclepro.2019.04.198.
Q1, IF (2019): 7.246. Environmental Sciences (19/265).
9. C. Ferreiro, N. Villota, J.I. Lombrana, M.J. Rivero. Heterogeneous catalytic ozonation of aniline-contaminated waters: a three-phase modelling approach using TiO₂/GAC. *Water*, 12, 12, 3448, 2020. DOI: 10.3390/w12123448.
Q2, IF (2020): 3.103. Water Resources (39/98).
10. P. Alfonso-Muniozguren, C. Ferreiro, E. Richard, M. Bussemaker, J.I. Lombrana, J. Lee. Analysis of ultrasonic pre-treatment for the ozonation of humic acids. *Ultrasonics Sonochemistry*, 71, 105359, 2021. DOI: 10.1016/j.ultsonch.2020.105359.
Q1, IF (2020): 7.491. Acoustics (1/32).
11. C. Ferreiro, I. Gómez-Motos, J.I. Lombrana, A. de Luis, N. Villota, O. Ros, N. Etxebarria. Contaminants of emerging concern removal in an effluent of wastewater treatment plant under biological and continuous mode ultrafiltration treatment. *Sustainability*, 12, 2, 725, 2020. DOI: 10.3390/su12020725.
Q2, IF (2020): 3.251. Environmental Sciences (124/274).
12. C. Ferreiro, N. Villota, A. de Luis, J.I. Lombrana, N. Etxebarria, J.M. Lomas. Water reuse study from urban WWTPs via c-ultrafiltration and ozonation technologies: basis for resilient cities and agriculture. *Agronomy*, 11, 2, 322, 2021. DOI: 10.3390/agronomy11020322.
Q1, IF (2020): 3.417. Agronomy (21/122).



Eskertza

Tesi honekin, ingeniari kimiko batek izan dezakeen etapa akademikorik garrantzitsuena amaitu da. Hasieran, 2015. urtean, zalantzak izan banituen ere, ez dut uste gaizki aukeratu nuenik nire bizitzaren 5 urte hauek lan honetan erabiltzea erabaki nuenean. Beste edozein proiektu esperimental eta berritzailek bezala, honek ere gorabeherak izan baditu ere, orduan jarritako helburuetatik haratago iristea lortu dut azkenean.

Pertsona askok lagundu didate lan hau gauzatzen. Hasteko, nire gurasoei eskerrak eman nahi dizkiet emandako laguntzarengatik eta ikasteko grina pizteagatik, ahalegindu gabe ezer lortzen ez dela erakusteagatik, eta, batez ere, hau guztia lortzeko baliabideak emateagatik.

Halaber, eskerrak eman nahi dizkiet nire zuzendariei, Iñaki Lombraña eta Maria José Rivero irakasleei, proiektu honetan sinesteagatik eta ikerketaren munduan sartzeko aukera emateagatik, baita urte hauetan ikerketa talde txiki batean ikasi dudan guztiagatik ere. Haiekin guztiekin partekatu ahal izan ditut etapa honetako ilusioa eta proiektuak.

Nire eskerrak Verónica-ri eta J.M. Rituerto-ri emandako laguntza tekniko eta materialarengatik, eta General Química S.A.U.-ren instalazioak uzteagatik ikerketa honen zati bat egiteko.

Eskerrak eman nahi dizkiet Txileko Universidad Católica de la Santísima Concepción (UCSC) unibertsitateko Teknologia Garbien laborategiko lankideei eta, bereziki, Hectorri, egindako iruzkinengatik eta haien unibertsitatean ongietorria emateagatik, gure bizitza hainbeste aldatu den urte honetan.

Nire eskerronik beroena eman nahi diet Mónica eta Txebi-ri zailtasunik handieneko egoeretan aurrera egiten lagundu didatelako, bideratu egin nautelako eta, zalantzak agertzean, iradokizun baliagarriak eman dizkidatelako.

Azkenik, baina ez garrantzi gutxiago izateagatik, eskerrak eman nahi dizkiet SGIker-eko langileei (Loli, Alfredo, Aitor, Javier, Alicia eta Ricardo) emandako aholkularitza zientifiko-teknikoagatik, eta mantentze-lanetako langileei (Humberto, Mikel eta Antonio-ri) behar izan ditudan ekipamendu konplexuak muntatzen izan duten pazientziagatik eta eman didaten laguntzagatik.

Estimutzen nauten pertsonak, lagunek eta familiako kideek eman didaten aintzatespenari eta laguntzari esker egin ahal izan dut ikerketa-lan hau. Haiek gabe ez nuke izango pertsona gisa eta, batez ere, profesional gisa hazten laguntzen didan indarra eta energia.

Guztiori, mila esker.

LABURPENA	1
1. SARRERA	4
1.1. URA, INGURUMEN-KUDEAKETAREN OINARRIZKO BALIABIDEA	5
1.2. PROZESU FOTOKIMIKO PRIMARIOAK ETA KATALITIKOAK	9
1.2.1. UV/H ₂ O ₂ -AN OINARRITUTAKO PROZESUAK	9
1.2.2. FOTOFENTON SISTEMAN OINARRITUTAKO PROZESUAK	11
1.2.3. FOTOKATALISI HETEROGENEOA	13
1.3. OZONIZAZIOAN OINARRITUTAKO PROZESU EZ-FOTOKIMIKOAK	17
1.3.1. OZONIZAZIO KATALITIKOA	17
1.3.2. ULTRASOINUEN TEKNOLOGIA, OZONIZAZIOAREN AURRETIKO TRATAMENDUA	20
1.3.3. OZONIZAZIOAN ULTRAIRAGAZKETA-PROZESUAK TXERTATZEA, SORTZEN ARI DIREN POLUITZAILE BERRIAK DEUSEZTATZEKO	21
1.4. IKATZ AKTIBATUZKO MATERIALETAN OINARRITUTAKO KONPOSITE BERRIEN SINTESIA	23
1.5. PROZESUEN AREAGOTZEA	24
1.6. TESIAREN ESPARRUA ETA HELBURUA	25
1.7. ERREFERENTZIAK	26
2. MATERIALAK ETA METODOAK	38
2.1. ERREAKTIBOAK	39
2.2. FOTOKATALIZATZAILEEN ETA KATALIZATZAILEEN SINTESIA	41
2.2.1. TiO ₂ /GAC KONPOSITEEN SINTESIA	41
2.2.2. MnO ₂ /GAC FOTOKATALIZATZAILEAREN SINTESIA	42
2.3. MATERIALEN KARAKTERIZAZIOA	43
2.4. METODOLOGIA ESPERIMENTALA	45
2.4.1. UV/H ₂ O ₂ SISTEMA ESPERIMENTALA	45
2.4.2. FOTOFENTON SISTEMA ESPERIMENTALA	45
2.4.3. KATALIZATZAILEAK ATXIKITA ETA ESEKIDURAN DITUEN SISTEMA FOTOKATALITIKO HIBRIDOA	46
2.4.4. SISTEMA FBR FOTOKATALITIKOA	47
2.4.5. OZONIZAZIO ERDIJARRAITUKO SISTEMA ESKALA PILOTUAN	48
2.4.6. OZONIZAZIO JARRAITUKO SISTEMA OHANTZE FINKOAN	49
2.4.7. SLURRYMOTAKO OZONIZAZIO KATALITIKO ERDIJARRAITUKO SISTEMA	50
2.4.8. ULTRASOINUEN BIDEZ AURRETRATATZEKO SISTEMA	51
2.4.9. OZONIZAZIO-EKIPAMENDUARI ATXIKITAKO ULTRAIRAGAZTE-SISTEMA JARRAITUA ESKALA PILOTUAN	52
2.5. ERREFERENTZIAK	54
3. ARGITALPEN ZIENTIFIKOAK	55
3.1. 1. ARGITALPENA. KINETIC MODELLING FOR CONCENTRATION AND TOXICITY CHANGES DURING THE OXIDATION OF 4-CHLOROPHENOL BY UV/H ₂ O ₂	57
3.2. 2. ARGITALPENA. TURBIDITY CHANGES DURING CARBAMAZEPINE OXIDATION BY PHOTO-FENTON	58
3.3. 3. ARGITALPENA. COLOUR CHANGES DURING THE CARBAMAZEPINE OXIDATION BY PHOTO-FENTON	59
3.4. 4. ARGITALPENA. ANALYSIS OF A HYBRID SUSPENDED-SUPPORTED PHOTOCATALYTIC REACTOR FOR THE TREATMENT OF WASTEWATER CONTAINING BENZOTHAZOLE AND ANILINE	60
3.5. 5. ARGITALPENA REMOVAL OF ANILINE AND BENZOTHAZOLE WASTEWATERS USING AN EFFICIENT MnO ₂ /GAC CATALYST IN A PHOTOCATALYTIC FLUIDISED BED REACTOR	61

3.6.	6. ARGITALPENA. ANALYSIS OF THE EFFECT OF THE OPERATIONAL CONDITIONS IN A COMBINED ADSORPTION-OZONATION PROCESS WITH GRANULAR ACTIVATED CARBON FOR THE TREATMENT OF PHENOL WASTEWATER	62
3.7.	7. ARGITALPENA APPLICATION OF A COMBINED ADSORPTION-OZONATION PROCESS FOR PHENOLIC WASTEWATER TREATMENT IN A CONTINUOUS FIXED-BED REACTOR	63
3.8.	8. ARGITALPENA. AN EFFICIENT CATALYTIC PROCESS FOR THE TREATMENT OF GENOTOXIC ANILINE WASTEWATER USING A NEW GRANULAR ACTIVATED CARBON-SUPPORTED TITANIUM DIOXIDE COMPOSITE	64
3.9.	9. ARGITALPENA. HETEROGENEOUS CATALYTIC OZONATION OF ANILINE-CONTAMINATED WATERS: A THREE-PHASE MODELLING APPROACH USING TiO₂/GAC	65
3.10.	10. ARGITALPENA. ANALYSIS OF ULTRASONIC PRE-TREATMENT FOR THE OZONATION OF HUMIC ACIDS	66
3.11.	11. ARGITALPENA. CONTAMINANTS OF EMERGING CONCERN REMOVAL IN AN EFFLUENT OF WASTEWATER TREATMENT PLANT UNDER BIOLOGICAL AND CONTINUOUS MODE ULTRAFILTRATION TREATMENT	67
3.12.	12. ARGITALPENA. WATER REUSE STUDY FROM URBAN WWTPs VIA C-ULTRAFILTRATION AND OZONATION TECHNOLOGIES: BASIS FOR RESILIENT CITIES AND AGRICULTURE	68
4.	<u>ONDORIOAK ETA ETORKIZUNeko AUKERAK</u>	69
4.1.	ONDORIOAK	70
4.1.1.	UV/H ₂ O ₂ -AN OINARRITUTAKO PROZESUAK	70
4.1.2.	FOTOFENTON SISTEMAN OINARRITUTAKO PROZESUAK	70
4.1.3.	FOTOKATALISI HETEROGENEOA ERREAKTORE HIBRIDOETAN ETA FBRAN	71
4.1.4.	OZONIZAZIO KATALITIKOA	73
4.1.5.	ULTRASOINUEN BIDEZKO AURRETRATAMENDUAK OZONIZAZIO-PROZESUETAN DUEN ERAGINA	75
4.1.6.	ULTRAIRAGAZKETA ETA OZONIZAZIO PROZESUEN INTEGRAZIOA	75
4.2.	ETORKIZUNeko AUKERAK	77
	<u>ERANSKINA</u>	79
A.1.	BILTZAR ZIENTIFIKOETAN EGINDAKO EKARPENAK	80
A.2.	BESTELAKO EKARPENAK	81
A.3.	MATERIAL OSAGARRIA	82
A.3.1.	1. ARGITALPENAREN MATERIAL OSAGARRIA	82
A.3.2.	5. ARGITALPENAREN MATERIAL OSAGARRIA	83
A.3.3.	7. ARGITALPENAREN MATERIAL OSAGARRIA	84
A.3.4.	8. ARGITALPENAREN MATERIAL OSAGARRIA	85
A.3.5.	9. ARGITALPENAREN MATERIAL OSAGARRIA	86
A.3.6.	10. ARGITALPENAREN MATERIAL OSAGARRIA	87

Laburpena

Ura bizitzarako beharrezkoa den baliabiderik garrantzitsuena da. Ur-eskaera gero eta handiagoa da, industriako sektoreek gero eta poluitzaile gehiago isuritzen dituzte, nekazaritzan pestizidak erabiltzen dira era masiboan, meatzaritzak, hirietako erabilerak eta baliabidearen urritasunak, horiek guztiek zalantzan jartzen dute uraren jasangarritasuna. Poluzioak ingurumena hondatzen du, eta, beraz, baita ekosistemak ere. Egoera zaildu egiten da ur-eskasia badago, ezin baitira erabili eskasia-garaietan aldi baterako arazoa gainditzen lagundu dezaketen ordeko ur-baliabideak.

Hori dela eta, gizarte osoaren ardura da ingurumena zaintzea. Horretarako, ezinbestekoa da ingurumenaren kudeaketa eta administrazioa era publikoan kontrolatzea. Uraren zikloaren ingurumen-kontrola are erronka handiagoa bilakatzen da klima-aldaketaren testuinguruan. Garapen Jasangarriaren Helburuek (GJH) uraren funtzioa nabarmentzen dute, trantsizio ekologikoaren politika publikoen esparruan; batez ere, 6. GJHaren bidez (Ur garbia eta saneamendua).

Frogatuta dago tratamendu konbentzionalak ez direla nahikoa bermatzeko ura ingurumenetik hartzean zuen kalitate-maila berarekin ondoren itzultzeko ingurumenera. Uretan dauden poluitzaileen askotariko egoerak eta izaera kimikoak kontuan hartuta, arazo horri erantzutea da tesi honen helburua. Horretarako, oxidazio-prozesu aurreratuetatik (AOP, *advanced oxidation process*,) aplikatzeko aukera gehien dituztenetatik, haien areagotzea izan da egiteko nagusia. AOPen barruan, bi multzo bereizi ziren: fotokimikoak eta ozonoan oinarritutako ez-fotokimikoak. **AOPen 12 kasu aztertu ziren (3. kapituluko atalak), eta haien eraginkortasuna handitzeko ekarpenak egin ziren** alderdi hauen bidez: AOP teknologiaren oinarrian sakontzea haren eredu sortzeko (3.1, 3.6, 3.7 eta 3.9 kasuak), prozesuaren aldagaiak aztertzea eta eragiketa-estrategia onuragarrienak hautatzea (3.2, 3.3 kasuak), erreakzio-ekipamenduan eraldaketak txertatzea (3.4 kasua) edo katalizatzaile berriak garatzea (3.5 eta 3.8 kasuak) eta tratamendu-sistema orokor konplexuagoetan integratzea (3.10, 3.11 eta 3.12 kasuak).

AOP fotokimikoen barruan, 4-klorofenola zuen jatorri industrialeko ur oso toxikoa aztertu zen 3.1 kasuan. Arazoari aurre egiteko, UV/H₂O₂ tratamendua proposatu zen efluentearen toxikotasuna gutxitzeko, eta, hala, sistema biologiko baten bidez tratatzeko moduko egoera lortzeko. Horretarako, **bigarren ordenako eredu zinetiko bat proposatuta** aztertu zen sistema. Degradazio-konposatuak taldetan edo *lumpetan* multzokatu ziren, 4-klorofenolaren bilakaera eta tratatutako efluentearen toxikotasuna aurreratzeko asmoz.

Aurrekoaren bide beretik eta prozesu fotokimikoen barruan jarraituz, 3.2 eta 3.3 kasuetan, karbamazepina deuseztatzeko aukera aztertu zen. Karbamazepina botika maiz agertzen den etxeko hondakin-uren efluyenteetan dugu. Kasu horretan, fotofenton sistema baten bidezko oxidazioa proposatu zen. Ura tratatzeko lehendik dauden instalazioetan erraz ezar daitekeen prozesu bat da, fotolisia edo ozonizazioan oinarritutako beste AOP batzuk baino erreakzio-denbora eta hautagarritasun handiagoa du, eta Fenton prozesu arrunta baino jasangarriagoa da. Prozesuan eragiten duten aldagaiak aztertu ziren **deuseztatze-errendimendu handiagoa duten eragiketa-estrategiak** ezartzeko. Halaber, poluitzailearen eta haren oxidazio-produktu nagusien degradazio-mekanismo posible bat proposatu zen. Horrez gain,

karbamazepinaren tasa txikiak deuseztatzearen arrazoiak ebaluatu ziren, hainbat parametro fisiko-kimikoren bidez, hala nola kolorea eta uhertasuna.

Anilina eta bentzotiazola zituzten efluente industrialen arazoari ere erantzuna ematen saiatu zen. Ur horiek kautxuaren industriatik zetorren, batez ere. 3.4 eta 3.5 kasuetan aztertu zen arazo hori. Asko aztertutako prozesu fotokatalitikoetan oinarritutako bi soluzio proposatu ziren. Alde batetik, **lehendik bazegoen fotorreaktore komertziala hobetzea** erabaki zen, erreaktorearen hormetan immobilizatutako TiO_2 -a ezarrita. Era hibridoan erabiltzea erabaki zen, esekiduran dagoen TiO_2 -aren kontzentrazio txikiak gehituta. Hala ere, eragiketa-kostuak eta sistema hori eskala industrialean erabiltzeak izan ditzakeen zailtasunak ikusita, material katalitikoak bilatzera birbideratu zen ikerketa. Material hori eraginkorra izan beharko litzateke konposatu erregogorrek eta iraunkorrak degradatzen eta mineralizatzen, eta, aldi berean, merkea, berreskuratzeko erraza eta eguzki-argiarekin aktibatzeke aukera ematen zuenak. Oro har, material jasangarriagoa bilatzea zen helburua. Horri lotuta, 3.5 kasuan, **ikatz aktibatu pikortsuan atxikitako MnO_2 -a duen fotokatalizatzaile berritzaile bat sintetizatu zen (MnO_2/GAC)**, teknika hidrotermalaren bidez. Katalizatzaile horren propietate fisikoak eta kimikoak egokiak zirenez, **ohantze fluidizatuan (FBR, *fluidised bed reactor*) gauzatutako erreakzio-sistema bat diseinatu zen**, eskura dagoen literaturan oinarrituta. Sistema hori prozesu fotokatalitiko bati egokituta zegoen, UV izpien irradiazioa hobetzeko eta fotokatalizatzailean poluitzaileen adsortzioa hobetzeko. Konposite berri horrekin lortutako emaitza onei esker, %80ra arteko mineralizazio-errendimendua lortu ahal izan zen.

Ikatz aktibatuak eta MnO_2 -aren oxidoak sinergia positiboak zituztenez, proposatu zen ikatz aktibatu pikortsuetan (GAC, *granular active carbon*) beste oxido batzuk ere erabiltzea (TiO_2 -a, adibidez) ozonizazio-prozesuetan. Hala, 3.6 eta 3.7 kasuetan, xehetasunez aztertu zen ikatz aktibatuarekin egindako adsortzioa eta ondoren egindako ozonizazio katalitiko (Ad/Ox prozesua, alegia), eta poluitzaile industrial ohikoak (fenola, kasurako) deuseztatzeke halako tratamenduen oinarritzko erreferentzia gisa erabili zen. Ohantze finkoko sistema erdijarraituan nahiz jarraituan, aztertu zen nolako eragina zuten eragiketa-aldagaiak deuseztatze- eta mineralizazio-errendimenduetan. **Ad/Ox prozesurako eredu zinetiko trifasiko bat** proposatu zen —adsortzio-fenomenoa, G-L eta L-S materia-transferentzia eta erreakzio kimikoa, likido zein solido mailan, barne hartzen zituena—. Datu esperimentalen doikuntza egin ondoren, proposatutako eredu aldagaiak aztertzeko eta **eragiketa-estrategiak hautatzeko** tresna bihurtu zen, ereduko konstanteak eta parametroak interpretatuz.

Ad/Ox-rekin emaitza onak lortu zirenez, 3.8 eta 3.9 kasuetan, dopatutako GACen garapena landu zen, ozonizazio katalitikoan erabili ahal izateko. Horretarako, **ikatz aktibatu pikortsuan atxikitako TiO_2 -a duen katalizatzaile berri bat (TiO_2/GAC) garatzea proposatu zen**, 3.5 kasuan katalizatzaileak sintetizatzeke eta garatzeko hartutako esperientzia aprobeztatuz. Katalizatzaile berri hori prestatzeko, metodologia berriak garatu ziren, besteak beste, hauspeatze-metodoak, murgiltze bidezko inpregnazioa eta teknika hidrotermala. TiO_2/GAC konposite berritzaile hori erabili zen ozonizazio katalitikoan, anilina zuten urak tratatzeko. Deuseztatze-maila handiagoa lortu zen erreakzio-denbora laburragoarekin eta ozono-dosi eta eragiketa-kostu txikiagoarekin, 3.5 kasuan ikusitako prozesu fotokatalitikoarekin alderatuz gero. Halaber, prozesua xehetasunez aztertu zen **Ad/Ox prozesurako eredu zinetiko**

trifasikoa formulatuta. Haren bidez, adsortzio-prozesuari, likidoan gertatutako oxidazioari eta katalizatzaile solidoan gertatutakoari erreferentzia egiten zioten hiru koefizienteen bidez zehaztu ahal izan zen erreazio-mekanismo nagusia: Langmuir-Hinshelwood mekanismoa edo Eley-Rideal eraldatua.

Ikatz aktibatu pikortsuan atxikitako oxido metalikoetan oinarritutako ozonizazio-teknologiarekin lortutako emaitzak onak izan baziren ere, ikusi zen azido humikoak, fulbikoak eta beste konposatu batzuk tratamenduarekiko erresistenteak zirela. Hori dela eta, 3.10 kasuan, **ozonizazioarekin konbinatutako ultrasoinuen (US) teknologia erabiltzea** proposatu zen. Aurretratamendu gisa US aplikatuta, azido humikoaren makromolekula apurtu eta molekula txikiago eta erreaktiboagoak sortuko lirateke, eta ozono bidezko tratamendua eraginkorragoa izango litzateke. Hala ere, US-ozonoa konbinazioak azido humikoaren egitura kimikoan izandako eragina ez zen ozonizazio arruntarekin lortutakoa baino hobea izan, makromolekula horren deuseztatzeari zegokionez, karbono organiko guztiaren (TOC, *total organic carbon*) neurketaren arabera. Edonola ere, biodegradagarritasunaren hobekuntza arina eragin zuten aldaketa kimikoen balorazio positiboa egin zen, eta adsortzio-prozesuetan eta/edo prozesu biologikoetan oinarritutako tratamendu alternatiboetarako bidea ireki zuen.

Azkenik, 3.11 eta 3.12 kasuetan, **ozonizazioaren aurretik ultrairagazketa integratzea** proposatu zen hondakin-uren araztegi (HUA) erreal batetik datorren efluente sekundarioko poluitzaile berriak deuseztatzeke. Prozesu biologikoaren bidez eta ultrairagazketa bidez lortutako errendimenduak aztertu ziren, maiz agertzen diren 39 poluitzaile berriren kasurako. Ultrairagazketa egin ondorengo errefus-korrontea ozonizazioaren bidez tratatu zen. Tratamendu integratu horren ondoren ozonizazioa aplikatuta, lortu zen mikropoluitzaileak ia guztiz deuseztatzea (%98 inguruko berreskurapen-faktore batez). Efluentearen toxikotasuna, esekiduran dauden solidoak eta uhertasuna ere ia erabat desagerrarazi ziren, Europako Batasunak onartutako ura berrerabiltzeko araudi berria betez (2020/741 EB). Prozesu integratuaren balorazio ekonomikoa egin zen, HUA bateko efluentea berrerabiltzeari zegokionez, eta ikusi zen tratamendu tertziario konbentzional batek (dekantazio lamelarra, UV argiarekin egindako desinfekzioa eta sodio hipokloritoarekin egindako klorazioa) baino kostu apur bat baxuagoa zuela. Horrenbestez, prozesu horrek aukera handiak zituen ur-kontsumitzaile handiek erabiltzeko (nekazaritzak, adibidez).

1. Sarrera



1.1. Ura, ingurumen-kudeaketaren oinarrizko baliabidea

Ura bizitzarako baliabide sozioekonomiko urria eta ezinbestekoa da. Naturan gertatzen diren prozesu biologikoak nahiz fisikoak garatzeko baliabiderik garrantzitsuena da, eta planetako bizitza mota guztien oinarria [1]. Hala ere, azkenaldian egon den eskaer-igoerak eta sektore industrialetan eta etxeetan duen parte-hartze zuzenak eta ez-zuzenak gainazaleko eta lur azpiko ur gezaren jasangarritasuna mehatxatu egin dute. Urak halako eragina du eguneroko bizitzan ezen gero eta murrizketa eta ingurumen-arau zorrotzagoak ezartzen ari baitira sektore garrantzitsuetan, hala nola nekazaritzan, basogintzan, janari-industrian eta manufaktura-industrian [2]. Hori horrela, ezinbestekoa da ur-baliabideak era estrategikoan eta jasangarrian kudeatzea eta erabiltzea.

Lehen sektorearekin erlazionatutako jarduera ekonomiko askotan, urak baldintzatzen du zer produktu mota, zenbat eta zer kalitatekin sor daitekeen. Bigarren eta hirugarren sektoreetan, berriz, lehengaien eraldaketarekin dago lotuta ura. Hozgarri eta garbigarri gisa erabiltzen da, baita beste hainbatetarako ere turismo- eta aisialdi-industrian [3].

Munduan gaur egun urarekin dauden arazoetan, faktore ugari eragiten dute. Horietako bat ur-eskasiarekin lotuta dago. Arazoa gero eta handiagoa da, urtez urte munduko populazioa handitzen joan delako: egun 7.800 milioi pertsona gara, eta 11.000 milioi pertsona izatera iritsiko gara mende amaierarako [4]. Horrez gain, populazioa hirigune handietan pilatzearen ondorioz, desoreka sortu da eskuragarri dagoen ur gezaren kantitatearen eta Lurreko gizakiek kontsumitzen dutenaren artean. Arazo horrekin lotuta, efekturik nabarmenenak akuiferoetan daude, putzuen bidez gehiegi ustiatzen dira eta. 1960ko hamarkadaz geroztik % 60 areagotu da akuiferoen ustiapena, eta, kasu batzuetan, haiek agortzea eragin du [5]. Ikus daitekeen beste eraginetako bat desertifikazioa da. Zuhaitz-mozketa masiboan, gehiegizko abeltzaintzaren eta suteen ondorioz, baso-masa handia galdu da. Horren guztiaren ondorioz, halako ekosistemen erdia galdu da 1960ko hamarkadaz geroztik, eta asko murriztu da lurrek ura atxikitzeo duten gaitasuna [6,7]. Azkenik, hirietako eta nekazaritza-guneetako hornikuntza-sareetan dauden ur-galera eta -ihes handiak ur-urritasuna eragin duten beste faktore erabakigarri bat dira. Horrenbestez, litekeena da ur-baliabideen urritasuna berehalako errealtate bihurtzea datorren hamarkadan [8].

Hala ere, egungo arazoak eragin dituen beste faktore bat uraren poluzioarekin eta degradazioarekin erlazionatuta dago. Industria- eta meatzaritza-jarduerak eta nekazaritzako pestiziden erabilera masiboek eragindako poluzioa da, neurri handi batean. Horrez gain, hondakin-uren araztegiak edo ur horiek tratatzeko baliabiderik ez duten herrietan gertatzen diren kontrolik gabeko isurketek ere poluitu egiten dituzte gainazaleko eta lur azpiko urak [9,10].

Testuinguru horretan, ingurumenaren kudeaketa eta administrazioa era publikoan kontrolatu behar da hura babestea nahi badugu, gizarte osoak baitu ingurumena zaintzeko ardura. Izaera publiko hori argi ikusten da baliabide hain garrantzitsuak kudeatzeko ezarrita dagoen araudi-esparru zabal eta konplexuan. Arazo horren jakitun, Europako Parlamentua eta haren kide diren estatuetakoko parlamentu nazionalak ur-baliabideak kudeatzeari eta kontserbatzeari buruzko gaien inguruko legeak ezartzen ari dira azken bi hamarkadetan, eta gero eta muga zorrotzagoak jartzen ari dira. 2000/60/EE Uraren Esparru Zuzentarauan eta duela gutxi onartutako ura berrerabiltzeari buruzko

2020/741/EB zuzentarauan oinarrituta dagoen 817/2015 Errege Dekretuaren bidez gauzatu dute hori, Espainiako ordenamendu juridikoko errege dekretuen bidez aplikatu diren [11–13] Europako zuzentaruetan hain zuzen. Uraren aprobetxamendua oztopatzen edo ekosistemak kaltetzen dituzten poluitzaileetako asko Europako Batasunak erregulatzen ditu Europako Ingurumen Agentziaren (EIA) bidez, 2013/39/EB zuzentaruaren bidez, eta 2015/495/EB eta 2018/840/EU erabakietan jasotako lehenetsuneko substantzien zerrendaren bidez. Halaber, atzerriko beste agentzia batzuek ere erregulatu dituzte. AEBko Ingurumena Babesteko Agentziak (IBA), adibidez, *Contaminants Candidate List* (CCL) delakoaren bidez erregulatu ditu [14,15].

Horrenbestez, ura errealitate ekonomiko bat eta ekosistemak mantentzeko ezinbesteko baliabide bat da, baina, batez ere, gizakien bizitzaren eta duintasunaren oinarritzko eskubide bat da. 2015ean aintzatetsi zuen eskubide hori Nazio Batuen erakundeak, garapen jasangarrirako helburuetan (GJH) eskubide hori sartzean. Helburuen artean jaso zen 2030erako uraren eta saneamenduaren oinarritzko eskuragarritasun unibertsala giza eskubide bat izango zela, eta uraren egoera bizitzaren eta ekonomiaren oinarria eta ongizate komuna bermatzen duen ondasun publiko bat izatearekin erlazionatu zuen. Penintsulako lurraldearen zati handi bat elkorra edo ia elkorra denez, eta desertifikazioa gero eta arazo handiagoa denez, lehen aipatu bezala, 6.GJHa (Ur garbia eta saneamendua) klima-aldaketaren aurkako borrokari dagokion 13. GJHarekin (Klimaren aldeko ekintza) bereziki erlazionatuta egongo litzateke [16,17]. Ondorioz, uraren kudeaketa erronka handi bat da, eta klima-aldaketaren testuinguruan are handiagoa bilakatuko dela aurreikusten da. Hori dela eta, ur-baliabideen kudeaketak garrantzi handia izango du trantsizio ekologikoko politika publikoen esparruan.

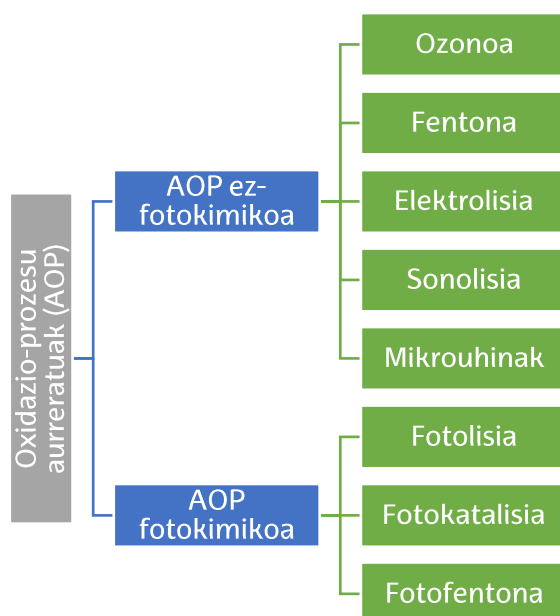
Hondakin-uren esparruan dauden soluzio aurreratuen maila baxuak argi erakusten du teknologia berriak ikertzeko behar larria dagoela. Teknologia horien artean daude, besteak beste, oxidazio-teknologia aurreratuak [18,19] edo mintz bidezko bereizketa-prozesuak [20,21]; izan ere, fenola, bentzotiazola, 4-klorofenola, anilina, materia organiko naturala eta beste poluitzaile batzuk dituzten hondakin-uren tratamendua hobetuko lukete. Gainera, sortzen ari diren poluitzaile berriek [22,23] —karbamazepinak, adibidez— argi erakusten dute ikerketa hori egitea behar-beharrezkoa dela konposatu horien izaera ulertzeko eta horiek ur-baliabideetan eta, beraz, ingurumenean dituzten ondorioak zein diren jakiteko. Horri dagokionez, argian edo ozonoan oinarritutako oxidazio-teknologia aurreratuak [24] aukera eraginkorrenetako batzuk dira, erazteko zailak diren gai toxikoekin poluitutako urak prozesu konbentzionalen bidez tratatzeko. Oxidazio-teknologia horiek beste bereizte-prozesu batzuetan integra daitezke —mintz bidezko prozesuetan, adibidez—, poluitzaileak guztiz deuseztatzeko eta ura jaso zen egoera berean bueltatzeko ingurumenera [18,20].

Oxidazio-prozesu aurreratuak (*advanced oxidation process*, AOP) oso ezagunak dira hondakin-ur organikoen tratamenduaren esparruan. Oso teknologia eraginkorrak dira hainbat poluitzaile mota tratatzeko, hala nola poluitzaile organiko toxiko eta iraunkorrak, sortzen ari diren poluitzaile berriak, poluitzaile naturalak, pestizidak, tindagaiak eta bestelako poluitzaile kaltegarriak. Beste metodo kimiko batzuekin alderatuz, AOPak oso prozesu eraginkorrak dira, eta ez dute bigarren mailako poluziorik eragiten [25]. AOPen barruan sartzen dira, besteak beste, Fenton-en erreakzioak, fotofentona, oxidazio fotokatalitikoak, ozonizazioa, oxidazio-erreakzio elektrokimikoak, oxidazio sonokimikoak, oxidazio-prozesu superkritikoak eta beste hainbat. Prozesu

horiek poluitzaile organikoak guztiz edo zati batean degradatzeko gai dira erradikal oso aktiboak sortuta [26–28].

Prozesu horietan, esan bezala, hidroxilo erradikalak sortzen dira, uretan dauden poluitzaileak oxidatu eta suntsitzeko behar beste. Hidroxilo erradikala ura tratatzeko erabiltzen den espezie oxidatzailerik errektiboena da. 2,80 V-eko potentziala du, ohiko beste oxidatzaile batzuk baino askoz handiagoa; ozonoak $E^\circ = 2,08 \text{ V}$ du, eta oxigenoak, berriz, $E^\circ = 1,23 \text{ V}$ [29]. Oro har, poluitzaile organikoek hidroxilo erradikalarekin izaten duten interakzioan hidrogeno bat irabazi edo galdu egiten da. Horren ondorioz, karbonoan oinarritutako erradikal bat sortzen da (elektroien transferentzia-erreakzioen bidez sortua), eta, ondoren, oxigeno molekularrekin erreaktionatzen du eta peroxilo erradikal bat sortzen du. Azkenik, peroxiloak poluitzailearekin erreaktionatzen du. Zetonak, aldehidoak edo alkoholak izan ohi dira oxidazioaren produktuak [30]. Oxidazioaren produktu horiek, oro har, ez dira hain toxikoak izaten eta biodegradatzeko errazagoak izaten dira [31].

AOP oxidazio-prozesu garrantzitsuenen sailkapen posible bat dago 1. irudian. Oxidazio-prozesu aurreratuetan, agente oxidatzaile sendoak erabili ohi dira—adibidez, hidrogeno peroxidoa (H_2O_2), ozonoa (O_3) edo katalizatzaileak (oxido metalikoak, erdieroaleak eta abar)—, eta argi ultramorearen, eguzki-argiaren edo ultrasoinuen bidezko irradiazioa ere erabili ohi da, bi prozesuak bereizita zein konbinatuta [32].



1. irudia Argiarekin eta argirik gabe gertatzen diren AOPen sailkapena.

Gaur egun, argia eta ozonoa erabiltzen duten AOPak dira hondakin-urak tratatzeko metodorik erakargarrienak, eraginkortasun handikoak eta jasagarriak direlako. Ezarpen industrial handia duten teknologiak dira biak, eta, horri esker, ekonomia zirkularra sustatzen eta hondakinak murrizten laguntzen dute [18]. Horrez gain, bi AOP edo gehiago batera erabiliz prozesuak indartzen dira, eta estrategia hori gero eta gehiago erabiltzen da oxidazio-gaitasuna handitzeko. Hala eginda, espezie oxidatzaile gehiago sortzen dira, prozesuan espezie gehiagok parte hartzen duelako (HO^\bullet , HO_2^\bullet , $\text{O}_2^{\bullet-}$) eta banakako prozesuen artean efektu sinergikoa sortzen delako (ikus 1. taula) [33].

1. taula AOP bakoitzean sortutako espezie oxidatzaileak [34].

AOPa	Espezie oxidatzaileak
<i>Fotokimikoa</i>	
Fentona	HO [•] , HO ₂ [•]
Fotofentona	HO [•]
UV/H ₂ O ₂	HO [•] , O ₂ ^{-•} , HO ₂ [•]
UV	HO [•] , H ⁺ , e ⁻
Fotokatalisia	HO [•] , h ⁺ , e ⁻ , O ₂ ^{-•} , HO ₂ [•]
<i>Ez-fotokimikoa</i>	
Ozonizazioa	HO [•] , O ₂ ^{-•} , HO ₂ [•] , HO ₃ [•] , O ₃ ^{-•}
Sonolisia	HO [•] , H [•]

1. taulan jasotakoaren arabera, *in situ* sortzen diren eta prozesuan parte hartzen duten erradikalen sortze-mekanismoen mende eta erasoaren eta degradazioaren eraginkortasunaren mende dago AOP oxidazio-prozesu bakoitzaren efektibotasuna. Eraginkortasuna, halaber, prozesuko eragiketa-aldagaien, ur-kalitatearen eta erradikal-kaptadoreen mende dago. Hala ere, kasu batzuetan AOP bat baino gehiago integratzeak inhibizio-efektuak eragin ditzake, nahiz eta oso ohikoa ez izan. Hala gertatzean, degradazioaren abiadura eta gaitasuna gutxitu egiten dira. Hori gertatzearen arrazoietako bat da espezie oxidatzaile asko sortzearen eraginez *scavenger* gisa jokatzeko hasten direla, erradikalak ez baitira oso espezie selektiboak [35,36].

Laburbilduz, hondakin-uren tratamendurako prozesu konbentzionaletan lortzeko zailak diren abantaila operatibo asko dituzte AOPek. Teknologia horiek erabiltzearen abantaila nagusiak 2. taulan jaso dira. Taula horretan ikus daitekeenez, AOPek, oro har, hainbat abantaila dituzte, hala nola erreazio-abiadura handia eta hainbat motatako poluitzaile organikoren toxikotasuna murrizteko eta guztiz mineralizatzeko gaitasun handia. Gainera, ez dituzte hondakinak kontzentratzen ezta medio batetik bestera transferitzen ere. Fenton-en teknologiak salbu, gainerako AOPek ez dute sortzen aurrerago tratatu behar izaten den lohirik. Bestalde, AOPek ez dutenez talde funtzional jakin bat era selektiboan erasotzen, hainbat izaeratako poluitzaileak trata daitezke aldi berean. Azkenik, esan behar da uren tratamendurako instalazioetan halako prozesuak ezartzeko kostua baxua dela. Hala ere, tratatu beharreko uraren ezaugarrien eta kontzentrazioen arabera, baita araztutako uraren helburuaren arabera ere, AOP bat edo beste bat ezartzeak abantaila gehiago izango ditu. Hurrengo bi ataletan azalduko dugu hori, teknologia bakoitzaren egokitasuna zehazten dugunean.

2. taula AOP batzuen abantaila eta desabantaila nagusiak [37].

Teknologia	Abantaila	Desabantaila
Fotolisia	<ul style="list-style-type: none"> - Oso eraginkorra hainbat motatako konposaturekin - Erabiltzeko erraza - Beste oxidatzaile arrunt batzuekin indartu daiteke; hidrogeno peroxidoarekin, adibidez 	<ul style="list-style-type: none"> - pH baxua behar da - Kondentsazio-konposatuak sortzen dira - Erreakzio-denbora oso luzeak
Fotokatalisia	<ul style="list-style-type: none"> - Kostu-eraginkortasun erlazio ona - Ez du toxikotasun handiagoa sortzen - Ez dago mugarik materia-transferentzian - Kimikoki prozesu egonkorra da eta giro-tenperaturan egin daiteke 	<ul style="list-style-type: none"> - Bereizte-etapa bat behar du katalizatzailea berreskuratzeko, <i>slurry</i> motako errektore batean egiten bada - Argi ultramorea (UV) behar du fotokatalizatzailearen gainazala aktibatzeko
Fotofentona	<ul style="list-style-type: none"> - Mineralizazio azkarra - Erreakzio-abiadura handia - Lohi ferrikoen ekoizpen txikia 	<ul style="list-style-type: none"> - Eragiketa-kostu handia - UV-ikusgaiaren espektroan funtzionatzen duten lanparak behar ditu - Lohiak sortzen dira
Ozonizazioa	<ul style="list-style-type: none"> - Konposatu organikoak hain toxikoak ez diren azpiproduktu biodegradagarriagoetara oxidatzeko gaitasuna - Selektiboa da - Hainbat poluzio-kargarekin eta emarirekin erabil daiteke - Ez du hondakinik sortzen - Haren ekintza indartu daiteke oxido metalikoetan oinarritutako katalizatzaileak erabilita 	<ul style="list-style-type: none"> - Ozonoak osagai erregogor jakin batzuekiko duen erreaktibotasuna mugatua da - Teknologia konplexua da behar dituen instalazioengatik - Ozonoa sortzearen energia-kostua
Ultrasoinuak	<ul style="list-style-type: none"> - Ez du kanpo-erreaktiborik behar erreakzioa abiarazteko - Parte hartzen duten faseen arteko materia-transferentzia hobetzen du 	<ul style="list-style-type: none"> - Aplikazio mugatua du eskala errealean - Tratamenduaren eraginkortasuna hobetu egin behar da - Energia asko behar da degradazio-maila esanguratsua lortzeko.

1.2. Prozesu fotokimiko primarioak eta katalitikoak

1.2.1. UV/H₂O₂-an oinarritutako prozesuak

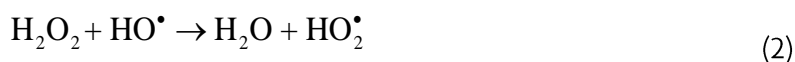
Argia ultramorearen erabileran oinarritutako prozesu fotokimikoak oso teknologia finkatuak dira, bai ur edangarriaren tratamenduan, bai hondakin-uren tratamenduan. Are gehiago, munduan aplikazio gehien dituzten eta gehien eskalatu diren tratamenduak dira [38]. Teknologia hori oso erabilgarria da hainbat hondakin-ur motatan kontzentrazio txikitzen dauden produktu farmazeutikoak tratatzeko. Alabaina, prozesu fotolitikoak direnez, oxigeno-eskaera kimiko (OEK) txikia duten konposatu fotosentikorretan soilik aplika daitezke. Prozesu industrialetatik datozen eta poluitzaile-karga handia duten efluenteen kasuan, fotolisia ez da eraginkorra, kontzentrazio altuek inhibitu egin baitezakete fotodegradazio-prozesua [39].

Beste efektu batzuek —hondakin-ur industrialetan gai solidoak esekiduran izateak eragiten duen iluntasunak, adibidez— argi ultramorearen eraginkortasuna gutxitzea eragin dezakete. Halakoetan, hidrogeno peroxidoa gehituz fotolisi-prozesua indartzea aukera ona izan daiteke poluitzaile organiko fenolikoak, klorodunak eta abar deuseztatzeko.

Hidrogeno peroxidoa, bestalde, oxidatzaile kimiko seguru bat da, ugaria eta erabiltzeko erraza. 1,78 V-eko oxidazio-potentziala du (E°), eta asko erabiltzen da industrian poluitzaile ugari deuseztatzeko. Hala ere, beste oxidatzaile batzuekin alderatuz gero (ozonoarekin, adibidez), ez ditu bere horretan oxidazio-ezaugarri onak. Hori dela eta, beste substantzia batzuekin, argi ultramorearen iturriekin edo katalizatzaileekin konbinatu behar da eraginkorragoa izan dadin [40,41]. Argi ultramore (UV) erabiltzen duten prozesuetan hidrogeno peroxidoa erabilia areagotu egiten da AOParen gaitasun fotolitikoa, zeharkako erreakzioak gehitzen baitira. Erreakzioaren abiadura handitze hori hidroxilo erradikal asko sortzeak eragiten du; izan ere, halako erradikal asko sortzen dira hidrogeno peroxidoaren O–O loturaren haustura homolitikoa gertatzean [42], 1. ekuazioan ikus daitekeenez:



Prozesu horretan errendimendu kuantikoa oso handia bada, gehienez bi hidroxilo erradikal sortuko dira. H_2O_2 -aren deskonposizio hori fotoinduzitu egin daiteke Haber-Weissen erradikal-mekanismoaren bidez, hedapen-urrats hauei jarraituta [43]:



Azkenik, hainbat amaitze-erreakzio gertatzen dira, erradikalen errekonbinazio-erreakzioen bidez:



Aldi berean, konposatu organikoaren beraren disoziazio-orekak gerta daitezke, baita sortutako tarteko konposatuenak ere (hidroxilo erradikalak, hidroperoxidoa eta abar), 7. eta 8. ekuazioen arabera:



Laburbilduz, hidrogeno peroxidoaren deskonposizio- eta sorrera-ziklo bat sor daiteke. Ziklo horrek izan dezakeen emaitza globala eragiketa-parametroen mende egongo da, besteak beste, erradiazio ultramorearen intentsitatearen, temperaturaren, pH-aren eta konposatu organikoaren izaeraren mende.

Sistema honetan erabiltzeko moduko poluitzaile aproposa 4-klorofenola izan daiteke. Toxikotasun handiko poluitzaile bat da, eta pestizida, desinfektatzaile eta antiseptiko ugari dituzten efluente industrialetan aurkitu ohi da. Gainera, poluitzaile honek beste berezitasun bat du. Hura oxidatzean sortzen diren azpiproduktuak hasierako poluitzailea baino toxikoagoak izan daitezke jarraitzen duten degradazio-ibilbidearen

arabera. Prozesu fotokimikoek funtzio garrantzitsua dute horiek deuseztatzen, 3. taulan ikus daitekeenez.

3. taula 4-klorofenola deuseztatzeko helburuarekin hondakin-ur industrialak tratatzeko metodoak

AOPa	Oharrak	Erreferentzia
Fotofentona	Lehen etapan, erreazio heterogeneo bat gertatu zen burdinaren gainazalean erradikalen bidetik, eta 4-klorokatekola deuseztatzeko eraginkorra izan zen. Bigarren etapan, erreazio homogeneo bat gertatu zela ikusi zen (Fenton-en erreazioa), eta <i>orto</i> eta <i>paraklorofenolperoxilo</i> erradikalek eta O ₂ -ak parte hartu zuten erreazio horretan. Ez zen lortu toxikotasun-maila onargarririk.	[44]
UV/TiO ₂	Ikusi zenez, TiO ₂ kristalen tamaina handitzeak (kaltzinazio-tenperaturaren efektuaren ondorioz) erraztu egiten zuen 4-klorofenola deuseztatzea. Hala ere, degradazio-bitartekariak hasierako poluitzaileak baino toxikotasun-maila apur bat handiagoa zuten.	[45]
UV/ZnO	4-klorofenola deuseztatzeko aldaera operatiboek pseudo-zero ordenako zinetikarekiko zuten mendekotasuna ikertu zen. Ikusi zenez, uretan ohikoak diren anioi inorganiko batzuek (Cl ⁻ eta SO ₄ ²⁻) gune aktiboen blokeatzaile gisa jokatzen zuten. O-hidroxilazio batean oinarritutako erreazio bat proposatu zen, eta horrek oso toxikoak ziren konposatu ugari eta katekola sortzea ekarri zuen.	[46]
UV/O ₃ /H ₂ O ₂	Ozonoa deskonposatzean hidroxilo erradikalak sortu ziren. Hala ere, hidroxilo erradikalak agertzeak ez zuen oxidazio-tasa igorazi pH = 9an. 7 eta 12 arteko pH-tartean neurtu ziren pseudo-lehen ordenako (klorofenolaren degradazio-erreazioa) konstante zinetikoen balioak ez ziren izan bata bestearekiko oso ezberdinak izan.	[47]
UV/H ₂ O ₂	Egjaztatu zen H ₂ O ₂ gehituta magnitude-orden batean handitzen zela erreazio-fotolitikoaren abiadura, fotolisiarekin ez bezala. Prozesua hobetu egin zen 4-klorofenolaren mineralizazioari dagokionez, eta konposatu biodegradagarriak ekoitzi ziren batez ere.	[48]

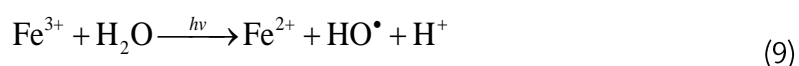
2. taulan erakutsitako AOP prozesuen artean, UV/H₂O₂ sistemak dituen abantailak azpimarratuko genituzke. Çatalkaya et al. taldearen iritziz [48], beste teknologia batzuk aplikatzeak izango lituzketen eragozpenekin alderatuz, eragiketa-kondizio egokietan (oxidatzaile-dosia, irradiazio-denbora, pH-a eta abar) egindako UV/H₂O₂ prozesuak efluentearen toxikotasuna eraginkortasunez murriztuko luke, haren biodegradagarritasuna eta mineralizazioa hobetuko lituzke eta uraren kolorearen intentsitatea jaisten lagunduko luke. Testuinguru horretan, prozesu biologiko batek onartzeko moduko toxikotasun-maila lortu arteko oxidazioa egingo balitz aurrez UV/H₂O₂ sistema baten bidez, guztiz oxidatuko litzateke efluente industrialaren karga organikoa, bat ere oxidazio-azpiprodukturik sortu gabe; besteak beste, kinonak, zeinak hasierako poluitzailea bera baino toxikoagoak baitira.

1.2.2. Fotofenton sisteman oinarritutako prozesuak

Fenton erreaktiboaren teknologia luze eta zabal erabiltzen da industrian poluitzaile organikoak degradatzeko, konposatu aromatikoak eta alifatikoak barne [48]. Fe-a bertan dela hidrogeno peroxidoa pH azido edo neutroan deskonposatzean eta hidroxilo erradikalak ekoiztean oinarritzen dira Fenton prozesuak [49]. Fenton prozesuek abantaila hauek dituzte: konposatu iraunkorrak modu eraginkorrean deuseztatzen dituzte, erabiltzeko errazak dira eta giro-tenperaturan eta presio atmosferikoan egin daitezke [44]. Horrez gain, erreaktiboak oso erraz eskuratu daitezke eta oso erabilerrazak dira, eta hori ere nabarmentzekoa da. Halaber, erraz aplikatu daitezke

prozesuok, ekipo berezirik behar izan gabe, eta erraz integra daitezke lehendik erabiltzen diren ur-tratamenduetan, besteak beste, koagulazioan, iragazketan edo oxidazio biologikoan [50,51]. Beste AOP batzuek ez bezala, Fenton teknologiak erreazio-abiadura laburra du, laburrenetakoa. Fenton prozesu homogeneoen desabantaila nagusiei dagokienez, aipatzekoa da prozesuaren amaieran metalak dituzten lohi ugari sortzen direla [27]. Horrek esan nahi du ingurumenerako kaltegarriak diren efektuak egongo direla. Efluentean metal katalitiko ugari isurtzen denez, berreskuratze-etapak txertatu behar dira prozesuan, eta horrek garestitu egiten du eragiketaren kostua.

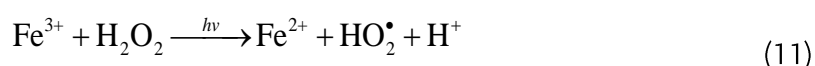
Hala ere, beste teknika batzuekin konbinatuz gero —argi ultramorearekin, adibidez— hobetu egin daiteke prozesuaren eraginkortasuna. Fotofenton izenez ezagutzen da prozesu hori [48,54]. Oso poluituta dauden hondakin-urak tratatzeko moduetatik etorkizun handiena duenetako bat da sistema hori. Ohiko fenton prozesuan ez bezala, sistema honetan, hidrogeno peroxidoaren fotolisia egiten da hasieran, 1. ekuazioaren arabera. Ondoren, Fe-a duen katalizatzailean irradiazio ultramoreak aplikatuta, Fe³⁺ ioia Fe²⁺-ra erreduzitzen da, eta hidroxilo erradikalak sortzen dira, 9. ekuazioaren arabera [54]:



Gero, 10. ekuazioan ikus daitekeenez, Fe²⁺-aren eta hidrogeno peroxidoaren artean erreazio azkar bat gertatzen da, eta hidroxilo erradikal gehigarriak sortzen dira Fenton-en erreazio arruntaren bidez. Hala, sortutako ioi ferroso berriek berriro erreazionatzen dute hidrogeno peroxidoarekin, eta hidroxilo erradikalak eta ioi ferrikoak sortzen dituzte, eta, hala, berriro elikatzen dute zikloa.



Aipatutako abantailaz gain, Fe³⁺-ak hidrogeno peroxidoarekin erreazona dezake eta erradikal-espezie gehiago eta Fe²⁺-a sortu, 11. ekuazioaren arabera.



Fotofenton teknologiaren onurak eta desabantailak kontuan hartuta, farmazeutikoki aktiboak diren produktuak dituzten urak egokiak lirateke AOP prozesu honen bidez tratatzeko. Horren arabera, karbamazepina eta antzeko botikak deuseztatzeko tratamendu gisa erabili ahal izango litzateke.

Hondakin-uren araztegian (HUA) arazo gehien sortzen ari den botiketako bat da karbamazepina. Sistema konbentzionalek instalazioetara sartzen diren uretan dagoen karbamazepinaren % 10 baino gutxiago deuseztatzeko gaitasuna dute [55]. Botika hori asko erabiltzen da gaixotasun neurologikoak tratatzeko, besteak beste, epilepsia, depresioa edo nahasmendu bipolarra. Gizakietan, % 72 xurgatzen eta metabolizatzen da gibelean, eta % 28 iraitzen da gorotzen bidez. Hori dela eta, hiriko hondakin-uretan maiztasun handiz atzematen diren konposatu farmazeutikoetariko bat da [56].

Hori horrela, HUAetan tratamendu tertziario bezala txerta daitezke AOPak, halako botikak eraginkortasunez deuseztatzeko. Aplikazio gehien dituzten AOPen artean, nabarmentzekoak dira prozesu hauetan oinarritutakoak: ozonoaren bidezko oxidazioa [57], oxidazio elektrokimikoa, UV prozesuen erabileran oinarritutako fotokatalisia, fentona eta fotofentona [58]. Horiez gain, aipatu behar da ozonoaren bidezko oxidazioa

oso errektiboa den arren olefinak edo aminak barne-egituran dituzten konposatu organikoekin, ez dela hain eraginkorra karbamazepinaren degradazioan aplikatzen denean [59]. Oxidazio elektrokimikoari dagokionez, elektrodoen osagaiak faktore ekonomiko mugatzailea dira era industrialean aplikatzeko garaian, eta hori dela eta ez da oso prozesu arrakastatsua izan.

Konposatu organiko mota ugari degradatzeko eta hidroxilo erradikalak sortzeko gai diren Fenton eta antzeko prozesuen kasuan, Fe^{2+} -a etengabe hornitu behar da. Horren eraginez, burdina ugari duten lohi gehiegi sortzen da [60]. Arazo hori arintzeko, fotofenton teknologia erabil daiteke, zeinaren bidez Fe(II) kontzentrazio txikiagoa erabil baitaiteke Fenton-en erreakzio konbentzional batean baino. Hori dela eta, fotofenton teknologia aukera eraginkorragoa, jasangarriagoa eta ingurumenerako egokiagoa litzateke karbamazepina eta antzeko botikak dituzten urak tratatzeko.

1.2.3. Fotokatalisi heterogeneoa

Kostu baxua duen eta ingurumenarekiko egokia den teknologia moldakor bat da fotokatalisi heterogeneoa. Poluitzaile ugari deuseztatzeko erabil daiteke, gainera. Azken lau hamarkadetan azkar hedatu den AOP bat da, eta hainbat garapen izan ditu, batez ere energiarekin eta ingurumenarekin erlazionatutako eremuetan [24,61].

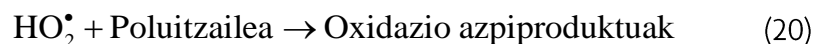
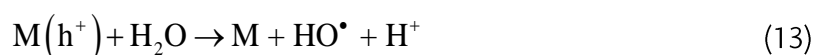
Azken hamarkadetan, fotokatalisiak eragin duen interesak bultzatuta, material erdieroaleak erabili dira fotokatalizatzaile gisa, bai ur- edo gas-fasean dauden sistemetako espezie organikoak eta inorganikoak deuseztatzeko, bai beste aplikazio batzuetarako, hala nola ingurumena garbitu edo edateko ura zein ur industrialak eta hondakin-urak tratatzeko [19,37]. Gehien ikertu diren materialen artean, TiO_2 -a dago [63]. Konposatu hori inerte da ingurumenean, fotokimikoki egonkorra da, eta erredox prozesuen bidez aireko eta uretako substratu organikoak eta inorganikoak oxidatzeko gaitasun bikaina du [25].

Oro har, fotokatalizatzaileek eguzki-argiaren edo argi artifizialaren erradiazio ultramoreak aprobetxatzen dituzte erradikal-espezieak sortzeko; ondoren, erradikal horiek arduratuko dira hainbat substantzia deskonposatzeaz, besteak beste, azido organikoak, estrogenoak, pestizidak, tindagaiak, konposatu aromatikoak eta abar [63,64]. Nanopartikulak uretan ez daudela ziurtatzeko, substratu baten bidez immobilizatzen dira. Horri dagokionez, duela gutxi egindako ikerketa batzuetan ikusi da nola immobilizatu TiO_2 nanopartikulak fotorreaktorearen hormen gainean euskarri gisa balio duten film meheetan atxikita [65,66]. Hala ere, efluentean dauden poluitzaileen kontzentrazio-aldaketek mugatu egiten dute konposatuaren erabilera. Horregatik, TiO_2 nanopartikulak gehitzea irtenbide bat izan daiteke une puntualetan; adibidez, efluentearen poluitzaile-kargaren piko puntualetan erreakzio-sistema hori (TiO_2 immobilizatuko katalizatzailea duena) diseinatzean aurreikusi ziren baldintzak gainditzen dituztenean.

Fotokatalizatzailea immobilizatuta edo esekiduran egon, ezinbestekoa da erdieroalea aktibatzea argi ultramorearekin, eguzki-argiarekin edo argi artifizialarekin irradiatuta. Material jakin bakoitzean debekatuta dagoen energia-bandaren arabera erabakiko da zer argi motarekin aktibatzen den. Material bakoitzaren ezaugarri elektronikoen mende dago banda-zabalera optikoaren balio hori. Debekatutako banda-energiaren balioa zenbat eta baxuagoa izan, orduan eta aukera gehiago izango du materialak argi ikusgaiaren/UV hurbilaren bidez aktibatzeko [67].

Materialaren eraginkortasun kuantiko hori optimizazio-tekniken bidez hobetu daiteke. Katalizatzaileen propietateak hobetzeko gehien erabiltzen den aukeretako bat dopatzeko mekanismoak dira [68]. Mekanismo horien artean, hauek daude: heterolotura-metodoak, banda ezberdinak dituzten bi erdieroale lotzean dautzena (NiTiO₃, TiO₂-MnO₂ eta abar); metal nobleak jalkitzea haien propietate elektroniko egokiak aprobetxatuta; morfologiaren kontrola; eta elementu metalikoekin (Fe, Co, Ni, Mn) eta ez-metalikoekin (karbonoa, adibidez) dopatzea [50,69].

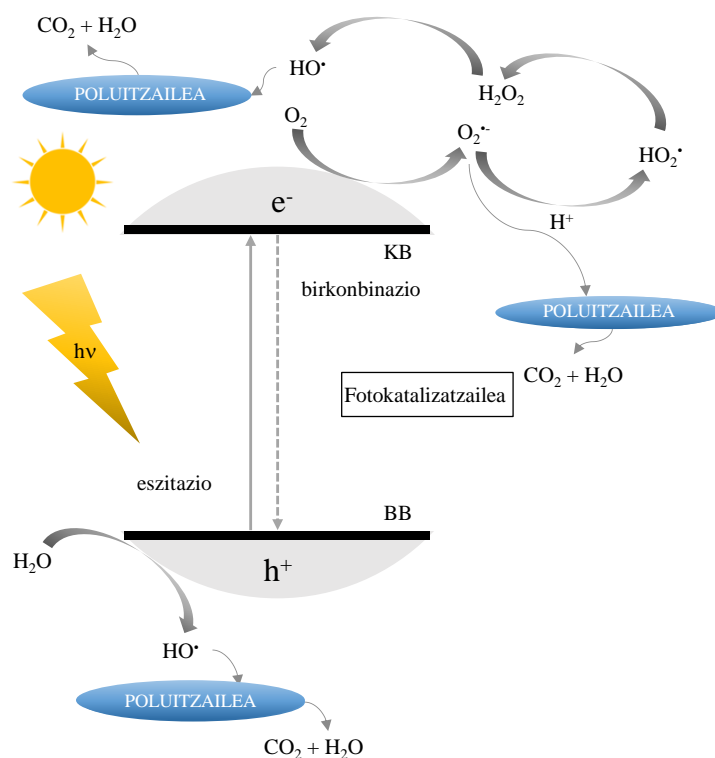
M erdieroale baterako fotokatalisi-teknologiaren erreakzio-mekanismoa 12-20 ekuazioen bidez deskriba daiteke [70].



2. irudiaren arabera, fotokatalisi-prozesuaren lehen erreakzioan, katalizatzaileak UV erradiazioak xurgatu zituen eta elektroio pare hutsak sortu ziren (h^+/e^-). Ondoren, elektroiek duten erredukzio-gaitasun handia dela eta, fotokatalizatzailearen gainazalean adsorbatutako oxigenoa erreduzitzen dute. Hala, superoxido ioia sortzen da ($O_2^{\bullet-}$). Gero, ura eta HO^- -aren espezie adsorbatuak oxidatzeaz arduratzen dira elektroio hutsak, eta hidroxilo erradikalak sortzen dira. Hidroxilo erradikal horiek arduratuko dira geroago poluitzaile organikoak oxidatzeaz. Gainera, poluitzaileak katalizatzailearen gainazalean adsorbatuta daudenean, gerta daiteke katalizatzailea zuzenean oxidatzea katalizatzailearen elektroio bat errebox erreakzioen bidez zuzenean transferituta.

Aztertutako material katalitikoaren artean, material karbonosoetan oinarritutako katalizatzaileek arreta handia erakarri dute MnO₂-aren oxidoen euskarri katalitiko gisa, MnO₂-AC konposite berrien sintesian [71-73]. Izan ere, konbinazio horrek propietate elektriko eta egitura-propietate egokiak ekartzen ditu berekin, eta, gainera, propietate horiek bakarrak eta kontrolatzeko modukoak dira [62]. Abantaila horiei esker, hauek hobetu dira: (i) debekatutako energia-banda sintonizatzea, kitzikapeneko uhin-luzera hedatzeko aukera emanez; (ii) elektroio-hutsunaren errekonbinazioa atzeratzea, eta (iii) erreaktiboak eta gune aktiboak adsorbatzeko gainazal zabala ematea. Manganeso oxidoek beste abantaila batzuk ere badituzte: poluitzaile iraunkorrak eraginkortasun handiz deuseztatzen dituzte [74,75], lurrazalean ugari daude, fabrikazio-kostu txikia

dute (TiO_2 -a baino % 75 merkeago, gutxi gorabehera) [76], fabrikatzeko prozesuan erraz erreproduzitzeko aukera dute, adsortzio-propietate onak dituzte, toxikotasun baxua, azidoekiko erresistentzia, erreodox potentziala eta ingurumenari ez diote kalterik eragiten [36,71,77]. Gainera, MnO_2 -ak 1-2 eV arteko banda-energia debekatua du, sintesi-prozesuan lortutako kristalaren egituraren arabera. Horri esker, eskualde ikusgai aktibatzen da, eta oxido metaliko klasikoek oso lehiakide gogorra bihurtu da katalizatzaile-funtzioa betetzeko garaian [78,79].



2. irudia Fotokatalisi heterogeneoaren printzipioak, material katalizatzaile erdieroaleekin.

Hala ere, teknologia mota honetan erreazio-sistema bera ere kontuan hartu behar da. Erreaktore motak alderatzeko egin diren azken ikerketetan ondorioztatu denez, ohantze trinko, finko eta fluidizatuko erreaktoreek (FBR, *fluidized bed reactor*) eskala handiko eragiketarako egiteko aukera ematen dute, eta oxidatzaile- edo katalizatzaile-karga txikiagoa behar dute poluitzaileak degradatzeko [80]. Tian et al. [81] eta Bello et al. [74] taldeek ikusi zuten ohantze trinko eta finkoko erreaktoreak ez zirela egokienak prozesu fotokatalitikoak egiteko. Petrokimika, errekuntza edo gasifikazio-aplikazioetan asko erabiltzen diren ohantze fluidizatuen kasuan, aldiz, desabantaila horiek gaitu egingo lirarteke, besteak beste, abantaila hauek izango lituzketelako: materia-transferentziaren tasa eta likido-solido (L-S) kontaktuaren nahaste uniformea, hasierako efluentean gerta daitezkeen aldaketetarako diseinu sendoa, ur-bolumen handiak prozesatzeko gaitasuna, operazio-kostu baxua eta erabiltzeko, eskalatzeko eta eraikitzeko erraztasuna [82,83].

Argitaratutako ikerketa gehienek erakutsi dute prozesuaren errendimendua hobetu egiten dela FBRa aplikatuta. Kanki et al. [84] taldeak, FBR batean zeramikazko euskarria zuten TiO_2 partikulak erabilita, fenolaren eta A bisfenolaren degradazio fotokatalitikoaz aztertu zuten. Ikusi zuten, oxidazio-kondizio berdinetan, poluitzaileak lau aldiz azkarrago deuseztatzen zirela erreaktorearen beste konfigurazio batzuetan baino. Huang & Huang [85] taldeak fenola zuten ur-korrente batean % 98 mineralizatzea lortu zuten FBR

fotokatalitiko batekin, beirazko esferen gainean jarritako FeOOH-a erabilia. Bi kasuetan ondorioztatu zuten hobetu egiten zela argiaren sartze-maila eta poluitzaileak euskarri-materialetan adsorbatzeko aukera, FBR sistema prozesu fotokatalitikoari egokituta.

Poluitzaile iraunkorrak dituzten efluente industrialak tratatzeko teknologia erabiltzeak baditu onurak, desabantailak eta aukerak. Horiek guztiak kontuan hartuta, bada teknologia bat anilina, bentzotiazolak eta antzeko konposatuak dituzten efluenteak tratatzeko aproposa izan daitekeena: fotokatalisi heterogeneoa. Teknika horrek TiO₂-katalizatzaileak erabil ditzake laguntza osagarri gisa sistema hibrido batean, edo MnO₂-katalizatzaileak erabil ditzake ikatz aktibatu pikortsuaren gainean atxikiak, ohantze fluidizatuko errektore batean.

Anilina eta bentzotiazola poluitzaile iraunkorrak dira, eta larruaren eta zuraren industrian agertu ohi dira, baita kautxuaren ekoizpenean ere bulkanizazioaren azeleratzaile gisa [86]. Bi poluitzaile horien kasuan, gainera, ur-ingurumeneko organismoen osasunean eragiteaz gain, tumoreak eta alergia indultzeko gaitasuna izan dezaketela aipatu da [87,88]. Gaur egun, azala sentibilizatzen duen agente kimiko gisa sailkatuta dago Europako Gai Kimikoen Agentzian [11,89]. Azalean, biriketan edo digestio-aparatuan anilinarekin kontaktua izanez gero, oxigenoa ehunetara garraiatzeko prozesuari eragiten dion aldaketa gertatzen da odolean. Aldaketa horrek ondorio arinak edo larriak izango ditu kontaktuaren iraupenaren eta magnitudearen arabera [90]. Gainera, duela gutxi egindako azterketa batean frogatu da genotoxikoa dela eta hazkuntza inhibitzen duela gari-landaketetan [91]. Gainera, etxeko hondakin-uretan eta aireportuko jariatze-uretan ere atzeman da bentzotiazola (*Contaminant Candidate List 4* zerrendan dago) [25,92,93].

Hemen proposatutako tratamenduaren parekoak diren ordezkoei dagokienez, biorremediatzeari buruzko ikerketek zalantzak agertu zituzten bi konposatuen biodegradazioaren inguruan, batez ere anilinari dagokionez, genotoxikoa baita. Horren ondorioz, tratamendu biologiko konbentzionalak edo lohi aktiboak ez dira gai izan haiek guztiz metabolizatzeke eta deuseztatzeke [94,95]. Urak tratatzeko beste teknologia batzuk erabili izan dira anilina edo bentzotiazola duten urak tratatzeko, hala nola koagulazioa [96], ikatz aktibatuen bidezko adsortzioa [97–99], ozonizazioa [88,100,101], fotokatalisia [25,102,103], oxidazio hezea [104,105] edo mintz bidezko bereizketa [23,106].

Sánchez et al. [107] taldeak TiO₂-a duen ur-esekiduran anilinaren oxidazio fotokatalitikoaz aztertu zuen, argi ultramorea erabilia. Shahrezaei et al. [63] taldeak, berriz, UV/TiO₂ fotokatalisia aplikatzeko aukera aztertu zuen anilina duten efluenteak tratatzeko. Azkenik, Anotai et al. [108] taldeak anilinaren oxidazioa ikertu zuen argi ikusgaiarekin aktibatutako titanio oxidoa erabilia. Hala ere, teknologia horiek bideraezinak izatea eragiten duten hainbat mugarekin egin dute topo teknologia horiek industrian ezartzeko garaian. Muga aipagarrienen artean daude, besteak beste, adsorbatzailearen adsortzio-gaitasuna, energia-kontsumo handia eta eraginkortasun baxua. Kasu batzuetan, arazo nagusia da toki bateko poluitzaile-karga beste poluzio mota batera (hondakin solidora) transferitzen duten teknologiak direla [109].

Horrenbestez, fotokatalisi heterogeneoa —dela ikatz aktibatu pikortsuko partikuletan atxikitako MnO₂-a erabilia, dela TiO₂ molekulen esekidura erabilia— ur horiek tratatzeko aukera berde eta jasangarria izango litzateke, hondakin-ur industrialetan

biodegradatzeko gaitasun txikia duten poluitzaile organikoak eta inorganikoak degradatzeko gaitasuna baitu.

1.3. Ozonizazioan oinarritutako prozesu ez-fotokimikoak

1.3.1. Ozonizazio katalitikoak

Ozonizazioa urte luzez erabili da hondakin-ur poluitu mota ugari tratatzeko. Ozonoa oso agente oxidatzaile sendoa da, 2,07 V-eko oxidazio-potentziala du, eta poluitzaile organiko eta inorganiko ugarirekin erreakzionatzeko gaitasuna du [29]. Bi mekanismo nagusiren bidez gertatzen da poluitzaile organikoen oxidazioa. Oxidazio hori zuzenean egin daiteke ozonoa disolbatuta, edo zeharka, hidroxilo erradikalak sortuta [35]. Oxidazio zuzenean, ozono molekularrak era selektiboan erreakzionatzen du fenolekin, konposatu aromatiko aktibatuekin, protonatu gabeko aminekin eta olefinekin; erreakzio horien konstante zinetikoak 1 eta $10^7 \text{M}^{-1} \text{s}^{-1}$ bitartekoak izaten dira. Zeharkako erreakzioetan, ostera, ozonoa hain selektiboak ez diren hidroxilo erradikal errektiboagotan deskonposatzen da pH-balio basikoetan. Azken kasu horretan, molekula organiko ia guztiekin erreakzionatzen dute erradikalek. Ez da prozesu selektibo bat, eta erreakzio-konstanteak 10^9 – $10^{10} \text{M}^{-1} \text{s}^{-1}$ ingurukoak dira [110].

Sistemaren eraginkortasuna hobetzeko helburuari begira, ozonizazio katalitiko heterogeneoek garrantzia berezia lortu dute. Halako prozesu katalitikoek poluitzaile organiko erregogorren ozonizazioa hobetzen dute katalizatzaile solido bat erabilita. Ozonizazioan erabilitako katalizatzaile horien artean daude, besteak beste, oxido metalikoak, zeinak erabil baitaitezke nanopartikula gisa, beste oxido metaliko batzuetan atxikita [36,111] (adibidez, TiO_2 , MnO_2 , Fe_2O_3 , CuFe_2O_4 , ZnFe_2O_4 eta MgO) edo material porotsu batzuetan atxikita, hala nola ikatz aktibatuan [112] edo zeolitetan [113].

Edonola ere, azken hamarkadan gehien erabili diren katalizatzaileetako batzuk karbonodun materialak dira. Ikatx aktibatuaren abantailletako batzuk adsorbatzeko gaitasun handia eta erreakzioan erraz oxidatzeko gaitasuna dira. Ikatx aktibatuaren gainazaleko oxidazioak ozonoaren deskonposaketa abiarazi edo sustatzen du, erradikal-espezieak sor daitezten. Izan ere, ozonizazioak aldatu egiten ditu ikatz aktibatuaren gainazaleko propietate kimikoak. Ikatx aktibatuen jarduera katalitikoak Nawrocky et al. taldeak proposatutako mekanismoaren bidez azaldu daitezke [114], disoluzioaren pH-aren arabera (21-34 ekuazioak).

- Erreakzio homogeneoa

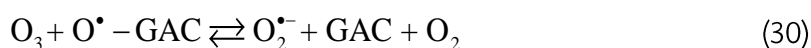
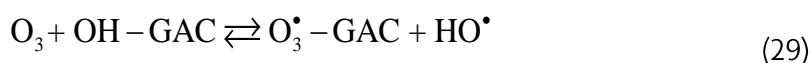
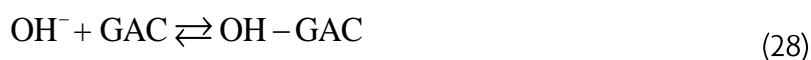


- Erreakzio heterogeneoa

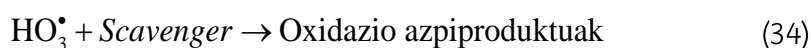
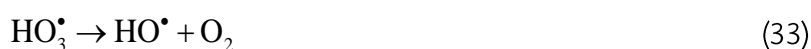
pH azidoan:



pH basikoan:



- Hedapen- eta amaitze-erreakzio homogeneoak



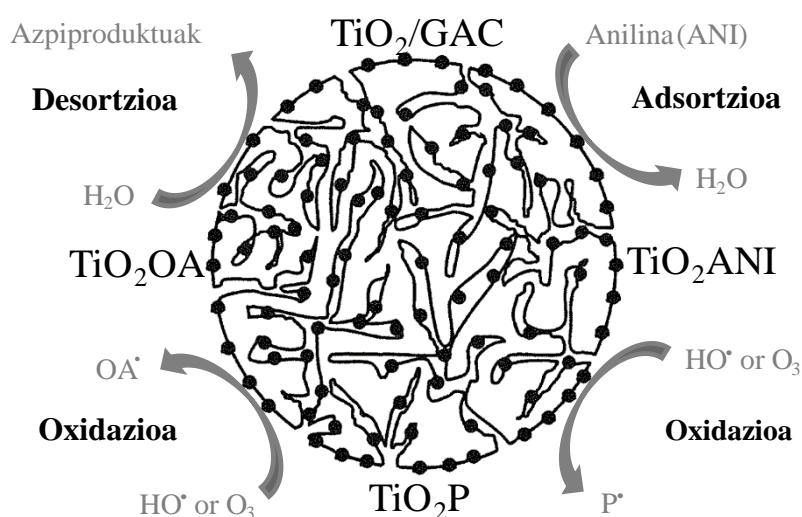
25-30 ekuazioen arabera, ozonoa ikatz aktibatuaren gainazalean adsorbatzen da hasieran. Ondoren, ikatz aktibatuak ozonoaren deskonposaketa abiarazten du, eta hidroxilo erradikalak askatzen ditu. Segidan, ozonoak gainazaleko taldeekin erreakzionatzen du, eta H₂O₂-a sortzen. Azken horrek uretan disolbatutako ozonoarekin erreakzionatzen du, eta hidroxilo erradikal gehiago ekoizten ditu.

Ikatx aktibatudun katalizatzaileak erabiltzen dituen teknologia honen aplikazio praktikoa bat fenola duten hondakin-ur industrialen tratamendua litzateke; zelulosaren industrian, petrolioaren birfintzean, industria metalurgikoan eta plastikoen industrian sortzen diren hondakin-uren tratamendua, hain zuzen ere [115]. EPAren lehentasunezko konposatu bat da fenola, eta *Contaminant Candidate List 4* (CCL4) [15] zerrendan jasota dago, gizakientzat eta uretako biziarentzat toxikotasun handikoa baita. Ikusienez, fenolak azaleko narriturak eta giltzurrunetako arazoak eragin ditzake gizakietan, eta leuzemia eta beste gaixotasun mutageniko batzuekin erlazionatuta egon daiteke [116].

Literaturan hainbat tratamendu-metodo proposatu dira fenolak hondakin-uretatik deuseztatzeko; adibidez, Fenton-en erreaktiboaren bidezko oxidazio kimikoa, adsortzioa, emultsioan dagoen mintz likido baten bidez erazte, koagulatzea eta hauspeatzea edo lohi aktiboak erabiltzea. Horiek dira gehien aipatzen diren tratamenduak [115,117,118]. Lohi aktiboaren kasuan, merkea eta erabiltzeko erraza izateagatik gehien erabiltzen den tratamendua bada ere, aplikazio mugatua du; izan ere,

lohian dauden mikroorganismoek, kondizio horietara egokituta ere, ezin dute 100 mg L^{-1} -tik gorako fenol-kontzentrazioak tratatu. Efluente horiek biodegradatzeko duten gaitasun txikiagatik eta halako fenol-kontzentrazioek mikroorganismoengan eragiten dituzten inhibizioengatik gertatzen da hori [119]. Zoritxarrez, industria kimikoko eta petrokimikoko hondakin-urek sarri gainditzen dituzte kontzentrazio horiek. Adibidez, kokearen industrian ohikoa da $28\text{-}3.900 \text{ mg L}^{-1}$ -ko kontzentrazioak aurkitzea, eta instalazio petrokimikoetan, berriz, $2,8\text{-}1.220 \text{ mg L}^{-1}$ tartekoak [112]. Testuinguru horretan, ikatz aktibatuekin batera ozonizazioa eta adsortzioa konbinatuz gero, tratamendu eraginkorragoa eta jasangarriagoa lortuko litzateke, ozonizazio sinplea edo prozesu fotokimikoetan oinarritutako beste AOP batzuk erabiltzearekin alderatuta.

Hala ere, lehenago azaldu den bezala, ikatz aktibatuekin egindako ozonizazio katalitikoaren errendimendua hobetu egin daiteke ikatz aktibatuen euskarrian oxido metalikoak atxikita. Horri dagokionez, literaturako egile batek baino gehiagok aipatu dituzte TiO_2/GAC katalizatzaileak, ozonizazio-teknologiekin konbinatuta erabiltzean lor daitekeen efektu sinergikoa dela eta [120,121]. Erreakzio-zinetika azkarrei eta mineralizazio-errendimendu altuari (% 70etik gorakoari) esker, erraza izan daiteke tratamendu hori eskala industrialean ezartzea. Arrazoi hauek egon daitezke mineralizazio-errendimendu altu horien atzean: i) euskarriaren aukeraketa, nahikoa azalera eta egitura porotsu egokia eman beharko luke; ii) katalizatzailearen osagai aktiboak; eta iii) katalizatzailea prestatzeko metodoa. Horrenbestez, prestatzeko metodoak eragina izan dezake katalizatzailean jalkitako fase aktiboaren egituran eta banaketan. Mekanismoari dagokionez, ozonoaren deskonposaketa katalitikoak Nawrocky et al. taldeak proposatutakoaren antzekoa izango litzateke [114], baina, oraingoa, katalizatzaileko oxido metalikoak ozonoaren materia fase likidotik solidora transferitzeko aukera erraztuko luke eta ozonoaren deskonposaketan lagunduko luke, hidroxilo erradikalak sortu ahal izateko, 3. irudian ikus daitezkeenez [122].



3. irudia Anilina duten hondakin-uren ozonizazio katalitikoan TiO_2/GAC konpositeek duten ekintza katalitikoaren mekanismoa [87].

Ozonizazio katalitikoetan, TiO_2/GAC katalizatzailea erabilgarria izan daiteke jatorri industrialeko uretako anilina deuseztatzeko.

Ozonizazio katalitikoa, horrenbestez, poluitzaile erregogorrek (anilina, adibidez) guztiz mineralizatzeko teknologia alternatibo bat da, AOP horrek oxidazio-gaitasun handia baitu [111]. Erabil daitezkeen katalizatzaile metalikoetatik titanio oxidoa proposatu zuten Beltrán et al. [123] eta Song et al. [124] taldeek, besteak beste, hainbat motatako poluitzailearen ozonizazio-prozesua azkartuko lukeen material aktibo gisa. Gainera, Beltrán-ek [29] 40 aldiz konbertsio handiagoa lortu zuen ozonizazio katalitikoarekin ozonizazio sinplearekin baino.

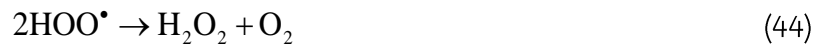
Beraz, TiO₂/GAC konpositeekin egindako ozonizazio katalitikoak erabiltzea izan daiteke anilina duten efluente industrialak arazteko tratamendurik eraginkor eta jasangarriena eta ozono gutxien kontsumitzen duena.

1.3.2. Ultrasoinuen teknologia, ozonizazioaren aurretiko tratamendua

Ultrasoinuen teknologia AOP alternatibo bat da, uretan dauden poluitzaile erregogorrek degradatzeko eta arrisku mikrobiologikoak deuseztatzeko potentziala duena. Beste AOP batzuekin alderatuz gero, ultrasoinuek abantaila bereziak dituzte: ez da errektiborik gehitu behar, erabiltzeko erraza da eta selektiboa da poluitzaileak deuseztatzeko garaian [125,126].

Ultrasoinuak hiru multzo handitan sailka daitezke haien maiztasunen arabera. Maiztasun baxuak (20-100 kHz) eta altuak (200-1.000 kHz) erabiltzen dira gehien prozesu kimikoetan [127]. Intentsitate altuko ultrasoinu-uhinak erabiltzen direnean, ultrasoinuek eta likidoan disolbatuta dauden gasek elkarri eragiten diote, eta kabitazio akustiko deritzona sustatzen da. Hori gertatzen da uhina sortu ondoren agertutako burbuilen hazkundera eta ondorengo kolapso inplosiboa gertatzen delako. Konpresio- eta hedakuntza-zikloak dituzte uhin horiek. Hedakuntzan burbuilak sortzen dira, baldin eta uhinek likidoaren indar molekularrak gainditzeko besteko intentsitatea badute. Hori dela eta, burbuilak likidoko gasaren edo lurrunaren difusioz hazten dira tamaina kritikora iritsi arte, eta, gero, apurtu egiten dira, eta konpresio- eta hedakuntza-ziklo txandakatuak sortzen dituzte. Ziklo horiek direla eta, likidoan poluitzaile organikoren bat badago, loturak hautsi egiten dira. Ur molekularak, adibidez, hautsi, eta hidrogeno atomo bat eta hidroxilo erradikal bat sortuz deskonposa daitezke; berdin gertatuko litzateke hainbat motatako poluitzailearekin eta disolbatutako gasekin, halakorik balego [24]. Ultrasoinu-sistema batean erradikalak sortzeko mekanismoa Adewuyi et al. taldeak egindako proposamenaren bidez azaldu daiteke: [128]:





Sistema sonolitiko batean, hiru eskualde bereizi daitezke [129,130]: (i) disoluzioaren *bulka*, (ii) kabitazio-burbuilaren interfasea eta (iii) burbuilaren barnealdea. Poluitzailearen izaera hidrofiliiko edo hidrofobikoaren arabera, konposatua eskualde batean edo beste batean kokatuko da. Horrek zuzenean baldintzatuko du poluitzaileak sonolisian jarraituko duen degradazio-ibilbidea.

Ultrasoinuak hainbat konposatu organiko arrakastaz degradatzeko gai badira ere, mineralizazio-maila txikia lortzen da, eta hori da, hain zuzen, haien desabantaila nagusia. Mineralizazioaren errendimenduak ez du %10 gaintzen maiz, sortzen diren degradazio-produktuak hidrofiloak eta ez-lurrunkorrak izaten direlako, eta ezaugarri horiek mugatu egiten dute guztiz deuseztatzeko aukera [125]. Gainera, prozesuak energia elektriko asko behar duenez, kostu ekonomiko handia du. Horrenbestez, tratamendu-denborek laburrak izan behar dute, baina, aldi berean, poluitzaile organiko erregogor eta toxikoak konposatu ez-kaltegarri edo jatorrizkoak baino biodegradagarriago bihurtzeko gai izan behar dute. Zailtasun horiek gaintzeko, ultrasoinuak beste oxidazio-prozesu aurreratu batzuekin konbina daitezke; ozonizazioarekin, adibidez [131].

Horri dagokionez, substantzia humikoz poluitutako uren kasuan, ultrasoinuen teknologiaren bidezko aurretratamendu bat eta, ondoren, ozonizazioa aplikatzeko aukera dago. Azido humikoak pisu molekular handiko konposatu naturalak dira, eta ur naturaletan maiz agertzen dira [26]. Are gehiago, ur naturalen materia organikoaren osagai nagusia dira, eta urak desinfektatzeko prozesuetan agertzen diren trihalometanoen (THM-en) aitzindariak dira. Konposatu horiek guztiz mineralizatzeko zailak dira, ozonizazio arrunta eta antzeko teknologiak aplikatzean erregogor izateko joera baitute [132,133]. Ondorioz, ultrasoinuek azido humikoaren egitura molekularra aldatzen lagundu dezakete, baita biodegradatzeko aukera handitu ere, ondoren ozonizazioa errazteko.

1.3.3. Ozonizazioan ultrairagazketa-prozesuak txertatzea, sortzen ari diren poluitzaile berriak deuseztatzeko

Ur-eskari gero eta handiagoari erantzuteko ur-baliabide berriak lortzeko beharrak bultzatuta, Europako Erkidegoko agintariak ura berroneratzeko eskema berrietan pentsatzen hasi dira, hirietako HUAetako tratamendu sekundariotik datorren ura berroneratzeko [134]. Klima-aldaketak, populazioaren hazkundeak eta uraren gehiegizko kontsumoak azkartu egin dituzte joera horiek, eta, gaur egun, ezinbestekoa da ura berroneratzea [1]. Kontzeptu berri horrek hiri jasangarrien garapenaren eta tokiko nekazaritza jasangarri eta seguruaren arteko lotura sustatzen lagundu dezake, hirietako hondakin-urak behar bezala berrerabilita. Hala ere, HUAetako efluente horietan gero eta maizago agertzen dira 2013/39/EB zuzentarauak erregulatzen dituen poluitzaile sortu berriak (CEC, *contaminants of emerging concern*); esaterako, disruptore endokrinoak (EDC, *endocrine disruptor*), produktu farmazeutikoak (PhAC,

pharmaceutically active compound) eta zaintza pertsonaleko produktuak (PPCP, *pharmaceuticals and personal care products*). Eta horrek ardura handia sortzen du berroneratutako ur horien segurtasunari dagokionez [22].

Mintz bidezko prozesuak (osmosia, nanoiragazketa eta ultrairagazketa, esaterako) asko erabiltzen dira hondakin-urak tratatzeko prozesuetan [135]. Ezaugarri horiei esker, hondakin-uren tratamendu tertziariorako aukera bikaina dira, haiek bakarrik nahiz prozesu hibrido batean txertatuta.

Ultrairagazketaren eta mintz bidezko antzeko prozesuen abantaila nagusia da sortzen den iragazkina kalitate handikoa dela, halako prozesuek kantitate handian erauzten baitituzte CECak. Gainera, osmosiak, nanoiragazketak eta antzeko bereizketa-prozesuek behar duten baino bulkada-indar askoz txikiagoarekin erabil daitezke. CEC poluitzaileak mintz horietatik igarotzean, mintzaren gainazalera adsorbatzen dira, gero mintzean disolbatzen dira eta, azkenik, disolbatutako CEC molekula horiek difusioz garraiatzen dira mintzaren matrizean zehar [136,137]. Teknologia honek dituen desabantailetakoa bat da inkrustazioak. Ondorioz, *fouling*aren eragin negatiboen kontra egiten duen eta funtzionamendu arruntari laguntzen dion sistema bat izateak erraztu egingo luke teknologia hori HUAetan eskala handian ezartzea.

Hala ere, ultrairagazketan sortzen diren kontzentratuak arazo larria dira ingurumenerako, hainbat ezaugarri eta toxikotasun dituzten CECak baitituzte [21]. Arazo horri aurre egiteko, AOP oxidazio-prozesuek mikropoluitzaile horiek deuseztatzen lagundu dezakete [60,137–139]. Eskura dauden AOPen artean, hauek dira esanguratsuenak: ozonizazioa [142,143], UV/H₂O₂/Fe³⁺ erabiliz indartutako fotokatalisi-prozesuak [53] eta beste prozesu elektrokimiko batzuk [129]. Aipatutakoetatik ozonizazioa nabarmentzen da, CECak deuseztatzeko errendimendu altua duela erakutsi baita. Mota horretako molekulen % 90-100 deuseztatzen du oxidazio-abiadura handiz; izan ere, ozonoak eta hidroxilo erradikalek erreaktibotasun handia dute bertako konposatu organiko askorekiko (diklofenakoa edo A bisfenola, besteak beste) [142]. Hala ere, eragiketa-kondizio jakin batzuk behar dira horretarako; pH-a eta ozono-dosia dira garrantzitsuenak. Gainera, desinfektatzaile-funtzioa ere betetzen du ozonoak, bakterioak, birusak, protozoak eta bestelako patogeno ugari inaktiba baitituzte hondakin toxikorik utzi gabe [143]. Aipatutako abantaila horiei gehitu behar zaie AOP honek ez duela lohirik sortzen, eta ozonoa energia-iturri berriztagarriekin sortzeko aukera ematen duela [144].

Laburbilduz, ultrairagazpen etengabea, errefus-korrontea ozonizazioz tratatzearekin konbinatuta, alternatiba egokia izan daiteke, eta ohiko tratamendu tertziarioa — koagulazioa, malutapena eta, ondoren, argi ultramorearekin edo sodio hipokloritoarekin desinfektatzea— baino merkeagoa izan daiteke hiriko hondakin-uretan dauden CECak eta mikroorganismo patogenoak eraginkortasunez tratatzeko.

1.4. Ikatz aktibatuzko materialetan oinarritutako konposite berrien sintesia

Fotokatalisian eta ozonizazio heterogeneoan materia-transferentziako arazoak saihesteko, ohikoa da nanopartikula eraldatu eta hobetuen esekidurak erabiltzea. Nanopartikulak hobetzeko, aurrez aipatu ditugun dopatze-mekanismoak erabiltzen dira (heterolotura, elementuak dopatzea, fase kristalinoaren kontrola eta abar). Hala ere, esekidurak erabiltzean, beharrezkoa da erreakzio ostean katalizatzailea berreskuratzeko etapa gehiago izatea. Etapa horiek askotarikoak izan daitezke; adibidez, koagulatu eta, ondoren, hauspeatu daiteke, iragazi daiteke eta abar [72,145]. Gainera, nanopartikulak erabiltzea ingurumenerako arriskutsua izan daiteke [146]. Ondorioz, TiO_2 edo MnO_2 -aren oxido metalikoak immobilizatzeko teknikak aukeratu dira, hau da, 1,5 mm inguruko batez besteko diametroa duten ikatz aktibatu pikortsuzko (GAC, *granular active carbon*) partikulen gainean immobilizatzen dira [87,147]. Hala eginda, katalizatzailea hobeto erabiltzeko aukera izateaz gain, saihesten da material katalitikoa tratatutako efluenteetan galtzea.

Gainera, sistema fotokatalitikoetan, eta eskala industrialean, ohantze fluidizatuko errektore (FBR) batean egin ahal izango litzateke prozesua, erraz eraiki eta erabil daitekeelako, eragiketa-kostu txikia duelako eta malgutasun handia duelako fase likidoan eta solidoan egoteko denborari dagokionez. MnO_2 nanopartikulak porotamaina handiko GAC batean atxikita erabiltzeak hainbat abantaila ekarriko lituzke; adibidez, masa- eta bero-transferentzia handiagoa gertatuko litzateke FBR sistemari [82]. Gainera, prozesuak ez luke material katalitikoa berreskuratzeko etaparik behariko, fluidizatuta egongo liratekeelako eta errektorean eroriko liratekeelako prozesua etendu ondoren. Bestalde, konposite hau edo GACari atxikitako TiO_2 -a erabilia, ez litzateke birsortze-faserik behariko, katalizatzaile berritzaile hauek gai baitira GACen gainazalean adsorbatzen diren poluitzaileak eraginkortasunez deuseztatzeko [148]. Halaber, bi material katalitiko hauek hondakin solido gisa deusezta daitezke, haien bizitza erabilgarria amaitzean.

Aipagai ditugun bi katalizatzaileek ozonizazio- eta fotokatalisi-prozesuetan duten garrantzia dela eta, zeresan handia du zer teknika erabiltzen den katalizatzaileak prestatzeko, ahalik eta propietate fisiko-kimikorik onenak lortu behar baitira, ahalik eta jarduera katalitiko handiena lortzeko. Horretarako, solidoan eta disoluzioan oinarritutako metodoak daude. Solidoan oinarritutakoen artean, sonikazioa edo lurruntze termikoa daude, eta, disoluzioetan oinarritutakoen artean, berriz, sintesi hidrotermala, murgiltze bidezko inpregnazioa, hauspeatzea eta sol-gel teknika ezagunak daude [149–151].

Teknika fisiko batean (solidoan) oinarritutako metodoei dagokienez, indarra, energia edo presioa erabiltzen da materialak nahasteko edo haien egitura eraldatzeko [152]. Metodo horien abantailen artean, aipatzekoak dira, besteak beste, aplikatzeko errazak direla eta purutasun handiko katalizatzaileak lortzeko aukera ematen dutela. Hala ere, sintesi-metodo horren bidez zaila da katalizatzailearen osaera, forma eta tamaina kontrolatzea [153]. Hori dela eta, baztertu egin zen halako teknikak erabiltzeko aukera, ezinbestekoa baita fase kristalino jakin bat lortzea eta fase aktiboa asko sakabanatzea GACean.

Disoluzioetan oinarritutako metodoak, berriz, gehiagotan erabiltzen dira, ingurumenerako egokiagoak izateaz gain, erabilitako disolbatzailearen arabera,

metodo fisikoek baino energia gutxiago behar dutelako. Gainera, erabilitako errektiboak askoz merkeagoak dira [154]. Metodo honetan, prozesuan parte hartzen duten aldagaien eraginez, hainbat osaera, forma eta tamaina lortzen dira, eta horrek konpositearen errendimenduari eragin diezaioke [155,156].

Literaturan aurkitutako lanetan, metodo tradizioaletan oinarritutako teknikak erabili izan dituzte; adibidez, teknika hidrotermala edo sol-gel teknika. Ghasemi et al. [157] taldeak, adibidez, titanio dioxidozko nanopartikulak immobilizatu zituen, dentsitate txikiko GAC bat erabiliz euskarri porotsu gisa, eta furfurala fotokatalisi bidez degradatu zuten sol-gel metodo bakuna baliatuz, tetra-n-butil titanatoa aitzindari gisa erabilia. Noorimotlagh et al. [158] taldeak, berriz, ikatz aktibatu pikortsua dopatu zuen TiO_2 partikulekin, eta, horretarako, hauspeatze-teknikaren bidez argi ikusgaiarekin aktibatzeke aukera emango zien anataso/errutilo erlazio bat erabili zuen. Hori lortzeko, titanio (IV) isopropoxidoa erabili zuen titanioaren aitzindari gisa, nonilfenola fotokatalisi bidez deuseztatzeko. Cui et al. [159] taldeak, bere aldetik, manganeso dioxidoz estalitako ikatz aktibatuzko konposite bat (MnO_2/AC) sintetizatu zuen hauspeatze-teknikaren bidez, potasio permanganatozko disoluzio batetik abiatuta. Hondakin-uretako glifosatoa adsorbatzeko prozesuan erabiltzea zen helburua. Azkenik, Warsi et al. [155] taldeak MnO_2 -aren hainbat fase kristalino alderatu zituen; potasio permanganatozko disoluziotik abiatuta teknika hidrotermala erabiliz lortutako faseak ziren. Aurkitu zuten, fase kristalino desberdinak lortzen ziren sintesiaren diseinuan ezarritako kondizioen arabera. Karbonozko nanohodietan (CNT, *carbon nanotube*) atxikitako $\alpha\text{-MnO}_2$ partikulak erabilia, egitura hibridoaren azalera hobetzea lortzen zen, eta portaera hobea zuten argi ikusgaiarekin aktibatzean.

Oro har esanda, autoreek hainbat konposite lortu zituzten, GACaren gainazalean partikula metalikoen banaketa irregularra zutenak. Aipatutako teknikak gaitasun mugatua zuten GACaren poroen barnean TiO_2 -a edo MnO_2 -a jalkitzen zela ziurtatzeko; askotan, kanpoko geruza estaltzen zen. Kasu gehienetan, partikulek blokeatu egiten zituzten GACaren barneko poroak, eta ezbaian jartzen zuten haren jarduera katalitikoa. Horrenbestez, alderatu egin beharke lirateke prestaketa-teknikak (murgiltze bidezko inpregnazioa, hauspeatzea eta hidrotermala), eta aztertu zein den egokiena aplikazio bakoitzerako, teknika batetik bestera ager daitekeen aldakortasuna esanguratsua izan baitaiteke.

1.5. Prozesuen areagotzea

Gaur egun, prozesuen areagotzea Europako Ibilbide Orrian [160] jasota daukagu. Bertan berrikuntza aplikatutako printzipio garrantzitsuenak bilduta ditugu, hala nola abantaila berriak lortzeko prozesuen eraginkorrak eginez, errektiboan eta energiaren kontsumo arduratsu batekin, hondakin gutxiago sortzeari eraginduz eta prozesuetan segurtasun handiagoa izanez konplexutasun txikiagoko plantak eginez. Gainera, ekarriko digu kapital-gastu txikiagoko prozesuak [161].

Prozesu areagotzearen printzipioak Van Gerven & Stankiewicz [162] honela deskribatu zituzten: (i) Prozesu kimikoen eraginkortasuna handitzeko molekular mailan aldaketak sustatzea prozesu zinetikaren bidez. Pignatello et al. [163], hainbat eragiketa-estrategia erabiliz deuseztatze-errendimendu handiagoak lortzeko, fotofenton motako erreazio-mekanismoak aztertu zituzten. (ii) Materiala eta energia ahalik eta gutxien alferrik galtzea prozesuak idealtasunetik hurbil eragiketa eginez. (iii) Bultzatzaile-gradientearen optimizazioa masa-transferentzia hobetuz. Dijkstra et al. [164] errektore

baten hormetan TiO_2 katalizatzailea eutsi zuten azido formikoa deuseztatzeko. Katalizatzailea esekiduran zebiltzan sistemarekin, pareko oxidazio-erreakzioaren errendimendua lortu zuten. (IV) Prozesu partzialen integraziotik abiatuta, eragin sinergikoak lortzea. Orge et al. [165] TiO_2 -rekin aldatutako ikatz aktibo berri bat garatu zuten, anilina deuseztatzeko ozonizazio fotokatalitikoko prozesu baten bidez. Erabateko degradazioa eta %90eko mineralizazioa lortu zuten ozonizazio katalitiko eta fotokatalisi heterogeneoa konbinatuz, bakarkako prozesuekin alderatuta.

Lau printzipio horiek AOP-ei aplikatu dakizkieke, doktorego-tesi honetan nabarmentzen den bezala. Printzipio hauek hobetzeko eta laguntzeko modu bat izango litzateke, adibidez, argi-eraginkortasuna maximizatuz, errektorearen diseinua optimizatuz eta eragiketa-baldintzak aztertuz (FBR edo errektore hibrido bidez), G-L materia-transferentzia hobetuz atomizazio-sistema eraginkorak erabiliz ozonizazio errektoreetan, fotokatalizatzaile edo katalizatzaile berriak garatuz (MnO_2/GAC eta TiO_2/GAC) propietate berriak lortzeko, aktibitate katalitiko areagotzeko edota aktibazio-uhinaren luzera-tartea aldatzeko, aplikazio fotokimikoen kasuan. Prozesu fotokimikoetan zein ez fotokimikoetan, ikatz aktiboa euskarri porotsu bezala erabiliz poluitzaileen adsortzioa sustatzeko, AOP-ren errendimenduari lagun zezakeen. Aipatutako hobekuntzak prozesuan martxan jarritz, instalazioko ekipoen tamaina eta errektiboaren kantitatea murriztuko litzateke, energia gutxiago kontsumituko litzateke eta hondakin gutxiago sortuko lirateke. Azken finean, teknologia merkeagoak eta jasangarriagoak lortuko lirateke.

1.6. Tesiaren esparrua eta helburua

Hondakin-urek izan ditzaketen poluitzaileen aniztasuna, izaera kimikoa, kontzentrazioak eta tratatu beharreko bolumenak aldakorrak direnez, egokienak izan daitezkeen teknologiak aurkeztu dira lan honetan. Prozesu bakoitza hautatzeko eta haren eragiketa-konfigurazioa prestatzeko, deuseztatzeko eta mineralizatze eraginkortasun handiena ekarriko duten irizpideak aplikatu ziren, industriako eta hirietako hondakin-uren poluzio-kasu adierazgarriak aztertzeko.

Tesi honen helburua hondakin-uren tratamenduaz dagoen ezagutza zabaltzea zen, hainbat eragiketa-estrategia eta zenbait katalizatzaile berriren konfigurazioa eta garapena aztertuta. Halaber, oxidazio-prozesu aurreratuen erabilera indartzea zen helburu, industrian eta hirietan adierazgarriak diren hainbat izaeratako efluenteetan aplikatzeko.

Tesi honetan hautatu den ekintza-esparrua kontuan hartuta, helburu nagusi hauek definitu dira:

- Oxidazio-prozesu aurreratuak identifikatzea eta hautatzea, tratatu beharreko hondakin-uretako poluitzaileen karga, izaera eta erregogortasun-mailaren arabera.
- Katalizatzaile berriak garatzea, ikatz aktibatu pikortsuan immobilizatutako titanio eta manganeso oxidoetan oinarrituta, fotokatalisi heterogeneoko eta ozonizazio katalitikoko prozesuak indartzeko, uretan dauden poluitzaileen degradazio osoa eta mineralizazio-maila altua lortu asmoz.
- Ozonizazio katalitikoaren teknologian parte hartzen duten eragiketa-aldagaien eragina ebaluatzea, prozesu trifasiko baten eredu proposatuz. Eredu horrek fase likidoan eta solidoan gertatzen den materia-transferentzia, adsortzioa eta

oxidazio kimikoa erlazionatuko lituzke poluitzaile organikoen degradazioarekin eta mineralizazioekin.

- Hautatutako prozesuen eragiketa-estrategiak definitzea, jasangarritasunaren ikuspegitik haien bideragarritasuna aztertzeko.

Aztertutako poluzio-kasuen emaitzak erabilitako oxidazio-teknologia aurreratu motaren arabera multzokatu dira. Zehazki, bi bloke handitan antolatu dira: teknologia fotokimikoak eta ez-fotokimikoak. Bloke bakoitza hiru azpikategoriatan banatu da, eskema honen arabera:

- Prozesu fotokimikoak
 - UV/H₂O₂-an oinarritutako prozesuak (1. argitalpena)
 - Fotofenton sisteman oinarritutako prozesuak (2. eta 3. argitalpenak)
 - Fotokatalisi heterogeneoa (4. eta 5. argitalpenak)
- Ozonizazioan oinarritutako prozesu ez-fotokimikoak
 - Ozonizazio katalitikoak (6., 7., 8. eta 9. argitalpenak)
 - Ultrasoinuen teknologia, ozonizazioaren aurretiko tratamendua (10. argitalpena)
 - Ozonizazioan ultrairagazketa-prozesuak txertatzea, sortzen ari diren poluitzaile berriak deuseztatzeko (11. eta 12. argitalpenak)

1.7. Erreferentziak

1. Aitken, D.; Rivera, D.; Godoy-Faúndez, A.; Holzapfel, E. Water Scarcity and the Impact of the Mining and Agricultural Sectors in Chile. *Sustainability* **2016**, *8*, 128, doi:10.3390/su8020128.
2. Valdes Ramos, A.; Aguilera Gonzalez, E.N.; Tobon Echeverri, G.; Samaniego Moreno, L.; Diaz Jimenez, L.; Carlos Hernandez, S. Potential Uses of Treated Municipal Wastewater in a Semiarid Region of Mexico. *Sustainability* **2019**, *11*, 2217, doi:10.3390/su11082217.
3. Busari, I.T.; Senzanje, A.; Odindo, A.O.; Buckley, C.A. The Impact of Irrigation Water Management Techniques on the Performance of Rice Using Treated Wastewater Reuse in Durban, South Africa. *Water Sci. Technol.-Water Supply* **2019**, *19*, 1604–1611, doi:10.2166/ws.2019.031.
4. Mayhew, S.; Hanefeld, J. Planning Adaptive Health Systems: The Climate Challenge. *Lancet Glob. Health* **2014**, *2*, E625–E626, doi:10.1016/S2214-109X(14)70313-4.
5. Ricart, S.; Villar-Navascues, R.A.; Hernandez-Hernandez, M.; Rico-Amoros, A.M.; Olcina-Cantos, J.; Molto-Mantero, E. Extending Natural Limits to Address Water Scarcity? The Role of Non-Conventional Water Fluxes in Climate Change Adaptation Capacity: A Review. *Sustainability* **2021**, *13*, 2473, doi:10.3390/su13052473.
6. Fornes, J.M.; Lopez-Gunn, E.; Villarroya, F. Water in Spain: Paradigm Changes in Water Policy. *J. Sci. Hydrol.* **2021**, *66*, 1113–1123, doi:10.1080/02626667.2021.1918697.
7. Jodar-Abellan, A.; López-Ortiz, M.I.; Melgarejo-Moreno, J. Wastewater Treatment and Water Reuse in Spain. Current Situation and Perspectives. *Water* **2019**, *11*, 1551, doi:10.3390/w11081551.
8. Chowdhary, P.; Bharagava, R.N.; Mishra, S.; Khan, N. Role of Industries in Water Scarcity and Its Adverse Effects on Environment and Human Health. In *Environmental Concerns and Sustainable Development: Volume 1: Air, Water*

- and Energy Resources; Springer, Singapore, **2020**; pp. 235–256 ISBN 9789811358890.
9. Bodzek, M.; Konieczny, K. Membranes in Organic Micropollutants Removal. *Curr. Org. Chem.* **2018**, *22*, 1070–1102, doi:10.2174/1385272822666180419160920.
 10. James, C.P.; Germain, E.; Judd, S. Micropollutant Removal by Advanced Oxidation of Microfiltered Secondary Effluent for Water Reuse. *Sep. Purif. Technol.* **2014**, *127*, 77–83, doi:10.1016/j.seppur.2014.02.016.
 11. *Real Decreto 817/2015, de 11 de septiembre, por el que se establecen los criterios de seguimiento y evaluación del estado de las aguas superficiales y las normas de calidad ambiental*; BOE núm. 219, de 12 de septiembre de 2015, páginas 80582 a 80677, **2015**, BOE-A-2015-9806.
 12. *Directive 2000/60/EC of the European Parliament and of the Council of 23 October 2000 Establishing a Framework for Community Action in the Field of Water Policy*; **2000**.
 13. *Regulation (EU) 2020/741 of the European Parliament and of the Council of 25 May 2020 on Minimum Requirements for Water Reuse (Text with EEA Relevance)*; **2020**; Vol. 177.
 14. Mestankova, H.; Parker, A.M.; Bramaz, N.; Canonica, S.; Schirmer, K.; von Gunten, U.; Linden, K.G. Transformation of Contaminant Candidate List (CCL3) Compounds during Ozonation and Advanced Oxidation Processes in Drinking Water: Assessment of Biological Effects. *Water Res.* **2016**, *93*, 110–120, doi:10.1016/j.watres.2015.12.048.
 15. US Environmental Protection Agency. Contaminant Candidate List 4-CCL 4. <https://www.epa.gov/ccl/contaminant-candidate-list-4-ccl-4-0> (Kontsultatuta 2021ko irailaren 9a).
 16. Hering, J.G.; Maag, S.; Schnoor, J.L. A Call for Synthesis of Water Research to Achieve the Sustainable Development Goals by 2030. *Environ. Sci. Technol.* **2016**, *50*, 6122–6123, doi:10.1021/acs.est.6b02598.
 17. United Nations About the Sustainable Development Goals. <https://www.un.org/sustainabledevelopment/sustainable-development-goals/> (Kontsultatuta 2021ko irailaren 9a).
 18. Boczkaj, G.; Fernandes, A. Wastewater Treatment by Means of Advanced Oxidation Processes at Basic pH Conditions: A Review. *Chem. Eng. J.* **2017**, *320*, 608–633, doi:10.1016/j.cej.2017.03.084.
 19. Daniel, D.; Fabrizio, C. *Handbook Of Advanced Methods And Processes In Oxidation Catalysis: From Laboratory To Industry*; World Scientific, Singapore, **2014**; ISBN 978-1-78326-334-9.
 20. Chen, W.; Gu, Z.; Wen, P.; Li, Q. Degradation of Refractory Organic Contaminants in Membrane Concentrates from Landfill Leachate by a Combined Coagulation-Ozonation Process. *Chemosphere* **2019**, *217*, 411–422, doi:10.1016/j.chemosphere.2018.11.002.
 21. Couto, C.F.; Lange, L.C.; Santos Amaral, M.C. A Critical Review on Membrane Separation Processes Applied to Remove Pharmaceutically Active Compounds from Water and Wastewater. *J. Water Process. Eng.* **2018**, *26*, 156–175, doi:10.1016/j.jwpe.2018.10.010.
 22. Mijangos, L.; Ziarrusta, H.; Ros, O.; Kortazar, L.; Angel Fernandez, L.; Olivares, M.; Zuloaga, O.; Prieto, A.; Etxebarria, N. Occurrence of Emerging Pollutants in Estuaries of the Basque Country: Analysis of Sources and Distribution, and Assessment of the Environmental Risk. *Water Res.* **2018**, *147*, 152–163, doi:10.1016/j.watres.2018.09.033.
 23. Ferreira, C.; Gómez-Motos, I.; Lombraña, J.I.; de Luis, A.; Villota, N.; Ros, O.; Etxebarria, N. Contaminants of Emerging Concern Removal in an Effluent of

- Wastewater Treatment Plant under Biological and Continuous Mode Ultrafiltration Treatment. *Sustainability* **2020**, *12*, 725, doi:10.3390/su12020725.
24. Ameta, S. *Advanced Oxidation Processes for Wastewater Treatment: Emerging Green Chemical Technology*; Academic Press, San Diego, CA, USA, **2018**; ISBN 978-0-12-810499-6.
 25. Ferreiro, C.; Villota, N.; Lombraña, J.I.; Rivero, M.J.; Zúñiga, V.; Rituerto, J.M. Analysis of a Hybrid Suspended-Supported Photocatalytic Reactor for the Treatment of Wastewater Containing Benzothiazole and Aniline. *Water* **2019**, *11*, 337, doi:10.3390/w11020337.
 26. Alfonso-Muniozgueren, P.; Ferreiro, C.; Richard, E.; Bussemaker, M.; Ignacio Lombraña, J.; Lee, J. Analysis of Ultrasonic Pre-Treatment for the Ozonation of Humic Acids. *Ultrason. Sonochem.* **2020**, *71*, 105359, doi:10.1016/j.ultsonch.2020.105359.
 27. Expósito, A.J.; Monteagudo, J.M.; Durán, A.; San Martín, I.; González, L. Study of the Intensification of Solar Photo-Fenton Degradation of Carbamazepine with Ferrioxalate Complexes and Ultrasound. *J. Hazard. Mater.* **2018**, *342*, 597–605, doi:10.1016/j.jhazmat.2017.08.069.
 28. Brillas, E.; Bastida, R.M.; Llosa, E.; Casado, J. Electrochemical Destruction of Aniline and 4-chloroaniline for Wastewater Treatment Using a Carbon/PTFE O₂ Fed Cathode. *J. Electrochem. Soc.* **1995**, *142*, 1733, doi:10.1149/1.2044186.
 29. Beltran, F.J. *Ozone Reaction Kinetics for Water and Wastewater Systems*; CRC Press, Boca Raton, FL, USA, **2003**; ISBN 978-0-203-50917-3.
 30. Liu, C.; Tang, X.; Kim, J.; Korshin, G.V. Formation of Aldehydes and Carboxylic Acids in Ozonated Surface Water and Wastewater: A Clear Relationship with Fluorescence Changes. *Chemosphere* **2015**, *125*, 182–190, doi:10.1016/j.chemosphere.2014.12.054.
 31. Kusic, H.; Koprivanac, N.; Bozic, A.L. Treatment of Chlorophenols in Water Matrix by UV/Ferri-Oxalate System: Part II. Degradation Mechanisms and Ecological Parameters Evaluation. *Desalination* **2011**, *280*, 208–216, doi:10.1016/j.desal.2011.07.005.
 32. Rodríguez, A.; Rosal, R.; Perdigón-Melón, J.A.; Mezcuca, M.; Agüera, A.; Hernando, M.D.; Letón, P.; Fernández-Alba, A.R.; García-Calvo, E. Ozone-Based Technologies in Water and Wastewater Treatment. In *Emerging Contaminants from Industrial and Municipal Waste*; Springer, Heidelberg, Germany, **2008**; Vol. 5S/2, pp. 127–175 ISBN 978-3-540-79209-3.
 33. O'Shea, K.E.; Dionysiou, D.D. Advanced Oxidation Processes for Water Treatment. *J. Phys. Chem. Lett.* **2012**, *3*, 2112–2113, doi:10.1021/jz300929x.
 34. Bhat, A.P.; Gogate, P.R. Degradation of Nitrogen-Containing Hazardous Compounds Using Advanced Oxidation Processes: A Review on Aliphatic and Aromatic Amines, Dyes, and Pesticides. *J. Hazard. Mater.* **2021**, *403*, 123657, doi:10.1016/j.jhazmat.2020.123657.
 35. Von Sonntag, C.; Von Gunten, U. *Chemistry of Ozone in Water and Wastewater Treatment: From Basic Principles to Applications*; Iwa Publishing, London, United Kingdom, **2012**; ISBN 978-1-84339-313-9.
 36. Wang, B.; Zhang, H.; Wang, F.; Xiong, X.; Tian, K.; Sun, Y.; Yu, T. Application of Heterogeneous Catalytic Ozonation for Refractory Organics in Wastewater. *Catalysts* **2019**, *9*, 241, doi:10.3390/catal9030241.
 37. Litter, M.I.; Candal, R.J.; Meichtry, J.M. *Advanced Oxidation Technologies: Sustainable Solutions for Environmental Treatments*; CRC Press, Boca Raton, FL, USA, **2014**; ISBN 978-1-138-00127-5.
 38. Shu, Z.; Singh, A.; Klamerth, N.; McPhedran, K.; Bolton, J.R.; Belosevic, M.; Gamal El-Din, M. Pilot-Scale UV/H₂O₂ Advanced Oxidation Process for Municipal Reuse Water: Assessing Micropollutant Degradation and Estrogenic Impacts on

- Goldfish (*Carassius Auratus L.*). *Water Res.* **2016**, *101*, 157–166, doi:10.1016/j.watres.2016.05.079.
39. Baxendale, J.H.; Wilson, J.A. The Photolysis of Hydrogen Peroxide at High Light Intensities. *Trans. Faraday Soc.* **1957**, *53*, 344–356, doi:10.1039/TF9575300344.
 40. Bensalah, N.; Chair, K.; Bedoui, A. Efficient Degradation of Tannic Acid in Water by UV/H₂O₂ Process. *Sustain. Environ. Res.* **2018**, *28*, 1–11, doi:10.1016/j.serj.2017.04.004.
 41. De Luis, A.M.; Lombraña, J.I.; Menéndez, A.; Sanz, J. Analysis of the Toxicity of Phenol Solutions Treated with H₂O₂/UV and H₂O₂/Fe Oxidative Systems. *Ind. Eng. Chem. Res.* **2011**, *50*, 1928–1937, doi:10.1021/ie101435u.
 42. De, A.K.; Chaudhuri, B.; Bhattacharjee, S. A Kinetic Study of the Oxidation of Phenol, o-Chlorophenol and Catechol by Hydrogen Peroxide between 298 K and 333 K: The Effect of pH, Temperature and Ratio of Oxidant to Substrate. *J. Chem. Technol. Biotechnol.* **1999**, *74*, 162–168.
 43. Benitez, F.J.; Beltran-Heredia, J.; Acero, J.L.; Rubio, F.J. Contribution of Free Radicals to Chlorophenols Decomposition by Several Advanced Oxidation Processes. *Chemosphere* **2000**, *41*, 1271–1277, doi:10.1016/S0045-6535(99)00536-6.
 44. Zhou, T.; Li, Y.; Ji, J.; Wong, F.-S.; Lu, X. Oxidation of 4-Chlorophenol in a Heterogeneous Zero Valent Iron/H₂O₂ Fenton-like System: Kinetic, Pathway and Effect Factors. *Sep. Purif. Technol.* **2008**, *62*, 551–558, doi:10.1016/j.seppur.2008.03.008.
 45. Sharma, S.; Mukhopadhyay, M.; Murthy, Z.V.P. Treatment of Chlorophenols from Wastewaters by Advanced Oxidation Processes. *Sep. Purif. Rev.* **2013**, *42*, 263–295, doi:10.1080/15422119.2012.669804.
 46. Gaya, U.I.; Abdullah, A.H.; Zainal, Z.; Hussein, M.Z. Photocatalytic Treatment of 4-Chlorophenol in Aqueous ZnO Suspensions: Intermediates, Influence of Dosage and Inorganic Anions. *J. Hazard. Mater.* **2009**, *168*, 57–63, doi:10.1016/j.jhazmat.2009.01.130.
 47. Pera-Titus, M.; García-Molina, V.; Baños, M.A.; Giménez, J.; Esplugas, S. Degradation of Chlorophenols by Means of Advanced Oxidation Processes: A General Review. *Appl. Catal. B.* **2004**, *47*, 219–256, doi:10.1016/j.apcatb.2003.09.010.
 48. Çatalkaya, E.Ç.; Bali, U.; Engül, F. Photochemical Degradation and Mineralization of 4-Chlorophenol. *Environ. Sci. Pollut. Res.* **2003**, *10*, 113–120, doi:10.1065/espr2002.10.135.
 49. Arzate, S.; Campos-Mañas, M.C.; Miralles-Cuevas, S.; Agüera, A.; García Sánchez, J.L.; Sánchez Pérez, J.A. Removal of Contaminants of Emerging Concern by Continuous Flow Solar Photo-Fenton Process at Neutral pH in Open Reactors. *J. Environ. Manage.* **2020**, *261*, 110265, doi:10.1016/j.jenvman.2020.110265.
 50. Ma, D.; Yi, H.; Lai, C.; Liu, X.; Huo, X.; An, Z.; Li, L.; Fu, Y.; Li, B.; Zhang, M.; et al. Critical Review of Advanced Oxidation Processes in Organic Wastewater Treatment. *Chemosphere* **2021**, *275*, 130104, doi:10.1016/j.chemosphere.2021.130104.
 51. Prada-Vasquez, M.A.; Estrada-Florez, S.E.; Serna-Galvis, E.A.; Torres-Palma, R.A. Developments in the Intensification of Photo-Fenton and Ozonation-Based Processes for the Removal of Contaminants of Emerging Concern in Ibero-American Countries. *Sci. Total Environ.* **2021**, *765*, 142699, doi:10.1016/j.scitotenv.2020.142699.
 52. Ruppert, G.; Bauer, R.; Heisler, G. UV-O₃, UV-H₂O₂, UV-TiO₂ and the Photo-Fenton Reaction - Comparison of Advanced Oxidation Processes for Wastewater Treatment. *Chemosphere* **1994**, *28*, 1447–1454, doi:10.1016/0045-6535(94)90239-9.

53. De la Cruz, N.; Esquius, L.; Grandjean, D.; Magnet, A.; Tungler, A.; de Alencastro, L.F.; Pulgarin, C. Degradation of Emergent Contaminants by UV, UV/H₂O₂ and Neutral Photo-Fenton at Pilot Scale in a Domestic Wastewater Treatment Plant. *Water Res.* **2013**, *47*, 5836–5845, doi:10.1016/j.watres.2013.07.005.
54. Sánchez Pérez, J.A.; Arzate, S.; Soriano-Molina, P.; García Sánchez, J.L.; Casas López, J.L.; Plaza-Bolaños, P. Neutral or Acidic pH for the Removal of Contaminants of Emerging Concern in Wastewater by Solar Photo-Fenton? A Techno-Economic Assessment of Continuous Raceway Pond Reactors. *Sci. Total Environ.* **2020**, *736*, 139681, doi:10.1016/j.scitotenv.2020.139681.
55. Villota, N.; Ferreiro, C.; Qulatein, H.A.; Lomas, J.M.; Lombraña, J.I. Turbidity Changes during Carbamazepine Oxidation by Photo-Fenton. *Catalysts* **2021**, *11*, 894, doi:10.3390/catal11080894.
56. Bahlmann, A.; Brack, W.; Schneider, R.J.; Krauss, M. Carbamazepine and Its Metabolites in Wastewater: Analytical Pitfalls and Occurrence in Germany and Portugal. *Water Res.* **2014**, *57*, 104–114, doi:10.1016/j.watres.2014.03.022.
57. Villota, N.; Lombraña, J.I.; Cruz-Alcalde, A.; Marcé, M.; Esplugas, S. Kinetic Study of Colored Species Formation during Paracetamol Removal from Water in a Semicontinuous Ozonation Contactor. *Sci. Total Environ.* **2019**, *649*, 1434–1442, doi:10.1016/j.scitotenv.2018.08.417.
58. Villota, N.; Lomas, J.M.; Camarero, L.M. Kinetic Modelling of Water-Color Changes in a Photo-Fenton System Applied to Oxidate Paracetamol. *J. Photochem. Photobiol. A* **2018**, *356*, 573–579, doi:10.1016/j.jphotochem.2018.01.040.
59. Ferreiro, C.; Villota, N.; de Luis, A.; Lombraña, J.I.; Etxebarria, N.; Lomas, J.M. Water Reuse Study from Urban WWTPs via C-Ultrafiltration and Ozonation Technologies: Basis for Resilient Cities and Agriculture. *Agronomy* **2021**, *11*, 322, doi:10.3390/agronomy11020322.
60. Oturan, M.A.; Aaron, J.-J. Advanced Oxidation Processes in Water/Wastewater Treatment: Principles and Applications. A Review. *Crit. Rev. Environ. Sci. Technol.* **2014**, *44*, 2577–2641, doi:10.1080/10643389.2013.829765.
61. Corredor, J.; Rivero, M.J.; Ortiz, I. New Insights in the Performance and Reuse of RGO/TiO₂ Composites for the Photocatalytic Hydrogen Production. *Int. J. Hydrog. Energ.* **2021**, *46*, 17500–17506, doi:10.1016/j.ijhydene.2020.01.181.
62. Amorós-Pérez, A.; Lillo-Ródenas, M.Á.; Román-Martínez, M. del C.; García-Muñoz, P.; Keller, N. TiO₂ and TiO₂-Carbon Hybrid Photocatalysts for Diuron Removal from Water. *Catalysts* **2021**, *11*, 457, doi:10.3390/catal11040457.
63. Shahrezaei, F.; Mansouri, Y.; Zinatizadeh, A. a. L.; Akhbari, A. Photocatalytic Degradation of Aniline Using TiO₂ Nanoparticles in a Vertical Circulating Photocatalytic Reactor. *Int. J. Photoenergy* **2012**, 430638, doi:10.1155/2012/430638.
64. Rancaño, L.; Rivero, M.J.; Mueses, M.Á.; Ortiz, I. Comprehensive Kinetics of the Photocatalytic Degradation of Emerging Pollutants in a LED-Assisted Photoreactor. S-Metolachlor as Case Study. *Catalysts* **2021**, *11*, 48, doi:10.3390/catal11010048.
65. Elfalleh, W.; Assadi, A.A.; Bouzaza, A.; Wolbert, D.; Kiwi, J.; Rtimi, S. Innovative and Stable TiO₂ Supported Catalytic Surfaces Removing Aldehydes under UV-Light Irradiation. *J. Photochem. Photobiol. A* **2017**, *343*, 96–102, doi:10.1016/j.jphotochem.2017.04.029.
66. Rioja, N.; Zorita, S.; Peñas, F.J. Effect of Water Matrix on Photocatalytic Degradation and General Kinetic Modeling. *Appl. Catal. B* **2016**, *180*, 330–335, doi:10.1016/j.apcatb.2015.06.038.

67. Dette, C.; Pérez-Osorio, M.A.; Kley, C.S.; Punke, P.; Patrick, C.E.; Jacobson, P.; Giustino, F.; Jung, S.J.; Kern, K. TiO₂ Anatase with a Bandgap in the Visible Region. *Nano Lett.* **2014**, *14*, 6533–6538, doi:10.1021/nl503131s.
68. Ribao, P.; Rivero, M.J.; Ortiz, I. TiO₂ Structures Doped with Noble Metals and/or Graphene Oxide to Improve the Photocatalytic Degradation of Dichloroacetic Acid. *Environ. Sci. Pollut. Res. Int.* **2017**, *24*, 12628–12637, doi:10.1007/s11356-016-7714-x.
69. Ribao, P.; Corredor, J.; Rivero, M.J.; Ortiz, I. Role of Reactive Oxygen Species on the Activity of Noble Metal-Doped TiO₂ Photocatalysts. *J. Hazard. Mater.* **2019**, *372*, 45–51, doi:10.1016/j.jhazmat.2018.05.026.
70. Ali, M.A.; Idris, M.R.; Quayum, M.E. Fabrication of ZnO nanoparticles by solution combustion method for the photocatalytic degradation of organic dye. *J. Nanostruct. Chem.* **2013**, *3*, 36, doi:10.1186/2193-8865-3-36.
71. Lin, H.; Chen, D.; Liu, H.; Zou, X.; Chen, T. Effect of MnO₂ Crystalline Structure on the Catalytic Oxidation of Formaldehyde. *Aerosol Air Qual. Res.* **2017**, *17*, 1011–1020, doi:10.4209/aaqr.2017.01.0013.
72. Kamran, U.; Heo, Y.-J.; Lee, J.W.; Park, S.-J. Chemically Modified Activated Carbon Decorated with MnO₂ Nanocomposites for Improving Lithium Adsorption and Recovery from Aqueous Media. *J. Alloys Compd.* **2019**, *794*, 425–434, doi:10.1016/j.jallcom.2019.04.211.
73. Zhou, J.; Wu, M.; Zhang, Y.; Zhu, C.; Fang, Y.; Li, Y.; Yu, L. 3D Hierarchical Structures MnO₂/C: A Highly Efficient Catalyst for Purification of Volatile Organic Compounds with Visible Light Irradiation. *Appl. Surf. Sci.* **2018**, *447*, 191–199, doi:10.1016/j.apsusc.2018.03.183.
74. Bello, M.M.; Abdul Raman, A.A.; Purushothaman, M. Applications of Fluidized Bed Reactors in Wastewater Treatment – A Review of the Major Design and Operational Parameters. *J. Clean. Prod.* **2017**, *141*, 1492–1514, doi:10.1016/j.jclepro.2016.09.148.
75. Ghatak, H.R. Advanced Oxidation Processes for the Treatment of Biorecalcitrant Organics in Wastewater. *Crit. Rev. Environ. Sci. Technol.* **2014**, *44*, 1167–1219, doi:10.1080/10643389.2013.763581.
76. Chiam, S.-L.; Pung, S.-Y.; Yeoh, F.-Y. Recent Developments in MnO₂-Based Photocatalysts for Organic Dye Removal: A Review. *Environ. Sci. Pollut. Res.* **2020**, *27*, 5759–5778, doi:10.1007/s11356-019-07568-8.
77. Tang, N.; Tian, X.; Yang, C.; Pi, Z.; Han, Q. Facile Synthesis of α-MnO₂ Nanorods for High-Performance Alkaline Batteries. *J. Phys. Chem. Solids* **2010**, *71*, 258–262, doi:10.1016/j.jpccs.2009.11.016.
78. Das, M.; Bhattacharyya, K.G. Oxidation of Rhodamine B in Aqueous Medium in Ambient Conditions with Raw and Acid-Activated MnO₂, NiO, ZnO as Catalysts. *J. Mol. Catal. A Chem.* **2014**, *391*, 121–129, doi:10.1016/j.molcata.2014.04.019.
79. Zhu, K.; Wang, C.; Camargo, P.H.C.; Wang, J. Investigating the Effect of MnO₂ Band Gap in Hybrid MnO₂-Au Materials over the SPR-Mediated Activities under Visible Light. *J. Mater. Chem. A* **2019**, *7*, 925–931, doi:10.1039/C8TA09785B.
80. Shih, Y.-J.; Tsai, M.-T.; Huang, Y.-H. Mineralization and Defluoridation of 2,2,3,3-Tetrafluoro-1-Propanol (TFP) by UV Oxidation in a Novel Three-Phase Fluidized Bed Reactor (3P-FBR). *Water Res.* **2013**, *47*, 2325–2330, doi:10.1016/j.watres.2013.02.007.
81. Tian, S.H.; Tu, V.T.; Chen, D.S.; Chen, X.; Xiong, Y. Degradation of Acid Orange II at Neutral pH Using Fe₂(MoO₄)₃ as a Heterogeneous Fenton-like Catalyst. *Chem. Eng. J.* **2011**, *169*, 31–37, doi:10.1016/j.cej.2011.02.045.
82. Tisa, F.; Abdul Raman, A.A.; Wan Daud, W.M.A. Applicability of Fluidized Bed Reactor in Recalcitrant Compound Degradation through Advanced Oxidation

- Processes: A Review. *J. Environ. Manag.* **2014**, *146*, 260–275, doi:10.1016/j.jenvman.2014.07.032.
83. Moussavi, G.; Aghapour, A.A.; Yaghmaeian, K. The Degradation and Mineralization of Catechol Using Ozonation Catalyzed with MgO/GAC Composite in a Fluidized Bed Reactor. *Chem. Eng. J.* **2014**, *249*, 302–310, doi:10.1016/j.cej.2014.03.059.
 84. Kanki, T.; Hamasaki, S.; Sano, N.; Toyoda, A.; Hirano, K. Water Purification in a Fluidized Bed Photocatalytic Reactor Using TiO₂-Coated Ceramic Particles. *Chem. Eng. J.* **2005**, *108*, 155–160, doi:10.1016/j.cej.2005.01.014.
 85. Huang, C.-P.; Huang, Y.-H. Application of an Active Immobilized Iron Oxide with Catalytic H₂O₂ for the Mineralization of Phenol in a Batch Photo-Fluidized Bed Reactor. *Appl. Catal. A* **2009**, *357*, 135–141, doi:10.1016/j.apcata.2008.12.043.
 86. Chen, H.; Zhuang, R.; Yao, J.; Wang, F.; Qian, Y.; Masakorala, K.; Cai, M.; Liu, H. Short-Term Effect of Aniline on Soil Microbial Activity: A Combined Study by Isothermal Microcalorimetry, Glucose Analysis, and Enzyme Assay Techniques. *Environ. Sci. Pollut. Res.* **2014**, *21*, 674–683, doi:10.1007/s11356-013-1955-8.
 87. Ferreira, C.; Villota, N.; Lombraña, J.I.; Rivero, M.J. An Efficient Catalytic Process for the Treatment of Genotoxic Aniline Wastewater Using a New Granular Activated Carbon-Supported Titanium Dioxide Composite. *J. Clean. Prod.* **2019**, *228*, 1282–1295, doi:10.1016/j.jclepro.2019.04.198.
 88. Valdés, H.; Zaror, C.A.; Jekel, M. Removal of Benzothiazole from Contaminated Waters by Ozonation: The Role of Direct and Indirect Ozone Reactions. *J. Adv. Oxid. Technol.* **2016**, *19*, 338–346, doi:10.1515/jaots-2016-0218.
 89. European Commission *European Union Risk Assessment Report Aniline*; Office for Official Publications of the European Communities, Luxembourg, **2004**; Vol. 50.
 90. Harbison, R.D.; Bourgeois, M.M.; Johnson, G.T. *Hamilton and Hardy's Industrial Toxicology*; John Wiley & Sons, Hoboken, NJ, USA, **2015**; ISBN 978-1-118-83421-3.
 91. Tao, N.; Liu, G.; Bai, L.; Tang, L.; Guo, C. Genotoxicity and Growth Inhibition Effects of Aniline on Wheat. *Chemosphere* **2017**, *169*, 467–473, doi:10.1016/j.chemosphere.2016.11.063.
 92. Seitz, W.; Winzenbacher, R. A Survey on Trace Organic Chemicals in a German Water Protection Area and the Proposal of Relevant Indicators for Anthropogenic Influences. *Environ. Monit. Assess.* **2017**, *189*, 244, doi:10.1007/s10661-017-5953-z.
 93. Ribeiro, A.R.; Nunes, O.C.; Pereira, M.F.R.; Silva, A.M.T. An Overview on the Advanced Oxidation Processes Applied for the Treatment of Water Pollutants Defined in the Recently Launched Directive 2013/39/EU. *Environ. Int.* **2015**, *75*, 33–51, doi:10.1016/j.envint.2014.10.027.
 94. De Wever, H.; Verachtert, H. Biodegradation and Toxicity of Benzothiazoles. *Water Res.* **1997**, *31*, 2673–2684, doi:10.1016/S0043-1354(97)00138-3.
 95. Felis, E.; Sochacki, A.; Magiera, S. Degradation of Benzotriazole and Benzothiazole in Treatment Wetlands and by Artificial Sunlight. *Water Res.* **2016**, *104*, 441–448, doi:10.1016/j.watres.2016.08.037.
 96. Mei-yan, X.; Can, D.; Godefroid, B.; Jian, Y. Treatment of Pharmaceutical Wastewater Containing Recalcitrant Compounds in a Fenton-Coagulation Process. *J. Environ. Sci.* **2006**, *18*, 459–463.
 97. Suresh, S.; Srivastava, V.C.; Mishra, I.M. Adsorptive Removal of Aniline by Granular Activated Carbon from Aqueous Solutions with Catechol and Resorcinol. *Environ. Technol.* **2012**, *33*, 773–781, doi:10.1080/09593330.2011.592228.

98. Liu, Q.; Zhang, L.; Hu, P.; Huang, R. Removal of Aniline from Aqueous Solutions by Activated Carbon Coated by Chitosan. *J. Water Reuse Desalin.* **2015**, *5*, 610–618, doi:10.2166/wrd.2015.097.
99. Sumegova, L.; Derco, J.; Melicher, M. Degradation of Benzothiazole by Ozonation and Adsorptive Ozonation. *Chem. Biochem. Eng. Q.* **2015**, *29*, 63–66, doi:10.15255/CABEQ.2014.2128.
100. Jing, Z.; Cao, S.; Yu, T.; Hu, J. Degradation Characteristics of Aniline with Ozonation and Subsequent Treatment Analysis. *J. Chem.* **2015**, 905921, doi:10.1155/2015/905921.
101. Ferreiro, C.; Villota, N.; Lombraña, J.I.; Rivero, M.J. Heterogeneous Catalytic Ozonation of Aniline-Contaminated Waters: A Three-Phase Modelling Approach Using TiO₂/GAC. *Water* **2020**, *12*, 3448, doi:10.3390/w12123448.
102. Canle L., M.; Santaballa, J.A.; Vulliet, E. On the Mechanism of TiO₂-Photocatalyzed Degradation of Aniline Derivatives. *J. Photochem. Photobiol. A* **2005**, *175*, 192–200, doi:10.1016/j.jphotochem.2005.05.001.
103. Reddy, P.A.K.; Reddy, P.V.L.; Kwon, E.; Kim, K.-H.; Akter, T.; Kalagara, S. Recent Advances in Photocatalytic Treatment of Pollutants in Aqueous Media. *Environ. Int.* **2016**, *91*, 94–103, doi:10.1016/j.envint.2016.02.012.
104. Gomes, H.T.; Machado, B.F.; Ribeiro, A.; Moreira, I.; Rosário, M.; Silva, A.M.T.; Figueiredo, J.L.; Faria, J.L. Catalytic Properties of Carbon Materials for Wet Oxidation of Aniline. *J. Hazard. Mater.* **2008**, *159*, 420–426, doi:10.1016/j.jhazmat.2008.02.070.
105. Zhou, L.; Xie, Y.; Cao, H.; Guo, Z.; Wen, J.; Shi, Y. Enhanced Removal of Benzothiazole in Persulfate Promoted Wet Air Oxidation via Degradation and Synchronous Polymerization. *Chem. Eng. J.* **2019**, *370*, 208–217, doi:10.1016/j.cej.2019.03.201.
106. Application of Reverse Osmosis to Remove Aniline from Wastewater. *Desalination* **2009**, *245*, 687–693, doi:10.1016/j.desal.2009.02.038.
107. Sánchez, L.; Peral, J.; Domènech, X. Photocatalyzed Destruction of Aniline in UV-Illuminated Aqueous TiO₂ Suspensions. *Electrochim. Acta* **1997**, *42*, 1877–1882, doi:10.1016/S0013-4686(96)00400-8.
108. Anotai, J.; Jevprasesphant, A.; Lin, Y.-M.; Lu, M.-C. Oxidation of Aniline by Titanium Dioxide Activated with Visible Light. *Sep. Purif. Technol.* **2012**, *84*, 132–137, doi:10.1016/j.seppur.2011.09.035.
109. Rahmat, M.; Rehman, A.; Rahmat, S.; Bhatti, H.N.; Iqbal, M.; Khan, W.S.; Bajwa, S.Z.; Rahmat, R.; Nazir, A. Highly Efficient Removal of Crystal Violet Dye from Water by MnO₂ Based Nanofibrous Mesh/Photocatalytic Process. *J. Mater. Res. Technol.* **2019**, *8*, 5149–5159, doi:10.1016/j.jmrt.2019.08.038.
110. Buhler, R.; Staehelin, J.; Hoigne, J. Ozone Decomposition in Water Studied by Pulse-Radiolysis. 1. HO₂/O₂⁻ and HO₃/O₃⁻ as Intermediates. *J. Phys. Chem.* **1984**, *88*, 2560–2564.
111. Ghuge, S.P.; Saroha, A.K. Catalytic Ozonation for the Treatment of Synthetic and Industrial Effluents - Application of Mesoporous Materials: A Review. *J. Environ. Manage.* **2018**, *211*, 83–102, doi:10.1016/j.jenvman.2018.01.052.
112. Ferreiro, C.; Villota, N.; Luis, A. de; Lombrana, J.I. Analysis of the Effect of the Operational Variants in a Combined Adsorption-Ozonation Process with Granular Activated Carbon for the Treatment of Phenol Wastewater. *React. Chem. Eng.* **2020**, *5*, 760–778, doi:10.1039/C9RE00424F.
113. Valdés, H.; Tardón, R.F.; Zaror, C.A. Cationic Dyes Removal Using Ozone, Natural Zeolite, and Ozone/Zeolite. *Ingeniare, Rev. chil. Ing.* **2009**, *17*, 360–364, doi:10.4067/S0718-33052009000300009.

114. Nawrocki, J. Catalytic Ozonation in Water: Controversies and Questions. Discussion Paper. *Appl. Catal. B* **2013**, *142–143*, 465–471, doi:10.1016/j.apcatb.2013.05.061.
115. Guelli Souza, S.; Souza, F.; Souza, A. Application of Individual and Simultaneous Ozonation and Adsorption Processes in Batch and Fixed-Bed Reactors for Phenol Removal. *Ozone Sci. Eng.* **2012**, *34*, 259–268, doi:10.1080/01919512.2012.688711.
116. Babich, H.; Davis, D.L. Phenol: A Review of Environmental and Health Risks. *Regul. Toxicol. Pharmacol.* **1981**, *1*, 90–109, doi:10.1016/0273-2300(81)90071-4.
117. Ribeiro, H.B.; Bampi, J.; da Silva, T.C.; Dervanoski, A.; Milanesi, P.M.; Fuzinato, C.F.; de Mello, J.M.M.; da Luz, C.; Vargas, G.D.L.P. Study of Phenol Biodegradation in Different Agitation Systems and Fixed Bed Column: Experimental, Mathematical Modeling, and Numerical Simulation. *Environ. Sci. Pollut. Res.* **2020**, *27*, 45250–45269, doi:10.1007/s11356-020-10380-4.
118. Lin, S.H.; Wang, C.H. Ozonation of Phenolic Wastewater in a Gas-Induced Reactor with a Fixed Granular Activated Carbon Bed. *Ind. Eng. Chem. Res.* **2003**, *42*, 1648–1653, doi:10.1021/ie020545x.
119. De Luis, A.M.; Lombraña, J.I.; Menéndez, A.; Sanz, J. Analysis of the Toxicity of Phenol Solutions Treated with H₂O₂/UV and H₂O₂/Fe Oxidative Systems. *Ind. Eng. Chem. Res.* **2011**, *50*, 1928–1937, doi:10.1021/ie101435u.
120. Orge, C.A.; Faria, J.L.; Pereira, M.F.R. Photocatalytic Ozonation of Aniline with TiO₂-Carbon Composite Materials. *J. Environ. Manage.* **2017**, *195*, 208–215, doi:10.1016/j.jenvman.2016.07.091.
121. Orge, C.A.; Sousa, J.P.S.; Gonçalves, F.; Freire, C.; Órfão, J.J.M.; Pereira, M.F.R. Development of Novel Mesoporous Carbon Materials for the Catalytic Ozonation of Organic Pollutants. *Catal. Lett.* **2009**, *132*, 1–9, doi:10.1007/s10562-009-0029-5.
122. Legube, B.; Karpel Vel Leitner, N. Catalytic Ozonation: A Promising Advanced Oxidation Technology for Water Treatment. *Catal. Today* **1999**, *53*, 61–72, doi:10.1016/S0920-5861(99)00103-0.
123. Beltran, F.J.; Rivas, F.J.; Montero-de-Espinosa, R. A TiO₂/Al₂O₃ Catalyst to Improve the Ozonation of Oxalic Acid in Water. *Appl. Catal. B* **2004**, *47*, 101–109, doi:10.1016/j.apcatb.2003.07.007.
124. Song, S.; Liu, Z.; He, Z.; Zhang, A.; Chen, J. Impacts of Morphology and Crystallite Phases of Titanium Oxide on the Catalytic Ozonation of Phenol. *Environ. Sci. Technol.* **2010**, *44*, 3913–3918, doi:10.1021/es100456n.
125. Kidak, R.; Dogan, S. Medium-High Frequency Ultrasound and Ozone Based Advanced Oxidation for Amoxicillin Removal in Water. *Ultrason. Sonochem.* **2018**, *40*, 131–139, doi:10.1016/j.ultsonch.2017.01.033.
126. Rahdar, S.; Igwegbe, C.A.; Ghasemi, M.; Ahmadi, S. Degradation of Aniline by the Combined Process of Ultrasound and Hydrogen Peroxide (US/H₂O₂). *MethodsX* **2019**, *6*, 492–499, doi:10.1016/j.mex.2019.02.033.
127. Xiao, R.; He, Z.; Diaz-Rivera, D.; Pee, G.V.; Weavers, L.K. Sonochemical Degradation of Ciprofloxacin and Ibuprofen in the Presence of Matrix Organic Compounds. *Ultrason. Sonochem.* **2014**, *21*, 428–435, doi:10.1016/j.ultsonch.2013.06.012.
128. Adewuyi, V.G. Sonochemistry: Environmental Science and Engineering Applications. *Ind. Eng. Chem. Res.* **2001**, *40*, 4681–4715, doi:10.1021/ie010096l.
129. Serna-Galvis, E.A.; Silva-Agredo, J.; Giraldo, A.L.; Florez-Acosta, O.A.; Torres-Palma, R.A. Comparative Study of the Effect of Pharmaceutical Additives on the Elimination of Antibiotic Activity during the Treatment of Oxacillin in Water by the Photo-Fenton, TiO₂-Photocatalysis and Electrochemical Processes. *Sci. Total Environ.* **2016**, *541*, 1431–1438, doi:10.1016/j.scitotenv.2015.10.029.

130. Naddeo, V.; Secondes, M.F.N.; Borea, L.; Hasan, S.W.; Ballesteros, F.; Belgiorno, V. Removal of Contaminants of Emerging Concern from Real Wastewater by an Innovative Hybrid Membrane Process – UltraSound, Adsorption, and Membrane Ultrafiltration (USAMe®). *Ultrason. Sonochem.* **2020**, *68*, 105237, doi:10.1016/j.ultsonch.2020.105237.
131. Fan, X.-D.; Zhang, W.-L.; Xiao, H.-Y.; Qiu, T.-Q.; Jiang, J.-G. Effects of Ultrasound Combined with Ozone on the Degradation of Organophosphorus Pesticide Residues on Lettuce. *RSC Adv.* **2015**, *5*, 45622–45630, doi:10.1039/c5ra03024b.
132. Larose, J.; Lègeron, J.P. Elimination of Humic Materials. *Ozone Sci. Eng.* **1982**, *4*, 80–90, doi:10.1080/01919518208550944.
133. Chiang, Y.-P.; Liang, Y.-Y.; Chang, C.-N.; Chao, A.C. Differentiating Ozone Direct and Indirect Reactions on Decomposition of Humic Substances. *Chemosphere* **2006**, *65*, 2395–2400, doi:10.1016/j.chemosphere.2006.04.080.
134. Jeong, H.; Bhattarai, R.; Adamowski, J.; Yu, D.J. Insights from Socio-Hydrological Modeling to Design Sustainable Wastewater Reuse Strategies for Agriculture at the Watershed Scale. *Agric. Water Manage.* **2020**, *231*, 105983, doi:10.1016/j.agwat.2019.105983.
135. Maiolo, M.; Pantusa, D. A Proposal for Multiple Reuse of Urban Wastewater. *J. Water Reuse Desalin.* **2018**, *8*, 468–478, doi:10.2166/wrd.2017.144.
136. Cuartucci, M. Ultrafiltration, a Cost-Effective Solution for Treating Surface Water to Potable Standard. *Water Pract. Technol.* **2020**, *15*, 426–436, doi:10.2166/wpt.2020.039.
137. Van der Bruggen, B.; Vandecasteele, C.; Van Gestel, T.; Doyen, W.; Leysen, R. A Review of Pressure-Driven Membrane Processes in Wastewater Treatment and Drinking Water Production. *Environ. Prog.* **2003**, *22*, 46–56, doi:10.1002/ep.670220116.
138. Nasirabadi, P.S.; Saljoughi, E.; Mousavi, S.M. Membrane Processes Used for Removal of Pharmaceuticals, Hormones, Endocrine Disruptors and Their Metabolites from Wastewaters: A Review. *Desalination Water Treat.* **2016**, *57*, 24146–24175, doi:10.1080/19443994.2016.1140081.
139. Wang, J.; Tian, Z.; Huo, Y.; Yang, M.; Zheng, X.; Zhang, Y. Monitoring of 943 Organic Micropollutants in Wastewater from Municipal Wastewater Treatment Plants with Secondary and Advanced Treatment Processes. *J. Environ. Sci.* **2018**, *67*, 309–317, doi:10.1016/j.jes.2017.09.014.
140. Kudlek, E. Decomposition of Contaminants of Emerging Concern in Advanced Oxidation Processes. *Water* **2018**, *10*, 955, doi:10.3390/w10070955.
141. Marquez, G.; Rodriguez, E.M.; Beltran, F.J.; Alvarez, P.M. Solar Photocatalytic Ozonation of a Mixture of Pharmaceutical Compounds in Water. *Chemosphere* **2014**, *113*, 71–78, doi:10.1016/j.chemosphere.2014.03.093.
142. Muhamad, M.S.; Salim, M.R.; Lau, W.J.; Yusop, Z.; Hadibarata, T. The Removal of Bisphenol A in Water Treatment Plant Using Ultrafiltration Membrane System. *Water Air Soil Pollut.* **2016**, *227*, 250, doi:10.1007/s11270-016-2951-7.
143. Liu, P.; Zhang, H.; Feng, Y.; Yang, F.; Zhang, J. Removal of Trace Antibiotics from Wastewater: A Systematic Study of Nanofiltration Combined with Ozone-Based Advanced Oxidation Processes. *Chem. Eng. J.* **2014**, *240*, 211–220, doi:10.1016/j.cej.2013.11.057.
144. Gomes, J.; Matos, A.; Gmurek, M.; Quinta-Ferreira, R.M.; Martins, R.C. Ozone and Photocatalytic Processes for Pathogens Removal from Water: A Review. *Catalysts* **2019**, *9*, 46, doi:10.3390/catal9010046.
145. Shahidi, S. Magnetic Nanoparticles Application in the Textile Industry—A Review. *J. Ind. Text.* **2021**, *50*, 970–989, doi:10.1177/1528083719851852.

146. Shah, S.N.A.; Shah, Z.; Hussain, M.; Khan, M. Hazardous Effects of Titanium Dioxide Nanoparticles in Ecosystem. *Bioinorg. Chem. Appl.* **2017**, doi:10.1155/2017/4101735.
147. Khan, I.; Sadiq, M.; Khan, I.; Saeed, K. Manganese Dioxide Nanoparticles/Activated Carbon Composite as Efficient UV and Visible-Light Photocatalyst. *Environ. Sci. Pollut. Res.* **2019**, *26*, 5140–5154, doi:10.1007/s11356-018-4055-y.
148. Colmenares, J.C.; Varma, R.S.; Lisowski, P. Sustainable Hybrid Photocatalysts: Titania Immobilized on Carbon Materials Derived from Renewable and Biodegradable Resources. *Green Chem.* **2016**, *18*, 5736–5750, doi:10.1039/C6GC02477G.
149. Martins, A.C.; Cazetta, A.L.; Pezoti, O.; Souza, J.R.B.; Zhang, T.; Pilau, E.J.; Asefa, T.; Almeida, V.C. Sol-Gel Synthesis of New TiO₂/Activated Carbon Photocatalyst and Its Application for Degradation of Tetracycline. *Ceram. Int.* **2017**, *43*, 4411–4418, doi:10.1016/j.ceramint.2016.12.088.
150. Campanati, M.; Fornasari, G.; Vaccari, A. Fundamentals in the Preparation of Heterogeneous Catalysts. *Catal. Today* **2003**, *77*, 299–314, doi:10.1016/S0920-5861(02)00375-9.
151. Liu, S.X.; Chen, X.V.; Chen, X. A TiO₂/AC Composite Photocatalyst with High Activity and Easy Separation Prepared by a Hydrothermal Method. *J. Hazard. Mater.* **2007**, *143*, 257–263, doi:10.1016/j.jhazmat.2006.09.026.
152. Król, A.; Pomastowski, P.; Rafiska, K.; Railean-Plugaru, V.; Buszewski, B. Zinc Oxide Nanoparticles: Synthesis, Antiseptic Activity and Toxicity Mechanism. *Adv. Colloid Interface Sci.* **2017**, *249*, 37–52, doi:10.1016/j.cis.2017.07.033.
153. Rokesh, K.; Nithya, A.; Jeganathan, K.; Jothivenkatachalam, K. A Facile Solid State Synthesis of Cone-like ZnO Microstructure an Efficient Solar-Light Driven Photocatalyst for Rhodamine B Degradation. *Mater. Today: Proc.* **2016**, *3*, 4163–4172, doi:10.1016/j.matpr.2016.11.091.
154. Cao, Y.; Lei, X.; Chen, Q.; Kang, C.; Li, W.; Liu, B. Enhanced Photocatalytic Degradation of Tetracycline Hydrochloride by Novel Porous Hollow Cube ZnFe₂O₄. *J. Photochem. Photobiol. A* **2018**, *364*, 794–800, doi:10.1016/j.jphotochem.2018.07.023.
155. Warsi, M.F.; Bilal, M.; Zulfiqar, S.; Khalid, M.U.; Agboola, P.O.; Shakir, I. Enhanced Visible Light Driven Photocatalytic Activity of MnO₂ Nanomaterials and Their Hybrid Structure with Carbon Nanotubes. *Mater. Res. Express* **2020**, *7*, 105015, doi:10.1088/2053-1591/abbf8d.
156. Vinoth Kumar, J.; Karthik, R.; Chen, S.-M.; Chen, K.-H.; Sakthinathan, S.; Muthuraj, V.; Chiu, T.-W. Design of Novel 3D Flower-like Neodymium Molybdate: An Efficient and Challenging Catalyst for Sensing and Destroying Pulmonary Toxicity Antibiotic Drug Nitrofurantoin. *Chem. Eng. J.* **2018**, *346*, 11–23, doi:10.1016/j.cej.2018.03.183.
157. Ghasemi, B.; Anvaripour, B.; Jorfi, S.; Jaafarzadeh, N. Enhanced Photocatalytic Degradation and Mineralization of Furfural Using UVC/TiO₂/GAC Composite in Aqueous Solution. *Int. J. Photoenergy* **2016**, 2782607, doi:10.1155/2016/2782607.
158. Noorimotlagh, Z.; Kazeminezhad, I.; Jaafarzadeh, N.; Ahmadi, M.; Ramezani, Z.; Silva Martinez, S. The Visible-Light Photodegradation of Nonylphenol in the Presence of Carbon-Doped TiO₂ with Rutile/Anatase Ratio Coated on GAC: Effect of Parameters and Degradation Mechanism. *J. Hazard. Mater.* **2018**, *350*, 108–120, doi:10.1016/j.jhazmat.2018.02.022.
159. Cui, H.; Li, Q.; Qian, Y.; Zhang, Q.; Zhai, J. Preparation and Adsorption Performance of MnO₂/PAC Composite towards Aqueous Glyphosate. *Environ. Technol.* **2012**, *33*, 2049–2056, doi:10.1080/09593330.2012.660641.

160. European Roadmap for Process Intensification (**2007**). Creative energy-energy transition. <https://efce.info/EUROPIN.html> (Kontsultatuta 2021ko irailaren 9a).
161. Van Gerven, T.; Mul, G.; Moulijn, J.; Stankiewicz, A. A Review of Intensification of Photocatalytic Processes. *Chem. Eng. Process.* **2007**, *46*, 781–789, doi:10.1016/j.cep.2007.05.012.
162. Van Gerven, T.; Stankiewicz, A. Structure, Energy, Synergy, Time—The Fundamentals of Process Intensification. *Ind. Eng. Chem. Res.* **2009**, *48*, 5, 2465–2474, doi:10.1021/ie801501y.
163. Pignatello, J.J.; Oliveros, E.; Mackay, A. Advanced Oxidation Processes for Organic Contaminant Destruction Based on the Fenton Reaction and Related Chemistry. *Crit. Rev. Environ. Sci. Technol.* **2006**, *36*, 1, 1–84, doi:10.1080/10643380500326564.
164. Dijkstra, M.F.J.; Michorius, A.; Buwalda, H.; Panneman, H.J.; Winkelman, J.G.M.; Beenackers, A.A.C.M. Comparison of the efficiency of immobilized and suspended systems in photocatalytic degradation. *Catal. Today* **2001**, *66*, 487–494, doi: 10.1016/S0920-5861(01)00257-7.

2. Materialak eta metodoak



Atal honetan, TiO₂/GAC eta MnO₂/GAC konposateak lortzeko erabili ziren materialak, metodologia esperimentalak eta sintesi-prozesua azalduko dira, labur. Informazio zehatzagoa nahi izanez gero, joan argitalpen zientifikoei dagokien 3. atalera.

2.1. Erreaktiboak

4. taulan ikus daitezke erabilitako erreaktibo nagusiak. Ur desionizatua ura purifikatzeko Milli-Q[®] unitate batek hornitu zuen.

4. taula Esperimentazioan erabilitako erreaktibo kimikoen zerrenda.

Erreaktiboak	Formula kimikoa	Purutasuna	Hornitzailea
2-hidroxibenzotiazola	C ₇ H ₅ NOS	Erreferentziazko material ziurtatua	SIGMA-ALDRICH
4-klorokatekola	C ₁₂ H ₃ (OH) ₂	% 97	SIGMA-ALDRICH
4-klorofenola	C ₁₂ H ₄ OH	≥% 99	SIGMA-ALDRICH
Potasio azesulfamoak	C ₄ H ₄ KNO ₄ S	Erreferentziazko material ziurtatua	SUPELCO
Azetaminofenoak	C ₈ H ₉ NO ₂	Erreferentziazko material ziurtatua	FLUKA
Etil azetatoak	C ₄ H ₈ O ₂	% 99,8	LABSCAN
Azido azetikoa	CH ₃ COOH	% 100	MERCK
Azido klofibrikoak	C ₁₀ H ₁₁ ClO ₃	Erreferentziazko material ziurtatua	MP BIOMEDICALS
Azido klorhidrikoak	HCl	% 33	SIGMA-ALDRICH
Azido formikoak	CH ₂ O ₂	% 99,0	ACROS ORGANICS
Azido fumarikoak	HOOCCH=CHCOOH	% 99,5	FLUKA CHEMIKA
Azido humikoak	HA	Teknikoa	SIGMA-ALDRICH
Azido maleikoak	HO ₂ CCH=CHCO ₂ H	≥% 99	ACROS ORGANICS
Azido nitrikoak	HNO ₃	% 69	ACROS ORGANICS
Azido ortofosforikoak	H ₃ PO ₄	% 85	MERCK
Azido perfluoro-n- oktanoikoak	C ₈ HF ₁₅ O ₂	Erreferentziazko material ziurtatua	SIGMA-ALDRICH
Azido sulfurikoak	H ₂ SO ₄	% 98	SIGMA-ALDRICH
Aeroxide [®] P25	TiO ₂	Komertziala	EVONIK INDUSTRIES
Aeroxide [®] P90	TiO ₂	Komertziala	EVONIK INDUSTRIES
Anilina	C ₆ H ₅ NH ₂	% 99,5	ACROS ORGANICS
Atrazina	C ₈ H ₁₄ ClN ₅	Erreferentziazko material ziurtatua	FLUKA
Bentzokinona	C ₆ H ₄ O ₂	Erreferentziazko material ziurtatua	SUPELCO
Bentzotiazola	C ₇ H ₅ NS	% 97	SIGMA-ALDRICH
Bezafibratoak	C ₁₉ H ₂₀ ClNO ₄	Erreferentziazko material ziurtatua	MP BIOMEDICALS
Butilparabenoak	C ₁₁ H ₁₄ O ₃	Erreferentziazko material ziurtatua	SIGMA-ALDRICH
Kafeina	C ₈ H ₁₀ N ₄ O ₂	Erreferentziazko material ziurtatua	SIGMA-ALDRICH
Karbamazepina	C ₁₅ H ₁₂ N ₂ O	% 99,1	FAGRON
Ikatz aktibatua hauts- formatuan	PAC	Komertziala	PANREAC

4. taula Esperimentazioan erabilitako errektibo kimikoen zerrenda (jarraipena).

Errektiboa	Formula kimikoa	Purutasuna	Hornitzailea
Amitriptilina klorhidratoa	C ₂₀ H ₂₃ N	Erreferentziazko material ziurtatua	SIGMA-ALDRICH
Zirprofloxazina klorhidratoa	C ₁₇ H ₁₉ ClFN ₃ O ₃	Erreferentziazko material ziurtatua	FLUKA
Klomipramina klorhidratoa	C ₁₉ H ₂₄ Cl ₂ N ₂	Erreferentziazko material ziurtatua	SIGMA-ALDRICH
Imipramina klorhidratoa	C ₁₉ H ₂₄ N ₂	Erreferentziazko material ziurtatua	SIGMA-ALDRICH
Norfloxazina klorhidratoa	C ₁₆ H ₁₉ ClFN ₃ O ₃	Erreferentziazko material ziurtatua	FLUKA
Nortriptilina klorhidratoa	C ₁₉ H ₂₁ N	Erreferentziazko material ziurtatua	SIGMA-ALDRICH
Propanolol klorhidratoa	C ₁₆ H ₂₁ NO ₂	Erreferentziazko material ziurtatua	MP BIOMEDICALS
Sodio kloruroa	NaCl	% 99,8	VWR
Titanio (IV) kloruroa	TiCl ₄	Sintesia	MERCK
Diklorometanoa	CH ₂ Cl ₂	>% 99,9	MERCK
Difenilamina	C ₁₂ H ₁₁ N	% 99	MERCK
Diurona	C ₉ H ₁₀ Cl ₂ N ₂ O	Erreferentziazko material ziurtatua	FLUKA
Mesilato eprosartana	C ₂₄ H ₂₈ N ₂ O ₇ S ₂	Erreferentziazko material ziurtatua	SOLVAY PHARMACEUTICALS
Etanol absolutua	C ₂ H ₆ O	% 100	PANREAC
Fenitoina	C ₁₅ H ₁₂ N ₂ O ₂	Erreferentziazko material ziurtatua	SIGMA-ALDRICH
Fenola	C ₆ H ₅ OH	≥% 99,0	SIGMA-ALDRICH
Fosfato sodiko dibasikoa, heptahidratatua	HNa ₂ O ₄ P·H ₂ O	% 99	FISHER
Fosfato sodiko monobasikoa	H ₂ O ₄ PNa·H ₂ O	% 98	FISHER
Genisteina	C ₁₅ H ₁₀ O ₅	Erreferentziazko material ziurtatua	EXTRASYNTHESE
Genistina	C ₂₁ H ₂₀ O ₁₀	Erreferentziazko material ziurtatua	EXTRASYNTHESE
Glizitina	C ₂₂ H ₂₂ O ₁₀	Erreferentziazko material ziurtatua	EXTRASYNTHESE
Hidrokinona	C ₆ H ₆ O ₂	Erreferentziazko material ziurtatua	SUPELCO
Sodio hidroxidoa	NaOH	≥% 97,0	LABKEM
Hydroarco® 3000	Ikatz aktibatu pikortsua	Komertziala	Cabot Corporation
Irbesartana	C ₂₅ H ₂₈ N ₆ O	Erreferentziazko material ziurtatua	SANOFI
Isoproturona	C ₁₂ H ₁₈ N ₂ O	Erreferentziazko material ziurtatua	FLUKA
Kemisorb® 530 GR 12x40	Ikatz aktibatu pikortsua	Komertziala	Kemira
Ketoprofenoa	C ₁₆ H ₁₄ O ₃	Erreferentziazko material ziurtatua	MP BIOMEDICALS
Losartan potasikoa	C ₂₂ H ₂₂ ClKN ₆ O	Erreferentziazko material ziurtatua	MERCK
Metanola, HPLC kalitatekoa	CH ₃ OH	>% 99,99	ACROS ORGANICS
Metilparabenoa	C ₈ H ₈ O ₃	Erreferentziazko material ziurtatua	SIGMA-ALDRICH
n-hexanoa, HPLC kalitatekoa	C ₆ H ₁₄	% 95	LABSCAN
Norit® GAC 1240 Plus	Ikatz aktibatu pikortsua	Komertziala	Cabot Corporation
Norit® ROX 0.8	Ikatz aktibatu pikortsua	Komertziala	Cabot Corporation
Potasio perfluoro-1-butanosulfonatoa	C ₄ F ₉ KO ₃ S	Erreferentziazko material ziurtatua	SIGMA-ALDRICH

4. taula Esperimentazioan erabilitako errektibo kimikoen zerrenda (jarraipena).

Errektiboa	Formula kimikoa	Purutasuna	Hornitzailea
Potasio perfluoro-1-oktanosulfonatoa	C ₈ F ₁₇ KO ₃ S	Erreferentziazko material ziurtatua	SIGMA-ALDRICH
Potasio permanganatoa	KMnO ₄	>% 99	PROBUS
Hidrogeno peroxidoa	H ₂ O ₂	% 30 (bol./bol.)	LABREM
Pirokatekola	C ₆ H ₆ O ₂	≥% 99	FLUKA CHEMIKA
Progesterona	C ₂₁ H ₃₀ O ₂	Erreferentziazko material ziurtatua	SIGMA-ALDRICH
Diklofenakoaren gatz sodikoa	C ₁₄ H ₁₀ Cl ₂ NNaO ₂	Erreferentziazko material ziurtatua	SIGMA-ALDRICH
Etilendiaminotetrazetikoaren gatz sodikoa	Na ₂ EDTA	% 99,0–101,1	PANREAC
Simazina	C ₇ H ₁₂ ClN ₅	Erreferentziazko material ziurtatua	FLUKA
Amoniako-disoluzioa	NH ₃	% 25	PANREAC
Sukralosa	C ₁₂ H ₁₉ Cl ₃ O ₈	Erreferentziazko material ziurtatua	SUPELCO
Sulfadiazina	C ₁₀ H ₁₀ N ₄ O ₂ S	Erreferentziazko material ziurtatua	SIGMA-ALDRICH
Sulfametoxazola	C ₁₀ H ₁₁ N ₃ O ₃ S	Erreferentziazko material ziurtatua	FLUKA
Burdina sulfato heptahidratatua	FeSO ₄ ·7H ₂ O	% 99,0	PANREAC
Sodio sulfitoa	Na ₂ SO ₃	% 58,5	SIGMA-ALDRICH
Perfluorooktano sulfonamida	C ₈ H ₂ F ₁₇ NO ₂ S	Erreferentziazko material ziurtatua	DR. EHRENSTORFER
Telmisartana	C ₃₃ H ₃₀ N ₄ O ₂	Erreferentziazko material ziurtatua	BOEHRINGER
Testosterona	C ₁₉ H ₂₈ O ₂	Erreferentziazko material ziurtatua	SIGMA-ALDRICH
Trimetoprima	C ₁₄ H ₁₈ N ₄ O ₃	Erreferentziazko material ziurtatua	FLUKA
Valsartana	C ₂₄ H ₂₉ N ₅ O ₃	Erreferentziazko material ziurtatua	BOEHRINGER
Potasio ioduroa	KI	% 99	PANREAC

2.2. Fotokatalizatzaileen eta katalizatzaileen sintesia

2.2.1. TiO₂/GAC konpositeen sintesia

- Hauspeatze-metodoa

Ikatz aktibatua HCl-arekin (% 37) aurretratu zen 30 minutuz, eta ur desionizatuarekin garbitu zen. Ondoren, 440 mL etanol absoluturi 10 mL TiCl₄ gehitu zitzaizkion tantaka, 30 minutuz, 23 °C-an, disoluzio hori bat lortu arte. Aeroxide® P90 TiO₂-aren 2,0 mg disolbatu ziren 50 mL etanoletan, eta 15 minutuz sonikatu zen. Gero, TiCl₄-EtOH zuen disoluzioari gehitu zitzaion. Ondoren, aurrez tratatutako 14,0 g GAC gehitu ziren, eta poliki irabiatu zen 45 minutuz. Azkenik, 19,2 mL NaOH (% 50) isuri ziren erreaktorera 2 orduan. Konpositea HNO₃ (% 10) eta ur desionizatua erabiliz garbitu zen. Ondoren, estufa batean lehortu zen, 90 °C-an, 12 orduz, eta, azkenik, aire-atmosfera batean kaltzinatu zen, 400 °C-an, ordubetez.

- Murgiltze bidezko inpregnazioa

Ikatz aktibatua HCl-arekin (% 37) aurretratu zen 30 minutuz, eta ur desionizatuarekin garbitu zen. Aeroxide® P90 TiO₂-aren 1,0 g disolbatu zen 400 mL ur desionizatutan, eta

15 minutuz sonikatu zen. Disoluzioa erreaktore esferiko batera eraman zen, eta, han, aurrez tratatutako GACaren 14,0 g gehitu eta 12ra doitu zen pH-a, NaOH-a (% 50) gehituta. Ikatz aktibatua ordubetez utzi zen TiO₂-dun disoluzioan, etengabe irabiatuz giro-tenperaturan. Lortutako disoluzioa bainu termostatiko batean berotu zen 100 °C-an, disoluzioaren 264 mL lurrundu arte. TiO₂/GAC konposatua ur desionizatuarekin garbitu, eta estufa batean lehortu zen, 90 °C-an 12 orduz. Azkenik, aire-atmosfera batean kaltzinatu zen, 400 °C-an ordubetez.

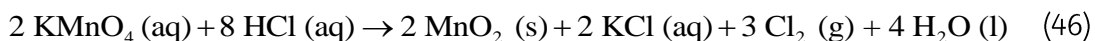
- Metodo hidrotermala

Ikatz aktibatua HCl-arekin (%37) aurretratatu zen 30 minutuz. Ondoren, ur desionizatuarekin garbitu zen, eta estufa batean lehortu, 80 °C-an 24 orduz. Aeroxide® P90 TiO₂-aren 1,0 g dispertsatu zen 400 mL ur desionizatutan, eta 15 minutuz sonikatu zen. Ondoren, Teflon®-ez egindako edukiontzi batera transferitu zen. Aurretratutako GACaren 14,0 g gehitu zitzaizkion nahasteari, eta etengabe irabiatu zen, 2 orduz, 20 °C-an. Ondoren, Teflon®-ezko edukiontzia itxi, eta estufa batean jarri zen, 120 °C-an, 3 orduz. Gaineko geruza kendu, eta solidoa ur desionizatuarekin garbitu zen. Estufa batean lehortu zen, 50 °C-an, 12 orduz.

2.2.2. MnO₂/GAC fotokatalizatzailearen sintesia

MnO₂/GAC konpositearen materiala sintetizatzeke, prestaketa-teknika hidrotermala erabili zen. Hainbat arrazoi zeuden metodo horren alde egiteko: prozesua sinplea zen, errepikakortasun ona zuen, fidagarritasun altua zuen eta erraza zen nanoegituraren tamaina eta morfologia ikatz aktibatu pikortsuzko euskarriari egokitzea.

Ikatz aktibatua disoluzio oso oxidatzaile batekin aurretratatu zen. H₂SO₄ eta H₂O₂ konposatuen nahasteaz (70:30 v/v) egindako disoluzio bat erabili zen, eta 24 orduz tratatu zen GACa. Haren fabrikazio-prozesuan sortutako ezpurutasunak kentzeko eta, hala, GACaren gainazala fase aktiboa jalkitzeko prest uzteko [1]. Ondoren, ur desionizatuarekin garbitu, eta estufan lehortu zen, 80 °C-an. Hurrengo pausuan, 9,97 g KMnO₄ disolbatu ziren 228,36 mL ur desionizatutan, eta disoluzioa 5 minutuz irabiatu zen. Ondoren, HCl kontzentratuaren 21,19 mL erantsi zitzaizkion tantaka permanganatozko disoluzioari, 15 minutuz. Nahitaezko HCl kantitate minimoa erabili zen, azken produktuaren kristalinitatea galtzeko arriskua eta nahi ez diren oxidoak (hausmannita, adibidez) sortzeko arriskua saihesteko [2]. Giro-tenperaturan egindako sintesian, honako erreakzio hau gertatu zen:



Erreakzioaren azpiproduktu nagusia KCl zen. Ondoren, irabiatze geldoz eta 1,25 orduko kontaktu-denboraz aurretratutako GACaren 14,0 g gehitu zitzaizkion disoluzioari. Segidan, autoklabe bateko Teflon®-ezko ontzi hermetiko batean sartu zen nahastea, eta estufa batean utzi zen, 180 °C-an, 12 orduz. Horrela lortutako MnO₂/GAC-3 konposita hainbat aldiz garbitu zen ur desionizatuarekin, soberako MnO₂ molekulak eta nahi ez diren azpiproduktuak kendu arte. Gero, estufa batean lehortu zen, 80 °C-an, 12 orduz. MnO₂/GAC-1 eta MnO₂/GAC-2 material katalitikoak, hurrenez hurren, 1,94 g eta 18,41 g KMnO₄-arekin sortu ziren, KMnO₄ eta HCl-aren arteko erlazio estekiometrikoak errespetatuz, 40. ekuazioaren arabera. Nanopartikulen (NP) sintesiari dagokionez, MnO₂/GAC-3 konposita lortzeko erabili zen prozedura bera jarraitu zen, ikatz aktibatuzko euskarria gehitu gabe.

2.3. Materialen karakterizazioa

Material katalitikoak (konpositeak) hainbat teknika analitiko instrumentalen bidez karakterizatu ziren, haien propietate fisikoak eta kimikoak aztertzeko.

Lagin bakoitzeko tamaina txikieneko partikulen morfologia eta mikroegitura aztertzeko, bereizmen handiko transmisiozko mikroskopia elektronikoa (HRTEM, *high-resolution transmission electron microscopy*) erabili zen, Philips CM200 modelokoa (Philips, Eindhoven, Herbehereak). Elektro-iturri gisa LaB₆ hari bat erabili zen, eta 200 kV-eko azelerazio-tentsioa. Mikroskopiaari akoplatuta, energia sakabanatzen zuen X izpiko espektroskopia bat zegoen, EDAX Genesis 4000 (AMETEK GmbH, Weiterstadt, Alemania). Espektroskopiaok Si(Li) motako detektagailu bat zuen, leiho superultramehe bat zuena, GAC garbien nahiz konpositedunen osaera kimikoa aztertzeko. Espektroak eta irudiak EDAM IV (AMETEK GmbH, Weiterstadt, Alemania) softwarearen bidez lortu ziren. Laginak etanol-ur nahaste ekimolarrean sakabanatu ziren ultrasoinuekin. Konpositetako partikularik txikienen eta oxido metalikoko nanopartikulen gainazaleko morfologia hobeto ikusteko, indar atomikoko mikroskopia (AFM, *atomic force microscope*) erabili zen. Mikroskopia Nanoscope V Bruker MULTIMODE 8 modeloa zen (Azbil Telstar Technologies, Terrassa, Espainia). Horrez gain, laginen irudiak hartu ziren ekorketazko mikroskopia elektronikoa bat (SEM, *scanning electron microscope*) erabilita; hain zuzen hau: JEOL JSM-7000F (JEOL B.V., Nieuw-Vennep, Herbehereak).

Konpositen ezaugarri granulometrikoak aztertzeko, Malvern Panalytical Mastersizer 3000 bat erabili zen (Malvern Panalytical, Malvern, Britainia Handia). Beste propietate fisiko batzuk (poroaren tamaina edo azalera espezifikoak, adibidez) purutasun handiko nitrogenoaren (N₂) irakite-tenperaturako (-196 °C) adsortzio-desortzioa analizatuz zehaztu ziren, eta, horretarako, Micromeritics ASAP 2010 gas-adsortzioko analizatzaile automatikoa erabili zen (Micromeritics France SA, Verneuil Halatte, Frantzia). Adsortzio-esperimentuak egin aurretik, lagina desgasifikatu egin zen, 383 K-n, 3 orduz. Katalizatzaile berrien poro-tamainaren banaketa BJH (Barret-Joyner-Halenda) metodoaren bidez zehaztu zen [3].

Fase kristalinoa eta kristalaren tamaina X izpien difrakzio-teknikaren bidez (XRD, *X-Ray Diffraction*) zehaztu zen Philips PW1710 difraktometroa erabilita (Philips, Eindhoven, Herbehereak). Laginak eho egin ziren, eta CuK α erradiazioa aplikatu zitzaion, ekorketa jarraitua eginez 5°-tik 70°-ra. 2 θ angeluaren ekorketa-abiadura 0,026° s⁻¹ izan zen. Datuen tratamendua Winplotr® (Institut des Sciences Chimiques de Rennes, Rennes, Frantzia) softwarearen bidez egin zen. Katalizatzailearen faseak identifikatzeko, haien ezaugarri ziren erpinak Joint Committee on Powder Diffraction Standards (JCPDS) datu-basearekin alderatu ziren.

Jalkitako oxido metalikoaren edukia X izpien fluoreszentsiazko espektroskopia bidez neurtu zen (XRF, *X-Ray Fluorescence*). Birrindutako lagin bakoitzetik abiatuta, borodun beirazko perla bat prestatu zen indukziozko mikrolabe batean egindako fusioaren bidez. Spectromelt A12 (Merck KGaA, Darmstadt, Alemania) urgarria eta lagina nahastu ziren 20:1 proportzioan. Agente oxidatzaile bat gehitu zitzaion, ikatzaren zati organiko guztia kentzeko (prozesuaren oxidazio-faseetan) eta oxido inorganikoak finkatzeko. Perlen analisi kimikoa hutsezko atmosferan egin zen, uhin-luzeraren barreiradura bidezko X izpien fluoreszentsiazko espektrometro sekuentzial bat (WDXRF, *wavelength dispersive X-ray fluorescence*) erabilita (Panalytical, AXIOS modeloa). Fluorimetroak Rh hodi bat

eta hiru detektagailu zituen (gas-fluxua, izarnadura eta Xe zigilatzea) (Malvern Panalytical, Malvern, Britainia Handia).

GACan jalkitako fase aktibo metalikoaren (MnO_2) dispersioa H_2 -aren kimisortzioaren bidez zehaztu zen, Micromeritics ASAP 2020 Plus analizatzailea erabilia (Micromeritics France S.A., Verneuil Halatte, Frantzia). Erredukzioa egiteko, 0,35 g katalizatzaile 300°C -an desgasifikatu zen 60 minutuz, eta, ondoren, erreduzitu egin zen 50 mL min^{-1} -ko abiadurako H_2/Ar gas-korrante batekin (% 5), 350°C -an, 2 orduz. Adsortzioaren isoterma H_2 -arekin egin zen 35°C -an. Kimisortzioa jasan duen H_2 kantitatea kalkulatzeko, adsortzio-isoterma errepikatu zen lagina 60 minutuz berriro gasifikatuta, bi isoterma arteko ezberdintasuna zehazteko.

Ikatz aktibatu garbien eta konpositeen gainazaleko ezaugarri kimikoak identifikatzeko, Fourierren transformatuaren espektroskopia infragorria (FTIR, *Fourier-transform infrared spectroscopy*) erabili zen. Agatazko almaiz batean eho ziren laginak. Ondoren, birrindutako lagina KBr anhidroarekin nahastu zen, GACaren %0,5 m/m nahastea lortzeko. Nahastutako laginaren disko prentsatu jarri zen JASCO 4200 (JASCO Corporation, Tokyo, Japonia) espektrometroaren disko-euskarrian. Gailuak L-alanina deuteratuz dopatutako triglizenozko detektagailu bat zuen (DLATGS). Espektroak transmitantzia moduan lortu ziren, $4.000\text{--}400\text{ cm}^{-1}$ -ko tartean; batez beste, 64 eskaneo egin ziren, eta 4 cm^{-1} -ko bereizmena lortu zen Spectra Manager V 2.14.02 (JASCO Corporation, Tokyo, Japonia) softwarea erabilia. KBr purudun disko prentsatu bat erabili zen zuri gisa, neurketa bakoitza egiteko.

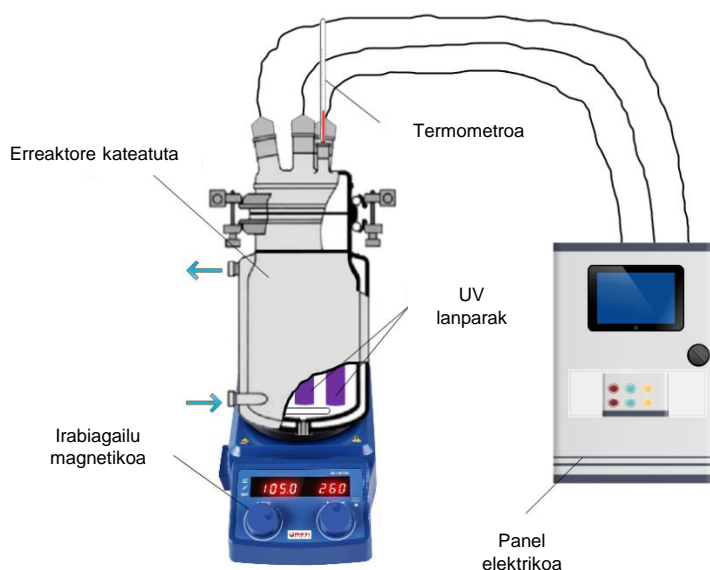
GACaren euskarrian jalkitako MnO_2 -aren egoera kimikoa zein zen ikusteko, X izpien espektroskopia fotoelektronikoa erabili zen (XPS, *X-ray photoelectron spectroscopy*). Leybold-Heraeus LHS-10 (Leybold GmbH, Munich, Germany) espektrometro ez-monokromatikoa erabili zen, X izpien iturri batekin, Al/Mg-arekin, anodo bikoitzarekin eta elektroien energia-analizatzaile hemisferikoarekin (HSA). XPS neurketak 150 W-eko X izpien iturriarekin egin ziren, erreferentzia gisa C_{1s} ($284,8\text{ eV}$) erpina hartuta, $0,2\text{ eV}$ -eko ziurgabetasunarekin. Huts handiarekin bateragarria den bi aldetako zinta itsasgarrian prestatu ziren laginak. XPSren emaitzak doitzeko XPSPEAK41 programa erabili zen (Leybold GmbH, Munich, Alemania). Laginak bi aldiz neurtu ziren sistemaren kontaminazioaren eraginez sortutako artefaktuak saihesteko. Espektroaren erpinaren dekonboluzioa egin zen, lineala ez den Shirley oinarri-lerroa erabilia (hondoa kentzeko) eta uhin Gaussiarren eta Lorentziarren konbinazio bat erabilia. Zero karga-puntua (PZC, *point of zero charge*) zehazteko, Ferreira et al. taldeak deskribatutako metodoa erabili zen [3]. NaCl disoluzio bati $0,100\text{ g}$ konposite gehitu zitzaion, eta pH-a neurtu zen CRISONen GLP 22 pH-metroa erabilia (Hach Lange Spain, L'Hospitalet de Llobregat, Espainia).

Material berrien propietate optikoak karakterizatzeko (*bandgap* jauzia), UV-Ikus ($200\text{--}2.200\text{ nm}$) absortzio-espektroak erabili ziren giro-tenperaturan, UV-vis-NIR Cary 5000 Agilent espektrometroa erabilia (Agilent, CA, AEB).

2.4. Metodologia esperimentalak

2.4.1. UV/H₂O₂ sistema esperimentalak

Esperimentuak 2 L-ko fotorreaktore batean egin ziren. 100 mm baino gutxiagoko barne-diametroa eta 270 mm-ko altuera zuen fotorreaktoreak (4. irudia). Temperatura 25 °C-an mantendu zen, atorraren bidez ura birzirkularazten zuen sistema termostatikoko bati esker. Argi ultramorearen sistema presio baxuko (254 nm) merkuriozko hiru UV-C lanparak osatuta zegoen, eta 8 W-eko potentzia nominala kontsumitzen zuen (PHILIPS TUV 8W G8T5, PHILIPS, Madril, Espainia). Lanparak errektorearen erdigunean zeuden, bata bestearekiko distantziakide. Lanpara bakoitza kuartzozko hodi baten barruan jarri zen. Neurketa aktinometrikoen bidez, ikusi zen fluxu fotoniko erasotzailea (I_0) $3,17 \times 10^{-5}$ Einstein s⁻¹ zela. Erradiazioaren ibilbide eraginkorra (L) 5,85 cm izan zen.



4. irudia Entsegu fotolitikoak egiteko muntaia esperimentalak [4].

Esperimentu bakoitzean, 4-klorofenola uretan disolbatu zen (1,7 L), 200 mg L⁻¹-ko kontzentrazioa duen disoluzioa ekoizteko. Disoluzioa errektorean jarri zen, eta nahastea irabiatu egin zen irabiagailu magnetiko batez, nahaste erreakzionatzaile behar bezain homogeneoa lortu arte. Ondoren, bainu termostatikoa piztu zen, disoluzioak 25±1 °C-ko temperatura lor zezan. H₂O₂-aren eta 4-klorofenolaren hasierako proportzioa—UV/H₂O₂ prozesuaren proportzio molarra (R)— 2 eta 400 artekoa izan zen. Hasierako pH-a esperimentuaren arabera doitu zen. Disoluzioa 5 minutuz behar bezala homogeneizatu ondoren jaso zen kontrol-lagina. Ondoren, UV-C lanparak piztu, eta laginak jaso ziren denbora-tarte jakinetan. Esperimentu guztiak hiru aldiz egin ziren. Desbideratze estandarra % 5etik beherakoa izan zen.

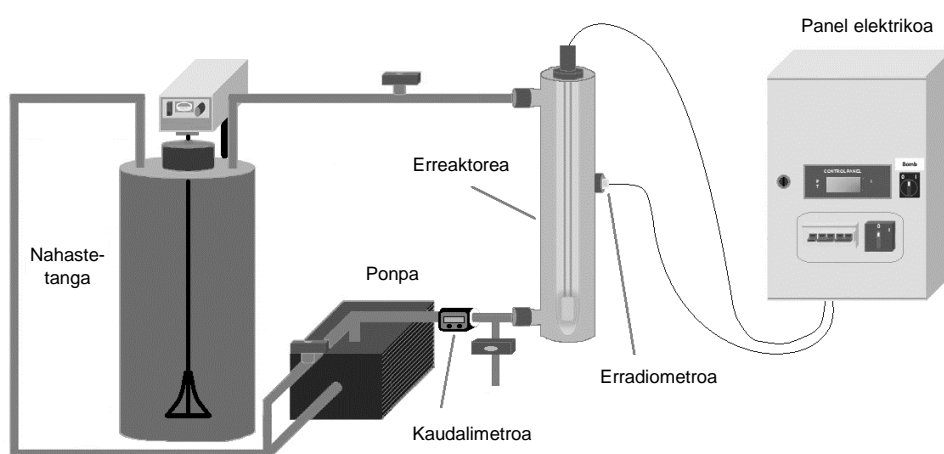
2.4.2. Fotofenton sistema esperimentalak

Karbamazepinaren 50,0 mg L⁻¹ ur-disoluzioaren laginak hartu, eta 1,0 L-ko errektore fotokatalitiko batean aztertu ziren. Erreaktoreak presio ertaineko merkuriozko UV-150W lanpara bat zuen (Heraeus, % 95eko transmisioa 300 eta 570 nm artean). Esperimentuen hasieran, ioi ferroso forman gehitu zen burdin katalizatzailea ((Fe), mg L⁻¹), tarte honekin: (Fe)₀ = 5,0-40,0 mg L⁻¹. Esperimentu multzo bakoitzean, 0-15,0 mM bitarteko oxidatzaile-dosia (H₂O₂) erabili zen. Esperimentu guztiak 40 °C-an

egin ziren funtzionamenduan egotean litzuketen kondizioak simulatzeko, erreakzionatzen zuen nahasteak lanpara ultramoreak igorritako beroa xurgatzen baitzuen. Hasierako pH-balio ezberdinekin egin ziren esperimentuak (2,0 eta 5,0 arteko pH-an), eta, hala, karbamazepina zuten ur-disoluzioak oxidatzean parametro horrek kolorean eta uhertasunean duen eragina ebaluatu.

2.4.3. Katalizatzaileak atxikita eta esekiduran dituen sistema fotokatalitiko hibridoa

Anilina eta bentzotiazola deuseztatzeko saiakera AOP 1 unitate esperimentalean egin zen (h₂O₂.TITANIUM®-ena). Sistema esperimental horrek elementu hauek zituen: hodi-formako erreaktore bat, merkurio-lanpara bat eta dagokion elikatze-iturria, 16,0 L-ko nahaste-tanga bat eta ponpa zentrifugoa (ikus 5. irudia).



5. irudia Anilinarekin eta bentzotiazolarekin proba fotolitikoak egiteko erabili den sistema esperimentalaren eskema [5].

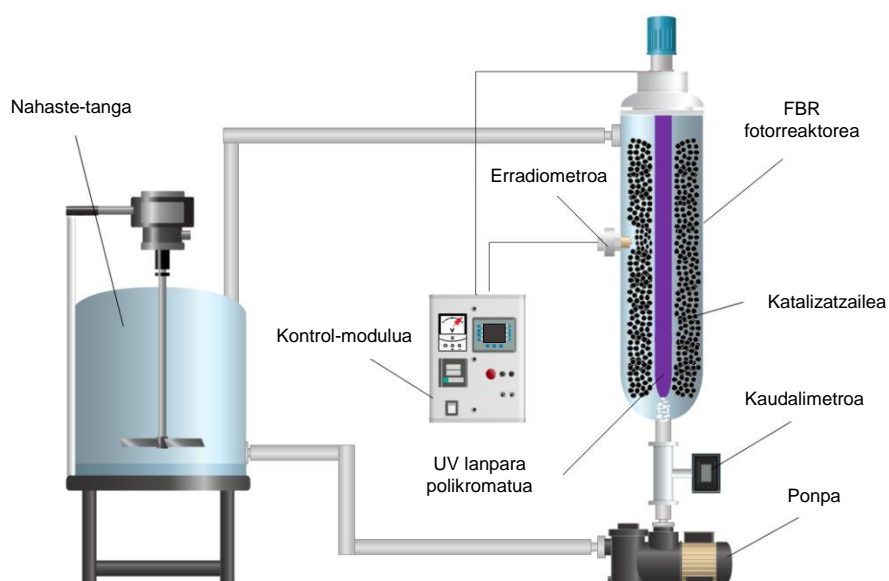
Erreaktorea titanio sinterizatuzko monobloke bat zen; 2,15 L-ko bolumena, 473 mm-ko luzera, 76 mm-ko diametroa eta 5 mm-ko lodiera zituen. Erreaktorearen estalduran jalkita 2,3 mg TiO₂ cm⁻² zituen. Fotorreaktorearen kokapenari zegokionez, bertikalean jarrita zegoen. Efluentearen sarrera-zuloa beheko aldean zuen; goiko aldean, bi zulo, eta alboan bat. Alboko zulotik, tenperatura infragorrien bidez neurtzen zuen gailu konpaktu bat zuen zunda sartu zitzaion, erradiometroarekin batera (PLS Systems AB, Sloga Ingenieros S.L., Puertollano, Espainia). Beste bi zuloak tratatu beharreko ura zeraman hodia konektatzeko erabili ziren. Erreaktoreak presio baxu eta ertaineko merkuriozko UVC lanpara bat zuen, 26 W-ekoa (GPH436T5L/4-Eubizz Water, Eubizz Water, Høyanger, Norvegia); lanparak 254 nm-an zuen gehieneko emisio-banda, eta kuartzozko karkasa baten barruan zegoen. Instalazioak kaudalimetro bat zuen erreaktorearen hasieran (GPI Electronic Digital Meter, NJ, AEB), eta ponpa zentrifugo bat (Pool Pump-72512, The Pool Shop, Tauranga, Zeelanda Berria) 0,5 m³ h⁻¹-ko emaria zuen efluentea erreaktorearen homogeneousazio-tangatik bultzatzeko.

25,0 °C-ko tenperatura konstantean egin ziren esperimentuak, anilina edo bentzotiazola edo bien nahastea zuten disoluzio sintetikoaren 16,0 L tratatzeko. Hasierako kontzentrazioa 22,0 mg L⁻¹ zen, pH konstanteari eutsi zitzaion eta Aeroxide® P25 katalizatzailearen 20,0-120,0 mg L⁻¹ bitarteko kontzentrazioa gehitu zitzaion. Disoluzioa nahaste-tangara eraman zen lanpara itzalita zegoela, eta ilunetan, adsortzio-oreka

lortzeko. Disoluzio sintetikoaren pH-a NaOH edo HCl-arekin doitu zen esperimentuaren arabera, eta konstante mantendu zen esperimentuak iraun zuen denboran. Ponpa eta irabiagailua 1750 b/m-ko abiadura jarri ziren abian. Ordubete igaro ondoren, adsortzio-oreka lortu zen. Ondoren, argi ultramorea piztu zen. Nahaste errektiboa 22 orduz irradiatu zen. Tarteka laginak hartu ziren, erreakzio fotokatalitikoaren bilakaeraren jarraipena egiteko.

2.4.4. Sistema FBR fotokatalitiko

FBR fotorreaktore batean egin zen anilina eta bentzotiazola deuseztatzeko esperimentua. Erreaktorea eskala pilotuko AOP 1 modelo zen, h₂O.TITANIUM®-ena (US20030059549A1 patentea) [6]. Erreaktorea aldatu egin zen gero, ohandte fluidizatuan erabiltzeko (ikusi 6. irudia).



6. irudia FBR erreaktorearen eskala pilotuko eskema. Hondakin-ur industrialetatik anilina eta bentzotiazola deuseztatzeko esperimentu fotokatalitiko eta adsortzio-esperimentuetan erabilakoa [7].

Osagai hauek zituen instalazio pilotuak: 2,15 L-ko edukiera eta 47,3 cm-ko luzera zuen altzairu herdoilgaitzezko erreaktore bat, 25 W-eko UVA lanpara polikromatikoa zuena (BL368/4-Eubizz Water, Eubizz Water, Høyanger, Norvegia). Lanpara kuartzozko hodi batek babesten zuen ($\varnothing_{barne} = 3,7$ cm), eta ardatzarekiko paralelo kokatuta zegoen altzairu herdoilgaitzezko fotorreaktore zilindriko batean ($\varnothing_{barne} = 7,6$ cm). Ikerketa honetan, modu ez-jarraituan jardun zen, 10 L-ko bolumen osoarekin. Ponpa zentrifugo batek (Pool Pump-72512, The Pool Shop, Tauranga, Zeelanda Berria) 0,75 m³ h⁻¹-ko birzirkulazio-emaria hornitu zuen. Ponpaketa-emaria neurtzeko, instalazioak zekarren emari-neurgailua erabili zen (GPI Electronic Digital Meter, NJ, AEB).

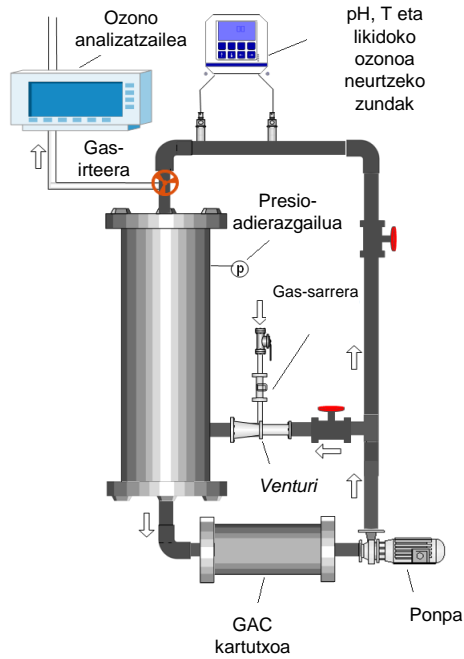
Esperimentu fotokatalitikoak 26,0 °C-ko tenperatura konstantean egin ziren, eta esperimentuak iraun zuen bitartean birzirkulazio-emari eta pH konstanteak mantendu ziren. Tratatu beharreko disoluzioa irabiagailu mekaniko bat zuen nahaste-tanga batean prestatu zen; guztiz homogeneizatu arte irabiatu zen (10 minutuz). Hasieran, lagin bat hartu zen, anilina- eta bentzotiazol-kontzentrazioak egiaztatzeko. Ondoren, ohandte fluidizatuko fotorreaktorean katalizatzailearen dosi egokia gehitu zen, eta

birzirkulazio-sistemara konektatu zen, adsortzio-oreka lortu arte (0,12 h). Segidan, UV-A lanpara piztu zen, eta hasiera eman zitzaion esperimenterari. Denbora-tarte erregularretan hartutako laginetan, anilina eta bentzotiazolaren degradazioa aztertu zen, baita beste parametro fisiko-kimiko orokor batzuk neurtu ere. Esperimentu guztiak hirutan egin ziren %5,3 baino errore txikiagoarekin. Halaber, hartutako lagin guztiak 0,45 µm-ko MF-Millipore (Merck KGaA, Darmstadt, Alemania) iragazki batekin iragazi ziren aztertu aurretik.

2.4.5. Ozonizazio erdijarraituko sistema eskala pilotuan

Ad/Ox bidez fenola deuseztatzeko prozesua gas-likido kontaktore batean egin zen, ikatz aktibatu hautsa eta ikatz aktibatu pikortsua (Kemisorb[®] 530) erabiliz. Ozonizazio-sistema esperimentalak 30,41 L-ko zutabe zilindriko bat zuen, eta han ezarri zen tratatu beharreko disoluzioa. Birzirkulazio-korrontean instalatutako *venturi* baten bidez sartu zen ozonoa erreaktorean, sistemaren homogeneizazio perfektua ziurtatzeko. Beheranzko likidoaren eta goranzko gasaren arteko kontaktua hobetzeko, lainoztagailu bat zegoen zutabearen goiko aldean, likidoa atomizatzeke (ikus 7. irudia). Disoluzioaren zati bat birzirkulatu egin zen, sistema hain biziki irabiatuta sor zitekeen aparra kentzeko. Sistema behar bezala nahasten zela bermatzeko bezain beste irabiatu zuen birzirkulazio-sistemak. 7. irudian ikus daitekeenez, erreakzio-likidoak interakzioa zuen kartutxo batean paketatutako GACaren karga jakin batekin.

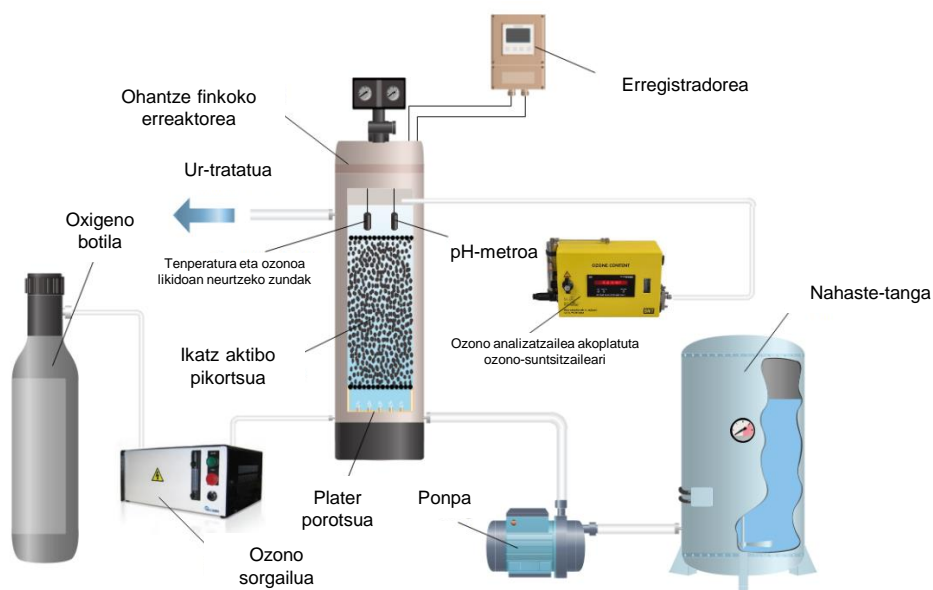
Esperimentuak 20,0 °C-ko tenperatura konstantean egin ziren, fenol-disoluzioen 10,0 L inguruko kargak erabiliz. Disoluzioen hasierako kontzentrazioa 1.000 mg L⁻¹ izaten zen. Esperimentu guztiak gas-emari konstantearekin egin ziren ($Q_G=4,0$ L min⁻¹). Gainera, gas-faseko ozonoaren kontzentrazio konstantea erabili zen sarreran ($C_{O_3,G}=19,0$ mg L⁻¹), 6,5eko pH-a eta ikatz aktibatuaren 250,0 edo 500,0 g-ko masa. Ozonoa ekoizteko, oxigeno oso purua eta TRIOGEN LAB2B sorgailua (BIO UV, Lunel, Frantzia) erabili ziren. Bainu hozgarri baten bidez kontrolatu zen tenperatura. Gas-faseko ozono-kontzentrazioa BMT 964C ozono-analizatzaile batekin (BMT MESSTECHNIK GMBH, Stahnsdorf, Alemania) kontrolatu zen. Fase likidoko ozonoaren kontzentrazioa eta tenperatura neurtzeko, Rosemount Analytical zunda bat erabili zen (499AOZ-54 modelo; Emerson, Alcobendas, Espainia), birzirkulatzen ari zen likidoaren goiko hodian txertatua. pH-a kontrolatzeko, berriz, Rosemount Analytical-en 399-09-62 zunda (Emerson, Alcobendas, Espainia) erabili zen, ozono-zundarekin batera Rosemount Analytical Solu Comp II erregistratzaile batean txertatua (Emerson, Alcobendas, Espainia). Erreaktoretik ateratzen zen gas-faseko ozonoa Zonosistem gailu termokatalitiko ozono-suntsitzaile batez deuseztatu zen (Ingeniería del Ozono S.L.U, Cádiz, Espainia).



7. irudia Fenolaren ozonizazio-esperimentuetarako erabilitako Ad/Ox ekipamendu esperimentalak [8].

2.4.6. Ozonizazio jarraituko sistema ohandze finkoan

Ad/Ox jarraituaren bidez fenola deuseztatzeko, GACez betetako kloruro polibinilozko (PVC) zutabe bat erabili zen. Zutabearen kanpoko diametroa 25 mm zen, barne-diametroa 21,2 mm, eta luzera 40 cm (ikus 8. irudia). Ozonizazio arruntaren eta Ad/Ox prozesuaren esperimentuak ozono-emari jarraituarekin egin ziren ($Q_G = 0,05 \text{ L h}^{-1}$), 20°C -an, 60,5 g-ko GACdun ohandzean eta disoluzioaren $Q_L = 12 \text{ mL min}^{-1}$ ponpatze-emariarekin. Hasierako hainbat pH-balio erabili ziren (3,0 eta 11,0 bitartean), fenolaren hainbat kontzentrazio ($250, 500, 750$ eta 1.000 mg L^{-1}) eta 1,0 eta 2,5 atm-ko bitarteko presioa (esperimentuaren arabera).



8. irudia Ad/Ox jarraituan ozonizazio katalitikoa egiteko erabilitako gailu esperimentalak [9].

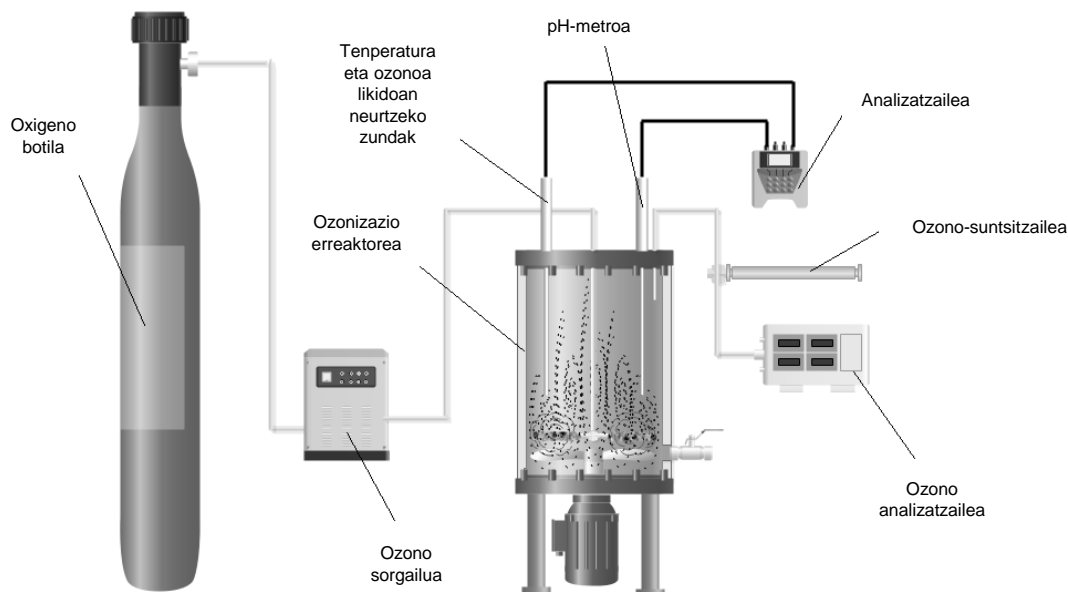
Ad/Ox edo ozonizazio arrunteko esperimentu bat egiteko, ohandzearen zutabeko beheko aldean jarritako plater porotsu batean zehar sartu zen *in situ* sortutako ozonoa —oxigeno ultrapurutik abiatuta eta TRIOGEN LAB2B (BIO UV, Lunel, Frantzia) ozono-sorgailua erabilia—. Ondoren, fenola zuen disoluzioaren fluxu likidoa hartu, eta PRECIFLOW (LAMBDA Laboratory Instruments, Baar, Suitza) ponpa peristaltiko baten bidez sartu zen, zutabearen alboko beheko sarreratik. Gas eta likidozko fluxuek, zutabetik gora egiterakoan, ikatz aktibatu pikortsuzko ohandzea zeharkatu zuten. Ondoren, GAC paketatuzko ohandzearen ondoren kokatutako irteera batean jaso zen fluxu likidoa.

Gas-fasean zegoen ozono-kontzentrazioa neurtzeko, zutabearen kokatutako BMT 964C ozono-analizatzailea erabili zen (BMT MESSTECHNIK GMBH, Stahnsdorf, Alemania). Disolbatutako ozonoaren kantitatea eta tenperatura neurtzeko, Rosemount 499AOZ-54 (Emerson, Alcobendas, Espainia) sentsore disolbatua erabili zen. pH-a neurtzeko, Rosemount Analytical Solu Comp II (Emerson, Alcobendas, Espainia) erregistratzailean txertatutako Rosemount Analytical 399 sentsorea erabili zen. Ozono-gas erresiduala suntsitzeko, Zonosistem (Ingeniería del Ozono S.L.U, Cádiz, Espainia) gailu termokatalitiko ozono-suntsitzailea erabili zen.

2.4.7. *Slurry* motako ozonizazio katalitiko erdijarraituko sistema

Disoluzio sintetikoetako anilina deuseztatzeko, hiru TiO₂/GAC konposite erabili ziren, hauspeatze-metodoa, murgiltze bidezko inpregnazioa eta metodo hidrottermala erabiliz sortuak. Konposite bakoitza bi ikatz aktibatu motarekin prestatu zen (Norit® GAC 1240 Plus eta Norit® ROX 0,8). Esperimentuetan, 7,5eko pH-a erabili zen hasieran, 11,3 mg L⁻¹-ko ozono-dosia eta 2,5 g O₃ h⁻¹-ko gas-fluxua. Operazio-aldagaien efektua aztertu zen hainbat ozonizazio pH-tan (3,0; 5,0; 7,0 eta 9,0) eta hainbat ozono-dositari (3,7; 5,4; 11,3 eta 20,1 mg L⁻¹), eta bi parametroak konstante mantendu ziren esperimentu guztian zehar. Atorraz estalitako 2 L-ko errektore batean egin ziren ozonizazio-esperimentuak; irabiagailua eta ozono-lainoztagailuak zituen errektoreak (ikus 9. irudia).

Esperimentu bakoitzean, 20,0 mg/L-ko kontzentrazioa zuen anilinazko disoluzioaren 1,5 L-rekin bete zen errektorea, esperimentu bakoitzari zegokion pH-an, eta 5,0 g katalizatzaile erabilia. Gas-emari jarraituarekin egin ziren esperimentuak, sarrerako ozono-kontzentrazio konstantearekin, 18 °C-an eta 1 atm-ko presioan. Etengabe irabiatu zen 60 b/min abiaduran, nahaste homogenea ziurtatzeko. Oxigeno oso purutik ekoiztu zen ozonoa TRIOGEN LAB2B sorgailuan (BIO UV, Lunel, Frantzia). Bainu hozgarri baten bidez kontrolatu zen tenperatura. Gas-faseko ozono-kontzentrazioa BMT 964C ozono-analizatzaile (BMT MESSTECHNIK GMBH, Stahnsdorf, Alemania) batekin kontrolatu zen. Fase likidokoa disolbatutako ozonoaren kontzentrazioa eta tenperatura neurtzeko, Rosemount Analytical zunda bat erabili zen (499AOZ-54 modelo; Emerson, Alcobendas, Espainia). pH-a kontrolatzeko, Rosemount Analytical-en 399-09-62 zunda (Emerson, Alcobendas, Espainia) erabili zen, ozono-zundarekin batera Rosemount Analytical Solu Comp II erregistratzaile batean txertatua (Emerson, Alcobendas, Espainia). Errektoretik ateratzen zen gas-faseko ozonoa Zonosistem (Ingeniería del Ozono S.L.U, Cádiz, Espainia) gailu termokatalitiko ozono-suntsitzaile batez deuseztatu zen.



9. irudia Anilinaren ozonizazio katalitikoko esperimentuetan erabiliko ekipamendua [3].

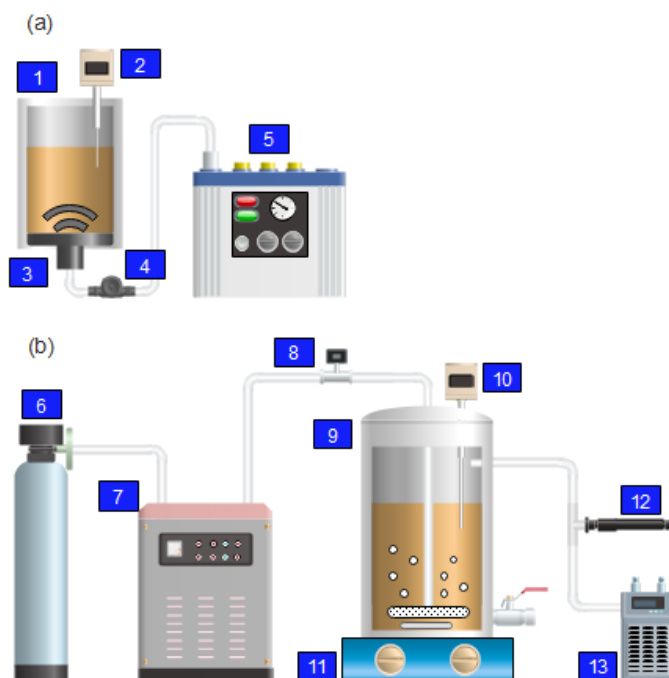
2.4.8. Ultrasoinuen bidez aurretratatzeke sistema

Prozedura honen arabera prestatu zen azido humikoaren lagina. Hasteko, 100 mg azido humiko eta 2 L ur desionizatu nahastu ziren (50 mg L^{-1}), eta, 0,25 M NaOH gehituz, pH-a 11ra igota disolbatu ziren. Disoluzioa 30 minutuz irabiatu zen 400 b/min-ra. Sonikazio-esperimentuei ekin aurretik, pH-a azidotu egin zen 7raino, 0,1 M H_2SO_4 gehituta.

Ultrasoinuen bidezko aurretratamendu-esperimentuak (ikusi 10. irudia) atorradun beirazko ontzi zilindriko batean egin ziren; ontziak 15 cm-ko altuera eta 6,7 cm-ko barne-diametroa zuen. Ontziaren hondoan jarri zen ultrasoinuen transduktorea (Honda Electronics Co. LTD, Disvent Ingenieros S.A., Bartzelona, Espainia), eta AG1006 potentzia-anplifikagailu batekin elikatu zen (T&C Power Conversion, Rochester, NY, AEB). Hiru maiztasun (98 kHz, 300 kHz eta 1 MHz) erabili ziren lau potentzietarako (10, 20, 30 eta 40 W), eta laginaren bolumena ere aldatu zen, 150 mL-tik 400 mL-ra. Azido humikoaren laginei sonikazioa aplikatu zitzairen 10, 20 eta 30 minutuz. pH-a eta temperatura etengabe kontrolatu ziren (Crison-en GLP 22 modelo, Bartzelona, Espainia) sonikazio-esperimentuen aurretik eta ondoren.

Sonikatutako efluenta ozonoarekin tratatu zen ondoren, 2 L-ko beirazko errektore zilindriko batean. Bi ozono-difusore eta irabiagailu magnetiko bat jarri ziren errektorearen hondoan. Ozonoaren emaria konstante mantendu zen $4,76 \text{ L min}^{-1}$ -ko abiadura konstantean, eta 60 b/min-ko irabiatze-abiaduran. Oxigeno oso purutik ekoiztu zen ozonoa *in situ* TRIOGEN LAB2B sorgailuan (BIO UV, Lunel, Frantzia). Aurrez sonikatutako azido humikoaren 1 L disoluzio ozonizatu zen, 30 eta 120 minutuz, lau ozono-dosirekin: 5,4; 7,4; 11,3 eta $19,7 \text{ mg L}^{-1}$. Etengabe kontrolatu ziren disolbatutako ozonoa (Rosemount Analytical modelo 499AOZ-54 zunda; Emerson, Alcobendas, Espainia) eta gaseko ozonoa (BMT 964C ozono-analizatzailea; BMT MESSTECHNIK GMBH, Stahnsdorf, Alemania), baita disolbatutako oxigenoa (Rosemount Analytical Solu Comp II erregistragailua; Emerson, Alcobendas, Espainia), pH-a eta temperatura (Rosemount Analytical zunda, 399-09-62 modelo; Emerson, Alcobendas, Espainia) ere.

Hondar-ozonoa suntsitzeko, Zonosistem gailu termokatalitiko erabili zen (Ingeniería del Ozono S.L.U, Cádiz, Espainia). Esperimentu guztiak gutxienez bi aldiz egin ziren.



10. irudia Ultrasoinuen (a) eta ozonizazio arruntaren (b) esperimentuak egiteko ekipamenduaren eskema [10].

(a) Ultrasoinu gailua; (1) Sonikazio-ontzia, (2) Parametro ugaitarako zunda, (3) Plaka-transduktorea, (4) Deskarga, (5) Potentzia-anplifikagailua. (b) Ozonizazio-eraketa; (6) O₂-botila, (7) O₃ sorgailua, (8) Kaudalimetroa, (9) O₃-erreaktorea, (10) Parametro ugaitarako zunda, (11) Irabiagailu magnetikoa, (12) O₃-suntsitzailea, (13) O₃-analizatzailea.

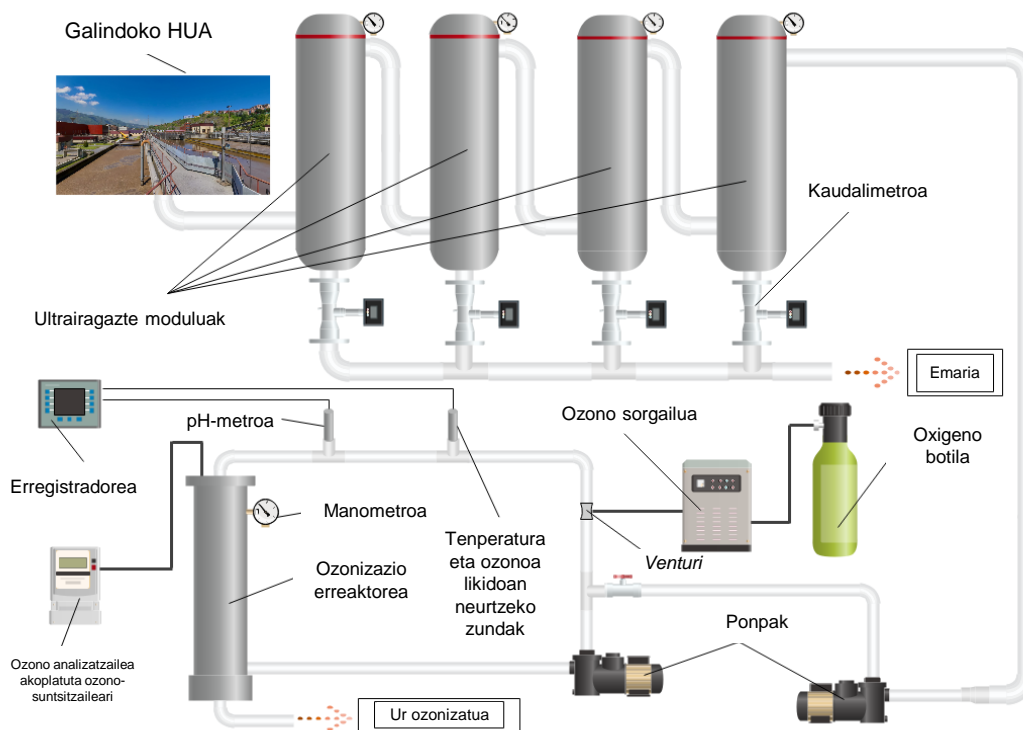
2.4.9. Ozonizazio-eraketa atxikitako ultrairagazte-sistema jarraitua eskala pilotuan

Ultrairagazte-sistema jarraitua erabiltzeko era bi modu edo egoeratan bereiztu zen: iragazte modua eta garbiketa modua. Iragazte moduan, barrura-kanpora konfiguraziodun *dead-end* iragazketa bat egin zen. Hala, ur guztia mintza zeharkatzera behartu zen barrutik kanpora, eta esekiduran zeuden solidoak eta solutuak (CECak, mikroorganismo patogenoak) zuntzen barneko gainazalean harrapatuta geratu ziren.

Tratamendu sekundariora konektatutako elikadura-adar baten bidez elikatu zen ultrairagazte-sistema jarraitua, 3,3 m³ h⁻¹ abiadurarekin, ekipamenduaren beheko zatian kokatutako ponpa zentrifugo baten bidez (ZMR02.30 S GF V BS8 B EN3, Argal Pumps, Brescia, Italia). Modulu bakoitzean lortutako iragazkina (41,5 L m⁻² h⁻¹ abiadurako fluxuarekin) iragazitako produktuaren hodian bertan bildu zen. Etengabe neurtu zen parametro hori emari-neurgailuen bidez (FLS F3.80, aliaxis, Okondo-Araba, Espainia), mintza zikintzea kontrolatzeko eta tratatutako uraren ekoizpena konstante izateko (ikus 11. irudia). Iragazketa-operazio ziklo bakoitzak 47 minutu iraun zituen. Ziklo bakoitzaren amaieran, mintzean zeharreko presioa hasierako 0,6 bar izatetik 2,3 bar-ekoa izatera iristen zen.

Bigarren modua garbiketari dagokio. Modu honetan, garbiketa-sekuentzia bat egin zen —*flushing*, atzeragarbiketa eta *Chemical Enhanced Flushing* (CEF) eta *Cleaning In Place* (CIP) garbiketa bat—. Sekuentziaren helburua da mintza jatorrizko egoerara

itzularaztea. Modu horri esker, zuntzen barnealdeko gainazalean jalkitako solidoak edo inkrustazioak eraginkortasunez kendu ziren. Garbiketa-sekuentzia moduluz modulu edo bikoteka egin zen, iragazitako emaria konstante izateko. Prozesuak 9 minutu iraun zituen, eta amaieran mintzean zeharreko presioa 0,6 bar-ekoa zen.



11. irudia Errefus-korrontea tratatzeko ultrairagazpen-prozesuaren eskema, ozonizazio-sistemari atxikia [11].

Errefus-korronteari ozonizazio arrunta aplikatzeko esperimientuetarako, erregimen ez-jarraitua erabili zen. Horretarako, ozonizazio-kontaktorea errefus-korrontetik zetorren uraren 30 L-rekin bete zen. Ondoren, ozonoa sartu zen kontaktorean birzirkulazio-begiztan kokatutako *venturi* baten bidez. Haren ondoren irabiagailu estatiko bat zegoen. Gainera, kontaktoreak likido-atomizagailu bat zuen goiko aldean, gas-likido kontaktua hobetzeko, 11. irudian ikus daitekeenez. Esperimentuak egiteko, 15,0°C-ko tenperatuta, 9,0ko pH-a, 1,5 bar-eko presioa, ozono-emari jarraitua (4 L min^{-1}) eta $6,4 \text{ mg L}^{-1}$ -ko ozono-dosia erabili ziren 180 minutuz. Manometro baten bidez kontrolatu zen sistemaren presioa (111.10, Wika Instruments, Bartzelona, Espainia), eta gas-faseko ozono-kontzentrazioa analizatzaile bidez kontrolatu zen (BMT 964C, BMT MESSTECHNIK GMBH, Stahnsdorf, Alemania). Likidoan disolbatutako ozonoaren kantitatea eta tenperatura neurtzeko, zunda anperometrikoa erabili zen (Rosemount 499AOZ-54, Emerson, Alcobendas, Espainia). pH-a neurtzeko, datu-erregistragailu bati (Rosemount Solu Comp II, Emerson, Alcobendas, Espainia) konektatutako pH-metro bat erabili zen (Rosemount 399-09-62, Emerson, Alcobendas, Espainia). Hondar-ozonoa suntsitzeko, ozono-suntsitzaile termokatalitiko bat erabili zen (KVM 20-2, ZonoSistem, El Puerto de Santa María, Espainia).

2.5. Erreferentziak

1. Al Mgheer, T.; H Abdulrazzak, F. Oxidation of Multi-Walled Carbon Nanotubes in Acidic and Basic Piranha Mixture. *Front. Nanosci. Nanotech.* **2016**, *2*, doi:10.15761/FNN.1000127.
2. Feng, X.H.; Liu, F.; Tan, W.F.; Liu, X.W. Synthesis of Birnessite from the Oxidation of Mn^{2+} by O_2 in Alkali Medium: Effects of Synthesis Conditions. *Clays Clay Miner.* **2004**, *52*, 240–250, doi:10.1346/CCMN.2004.0520210.
3. Ferreiro, C.; Villota, N.; Lombraña, J.I.; Rivero, M.J. An Efficient Catalytic Process for the Treatment of Genotoxic Aniline Wastewater Using a New Granular Activated Carbon-Supported Titanium Dioxide Composite. *J. Clean. Prod.* **2019**, *228*, 1282–1295, doi:10.1016/j.jclepro.2019.04.198.
4. Ferreiro, C.; Sanz, J.; Villota, N.; de Luis, A.; Lombraña, J.I. Kinetic Modelling for Concentration and Toxicity Changes during the Oxidation of 4-Chlorophenol by UV/ H_2O_2 . *Sci. Rep.* **2021**, *11*, 15726, doi:10.1038/s41598-021-95083-7.
5. Ferreiro, C.; Villota, N.; Lombraña, J.I.; Rivero, M.J.; Zúñiga, V.; Rituerto, J.M. Analysis of a Hybrid Suspended-Supported Photocatalytic Reactor for the Treatment of Wastewater Containing Benzothiazole and Aniline. *Water* **2019**, *11*, 337, doi:10.3390/w11020337.
6. US Patent Application for TiO_2 Base coagulant and its application. Patent Application US20170137306 (Erregistratua 2017ko maiatzaren 18a).
7. Ferreiro, C.; Villota, N.; Lombraña, J.I.; Rivero, M.J.; Zúñiga, V.; Rituerto, J.M. Removal of Aniline and Benzothiazole Wastewaters Using an Efficient MnO_2 /GAC Catalyst in a Photocatalytic Fluidised Bed Reactor. *Materials* **2021**, *14*, 18, 5207, doi:10.3390/ma14185207.
8. Ferreiro, C.; Villota, N.; Luis, A. de; Lombrana, J.I. Analysis of the Effect of the Operational Variants in a Combined Adsorption-Ozonation Process with Granular Activated Carbon for the Treatment of Phenol Wastewater. *React. Chem. Eng.* **2020**, *5*, 760–778, doi:10.1039/C9RE00424F.
9. Ferreiro, C.; de Luis, A.; Villota, N.; Lomas, J.M.; Lombraña, J.I.; Camarero, L.M. Application of a Combined Adsorption–Ozonation Process for Phenolic Wastewater Treatment in a Continuous Fixed-Bed Reactor. *Catalysts* **2021**, *11*, 1014, doi:10.3390/catal11081014.
10. Alfonso-Muniozgueren, P.; Ferreiro, C.; Richard, E.; Bussemaker, M.; Ignacio Lombraña, J.; Lee, J. Analysis of Ultrasonic Pre-Treatment for the Ozonation of Humic Acids. *Ultrason. Sonochem.* **2020**, *71*, 105359, doi:10.1016/j.ultsonch.2020.105359.
11. Ferreiro, C.; Villota, N.; de Luis, A.; Lombraña, J.I.; Etxebarria, N.; Lomas, J.M. Water Reuse Study from Urban WWTPs via C-Ultrafiltration and Ozonation Technologies: Basis for Resilient Cities and Agriculture. *Agronomy* **2021**, *11*, 322, doi:10.3390/agronomy11020322.

3. Argitalpen zientifikoak



Tesi honetan, prozesu fotokimikoei eta ozonoan oinarritutako prozesu ez-fotokimikoei dagozkien 12 AOP laburtu dira, eta 5. taulan jasotako alderdietan sakondu da. **AOPen 12 kasu aztertu ziren (3. kapituluko atalak), eta haien eraginkortasuna eta jasangarritasuna handitzeko ekarpenak egin ziren** alderdi hauen bidez: AOP teknologiaren oinarrian sakontzea haren eredia sortzeko (3.1, 3.6, 3.7 eta 3.9 kasuak), prozesuaren aldagaiak aztertzea eta eragiketa-estrategia onuragarrienak hautatzea (3.2, 3.3 kasuak), erreakzio-ekipamenduan eraldaketak txertatzea (3.4 kasua) edo katalizatzaile berriak garatzea (3.5 eta 3.8 kasuak) eta tratamendu-sistema orokor konplexuagoetan integratzea (3.10, 3.11 eta 3.12 kasuak).

5. taula Aztertutako kasu bakoitzerako eman diren ekarpenen laburpena.

	Kasuak	AOPa	Ekarpena
Prozesu fotokimikoak	3.1	UV/H ₂ O ₂	- AOP teknologiaren oinarrian sakontzea haren eredia sortzeko, bigarren ordenako eredu zinetiko bat proposatuta
	3.2	Fotofentona	- Prozesuaren aldagaiak aztertzea eta aldekoenak diren eragiketa-estrategiak hautatzea
	3.3		
	3.4		- Lehendik badagoen fotorreaktore komertzial bat hobetzea
	3.5	Fotokatalisi heterogeneoa	- Ikatz aktibatu pikortsuan atxikitako MnO ₂ -a duen fotokatalizatzaile berritzailea sintetizatzea (MnO ₂ /GAC) - Ohantze fluidizatuan (FBR) jarduten duen erreakzio-sistema diseinatzea
Ozonizazioan oinarritutako prozesu ez-fotokimikoak	3.6	Ozonizazio katalitikoa	- Eredu zinetiko trifasikoa garatzea Ad/Ox prozesurako
	3.7		- Eragiketa-estrategiak hautatzea
	3.8		- Ikatz aktibatu pikortsuan atxikitako TiO ₂ -a duen katalizatzaile berritzailea garatzea (TiO ₂ /GAC)
	3.9		- Eredu zinetiko trifasikoa formulatzea Ad/Ox prozesurako
	3.10	US + ozonoa	- Ultrasoinuen (US) teknologia ozonizazioarekin konbinatuta erabiltzea
	3.11	Ultrairagazketa ozonizazio-prozesuetan	- Ozonizazioaren aurretik ultrairagazketa integratzea poluitzaile berriak deuseztatzeko
	3.12		

3.1. 1. argitalpena. Kinetic modelling for concentration and toxicity changes during the oxidation of 4-chlorophenol by UV/H₂O₂

3.1 kapitulua artikulu honi dagokio:

C. Ferreiro, J. Sanz, N. Villota, A. de Luis, J.I. Lombraña. Kinetic modelling for concentration and toxicity changes during the oxidation of 4-chlorophenol by UV/H₂O₂. *Scientific Reports*, 11, 1, 15726, 2021. DOI: 10.1038/s41598-021-95083-7.



OPEN

Kinetic modelling for concentration and toxicity changes during the oxidation of 4-chlorophenol by UV/H₂O₂

Cristian Ferreiro^{1✉}, Josu Sanz², Natalia Villota³, Ana de Luis⁴ & José Ignacio Lombraña¹

This work develops a kinetic model that allow to predict the water toxicity and the main degradation products concentration of aqueous solutions containing 4-chlorophenol oxidised by UV/H₂O₂. The kinetic model was developed grouping degradation products of similar toxicological nature: aromatics (hydroquinone, benzoquinone, 4-chlorocatechol and catechol), aliphatics (succinic, fumaric, maleic and malonic acids) and mineralised compounds (oxalic, acetic and formic acids). The degradation of each group versus time was described as a mathematical function of the rate constant of a second-order reaction involving the hydroxyl radical, the quantum yield of lump, the concentration of the hydroxyl radicals and the intensity of the emitted UV radiation. The photolytic and kinetic parameters characterising each lump were adjusted by experimental assays. The kinetic, mass balance and toxicity equations were solved using the Berkeley Madonna numerical calculation tool. Results showed that 4-chlorophenol would be completely removed during the first hour of the reaction, operating with oxidant molar ratios higher than $R = 200$ at pH 6.0 and UV = 24 W. Under these conditions, a decrease in the rate of total organic carbon (TOC) removal close to 50% from the initial value was observed. The solution colour, attributed to the presence of oxidation products as *p*-benzoquinone and hydroquinone, were oxidised to colourless species, that resulted in a decrease in the toxicity of the solutions (9.95 TU) and the aromaticity lost.

List of symbols

Agitation	Stirring power, rpm
C_0	Initial concentration of 4-chlorophenol, mol L ⁻¹
C_{exp}	Concentration of a compound or lump <i>i</i> measured experimentally, mol L ⁻¹
C_i	Concentration of each lump <i>i</i> , mol L ⁻¹
C_j	Concentration of a given compound present in solution, mol L ⁻¹
$C_{HO\cdot}$	Concentration of hydroxyl radicals, mol L ⁻¹
Colour ₀	Initial colouration was attributed to the 4-chlorophenol in solution, AU
C_{sim}	Concentration of a compound or lump <i>i</i> obtained from the model, mol L ⁻¹
C_{TOC}	Concentration of total organic carbon, mol L ⁻¹
EC_{50}	Half maximal effective concentration, mol L ⁻¹
EC_{50i}	Average half maximal effective concentration, mol L ⁻¹
$EC_{50i exp}$	Experimentally determined average half maximal effective concentration, mol L ⁻¹
F_i	Fraction of UV radiation absorbed by compounds of lump <i>i</i> , dimensionless
I_0	Intensity of the emitted UV radiation, Einstein min ⁻¹
IC_{50}	Half maximal inhibitory concentration, mol L ⁻¹

¹Department of Chemical Engineering, Faculty of Science and Technology, University of the Basque Country UPV/EHU, Barrio Sarriena S/N, 48940 Leioa, Spain. ²Department of Mathematics and Science Didactics, Faculty of Education, Philosophy and Anthropology of Donostia-San Sebastián, University of the Basque Country UPV/EHU, Barrio Sarriena S/N, 48940 Leioa, Spain. ³Department of Chemical and Environmental Engineering, Faculty of Engineering of Vitoria-Gasteiz, University of the Basque Country UPV/EHU, Nieves Cano, 12, 01006 Vitoria-Gasteiz, Spain. ⁴Department of Chemical and Environmental Engineering, Faculty of Engineering in Bilbao, University of the Basque Country UPV/EHU, Plaza Ingeniero Torres Quevedo, 1, 48013 Bilbao, Spain. ✉email: cristian.ferreiro@ehu.eus

k'_1, k'_2, k'_3, k'_4 and k'_5	Pseudo-first-order kinetic constant of each lump, s^{-1}
k_i	Zero-order kinetic constant (oxidation), $s^{-1} \text{ mol}^{-1} \text{ L}$
\bar{k}_i	Second order kinetic constant, $s^{-1} \text{ L mol}^{-1}$
L	Effective path length of the photoreactor, m
N	Number of experimental values
R	Peroxide/4-chlorophenol molar ratio, dimensionless
t	Time, s
T	Temperature, $^{\circ}\text{C}$
Toxicity	Toxicity, TU
V_{reac}	Volume of dissolution, L

Greeks

ε	Molar extinction coefficient, $\text{M}^{-1} \text{ m}^{-1}$
α	Fraction of all photolytically degraded 4-chlorophenol (group B ₁)
σ	Weighted standard deviation
Φ_i	Quantum yield for lump i, mol Einstein ⁻¹

Subscripts

0	Refers to a time or initial state
A	Refers to the lump formed by 4-chlorophenol
B ₁	Refers to the lump formed by hydroquinone, <i>p</i> -benzoquinone and other unknown that are more toxic than 4-chlorophenol
B ₂	Refers to the lump formed by 4-chlorocatechol, catechol, and other unknown compounds that are less toxic than 4-chlorophenol
C	Refers to the lump formed by formic acid, acetic acid, oxalic acid, and other compounds of similar nature
D	Refers to the lump formed by CO ₂ and H ₂ O
exp	Refers to an experimentally obtained parameter
i	Refers to a certain lump i
j	Refers to the different compounds present in the solution
sim	Refers to a parameter obtained from the kinetic model

Chlorophenols are catalogued as one of the priority pollutants (Clean Water Act and by European Directive 2013/39/EU) according to the United States Environmental Protection Agency (US EPA)^{1–3} because they are toxic and potentially carcinogenic compounds². They are considered one of the most important classes of water contaminants due to they are difficult to remove from the environment^{2–5} and they can appear in drinking water when hypochlorite reacts during water disinfection⁴. Thus, they are of great concern.

It has been selected 4-chlorophenol as the representative member of this family of harmful compounds. Levels of 4-chlorophenol have been reported as ranging from 150 $\mu\text{g L}^{-1}$ ⁶ to 100–200 mg L^{-1} ^{7,8} in contaminated environments.^{10,11}

Advanced oxidation processes (AOPs) could help in the effective removal of these recalcitrant compounds from wastewater^{9–11}. However, the cost-inefficiency of these methods limits the practical application of these technologies^{12,13}. Moreover, persistent byproducts produced during the oxidation process can be released into the environment^{14,15}. Thus, AOPs may be made suitable for industrial applications, if they are adequately integrated with the biological processes by combined treatments. Thus, the complete removal of water pollutants by AOPs could be combined by more environment friendly treatments leading easily biodegradable species. This propose considers that the biological oxidation process could be the last step into a combined oxidation process that results in the complete oxidation of organic load^{16,17}.

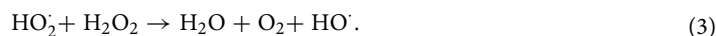
Thus, it is important to develop models that can predict the toxicities of treated solutions for developing integration strategies involving AOPs and biological processes. This tool can be used for the determination of the operating conditions necessary to reduce the toxicity of the system. In this way, it is possible to achieved a water toxicity level that allow the implantation of biological processes where occur the complete degradation of the remaining pollutant load, developing in this way, a cost-effective, integrated wastewater treatment method.

The photochemical degradation of chlorophenols is a well documented process (see Supplementary Table S1). Çatalkaya et al.¹⁸ reported that the UV/H₂O₂ process could effectively reduce the toxicity of the system. This process can also improve biodegradability, decrease the intensity of the colour, and assist in the removal of micropollutants. The use of UV/H₂O₂ is more advantageous than semiconductor photocatalysis due to economic and feasible to implement in an industrial installation. Moreover, the use of a catalyst can lead to some operation problems such as solids management, separation and contamination in the treated water. Other effects such as screening, caused by the presence of suspended solids in industrial wastewaters would lead to a reduction of the efficiency of UV light.

The photolytic decomposition via bond cleavage occurs via a radical mechanism. The hydroxyl radicals (in the presence of oxidants such as H₂O₂) take part in the process as follows^{19,20}:



The decomposition of H_2O_2 can be photoinduced by the Haber–Weiss radical mechanism. The propagation steps are as follows:



Finally, different termination reactions take place through radical recombination reactions:



At the same time, dissociation equilibria of the organic compound itself and of the various intermediates formed, such as hydroxyl, hydroperoxide radicals, etc., according to the following:



Like other phenolic compounds, chlorophenols could be degraded to toxic byproducts during the initial stages of the oxidation pathway^{3,21}, checking that the oxidation intermediates generated could be more toxic than the own parent pollutant (for example quinone like compounds). The formation of these byproducts could be attributed to direct photolysis or the use of low oxidant dosages^{22,23}. Then, the efficiency of the oxidant process is generally determined by recording the oxidant dosage per pollutant load containing water. Thus, special attention should be paid to remove completely these toxic intermediates achieving acceptable water quality levels²⁴. Consequently, it is necessary operating with excess of oxidant ratios (or an over stoichiometric addition of the oxidant) to avoid the formation of these refractory intermediates, considering that high amounts of oxidant can produce counter-effects leading to increased treatment costs. In this way, the cost-effectiveness of degradation process could be realised by optimising the amount of oxidant to reduce the wastewater toxicity.

Thus, the aim of this work consist of developing a kinetic model based on the oxidant dosage effect allow to predict the toxicity of 4-chlorophenol aqueous solutions oxidised by UV/ H_2O_2 . Consequently, the water toxicity and the formation of the different reaction intermediates were analysed during the oxidation of 4-chlorophenol. The kinetic model developed grouping three lumps of degradation byproducts as a function of their toxicity degree. The photolytic and kinetic parameters characterising each lump were adjusted in the proposed oxidation assays, obtaining a kinetic model that predict the water toxicity as a function of oxidant dose and the UV exposure time.

Results and discussion

Effect of oxidant dosage on water-quality parameters. Several experiments of 4-chlorophenol oxidation by H_2O_2 /UV were carried out at pH 6.0, varying the molar ratios of hydrogen peroxide to 4-chlorophenol between $R=0$ –400 mol H_2O_2 /mol 4-chlorophenol. The objective was to analyse the effect of the oxidant in the oxidation process, where the parameters considered as water quality indicators were the pollutant concentration (C , mg L^{-1}), total organic carbon (TOC, mg L^{-1}), colour (AU) and loss of aromaticity (AU).

Figure 1a shows that 4-chlorophenol would be completely removed from the system, during the first hour from the start of the reaction, operating with oxidant molar ratios higher than $R=200$. Under these conditions, a decrease in the rate of TOC removal close to 50% from the initial value was observed (Fig. 1b). These results agrees well with the results (R values in the range of 150–375) reported by Ec et al.²⁵. Operating under conditions of lower hydrogen peroxide concentration ($R < 200$), an insufficient amount of hydroxyl radicals is generated, being the photolytic pathway that dominates the radical pathway²⁶. As the molar ratio of H_2O_2 to 4-chlorophenol increases, large amounts of the oxidant radicals are generated that assists the effective degradation of 4-chlorophenol. With the dose ratio of H_2O_2 used in this work, as shown in Fig. 1, primary degradation (100%) and mineralisation rate (45% of TOC removal) are achieved, in the same order of variety advanced oxidation techniques, including heterogeneous photocatalytic variants; i.e. with heterojunction^{27,28} and hybrid biomaterials²⁹.

Under conditions of high reactant doses ($R > 200$), hydroxyl radicals were produced in large amounts. The excess H_2O_2 was converted into the hydroperoxyl radical, which exhibits less oxidative power than the hydroxyl radical (Eqs. 2, 7, 8). Additionally, the excess of peroxide was consumed by water and recombination reactions³⁰. The solution colour changes during the degradation of 4-chlorophenol (Fig. 1c). Different water colours (purplish-red, reddish-orange, orange, yellow, red-brown, and light yellow) of 4-chlorophenol aqueous solutions oxidised by AOPs have been previously reported^{23,31}, checking that water colour could be attributed to the presence of degradation by products generated during the oxidation process. The analyses carried out showed that the main by products formed during the oxidation pathways would be *p*-benzoquinone and hydroquinone³². The presence of these species would demonstrate that the colour formation is due to the formation of new chromophore groups in benzene rings, causing the generation of quinones and their derivatives³³. Operating at $R=200$, colour compounds were oxidized to colourless species, remaining in minor amounts, that resulted in a decrease in the toxicity of the solutions.

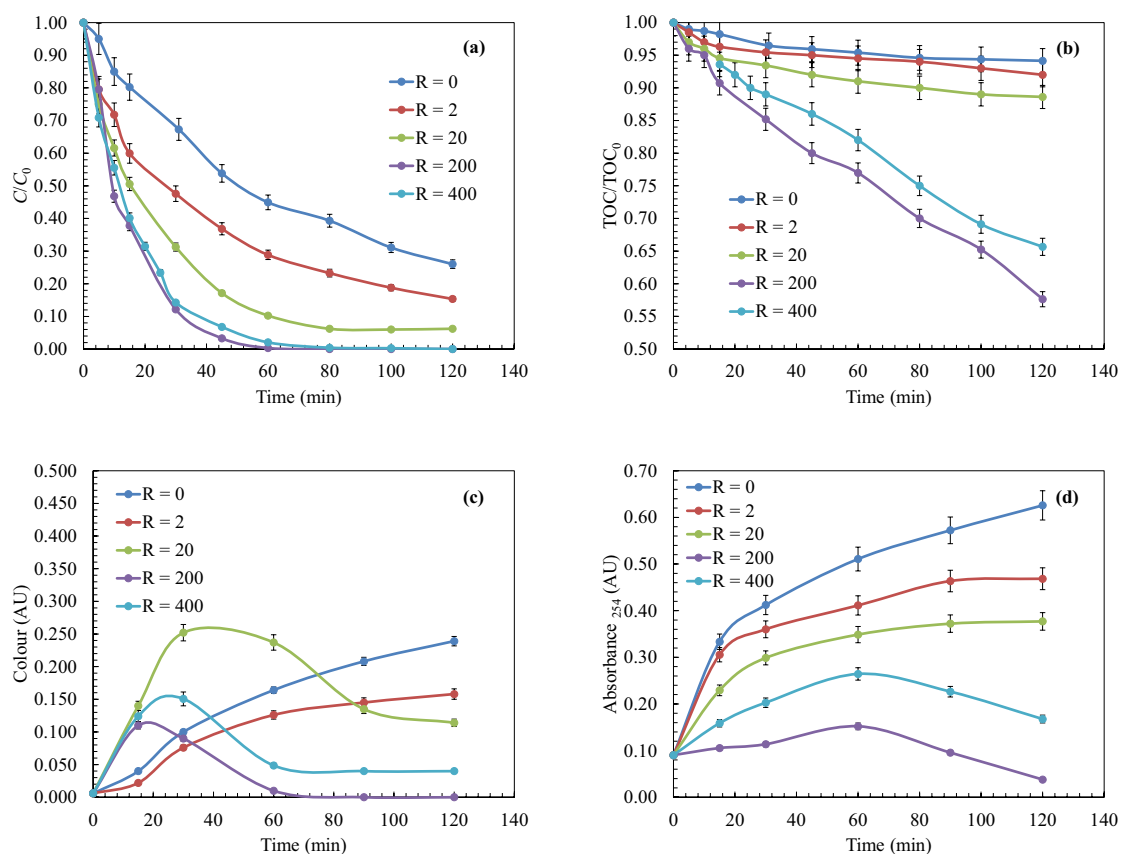


Figure 1. Study of the effect of peroxide dose during the UV/H₂O₂ oxidation of 4-chlorophenol. **(a)** Primary oxidation of 4-chlorophenol; **(b)** Mineralisation; **(c)** Colour induction; **(d)** Aromatic ring rupture. Experimental conditions: $T = 25\text{ }^{\circ}\text{C}$; $C_0 = 200\text{ mg L}^{-1}$; $\text{pH} = 6.0$; Agitation = 700 rpm; $V_{\text{reac}} = 1.7\text{ L}$.

The decreased in the loss of aromaticity, analysed at 254 nm, described in Fig. 1d could be attributed to the rupture of the aromatic rings and could indicate the degradation of the aromatic compounds. The loss of aromaticity decreases when $R = 200$, checking that the aromatic rings ruptured and chromophore groups degraded resulting in more favourable oxidation conditions.

Degradation pathway of 4-chlorophenol. Prior to the development of the kinetic model, the pollutant degradation compounds were analysed. Figure 2 shows the degradation of 4-chlorophenol, as well as the formation of their main oxidation intermediates. Results show that the oxidation of 4-chlorophenol leads to the formation of intermediate species of aromatic nature such as 4-chlorocatechol, catechol, hydroquinone and *p*-benzoquinone, as well as the formation of aliphatic species, such as maleic, fumaric, formic and acetic acids. The results obtained allow to verify that the action of UV light is capable of degrading the 4-chlorophenol rings to dihydroxylated rings (Fig. 2a). However, UV light did not prove effectiveness during the degradation of dihydroxylated intermediates to quinone-like compounds and carboxylic acids (Fig. 2b).

Thus, with the aim of degrade 4-chlorophenol until achieve higher oxidation levels, it is necessary to combine UV light with the action of an oxidant (hydrogen peroxide). Figure 1c,e show that the main degradation pathway of 4-chlorophenol evolves towards the formation of chlorosubstituted intermediates (chlorocatechol). On the other hand, once the aromatic intermediates have been degraded until carboxylic acids, it can be checked that using oxidant ratios of $R = 200$, 4-chlorophenol was completely degraded until formic acid.

The analysis performed suggests two possible reaction pathways³⁴. In the first, the hydroxyl radicals attacks the aromatic rings in the *ortho*-substituted position, and displaces hydrogen, which promotes the formation of 4-chlorocatechol. In the second, the attack of hydroxyl radicals can occur in the *para*-substituted position, which cause the displacement and substitution of the chloride ion, causing the formation of hydroquinone, which is oxidised to benzoquinone (see Fig. 3).

Kinetic modelling of the reaction intermediates pathway. Determination of the reaction kinetics of such complex oxidation processes can be simplified using a lumped model where all the species exhibiting similar characteristics are grouped. Thus, each group was regarded as a unique compound³⁵. The contributions of different oxidation intermediates towards the total toxicity of the system depend on their individual toxicities. Then, all the oxidation intermediates do not contribute equally to the total toxicity of the system. The oxidation by products are grouped into five main groups based on their toxicity. The lumped model was constructed fol-

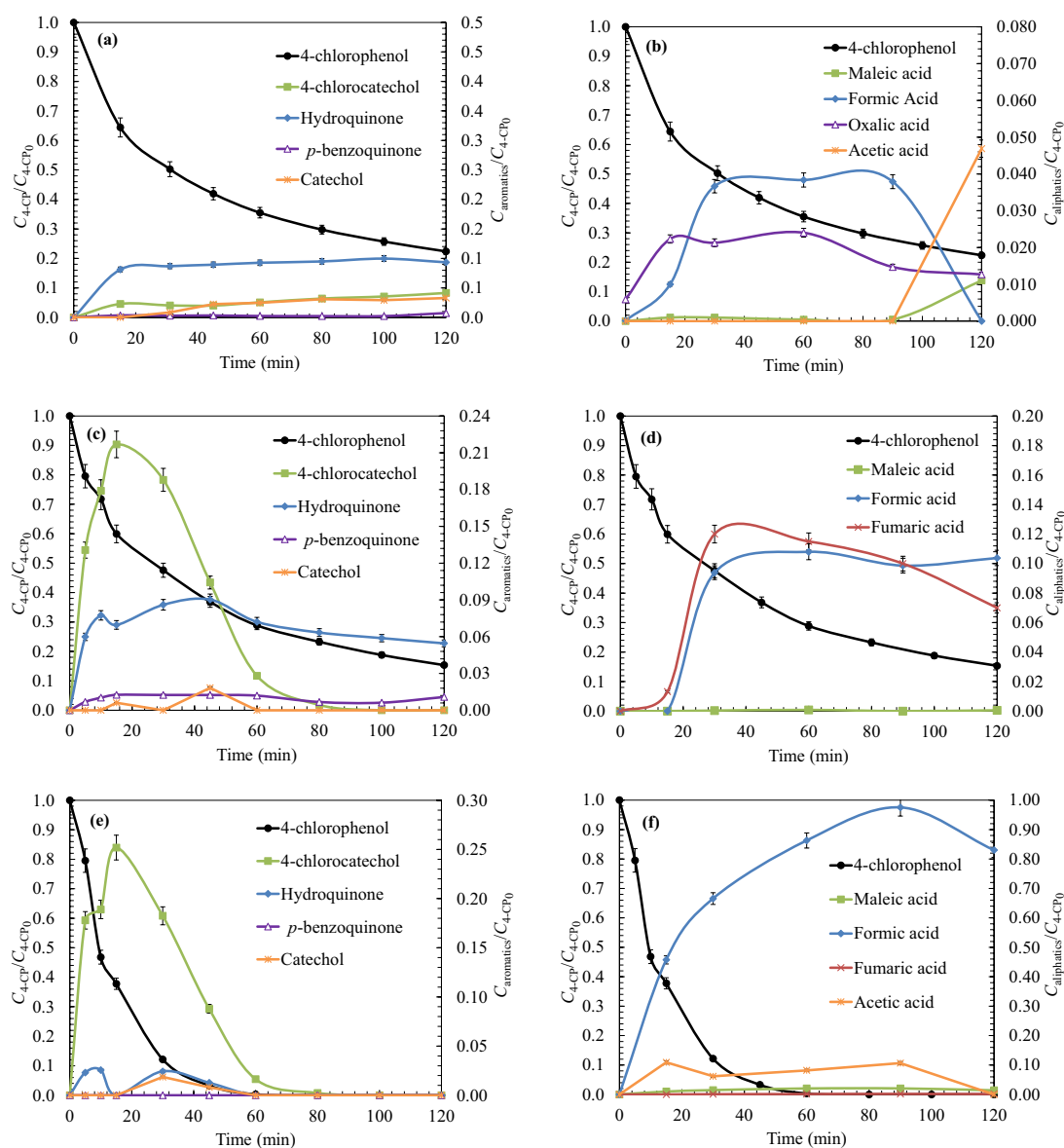


Figure 2. Analysis of the main degradation intermediates (left: aromatic compounds; right: aliphatic oxidation products) produced during the oxidation of 4-chlorophenol (UV/H₂O₂ process) under different peroxide doses: (a)/(b) $R=0$; (c)/(d) $R=2$; (e)/(f) $R=200$. Experimental conditions: $T=25\text{ }^{\circ}\text{C}$; $C_0=200\text{ mg L}^{-1}$; $\text{pH}=6.0$; Agitation = 700 rpm; $V_{\text{react}}=1.7\text{ L}$.

lowing previously reported protocols²⁴. The mechanisms proposed by Kusic et al.³⁶ and Gomez et al.³ have been presented in Fig. 4.

A common photolytic process forms the basis of the first stage of the oxidation process (4-chlorophenol oxidation; assigned as A). Direct photolysis promotes hydroxylation and dechlorination reactions. The highly toxic *p*-benzoquinone ($EC_{50}=0.035\text{ mg L}^{-1}$) and/or hydroquinone ($EC_{50}=0.088\text{ mg L}^{-1}$) intermediates³⁷, and comparatively less toxic 1,2,4-trihydroxybenzene ($EC_{50}=1.03\text{ mg L}^{-1}$) and/or resorcinol ($EC_{50}=9.02\text{ mg L}^{-1}$) were produced in small amounts³⁵.

The hydroxyl radicals turned the oxidation process via another oxidation pathway that results in the formation of other substances like hydroquinone. Chlorinated compounds and *p*-benzoquinone were also formed during the process. Aromatic compounds of varying toxicities were formed in the first step of the oxidation process. Group B₁ consists of *p*-benzoquinone and hydroquinone. These compounds are believed to contribute the most maximum towards the global toxicity of treated wastewater as these compounds are abundant²⁴. Several researchers have reported that condensation products were formed within minutes (from the start of the reaction) in the absence of oxidants (or under conditions of oxidant deficiency). The majority of the by products formed, were two-ring aromatic chlorinated compounds such as chlorinated hydroxylated biphenyls, dichlorodiphenyl ethers, and dichlorodibenzodioxins. These chlorinated compounds significantly raise the toxicity of the system²².

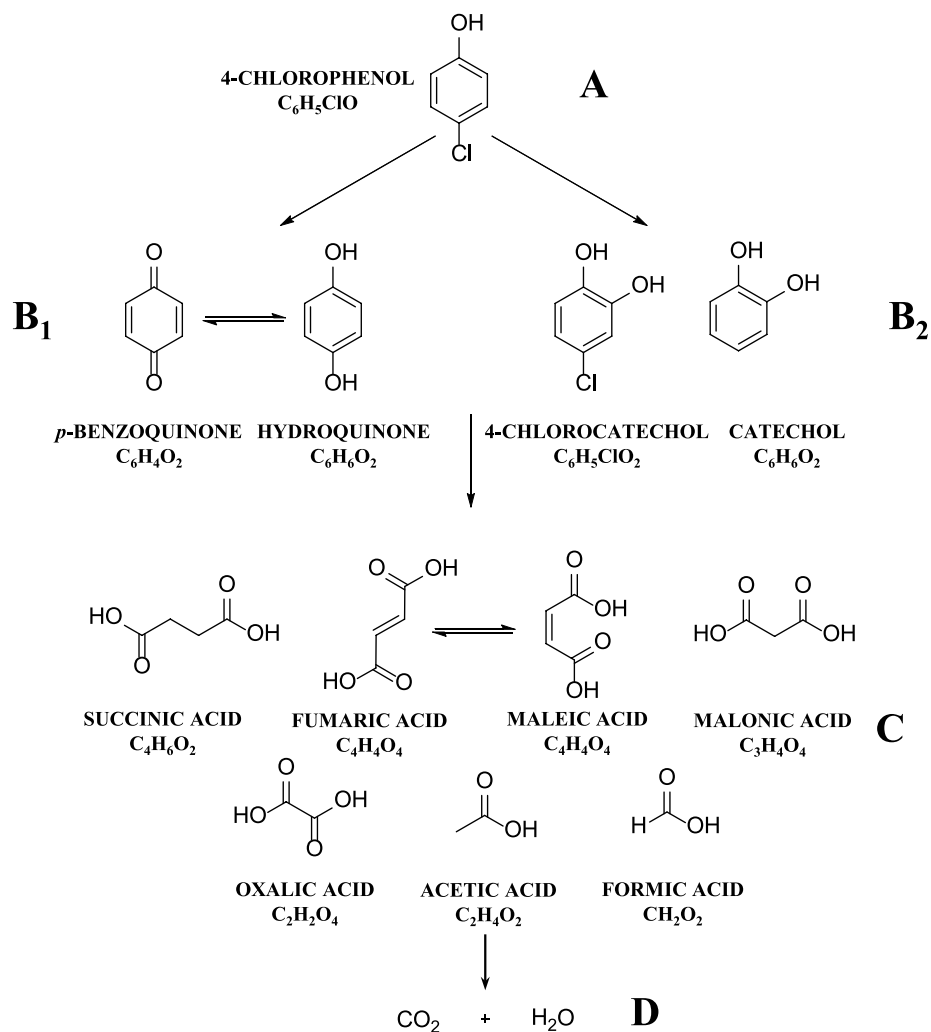


Figure 3. Proposed oxidation pathway for the oxidation of 4-chlorophenol via UV/H₂O₂ process.

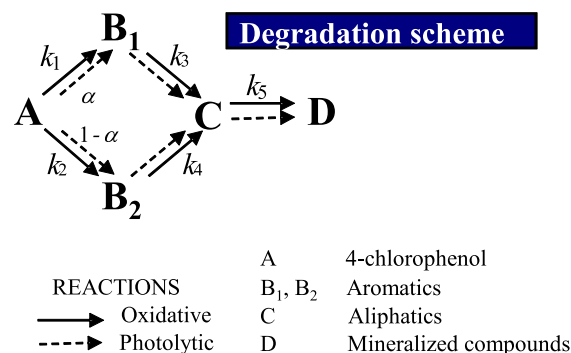


Figure 4. Proposed parallel reaction model for the oxidation of 4-chlorophenol using the UV/H₂O₂ technology.

In this case, water appeared yellow–brown, indicating the presence of these chromophoric toxic compounds with high molecular weight³².

The aromatic 4-chlorocatechol and catechol compounds formed as by products via the radical pathway are members of the B₂ group. These compounds are less toxic than the parent compounds. In the next step of oxidation, aromatic compounds were converted to unsaturated acids (fumaric acid and maleic acid) that are subsequently converted to saturated carboxylic acids (formic acid and acetic acid). Among these, formic acid,

acetic acid, fumaric acid, and maleic acid are members of group C. The constituents of this group were less toxic than the constituents of the previously described groups. Further oxidation results in CO₂ mineralisation and formation of water (group D)^{36,38}.

The change in the concentrations of the species of each group over time and the variation in toxicity over time can be determined using a kinetic model. The model was proposed by studying the reaction mechanism presented in Fig. 4. Various factors were considered for developing the kinetic model:

- Three groups (lumps) of oxidation intermediates (B₁, B₂, and C) were defined. Group B₁ primarily consisted of hydroquinone, *p*-benzoquinone, and some unknown compounds (of similar structure) that exhibited high toxicity²⁴. Groups B₂ and C consisted of compounds that exhibited lower toxicity levels. The toxicity levels and the constituents were experimentally determined. Group B₂ consisted of 4-chlorocatechol and catechol and group C consisted of various carboxylic acids (acetic acid, oxalic acid, formic acid, succinic acid, malonic acid, maleic acid, and fumaric acid).
- The degradation of 4-chlorophenol proceeds via a two ways parallel reaction mechanism. The mechanism has been previously reported by Azevedo et al.³⁹ (Fig. 4). B₁ and B₂ are the reference lumps of each route.
- The degradation of each group proceeds via the photolytic (zero-order kinetic (k_i)) and radical (pseudo-first-order kinetic (k'_i)) pathways.
- The average toxicity (EC_{50}), photolytic parameters, and kinetics constants have been determined for each lump. The experimentally obtained values of toxicity and concentration were fitted using the appropriate analysis model.

The degradation of each group versus time is described by Eq. (9), which considers the contributions of the direct photolysis and hydroxyl-radical attack processes^{3,35,40}. The relation can be expressed as follows:

$$-\frac{dC_i}{dt} = I_0 \times \Phi_i \times F_i \times \left(1 - \exp\left(-2.303 \times L \times \sum (\epsilon_j \times C_j)\right)\right) + \bar{k}_i \times C_i \times C_{HO^\cdot}, \quad (9)$$

where \bar{k}_i is the rate constant of a second-order reaction involving the hydroxyl radical in group *i*, Φ_i denotes the quantum yield of lump *i*, C_{HO^\cdot} denotes the concentration of the hydroxyl radicals, and I_0 represents the intensity of the emitted UV radiation. F_i (incident radiation) denotes the radiation absorbed partially by each group. This can be expressed by Eq. (10) as follows:

$$F_i = \frac{\sum (\epsilon_j \times C_j)_i}{\sum \epsilon_j \times C_j}. \quad (10)$$

Equation (9) could be simplified if it was assumed that the reaction between hydroxyl radicals and 4-chlorophenol is a pseudo-first-order reaction (k'_i)^{19,41}. Under this condition, mass balance equations can be formulated for 4-chlorophenol (group A). The other four degradation products are grouped (groups B₁, B₂, C, and D) based on the total organic carbon (TOC) values. The simplified equations can be expressed as follows:

$$\frac{dC_A}{dt} = -I_A \times \Phi_A \times F_A - k'_1 \times C_A - k'_2 \times C_A, \quad (11)$$

$$-\frac{dC_{B_1}}{dt} = \alpha \times I_A \times \Phi_A \times F_A - I_{B_1} \times \Phi_{B_1} \times F_{B_1} + k'_1 \times C_A - k'_3 \times C_{B_1}, \quad (12)$$

$$-\frac{dC_{B_2}}{dt} = (1 - \alpha) \times I_A \times \Phi_A \times F_A - I_{B_2} \times \Phi_{B_2} \times F_{B_2} + k'_2 \times C_A - k'_4 \times C_{B_2}, \quad (13)$$

$$-\frac{dC_C}{dt} = I_{B_1} \times \Phi_{B_1} \times F_{B_1} + I_{B_2} \times \Phi_{B_2} \times F_{B_2} - I_C \times \Phi_C \times F_C + k'_3 \times C_{B_1} + k'_4 \times C_{B_2} - k'_5 \times C_C, \quad (14)$$

$$-\frac{dC_D}{dt} = I_C \times \Phi_C \times F_C + k'_5 \times C_C, \quad (15)$$

$$-\frac{dC_{TOC}}{dt} = k'_1 \times C_A + k'_2 \times C_{B_1} + k'_3 \times C_{B_2} + k'_4 \times C_C + k'_5 \times C_D, \quad (16)$$

where α denotes the photolytically degraded fraction of 4-chlorophenol to group B₁ and C_i denotes the concentration of each lump *i*. The change in toxicity over time can be predicted by studying the toxicities exhibited by each lump. The concentration at any given time and the average toxicity of each group was predicted by preliminary calculations and validated from results reported in the literature (Table 1). Group D was excluded from the calculations as mineralised CO₂ and water were present in the system. It did not contribute to the overall toxicity of the system. Toxicity was determined by Eq. (17), which was derived from Eq. (19). The equation derived to determine the toxicity of the system takes into account the fraction of unknown compounds belonging to group B₁. The following equation was proposed to determine the toxicity of the system based on the above assumptions²⁴:

Substance group	Compound	EC ₅₀ (mg L ⁻¹)		ε (M ⁻¹ cm ⁻¹)		Φ (mol Einstein ⁻¹)	
		Individual	Lump	Individual	Lump	Individual	Lump
A	4-chlorophenol	5.654	5.654	510.0	510.0	0.017	0.017
B ₁	Hydroquinone	0.088	0.0615	307.2	2044.9	0.047	0.025
	<i>p</i> -benzoquinone	0.035		13,612.0		0.025	
B ₂	4-chlorocatechol	5.932	6.892	381.3		0.057	0.0024
	Catechol	7.853		504.1		0.0001	
C	Maleic acid	3.852	63.154	769.9	1172.0	0.048	0.0351
	Fumaric acid	15.79		894.0		0.063	
	Malonic acid	12.28		697.0		0.27	
	Oxalic acid	817.2		630.9		0.15	
	Acetic acid	273.2		3159.2		0.028	
	Formic acid	235.6		504.1		0.006	
	Succinic acid	102.0		6300.0		0.0032	

Table 1. Toxicity and photolytic properties of individual and grouped substances produced during the oxidation of 4-chlorophenol (UV/H₂O₂ oxidation mechanism)^{36,38,42–44}.

Group	ε (M ⁻¹ cm ⁻¹)	Φ (mol Einstein ⁻¹)	EC ₅₀ (mg L ⁻¹)
A	409	0.022	4.068
B ₁	480	0.015	0.075
B ₂	325	0.007	6.240
C	1485	0.005	73.300
D	–	–	–

Table 2. Photolytic and toxicity properties determined using the proposed toxicity–kinetic model. Experimental conditions: *T* = 25 °C; *C*₀ = 200 mg L⁻¹; pH = 6.0; Agitation = 700 rpm; *V*_{reac} = 1.7 L.

$$-\frac{d\text{Toxicity}}{dt} = k'_1 \times \frac{C_A}{EC_{50A}} + k'_2 \times \left(\frac{C_{B1}}{EC_{50B1}} + \frac{C_{B1\text{lump}}}{EC_{50B1}} \right) + k'_3 \times \frac{C_{B2}}{EC_{50B2}} + k'_4 \times \frac{C_C}{EC_{50C}} \quad (17)$$

Validation of the kinetic model. The model proposed was based on the lumped mechanism described by Kusic et al.³⁶ and Li et al.⁴⁵. The kinetic, mass balance, and toxicity equations were solved using the Berkeley Madonna numerical calculation tool (Eqs. 10–17). The change in the concentration of each lump over time was determined using this method.

The simultaneous fitting of experimental and simulated data helped to determine the simulated photolytic, kinetic, and toxicity values of each lump. The determination of these values and the EC₅₀ values of the compounds can potentially help to predict the toxicity of wastewater during the UV/H₂O₂ treatment process, carried out under different operational conditions. The adjustment minimises the sum of squared residuals. The goodness of fit was determined by calculating the weighted standard deviation, *σ*, given by Eq. (18) as follows³⁰:

$$\sigma = \sqrt{\frac{\sum_{i=1}^N \left(\frac{C_{\text{exp}} - C_{\text{sim}}}{C_{\text{exp}}} \right)^2}{N - 1}}, \quad (18)$$

where *N* was the number of experimental values and *C*_{exp} and *C*_{sim} denote the concentration (of the compound or lump (*i*)) determined experimentally and the concentration determined using the model, respectively. The data obtained from the direct photolysis experiments (*R* = 0) were used to determine the values of the photolytic parameters (quantum yield and extinction coefficient). The process of direct photolysis only affects the rate of disappearance of each lump. The photolytic contribution can be determined from the Lambert–Beer law. The initial values of the quantum yield (Φ) and extinction coefficient (ε) were presented in Table 1. After determining the photolytic parameters (Table 2), the experimental data were modelled in the presence of H₂O₂ to determine the values of the pseudo-first-order rate constants (*k*'₁, *k*'₂, *k*'₃, *k*'₄, and *k*'₅). The constants can be estimated by studying the reactions between the hydroxyl radicals and the lumps (except D; Eqs. 11–14). For the direct photolysis process (*R* = 0), the zero-order kinetic constants (*k*_i) and the condition of total mass balance (Eq. 16) were considered for determining the experimental and theoretical concentrations of each group. The simulated constants were presented in Table 2. Following this, it was determined if the EC_{50i sim} values of each group (obtained by fitting the simulated toxicity data) agreed well with the experimentally obtained EC_{50i exp} values of each lump. The initial EC_{50i} values were determined using the EC₅₀ values of the individual species

Parameter	UV alone process			
k_1 ($s^{-1} \text{ mol L}^{-1}$)	2.12×10^{-5}			
k_2 ($s^{-1} \text{ mol L}^{-1}$)	0.99×10^{-5}			
k_3 ($s^{-1} \text{ mol L}^{-1}$)	1.30×10^{-5}			
k_4 ($s^{-1} \text{ mol L}^{-1}$)	4.64×10^{-5}			
k_5 ($s^{-1} \text{ mol L}^{-1}$)	1.48×10^{-5}			
α	0.37			
σ	0.054			
UV/H ₂ O ₂ process				
	R = 2	R = 20	R = 200	R = 400
k'_1 (s^{-1})	2.46×10^{-5}	1.51×10^{-4}	6.87×10^{-4}	2.05×10^{-4}
k'_2 (s^{-1})	1.07×10^{-5}	1.16×10^{-3}	1.25×10^{-3}	1.19×10^{-3}
k'_3 (s^{-1})	1.54×10^{-5}	5.83×10^{-5}	1.23×10^{-4}	8.56×10^{-5}
k'_4 (s^{-1})	4.96×10^{-5}	1.65×10^{-4}	1.14×10^{-3}	4.44×10^{-4}
k'_5 (s^{-1})	1.67×10^{-5}	4.50×10^{-5}	9.10×10^{-5}	6.82×10^{-5}
α	0.35	0.21	0.16	0.19
σ	0.057	0.043	0.052	0.049

Table 3. Kinetic parameters predicted using the proposed toxicity–kinetic model at different H₂O₂/4-chlorophenol ratios. Experimental conditions: $T = 25$ °C; $C_0 = 200$ mg L⁻¹; pH = 6.0; Agitation = 700 rpm; $V_{\text{reac}} = 1.7$ L.

reported in the literature^{36,38,42–44}. The values obtained from literature reports have been presented in Table 1. It is worth mentioning that the toxicities exhibited by the substances (belonging to the same group) were similar (EC_{50} values of the same order of magnitude). This was the primary criterion of lumped modelling.

High quantum yields were recorded for groups A and B₁ (0.022 and 0.015 mol Einstein⁻¹, respectively; Table 2). The data revealed that 4-chlorophenol could be easily degraded by the process of direct photolysis⁴¹. The branch mechanism is favoured when the photolytic pathway is the predominant mechanistic pathway. It was observed that a satisfactory adjustment between the simulated and experimental results could be achieved ($\sigma \cong 0.05$) if a quantum yield value (for the reaction involving the photolysis of 4-chlorophenol), that is close to that reported by Pera-Titus et al.⁴⁶ is used for the calculations. The quantum yield recorded for group C ($\Phi = 0.005$ mol Einstein⁻¹), which consists of aliphatic compounds, agreed well with the quantum yield reported by Kralik et al. for the same group⁴⁰.

As mentioned before, the theoretical toxicity of each group was represented as a function of the EC_{50} values of the identified species. The Microtox toxicity bioassay was used to determine the values presented in Table 2. The experimentally determined values were compared with the values presented in the literature (Table 1).

Table 3 presents the values of the kinetic constants determined using the proposed kinetic model. The value of α (the coefficient that correlates the production of substances (by photolytically degrading A) belonging to group B₁ to the compounds belonging to group B₂) was found to be 0.37. It must be remembered that the models comprised of compounds that exhibited similar toxicological properties. Group B₁ comprised of all unknown aromatic compounds.

The results reveal that in the absence of oxidants, the highly toxic compounds, such as double-ringed chlorinated compounds (except *p*-benzoquinone and hydroquinone), were produced⁴⁷. This was because, during the photolytic oxidation process, the formation of hydroquinone or *p*-benzoquinone was favoured over the formation of 4-chlorocatechol³⁶. The experimental results presented in Table 3 validate this result. The coefficient α , determined using the simulation method, helps in understanding the nature of the unidentified products. The value of α (0.37) indicates that under these conditions, oxidation products that were more toxic than the parent pollutants were formed. Among all the identified compounds, hydroquinone was found to be present in the highest amount⁴⁸. On the other hand, the value of this fraction decreased to 0.16 (at $R = 200$) when experiments were carried out in the presence of H₂O₂.

The values of the kinetic constants indicate that k_1 ($2.12 \times 10^{-5} \text{ s}^{-1} \text{ mol L}^{-1}$) was higher than k_2 ($0.99 \times 10^{-5} \text{ s}^{-1} \text{ mol L}^{-1}$) (under conditions of all oxidant dosages). The differences between k'_1 and k'_2 increased as the peroxide concentration increases. At conditions of $R = 200$, this difference increased by two orders of magnitude ($k'_2 = 1.25 \times 10^{-3} \text{ s}^{-1}$ versus $k'_3 = 1.23 \times 10^{-4} \text{ s}^{-1}$; Table 3). These results reveal that the radical pathway promotes the formation of the constituents of group B₂ (over the constituents of group B₁). This result has been previously reported by other groups^{35,40,49}. It has been hypothesised that when the oxidation reaction occurs in the presence of hydroxyl radicals, the hydroxylation reaction was favoured over the chlorination reaction. This was because the *para*-position of chlorophenol is highly susceptible to attack during the direct photolysis reactions. The photoreactivity of the chlorine atom is higher than that of the hydroxyl group. In the presence of peroxides, chlorophenols react rapidly under conditions of UV radiation⁴¹.

Under maximum dosage conditions, a large amount of 4-chlorocatechol was degraded and less amounts of *p*-benzoquinone (or hydroquinone) was produced. Similar results were obtained when the k'_1 values at different H₂O₂ dosages were compared with each other. The value of k'_1 increased as the value of R increase (from

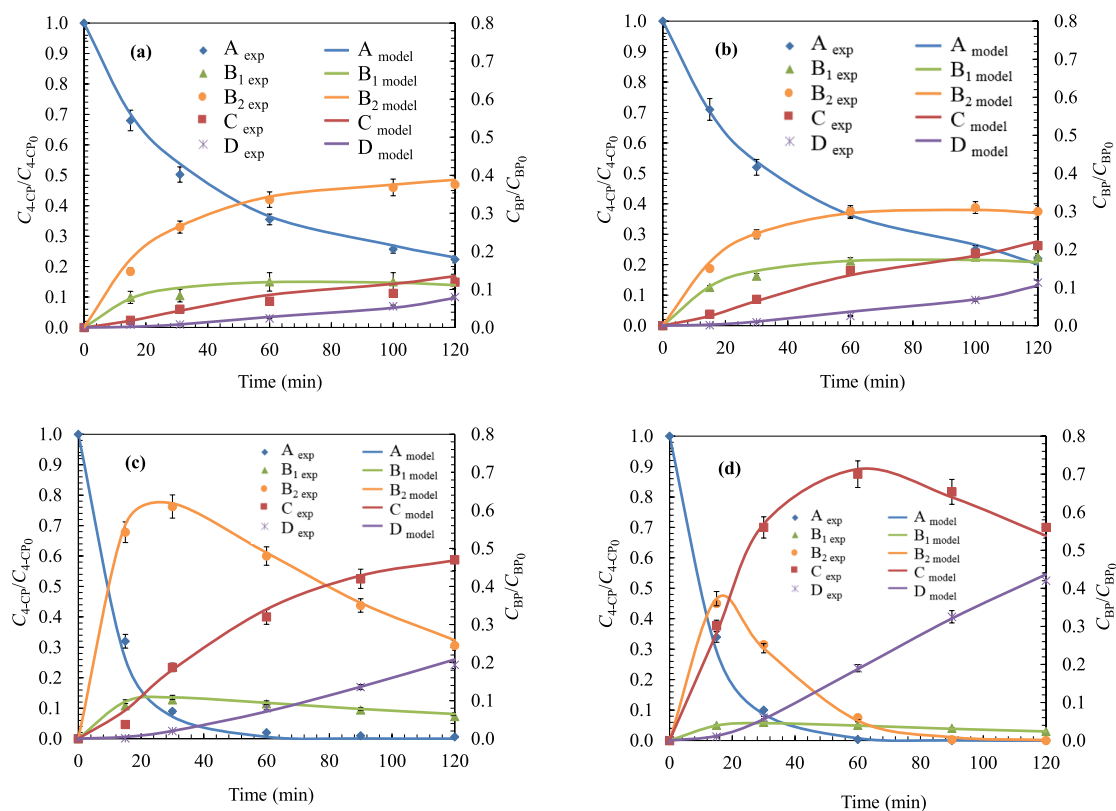


Figure 5. Evolution of the dimensionless concentration of each lump during the oxidation of 4-chlorophenol. Data fitted to the kinetic model at different doses of H_2O_2 : (a) $R=0$; (b) $R=2$; (c) $R=20$; (d) $R=200$. Experimental conditions: $T=25\text{ }^\circ\text{C}$; $C_0=200\text{ mg L}^{-1}$; $\text{pH}=6.0$; Agitation = 700 rpm; $V_{\text{reac}}=1.7\text{ L}$.

$R=2$ ($2.46 \times 10^{-5}\text{ s}^{-1}$) to $R=20$ ($1.51 \times 10^{-4}\text{ s}^{-1}$). A slight drop in value was observed when R was in the range of 200–400 ($R=200$ ($6.87 \times 10^{-4}\text{ s}^{-1}$); $R=400$ ($2.05 \times 10^{-4}\text{ s}^{-1}$)). The amount of hydroxyl radicals present in the media ($R \geq 200$) hindered the production of the compounds constituting group B_1 . Simultaneously, the formation of the compounds constituting group B_2 was promoted (Fig. 5). The values of k'_1 and k'_2 indicated the efficiency with which 4-chlorophenol was degraded.

The results revealed that the values of the kinetic constants (k'_1 and k'_2) increase till $R=200$ and become constant thereafter. It was observed that the amounts of degraded compounds did not increase with the increase in the amount of oxidant under conditions of constant radical concentration. A lower concentration of the generated hydroxyl radicals under steady-state conditions did not promote the efficiency of the reaction. The oxidant dosage under these conditions was known as the critical dose. When the critical R -value was reached, an increase in the peroxide dosage can potentially hinder the oxidation reaction, as the excess hydroxyl radicals can potentially react with H_2O_2 (scavenger reactions)^{1,18}. Similar observations were made when the change in the concentration of 4-chlorophenol with time was experimentally studied under conditions of $R=20$ (Fig. 5c) and 200 (Fig. 5d).

The critical dose under which the process of mineralisation or complete degradation was not promoted, was approximately 200 ($R=200$). Although the reaction kinetics (direct oxidation of 4-chlorophenol) was not improved when the dosage was increased above 20, the analysis of the experimental results revealed that rate of mineralisation increased with the increase in the oxidant dosage. The concentration of the different oxidation products decreased at a higher rate under the experimental conditions. This was validated by the k'_4 and k'_5 values determined by the simulation experiments (Table 3). The values of the constants k'_4 and k'_5 indicated that when the dose of H_2O_2 was increased, the rate of mineralisation increased. This was reflected by the increase in the amounts of low molecular weight compounds (such as fumaric acid). The values of the constants k'_1 and k'_2 , directly related to the primary degradation of *p*-chlorophenol, remained constant ($R \geq 20$). However, the values of the other constants increased under similar conditions.

Aromatic compounds (constituents of groups B_1 and B_2) were the reactants in the second step of the oxidation reaction. The rate of the final step (group D; CO_2 and H_2O) rapidly increased at $R=200$. The critical R for mineralisation was reached at dosages ≥ 200 , though the maximum amounts of the compounds that belong to group B_2 were formed within the first 20 min of the reaction. On the other hand, the amounts of compounds (carboxylic acids and low molecular weight compounds) constituting group C increased (Fig. 5d) till the first 60 min. Following this, the amounts of the compounds decreased as hydroxyl radicals (generated from H_2O_2) increased. These radicals could effectively react with these compounds to produce increased amounts of CO_2 and H_2O (group D).

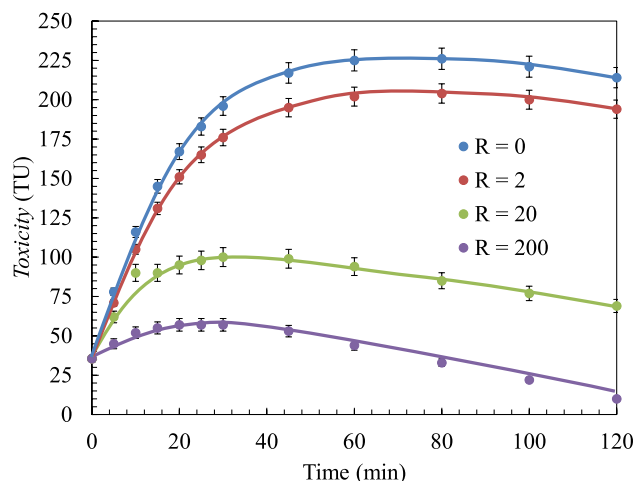


Figure 6. Prediction of the toxicity of the mixture during the oxidation of 4-chlorophenol (UV/H₂O₂ process) varying H₂O₂ dose.

Figure 6 showed the change in toxicity over time, determined using the kinetic model, at four different doses of peroxide during the process of photolysis. Good fitting results were obtained and the mean standard deviation was approximately 0.057 ($\sigma \cong 0.057$). The toxicity was found to increase during the first 20 min of the reaction. Compounds belonging to group B₁ (such as hydroquinone and *p*-benzoquinone) that were more toxic than 4-chlorophenol were produced under these conditions. An increase in the dose of H₂O₂ resulted in a decrease in the amounts of the compounds. The degradation compounds belonging to groups B₁ and B₂ were removed from the system under these conditions and by products (such as formic acid or fumaric acid) belonging to group C (less toxic compounds) were formed.

This increase in toxicity was also reported by Muñoz et al.²² and Karci et al.²³ that they concluded that in the absence of oxidant or under conditions of inadequate oxidant dose, toxic substances (such as hydroquinone and *p*-benzoquinone) and condensation by products were formed. According to Ronco et al.⁵⁰, a toxicity value of less than 1 TU indicated that the effluent was non-toxic or exhibited low toxicity. The values in the range of 1–10 TU correspond to slightly toxic effluents. When the value $\hat{>}$ 11 TU, the effluent was considered to be highly toxic. At $R = 200$, a value of 9.95 TU was recorded for the wastewater under study. This sample could be used for biodegradation. The degradation pathway led to the formation of the compounds constituting group B₁ under conditions of inadequate doses of oxidants. Under these conditions, the original wastewater sample was found to be more toxic and the chemical degradation pathway could not be complemented by a biological process.

Methods

Reagents. 4-Chlorophenol (ClC₆H₄OH, Sigma-Aldrich, $\geq 99\%$), hydrogen peroxide (H₂O₂, Labkem, 30%, (v/v)), hydrochloric acid (HCl, Sigma-Aldrich, 33%), sodium hydroxide (NaOH, Labkem, $\geq 97.0\%$), sodium sulfite (Na₂SO₃, Sigma-Aldrich, 58.5%), *ortho*-phosphoric acid (H₃PO₄, Merck, 85%), and HPLC-grade methanol (CH₃OH, Acros Organics, $> 99.99\%$) were used as received. The following were used as calibration standards: 4-chlorocatechol (ClC₆H₃(OH)₂, Sigma-Aldrich, 97%), hydroquinone (Supelco, certified reference material), benzoquinone (Supelco, certified reference material), pyrocatechol (Fluka Chemika, $\geq 99\%$), maleic acid (HO₂CCH=CHCO₂H, Acros Organics, $\geq 99\%$), fumaric acid (HOOCCH=CHCOOH, Fluka Chemika, 99.5%), and formic acid (CH₂O₂, Acros Organics, 99.0%). Deionised water was collected from a Milli-Q water purification unit supplied by Merck.

Analytical techniques. The intermediates produced during the oxidation of 4-chlorophenol were detected using the high-performance liquid chromatography (HPLC) technique. The Waters Alliance 2695 system (WATERS, Milford, CT, USA) equipped with the Waters 2487 Dual λ Absorbance Detector (Waters, Milford, CT, USA) was used for the same. An INERTSIL ODS-3 column (150 mm \times 4.6 mm, 5 μ m) (GL Sciences, Torrance, CA, USA) was used to detect 4-chlorophenol (CP) and 4-chlorocatechol (4Cl-CC). The methanol:water (30:70, v/v) solvent system buffered with *o*-H₃PO₄ at pH 3 was used as the mobile phase. The flow rate was maintained at 1.0 mL min⁻¹ and the sample volume was 1.0 μ L. The analytes were detected at 280 nm. Other aromatic compounds such as hydroquinone (HQ), benzoquinone (BQ), and pyrocatechol (CC) were detected under the same conditions. The methanol:water (20:80, v/v) solvent system was used as the mobile phase for eluting the aromatic compounds. The experiments to detect BQ were carried out at a wavelength of 245 nm.

The aliphatic substances (maleic acid, fumaric acid, acetic acid, and formic acid) were separated on the INERTSIL ODS-4 column (250 mm \times 4.6 mm, 5 μ m) (GL SCIENCES, Torrance, CA, USA). The mobile phase consisted of (NH₄)₂HPO₄ (20 mM) at pH 2. The compounds were detected at a wavelength of 214 nm. The flow rate was maintained at 1.0 mL min⁻¹.

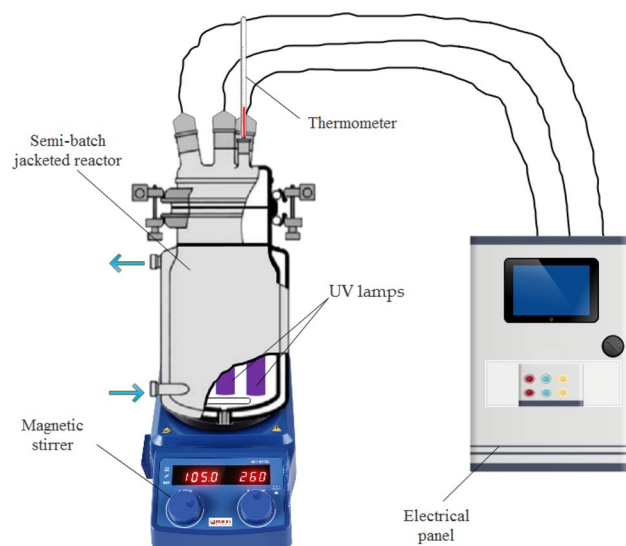


Figure 7. Experimental set-up used to carry out photolytic assays.

The concentration of unreacted H_2O_2 was determined spectrophotometrically at 420 nm, following the procedure outlined by Eisenberg⁵¹. The variation in the colour intensity was determined by recording the absorbance at 455 nm⁵². The rupture of the aromatic ring was detected by recording the absorbance of the sample at 254 nm using the PerkinElmer Lambda 10 UV/Vis spectrophotometer (PerkinElmer España, Madrid, Spain)⁹. The extent of oxidation was determined as the difference of the initial and final total organic carbon (TOC) using the Shimadzu TOC-VCSN analyser (Izasa Scientific, Alcobendas, Spain) to determine the efficiency of the water treatment process.

The variation in toxicity over time was determined by conducting a MICROTOX toxicity test (ISO 11348-3 (1998); Water Quality—Determination of the inhibitory effect of water samples on the light emission of *Aliivibrio fischeri* (Luminescent bacteria test)—Part 3: Method using freeze-dried bacteria⁵³) using a Microtox SDY 500 Analyzer (Microbics Corp., New Castle, DE, USA). The reported method takes into account the changes in the luminescence emission of the luminescent *Aliivibrio fischeri* bacteria when it was exposed to toxic compounds. Toxicity values were expressed in terms of their inhibitory concentration (IC_{50}) or variant effective concentration (EC_{50}) (from the initial concentration of the pollutant (C_i); the dilution necessary to reduce 50% the initial luminescence of the bacteria). These were most commonly expressed in toxicity units (TU) as follows (Eq. 19)^{24,26}:

$$\text{Toxicity} = \frac{100}{IC_{50}} = \frac{C_i}{EC_{50}}. \quad (19)$$

All samples were treated with excess Na_2SO_3 to remove the residual H_2O_2 present in the system before analysing their toxicities. The samples were aerated to convert the residual sulfite to sulfate³⁸.

All numerical calculations were performed using the Berkeley Madonna software (version 8.0; UC Berkeley, Berkeley, CA, USA). This software can be used to efficiently solve differential equations to predict the variation in concentrations and toxicities of each group of species over time. In addition, the program used the trial-and-error method to fit experimental and theoretical data to obtain the values of the photolytic, kinetic, and toxicological parameters of grouped substances. The method has been explained in the forthcoming sections.

Experimental set-up. Experiments were performed in a photochemical reactor (2 L batch mode) consisting of a Pyrex mixing vessel. The inner diameter was 100 mm and the height was 270 mm (Fig. 7). The temperature was maintained at 25 °C using a jacketed water recirculating thermostatic system. Three low-pressure mercury UV-C lamps (254 nm) that consume a nominal power of 8 W (Philips TUV 8 W G8T5, Philips, Madrid, Spain) were used for irradiation. UV irradiation was used instead of a visible or solar light source because these two sources emit only 5% of the UV irradiation required for the decomposition of hydrogen peroxide. The lamps were equidistant from each other and placed at the centre of the reactor. Each of the lamps was placed inside a quartz tube. Actinometrical measurements, revealed that the incident photonic flux (I_0) was 3.17×10^{-5} Einstein s^{-1} . The effective radiation path (L) was 5.85 cm.

Experimental procedure. 4-chlorophenol was dissolved in water (1.7 L) to obtain a solution of concentration 200 mg L^{-1} . The solution was placed in the reactor and the mixture was stirred using a magnetic stirrer to produce a homogenous solution. Following this, the thermostatic bath was switched on to allow the solution to reach a temperature of 25 ± 1 °C. The initial ratio of H_2O_2 to 4-chlorophenol (molar ratio (R); UV/ H_2O_2 process) ranged from 2 to 400. The initial pH was adjusted as needed. The control sample was collected after adequately

homogenising the solution (homogenisation time: 5 min). Subsequently, the UV-C lamp was switched on and the samples were collected at different time intervals. During the reaction, the temperature of the thermostatic bath was regulated such that the final temperature of the solution was 25 ± 1 °C. All the experiments were conducted thrice. The average standard deviation was less than 5%.

Conclusions

A kinetic model has been proposed to study the changes in the concentration and toxicity during the oxidation process of 4-chlorophenol by UV/H₂O₂. The effect of peroxide dose on degradation was studied to establish the operational conditions that promote the formation of non-toxic or slightly toxic effluents that can be subsequently treated via a biological pathway. The efficiency of the proposed model was calibrated using the experimental data, checking that the mean standard deviation was <0.05.

Based on the identification and analysis of the degradation products, two possible oxidative pathways were proposed, which occur simultaneously. The dose of the oxidant used and the reaction time indicated which of the two pathways would be predominantly operative. The main oxidation intermediates were grouped in different lumps based on various parameters: toxicity, extinction coefficient, and quantum yield.

The model allowed the determination of the kinetic and photolytic parameters. The estimation of these constants allowed the determination of the conditions under which more toxic and recalcitrant by products were formed. Conditions under which less toxic and easily degradable compounds were formed were also determined.

A less toxic effluent (9.95 TU) was produced at a pH of 6.0 when the dose of H₂O₂ was 200 ($R = 200$). Under these conditions, 4-chlorophenol could be degraded completely within 120 min from the start of the reaction. The percentage of mineralisation was approximately 40% and a total loss in colour was observed. This model can be potentially used in industries for the prediction of the operational behaviour of the UV/H₂O₂ system under different working conditions. The model can be used in association with a biological system. Moreover, the behaviour in terms of intermediate formation and toxicity can serve as a reference for other advanced oxidation techniques, including photocatalytic ones, with primary degradation and mineralisation rates similar to those studied here.

Data availability

The datasets generated during and/or analysed during the current study are available from the corresponding author on reasonable request.

Received: 22 March 2021; Accepted: 21 July 2021

Published online: 03 August 2021

References

- Murcia, M. D. *et al.* Assessing combination treatment, enzymatic oxidation and ultrafiltration in a membrane bioreactor, for 4-chlorophenol removal: Experimental and modeling. *J. Membr. Sci.* **342**, 198–207 (2009).
- Zhou, T., Li, Y., Ji, J., Wong, F.-S. & Lu, X. Oxidation of 4-chlorophenol in a heterogeneous zero valent iron/H₂O₂ Fenton-like system: Kinetic, pathway and effect factors. *Sep. Purif. Technol.* **62**, 551–558 (2008).
- Gomez, M. *et al.* A KrCl exciplex flow-through photoreactor for degrading 4-chlorophenol: Experimental and modelling. *Appl. Catal. B* **117–118**, 194–203 (2012).
- Leyva, E., Crispin, I., Moctezuma, E. & Leyva, S. Selective chemical oxidation or reduction of chlorophenols with potassium nitrosodisulfonate. *ARKIVOC* **2003**, 203–212 (2004).
- Chung, S.-G. *et al.* Photocatalytic degradation of chlorophenols using star block copolymers: Removal efficiency, by-products and toxicity of catalyst. *Chem. Eng. J.* **215–216**, 921–928 (2013).
- Valo, R. J., Häggblom, M. M. & Salkinoja-Salonen, M. S. Bioremediation of chlorophenol containing simulated ground water by immobilized bacteria. *Water Res.* **24**, 253–258 (1990).
- Ettala, M., Koskela, J. & Kiesilä, A. Removal of chlorophenols in a municipal sewage treatment plant using activated sludge. *Water Res.* **26**, 797–804 (1992).
- Rafiee, M., Mesdaghinia, A., Ghahremani, M. H., Nasser, S. & Nabizadeh, R. 4-Chlorophenol inhibition on flocculent and granular sludge sequencing batch reactors treating synthetic industrial wastewater. *Desalin. Water Treat.* **49**, 307–316 (2012).
- Ferreiro, C., Villota, N., Lombrana, J. I. & Rivero, M. J. An efficient catalytic process for the treatment of genotoxic aniline wastewater using a new granular activated carbon-supported titanium dioxide composite. *J. Clean. Prod.* **228**, 1282–1295 (2019).
- Ferreiro, C., Villota, N., de Luis, A. & Lombrana, J. I. Analysis of the effect of the operational variants in a combined adsorption-ozonation process with granular activated carbon for the treatment of phenol wastewater. *React. Chem. Eng.* **5**, 760–778 (2020).
- Alfonso-Muniozguren, P. *et al.* Analysis of ultrasonic pre-treatment for the ozonation of humic acids. *Ultrasonics Sonochem.* **105359**. <https://doi.org/10.1016/j.ultsonch.2020.105359> (2020).
- Ferreiro, C. *et al.* Analysis of a hybrid suspended-supported photocatalytic reactor for the treatment of wastewater containing benzothiazole and aniline. *Water* **11**, 337 (2019).
- James, C. P., Germain, E. & Judd, S. Micropollutant removal by advanced oxidation of microfiltered secondary effluent for water reuse. *Sep. Purif. Technol.* **127**, 77–83 (2014).
- Dixit, A., Tirpude, A. J., Mungray, A. K. & Chakraborty, M. Degradation of 2, 4 DCP by sequential biological-advanced oxidation process using UASB and UV/TiO₂/H₂O₂. *Desalination* **272**, 265–269 (2011).
- de Luis, A. & Lombrana, J. I. pH-based strategies for an efficient addition of H₂O₂ during ozonation to improve the mineralisation of two contaminants with different degradation resistances. *Water Air Soil Pollut.* **229**, 372 (2018).
- Marco, A., Esplugas, S. & Saum, G. How and why combine chemical and biological processes for wastewater treatment. *Water Sci. Technol.* **35**, 321–327 (1997).
- Paul Guin, J., Bhardwaj, Y. K. & Varshney, L. Mineralization and biodegradability enhancement of Methyl Orange dye by an effective advanced oxidation process. *Appl. Radiat. Isotopes* **122**, 153–157 (2017).
- Çatalkaya, E. Ç., Bali, U. & Şengül, F. Photochemical degradation and mineralization of 4-chlorophenol. *Environ. Sci. Pollut. Res.* **10**, 113–120 (2003).
- Benitez, F. J., Beltran-Heredia, J., Acero, J. L. & Rubio, F. J. Contribution of free radicals to chlorophenols decomposition by several advanced oxidation processes. *Chemosphere* **41**, 1271–1277 (2000).
- Ameta, S. *Advanced Oxidation Processes for Wastewater Treatment: Emerging Green Chemical Technology*. (2018).

21. Du, P. *et al.* Transformation, products, and pathways of chlorophenols via electro-enzymatic catalysis: How to control toxic intermediate products. *Chemosphere* **144**, 1674–1681 (2016).
22. Munoz, M., de Pedro, Z. M., Casas, J. A. & Rodriguez, J. J. Assessment of the generation of chlorinated byproducts upon Fenton-like oxidation of chlorophenols at different conditions. *J. Hazard. Mater.* **190**, 993–1000 (2011).
23. Karci, A., Arslan-Alaton, I., Olmez-Hanci, T. & Bekbölet, M. Transformation of 2,4-dichlorophenol by H₂O₂/UV-C, Fenton and photo-Fenton processes: Oxidation products and toxicity evolution. *J. Photochem. Photobiol. A* **230**, 65–73 (2012).
24. Santos, A., Yustos, P., Rodriguez, S., Vicente, F. & Romero, A. Kinetic modeling of toxicity evolution during phenol oxidation. *Ind. Eng. Chem. Res.* **48**, 2844–2850 (2009).
25. Ec, C., U. B. & F. S. Photochemical degradation and mineralization of 4-chlorophenol. *Environ. Sci. Pollut. Res. Int.* **10**. <https://pubmed.ncbi.nlm.nih.gov/12729044/> (2003).
26. De Luis, A. M., Lombraña, J. I., Menéndez, A. & Sanz, J. Analysis of the toxicity of phenol solutions treated with H₂O₂/UV and H₂O₂/Fe oxidative systems. *Ind. Eng. Chem. Res.* **50**, 1928–1937 (2011).
27. Kumar, A., Sharma, S. K., Sharma, G., Naushad, M. & Stadler, F. J. CeO₂/g-C₃N₄/V₂O₅ ternary nano hetero-structures decorated with CQDs for enhanced photo-reduction capabilities under different light sources: Dual Z-scheme mechanism. *J. Alloys Compds.* **838**, 155692 (2020).
28. Kumar, A. *et al.* High-performance photocatalytic hydrogen production and degradation of levofloxacin by wide spectrum-responsive Ag/Fe₃O₄ bridged SrTiO₃/g-C₃N₄ plasmonic nanojunctions: Joint effect of Ag and Fe₃O₄. *ACS Appl. Mater. Interfaces* **10**, 40474–40490 (2018).
29. Kumar, A. *et al.* Bio-inspired and biomaterials-based hybrid photocatalysts for environmental detoxification: A review. *Chem. Eng. J.* **382**, 122937 (2020).
30. Ferreiro, C., Villota, N., Lombraña, J. I. & Rivero, M. J. Heterogeneous catalytic ozonation of aniline-contaminated waters: A three-phase modelling approach using TiO₂/GAC. *Water* **12**, 3448 (2020).
31. Zazo, J. A., Casas, J. A., Moledano, A. F., Gilarranz, M. A. & Rodriguez, J. J. Chemical pathway and kinetics of phenol oxidation by Fenton's reagent. *Environ. Sci. Technol.* **39**, 9295–9302 (2005).
32. Hirvonen, A., Trapido, M., Hentunen, J. & Tarhanen, J. Formation of hydroxylated and dimeric intermediates during oxidation of chlorinated phenols in aqueous solution. *Chemosphere* **41**, 1211–1218 (2000).
33. Trapido, M., Veressina, Y., Hentunen, J. K. & Hirvonen, A. Ozonation of chlorophenols: Kinetics, by-products and toxicity. *Environ. Technol.* **18**, 325–332 (1997).
34. Satuf, M. L., Brandi, R. J., Cassano, A. E. & Alfano, O. M. Photocatalytic degradation of 4-chlorophenol: A kinetic study. *Appl. Catal. B* **82**, 37–49 (2008).
35. Murcia, M. D. *et al.* A new substrate and by-product kinetic model for the photodegradation of 4-chlorophenol with KrCl exciplex UV lamp and hydrogen peroxide. *Chem. Eng. J.* **187**, 36–44 (2012).
36. Kusic, H., Koprivanac, N. & Bozic, A. L. Treatment of chlorophenols in water matrix by UV/ferri-oxalate system: Part II. Degradation mechanisms and ecological parameters evaluation. *Desalination* **280**, 208–216 (2011).
37. Hautaniemi, M., Kallas, J., Munter, R. & Trapido, M. Modelling of chlorophenol treatment in aqueous solutions. 1. Ozonation and ozonation combined with UV radiation under acidic conditions. *Ozone Sci. Eng.* **20**, 259–282 (1998).
38. Krebel, M., Kusic, H., Koprivanac, N., Meixner, J. & Bozic, A. L. Treatment of chlorophenols by UV-based processes: Correlation of oxidation by-products, wastewater parameters, and toxicity. *J. Environ. Eng.* **137**, 639–649 (2011).
39. Azevedo, E. B., de Neto, F. R. A. & Dezotti, M. Lumped kinetics and acute toxicity of intermediates in the ozonation of phenol in saline media. *J. Hazard. Mater.* **128**, 182–191 (2006).
40. Kralik, P., Kusic, H., Koprivanac, N. & Loncaric Bozic, A. Degradation of chlorinated hydrocarbons by UV/H₂O₂: The application of experimental design and kinetic modeling approach. *Chem. Eng. J.* **158**, 154–166 (2010).
41. Czaplicka, M. Photo-degradation of chlorophenols in the aqueous solution. *J. Hazard. Mater.* **134**, 45–59 (2006).
42. Mundi, C., Back, M. H. & Back, R. A. Photochemistry of the maleic—Fumaric acid system in aqueous solution at 254 nm. *J. Photochem. Photobiol. A* **67**, 13–22 (1992).
43. Vernon, A. A. & Forbes, G. S. An experiment to determine a photochemical quantum yield. *J. Chem. Educ.* **34**, 350 (1957).
44. Waldner, G., Pourmodjib, M., Bauer, R. & Neumann-Spallart, M. Photoelectrocatalytic degradation of 4-chlorophenol and oxalic acid on titanium dioxide electrodes. *Chemosphere* **50**, 989–998 (2003).
45. Li, X., Cubbage, J. W. & Jenks, W. S. Photocatalytic degradation of 4-chlorophenol. 2. The 4-chlorocatechol pathway. *J. Org. Chem.* **64**, 8525–8536 (1999).
46. Pera-Titus, M., García-Molina, V., Baños, M. A., Giménez, J. & Esplugas, S. Degradation of chlorophenols by means of advanced oxidation processes: A general review. *Appl. Catal. B Environ.* **47**, 219–256 (2004).
47. Bian, W., Song, X., Liu, D., Zhang, J. & Chen, X. The intermediate products in the degradation of 4-chlorophenol by pulsed high voltage discharge in water. *J. Hazard. Mater.* **192**, 1330–1339 (2011).
48. Beltrán, F. J., Rivas, F. J. & Gimeno, O. Comparison between photocatalytic ozonation and other oxidation processes for the removal of phenols from water. *J. Chem. Technol. Biotechnol.* **80**, 973–984 (2005).
49. Rayne, S., Forest, K. & Friesen, K. J. Mechanistic aspects regarding the direct aqueous environmental photochemistry of phenol and its simple halogenated derivatives. A review. *Environ. Int.* **35**, 425–437 (2009).
50. Ronco, A. E., Castillo, G. & DiAz-Baez, M. C. Development and application of microbioassays for routine testing and biomonitoring in Argentina, Chile and Colombia. in *New Microbiotests for Routine Toxicity Screening and Biomonitoring* (eds. Persoone, G., Janssen, C. & De Coen, W.) 49–61. https://doi.org/10.1007/978-1-4615-4289-6_5 (Springer, 2000).
51. Eisenberg, G. Colorimetric determination of hydrogen peroxide. *Ind. Eng. Chem. Anal. Ed.* **15**, 327–328 (1943).
52. Villota, N. *et al.* Colour changes during the carbamazepine oxidation by photo-fenton. *Catalysts* **11**, 386 (2021).
53. Association, A. P. H. *Standard Methods for the Examination of Water & Wastewater*. (American Public Health Association, 2005).

Acknowledgements

The authors are grateful to the University of the Basque Country (UPV/EHU) for their financial support of this study through the PPGA20/33 project, and C. Ferreiro's predoctoral PIF grant (PIF16/367).

Author contributions

J.S. and C.F.: Conceptualisation, Methodology, Investigation, Validation, Data curation, and final editing. N.V.: Write fundamentals and Writing-review. J.I.L. and A.d.L.: Funding acquisition, Resources, and Writing-review. All authors reviewed the manuscript.

Competing interests

The authors declare no competing interests.

Additional information

Supplementary Information The online version contains supplementary material available at <https://doi.org/10.1038/s41598-021-95083-7>.

Correspondence and requests for materials should be addressed to C.F.

Reprints and permissions information is available at www.nature.com/reprints.

Publisher's note Springer Nature remains neutral with regard to jurisdictional claims in published maps and institutional affiliations.



Open Access This article is licensed under a Creative Commons Attribution 4.0 International License, which permits use, sharing, adaptation, distribution and reproduction in any medium or format, as long as you give appropriate credit to the original author(s) and the source, provide a link to the Creative Commons licence, and indicate if changes were made. The images or other third party material in this article are included in the article's Creative Commons licence, unless indicated otherwise in a credit line to the material. If material is not included in the article's Creative Commons licence and your intended use is not permitted by statutory regulation or exceeds the permitted use, you will need to obtain permission directly from the copyright holder. To view a copy of this licence, visit <http://creativecommons.org/licenses/by/4.0/>.

© The Author(s) 2021

3.2. 2. argitalpena. Turbidity changes during carbamazepine oxidation by photo-Fenton

3.2 kapitulua artikulu honi dagokio:

N. Villota, C. Ferreiro, H.A. Qulatein, J.M. Lomas, J.I. Lombraña. Turbidity changes during carbamazepine oxidation by photo-Fenton. *Catalysts*, 11, 8, 894, 2021. DOI: 10.3390/catal11080894.

Article

Turbidity Changes during Carbamazepine Oxidation by Photo-Fenton

Natalia Villota ^{1,*} , Cristian Ferreiro ² , Hussein A. Qulatein ³ , Jose M. Lomas ¹ and Jose Ignacio Lombraña ² 

- ¹ Department of Environmental and Chemical Engineering, Faculty of Engineering of Vitoria-Gasteiz, University of the Basque Country, UPV/EHU, 01006 Vitoria-Gasteiz, Spain; josemaria.lomas@ehu.eus
- ² Department of Chemical Engineering, Faculty of Science and Technology, University of the Basque Country, UPV/EHU, 48940 Leioa, Spain; cristian.ferreiro@ehu.eus (C.F.); ji.lombrana@ehu.eus (J.I.L.)
- ³ Department of Chemical Engineering, Faculty of Engineering, Anadolu University, 26470 Eskişehir, Turkey; husseinqulatein@gmail.com
- * Correspondence: natalia.villota@ehu.eus; Tel.: +34-945013248

Abstract: The objective of this study is to evaluate the turbidity generated during the Fenton photo-reaction applied to the oxidation of waters containing carbamazepine as a function of factors such as pH, H₂O₂ concentration and catalyst dosage. The results let establish the degradation pathways and the main decomposition byproducts. It is found that the pH affects the turbidity of the water. Working between pH = 2.0 and 2.5, the turbidity is under 1 NTU due to the fact that iron, added as a catalyst, is in the form of a ferrous ion. Operating at pH values above 3.0, the iron species in their oxidized state (mainly ferric hydroxide in suspension) would cause turbidity. The contribution of these ferric species is a function of the concentration of iron added to the process, verifying that the turbidity increases linearly according to a ratio of 0.616 NTU L/mg Fe. Performing with oxidant concentrations at (H₂O₂) = 2.0 mM, the turbidity undergoes a strong increase until reaching values around 98 NTU in the steady state. High turbidity levels can be originated by the formation of coordination complexes, consisting of the union of three molecules containing substituted carboxylic groups (BaQD), which act as ligands towards an iron atom with Fe³⁺ oxidation state.

Keywords: BaQD; carbamazepine; ferric coordination complex; photo-Fenton; turbidity



Citation: Villota, N.; Ferreiro, C.; Qulatein, H.A.; Lomas, J.M.; Lombraña, J.I. Turbidity Changes during Carbamazepine Oxidation by Photo-Fenton. *Catalysts* **2021**, *11*, 894. <https://doi.org/10.3390/catal11080894>

Academic Editor: Enric Brillas

Received: 25 June 2021

Accepted: 21 July 2021

Published: 24 July 2021

Publisher's Note: MDPI stays neutral with regard to jurisdictional claims in published maps and institutional affiliations.



Copyright: © 2021 by the authors. Licensee MDPI, Basel, Switzerland. This article is an open access article distributed under the terms and conditions of the Creative Commons Attribution (CC BY) license (<https://creativecommons.org/licenses/by/4.0/>).

1. Introduction

Over the last decade, special attention has been paid to the presence in waters (in relation to both their distribution and concentration) of certain organic compounds that, until now, had not been considered significant dangerous species. This is related to the improvement of analytical technique, as formerly undetected organic components are being more widely observed, considering that they have the potential to cause adverse effects both environmentally and in living beings [1].

Specifically, preventive measures are being adopted to control the emissions of pharmaceutically active products (PhACs) on environmental systems due to the harmful impacts that they can cause both on aquatic life and on human health [2] because they are recalcitrant compounds that generate toxicity [3,4]. The frequent presence of PhACs in freshwater and wastewater has promoted the establishment of water quality standards for periodic monitoring [5]. Thus, carbamazepine (CBZ) is proposed as an anthropogenic marker of water contamination, caused by its persistence in conventional water treatment plants, also being perceptible in some freshwater systems [6–8].

CBZ is an anticonvulsive and mood-stabilizing drug, which is used primarily in the treatment of epilepsy and bipolar disorder [9]. After consumption, around 10% of CBZ is excreted from the human body [10]. Besides, CBZ is the main cause of Stevens–Johnson syndrome that can cause toxic epidermal necrolysis [11]. This skin condition is potentially fatal, with a mortality rate of 30%, in which cell death causes the epidermis to separate

from the dermis [12]. On the other hand, intrauterine exposure to CBZ is associated with a congenital defect of the spine and spinal cord, spina bifida [13] and problems with the neurodevelopmental embryo [14]. Moreover, higher fetal losses, as well as congenital malformation rates, have been reported among women consuming carbamazepine during pregnancy [15]. For these reasons, the presence of CBZ in drinking water and some groundwater is a cause for concern since it constitutes a risk factor as a possible route of access to the embryo and the infant through intrauterine exposure or breastfeeding.

A large part of the PhACs reach the wastewater through human body excretion and, if they are not effectively eliminated in the water treatment plants (WWTPs), both the effluent and the sludge lead to an important source of spreading PhACs in the environment [16,17]. In particular, conventional wastewater treatment plants remove less than 10% of the CBZ contained in the input influents [18–20]. Thus, WWTP effluents are an important gateway for CBZ accessing surface and groundwater. In general, the concentration of CBZ is higher in WWTPs than in exterior waters because the dilution phenomena and natural attenuation significantly reduce the concentration of these pollutants [21].

The need to effectively eliminate PhACs has promoted Advanced Oxidation Processes, known as AOPs [22]. Among the AOPs with the greatest applications stand out the technologies based on oxidation with ozone [23], electrochemical oxidation, photocatalysis based on the use of UV and Fenton processes [24] and photo-Fenton [25,26]. However, it should be noted that the oxidation with ozone, although highly reactive with organic compounds that have olefins or amines in their internal structure, is less effective when applied in the degradation of the CBZ and ibuprofen [27,28]. In electrochemical oxidation, the materials making up the electrodes are a limiting factor for industrial application. Besides, Fenton-like processes produce hydroxyl radicals, which are strong oxidizing agents capable of degrading a wide range of polluting organic compounds. However, the traditional Fenton reagent requires a continuous supply of Fe^{2+} , which produces an excess of iron in the generated sludge [29]. To alleviate this drawback, this work applies photo-Fenton technology since UV light increases the efficiency of the process. Therefore, the concentrations of Fe (II) utilized can be much smaller than in the conventional Fenton reaction.

This study evaluates the Fenton photo-reaction applied to the degradation of CBZ as a function of several factors, such as pH, hydrogen peroxide concentration and catalyst dosage. Experimental assays allow checking that during the oxidation treatment, the treated waters acquire high levels of turbidity depending on the operating conditions used in the tests. In this way, the aim of this work has been to establish the causes of turbidity in the treated water and the factors that affect it, relating the formation of turbidity with the degradation pathways and the main decomposition byproducts causing turbidity. Several references reported in the bibliography have studied the photo-Fenton treatment applied to carbamazepine degradation in domestic wastewater [30]. In general, the main objectives of these works are based on the intensification of ultraviolet technology combined with other AOPs as iron complexes or ultrasound waves [27,31] and the use of solar light improving the operational cost [32,33]. However, the novelty of this work is to analyze and establish the selectivity of the degradative routes of CBZ to water-turbidity generation as a function of the operating conditions.

2. Results

2.1. Turbidity Changes during Carbamazepine Oxidation

During the degradation of aqueous solutions containing different drugs, using a photo-Fenton process, it is found that turbidity appears in the treated water (see Figure 1a). The turbidity control of the water is closely related to the effectiveness of the disinfection processes, both chemical (chlorine or other biocides) and physical (UV radiation). This is due to the particles causing turbidity, which reduce the efficiency of the processes of chlorination in the elimination of pathogenic organisms, since they physically protect microorganisms from direct contact with the disinfectant. Although the direct effects of

turbidity on health are not known yet, it affects the organoleptic properties of the water, which is why it often causes the rejection of consumers.

As shown in Figure 1a, the turbidity generated is a function of the type of pollutant that the water contains, as well as the operating conditions used in the oxidation treatment. Comparing these results with those shown in Figure 1b for the case of carbamazepine oxidation, when carrying out photo-oxidation using oxidant concentrations (H_2O_2) = 15.0 mM, the oxidized water presents turbidity levels of 4.6 NTU. Meanwhile, when using (H_2O_2) = 2.0 mM, the turbidity of the water increases to levels of 19.0 NTU after 120 min of reaction. For this reason, it is necessary to perform specific studies for each kind of effluent, since the turbidity will be determined by the presence of PhACs contained in the water, as a consequence of the human activities in the emission sources.

Globally, the World Health Organization (WHO) Quality Guidelines for Water for Human Consumption recommends a maximum of 5 NTU as a reference value, although the WHO indicates that, to achieve efficient disinfection, the water must have average turbidity lower than or equal to 1 NTU. Considering Spain, turbidity is a parameter included in current regulations, where its maximum permitted limits are regulated in Royal Decree 140/2003 [34] on hygienic–sanitary criteria of water for human consumption and Royal Decree 1620/2007 [35] on reuse of purified waters.

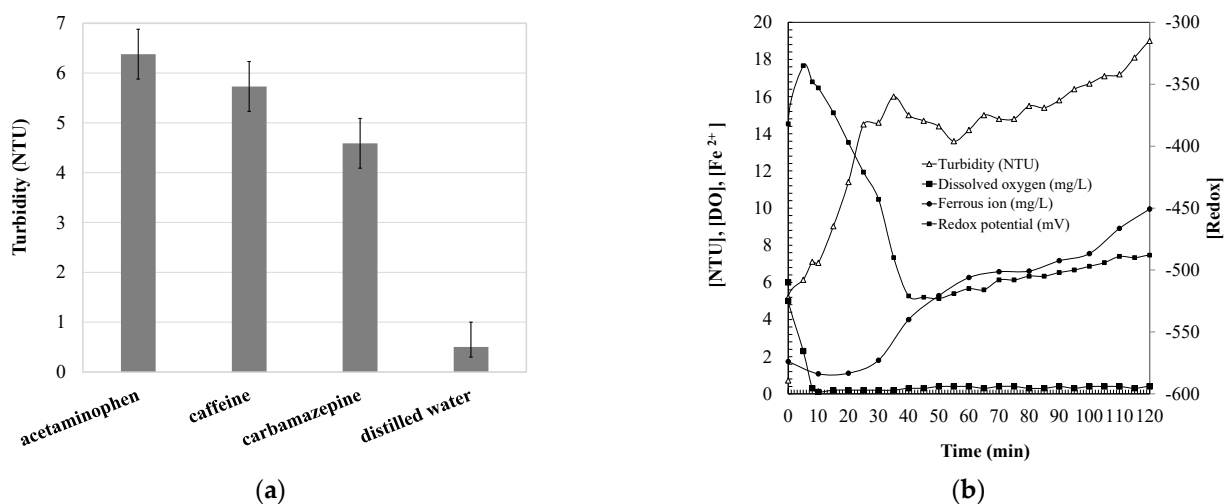


Figure 1. (a) Turbidity analyzed on aqueous solutions containing different PhACs oxidized by photo-Fenton. Experimental conditions: (C) = 50.0 mg/L; pH = 3.0; (H_2O_2) = 15.0 mM; (Fe) = 10.0 mg/L; (UV) = 150 W; T = 25 °C. (b) Water quality indicators analyzed during the carbamazepine oxidation by photo-Fenton. Experimental conditions: (CBZ) = 50.0 mg/L; pH = 3.0; (H_2O_2) = 2.0 mM; (Fe) = 10.0 mg/L; (UV) = 150 W; T = 25 °C.

On the other hand, Figure 1b represents turbidity as a function of other signs of water quality, such as the redox potential and the concentrations of ferrous ion and dissolved oxygen. As displayed, the results do not indicate a direct relationship with the formation of turbidity. Thus, a more in-depth analysis is necessary to estimate the effect of the main operating parameters of the photo-Fenton treatment on the formation of turbidity. In this work, pH, oxidant and catalyst dosage are considered.

2.2. pH Effect

Figure 2a shows the changes in turbidity of the aqueous solutions containing CBZ during their degradation, using the photo-Fenton process, where the pH of each test varied between pH = 2.0 and 5.0. It should be noted that the pH value has remained constant throughout the reaction. These results let verify that acidity affects the formation of turbidity in the water. However, its formation does not follow a linear relationship with the pH, but rather, three general ranges of operation are observed.

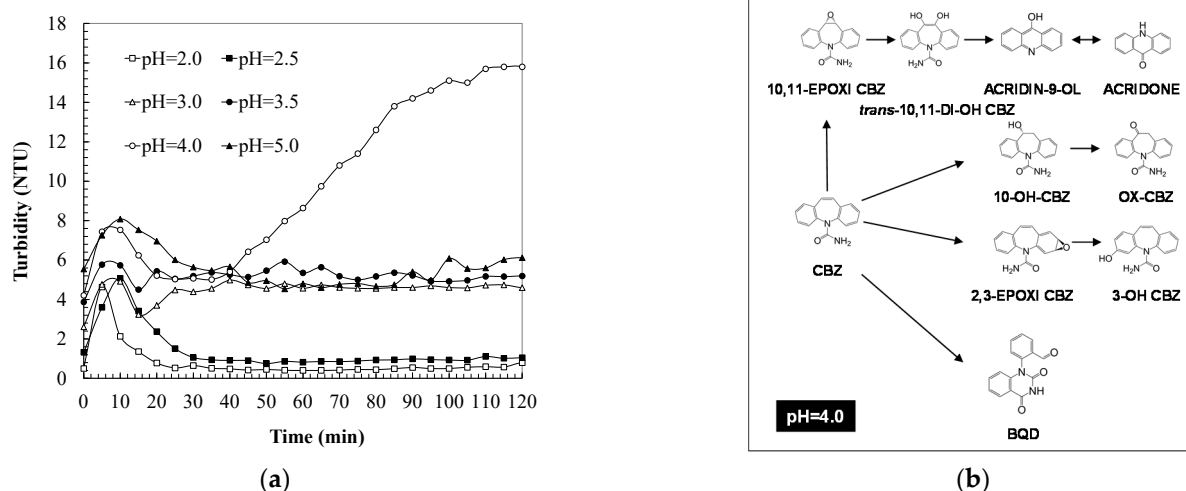


Figure 2. (a) pH effect on turbidity changes in a photo-Fenton system during the carbamazepine oxidation. (b) Equilibrium-species in carbamazepine aqueous solutions oxidized at pH = 4.0 by photo-Fenton treatment. Experimental conditions: (CBZ) = 50.0 mg/L; (H₂O₂) = 15.0 mM; (Fe) = 10.0 mg/L; (UV) = 150 W; T = 40 °C.

When applying acidity between pH = 2.0 and 2.5, the turbidity of the treated water is less than 1 NTU. This indicates that they are accepted by the legislation, which establishes the water quality criteria for both consumption and reuse. Oxidized water samples were analyzed to test carbamazepine degradation intermediates that coexist in the solution once a steady state is reached (see Appendix A, Table A1). The reason that these intermediate species cause low levels of turbidity is due to the fact that, performing at a controlled pH = 2.0–2.5, the iron species added in the form of a catalyst are present as ferrous ions. Iron species in their reduced state have a low capacity to react with organic matter, forming metallic complexes or inorganic hydroxides that cause turbidity.

The intermediates detected operating at pH = 2.0 allow proposing the degradation mechanism shown in Figure 3a, where CBZ would be oxidized through four main degradation routes. The dihydroxylation of the central benzene ring in the cis position of the hydroxyl groups, which would lead to obtaining acridones through the formation of hydroxylated acridines (Acridin-9-ol). On the other hand, the two benzene rings located at the extremes of the CBZ molecule would be hydroxylated, giving rise to the simultaneous formation of 3-hydroxy-carbamazepine (3-OH CBZ) and 2-hydroxy-carbamazepine (2-OH CBZ). Moreover, the attack of the aromatic ring of CBZ, according to the Criegee mechanism, would lead to the formation of 1-(2-benzaldehyde)-4-hydro-(1H,3H)-quinazoline-2-one (BQM) after intramolecular reactions and rearrangements. The reaction of BQM with hydroxyl radicals would lead to the formation of 1-(2-benzaldehyde)-(1H, 3H)-quinazoline-2,4-dione (BQD) [20,36]. Finally, the aldehyde group of the BQD could react with the hydroxyl radicals giving rise to the formation of the carboxyl group, generating the molecular structure 1-(2-benzoic acid)-(1H, 3H) -quinazoline-2,4-dione (BaQD), [37,38].

Conducting at pH values 3.0 and 3.5, turbidity around 5 NTU was observed, which would be the maximum limit value accepted by the water legislation. In tests performed at pH = 5.0, kinetic results were obtained that lead to similar turbidity. Besides, the intermediates that contain the oxidized CBZ samples were analyzed, operating at pH = 3.0 (see Table A2) and pH = 5.0 (see Table A4), in such a way that they allow to propose the potential degradation mechanisms of CBZ. It is found that, when carrying out the oxidation of CBZ both at pH = 3.0 and at pH = 5.0 controlled throughout the process, the four degradation pathways observed when operating at pH between 2.0 and 2.5 are kept, although with some nuances.

Figure 3b displays the CBZ degradation mechanism proposed for the assay conducted at a controlled pH = 5.0. In this case, the formation of the epoxide group in the central benzene ring, 10,11 epoxy-carbamazepine (10,11-Epoxy CBZ), is detected, which leads to the for-

mation of the two dihydroxylated isomers in cis positions 10,11-dihydroxycarbamazepine (cis 10,11-DiOH-CBZ) and trans 10,11-dihydroxycarbamazepine (trans 10,11-DiOH-CBZ). In turn, both are degraded, generating acridin-9-ol and acridone. On the other hand, the hydroxylation of the central benzene ring occurs, giving rise to the formation of 10-hydroxycarbamazepine (10-OH CBZ), as well as the hydroxylation of the lateral ring generating 2-hydroxycarbamazepine (2-OH CBZ). Moreover, the presence of (BQD) was tested. Given that the nature of the CBZ degradation intermediates analyzed does not present relevant structural differences with respect to the species detected in the previous case, operating at pH = 2.0, it should be considered that iron species could be the species directly affected by the change in the applied pH. In the case of conducting at pH = 3.0 and 5.0, iron would be found mainly in the form of ferric ions. However, when degrading intermediates of CBZ, the formation of metallic complexes between organic matter and ferric ions does not seem important. It would be more accurate to consider that the direct cause of turbidity formation would be the presence of ferric hydroxide in the solution, which would remain in suspension, and that would be a function of the concentration of iron added to the system. In this case, the tests were conducted at (Fe) = 10.0 mg/L, and the turbidity of the water was similar.

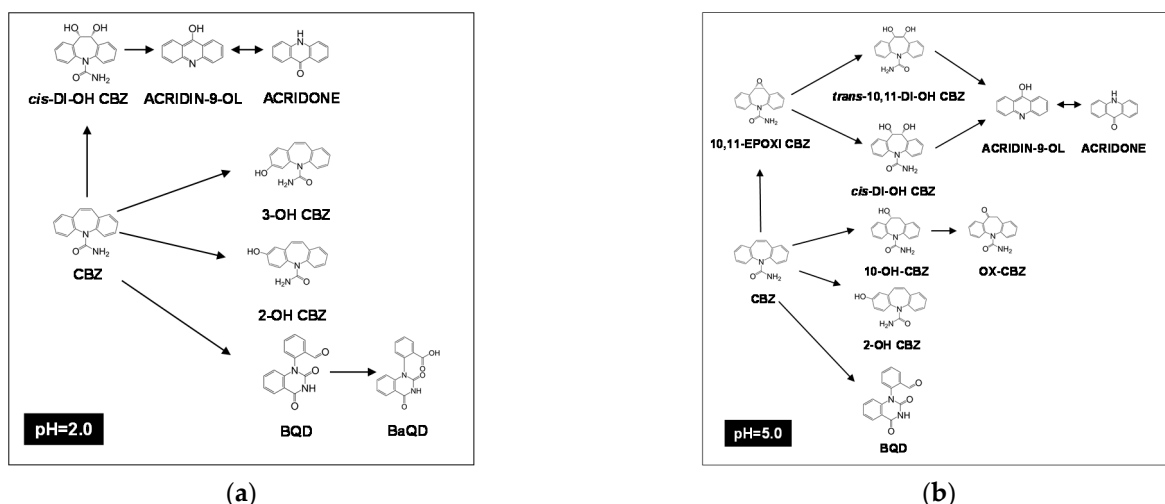


Figure 3. Equilibrium-species in carbamazepine aqueous solutions oxidized by photo-Fenton treatment. (a) Operating at pH = 2.0. (b) Operating at pH = 5.0. Experimental conditions: (CBZ) = 50.0 mg/L; (H₂O₂) = 15.0 mM; (Fe) = 10.0 mg/L; (UV) = 150 W; T = 40 °C.

When carrying out the treatment operating at pH = 4.0, Figure 2a shows that the turbidity potentially increases, reaching maximum values around 16 NTU at 120 min of reaction. However, it is noted that as the oxidation process progresses, the turbidity decreases, reaching values about 5 NTU in the steady state.

To explain this effect, the oxidized water was analyzed at pH = 4.0 (see Table A3), where, from the results obtained, the degradation mechanism shown in Figure 2b is proposed. In a similar way to the rest of the assays, four main degradation pathways are detected, towards the formation of acridon, in this case, through the trans isomer 10,11-DiOH-CBZ, as well as the hydroxylation pathways through the central and lateral benzene ring of CBZ, confirming the formation of BQD and its subsequent oxidation-generating BaQD.

It should be remarked that in all the tests performed during the first 30 min of reaction, a small turbidity peak occurs, whose maximum increases proportionally with the pH. In the case of operating at pH = 4.0, a second turbidity peak appears, with a larger area, which is not observed in the rest of the experiments. This significant increase in turbidity may be due to the formation of ferric species that remain in suspension during the first two

hours of the reaction. Afterward, they slowly precipitate until a solution is obtained with turbidity not exceeding 5 NTU.

These results allow us to consider that the iron species, mainly ferric hydroxide, cause turbidity changes when varying the operational pH. Therefore, when applying $\text{pH} = 4.0$, which means that iron is mainly found as a ferric ion, and since the same initial iron catalyst concentration is used ($[\text{Fe}] = 10.0 \text{ mg/L}$), the final turbidity of the treated water is similar to that of the oxidized samples at $\text{pH} = 3.0\text{--}5.0$, which fluctuate around 5 NTU.

The effect of hydrogen peroxide dosage on the formation of turbidity during the oxidation of CBZ was analyzed using a photo-Fenton treatment (see Figure 4a). The tests were performed varying the concentration of oxidant dosed between 2.0 and 15.0 mM, keeping steady the dosage of iron, added as a catalyst in the form of ferrous ion, at 10.0 mg/L and $\text{pH} = 0$. Checking turbidity in the water during the oxidation of CBZ shows three operating ranges that lead to similar turbidity levels. This fact could indicate that the dose of hydrogen peroxide would affect the selectivity of the oxidation pathways of CBZ, leading to the formation of degradation intermediates that cause turbidity.

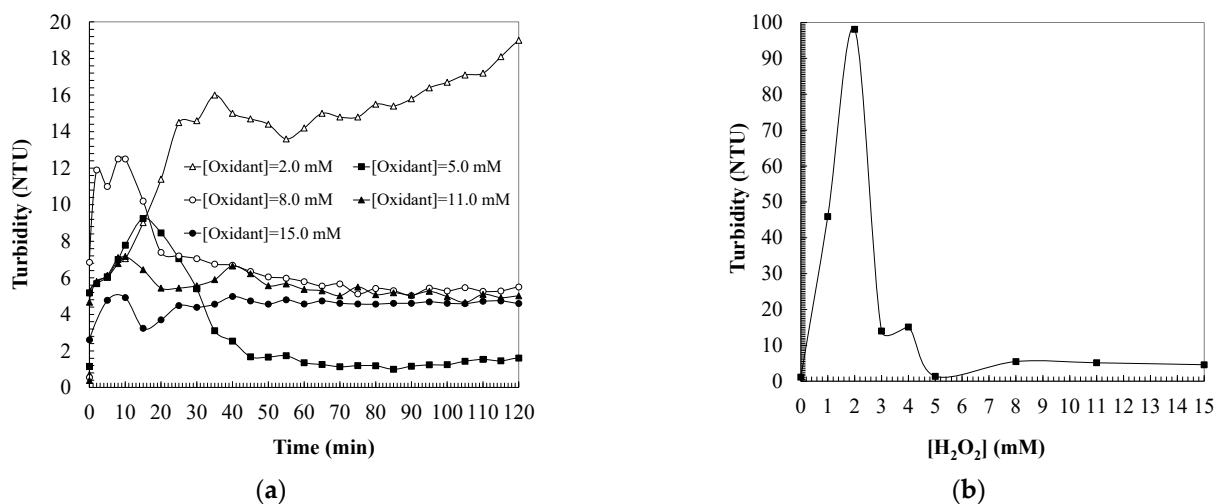


Figure 4. (a) Effect of hydrogen peroxide concentration ($[\text{Oxidant}]$, mM) on turbidity changes in a photo-Fenton system during the carbamazepine oxidation. (b) Effect of hydrogen peroxide on the solutions turbidity once achieved the steady state. Experimental conditions: $(\text{CBZ}) = 50.0 \text{ mg/L}$; $\text{pH} = 3.0$; $(\text{Fe}) = 10.0 \text{ mg/L}$; $(\text{UV}) = 150 \text{ W}$; $T = 40 \text{ }^\circ\text{C}$.

When applying oxidant concentrations between $(\text{H}_2\text{O}_2) = 8.0$ and 15.0 mM , a slight peak of turbidity appears during the first 20 min of the oxidation. It is verified that the maximum turbidity value of the peak is a function of the oxidant concentration. Therefore, that, using $(\text{H}_2\text{O}_2) = 8.0 \text{ mM}$, produces a maximum turbidity of 12.5 NTU. Meanwhile, $(\text{H}_2\text{O}_2) = 1.0 \text{ mM}$ produces 7.2 NTU and $(\text{H}_2\text{O}_2) = 15.0 \text{ mM}$ creates 5.0 NTU. Once the peak arises, the turbidity evolves according to the kinetics of parallel trend until it coincides in similar values. Besides, it happens that in the steady state (see Figure 4b), the water treated under these conditions presents turbidity around 5 NTU. This result could indicate that the turbidity-causing intermediates formed during the first 20 min, which are dependent on the oxidation degree of the CBZ reached by using different doses of oxidant, are degraded to species of a similar nature.

Experimenting with oxidant concentrations $(\text{H}_2\text{O}_2) = 5.0 \text{ mM}$, the formation of a turbidity peak is observed during the first 60 min of CBZ oxidation. In this case, the pinnacle is of greater area than in the previous interval. Moreover, it is verified that the turbidity evolves to values near 1.5 NTU in the steady state (see Figure 4b). Performing with oxidant concentrations $(\text{H}_2\text{O}_2) = 2.0 \text{ mM}$, the water turbidity undergoes a notable increase during the first 30 min of oxidation of the CBZ, following a linear ratio of 0.34 NTU/min . Subsequently, the turbidity increases over time, but more slowly, at a rate of 0.057 NTU/min , until reaching around 98 NTU in the steady state (see Figure 4b). This result would indicate

that CBZ degradation occurs through serial reactions that lead to the formation of species of a different nature, which cause turbidity.

Next, the treated water was analyzed using the oxidant dose (H_2O_2) = 2.0 mM to determine the degradative routes of CBZ towards the formation of species causing turbidity since it creates the highest turbidity in the tests conducted (see Figure 5a). These results allow us to verify that the four general pathways of CBZ degradation observed in the study of the effect of pH also occur here. The oxidation proceeds towards the production of acridones through the formation of the epoxide in the central benzene ring of CBZ, as well as the creation of the epoxide group in the lateral benzene ring, which leads to the development of hydroxylated species 2-OH-CBZ. On the other hand, hydroxylation reactions happen in the central benzene ring of CBZ, with the consequent formation of OX-CBZ and degradation towards the formation of BQD and BaQD.

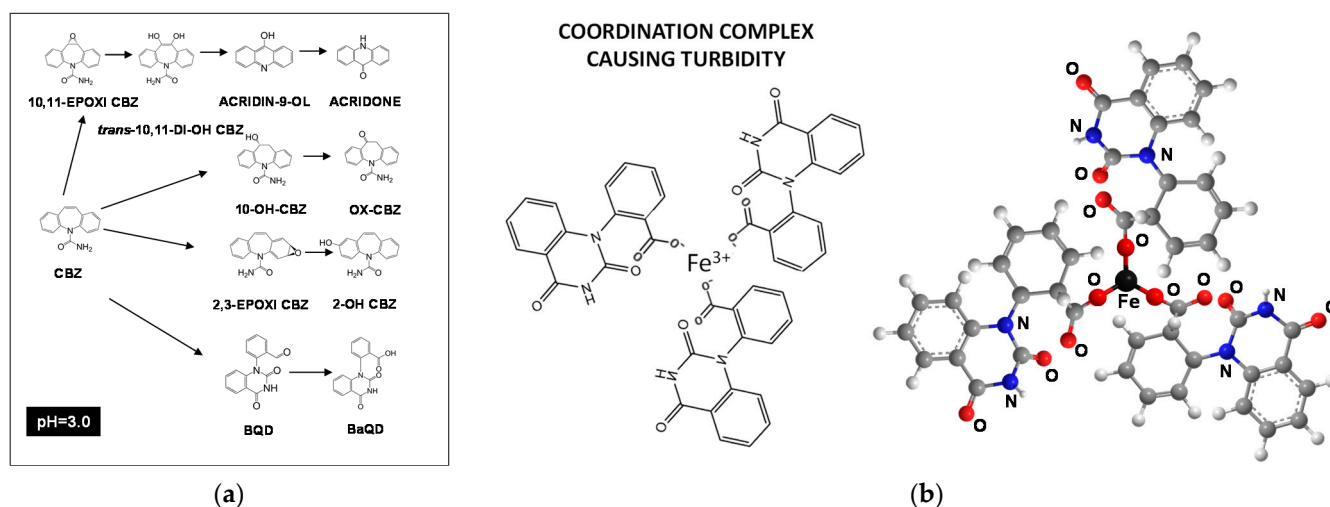


Figure 5. (a) Equilibrium-species in carbamazepine aqueous solutions oxidized by photo-Fenton treatment operating at pH = 3.0. (b) Molecular structure in 2D and 3D of possible coordination iron complex BaQD-Fe(III) causing turbidity in water. Experimental conditions: (CBZ) = 50.0 mg/L; pH = 3.0; (H_2O_2) = 2.0 mM; (Fe) = 10.0 mg/L; (UV) = 150 W; T = 40 °C.

Given the molecular structures of the species detected, it does not seem conceivable that the formation of intermolecular hydrogen bondings generates stable structures of a purely organic nature. In this case, it is contemplated that there are ferric species in the system, since the tests were performed at pH = 3.0, which determines the distribution of the iron species in the solution. Based on this premise, it is plausible that the high levels of turbidity generated in the water when using oxidant concentrations (H_2O_2) = 2.0 mM can be caused by the formation of coordination complexes. They consist of the union of three molecules containing substituted carboxylic groups (BaQD), which act as ligands towards an iron atom with oxidation state 3⁺, whose molecular structure is shown in Figure 5b.

2.3. Effect of Iron Catalyst

The effect of iron dosage, used as a catalyst, was studied, working with concentrations between (Fe) = 5.0 and 40.0 mg/L (see Figure 6a) and keeping steady the oxidant concentration and pH. The results indicate that the turbidity kinetics analyzed during the oxidation of CBZ show a parallel evolution in all the tests, where the turbidity increases linearly with the iron concentration according to a ratio of 0.616 NTU L/mg Fe (see Equation (1)). These results demonstrate that iron does not affect the CBZ degradation mechanism. Furthermore, by operating at a constant pH, the distribution of ferrous and ferric species in solution is kept constant. Finally, the concentration of iron species was analyzed, verifying that the catalyst is mainly found as ferric species (see Figure 6b).

$$[\text{NTU}] = [\text{NTU}]_0 + 0.6159 [\text{Fe}] \quad (r^2 = 0.9804) \quad (1)$$

Being that:

[NTU]₀: turbidity of the aqueous solution of CBZ (=0.2261 NTU);

[NTU]: water turbidity (NTU);

[Fe]: initial iron concentration (mg/L).

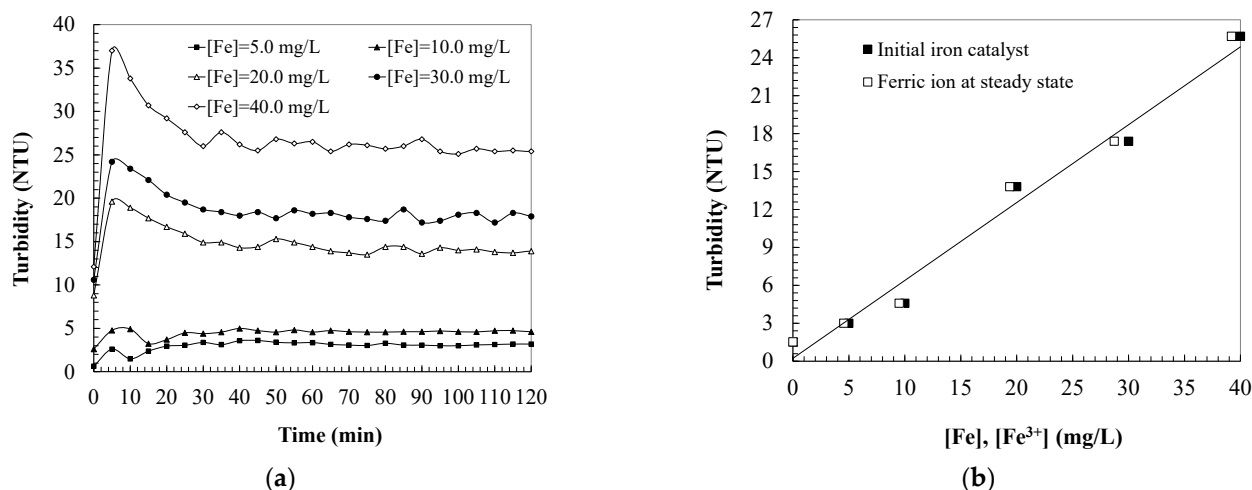


Figure 6. (a) Effect of iron catalyst on turbidity changes in a photo-Fenton system during the carbamazepine oxidation. (b) Effect of iron concentration on the solutions turbidity once the steady state is achieved. Experimental conditions: (CBZ) = 50.0 mg/L; pH = 3.0; (H₂O₂) = 15.0 mM; (UV) = 150 W; T = 40 °C.

3. Materials and Methods

3.1. Experimental Methods

Samples of carbamazepine aqueous solutions ((CBZ) = 50.0 mg/L, Fagron 99.1%) were studied in a photocatalytic 1.0 L reactor provided with a UV-150W mercury lamp of medium pressure (Heraeus, 95% transmission between 300 and 570 nm). Reactions began adding the iron catalyst as ferrous ion ((Fe), mg/L) operating between (Fe)₀ = 5.0–40.0 mg/L (FeSO₄ 7H₂O, Panreac 99.0%) and the oxidant dosage for each set of experiments, which varied between (H₂O₂) = 0–15.0 mM (Panreac, 30% w/v). All the experiments were carried out at around 40 °C in order to simulate real operating conditions, considering the heat absorbed by the water that is in direct contact with the ultraviolet lamp. Assays were performed operating under different initial pH conditions (pH between 2.0 and 5.0) in order to assess the effect of this parameter on color formation during oxidation of carbamazepine aqueous solutions. Acidity was kept constant, adding NaOH and HCl 0.1M.

3.2. Analytical Methods

Turbidity (NTU) was analyzed by a turbidimeter (100Q-Hach) and ferrous ion (Fe²⁺, mg/L) by the phenanthroline method at λ = 510 nm (Fortune, 1938) using a UV/Vis Spectrophotometer 930-Uvikon, Kontron Instruments (Mazowieckie, Poland). Dissolved oxygen (DO, mg/L) was assessed by a Polarographic Portable Dissolved Oxygen Meter HI9142, Hanna Instruments, S.L. (Eibar, Spain). Total dissolved solids (TDS, mg/L) were analyzed by a TDS Metter Digital and redox potential (V) by a conductimeter Basic 20 Crison, Hach (Derio, Spain).

3.3. Liquid Chromatography-Mass Spectrometry to Elucidate the Intermediates of Carbamazepine Degradation

Samples were stored after receipt under refrigeration. Samples were centrifuged and subsequently diluted before starting analysis. The analysis was carried out with an LC/Q-TOF, with ESI+ Agilent Jet Stream ionization source and the following conditions: column: Kinetex EVO C18 HPLC/UHPLC Core-Shell (100 × 3 mm) 2.6 μm (Phenomenex company, Tianjin, China). Mobile phase 0.1% formic acid (A): acetonitrile with 0.1% of

formic acid (B). Gradient: %B: 20; 20; 100; 100; 20 vs. time: 0; 2; 24; 28; 30. Flow: 0.3 mL/min. Column temperature: 35 °C. Injection volume: 5 μ L. Ionization: Gas T = 300 °C; drying gas 10 L/min; Nebulizer 20 psig; shealt gas T = 350 °C; shealt gas flow 11 L/min; frag 125 V. Vcap 3500 V.

A screening method was developed to allow the elution and ionization of the greater number of compounds present in the sample. The stabilization of the system, the reproducibility of the signals and the correction of the exact mass were checked before starting the analysis. The compounds were searched using the deconvolution algorithm "Find by molecular features" and subsequent filtering of the proposed compounds based on compounds detected in the blank, background noise and minimum abundance of the compound. The following chromatograms show the major compounds observed for each of the samples (Figure 7). Under the proposed conditions, the following chromatograms were obtained for each of samples at pH=2.0, 3.0, 4.0 and 5.0 (Figures 8–11).

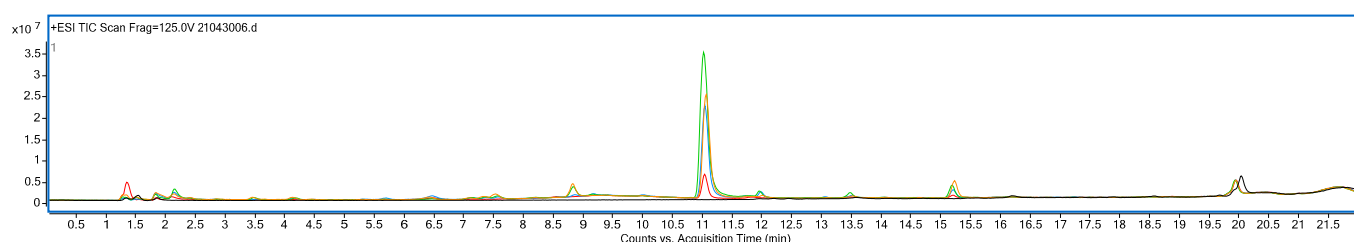


Figure 7. Chromatographic profile of a methanol blank (black line) and samples (red, blue, orange and green line).

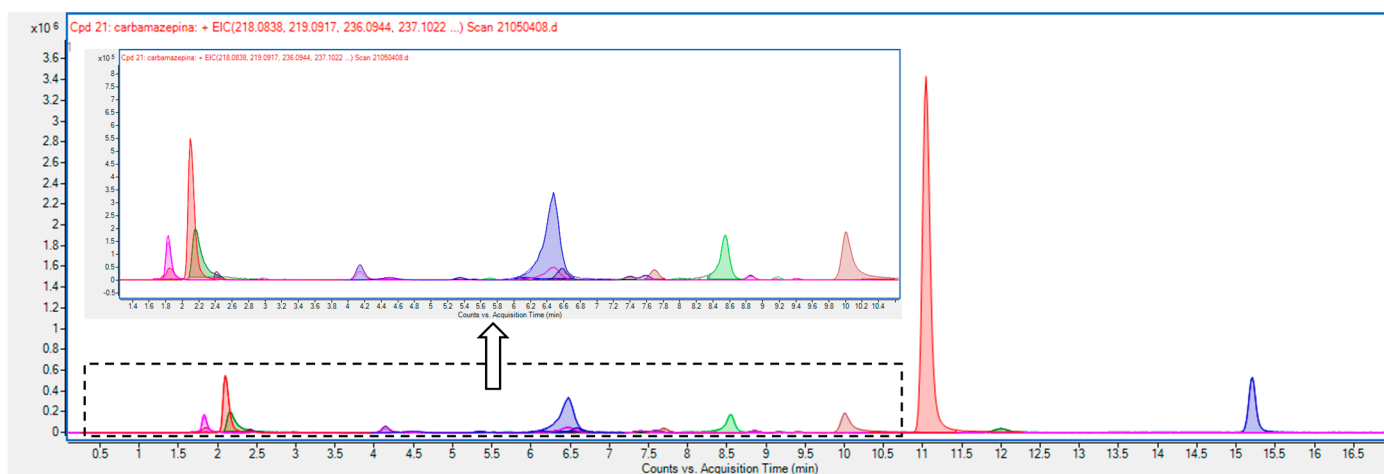


Figure 8. Chromatographic profile of the major compounds detected in the sample of carbamazepine oxidized to pH = 2.0. Experimental conditions: (CBZ) = 50.0 mg/L; (Fe) = 10 mg/L; (H₂O₂) = 15.0 mM; T = 25 °C; (UV) = 150 W.

In order to try to identify the greatest number of compounds, standards of possible carbamazepine degradation compounds were initially prepared to check their retention time and mass spectra. The following commercial standards were used: carbamazepine (CBZ), oxo-carbamazepine (Oxo-CBZ), carbamazepine 10, 12-epoxide (Epoxi-CBZ), 11-dihydro-10-hydroxycarbamazepine (10-OH CBZ), 9-acridanone, acridin-9-ol, 4-aminophenol, malonic acid (Figure 12).

Using the method developed for the screening, the following retention times (Tr) and characteristic ions or mass/charge ratios (m/z) were obtained for each compound (Table 1). Appendix A summarizes the predominant compounds found, as well as their characteristic ions (m/z) and the experimental masses calculated for each sample.

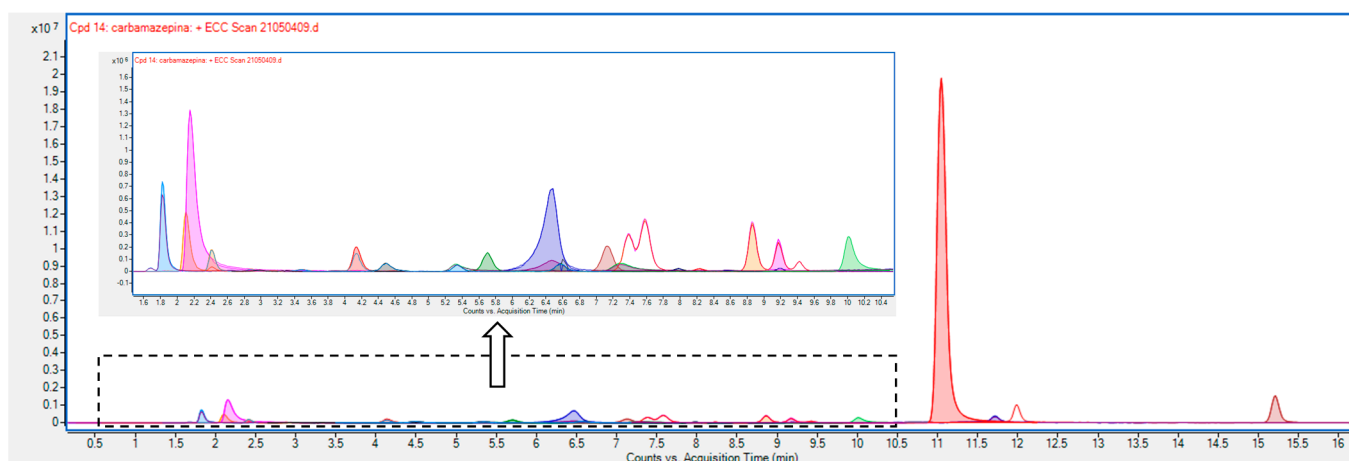


Figure 9. Chromatographic profile of the major compounds detected in the sample of carbamazepine oxidized to pH = 3.0. Experimental conditions: (CBZ) = 50.0 mg/L; (Fe) = 10 mg/L; (H₂O₂) = 15.0 mM; T = 25 °C; (UV) = 150 W.

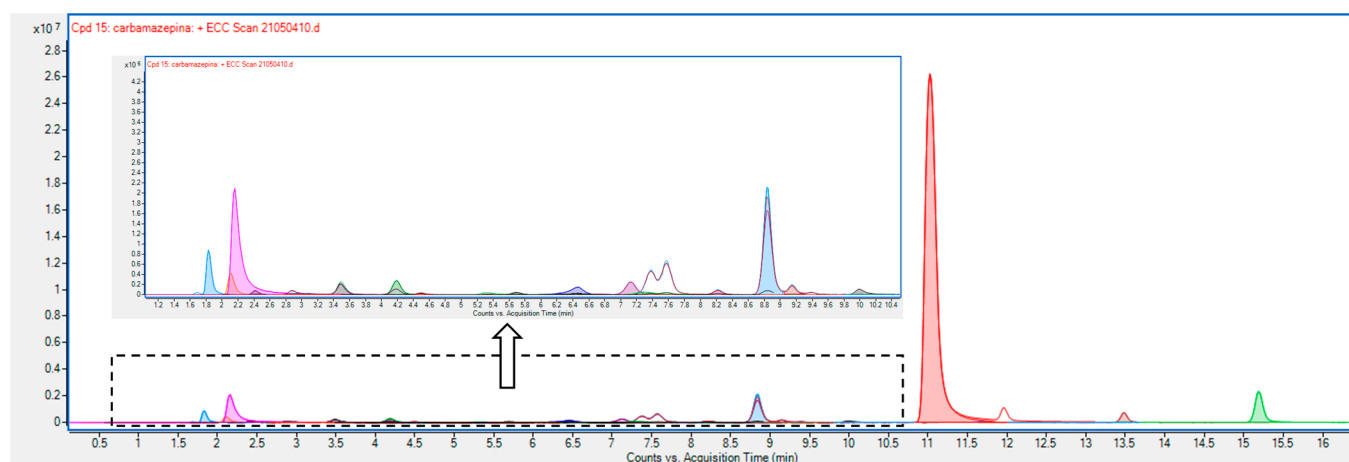


Figure 10. Chromatographic profile of the major compounds detected in the sample of carbamazepine oxidized to pH = 4.0. Experimental conditions: (CBZ) = 50.0 mg/L; (Fe) = 10 mg/L; (H₂O₂) = 15.0 mM; T = 25 °C; (UV) = 150 W.

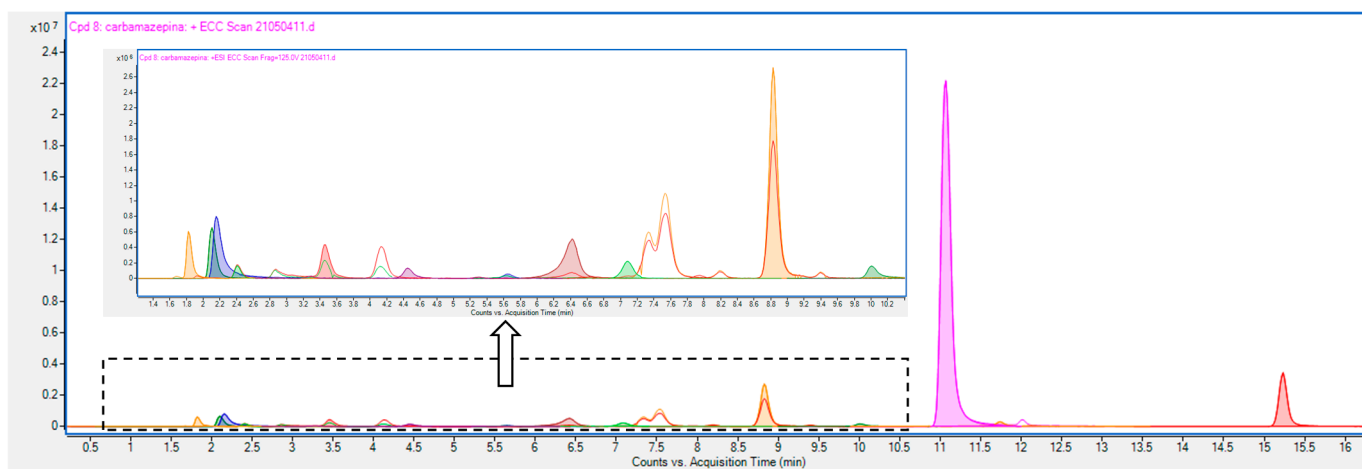


Figure 11. Chromatographic profile of the major compounds detected in the sample of carbamazepine oxidized to pH = 5.0. Experimental conditions: (CBZ) = 50.0 mg/L; (Fe) = 10 mg/L; (H₂O₂) = 15.0 mM; T = 25 °C; (UV) = 150 W.

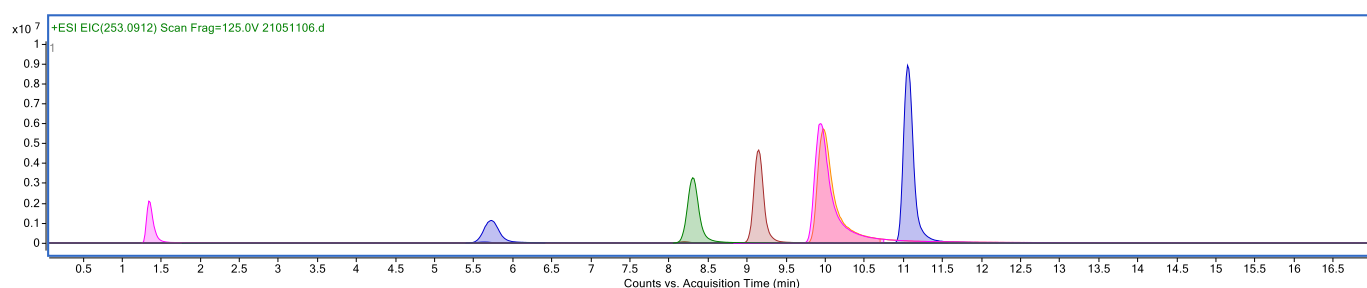


Figure 12. Excerpt chromatogram of standards (EIC) of 1 ppm CBZ, acridone, acridin, Oxo-CBZ, Epoxi-CBZ, 10-OH CBZ, malonic acid and 4-aminophenol.

Table 1. Standards analyzed.

Compound	Tr, min	m/z
4-aminophenol	1.3	110.0600
Malonic acid	1.8	105.0182
10-OH CBZ	5.8	255.1128
Epoxi-CBZ	8.2	253.0972
Oxo-CBZ	9.1	253.0972
9-acridanone	9.9	196.0757
Acridin-9-ol	9.9	196.0757
CBZ	11.2	237.1022

Once the majority of compounds were identified, and in order to determine the concentration of the degradation products in the samples (identified with the commercial standards), calibration was completed. The quantification of the samples was carried out using a calibration at concentrations between 0.001 and 5 $\mu\text{g}/\text{mL}$. The results obtained from the quantitative analysis are shown in Table 2.

Table 2. Results of quantitative analysis, concentrations in $\mu\text{g}/\text{mL}$.

Compound	pH = 2.0	pH = 3.0	pH = 4.0	pH = 5.0
CBZ	1.8	10.8	34.4	17.0
Oxo-CBZ	<LQL	0.25	0.21	0.037
Epoxi-CBZ	-	-	-	-
10-OH CBZ	<LQL	0.065	0.022	0.013
9-acridanone and acridin-9-ol	0.013	0.026	0.004	0.010
4-aminophenol	n.d.	n.d.	n.d.	n.d.
Malonic acid	n.d.	n.d.	n.d.	n.d.

n.d.: not detected, LQL: lower quantification limit (0.002 $\mu\text{g}/\text{mL}$).

Next is explained the validation of the method, wherein Tables 3–7 provide full validation process of the analysis of CBZ and its degradation products with the main validation parameters. The samples were subjected to drastic conditions to acid hydrolysis (1N HCl), basic hydrolysis (1N NaOH), sunlight and temperature (30 $^{\circ}\text{C}$). Subsequently, the amount recovered was determined in triplicate after 7 days.

Table 3. Limit of quantification values (LOQ) and limit of detection values (LOD) of CBZ and the detected degradation intermediates in water.

Compound	LOQ (ng/mL)	LOD (ng/mL)
CBZ	100	30
Oxo-CBZ	2	0.6
10-OH CBZ	2	0.6
9-acridanone	1	0.3
Acridin-9-ol	1	0.3

Table 4. Linearity values of CBZ and the detected degradation intermediates in water.

Compound	Range (µg/mL)	Regression Equation	R ²
CBZ	0.1–50	$y = 3.580x + 6.340$	0.998
Oxo-CBZ	0.002–0.5	$y = 2.933x + 5.480$	0.998
10-OH CBZ	0.002–0.5	$y = 2.008x + 3.146$	0.993
9-acridanone	0.001–0.5	$y = 5.298x + 9.636$	0.998
Acridin-9-ol	0.001–0.5	$y = 5.034x + 8.996$	0.998

Table 5. Specificity values of CBZ and the detected degradation intermediates in water.

Compound	Parameter	Amount Added (µg/mL)	Amount Recovered (µg/mL)	Degradation (%)
CBZ	Acidic degradation	25.05	24.58	1.87
	Alkaline degradation	25.05	24.29	3.04
	Solar light	25.05	24.87	0.71
OX-CBZ	Acidic degradation	0.251	0.246	2.03
	Alkaline degradation	0.251	0.241	3.87
	Solar light	0.251	0.249	0.98
10-OH CBZ	Acidic degradation	0.251	0.247	1.54
	Alkaline degradation	0.251	0.240	4.20
	Solar light	0.251	0.249	0.85
Acridanone	Acidic degradation	0.2505	0.2464	1.64
	Alkaline degradation	0.2505	0.2412	3.72
	Solar light	0.2505	0.2480	0.99
Acridin 9-ol	Acidic degradation	0.2505	0.2447	2.31
	Alkaline degradation	0.2505	0.2418	3.47
	Solar light	0.2505	0.2479	1.02

Table 6. Accuracy values of CBZ and the detected degradation intermediates in water.

Compound	Range (µg/mL)	Recovery (Mean ± % RSD)
CBZ	0.1–50	100.05 ± 0.023
Oxo-CBZ	0.002–0.5	100.24 ± 0.030
10-OH CBZ	0.002–0.5	100.56 ± 0.011
9-acridanone	0.001–0.5	100.08 ± 0.007
Acridin-9-ol	0.001–0.5	100.91 ± 0.024

Table 7. Precision values of CBZ and the detected degradation intermediates in water.

Compound	Concentration (µg/mL)	Standard Solution		Sample Solution		Mean	SD	% RSD
		Intraday Precision	Interday Precision	Intraday Precision	Inter-Day Precision			
CBZ	25.05	96.0190	96.9792	98.0188	98.9080	97.4812	98.7352	0.0128
OX-CBZ	0.251	6.2164	6.1542	6.0696	6.0908	6.1328	6.1988	0.0108
10-OH CBZ	0.251	3.6500	3.7595	3.8475	3.7264	3.7459	3.8279	0.0118
Acridanone	0.2505	10.9633	10.6344	10.8027	10.7996	10.8000	10.934	0.0124
Acridin 9-ol	0.2505	10.2570	10.1544	10.0560	10.3688	10.2091	10.3431	0.0131

4. Conclusions

This work checks the effect of the control parameters of photo-Fenton technology applied to CBZ oxidation. Experimental assays show that during the oxidation of aqueous solutions containing CBZ, the water turbidity shows great changes as a function of the operational conditions (pH, hydrogen peroxide and catalyst concentration). The relationship between turbidity and the control parameters of the photo-Fenton reaction would be caused by the degradation intermediates generated in water as a function of the oxidized

degree achieved in the treatment. The analysis of treated waters that show the higher turbidity levels allow establishing a general oxidation mechanism, where the CBZ would be oxidized through four main degradation routes. First, the formation of the epoxide (10,11-Epoxy CBZ) leads to the creation of two dihydroxylated isomers (cis and trans 10,11-DiOH-CBZ), which, in turn, degrade, generating acridin-9-ol and acridone. On the other hand, the creation of the epoxide (2,3-Epoxy CBZ) generates hydroxylated benzene rings (3-OH CBZ and 2-OH CBZ). Moreover, the attack of the aromatic ring of CBZ would lead to the production of BQM, where the reaction of BQM with hydroxyl radicals would direct the generation of BQD. Finally, the aldehyde group of BQD could react with the hydroxyl radicals, generating BaQD. Moreover, it has to be considered that in this system, the iron catalyst has the oxidized form Fe^{3+} . Then, the generation of high turbidity would be explained based on the molecular structure of the degradation intermediates detected, where it would be possible to propose the formation of coordination complexes with ferric ions that enhance the turbidity. This would be the case of coordination compounds between a ferric ion atom with three BaQD molecules that consist of stable supramolecular structures that reduce the passage of light through the water, causing turbidity.

Author Contributions: Experimental design, writing, review, conclusions, N.V.; translation, formatting, references, C.F.; experimental development, H.A.Q.; translation, review, J.M.L.; obtaining sponsors, obtaining funding, J.I.L. All authors have read and agreed to the published version of the manuscript.

Funding: Authors are grateful to the University of the Basque Country UPV/EHU for the financial support to carry out this research study through the scholarship Student Mobility for Traineeships in the Erasmus + Programme between the Anadolu University in Eskisehir (Turkey) and the Faculty of Engineering Vitoria-Gasteiz (Spain).

Acknowledgments: The authors thank for technical and human support provided by the Central Service of Analysis from Álava—SGiker—UPV/EHU.

Conflicts of Interest: The authors declare no conflict of interest.

Appendix A

Table A1. Results of screening of major compounds. Sample pH = 2.0. Experimental conditions: [CBZ] = 50.0 mg/L; [Fe] = 10.0 mg/L; [H₂O₂] = 15.0 mM; T = 25 °C; [UV] = 150 W.

Label	Tr, min	m/z	Mass	Height	Name	Score	Diff (DB,ppm)	Ions
Comp 1	1.8	224.0718	223.0645	146,262	-	-	-	3
Comp 2	1.8	163.0511	162.0438	41,946	-	-	-	2
Comp 3	2.1	147.0557	146.0485	501,215	-	-	-	2
Comp 4	2.2	180.0811	179.0739	172565	Acridine	99.09	-2.02	2
Comp 5	2.4	271.1054	270.0991	33,111	CIS-d iOH -CBZ	88.39	4.91	8
Comp 6	4.1	271.1092	270.1023	58,811	CIS-diOH-CBZ	94.64	-7.03	7
Comp 7	4.5	267.0781	266.0708	8828	BQD	87.11	-6.51	1
Comp 8	5.4	267.0779	266.0706	8275	BQD	89.7	-5.78	2
Comp 9	5.8	255.1158	254.1093	8104	-	-	-	-
Comp 10	6.5	251.0828	250.0755	269,555	T1251	92.29	-5.1	5
Comp 11	6.6	267.0778	266.0706	38,790	BQD	90.62	-5.5	2
Comp 12	7.3	224.0719	223.0639	1553	-	-	-	3
Comp 13	7.4	253.0989	252.0919	12,234	2-OH-CBZ	73.88	-7.86	2
Comp 14	7.6	253.0983	252.0911	16,164	2-OH-CBZ	80.87	-4.92	2
Comp 15	7.7	283.0727	282.0654	32,599	BaQD	93.23	-4.53	2
Comp 16	8.5	267.0779	266.0706	147,319	BQD	90.13	-5.65	3
Comp 17	8.9	253.0994	252.0928	15,599	3-OH-CBZ	77.71	-11.53	3
Comp 18	9.2	253.1034	252.096	3526	-	-	-	2
Comp 19	9.9	196.077	195.0697	184,640	Acridone or acridin-9-ol	96.9	-6.8	10
Comp 20	11.2	259.0863	236.0971	3,433,925	Carbamazepine	94	-9.09	7
Comp 21	12.0	318.2826	317.2753	29,688	-	-	-	2
Comp 22	15.2	226.0881	225.0808	402,491	-	-	-	5

Table A2. Results of screening of major compounds. Sample pH = 3.0. Experimental conditions: [CBZ] = 50.0 mg/L; [Fe] = 10.0 mg/L; [H₂O₂] = 15.0 mM; T = 25 °C; [UV] = 150W. The compounds indicated in grey are the possible species identified by the database.

Label	Tr, min	m/z	Mass	Height	Name	Score	Diff (DB,ppm)	Ions
Comp 1	1.8	224.0716	223.0644	632,743	-	-	-	3
Comp 2	2.1	147.0563	146.0491	436,509	-	-	-	3
Comp 3	2.2	180.0818	179.0745	1,149,862	Acridine	92.86	-5.76	3
Comp 4	2.4	271.1095	270.1017	147,566	TRANS-diOH-CBZ	86.39	-4.87	3
Comp 5	3.5	271.109	270.102	12,320	-	-	-	2
Comp 6	4.1	253.099	270.1023	169,843	TRANS-diOH-CBZ	93.57	-6.99	3
Comp 7	4.5	267.0774	266.0701	56,646	BQD	95.11	-3.92	2
Comp 8	5.3	267.0777	266.0704	45,947	BQD	91.98	-5.07	2
Comp 9	5.7	237.1033	254.1065	131,805	10-OH-CBZ	83.69	-4.02	2
Comp 10	6.5	251.0834	250.0761	544,371	T1251	84	-7.51	5
Comp 11	6.6	267.0776	266.0704	55,876	BQD	93.04	-4.7	2
Comp 12	7.1	269.0934	268.0861	141,392	-	-	-	4
Comp 13	7.3	224.0718	223.0644	52,554	-	-	-	3
Comp 14	7.4	253.0988	252.0916	256,182	2-OH-CBZ	95.43	-6.61	8
Comp 15	7.6	253.0989	252.0916	357,248	2-OH-CBZ	94.24	-6.77	5
Comp 16	7.7	283.0735	282.0662	9024	BaQD	82.12	-7.58	2
Comp 17	7.9	267.0784	266.0709	19,667	BQD	85.55	-6.92	3
Comp 18	8.2	253.0985	252.0914	17,230	EP-CBZ	73.45	-6.07	2
Comp 19	8.6	267.0795	266.0722	8216	-	-	-	2
Comp 20	8.8	253.0994	252.0921	330,535	2-OH-CBZ	90.52	-8.92	4
Comp 21	9.2	253.0988	252.0916	204,534	Oxcarbamazepine	94.32	-6.72	5
Comp 22	10.0	196.0772	195.0699	280,810	Acridone or acridin-9-ol	96.78	-7.92	6
Comp 23	11.2	237.1047	236.0974	10,672,680	Carbamazepine	88.67	-10.08	15
Comp 24	11.7	224.0733	223.066	276,891	-	-	-	5
Comp 25	11.9	473.1992	472.1919	639,344	-	-	-	6
Comp 26	15.2	226.0889	225.0816	1,183,745	-	-	-	5

Table A3. Results of screening of major compounds. Sample pH = 4.0. Experimental conditions: [CBZ] = 50.0 mg/L; [Fe] = 10.0 mg/L; [H₂O₂] = 15.0 mM; T = 25 °C; [UV] = 150W. The compounds indicated in grey are the possible species identified by the database.

Label	Tr, min	m/z	Mass	Height	Name	Score	Diff (DB,ppm)	Ions
Comp 1	1.8	224.0722	223.0649	755,262	-	-	-	3
Comp 2	2.1	147.0566	146.0493	372,649	-	-	-	3
Comp 3	2.2	180.0822	179.0749	1,818,336	Acridine	87.37	-7.78	3
Comp 4	2.4	271.109	270.1018	67,258	TRANS-diOH-CBZ	80.63	-5.01	2
Comp 5	3.5	271.1091	270.1017	178,694	TRANS-diOH-CBZ	96.59	-4.95	3
Comp 6	4.2	253.0988	270.1021	236,040	TRANS-diOH-CBZ	94.47	-6.47	3
Comp 7	4.5	267.0778	266.0705	26,250	BQD	90.8	-5.44	2
Comp 8	5.3	267.078	266.0707	9285	BQD	88.48	-6.13	1
Comp 9	5.7	255.1141	254.1069	31,349	10-OH-CBZ	80.45	-5.52	3
Comp 10	6.5	251.0825	250.0753	119,415	T1251	94.04	-4.46	3
Comp 11	6.6	267.0779	266.0706	13,942	BQD	89.97	-5.7	2
Comp 12	7.1	269.0935	268.0861	166,675	-	-	-	5
Comp 13	7.4	224.0716	223.0643	44,729	-	-	-	2
Comp 14	7.3	253.0985	252.0912	385,655	3-OH CBZ	96.47	-5.18	5
Comp 15	7.6	253.099	252.0917	514,816	3-OH CBZ	93.53	-7.24	8
Comp 16	7.9	267.0781	266.0708	12,768	BDQ	87.89	-6.29	2
Comp 17	8.2	253.099	252.0918	70,044	EP-CBZ	93.04	-7.69	3
Comp 18	8.8	253.0996	252.0923	1,397,381	3-OH-CBZ	89.34	-9.65	11
Comp 19	9.1	253.0989	252.0916	149,274	Oxcarbamazepine	78.9	-6.89	4
Comp 20	9.9	196.0767	195.0696	109,794	Acridone or acridin-9-ol	97.14	-5.92	4
Comp 21	11.2	237.105	236.0973	15,089,995	Carbamazepine	83.8	-9.81	9
Comp 22	11.7	224.0723	223.0653	95,064	-	-	-	2
Comp 23	11.9	473.1994	472.192	688,405	-	-	-	8
Comp 24	13.5	210.0931	209.0859	635,867	-	-	-	3
Comp 25	15.2	226.0889	225.0817	1,793,645	-	-	-	8

Table A4. Results of screening of major compounds. Sample pH = 5.0. Experimental conditions: [CBZ] = 50.0 mg/L; [Fe] = 10.0 mg/L; [H₂O₂] = 15.0 mM; T = 25 °C; [UV] = 150W. The compounds indicated in grey are the possible species identified by the database.

Label	Tr, min	m/z	Mass	Height	Name	Score	Diff (DB,ppm)	Ions
Comp 1	1.8	224.0718	223.0645	520,658	-	-	-	3
Comp 2	2.1	147.0568	146.0496	588,299	-	-	-	3
Comp 3	2.2	180.0822	179.0749	693,527	Acridine	87.18	-7.84	3
Comp 4	2.4	271.1092	270.1019	141,194	TRANS-diOH-CBZ	80.16	-5.49	2
Comp 5	3.5	271.1091	270.1019	432,132	CIS-diOH-CBZ	96.29	-5.38	7
Comp 6	4.1	271.1091	270.1018	409,566	CIS-diOH-CBZ	96.85	-5.13	9
Comp 7	4.5	267.0778	266.0705	114,157	BQD	91.47	-5.23	2
Comp 8	5.3	267.0779	266.0706	13,734	BQD	89.84	-5.73	1
Comp 9	5.7	255.114	254.1069	56,313	10-OH-CBZ	96.03	-5.69	10
Comp 10	6.4	251.0827	250.0755	398,550	T1251	92.37	-5.07	6
Comp 11	6.5	267.0782	266.0709	10,804	BQD	86.14	-6.77	2
Comp 12	7.1	269.0935	268.0862	148,854	-	-	-	8
Comp 13	7.3	224.0721	223.0648	51,741	-	-	-	4
Comp 14	7.3	253.0989	252.0916	473,737	2-OH-CBZ	95.34	-6.62	6
Comp 15	7.5	253.0995	252.0922	802,934	2-OH-CBZ	91.73	-9.17	10
Comp 16	7.9	267.0775	266.0701	34,402	BQD	95.57	-3.73	4
Comp 17	8.2	253.0985	252.0915	81,586	EP-CBZ	97.33	-6.51	8
Comp 18	8.8	253.0996	252.0924	1,722,757	2-OH-CBZ	90.91	-9.73	11
Comp 19	9.1	253.0983	252.0911	37,573	Oxcarbamazepine	80.73	-4.9	2
Comp 20	10.0	196.0773	195.07	158,961	Acridone or acridin-9-ol	95.31	-8.41	6
Comp 21	11.2	237.1048	236.0973	11,711,134	Carbamazepine	89.16	-9.9	15
Comp 22	11.7	224.0731	223.0663	207,462	-	-	-	5
Comp 23	12.0	473.1987	472.1915	239,021	-	-	-	7
Comp 24	15.2	226.0886	225.0814	2,443,394	-	-	-	11

References

- Lapworth, D.J.; Baran, N.; Stuart, M.E.; Ward, R.S. Emerging Organic Contaminants in Groundwater: A Review of Sources, Fate and Occurrence. *Environ. Pollut.* **2012**, *163*, 287–303. [[CrossRef](#)] [[PubMed](#)]
- Hai, F.L.; Yang, S.; Asif, M.B.; Sencadas, V.; Shawkat, S.; Sanderson-Smith, M.; Gorman, J.; Xu, Z.-Q.; Yamamoto, K. Carbamazepine as a Possible Anthropogenic Marker in Water: Occurrences, Toxicological Effects, Regulations and Removal by Wastewater Treatment Technologies. *Water* **2018**, *10*, 107. [[CrossRef](#)]
- Hughes, S.R.; Kay, P.; Brown, L.E. Global Synthesis and Critical Evaluation of Pharmaceutical Data Sets Collected from River Systems. *Environ. Sci. Technol.* **2013**, *47*, 661–677. [[CrossRef](#)]
- Gavrilescu, M.; Demnerová, K.; Aamand, J.; Agathos, S.; Fava, F. Emerging Pollutants in the Environment: Present and Future Challenges in Biomonitoring, Ecological Risks and Bioremediation. *New Biotechnol.* **2015**, *32*, 147–156. [[CrossRef](#)]
- Brack, W.; Dulio, V.; Ågerstrand, M.; Allan, I.; Altenburger, R.; Brinkmann, M.; Bunke, D.; Burgess, R.M.; Cousins, I.; Escher, B.I.; et al. Towards the Review of the European Union Water Framework Directive: Recommendations for More Efficient Assessment and Management of Chemical Contamination in European Surface Water Resources. *Sci. Total Environ.* **2017**, *576*, 720–737. [[CrossRef](#)]
- Kumar, A.; Batley, G.E.; Nidumolu, B.; Hutchinson, T.H. Derivation of Water Quality Guidelines for Priority Pharmaceuticals. *Environ. Toxicol. Chem.* **2016**, *35*, 1815–1824. [[CrossRef](#)] [[PubMed](#)]
- Marcelo, V.O.; Salette, R.; Jose, L.F.C.L.; Marcela, A.S. Analytical Features of Diclofenac Evaluation in Water as a Potential Marker of Anthropogenic Pollution. *Curr. Pharm. Anal.* **2016**, *13*, 39–47.
- Ferrer, I.; Thurman, E.M. Analysis of 100 Pharmaceuticals and Their Degradates in Water Samples by Liquid Chromatography/Quadrupole Time-of-Flight Mass Spectrometry. *J. Chromatogr. A* **2012**, *1259*, 148–157. [[CrossRef](#)] [[PubMed](#)]
- Arye, G.; Dror, I.; Berkowitz, B. Fate and Transport of Carbamazepine in Soil Aquifer Treatment (SAT) Infiltration Basin Soils. *Chemosphere* **2011**, *82*, 244–252. [[CrossRef](#)]
- Kasprzyk-Hordern, B.; Dinsdale, R.M.; Guwy, A.J. The Removal of Pharmaceuticals, Personal Care Products, Endocrine Disruptors and Illicit Drugs during Wastewater Treatment and Its Impact on the Quality of Receiving Waters. *Water Res.* **2009**, *43*, 363–380. [[CrossRef](#)]
- Chen, P.; Lin, J.-J.; Lu, C.-S.; Ong, C.-T.; Hsieh, P.F.; Yang, C.-C.; Tai, C.-T.; Wu, S.-L.; Lu, C.-H.; Hsu, Y.-C.; et al. Carbamazepine-Induced Toxic Effects and HLA-B*1502 Screening in Taiwan. *N. Engl. J. Med.* **2011**, *364*, 1126–1133. [[CrossRef](#)] [[PubMed](#)]
- Pereira, F.A.; Mudgil, A.V.; Rosmarin, D.M. Toxic Epidermal Necrolysis. *J. Am. Acad. Dermatol.* **2007**, *56*, 181–200. [[CrossRef](#)] [[PubMed](#)]

13. Jentink, J.; Dolk, H.; Loane, M.A.; Morris, J.K.; Wellesley, D.; Garne, E.; de Jong-van den Berg, L.; EUROCAT Antiepileptic Study Working Group. Intrauterine Exposure to Carbamazepine and Specific Congenital Malformations: Systematic Review and Case-Control Study. *BMJ* **2010**, *341*, c6581. [[CrossRef](#)] [[PubMed](#)]
14. Cummings, C.; Stewart, M.; Stevenson, M.; Morrow, J.; Nelson, J. Neurodevelopment of Children Exposed in Utero to Lamotrigine, Sodium Valproate and Carbamazepine. *Arch. Dis. Child.* **2011**, *96*, 643–647. [[CrossRef](#)] [[PubMed](#)]
15. Atkinson, D.E.; Brice-Bennett, S.; D'Souza, S.W. Antiepileptic Medication during Pregnancy: Does Fetal Genotype Affect Outcome? *Pediatr. Res.* **2007**, *62*, 120–127. [[CrossRef](#)]
16. Hai, F.I.; Nghiem, L.D.; Khan, S.J.; Price, W.E.; Yamamoto, K. Wastewater Reuse: Removal of Emerging Trace Organic Contaminants. In *Membrane Biological Reactors: Theory, Modeling, Design, Management and Applications to Wastewater Reuse*; IWA Publishing: London, UK, 2014; ISBN 978-1-78040-065-5.
17. Vieno, N.; Tuhkanen, T.; Kronberg, L. Elimination of Pharmaceuticals in Sewage Treatment Plants in Finland. *Water Res.* **2007**, *41*, 1001–1012. [[CrossRef](#)]
18. Ying, G.-G.; Kookana, R.S.; Kolpin, D.W. Occurrence and Removal of Pharmaceutically Active Compounds in Sewage Treatment Plants with Different Technologies. *J. Environ. Monit.* **2009**, *11*, 1498–1505. [[CrossRef](#)]
19. Tixier, C.; Singer, H.P.; Oellers, S.; Müller, S.R. Occurrence and Fate of Carbamazepine, Clofibrac Acid, Diclofenac, Ibuprofen, Ketoprofen, and Naproxen in Surface Waters. *Environ. Sci. Technol.* **2003**, *37*, 1061–1068. [[CrossRef](#)]
20. Wijekoon, K.C.; Hai, F.I.; Kang, J.; Price, W.E.; Guo, W.; Ngo, H.H.; Nghiem, L.D. The Fate of Pharmaceuticals, Steroid Hormones, Phytoestrogens, UV-Filters and Pesticides during MBR Treatment. *Bioresour. Technol.* **2013**, *144*, 247–254. [[CrossRef](#)]
21. Guo, Y.C.; Krasner, S.W. Occurrence of Primidone, Carbamazepine, Caffeine, and Precursors for N-Nitrosodimethylamine in Drinking Water Sources Impacted by Wastewater. *JAWRA J. Am. Water Resour. Assoc.* **2009**, *45*, 58–67. [[CrossRef](#)]
22. Luo, Y.; Guo, W.; Ngo, H.H.; Nghiem, L.D.; Hai, F.I.; Zhang, J.; Liang, S.; Wang, X.C. A Review on the Occurrence of Micropollutants in the Aquatic Environment and Their Fate and Removal during Wastewater Treatment. *Sci. Total Environ.* **2014**, *473*, 619–641. [[CrossRef](#)] [[PubMed](#)]
23. Villota, N.; Lombraña, J.I.; Cruz-Alcalde, A.; Marcé, M.; Esplugas, S. Kinetic Study of Colored Species Formation during Paracetamol Removal from Water in a Semicontinuous Ozonation Contactor. *Sci. Total Environ.* **2019**, *649*, 1434–1442. [[CrossRef](#)]
24. Mijangos, F.; Varona, F.; Villota, N. Changes in Solution Color During Phenol Oxidation by Fenton Reagent. *Environ. Sci. Technol.* **2006**, *40*, 5538–5543. [[CrossRef](#)] [[PubMed](#)]
25. Villota, N.; Lomas, J.M.; Camarero, L.M. Study of the Paracetamol Degradation Pathway That Generates Color and Turbidity in Oxidized Wastewaters by Photo-Fenton Technology. *J. Photochem. Photobiol. A Chem.* **2016**, *329*, 113–119. [[CrossRef](#)]
26. Villota, N.; Ferreira, C.; Qulatein, H.A.; Lomas, J.M.; Camarero, L.M.; Lombraña, J.I. Colour Changes during the Carbamazepine Oxidation by Photo-Fenton. *Catalysts* **2021**, *11*, 386. [[CrossRef](#)]
27. Sun, S.; Yao, H.; Fu, W.; Liu, F.; Wang, X.; Zhang, W. Enhanced Degradation of Carbamazepine in FeOCl Based Photo-Fenton Reaction. *J. Environ. Chem. Eng.* **2021**, *9*, 104501. [[CrossRef](#)]
28. Yao, W.; Qu, Q.; von Gunten, U.; Chen, C.; Yu, G.; Wang, Y. Comparison of Methylisoborneol and Geosmin Abatement in Surface Water by Conventional Ozonation and an Electro-Peroxone Process. *Water Res.* **2017**, *108*, 373–382. [[CrossRef](#)]
29. Oturan, M.A.; Aaron, J.-J. Advanced Oxidation Processes in Water/Wastewater Treatment: Principles and Applications. A Review. *Crit. Rev. Environ. Sci. Technol.* **2014**, *44*, 2577–2641. [[CrossRef](#)]
30. Ahmed, M.M.; Chiron, S. Solar Photo-Fenton like Using Persulphate for Carbamazepine Removal from Domestic Wastewater. *Water Res.* **2014**, *48*, 229–236. [[CrossRef](#)]
31. Expósito, A.J.; Monteagudo, J.M.; Durán, A.; San Martín, I.; González, L. Study of the Intensification of Solar Photo-Fenton Degradation of Carbamazepine with Ferrioxalate Complexes and Ultrasound. *J. Hazard. Mater.* **2018**, *342*, 597–605. [[CrossRef](#)] [[PubMed](#)]
32. Guo, Q.; Zhu, W.; Yang, D.; Wang, X.; Li, Y.; Gong, C.; Yan, J.; Zhai, J.; Gao, X.; Luo, Y. A Green Solar Photo-Fenton Process for the Degradation of Carbamazepine Using Natural Pyrite and Organic Acid with in-Situ Generated H₂O₂. *Sci. Total Environ.* **2021**, *784*, 147187. [[CrossRef](#)] [[PubMed](#)]
33. Casierra-Martinez, H.A.; Madera-Parra, C.A.; Vargas-Ramírez, X.M.; Caselles-Osorio, A.; Torres-López, W.A. Diclofenac and Carbamazepine Removal from Domestic Wastewater Using a Constructed Wetland-Solar Photo-Fenton Coupled System. *Ecol. Eng.* **2020**, *153*, 105699. [[CrossRef](#)]
34. BOE.Es—BOE-A-2003-3596 Royal Decree 140/2003, of February 7th, Establishing Sanitary Criteria for the Quality of Water for Human Consumption. Available online: <https://www.boe.es/buscar/doc.php?id=BOE-A-2003-3596> (accessed on 24 June 2021).
35. BOE.Es—BOE-A-2007-21092 Royal Decree 1620/2007, of December 7th, Establishing the Legal Regime for the Reuse of Purified Waters. Available online: <https://www.boe.es/buscar/doc.php?id=BOE-A-2007-21092> (accessed on 24 June 2021).
36. De Laurentiis, E.; Chiron, S.; Kouras-Hadef, S.; Richard, C.; Minella, M.; Maurino, V.; Minero, C.; Vione, D. Photochemical Fate of Carbamazepine in Surface Freshwaters: Laboratory Measures and Modeling. *Environ. Sci. Technol.* **2012**, *46*, 8164–8173. [[CrossRef](#)]

-
37. Krakstrom, M.; Saeid, S.; Tolvanen, P.; Kumar, N.; Salmi, T.; Kronberg, L.; Eklund, P. Ozonation of Carbamazepine and Its Main Transformation Products: Product Determination and Reaction Mechanisms. *Environ. Sci. Pollut. Res.* **2020**, *27*, 23258–23269. [[CrossRef](#)] [[PubMed](#)]
 38. McDowell, D.C.; Huber, M.M.; Wagner, M.; von Gunten, U.; Ternes, T.A. Ozonation of Carbamazepine in Drinking Water: Identification and Kinetic Study of Major Oxidation Products. *Environ. Sci. Technol.* **2005**, *39*, 8014–8022. [[CrossRef](#)] [[PubMed](#)]




3.3. 3. argitalpena. Colour changes during the carbamazepine oxidation by photo-Fenton

3.3 kapitulua artikulu honi dagokio:

N. Villota, C. Ferreiro, H.A. Qulatein, J.M. Lomas, L.M. Camarero, J.I. Lombraña. Colour changes during the carbamazepine oxidation by photo-Fenton. *Catalysts*, 11, 3, 386, 2021. DOI: 10.3390/catal11030386.

Article

Colour Changes during the Carbamazepine Oxidation by Photo-Fenton

Natalia Villota ^{1,*}, Cristian Ferreiro ², Hussein Ahmad Qulatein ³, Jose María Lomas ¹, Luis Miguel Camarero ¹ and José Ignacio Lombrana ²

¹ Department of Chemical and Environmental Engineering, Faculty of Engineering of Vitoria-Gasteiz, University of the Basque Country UPV/EHU, Nieves Cano 12, 01006 Vitoria-Gasteiz, Spain; josemaria.lomas@ehu.es (J.M.L.); luismiguel.camarero@ehu.es (L.M.C.)

² Department of Chemical Engineering, Faculty of Science and Technology, University of the Basque Country UPV/EHU, Barrio Sarriena s/n, 48940 Leioa, Spain; cristian.ferreiro@ehu.es (C.F.); ji.lombrana@ehu.es (J.I.L.)

³ Department of Chemical Engineering, Faculty of Engineering, Anadolu University, 26555 Eskisehir, Turkey; husseinquulatein@gmail.com

* Correspondence: natalia.villota@ehu.es; Tel.: +34-9450-13248

Abstract: The oxidation of aqueous solutions of carbamazepine is conducted using the Fenton reagent, combined with the photolytic action of a 150 W medium pressure UV lamp, operating at T = 40 °C. The effect of acidity is analysed at an interval pH = 2.0–5.0, verifying that operating at pH = 5.0 promotes colour formation (Colour = 0.15 AU). The effect of iron is studied, finding that the colour of the water increases in a linear way, Colour = 0.05 + 0.0075 [Fe]₀. The oxidising action of hydrogen peroxide is tested, confirming that when operating with [H₂O₂]₀ = 2.0 mM, the maximum colour is generated (Colour_{max} = 0.381 AU). The tint would be generated by the degradation of by-products of carbamazepine, which have chromophoric groups in their internal structure, such as oxo and dioxocarbazepines, which would produce tint along the first minutes of oxidation, while the formation of acridones would slowly induce colour in the water.

Keywords: acridone; carbamazepine; colour; oxo-carbamazepine; photo-Fenton



Citation: Villota, N.; Ferreiro, C.; Qulatein, H.A.; Lomas, J.M.; Camarero, L.M.; Lombrana, J.I. Colour Changes during the Carbamazepine Oxidation by Photo-Fenton. *Catalysts* **2021**, *11*, 386. <https://doi.org/10.3390/catal11030386>

Academic Editors: Gassan Hodaifa and Rafael Borja

Received: 24 February 2021
Accepted: 16 March 2021
Published: 18 March 2021

Publisher's Note: MDPI stays neutral with regard to jurisdictional claims in published maps and institutional affiliations.



Copyright: © 2021 by the authors. Licensee MDPI, Basel, Switzerland. This article is an open access article distributed under the terms and conditions of the Creative Commons Attribution (CC BY) license (<https://creativecommons.org/licenses/by/4.0/>).

1. Introduction

The study of emerging pollutants in wastewater, as well as its treatment and elimination, are receiving great attention in recent times due to their presence in many kinds of waters and their possible repercussions on the environment [1]. In almost all wastewater of both urban and industrial origin, different emerging pollutants have been detected in variable concentrations, depending on the activities conducted in the original areas of such waters. Recently, several governments are beginning to limit the presence of some of them, based on the Directive 2013/39/EU of the European Parliament, as well as the Council of 12 August 2013 Amending Directives 2000/60/EC and 2008/105/EC [2], although the effects that they cause or their content in the environment are largely unknown.

The main source of entry into the environment for these pollutants is through unprocessed wastewater and effluents from wastewater treatment plants (WWTPs). Conventional plants are not designed for the elimination of this type of micro-pollutants, so their removal in many cases is not complete. Based on this approach, a need arises for these studies, which seek to know the behaviour of emerging pollutants, which are selected based on European guidelines to be analysed in WWTPs. In this way, the aim of this work is to establish indicators of contamination throughout the different phases that form the treatment systems of these plants, being a key aspect to consider the degree of elimination of these contaminants in the different treatment processes currently used.

Among these priority substances, pharmaceutical products, being active biological substances, can affect living organisms in water even in small concentration. Pharmaceu-

ticals such as hormones, pain relievers, and antidepressants can have adverse influence on fish, crustaceans, and algae, because they have a similar kind of receptors as humans. The consequences on animals and plants can be very different from the pharmacological effects expected in humans. For this reason, there is a current need to develop new analysis methods that ensure the effectiveness of the AOPs, in order to conduct a correct design of the new processes [3].

Following the indications of Directive 2013/39/EU of the European Parliament, this work is part of a central line of research that is focussed on the development of techniques that allow the degradation of drugs, because there are resistant micro-pollutants contained in wastewater. The purpose is to prevent their transmission to water distribution networks based on the Commission Implementing Rule (EU) 2018/840 of 5 June 2018 [4].

This work focusses on the study of the degradation of the drug carbamazepine. This drug has been selected as a model pollutant of the study, due to its persistence in conventional treatment plants, as well as its wide presence in urban water [5]. Carbamazepine (CBZ) is a medicine utilised to treat neurological conditions such as epilepsy, depression, or bipolar disorder. In humans, around 72% is absorbed and metabolised in the liver, and 28% is excreted in feces. CBZ is one of the most frequently detected pharmaceutical compounds in urban aqueous systems [6,7]. On the other hand, the main metabolites detected in urine are BBZ-epoxide, CBZ-diol, CBZ-acridan, 2-OH-CBZ, and 3-OH-CBZ [5,8,9]. CBZ is a recalcitrant pollutant identified in the effluents of sewage treatment plants and in superficial waters, which has a potential impact on the environment due to its physico-chemical properties, since it is seldom eliminated in conventional water treatments [10].

Due to its potential effect on aquatic microorganisms and human health, there is a notable concern about its removal from water. Studies performed in the presence of CBZ in relevant concentrations show that it can induce disorders in lipid metabolism, as well as damage to mitochondria and DNA in fish [11,12]. Moreover, research published by Faisal et al. [5] shows that CBZ residues in drinking water could cause congenital malformations and/or neurological development problems after long-term intrauterine exposure or breastfeeding. On the other hand, analysis of UV-irradiated aqueous CBZ solutions reveals that acridine, a compound known to be carcinogenic, is one of the by-products formed [13].

Within this context, Advanced Oxidation Processes (AOPs) are presented as an alternative with great potential to effectively eliminate emerging pollutants. To perform the industrial implementation of AOPs, it is necessary to evaluate the different technologies to minimise toxic risks to human health [14], and to solve problems regarding technical feasibility, cost-effectiveness, and their own sustainability [15]. On the other hand, the low concentration levels in which these micro-pollutants are found in the waters limit the effectiveness of these treatments [16]. Assessing the effects induced by the discharge of these wastewaters into natural channels is a challenge, since it presents the difficulty of identifying numerous pollutants, metabolites, and transformation products in very low concentrations.

Among these technologies, this work tries to test the use of hydrogen peroxide combined with iron salts and ultraviolet (UV) light, called photo-Fenton Technology, in order to study the degradation of carbamazepine in aqueous solution. Ultraviolet light is a germicide emission that does not present any residual or secondary effects. Therefore, this technique has a great potential to become a useful tool with high viability. Nevertheless, it is necessary to develop a solid foundation of knowledge in the design of feasible processes for the degradation of emerging pollutants, which requires exhaustive research on the laboratory scale and in pilot plants.

2. Results

2.1. Colour Changes during Carbamazepine Oxidation

Figure 1 displays the colour changes that occur in the aqueous solution during the degradation of carbamazepine using the photo-Fenton process. The operating conditions in

the tests shown in Figure 1a lead to the formation of a tinted aqueous residue recalcitrant to oxidation. For this reason, it is chosen as a representative essay to analyse this phenomenon. The degradation of carbamazepine occurs during the first two hours of reaction following second-order kinetic guidelines. The generation of tint in the water occurs during the first 40 min of reaction until it reaches a maximum value that remains stable over time.

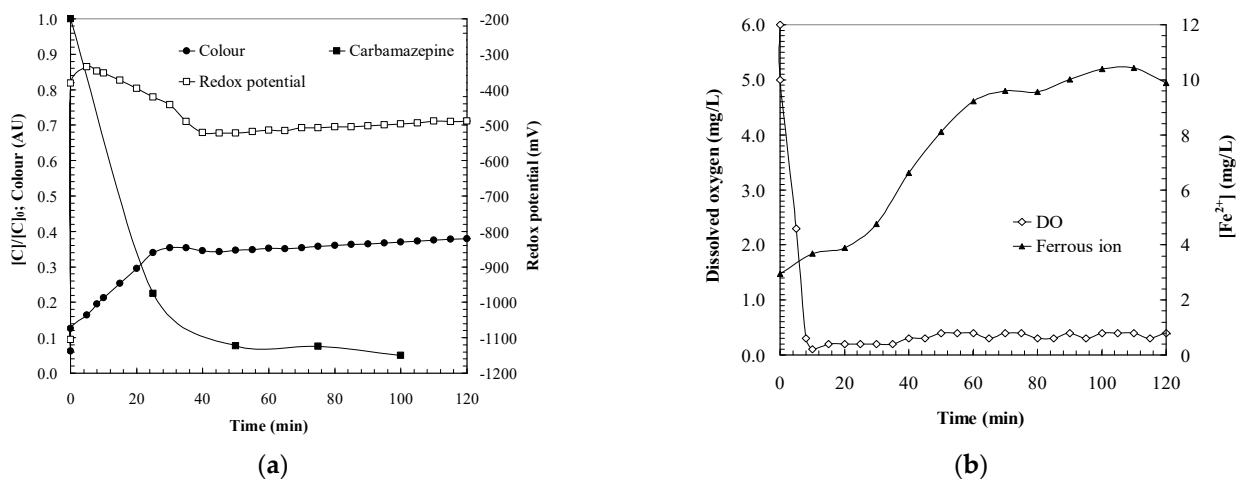


Figure 1. Water quality parameters analysed during carbamazepine oxidation by photo-Fenton: (a) Carbamazepine concentration, colour and redox potential. (b) Dissolved oxygen and ferrous ion. Experimental conditions: $[CBZ]_0 = 50.0$ mg/L; $pH = 3.0$; $[H_2O_2]_0 = 2.0$ mM; $[Fe]_0 = 10.0$ mg/L; $[UV] = 150$ W; $T = 40$ °C.

Analysing the redox potential values, an intense increase is observed during the first 5 min of the reaction until reaching a maximum value that decreases, arriving to a steady state after 40 min. This similar evolution between the colour and the redox potential changes makes it possible to associate the species that produce the hue changes in the water with the degradation intermediates of carbamazepine, which cause the redox potential values considered in the solution.

It should be noted that the increase in the redox potential during the first minutes of the reaction may be due to the oxidation of the ferrous ions to ferric, which is presented in Figure 1b. This allows verifying that approximately 70% of iron added to the reaction mixture in the form of ferrous ions is oxidised through the Fenton mechanism to ferric ions. Furthermore, during the course of the reaction, it is found that under the conditions tested, complete regeneration of the catalyst to ferrous ions occurs.

These results allow proposing a direct relationship between the redox potential and the reaction intermediates generated in the different stages of the carbamazepine oxidation mechanism. The substitution of groups of different nature (hydroxyl, oxo) in the aromatic rings affect the redox potential of the molecule, enlarging or reducing its value depending on the inducing effect of the substituent groups to accept or reject electrons in such a way that if the substitution in the ring is favored, they decrease the redox potential. In the case of hydroxylated carbamazepine molecules, when the aromatic ring loses the proton of the substituted hydroxyl group, electron delocalisation increases, thereby enlarging stability and causing the redox potential to decline [17]. Based on this hypothesis, it could be considered that the diminishment in redox potential would be related to the maximum concentration of dihydroxylated carbamazepines in the reaction medium, which would be contemplated as the precursor species of colour formation in water.

On the other hand, Figure 1b shows the evolution of dissolved oxygen (DO, mg O_2 /L). During the first 10 min of the reaction, there is a high consumption of oxygen dissolved in water, until reaching levels around (DO = 0.1 mg O_2 /L). This utilisation can be related to the oxidation process through the formation of strongly oxidising radical species. In this way, a highly oxidising environment is created that requires a large consumption of oxidising species. In addition, it is found that the moment when almost all the DO is

exhausted corresponds to the highest redox potential. This aspect can be associated to the maximum concentration of ferric ions generated in the Fenton reaction.

Next, the DO concentration begins to increase slightly until reaching levels of about 0.4 mg O₂/L after two hours of reaction. This behaviour is similar to that observed in studies reported in the bibliography during the oxidation of other organic pollutants [18], where this second stage of DO production presents a clear dependence on the nature of the oxidised species. In general, it is found that DO release is higher during the oxidation of organic matter that does not form organometallic complexes with iron, due to their molecular structure configuration. When the release of DO in the water is very slow, it is attributed to the fact that the degradation intermediates can form supramolecular structures with the ferric ions, preventing the iron regeneration.

In the case of the oxidation of carbamazepine shown in Figure 1b, it is observed that the DO release rate in water is very low ($k_{DO} = 0.0017$ mg O₂/L min), although the ferric ions are completely regenerated to ferrous. This result could be attributed to oxygen evolution reactions, where free radicals participate. The conditions that facilitate the formation of tint in the water are related to the use of scarce oxidant with respect to the contaminant load. This leads to partial oxidation of carbamazepine towards the formation of colour precursor intermediates. By conducting the reaction with a shortage of oxidant, it causes the generated radical load to be consumed through the processes of oxidation of organic matter and iron regeneration. As a result, the interradical reactions producing oxygen release in the water are relegated.

2.2. pH Effect

Figure 2 presents the effect of pH on water colour changes during the oxidation of aqueous carbamazepine solutions, operating between pH = 2.0 and 5.0. It should be noted that the acidity has remained stable throughout the reaction at the initial established value. In the tests conducted, it was found that during the first 5 min of the oxidation, tint was generated in the water until it reached a maximum value and then decreases to a stable value, around 30 min of reaction time. PH determines the value of the colour area as well as the residual hue of the oxidised water. On the other hand, it is observed that operating between pH = 2.0 and 3.5, the maximum colour formation occurs at around 5 min of reaction. However, at pH = 4.0 and 5.0 the maximum colour formation occurs between 10 and 15 min.

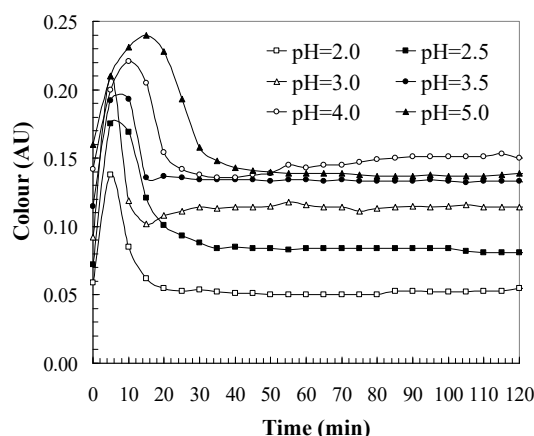


Figure 2. pH effect on colour changes in a photo-Fenton system during the carbamazepine oxidation. Experimental conditions: [CBZ]₀ = 50.0 mg/L; [H₂O₂]₀ = 15.0 mM; [Fe]₀ = 10.0 mg/L; [UV] = 150 W; T = 40 °C.

To analyse this result in more detail, Figure 3a represents the colour of the treated water once it has reached a steady state, together with the redox potential values. It is observed that both variables show a similar evolution regarding pH effect. By increasing the value from pH = 2.0 to 5.0, the intensity of the colour and the redox potential increases,

showing a maximum when carrying out the tests at pH = 5.0. As this pH increases, the colour and redox potential of the water decrease.

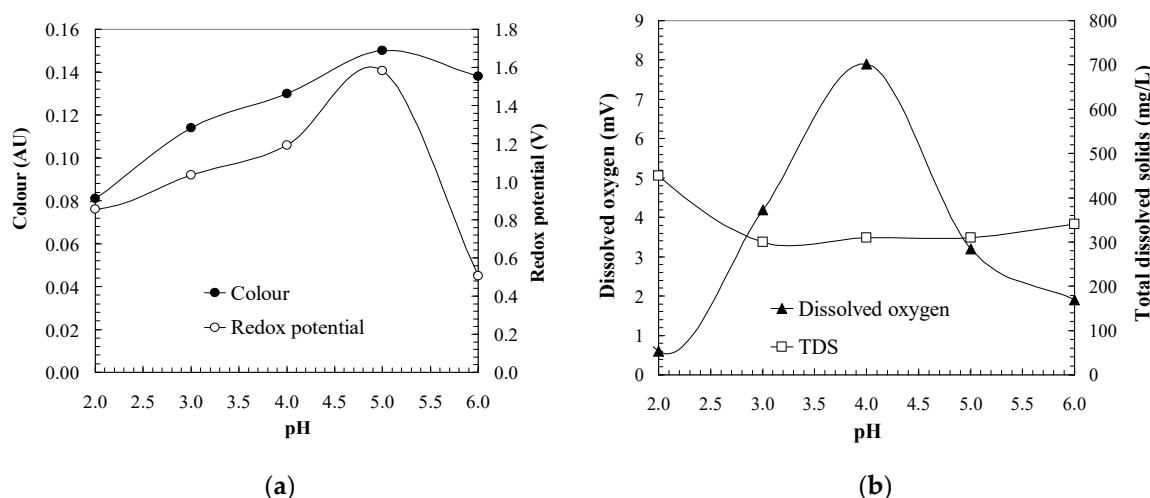


Figure 3. Indicator parameters of water quality analysed at the steady state: (a) Colour and redox potential. (b) Dissolved oxygen and total dissolved solids. Experimental conditions: $[CBZ]_0 = 50.0$ mg/L; $[H_2O_2]_0 = 15.0$ mM; $[Fe]_0 = 10.0$ mg/L; $[UV] = 150$ W; $T = 40$ °C.

To explain this effect, the speciation diagram of Fe (III) species as pH function in a photo-Fenton system [19] has been analysed. Then, it is found that the formation of the $Fe(OH)_2^-$ species in a photo-Fenton system potentially increases from pH = 2.0 until reaching its maximum at pH = 5.5. Thus, the effect of pH on colour formation could be associated with the presence of ferric hydroxide in the aqueous medium. The colour reduction operating at values higher than pH = 5.5 may be due to the fact that from this value, the formation of ferric hydroxide takes place, which would precipitate. This could cause a decrease in the concentration of iron dissolved, diminishing the aqueous tint.

Figure 3b displays the effect of pH on the concentration of DO in the water, which leads to verify a strong increase from pH = 2.0 to pH = 4.0, where the maximum concentration of DO occurs ($[DO] = 7.9$ mg O_2 /L), and then, it decreases from pH = 4.0 to 6.0. This effect could be explained with the Pourbaix diagram for iron, which presents the predominance of the various chemical species in water for an element. Analysing the redox potential diagram of the medium as a function of pH, it can be verified that the experimental redox potential values measured for each pH (see Figure 3a) indicate that within the interval between pH = 2.0 and 4.0, the iron would be in the Fe^{3+} form. Meanwhile, the values analysed at pH = 5.0 would indicate that iron would be in the FeO_4^{2-} form and at pH = 6.0 in the Fe_2O_3 form. This change in the nature of the iron species that would coexist in the system could be related with the reactions of oxygen release.

2.3. Effect of Hydrogen Peroxide Dosage

During the oxidation treatment of aqueous carbamazepine samples, it is found that the water acquires colour during the first 20 min of reaction (Figure 4a). It is verified that the intensity of the tint depends on the dose of oxidant used. The results present two clear trends in the kinetics of colour formation. On the one hand, operating with low concentrations of oxidant, around $[H_2O_2]_0 = 2.0$ mM, corresponding to stoichiometric ratios of 1 mol CBZ: 10 mol H_2O_2 , tint is generated in the water according to a ratio of 0.0086 AU/min, until reaching its maximum intensity ($Colour_{max} = 0.353$ AU) at 30 min of reaction. Subsequently, the hue continues increasing but much more slowly, following ratios of 0.0005 AU/min, until it arrives at the steady state ($Colour_{\infty} = 0.381$ AU).

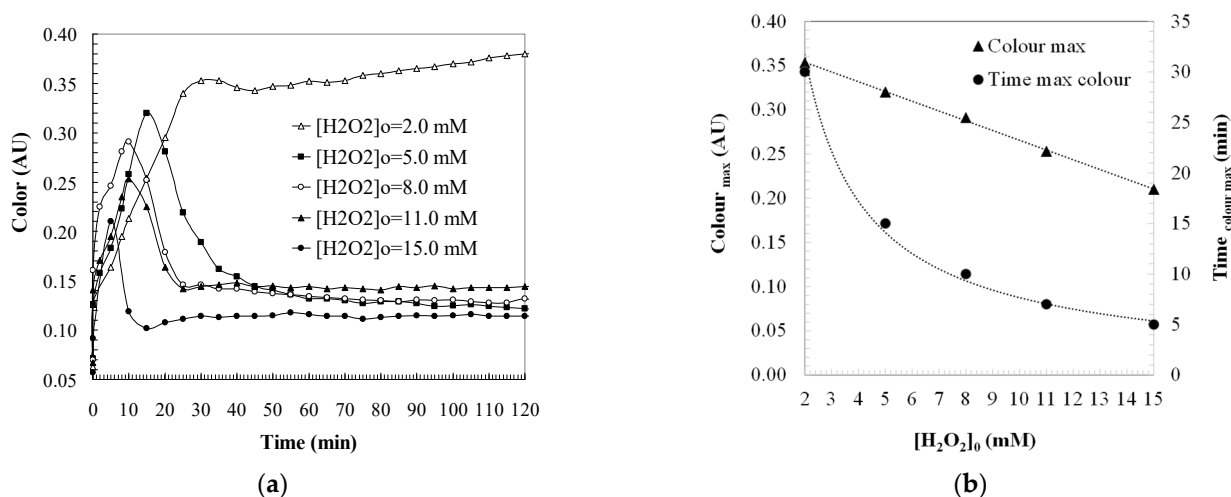


Figure 4. (a) Effect of hydrogen peroxide on colour changes in a photo-Fenton system during the carbamazepine oxidation. (b) Maximum colour formation (Colour_{\max} , AU) and time corresponding to the maximum colour formation ($\text{Time}_{\text{colour max}}$, min) as a function of the oxidant dosage. Experimental conditions: $[\text{CBZ}]_0 = 50.0 \text{ mg/L}$; $\text{pH} = 3.0$; $[\text{Fe}]_0 = 10.0 \text{ mg/L}$; $[\text{UV}] = 150 \text{ W}$; $T = 40 \text{ }^\circ\text{C}$

Performing with oxidant concentrations greater than $[\text{H}_2\text{O}_2]_0 = 5.0 \text{ mM}$, corresponding to stoichiometric ratios greater than 1 mol CBZ: 25 mol H_2O_2 , the colour formation follows the evolution of a reaction intermediate, with rapid colour formation during the first minutes of oxidation, until reaching a maximum value, and decreasing until obtaining a colourless solution. The oxidant dosage determines both the maximum colour generated (Equation (1)) and the time in which the formation of the highest colour intensity occurs (Equation (2)), as it is shown in Figure 4b. This result indicates that the stoichiometric ratio of oxidant utilised determines the degree of oxidation achieved—that is, the stage of the carbamazepine degradation mechanism reached and, consequently, the nature of the intermediates that coexist in solution. As a result, the higher the molar ratio of oxidant, the lower the intensity of the tint generated, so that the formation of coloured species is reduced. The fact that under these conditions, a colourless oxidised residue is obtained shows that operating in all conditions, the dose of oxidant is sufficient to degrade the intermediates that provide tint to colourless species.

$$\text{Colour}_{\max} = 0.3759 - 0.011 [\text{H}_2\text{O}_2]_0 \quad (r^2 = 0.9988) \quad (1)$$

$$t_{\text{colour max}} = 58.31 \times [\text{H}_2\text{O}_2]_0^{-0.8813} \quad (r^2 = 0.9916) \quad (2)$$

The results shown indicate the existence of two stages in colour formation based on the carbamazepine degradation mechanism proposed in Figure 5. The first step takes place during the first stages of decomposition and leads to the formation of highly tinted species. This stage would involve hydroxylation reactions through the electrophilic attack of the hydroxyl radicals to the olefinic double bond in the central and lateral heterocyclic rings of carbamazepine, conducting to the formation of the corresponding hydroxylated carbamazepines. The action of hydroxyl radicals can generate a new hydroxylation of the molecule, leading to the creation of cis and trans-dihydroxy-carbamazepine [20]. The formation of the rare cis isomer appears to be less than that of trans [21]. Finally, the oxidation of these species would produce colour precursors, oxo and dioxo-carbamazepines (10-OH-CBZ, 9-OH-CBZ, EP-CBZ, OX-CBZ), due to the presence of chromophore groups in their molecular structure.

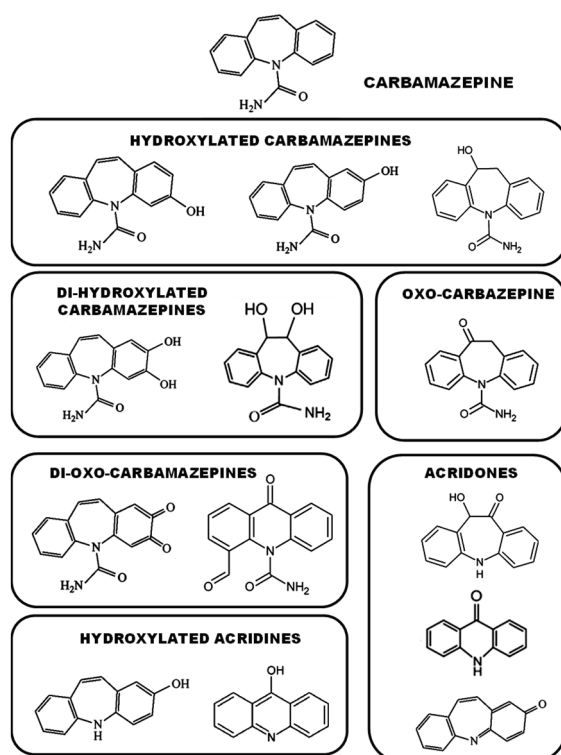


Figure 5. Reaction intermediates causing colour in oxidised carbamazepine solutions.

During the second stage, there would be the creation of additional species that coexist with those generated in the previous stage, which provide less intensity of tint to the water. In this case, it is possible to consider the formation of degradation by-products of the carbamazepine species, generating hydroxylated molecules of acridine (9-OH-acridine) and the corresponding acridones that cause the additional contribution of colour.

Figure 6 shows the effect of the oxidant concentration used on several parameters that indicate the quality of the water once it is treated. Analysing the tint of the oxidised water, it is found that operating with concentrations $[H_2O_2]_0 = 2.0$ mM, the oxidation of carbamazepine leads to the formation of highly coloured species. On the other hand, working with concentrations higher than $[H_2O_2]_0 = 5.0$ mM, a colourless water is obtained. Simultaneously, the redox potential shows an evolution characterised by a slight decrease until reaching a minimum value ($[Redox]_{min} = -0.489$ V) in $[H_2O_2]_0 = 2.0$ mM, when the maximum colour formation take place ($Colour_{max} = 0.381$ AU). Subsequently, it increases practically linear with respect to the concentration of oxidant applied.

To explain this minimum value of redox potential, a relationship can be established between the evolution of the potential and the reaction intermediates generated in the different stages of the oxidation mechanism. Studies carried out on the effect of the substitution of groups of different nature in aromatic rings indicate that they affect the value of the redox potential of the molecule, increasing or decreasing depending on the inducing effect of the substituent groups to accept or transfer electrons [17]. Therefore, if ring substitution is favored, the redox potential value diminishes.

In the case of carbamazepine, there is a small stabilisation by resonance, which is attributable to electronic delocalisation. When the ring loses the proton of the substituted hydroxyl group, electron delocalisation increases, thus favoring stability and reducing the redox potential. Therefore, based on these hypotheses, the minimum value observed would be related to the maximum concentration of hydroxylated and dihydroxylated carbamazepines in the reaction medium, which would be the precursors of the tint that the solution acquires. By increasing the oxidant ratio, these intermediates are degraded, increasing the degree of oxidation, and it is found that the redox potential of the system evolves to positive values, which would indicate the formation of quinones and acridines.

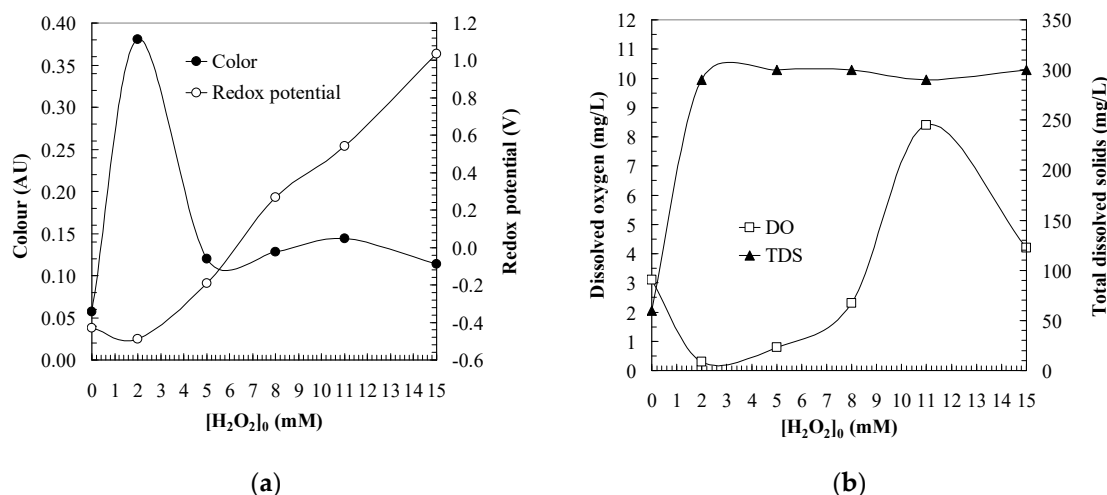


Figure 6. Indicator parameters of water quality analysed at the steady state: (a) Colour and redox potential. (b) Dissolved oxygen and total dissolved solids. Experimental conditions: $[CBZ]_0 = 50.0$ mg/L; pH = 3.0; $[Fe]_0 = 10.0$ mg/L; $[UV] = 150$ W; $T = 40$ °C.

The dissolved oxygen analysed in treated samples is consistent with their redox potential values. It is observed that the DO concentration in water increases as the treatment is conducted with higher concentrations of oxidant, up to a maximum operating point, which corresponds to $[H_2O_2]_0 = 11.0$ mM, with a DO = 8.4 mg O_2 /L. However, in the test carried out using $[H_2O_2]_0 = 15.0$ mM, the DO experienced a big decrease until values of DO = 4.2 mg O_2 /L. These lower levels of DO are observed throughout the course of the reaction, which could be due to operating with excess of oxidant with respect to the iron concentration. On the other hand, the concentration of Total Dissolved Solids (TDS, mg/L) remains constant in all the tests performed.

2.4. Effect of Iron Dosage

Figures 7 and 8 show the effect of catalyst concentration on the colour acquired by oxidised carbamazepine solutions. Operating with different iron concentrations (Figure 7a), it is observed that adding the iron dose established for each experiment increases tint to the initial carbamazepine solution ($Colour_0$, AU). The colour that the water gains shows a second degree polynomial increase (Equation (3)) with respect to the concentration of total iron supplied ($[Fe]_0$, mg/L). The initial iron added to the solution in the form of ferrous sulfate undergoes a series of equilibrium reactions between species, because the pH of the sample is adjusted to pH = 3.0 (Figure 7b). For this reason, one part of the iron ions is in a reduced state and the other is oxidised, being the ferric ions the providers of the tint to the water.

When the oxidant is added and the oxidation of the carbamazepine begins, the hue generated in the water increases until reaching a maximum value ($Colour_{max}$, AU) at 5 min after oxidation in all the tests conducted. This fact indicates that when using the same concentration of oxidant, the degradation intermediates of carbamazepine formed in water are similar species. Therefore, the colour peaks occur simultaneously, and following identical kinetics, they are displaced in parallel. This linear displacement is established by the iron concentration (Equation (4)).

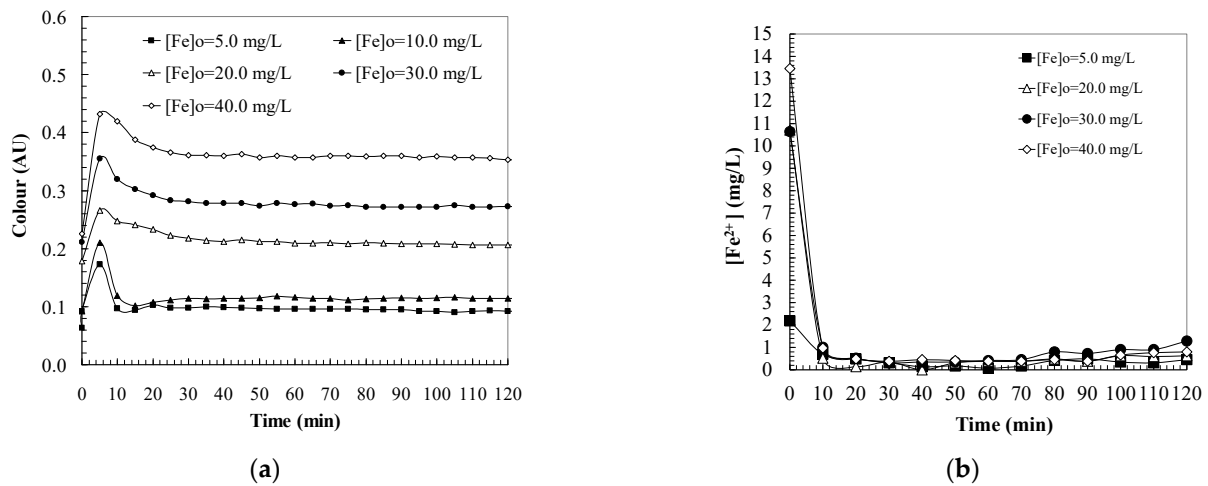


Figure 7. (a) Effect of iron on colour changes in a photo-Fenton system during the carbamazepine oxidation. (b) Ferrous ions concentration in water solution during carbamazepine oxidation. Experimental conditions: $[CBZ]_0 = 50.0$ mg/L; $pH = 3.0$; $[H_2O_2]_0 = 15.0$ mM; $[UV] = 150$ W; $T = 40$ °C.

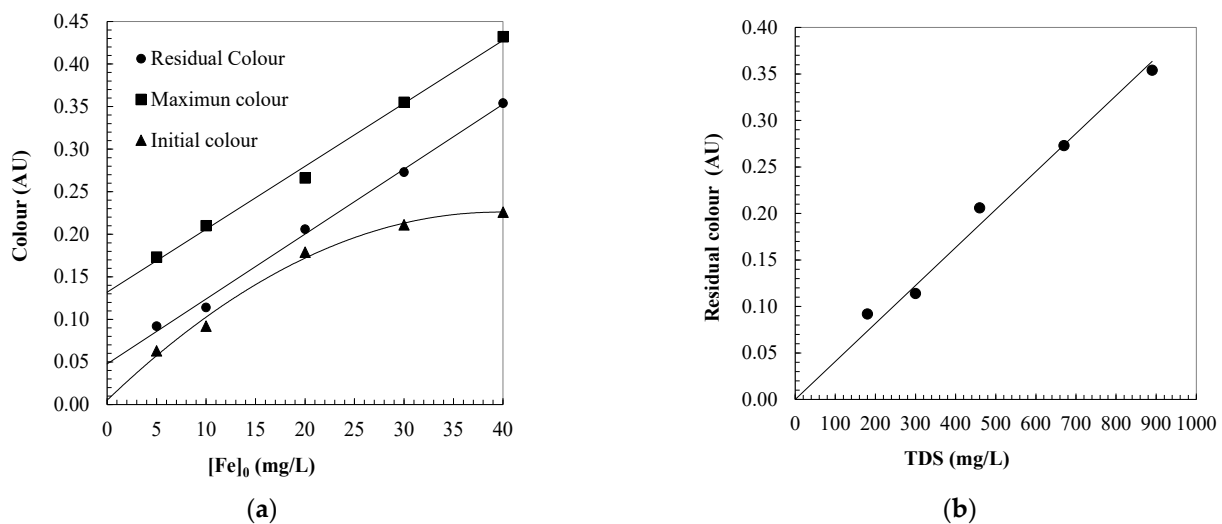


Figure 8. (a) Effect of iron dosage on water colour levels observed during the carbamazepine oxidation. (b) Relationship between total dissolved solids and the residual colour of water oxidized. Experimental conditions: $[CBZ]_0 = 50.0$ mg/L; $pH = 3.0$; $[H_2O_2]_0 = 15.0$ mM; $[UV] = 150$ W; $T = 40$ °C.

On the other hand, the persistent colour that lasts in the oxidised sample ($Colour_{\infty}$, AU) increases linearly with the iron concentration (Equation (5)). It is observed that both the maximum colour and the residual increase linearly with the total iron concentration, according to an average ratio of $k_{Fe} = 0.0075$ AU L/mg Fe. Furthermore, it is found that they remain constant in all the tests: a difference between the maximum colour and the residual of 0.0843 AU. This tint value is explained by the contribution of iron species that can interact with the organic load of the water, forming metallic complexes, which are degraded during oxidation. As shown in Figure 8b, the lasting residual colour is provided by the iron species in suspension, which contribute linearly (Equation (7)) to the total suspended solids (TDS, mg/L).

$$Colour_0 = 0.0117 [Fe]_0 - 0.0002 [Fe]_0^2 \quad (r^2 = 0.9901) \quad (3)$$

$$Colour_{max} = 0.132 + 0.0074 [Fe]_0 \quad (r^2 = 0.9946) \quad (4)$$

$$Colour_{\infty} = 0.0477 + 0.0076 [Fe]_0 \quad (r^2 = 0.9961) \quad (5)$$

$$[\text{TDS}] = 72.982 + 20.211 [\text{Fe}]_0 \quad (r^2 = 0.9974) \quad (6)$$

$$\text{Colour}_\infty = 0.0004 [\text{TDS}] \quad (r^2 = 0.9826) \quad (7)$$

3. Materials and Methods

3.1. Experimental Methods

Samples of carbamazepine aqueous solutions ($[\text{CBZ}]_0 = 50.0 \text{ mg/L}$, Fagron 99.1%) were studied in a photocatalytic 1.0 L reactor provided with an UV-150 W mercury lamp of medium pressure (Heraeus, 95%, transmission between 300 and 570 nm). Reactions started adding the iron catalyst as ferrous ion ($[\text{Fe}]_0$, mg/L), operating between $[\text{Fe}]_0 = 5.0\text{--}40.0 \text{ mg/L}$ ($\text{FeSO}_4 \cdot 7 \text{ H}_2\text{O}$, Panreac 99.0%) and the oxidant dosage for each set of experiments, which varied between $[\text{H}_2\text{O}_2]_0 = 0\text{--}15.0 \text{ mM}$ (Panreac, 30% w/v). All the experiments were conducted at around 40 °C in order to simulate real working conditions, considering the heat absorbed by the water that is in direct contact with the UV lamp. Assays were performed under different initial pH conditions (pH between 2.0 and 5.0) in order to assess the effect of this parameter on colour formation during the oxidation of carbamazepine aqueous solutions. Acidity was kept constant adding NaOH and HCl.

3.2. Analytical Methods

Carbamazepine concentration (CBZ, mg/L) was assessed along the reaction at $\lambda = 210 \text{ nm}$ by a High-Performance Liquid Chromatograph attached to a spectrophotometer UV/Vis (HPLC Agilent 1200). Analysis was performed by injecting manually 20.0 μL samples, which were dragged by a carrier of 1.0 mL/min flow, consisting of a mixture of methanol and distilled water MeOH/H₂O: 80/20, through a Column C₁₈, XBridge Phenyl 5 μm 4.6 \times 250 mm (Bridge Waters), with limit of detection 0.1 mg/L.

Colour expressed in Absorbance Units (AU) was quantified by the absorbance of the aqueous solution analysed at $\lambda = 455 \text{ nm}$ and ferrous ion ($[\text{Fe}^{2+}]$, mg/L) at $\lambda = 510 \text{ nm}$ by the phenanthroline method using an UV/Vis Spectrophotometer 930-Uvikon [22]. Dissolved oxygen (DO, mg/L) was measured by a DO-meter HI9142. Total dissolved solids (TDS, mg/L) were analysed by a TDS Metter Digital and Redox potential (V) by a conductimeter (Basic 20 Crison).

3.3. Liquid Chromatography-Mass Spectrometry to Elucidate the Intermediates of Carbamazepine Degradation

Samples were analysed by Liquid Chromatography-Mass Spectrometry to find the carbamazepine degradation pathways that induce high levels of colour in the water during the oxidation process. Analysis was performed with an LC/Q-TOF provided with an ionisation source ESI + Agilent Jet Stream, with the following conditions: Kinetex column EVO C18 (100 \times 3 mm) 2.6 μm . Moving phase 0.1% Formic Acid (A): Acetonitrile 0.1% Formic Acid (B). Gradient, %B: time (min): 20:0; 20:2; 100:24; 100:28; 20:30. Flow 0.3 mL/min. Column Temperature 35 °C. Injection volume 5 μL . Ionisation: Gas temperature 300 °C, drying gas 10 L/min, nebuliser 20 psig, shelf gas temperature 350 °C, shelf gas flow 11 L/min, frag 125 V. V_{cap} 3500 V.

A screening method was developed, allowing the elution and ionisation of the majority of compounds in the sample. Before starting the analysis, the stabilisation of the system, the reproduction in the signals, and the correction of the exact masses were checked. With the aforementioned conditions, the chromatogram shown in Figure 9 was attained.

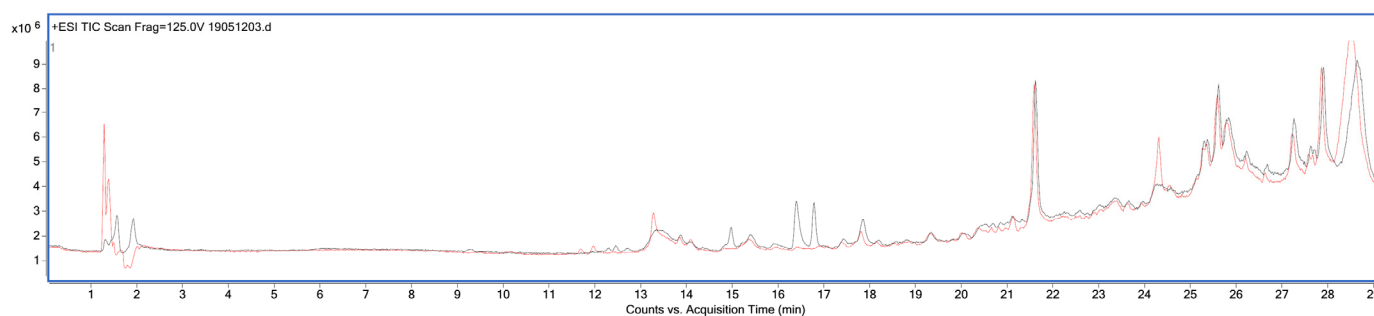


Figure 9. Chromatographic profile of a methanol blank (grey line) and of the sample (red line).

The search for compounds was performed using the Find deconvolution algorithm by molecular features and a subsequent screening of the proposed compounds, based on compounds detected in the blank, background noise, and minimum abundance of the compound (Figure 10). Appendix A summarises the major ions (m/z) and the experimental masses calculated for each of the compounds.

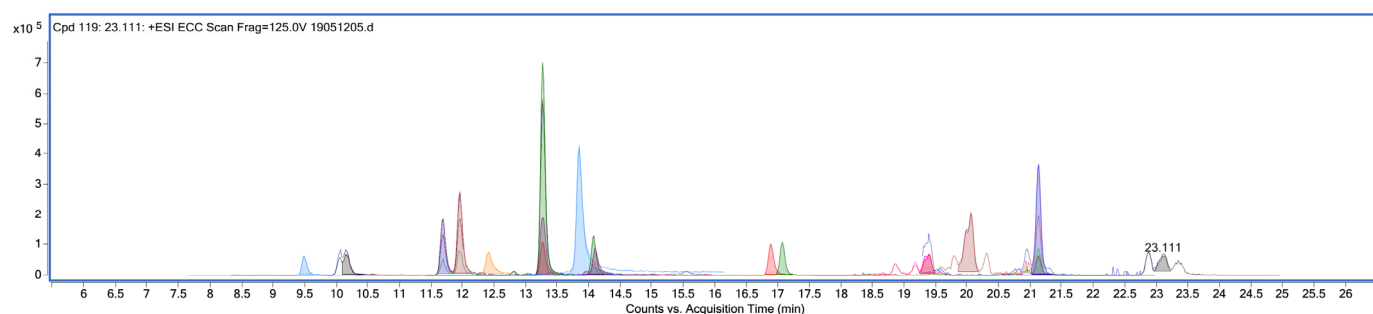


Figure 10. Chromatographic profile of the major compounds in the oxidised carbamazepine sample.

4. Conclusions

The stoichiometric ratio of oxidant determines the degree of oxidation achieved, that is, the nature of the intermediates that coexist in solution. Performing with low concentrations of oxidant, corresponding to stoichiometric ratios of 1 mol CBZ: 10 mol H_2O_2 , colour is generated in the water until it reaches its maximum intensity (oxo and dioxo-carbamazepines). Subsequently, the tint continues to increase more slowly, until arriving at the steady state, remaining a coloured aqueous residue that would contain hydroxylated acridines and acridones. Applying concentrations higher than 1 mol CBZ: 25 mol H_2O_2 , the colour formation follows the evolution of a reaction intermediate, obtaining a colourless solution.

The initial iron added to the solution, in the form of ferrous sulfate, undergoes a series of equilibrium reactions between species. This is due to the fact that the acidity of the sample is adjusted to pH = 3.0. Therefore, a part of the iron ions are found in a reduced state and the another in its oxidised, being the ferric ions that provide tint to the water. Both the maximum colour and the persistent colour increase with the concentration of iron used in the treatment, according to an average ratio of $k_{Fe} = 0.0075 \text{ AU L/mg Fe}$. The maximum tint would be generated by the iron species that interact with the organic load, forming metallic complexes, while the lasting colour would be generated by the iron species in suspension.

Author Contributions: Conceptualization, N.V. and J.M.L.; methodology, L.M.C. and H.A.Q.; software, J.M.L.; validation, C.F., J.I.L. and N.V.; formal analysis, J.I.L.; investigation, N.V., H.A.Q. and C.F.; resources, C.F.; data curation, N.V.; writing—original draft preparation, N.V., C.F. and H.A.Q.; writing—review and editing, J.M.L., L.M.C. and J.I.L.; visualization, N.V. and C.F.; supervision, L.M.C.; project administration, N.V. and J.I.L. and J.I.L. acquired the funding. All authors have read and agreed to the published version of the manuscript.

Funding: Authors are grateful to the University of the Basque Country UPV/EHU the financial support to carry out this research study through the scholarship Student Mobility for Traineeships in the Erasmus + Programme between the Anadolu University in Eskisehir (Turkey) and the Faculty of Engineering Vitoria-Gasteiz (Spain), and the research Project PPGA20/33.

Acknowledgments: The authors thank for technical and human support provided by Central Service of Analysis from Álava—SGIker—UPV/EHU.

Conflicts of Interest: The authors declare no conflict of interest.

Appendix A

Label	RT	m/z	Mass	Height	Name	Score	Diff (DB ppm)	Ions
Cpd 31: carbamazepina	13.276	237,1029	236,0956	500597	carbamazepina	96.87	-2.51	7
Cpd 76: 13.857	13.857	274,2747	273,2674	352024				3
Cpd 112: 21.134	21.134	320,2563	297,2671	162272				8
Cpd 14: 10-OH-CBZ	11.961	255,1133	254,106	157787	10-OH-CBZ	97.82	-2	5
Cpd 33: 13.277	13.277	377,2089	376,2016	147884				3
Cpd 12: 10-OH-CBZ	11.693	255,113	254,1057	111904	10-OH-CBZ	99.74	-0.69	4
Cpd 104: 20.044	20.044	318,2412	295,2519	104589				5
Cpd 81: 14.083	14.083	237,1027	236,0954	93089				3
Cpd 30: 13.276	13.276	275,0584	274,0511	85219				3
Cpd 93: 16.894	16.894	238,111	237,1027	75562				3
Cpd 83: 14.110	14.111	318,2306	317,233	89324				3
Cpd 115: 21.135	21.135	336,2303	335,223	85581				3
Cpd 17: 9-OH-acridine	12.421	196,0759	195,0686	63672	9-OH-acridine	99.55	-1.06	2
Cpd 91: 17.075	17.075	226,0865	225,0793	63218				5
Cpd 9: 10-OH-CBZ	10.167	255,1132	254,1059	56756	10-OH-CBZ	98.81	-1.47	2
Cpd 98: 19.375	19.375	280,2641	279,2569	55466				2
Cpd 6: 9.484	9.484	234,2067	233,1995	55020				2
Cpd 100: 19.384	19.384	320,2569	319,2497	54644				2
Cpd 119: 23.111	23.111	280,2638	279,2566	53960				2
Cpd 113: 21.134	21.134	356,3274	355,3201	50339				2
Cpd 86: 14.340	14.34	288,2895	287,2823	45206				2
Cpd 85: 14.155	14.155	210,0915	209,0842	42403				2
Cpd 35: 13.278	13.278	295,1557	294,1484	40689				2
Cpd 19: 13.263	13.263	261,1861	259,1788	36857				2
Cpd 111: 20.951	20.951	320,2565	297,2671	37049				6
Cpd 48: EP-CBZ	13.382	253,0975	252,0902	36822	EP-CBZ	99.19	-1.22	2
Cpd 105: 20.049	20.049	334,215	333,2077	35819				3
Cpd 78: 14.068	14.068	290,2698	289,2625	35753				2
Cpd 16: 12.147	12.147	264,2224	263,2251	35155				2
Cpd 95: 19.177	19.177	280,264	279,2568	34356				2
Cpd 15: 12.028	12.028	248,2431	245,2358	33414				2
Cpd 107: 20.311	20.311	318,2406	295,2511	33204				4
Cpd 80: 14.082	14.082	275,0585	274,0513	30799				3
Cpd 29: 13.275	13.275	617,1398	1232,2651	30685				3
Cpd 27: 13.239	13.239	606,1349	1210,2552	30129				3
Cpd 106: 20.056	20.056	354,3127	353,3054	29989				2
Cpd 94: 15.871	15.871	280,2638	279,2566	29484				2
Cpd 25: 13.202	13.202	593,1277	1188,2408	28796				3
Cpd 10: OX-CBZ	11.455	253,0974	252,0902	28240	OX-CBZ	99.39	-1.06	2
Cpd 79: 14.082	14.082	220,0761	219,0688	27418				2
Cpd 92: 18.868	18.868	320,2569	319,2496	27350				2
Cpd 38: 13.311	13.311	628,147	1254,2795	26627				3
Cpd 103: 19.794	19.794	318,2408	295,2515	26475				4
Cpd 23: 13.240	13.24	605,8839	1209,7633	26392				3
Cpd 60: 13.472	13.472	550,151	549,1437	26184				2
Cpd 26: 13.203	13.203	594,8776	1187,7406	26183				3
Cpd 89: 15.304	15.304	158,1537	157,1464	25035				2
Cpd 50: 13.409	13.409	532,5398	531,5325	24788				2
Cpd 82: 14.089	14.089	301,2856	300,2783	24337				2
Cpd 84: 14.126	14.126	239,118	238,1107	24171				2
Cpd 57: 13.443	13.443	541,3456	540,3383	24099				2
Cpd 75: EP-CBZ	13.706	253,097	252,0898	23905	EP-CBZ	99.85	0.53	2
Cpd 24: 13.164	13.164	584,1215	1166,2284	23833				3
Cpd 63: 13.503	13.503	558,9567	557,9494	23484				2
Cpd 87: 14.414	14.414	244,2638	243,2565	23224				2
Cpd 67: 13.533	13.533	567,762	566,7547	23093				2
Cpd 32: 13.277	13.277	616,8904	1231,7663	22863				3
Cpd 39: 13.312	13.312	627,8961	1253,7777	22613				3
Cpd 99: 19.383	19.383	336,2311	335,2238	22461				3
Cpd 41: 13.343	13.343	639,1532	1276,2919	22192				3
Cpd 8: 10.079	10.079	237,1025	236,0952	22176				2
Cpd 108: 20.338	20.338	293,2085	292,2012	22094				3
Cpd 47: 13.377	13.377	523,7354	522,7282	21838				2
Cpd 23: 13.163	13.163	583,871	1165,7274	21569				3
Cpd 18: 12.606	12.606	356,2799	355,2726	21417				2
Cpd 69: 13.562	13.562	576,5671	575,5598	21292				2
Cpd 4: 8.489	8.489	218,2118	217,2045	19862				2
Cpd 59: 13.471	13.471	550,3513	549,344	19427				2
Cpd 43: 13.361	13.361	263,0799	240,0905	19233				4
Cpd 48: 13.378	13.378	650,1607	1296,3068	19170				3
Cpd 110: 20.949	20.949	336,2306	335,2233	18835				2
Cpd 101: 19.382	19.382	316,2255	293,2362	18690				2
Cpd 70: 13.590	13.59	585,3719	584,3646	18102				2
Cpd 52: 13.410	13.41	532,7411	531,7338	17844				2
Cpd 61: 13.473	13.473	549,9508	548,9435	17777				2
Cpd 66: 13.531	13.531	567,9614	566,9542	17321				2
Cpd 22: 13.126	13.126	573,1151	1144,2156	17313				3
Cpd 42: 13.345	13.345	638,9041	1275,7937	17090				2
Cpd 55: 13.440	13.44	541,5456	540,5383	16747				2
Cpd 64: 13.503	13.503	559,9561	558,9488	16712				2
Cpd 62: 13.502	13.502	558,7568	557,7495	16704				2
Cpd 98: 13.444	13.444	541,1454	540,1382	16651				2
Cpd 7: 9.927	9.927	278,2328	277,2255	16503				2
Cpd 51: 13.410	13.41	661,1668	1320,319	16386				2
Cpd 53: 13.411	13.411	532,3405	531,3332	16342				2
Cpd 5: 9.370	9.37	282,2383	261,231	16255				2
Cpd 37: 13.309	13.309	505,923	504,9157	15944				2
Cpd 72: 13.615	13.615	594,1771	593,1699	15851				2
Cpd 36: 13.309	13.309	506,1242	505,1169	15539				2
Cpd 77: 14.042	14.042	288,2899	287,2826	15366				2
Cpd 46: 13.377	13.377	523,9355	522,9282	15213				2
Cpd 65: 13.530	13.53	567,9607	566,9534	14913				2
Cpd 44: 13.376	13.376	523,5355	522,5282	14899				2
Cpd 21: 13.125	13.125	572,8649	1143,7152	14659				2
Cpd 3: 5.852	5.852	120,0436	137,0473	14406				2
Cpd 2: 5.222	5.222	170,1176	187,1208	14396				2
Cpd 118: 22.908	22.908	336,3235	335,3163	14060				2
Cpd 45: 13.377	13.377	649,9099	1287,8052	13910				3
Cpd 73: 13.619	13.619	594,376	593,3687	13878				2
Cpd 68: 13.562	13.562	576,3662	575,3589	13754				2
Cpd 40: 13.343	13.343	514,7299	513,7226	13575				2
Cpd 34: 13.278	13.278	281,1401	280,1329	13193				2
Cpd 88: 14.862	14.862	224,1433	223,1361	13078				2
Cpd 102: 19.782	19.782	214,2174	213,2101	13071				2
Cpd 54: 13.412	13.412	660,9158	1319,8171	12993				3
Cpd 11: 13.546	13.546	339,2322	338,2349	12912				2
Cpd 1: 12.841	12.841	188,1018	173,1052	12774				2
Cpd 93: 18.869	18.869	336,2303	335,223	12673				2
Cpd 56: 13.443	13.443	672,1734	1342,3323	12590				2
Cpd 13: 11.958	11.958	220,0759	219,0686	12462				2
Cpd 97: 19.182	19.182	336,2305	335,2232	11979				2
Cpd 116: 21.404	21.404	431,1659	430,1586	11763				2
Cpd 71: 13.591	13.591	585,1719	584,1647	11328				2
Cpd 117: 22.123	22.123	429,3195	428,3122	11051				2
Cpd 74: 13.620	13.62	593,9763	592,969	10811				2
Cpd 95: 18.968	18.968	316,2252	293,2355	10142				3
Cpd 109: 20.479	20.479	483,3842	483,3769	10113				2
Cpd 20: 13.085	13.085	561,8572	1121,6998	10112				2
Cpd 114: 21.135	21.135	339,2996	338,2923	10052				2

Figure A1. Major ions (m/z) and experimental masses calculated for each of the intermediate compounds detected in a sample of carbamazepine oxidized by photo-Fenton treatment under operating conditions that lead to the formation of coloured solution.

5. Hai, F.I.; Yang, S.; Asif, M.B.; Sencadas, V.; Shawkat, S.; Sanderson-Smith, M.; Gorman, J.; Xu, Z.-Q.; Yamamoto, K. Carbamazepine as a Possible Anthropogenic Marker in Water: Occurrences, Toxicological Effects, Regulations and Removal by Wastewater Treatment Technologies. *Water* **2018**, *10*, 107. [[CrossRef](#)]
6. Arye, G.; Dror, I.; Berkowitz, B. Fate and Transport of Carbamazepine in Soil Aquifer Treatment (SAT) Infiltration Basin Soils. *Chemosphere* **2011**, *82*, 244–252. [[CrossRef](#)] [[PubMed](#)]
7. Al Aukidy, M.; Verlicchi, P.; Jelic, A.; Petrovic, M.; Barcelò, D. Monitoring Release of Pharmaceutical Compounds: Occurrence and Environmental Risk Assessment of Two WWTP Effluents and Their Receiving Bodies in the Po Valley, Italy. *Sci. Total Environ.* **2012**, *438*, 15–25. [[CrossRef](#)] [[PubMed](#)]
8. Badia-Fabregat, M.; Lucas, D.; Pereira, M.A.; Alves, M.; Pennanen, T.; Fritze, H.; Rodríguez-Mozaz, S.; Barceló, D.; Vicent, T.; Caminal, G. Continuous Fungal Treatment of Non-Sterile Veterinary Hospital Effluent: Pharmaceuticals Removal and Microbial Community Assessment. *Appl. Microbiol. Biotechnol.* **2016**, *100*, 2401–2415. [[CrossRef](#)] [[PubMed](#)]
9. Behera, S.K.; Kim, H.W.; Oh, J.-E.; Park, H.-S. Occurrence and Removal of Antibiotics, Hormones and Several Other Pharmaceuticals in Wastewater Treatment Plants of the Largest Industrial City of Korea. *Sci. Total Environ.* **2011**, *409*, 4351–4360. [[CrossRef](#)] [[PubMed](#)]
10. Tian, Y.; Xia, X.; Wang, J.; Zhu, L.; Wang, J.; Zhang, F.; Ahmad, Z. Chronic Toxicological Effects of Carbamazepine on *Daphnia Magna* Straus: Effects on Reproduction Traits, Body Length, and Intrinsic Growth. *Bull. Environ. Contam. Toxicol.* **2019**, *103*, 723–728. [[CrossRef](#)] [[PubMed](#)]
11. Xin, J.; Yan, S.; Hong, X.; Zhang, H.; Zha, J. Environmentally Relevant Concentrations of Carbamazepine Induced Lipid Metabolism Disorder of Chinese Rare Minnow (*Gobiocypris Rarus*) in a Gender-Specific Pattern. *Chemosphere* **2021**, *265*, 129080. [[CrossRef](#)] [[PubMed](#)]
12. Yan, S.; Chen, R.; Wang, M.; Zha, J. Carbamazepine at Environmentally Relevant Concentrations Caused DNA Damage and Apoptosis in the Liver of Chinese Rare Minnows (*Gobiocypris Rarus*) by the Ras/Raf/ERK/P53 Signaling Pathway. *Environ. Pollut.* **2021**, *270*, 116245. [[CrossRef](#)] [[PubMed](#)]
13. Almeida, Â.; Calisto, V.; Domingues, M.R.M.; Esteves, V.I.; Schneider, R.J.; Soares, A.M.V.M.; Figueira, E.; Freitas, R. Comparison of the Toxicological Impacts of Carbamazepine and a Mixture of Its Photodegradation Products in *Scrobicularia Plana*. *J. Hazard Mater.* **2017**, *323*, 220–232. [[CrossRef](#)] [[PubMed](#)]
14. Prasse, C.; Stalter, D.; Schulte-Oehlmann, U.; Oehlmann, J.; Ternes, T.A. Spoil for Choice: A Critical Review on the Chemical and Biological Assessment of Current Wastewater Treatment Technologies. *Water Res.* **2015**, *87*, 237–270. [[CrossRef](#)] [[PubMed](#)]
15. Benner, J.; Helbling, D.E.; Kohler, H.-P.E.; Wittebol, J.; Kaiser, E.; Prasse, C.; Ternes, T.A.; Albers, C.N.; Amand, J.; Horemans, B.; et al. Is Biological Treatment a Viable Alternative for Micropollutant Removal in Drinking Water Treatment Processes? *Water Res.* **2013**, *47*, 5955–5976. [[CrossRef](#)] [[PubMed](#)]
16. Magi, A.; Semeraro, R.; Mingrino, A.; Giusti, B.; D’Aurizio, R. Nanopore Sequencing Data Analysis: State of the Art, Applications and Challenges. *Brief. Bioinform.* **2018**, *19*, 1256–1272. [[CrossRef](#)] [[PubMed](#)]
17. Fieser, L.F.; Fieser, M. *Química Orgánica Superior*; Grijalbo: Barcelona, Mexico, 1966; Volume 2.
18. Villota, N.; Lomas, J.; Camarero, L. Changes of Turbidity during the Oxidation of Dihydroxylated Benzenes by Fenton Reagent and Effect on Dissolved Oxygen. *Desalination Water Treat.* **2018**, *127*, 2–7. [[CrossRef](#)]
19. De Luis, A. *Degradación de Compuestos Fenólicos En Disolución Acuosa Con Peróxido de Hidrógeno: Modelización de Los Sistemas de Generación de Radicales*; University of the Basque Country: Leioa, Spain, 1999.
20. Zhang, L.; Zhao, X.; Niu, C.; Tang, N.; Guo, H.; Wen, X.; Liang, C.; Zeng, G. Enhanced Activation of Peroxymonosulfate by Magnetic Co₃MnFeO₆ Nanoparticles for Removal of Carbamazepine: Efficiency, Synergetic Mechanism and Stability. *Chem. Eng. J.* **2019**, *362*, 851–864. [[CrossRef](#)]
21. Golan-Rozen, N.; Seiwert, B.; Riemenschneider, C.; Reemtsma, T.; Chefetz, B.; Hadar, Y. Transformation Pathways of the Recalcitrant Pharmaceutical Compound Carbamazepine by the White-Rot Fungus *Pleurotus Ostreatus*: Effects of Growth Conditions. *Environ. Sci. Technol.* **2015**, *49*, 12351–12362. [[CrossRef](#)] [[PubMed](#)]
22. Mijangos, F.; Varona, F.; Villota, N. Changes in Solution Color During Phenol Oxidation by Fenton Reagent. *Environ. Sci. Technol.* **2006**, *40*, 5538–5543. [[CrossRef](#)] [[PubMed](#)]

3.4. 4. argitalpena. Analysis of a hybrid suspended-supported photocatalytic reactor for the treatment of wastewater containing benzothiazole and aniline

3.4 kapitulua artikulu honi dagokio:

C. Ferreiro, N. Villota, J.I. Lombraña, M.J. Rivero, V. Zúñiga, J.M. Rituerto. Analysis of a hybrid suspended-supported photocatalytic reactor for the treatment of wastewater containing benzothiazole and aniline. *Water*, 11, 2, 337, 2019. DOI: 10.3390/w11020337.

Article

Analysis of a Hybrid Suspended-Supported Photocatalytic Reactor for the Treatment of Wastewater Containing Benzothiazole and Aniline

Cristian Ferreiro ^{1,*} , Natalia Villota ², José Ignacio Lombrana ¹ , María J. Rivero ³ ,
Verónica Zúñiga ⁴  and José Miguel Rituerto ⁴

¹ Department of Chemical Engineering, University of the Basque Country UPV/EHU, P.O. Box 644, E-48080 Bilbao, Spain; ji.lombrana@ehu.eus

² Department of Environmental and Chemical Engineering, Escuela Universitaria de Ingeniería Vitoria-Gasteiz, University of the Basque Country UPV/EHU, Nieves Cano, 12. 01006 Alava, Spain; natalia.villota@ehu.eus

³ Department of Chemical and Biomolecular Engineering, University of Cantabria, 39005 Santander, Spain; riveromj@unican.es

⁴ General Química, S.A.U. (Grupo Dynasol), 01213 Lantaron, Spain; veronica.zuniga@repsol.com (V.Z.); jrituertol@repsol.com (J.M.R.)

* Correspondence: cristian.ferreiro@ehu.eus; Tel.: +34-946-012-512

Received: 24 January 2019; Accepted: 13 February 2019; Published: 16 February 2019



Abstract: In this work, a study of the main operating variables affecting TiO₂/UV photocatalysis was carried out. The treatment of an industrial effluent containing aniline and benzothiazole from the manufacture of accelerants for vulcanization was performed in a TiO₂-supported commercial photoreactor. The degradation of both contaminants was monitored by GC-MS analysis. The proposed experiments were able to properly identify the phenomenon of adsorption, as well as to improve the performance of the commercial photoreactor by adding small amounts of TiO₂ in suspension. The removal performance, durability of the photocatalytic material, and energy costs were analysed. The results showed that the use of suspensions intensifies the degradation obtaining an improvement of 23.15% with respect to the use of the supported catalyst. For an aniline and benzothiazole solution, the best operating conditions were found at pH = 12.0, introducing 60.0 mg L⁻¹ of suspended TiO₂ together with the existing supported catalyst.

Keywords: aniline; benzothiazole; photocatalysis; adsorption mechanism; TiO₂/UV; supported catalyst; suspended catalyst; commercial photoreactor; water treatment

1. Introduction

The industrial scale of many production processes has generated increasing amounts of waste by-products that have been dumped into the environment assuming that nature itself would absorb them properly. However, many of these compounds such as aniline (ANI) and benzothiazole (BT) have been shown to affect the health of live organisms [1]. These pollutants are typical of effluents from industries related to the manufacture of dyes for textiles, accelerators for vulcanization, oil refining, biocides, paper and leather manufacturing, anticorrosive agents in antifreeze formulations, and photosensitizers in photography [2,3].

Aniline and benzothiazole are two pollutants of concern due to their effects on the environment and human health [4,5]. These chemicals are highly soluble in water, resistant to biodegradation and have toxic effects [6]. In addition, together with the scarcity of information about the toxicity of BT, which is known to cause acute toxicity in the aquatic environment, the US Environmental Protection

Agency has included it in the Contaminant Candidate List 4 (CCL4) [7]. Only in the USA BT's production was around 450 t in 2016 [4,8]. Many of these pollutants cannot be completely eliminated by conventional water treatment processes and consequently BT has been detected in drinking water distribution networks that reach household taps [9]. Moreover, a study has been published showing genotoxicity and growth inhibition caused by aniline in wheat crops. The low biodegradability, stable chemical structure, and toxicity of this type of organic compounds prevent their removal in a biological treatment [6].

The degradation of these non-biodegradable organic pollutants could be satisfactorily achieved using advanced oxidation processes (AOPs). These processes could remove these contaminants completely or make them less harmful to human health and the aquatic environment [10].

TiO₂/UV photocatalysis can be an alternative to conventional processes or other AOPs with low oxidation rates and high operating costs to treat recalcitrant and non-biodegradable contaminants [11]. This technology is proposed due to its low cost, operating temperature and atmospheric pressure, so it does not require complex installations. Among the most commonly used photoactive materials, TiO₂ stands out due to its high activity under UV radiation. Oxidation reactions take place near the catalytic surface of the semiconductor. The electrons of the valence band under UV light move to the conduction band generating a hollow electron pair. These electrons in contact with air reduce O₂ by forming superoxide ions. On the other hand, the generated holes oxidize the adsorbed water generating hydroxyl radicals (HO[•]) on the TiO₂ surface. Next, these generated radical species will be in charge of oxidizing the organic compounds present in the aqueous reaction medium to produce CO₂ [2,12]. The extent of the degradation can be conditioned by the adsorption of the organic compounds [13–15].

Although photocatalysis in suspension is becoming important within AOPs, the recovery of the catalyst has been always a challenge to its commercial implementation [2,16,17]. The immobilization of the catalyst on a support could overcome this limitation [12,16,18–22]. For example, in Kecskémét (Hungary) the Mercedes-Benz factory installed in 2016 a TiO₂-supported photocatalytic h₂o.TITANIUM® equipment to treat the flush water of the factory for chemical-free purposes [23]. Many studies indicate that TiO₂ can be supported on several materials such as pebbles, glass spheres, silica gel beads, or cellulose. However, the simultaneous use of the catalyst supported on the wall of a photoreactor as well as suspended has not been studied yet. This would be a way of improving the performance of a commercial reactor of supported catalytic configuration.

The present work focuses on the improvement of commercial photoreactors for industrial implementation, which have TiO₂ supported to remove aniline and benzothiazole. Therefore, TiO₂ suspensions will be introduced to increase the degradation in this hybrid system. The adsorption and degradation of synthetic solutions containing aniline or benzothiazole using TiO₂ catalyst under different experimental conditions have been investigated. The adsorption equilibrium and kinetic parameters were estimated from the adsorption experiments. In addition, a kinetic study of the main operating variables of the photocatalytic process has been carried out with synthetic solutions of aniline or benzothiazole, varying the initial pH of the solution, dose of catalyst in suspension, configuration of the TiO₂ and the effect of the mixture of both compounds was analysed. Finally, the operating variables that lead to a higher removal percentage without generating difficulties and higher costs in the recovery process of the catalytic particles of TiO₂ were selected.

2. Materials and Methods

2.1. Reagents

Aniline (C₆H₅NH₂, Acros Organics, 99.5%), benzothiazole (C₇H₅NS, Sigma-Aldrich, 97%), hydrogen chloride (HCl, Merck, 37%), sodium hydroxide (NaOH, Panreac, 50%), dichloromethane (CH₂Cl₂, Merck, >99.9%), and diphenylamine (C₁₂H₁₁N, Merck, 99%). Deionized water was supplied by a Milli-Q water purification unit from Merck. The TiO₂ Aeroxide®P25 catalyst was obtained from Evonik Industries.

2.2. Product Analysis

The quantification of each individual compound was determined by an Agilent 6890N gas chromatograph coupled to an Agilent 5975 mass spectrometer. The chromatograph was equipped with a 30.0 cm non-polar phase capillary column. The aqueous samples to be analysed, previously adjusted to pH = 11.0 for the determination of aniline and pH = 3.0 for benzothiazole, are subjected to an extraction with dichloromethane (with 0.1% diphenylamine as internal standard). A sample volume of 0.4 μL is then injected into the GC/MS chromatograph (Agilent, CA, USA) in a program consisting of an initial temperature of 60.0 $^{\circ}\text{C}$ for 2 min and a subsequent heating ramp of 12.0 $^{\circ}\text{C min}^{-1}$ until 280.0 $^{\circ}\text{C}$ is reached, a temperature that is maintained for 20 min. Other conditions: He is used as carrier gas with a flow rate of 1.0 mL min^{-1} ; split ratio, 1:50. pH monitoring was performed with a Knicks 911 pH meter. The degree of mineralization was quantified by Total Organic Carbon TOC analysis in a Shimadzu TOC-VCSH Analyzer (Izasa Scientific, Alcobendas, Spain).

2.3. Determination of pH_{pzc}

The point of zero charge of TiO_2 P25 was determined by acid-base titration method according to Silva et al. [24]. For this purpose, 50 mL of 0.01 M NaCl solution was transferred to 100 mL flask. The values of these solutions were adjusted between 2 and 12 using 0.1 M HCl or NaOH. Then, 0.15 g of TiO_2 were added to the solution. After a contact time of 24 h, the final pH was measured. The final pH measured were plotted against the initial pH. The point of intersection of the curve result in pH_{pzc} .

2.4. Adsorption Experiments

The adsorption experiments were performed in the dark to obtain equilibrium and kinetic data in the temperature ranged of 10–60 $^{\circ}\text{C}$, pH of 2.0–12.0 for aniline and benzothiazole. All experiments were carried out at constant temperature and pH. The isotherms were obtained by preparing suspensions in which 500.0 mL solutions of aniline or benzothiazole were dissolved with 0.05 g of TiO_2 catalyst powder in 0.5 L jacketed reactor provided with a stirrer. The agitation was maintained constant at 1750 rpm in order to keep perfect mixing. The temperature was controlled by a refrigerating bath. The adsorption equilibrium concentration was reached after the solutions were stirred magnetically for 24 h in the dark. To remove the catalyst particles, the solutions were filtered through a 0.45 μm membrane (MF-Millipore) before proceeding to the analysis of the concentration of each contaminant by GC/MS chromatography. The amount of aniline or benzothiazole adsorbed onto TiO_2 at equilibrium, q_e (mg g^{-1}), was calculated using the Equation (1):

$$q_e = \frac{(C_0 - C_e) \cdot V}{M} \quad (1)$$

where C_0 and C_e are the initial and equilibrium aniline or benzothiazole concentration in mg L^{-1} respectively, V is the volume of the solution (L) and M is the mass of TiO_2 (g). Similarly, the amount adsorption of pollutant at time t (min), was calculated by Equation (2):

$$q_t = \frac{(C_0 - C_t) \cdot V}{M} \quad (2)$$

where C_0 and C_t are the initial at any time aniline or benzothiazole concentration in mg L^{-1} respectively, V is the volume of the solution (L) and M is the mass of adsorbent (g). All adsorption experiments were performed in triplicate and the mean values were used for the adsorption study. The maximum standard deviation of measured concentrations was no greater than 0.052 mg L^{-1} .

2.5. Photocatalytic Experiments

The removal of aniline and benzothiazole was carried out in a photoreactor unit AOP 1 of h2o.TITANIUM®. The experimental system consists of a tubular reactor, a mercury lamp and its corresponding power supply, a 16.0 L mixing tank and a centrifugal pump (Figure 1).

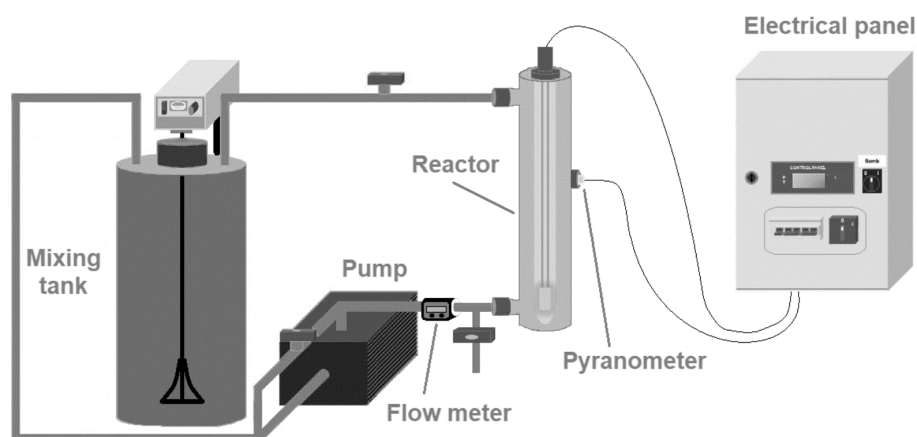


Figure 1. Schematic of the experimental equipment used to carry out the photocatalytic tests with aniline and benzothiazole.

The reactor consisted of a titanium sintered monobloc with a volume of 2.15 L, length of 473 mm, diameter 76 mm and thickness of 5 mm. The reactor had $2.3 \text{ mg TiO}_2 \text{ cm}^{-2}$ deposited therein on a structural substrate as a coating, as it is described in the patent US 2003/0059549A1 [25]. With regard to the photoreactor arrangement, it was oriented vertically with the entrance orifice of the effluent on the bottom, two orifices on the top and one on the side. The side one was used to insert the probe containing a compact infrared temperature meter, together with a radiometer (PLS Systems AB, Sloga Ingenieros S.L., Puertollano, Spain). The two remaining orifices were used to connect/disconnect the pipe with the water to be treated. The reactor is equipped with a 26 W low-medium pressure mercury UVC lamp (GPH436T5L/4-Eubizz Water, Eubizz Water, Høyanger, Norway) with a maximum emission band at 254 nm enclosed in a quartz casing which provides a minimum dose of 400 J m^{-2} , equivalent to an irradiation intensity of 25.8 W m^{-2} [26]. The installation has a flowmeter (GPI Electronic Digital Meter, GPImeters.com, NJ, USA) at the reactor inlet and a device (Pool Pump-72512, The Pool Shop, Tauranga, New Zealand) to pump out the effluent with a flow rate of $0.5 \text{ m}^3 \text{ h}^{-1}$, from the homogenization tank to the reactor.

The experiments were carried out at a constant temperature of $25.0 \text{ }^\circ\text{C}$ to treat 16.0 L of synthetic solutions of aniline or benzothiazole and mixtures of both with initial concentrations of 22.0 mg L^{-1} , maintaining a constant pH and adding TiO_2 P25 catalyst between 20.0 and 120.0 mg L^{-1} . The solution was transferred to the mixing tank with the lamp switched off and in darkness to achieve adsorption equilibrium. The natural pH of the synthetic solution of aniline ($\text{pH} = 6.23$), benzothiazole ($\text{pH} = 5.45$) and a mixture of both ($\text{pH} = 5.92$) was adjusted with NaOH at 50% or HCl at 33% according to the experiment and was kept constant throughout the experiment. The pump and agitator were switched on at 1750 rpm. After 1 h, the adsorption equilibrium was reached. Then, the UV light source was switched on. The reactive mixture was irradiated for 22 h. The samples collected for monitoring the evolution of the photocatalytic reaction were filtered with a $0.45 \text{ } \mu\text{m}$ (MF-Millipore) membrane (Merck KGaA, Darmstadt, Germany) for further analysis.

3. Results and Discussion

3.1. Characterization of TiO₂ P25

The efficiency of the catalyst to remove pollutants and adsorptive properties could be affected by its point of zero charge (PZC). When the surface of the catalyst is positively charged ($\text{pH} < \text{pH}_{\text{pzc}}$), interactions with anionic pollutants can be favoured (Equation (3)), whereas when it is negatively charged ($\text{pH} > \text{pH}_{\text{pzc}}$), interactions with cationic pollutants would be promoted (Equation (4)) [27].



The experimental curve obtained by the drift method for TiO₂ P25 shown in Figure 2. The point of zero charge, pH_{pzc} , of TiO₂ P25 was 3.5. The calculated value differs from the typical value of 6.5 based on two reasons. The first one is that the proportion of the existing groups on the TiO₂ surface (singly coordinated Ti_3O^0 , doubly coordinated $\text{Ti}_2\text{O}^{2/3-}$, and triply coordinated $\text{TiO}^{4/3-}$) with varying pK constants are capable of modifying the pH of the isoelectric point. Secondly, the increase in the size of the agglomerates is able to displace the zero point charged to lower pH values [28,29].

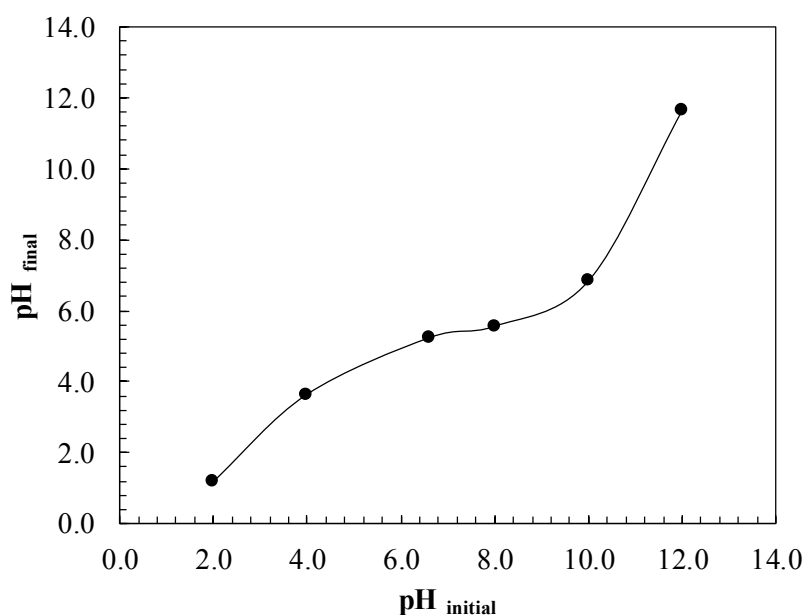


Figure 2. Isoelectric point of TiO₂ P25 catalyst determined by acid-base titration method.

Another important physical property of the catalyst is the surface area (S). It can be calculated from Equation (5) [30,31] from adsorption data.

$$S = q_{\text{max}} \cdot \text{CSA} \cdot N_A \quad (5)$$

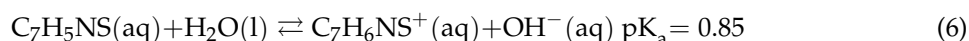
where q_{max} is the monolayer adsorption capacity ($\text{mg pollutant g}^{-1} \text{TiO}_2$) obtained from Langmuir isotherm model, CSA is the cross-sectional area occupied by aniline molecule (36.6 \AA^2) [32] and N_A is the Avogadro's number ($6.022 \times 10^{23} \text{ mol}^{-1}$). The specific surface area of TiO₂ P25 was found to be $50.03 \text{ m}^2 \text{ g}^{-1}$.

3.2. Effect of pH in Adsorption Process

The study of the effect of pH was carried out taking into account the load on the surface of TiO₂ with respect to its isoelectric point [27]. Figure 3 shows the effect of pH in the range of 2.0–12.0 for

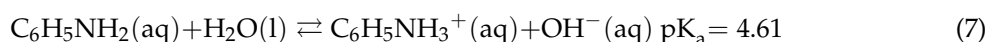
the adsorption of aniline or benzothiazole on TiO_2 starting from solutions of initial concentration of 22.0 mg L^{-1} .

As observed in Figure 3 the effect of pH on the adsorbed amount of benzothiazole in TiO_2 remains almost negligible in the studied pH range with a value of 23.5 mg g^{-1} . The fact that it remains unchanged can be related to the isoelectric point of TiO_2 found at $\text{pH}_{\text{pzc}} = 3.5$ and to the speciation of benzothiazole according to Equation (6):



According to the pK_a of the reaction in Equation (6), the observed in Figure 3 is due to the fact that benzothiazole in the pH range studied were in neutral form, therefore the effect of the electrical charge on the adsorption equilibrium of this compound in TiO_2 is very limited.

However, in the case of aniline adsorption a considerable increase in the amount adsorbed was observed from 17.1 mg g^{-1} to an alkaline pH at a maximum of 122.78 mg g^{-1} at $\text{pH} = 3.9$. This could be explained by aniline dissociation equilibrium [6]:



The pK_a of Equation (7) indicates that aniline at $\text{pK}_a > 4.61$ is in its neutral state. While at an acidic pH ($\text{pK}_a < 4.61$) it is in the form of anilinium cation. If the isoelectric point of TiO_2 is related to the latter with a $\text{pH}_{\text{pzc}} > 3.5$ the surface of the TiO_2 catalyst would be negatively charged so at a pH between 3.5 and 4.61 the aniline cation would be attracted by the negative charges of the external surface of TiO_2 , improving the adsorption.

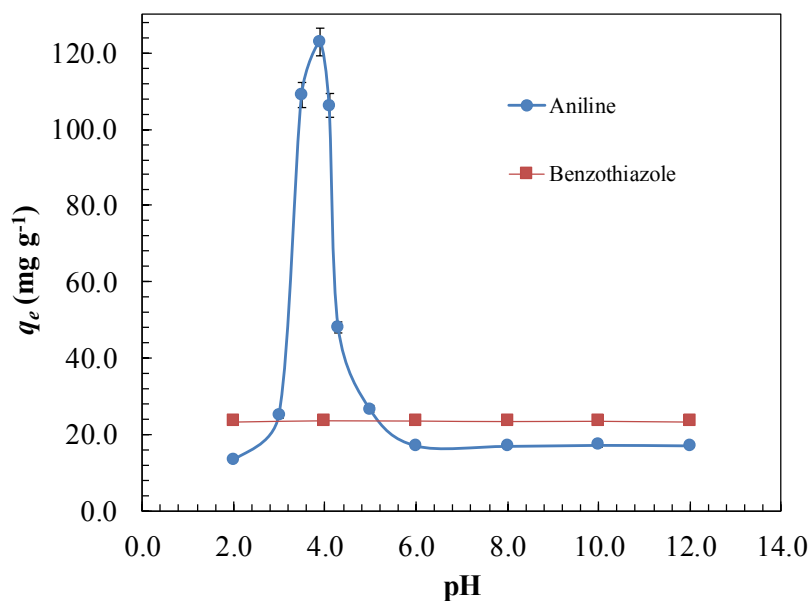


Figure 3. Effect of solution pH on aniline or benzothiazole adsorption on TiO_2 at equilibrium. Experimental conditions: $C_0 = 22.0 \text{ mg L}^{-1}$, $[\text{TiO}_2] = 100.0 \text{ mg L}^{-1}$, $T = 25.0 \text{ }^\circ\text{C}$.

3.3. Adsorption Isotherms

To analyse the process of adsorption, various isotherm models such as Langmuir, Freundlich, Temkin, Dubinin-Radushkevich, Elovich and Generalized isotherm were used to fit obtained experimental data. Figure 4 shows the adsorption isotherms of aniline and benzothiazole on TiO_2 at $10 \text{ }^\circ\text{C}$, $20 \text{ }^\circ\text{C}$, $40 \text{ }^\circ\text{C}$ and $60 \text{ }^\circ\text{C}$ at $\text{pH} = 12.0$ for aniline and at $\text{pH} = 8.0$ for benzothiazole [33].

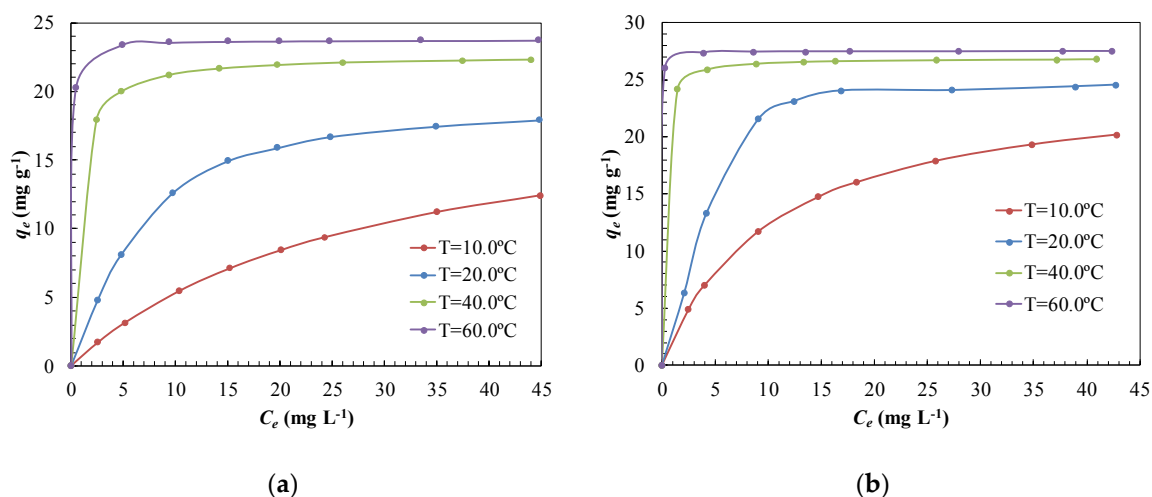


Figure 4. Adsorption isotherms of (a) aniline at pH = 12.0 and (b) benzothiazole at pH = 8.0 on TiO₂ P25 catalyst at different temperatures.

3.3.1. Langmuir Isotherm

This model assumes that the adsorbate forms a monolayer on the adsorbent surface and adsorption occurs over specific homogeneous sites on the adsorbent. There is also an absence of interaction between the adsorbed molecules. Langmuir isotherm model linearized is given by the Equation (8) [34]:

$$\frac{C_e}{q_e} = \frac{1}{q_{max} \cdot K_L} + \frac{1}{q_{max}} \cdot C_e \quad (8)$$

where K_L is the equilibrium constant related to the affinity of the binding sites ($L \text{ mg}^{-1}$). Model parameters can be calculated from slope and intercept of linear regression C_e/q_e versus C_e . According to Meena et al. [35] the characteristics of Langmuir isotherm can be described by a separation factor R_L . This separation factor could be calculated from Equation (9). This factor indicates the nature of adsorption according to the criteria shown on Table 1.

$$R_L = \frac{1}{1 + K_L \cdot C_0} \quad (9)$$

Table 1. Nature of adsorption from Langmuir isotherm fitted equilibrium data.

R_L values	Adsorption Nature
$R_L > 1$	Unfavourable
$R_L = 1$	Linear
$0 < R_L < 1$	Favourable
$R_L = 0$	Irreversible

Table 2 shows the Langmuir adsorption isotherm values. Since R_L values lie between 0 and 1 for aniline or benzothiazole adsorption onto TiO₂, the adsorption process is favourable. According to the values obtained of maximum adsorption capacity, the adsorption process shows an increase in adsorption capacity as temperature increases from 20.08 mg g^{-1} to 23.75 mg g^{-1} for aniline and from 25.06 mg g^{-1} to 27.47 mg g^{-1} for benzothiazole. This may be due to aniline or benzothiazole molecules acquiring enough energy to experience an interaction with the active site on the surface. The values of the Langmuir equilibrium constant suggest that there is a strong interaction between aniline or benzothiazole with the TiO₂ surface at high temperatures. However, at low temperatures the K_L value obtained (0.036 or 0.097 $L \text{ mg}^{-1}$) indicates that the interaction between adsorbate and adsorbent is somewhat weaker.

3.3.2. Freundlich Isotherm

This empirical model of multilayer adsorption assumes the existence of interactions between adsorbed molecules. Freundlich equation can be defined by the following expression in linear form:

$$\ln q_e = \ln K_F + \frac{1}{n} \cdot \ln C_e \quad (10)$$

where K_F (mg g^{-1}) (L mg^{-1})^{1/n} is the Freundlich constant, indicative of adsorption capacity, and n is the heterogeneity factor. Isotherm parameters can be calculated from slope and intercept of linear regression $\ln q_e$ versus $\ln C_e$. A value of n less than one indicates the irreversibility of the process and greater than one reveals favourable adsorption [36,37]. The values of the constants are presented in Table 2. The adsorption capacity of TiO_2 increases with temperature as it was observed with the Langmuir model. The value of $n > 1$ is indicative of a favourable adsorption. However, the adjustment coefficient is significantly lower, $R^2 \cong 0.920$, compared to the one obtained with the Langmuir model ($R^2 \cong 0.990$).

3.3.3. Temkin Isotherm

Temkin's model assume that the heat of adsorption decreases linearity with coverage due to adsorbent and adsorbate interactions. This adsorption differs from a uniform distribution of the bonding energies [37–39]. Temkin model can be applied in the linear form by the following expression:

$$q_e = B_1 \cdot \ln K_T + B_1 \cdot \ln C_e \quad (11)$$

where K_T (L mg^{-1}) is the equilibrium constant corresponding to maximum binding energy and B_1 is the variation of adsorption energy (kJ mol^{-1}). These constants can be obtained from plotting q_e versus $\ln C_e$ and are presented in Table 2. The increase of K_T equilibrium constant from 0.362 L mg^{-1} to 2.727 L mg^{-1} with the increase of the temperature in the case of aniline or from 0.931 L mg^{-1} to 2.459 L mg^{-1} for benzothiazole it could be related to heat of adsorption.

3.3.4. Dubinin-Radushkevich (D-R) Isotherm

This model describes the adsorption isotherms of single solute system. This isotherm is more general than Langmuir isotherm and it does not assume the homogeneity of the surface or constant adsorption potential [31,36,40]. The linear form of D-R model can be expressed from the following equation:

$$\ln q_e = \ln q_s - \beta \cdot \varepsilon^2 \quad (12)$$

where q_s (mg g^{-1}) is the maximum amount of pollutant that can be adsorbed on TiO_2 , β ($\text{mol}^2 \text{ kJ}^{-2}$) is the activity coefficient related to adsorption energy and ε is the Polanyi potential, which can be calculated from this correlation [40]:

$$\varepsilon = R \cdot T \cdot \ln \left(1 + \frac{1}{C_e} \right) \quad (13)$$

where R is the universal gas constant ($8.314 \text{ J mol}^{-1} \text{ K}^{-1}$), T is the absolute temperature (K). The mean adsorption free energy, E (kJ mol^{-1}) per molecule of adsorbate can be calculate using this expression:

$$E = \frac{1}{\sqrt{2 \cdot \beta}} \quad (14)$$

According to the obtained values of adsorption free energy, the adsorption energy of benzothiazole ($12.70 \text{ kJ mol}^{-1}$) is greater than the one obtained with aniline (2.50 kJ mol^{-1}) at 60°C . Regarding the quality of the adjustment of the experimental data, it would be behind Langmuir's model. Even so, the

quality of the fit suggests, based on the peculiarities of the D-R isotherm model, that the predominant mechanism is chemical adsorption in both cases.

3.3.5. Elovich Isotherm

This model assumes that adsorption sites increase exponentially with adsorption, implying a multilayer adsorption [41,42]. The linear form of the Elovich model is described in the following equation:

$$\ln \frac{q_e}{C_e} = \ln K_E \cdot q_{max} - \frac{1}{q_{max}} \cdot q_e \quad (15)$$

where Elovich constant, K_E ($L \text{ mg}^{-1}$) and maximum adsorption capacity can be calculated from the slope and intercept of $\ln (q_e/C_e)$ versus q_e . Modelized parameters are presented in Table 2.

3.3.6. Generalized Isotherm

The expression of the generalized equation is shown below:

$$\ln \left(\frac{q_{max}}{q_e} - 1 \right) = \ln K_G - N \cdot \ln C_e \quad (16)$$

where K_G (mg L^{-1}) is the saturation constant and N is the cooperative binding constant [36]. The parameters K_G and N have been calculated from the slope and intercept of the plot of $\ln (q_{max}/q_e - 1)$ versus $\ln C_e$. Table 2 gives these values of generalized adsorption isotherm.

Table 2. Values of adsorption isotherm models for adsorption of aniline or benzothiazole onto TiO_2 at different temperatures.

Adsorbate	Aniline				Benzothiazole			
	Temperature, °C							
	10	20	40	60	10	20	40	60
Langmuir								
$K_L, L \text{ mg}^{-1}$	0.036	0.138	1.568	13.314	0.097	0.419	5.958	61.528
$q_{max}, \text{mg g}^{-1}$	20.08	21.14	22.62	23.75	25.06	26.11	26.89	27.47
R^2	0.997	0.997	0.998	0.994	0.995	0.997	0.996	0.998
R_L values	0.56	0.25	0.03	3.4×10^{-3}	0.32	0.10	0.01	7.38×10^{-4}
Freundlich								
$K_F, (\text{mg g}^{-1})(L \text{ mg}^{-1})^{1/n}$	0.84	2.99	16.82	23.14	3.485	5.413	25.295	27.303
n	1.28	1.69	10.52	131.58	2.00	2.90	55.87	555.56
R^2	0.986	0.960	0.928	0.896	0.906	0.859	0.937	0.926
Temkin								
$K_T, L \text{ mg}^{-1}$	0.362	1.243	2.107	2.727	0.931	1.035	2.050	2.459
$B_T, \text{kJ mol}^{-1}$	4.34	4.78	5.42	6.11	5.5608	8.9068	10.115	15.192
R^2	0.995	0.994	0.907	0.895	0.998	0.974	0.945	0.958
Dubinin-Radushkevich								
$q_s, \text{mg g}^{-1}$	11.54	17.80	22.26	23.71	15.28	23.64	26.57	27.44
$\beta, \text{mol}^2 \text{kJ}^{-2}$	17.428	6.315	0.755	0.080	1.996	1.533	0.054	0.003
$E, \text{kJ mol}^{-1}$	0.17	0.28	0.81	2.50	0.50	0.57	3.05	12.70
R^2	0.990	0.942	0.965	0.993	0.908	0.977	0.967	0.999
Elovich								
$K_E, L \text{ mg}^{-1}$	0.064	4.733	18.415	33.360	0.300	2.254	24.890	37.601
$q_{max}, \text{mg g}^{-1}$	12.47	4.65	0.59	0.16	11.15	2.21	0.31	0.03
R^2	0.984	0.950	0.962	0.946	0.963	0.762	0.828	0.952
Generalized								
$K_G, \text{mg L}^{-1}$	27.79	8.06	0.64	0.08	10.339	5.277	0.168	0.016
N	1.07	1.04	1.01	1.00	1.36	1.28	1.21	1.08
R^2	0.999	0.989	0.986	0.995	0.903	0.920	0.952	0.991

According to the R^2 coefficient, the best fitting was obtained for the Langmuir isotherm model for all temperatures and pollutants studied. This good agreement can be attributed to the following causes according with Meena et al. [35]: (i) the formation of monolayer coverage on the surface of TiO_2 with minimal interaction among molecules of aniline or benzothiazole, (ii) all sites having the same adsorption energies, and (iii) the maximum adsorption corresponds to a saturated monolayer of aniline or benzothiazole on TiO_2 surface.

3.4. Adsorption Kinetics Models

In order to study adsorption kinetics, five possible models have been presented. The pseudo-first order equation, pseudo-second order equation, intraparticle diffusion, Elovich model and Bangham model have been studied. Figure 5 shows the adsorption kinetics of aniline and benzothiazole on TiO_2 at 10 °C, 20 °C, 30 °C, 40 °C and 60 °C at pH = 12.0 for aniline and at pH = 8.0 for benzothiazole.

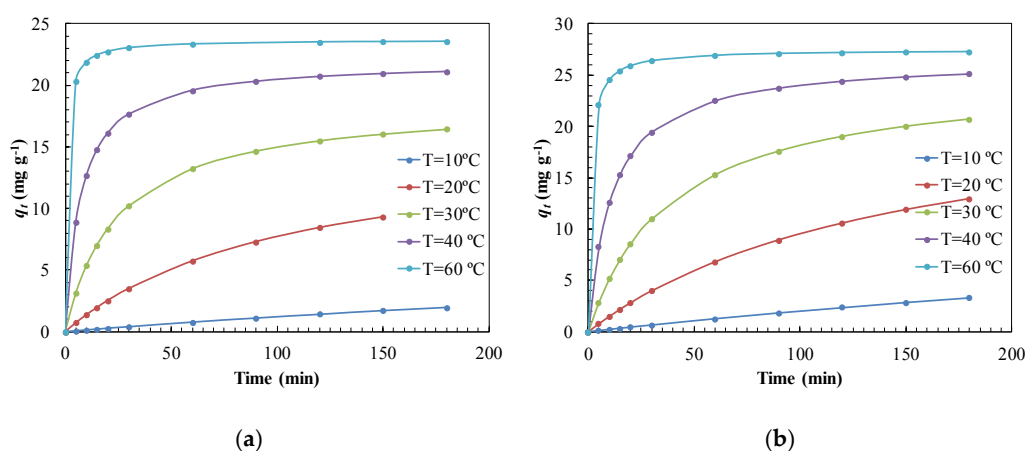


Figure 5. Evolution of the adsorbed capacity with time for effect of temperature (a) aniline at pH = 12.0 and (b) benzothiazole at pH = 8.0 on TiO_2 P25 catalyst.

3.4.1. Pseudo-First Order Kinetic Model

The pseudo-first order model is based on the consideration that adsorption occurs through a physisorption mechanism because the limiting stage is film diffusion. By controlling the velocity of diffusion into the film, the velocity of adsorption will vary inversely with particle size, film thickness and distribution coefficient. This model assumes: (i) the adsorption only occurs on localized sites, (ii) the energy of adsorption process does not depend on surface coverage, (iii) maximum adsorption corresponds to a saturated monolayer, and (iv) the concentration of aniline or benzothiazole is considered constant, because it is provided in great excess [43,44]. Lagergren's pseudo-first order equation can be expressed in the following terms:

$$\frac{dq_t}{dt} = k_1 \cdot (q_e - q_t) \quad (17)$$

where q_t ($mg\ g^{-1}$) is the amount of adsorbate adsorbed at time t , q_e ($mg\ g^{-1}$) is the adsorption capacity at equilibrium and k_1 (min^{-1}) is the pseudo first order rate constant. The integration of Equation (17) applying boundary conditions $t = 0$ to $t = t$ and $q_t = 0$ to $q_t = q_e$, leads to the following expression:

$$\log(q_e - q_t) = \log q_e - \frac{k_1}{2.303} \cdot t \quad (18)$$

The kinetic parameter can be obtained from the slope of a plot of $\log(q_e - q_t)$ versus t . The values of k_1 for the adsorption of aniline or benzothiazole onto TiO_2 are given in Table 3.

The correlation coefficient R^2 shows that the pseudo-first order kinetic model is not the most appropriate for adjusting experimental data ($R^2 \cong 0.980$), so physisorption does not appear to be the adsorption mechanism taking place for both aniline and benzothiazole.

3.4.2. Pseudo Second Order Kinetic Model

The pseudo second order model assumes that in this type of adsorption the chemical reaction seems significant, so the controlling stage is the velocity of the chemical reaction. Thus, the mechanism that takes place is chemisorption. In this mechanism the adsorption kinetics corresponds to a second order of a reversible reaction. The adsorption rate can be described as:

$$\frac{dq_t}{dt} = k_2 \cdot (q_e - q_t)^2 \quad (19)$$

where k_2 ($\text{g mg}^{-1} \text{min}^{-1}$) is the pseudo second order rate constant. Integrating Equation (19) for the boundary conditions $t = 0$ to $t = t$ and $q_t = 0$ to $q_t = q_t$ and linearization leads to following expression:

$$\frac{t}{q_t} = \frac{1}{k_2 q_e^2} + \frac{1}{q_e} \cdot t \quad (20)$$

The equilibrium adsorption capacity kinetic parameter can be obtained with the slope and k_2 is obtained from the intercept of a plot of t/q_t versus t . The values of k_2 for the adsorption of aniline or benzothiazole onto TiO_2 are given in Table 3. According to the correlation coefficient obtained ($R^2 = 0.990$) the pseudo second order kinetic model shows a greater fit than pseudo first order model ($R^2 \cong 0.980$). Contrary to the other models, this model predicts that the adsorption mechanism is chemisorption and consequently, the reaction is the rate controlling step [43]. This prediction agrees with the observation of an increase of adsorption of aniline or benzothiazole at high temperatures, variable strongly dependent on chemical reactions.

Table 3. Kinetic parameters for the adsorption of aniline or benzothiazole onto TiO_2 at different temperatures.

Adsorbate	Aniline					Benzothiazole				
	Temperature, °C					Temperature, °C				
Kinetic Model	10	20	30	40	60	10	20	30	40	60
Pseudo-1st order										
k_1, min^{-1}	0.001	0.006	0.026	0.053	0.084	0.001	0.005	0.019	0.043	0.097
R^2	0.949	0.979	0.955	0.939	0.966	0.969	0.940	0.952	0.960	0.962
Pseudo-2nd order										
$k_2, \text{g mg}^{-1} \text{min}^{-1}$	0.0002	0.0006	0.0021	0.0062	0.0513	7.87×10^{-5}	0.0003	0.001	0.0034	0.0305
R^2	0.993	0.996	0.999	0.991	0.998	0.995	0.997	0.998	0.991	0.999
Intraparticle diffusion										
$k_{dif}, \text{mg g}^{-1} \text{min}^{-0.5}$	0.17	0.89	1.16	1.83	1.67	0.29	1.14	1.88	3.45	1.27
$C, \text{mg g}^{-1}$	0.46	1.38	2.51	6.71	16.59	0.78	2.07	0.29	1.31	20.01
R^2	0.986	0.998	0.932	0.881	0.756	0.984	0.998	0.979	0.975	0.880
R_i	0.98	0.93	0.89	0.70	0.30	0.97	0.92	0.99	0.95	0.27
Elovich										
$\alpha_e, \text{mg g}^{-1} \text{min}^{-1}$	0.05	0.43	1.61	7.87	2.18×10^5	0.07	0.47	1.55	4.72	6.00×10^3
$\beta_e, \text{g mg}^{-1}$	3.654	0.497	0.242	0.231	0.656	3.366	0.570	0.222	0.159	0.419
R^2	0.880	0.932	0.995	0.978	0.950	0.931	0.948	0.981	0.999	0.956
Bangham										
k_B, g	0.36	5.58	44.03	174.70	469.67	0.58	6.47	44.35	193.85	573.80
A	0.935	0.755	0.445	0.220	0.036	0.950	0.757	0.484	0.235	0.035
R^2	0.999	0.990	0.946	0.884	0.800	0.999	0.994	0.973	0.938	0.896

3.4.3. Intraparticle Diffusion Kinetic Model

This empirical kinetic model explains the diffusion mechanism [37,39]. The functional relationship is represented as:

$$q_t = k_{dif} \cdot \sqrt{t} + C \quad (21)$$

where k_{dif} ($\text{mg g}^{-1} \text{min}^{-0.5}$) is the intraparticle diffusion rate constant. The values of the intercept, C (mg g^{-1}) give an idea about the thickness of the boundary layer [37]. Kinetic model parameters are shown in Table 3. Obtaining a value other than zero in parameter C is indicative of the coexistence of the external diffusion step along with the intraparticle diffusion. According to Adam [31], the value of C indicates that the amount is adsorbed in a short period of time. This magnitude can be measured by the initial adsorption factor R_i as shown below:

$$R_i = 1 - \frac{C}{q_{max}} \quad (22)$$

The criteria of R_i ratio of the initial adsorption amount is shown on Table 4:

Table 4. Initial adsorption factor means from intraparticle diffusion kinetic model fitted kinetic data.

R_i Values	
$R_i = 1$	No exist initial adsorption
$0.9 < R_i < 1$	Weak initial adsorption
$0.5 < R_i < 0.9$	Intermediately initial adsorption
$0.1 < R_i < 0.5$	Strong initial adsorption
$R_i < 0.1$	Approaching complete initial adsorption

The R_i values obtained from Table 3 were found between 0.96 and 0.30 for aniline or benzothiazole. This factor indicates that with increasing temperature the initial adsorption was stronger than at low temperatures.

3.4.4. Elovich Kinetic Model

This kinetic model assumes that the adsorption occurs on localized sites and the energy adsorption increases with the surface coverage. Additionally, the concentration of the TiO_2 is considered to be constant [42,44]. The linear form of Elovich model can be illustrated as follows:

$$q_t = \frac{1}{\beta_e} \cdot \ln(\alpha_e \cdot \beta_e) + \frac{1}{\beta_e} \cdot \ln t \quad (23)$$

where α_e is the initial adsorption rate ($\text{mg g}^{-1} \text{s}^{-1}$) and β_e is the constant related to the extent of surface coverage and activation energy for chemisorption (g mg^{-1}). Table 3 shows the parameters obtained from the Elovich model for experimental kinetic data. As can be seen, the initial adsorption becomes stronger in both cases the higher the temperature, going from 0.05 to $2.18 \times 10^5 \text{ mg g}^{-1} \text{min}^{-1}$. This may be due to the fact that at high temperature the diffusion control is much stronger in a film diffusion step.

3.4.5. Bangham Kinetic Model

This model allows to know how slow the adsorption stage in the process. The Bangham equation [36] is given by:

$$\log \left(\log \left(\frac{C_0}{C_0 - q_t \cdot M} \right) \right) = \log \left(\frac{k_B \cdot M}{2.303 \cdot V} \right) + A \cdot \log t \quad (24)$$

where k_B (g) and A are constants of the Bangham system. The Bangham model responds to a diffusion in the micropores [45]. Since the double logarithm is capable of modelling experimental data ($R^2 = 0.940$) it means that the diffusion of aniline or benzothiazole into the adsorbent pores is the phase that controls the rate of adsorption.

The best fit model was selected based on the determination coefficient R^2 . According to that criteria, the correlation coefficients were the highest ($R^2 = 0.990$) for the pseudo-second order kinetic model for all temperatures and pollutants studied. As described throughout this section, several adsorption steps may be involved in the kinetic control regime, along with the main chemisorption mechanism of aniline or benzothiazole. Some of these identified steps are summarized in the next sections: (i) external mass transfer from the aqueous medium to the boundary film (ii) Mass transfer from boundary film to TiO_2 external surface (iii) Mass transfer in the pores (iv) Adsorption onto TiO_2 active sites (strong initial adsorption at high temperatures) and (iv) Internal diffusion step (intraparticle diffusion).

3.5. Thermodynamic Parameters

The influence of the temperature of adsorption of aniline or benzothiazole on TiO_2 was studied in the range of 10–60 °C. As observed in Figures 4 and 5, the adsorption of aniline or benzothiazole increased with the temperature increase from 10 to 60 °C. This increase in TiO_2 adsorption capacity with temperature is indicative of endothermic processes [31,35,38]. This increase in adsorption can be attributed to the favourable intermolecular forces between the adsorbate, aniline or benzothiazole, and the adsorbent, TiO_2 , are much stronger than those between the adsorbate and the solvent. As a result of all this, the increase in temperature to 60 °C makes the adsorbate easier to be adsorbed. Increased adsorption can also be promoted by increasing the number of active sites available and decreasing the boundary layer. As the temperature increases, the diffusivity through the pores is enhanced and could contribute to increased adsorption. Other factors such as the external mass transfer could also be favoured with the increase of temperature. All these hypotheses can be corroborated from the evaluation of thermodynamic parameters.

The thermodynamic parameters: enthalpy, entropy and free energy changes, during adsorption, can be calculated using the following expressions [35]:

$$\Delta G = -R \cdot T \cdot \ln K_L \quad (25)$$

where ΔG is the free energy change (J mol^{-1}), R is the universal gas constant ($8.314 \text{ J mol}^{-1} \text{ K}^{-1}$), T is the absolute temperature (K) and K_L is the equilibrium constant (L mol^{-1}). The determination of enthalpy and entropy was carried out using Van't Hoff equation [38]:

$$\ln K_L = \frac{\Delta S}{R} - \frac{\Delta H}{R} \cdot \frac{1}{T} \quad (26)$$

where ΔS is the entropy change ($\text{J mol}^{-1} \text{ K}^{-1}$) and ΔH is the enthalpy change (J mol^{-1}). These parameters can be obtained from the slope and intercept of $\ln K_L$ versus $1/T$. Table 5 summarizes obtained thermodynamic parameters. The positive value of enthalpy change confirms that the adsorption of aniline or benzothiazole onto TiO_2 is endothermic. According with Adam [31], a value of enthalpy change less than 84 kJ mol^{-1} indicates a physisorption mechanism, while a chemisorption reaches typical enthalpy values between 84 and 420 kJ mol^{-1} . In this work, enthalpy values of 92.78 and $101.26 \text{ kJ mol}^{-1}$ for aniline and benzothiazole respectively confirm the hypothesis of a chemisorption mechanism. The positive values of entropy change indicate the increase of the randomness between solution and solid interface and, consequently, structural changes in the TiO_2 and aniline or benzothiazole. The negative values of free energy change in both cases indicate the feasibility and spontaneous nature of adsorption process [35].

From the kinetic data taken at different temperatures between 10 and 60 °C, the activation energy was estimated using the following expression [40]:

$$\ln k_2 = \ln k_0 - \frac{E_a}{R} \cdot \frac{1}{T} \quad (27)$$

where k_2 is the pseudo-second order adsorption kinetic constant ($\text{g mg}^{-1} \text{min}^{-1}$), k_0 is the frequency factor, R is the universal gas constant ($8.314 \text{ J mol}^{-1} \text{K}^{-1}$), T is the absolute temperature (K) and E_a is the activation energy for the adsorption process (J mol^{-1}). The activation energy was determined from the slope of $\ln k_2$ versus $1/T$ according with Equation (27). The activation energy indicates the type of adsorption. According to Fil et al. [40,42] an activation energy value between 0–88 kJ mol^{-1} indicates a physical adsorption while, between 88–400 kJ mol^{-1} , indicates chemical adsorption. The obtained values of activation energy for aniline (89.23 kJ mol^{-1}) and benzothiazole (93.67 kJ mol^{-1}) also confirm a chemisorption mechanism.

Table 5. Activation energy and thermodynamic parameters of aniline or benzothiazole onto TiO_2 .

Adsorbate	T °C	K_L L mol^{-1}	ΔH kJ mol^{-1}	ΔS $\text{J mol}^{-1} \text{K}^{-1}$	ΔG kJ mol^{-1}	E_a kJ mol^{-1}	k_0
Aniline	10	3.35×10^3	92.78	395.13	−19.11	89.23	4.92×10^{12}
	20	1.29×10^4			−23.06		
	40	1.46×10^5			−30.96		
	60	1.24×10^6			−38.86		
Benzothiazole	10	1.31×10^4	101.26	436.41	−22.31	93.67	1.44×10^{13}
	20	5.67×10^4			−26.68		
	40	8.05×10^5			−35.41		
	60	8.32×10^6			−44.13		

3.6. Adsorption Effect on the Photodegradation of Aniline and Benzothiazole

In order to identify the controlling step during the photocatalytic process, the kinetics of aniline and benzothiazole removal by adsorption and photocatalysis were adjusted to pseudo-first order (Equation (18)) and pseudo-second order models (Equation (20)). The results of kinetics parameters obtained by both models are presented in Table 6.

Table 6. Determined kinetic parameters of adsorption and photocatalysis processes for the removal of aniline or benzothiazole with TiO_2 catalyst. Experimental conditions: $C_0 = 22.0 \text{ mg L}^{-1}$; $T = 25.0 \text{ °C}$; $P = 1.0 \text{ atm}$; $[\text{TiO}_2] = 100.0 \text{ mg L}^{-1}$; pH = 12.0 (aniline removal); pH = 8.0 (benzothiazole removal).

Pollutant	Aniline		Benzothiazole	
	Process			
Kinetics Model	Adsorption	Photocatalysis ¹	Adsorption	Photocatalysis ¹
Pseudo-1st-order				
k_1 (min^{-1})	0.0124	0.0065	0.0097	0.0031
R^2	0.963	0.999	0.957	0.997
Pseudo-2nd-order				
k_2 ($\text{g mg}^{-1} \text{min}^{-1}$)	0.0035	0.00081	0.0005	7.39×10^{-6}
R^2	0.999	0.889	0.997	0.864

¹ Adsorption process with simultaneous photocatalysis.

According to Table 6, slight differences in the fitting of the experimental data were observed, with good results in general, except in the cases when the photocatalysis participates, and the pseudo second order model is considered ($R^2 < 0.890$). Supposing the overall photocatalysis process consist of an in-series combination of adsorption and photocatalysis steps, the lowest step kinetic will determine the rate of the overall process [46]. The pseudo first order model fitted the best overall process. Moreover,

since the kinetic constant referring the photocatalysis step ($k_1 = 0.0065 \text{ min}^{-1}$) is lower than that of adsorption only ($k_1 = 0.0124 \text{ min}^{-1}$), either for aniline or benzothiazole, the photocatalysis step is postulated as the controlling one of the overall process.

3.7. Effect of pH on Photodegradation

The effect of pH was analysed with synthetic solutions of aniline or benzothiazole with a $C_0 = 22.0 \text{ mg L}^{-1}$ and different initial pH using the supported configuration of the TiO_2 catalyst. Modelling the oxidation kinetics of aniline or benzothiazole requires a model approach that satisfactorily predicts profiles in which the oxidation rate increases with the irradiation time until reaching a point in which the velocity remains constant. This behaviour is reflected in the Langmuir-Hinshelwood (L-H) model, a model widely used in photocatalytic reactions [47]. This model considers that a surface reaction occurs in five consecutive steps: (i) diffusion of the reagent molecules to the surface of TiO_2 , (ii) adsorption on the surface, (iii) reaction on the surface on which product formation occurs, (iv) desorption of products and (v) diffusion of non-absorbed products away from the surface of TiO_2 . L-H model is expressed according to Equation (28):

$$r = -\frac{dC}{dt} = \frac{k \cdot K_{ad} \cdot C}{1 + K_{ad} \cdot C} \quad (28)$$

where, C is the aniline or benzothiazole concentration at time t (mg L^{-1}), K_{ad} is the L-H adsorption constant (L mg^{-1}), k is the kinetic constant ($\text{L mg}^{-1} \text{ h}^{-1}$) and r is the reaction rate ($\text{mg L}^{-1} \text{ h}^{-1}$). In this study, since the initial concentrations of benzothiazole and aniline were lower than $1.0 \times 10^{-3} \text{ mol L}^{-1}$, the product $K_{ad} \times C \ll 1.0$ and consequently Equation (28) could approximate to Equation (29) [48].

$$r = -\frac{dC}{dt} = k \cdot K_{ad} \cdot C \quad (29)$$

Integrating, Equation (30) is obtained:

$$\ln\left(\frac{C_0}{C}\right) = k \cdot K_{ad} \cdot t \approx k_{app} \cdot t \quad (30)$$

where k_{app} is the kinetic constant of pseudo-first order (h^{-1}). Figure 6 shows the removal kinetics obtained for aniline or benzothiazole solutions at different pHs with only supported TiO_2 .

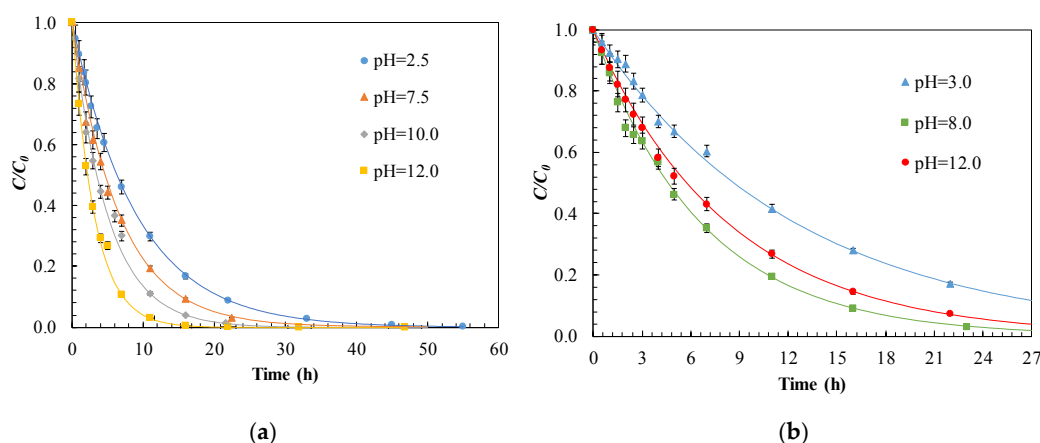


Figure 6. Effect of pH on the photocatalytic degradation of; (a) aniline and (b) benzothiazole, using only TiO_2 -supported catalyst. Experimental (dots) and pseudo-1st-order modelled (—) kinetic results. Conditions: $C_0 = 22.0 \text{ mg L}^{-1}$; $T = 25.0 \text{ }^\circ\text{C}$; $P = 1.0 \text{ atm}$.

Figure 6 shows that, in the case of aniline removal (Figure 6a), the photocatalytic oxidation rate is favoured at alkaline pH (above pH = 12.0). However, operating at pH = 2.5 results in less degradation rates, the formation of polyaniline on the lamp is induced [49]. This compound on the lamp surface prevents the passage of UV light reaches the reactor wall TiO₂ resulting in low degradation rate.

For the benzothiazole removal (Figure 6b), slower kinetics than those obtained in the case of aniline were obtained. In this case the elimination is favoured at pH = 8.0. The lower degradation of benzothiazole could be due to the presence of several oxidation intermediates by-products, negatively charged, that compete with the initial compound [50].

The dependence of the kinetic constants of pseudo-first order for the degradation of aniline or benzothiazole with pH are shown in Figure 7.

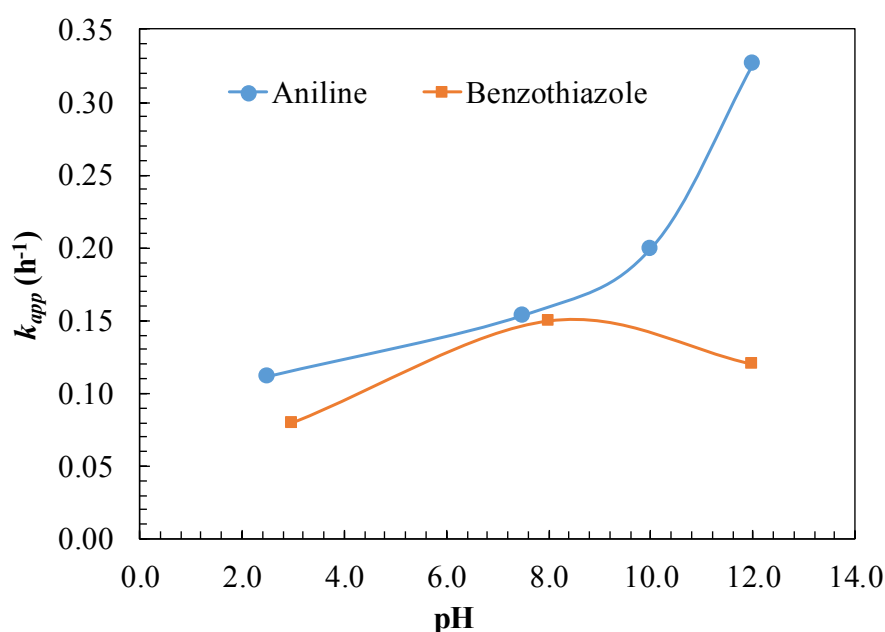


Figure 7. Pseudo-first order kinetic constants, k_{app} , at different pHs, for photocatalytic degradation of aniline or benzothiazole with only TiO₂-supported catalyst. Experimental conditions: $C_0 = 22.0 \text{ mg L}^{-1}$; $T = 25.0 \text{ }^\circ\text{C}$; $P = 1.0 \text{ atm}$.

In the case of aniline, there is an upward trend in the kinetic constant with pH, with a maximum value of $=0.327 \text{ h}^{-1}$ at pH = 12.0. This maximum can be attributed to the good interaction between the hydroxyl radicals located on the surface of the catalyst and aniline [50]. However, the decrease of k_{app} at acid pH led to observed minimum value of $=0.112 \text{ h}^{-1}$ at pH = 2.5. The appearance of condensation reactions that compete with oxidation reactions when polyaniline is deposited over the UV lamp [49] explains this behavior. In the elimination of benzothiazole at pH = 8.0, a maximum in the degradation rate was observed, with a value of $k_{app} = 0.150 \text{ h}^{-1}$.

3.8. Effect of TiO₂ Suspended Catalyst Loading

The concentration of TiO₂ in the photocatalytic reaction system directly affects the oxidation rate of aniline or benzothiazole, where the amount of TiO₂ catalyst is directly proportional to the overall photocatalytic reaction rate. In this type of systems, it is common that initially a linear dependence is maintained between introduced catalyst dose and oxidation rate until reaching a certain critical concentration, from which the reaction rate begins to decrease due to the light scattering effect [50]. Figure 8 shows the removal kinetics obtained for aniline or benzothiazole solutions at different doses of TiO₂ in a hybrid system with supported catalyst of TiO₂.

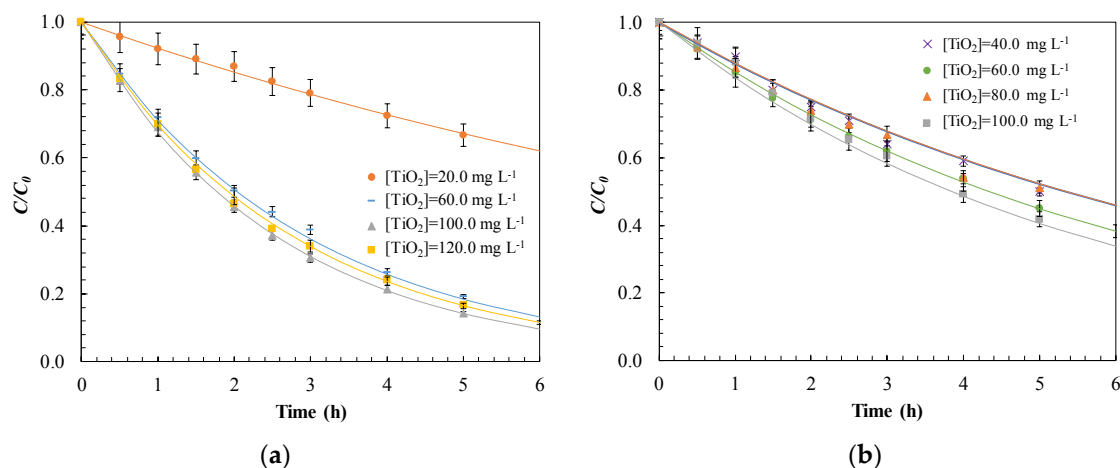


Figure 8. Experimental (dots) and pseudo-1st-order modelled (—) kinetic results for photocatalytic degradation of: (a) aniline operating at pH = 12.0 or (b) benzothiazole operating at pH = 8.0 carrying out the treatment in a hybrid system with supported catalyst of TiO₂ and different doses of TiO₂ in suspension simultaneously. Experimental conditions: C₀ = 22.0 mg L⁻¹; T = 25.0 °C; P = 1.0 atm.

In the case of aniline, a progressive increase in oxidation rate is observed when the existing supported catalyst in the photoreactor is used simultaneously with introduced TiO₂. Thus, with a hybrid supported suspended configuration, 82% aniline removal was achieved, using a dose of 100.0 mg L⁻¹ after 5 h of irradiation. However, with the addition of 20.0 mg L⁻¹ of TiO₂ only a 30% removal was achieved for the same time. In the case of benzothiazole, the differences observed in the degradation kinetics were not so relevant. Thus, with 100.0 mg L⁻¹ TiO₂ suspension a slight improvement was observed obtaining a 58% removal, for a reaction time of 5 h, clearly lower than that observed on aniline.

The effect of the simultaneous use of suspended and supported TiO₂ catalyst on the pseudo first order kinetic constants can be observed in Figure 9 according to the model proposed in Equation (30).

In the case of aniline, it is observed that initially a TiO₂ load between 20.0 and 80.0 mg L⁻¹, there is a linear tendency between the dose of catalyst used and the obtained apparent kinetic constant. Over a critical 100.0 mg L⁻¹ TiO₂ dose ($k_{app} = 0.408 \text{ h}^{-1}$), k_{app} begins to decrease. This phenomenon may be due to a screen effect. Catalytic particles leads to an increase in turbidity, covering each other and reducing the light received by the TiO₂ suspended and also that supported on the wall [50]. The consequences of this effect could be reduced with a reactor design in which the annular space between the UV lamp and the reactor wall was as small as possible in order to facilitate the efficiency of the UV light emitted [51].

In the degradation of benzothiazole, the influence of the catalyst dose on the apparent kinetic constant is smaller than for aniline. A kinetic constant of $k_{app} = 0.181 \text{ h}^{-1}$ was obtained with a TiO₂ dose of 100.0 mg L⁻¹. The lack of significant improvements in the degradation of benzothiazole suggests that the appearance of intermediate oxidation compounds, derived from the strong excision of the aromatic ring, would lead to the generation of ammonia, nitrate, amide compounds such as N-formyl-oxamic acid, and nitrous derivatives. These compounds of greater complexity than those derived from the oxidation of aniline could compete with benzothiazole for hydroxyl radicals and lead to a lower value of k_{app} [52,53].

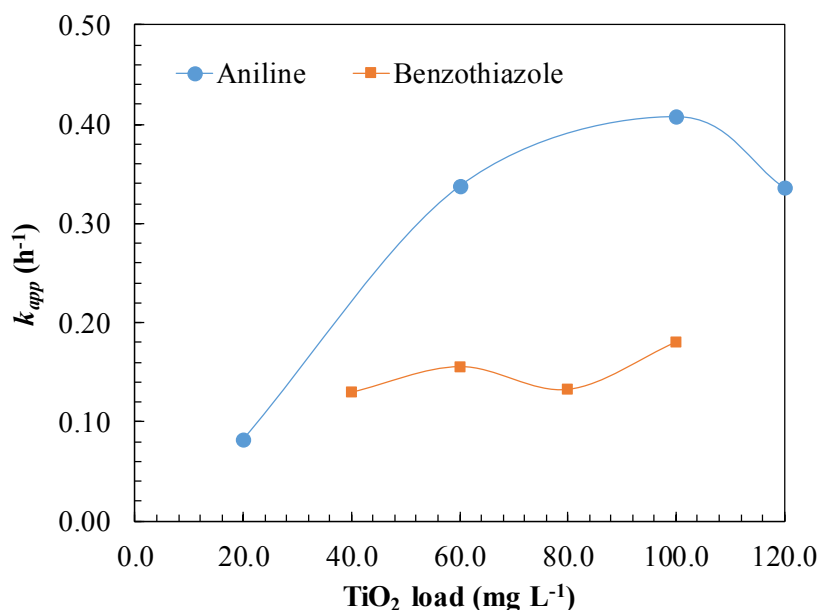


Figure 9. Effect of the suspended TiO₂ dosage on the pseudo-first order kinetic constants for the degradation of aniline or benzothiazole. Experimental conditions: C₀ = 22.0 mg L⁻¹; pH = 12.0 (aniline); pH = 8.0 (benzothiazole); T = 25.0 °C; P = 1.0 atm.

3.9. Photocatalytic Reactor Configuration

The reactors used for water treatment by photocatalysis can be classified into two main configurations: reactors with suspended photocatalytic particles and reactors with immobilized photocatalyst. Systems based on the use of suspended catalyst were preferred due to their large active surface area per unit volume and the ease of regenerating once used with a simple wash with deionized water [12,21,50]. The configuration supported does not require a downstream separation stage either by decanting tanks or a cross-flow filtration system, to allow the reactor to operate continuously, but requires maintenance processes for reuse the catalyst after each use as a result of fouling [19]. Catalyst fouling is due to the accumulation of adsorbed by-products on the surface and cavities of the TiO₂ support reducing received UV radiation. Besides, fouling also affects the blockage of the active adsorption sites resulting in significantly reduced catalytic activity [54]. Therefore, oxidizing fouling compounds would be required to fully recover the activity, with the consequent shutdown of the system; this is one of the great challenges posed by this configuration.

The progressive loss of activity of the photocatalyst after several cycles has to be considered, especially in the case of supported configurations [18,20,21], Figure 10 shows that the loss of activity can be compensated thanks to the use of hybrid form of the supported catalyst and the introduction of TiO₂ in suspension in small concentrations (<<1.0 g L⁻¹).

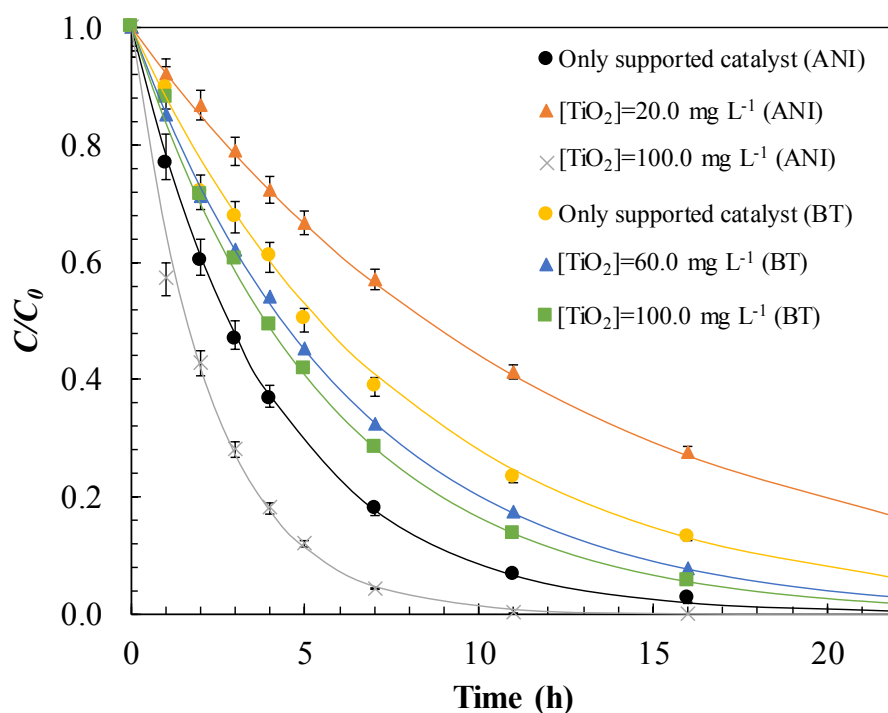


Figure 10. Comparison between only supported and suspended-supported TiO_2 for the degradation of: aniline or benzothiazole, through the experimental (dots) and modelled (—) pseudo-first order kinetics. Experimental conditions: $C_0 = 22.0 \text{ mg L}^{-1}$; $\text{pH} = 12.0$ (aniline); $\text{pH} = 8.0$ (benzothiazole); $T = 25.0 \text{ }^\circ\text{C}$; $P = 1.0 \text{ atm}$.

Figure 10 shows that adding the optimal dose of 100.0 mg L^{-1} of TiO_2 in suspension, for both compounds, achieves higher yields than with the exclusive use of the supported catalyst. The adjustment to a pseudo-first order kinetics of the C/C_0 profiles, in the case of aniline, gave an apparent kinetic constant variation from $k_{app} = 0.327 \text{ h}^{-1}$ to $k_{app} = 0.408 \text{ h}^{-1}$, while the degradation rate of benzothiazole increased from $k_{app} = 0.150 \text{ h}^{-1}$ to $k_{app} = 0.181 \text{ h}^{-1}$. This represents an improvement of 24.77% and 20.66%, respectively, respect to the only TiO_2 supported configuration. With the simultaneous use of both configurations, species that were previously adsorbed on the supported catalyst could be oxidized. Thus, there would be no accumulation of degradation by-products, avoiding blockage of the active sites and catalyst activity loss. The results obtained are promising since authors such as Santiago et al. [21] or Velmurugan et al. [54] conducted studies comparing the mineralization of imazalil and gelatin industry effluent using Evonik commercial suspension catalysts such as P25 and P90 and only supported configuration concluded that the suspension configuration resulted in a higher degree of mineralization. Kete et al. [20] also studied the three catalytic configurations exposed for the removal of RB19 dye. It obtained worse results in the hybrid configuration with respect to the supported or suspended configurations due to the annular space of the reactor was 5.0 cm compared to the 2.5 used in this work. Another relevant aspect to consider is the durability of catalyst, according with Verma et al. [19] studies, the suspended catalyst maintains almost intact its catalytic activity after more than 100 cycles compared to the supported catalyst that loses 20% of its activity. The proposed hybrid configuration would avoid long stoppages in an industrial treatment plant for the regeneration stage. Regarding the recovery of TiO_2 particles, using a concentration of 100.0 mg L^{-1} , instead of $2.0\text{--}3.0 \text{ g L}^{-1}$ dosage used by Bansal et al. [18], would considerably facilitate their separation by means of a tangential membrane filtration. Operating costs would not increase because of the improvement in degradation yields of approximately 25%, since there is no need of having to resort to a highly complex supported configuration using pebbles, glass spheres or silica gel beads [12,19–22].

3.10. Simultaneous Removal of Aniline and Benzothiazole

The effect of a synthetic aqueous matrix of aniline and benzothiazole on operational conditions was compared to each catalyst removal separately. In Figure 11, the oxidation of a mixture of both contaminants with $C_0 = 22.0 \text{ mg L}^{-1}$ was studied at $\text{pH} = 12.0$, and introducing 60.0 , 80.0 and 100.0 mg L^{-1} of catalyst in suspension.

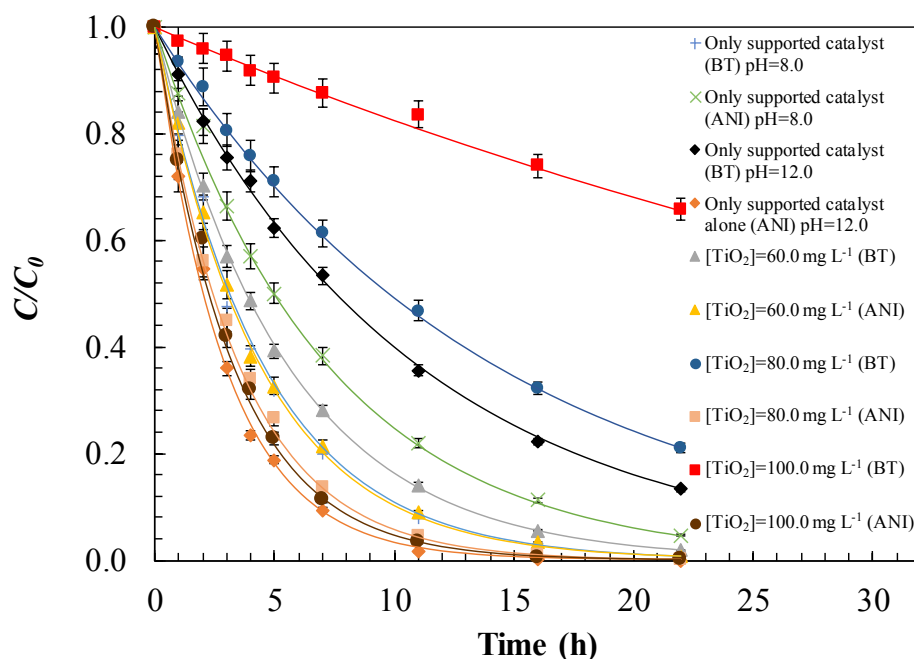


Figure 11. Effect of the matrix on photocatalytic oxidation of aniline and benzothiazole using the supported or supported configuration with addition of TiO_2 in suspension fitted to the pseudo-first order kinetic model (—). Experimental conditions: $C_0 = 22.0 \text{ mg L}^{-1}$; $T = 25.0 \text{ }^\circ\text{C}$; $P = 1.0 \text{ atm}$.

Figure 11 shows that the pH of the solution that $\text{pH} = 12.0$ gives rise to a higher removal efficiency with a $k_{app} = 0.341 \text{ h}^{-1}$, for aniline, and $k_{app} = 0.091 \text{ h}^{-1}$ for benzothiazole. Under these conditions, a higher generation of hydroxyl radicals is obtained compared to $\text{pH} = 8.0$, in which a $k_{app} = 0.138 \text{ h}^{-1}$ was obtained, for aniline, and $k_{app} = 0.228 \text{ h}^{-1}$ for benzothiazole. The mechanistic degradation route of this binary matrix generates oxidation byproducts such as nitrobenzene, phenol, nitrate and amidic compounds that compete with aniline and benzothiazole [13,52,53] for the hydroxyl radicals. Most intermediates present a positive charge, which facilitates the interaction with the surface of the TiO_2 catalyst. The introduction of a suspended catalyst did not behave in the same way as when each compound was studied separately. Therefore, it is necessary to reach an agreement that will lead to the highest levels of elimination of both aniline and benzothiazole. This break-even point is at a dose of $[\text{TiO}_2] = 60.0 \text{ mg L}^{-1}$ with $k_{app} = 0.220 \text{ h}^{-1}$ for aniline and $k_{app} = 0.181 \text{ h}^{-1}$ for benzothiazole. In any case, it seems to be evidenced that in global terms the introduction of TiO_2 suspensions in a photoreactor with internal TiO_2 supported walls leads to an improvement in the oxidation of aniline and benzothiazole, in addition to the advantages indicated in the previous section [18].

Additionally, the degree of mineralization obtained from the mixture of aniline with benzothiazole was monitored using the supported configuration together with the addition of 60.0 mg L^{-1} of TiO_2 in suspension at $\text{pH} = 12.0$. Figure 12 shows the evolution of total organic carbon (TOC).

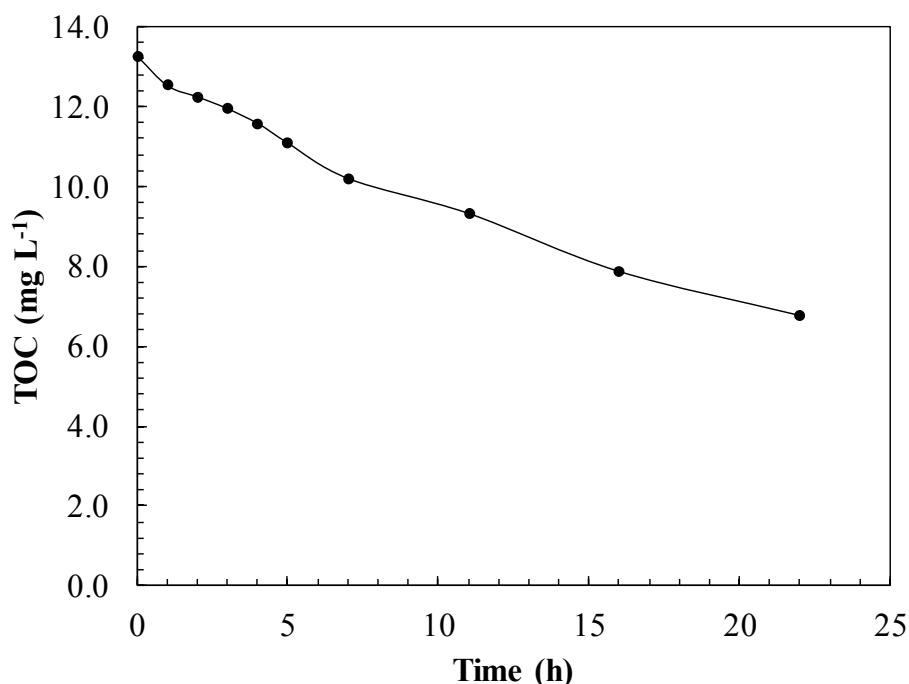


Figure 12. Photocatalytic oxidation of aniline and benzothiazole mixtures monitored by total organic carbon (TOC) with hybrid suspended-supported TiO₂ configuration. Experimental conditions: C₀ = 22.0 mg L⁻¹; [TiO₂] = 60.0 mg L⁻¹; pH = 12.0; T = 25.0 °C; P = 1.0 atm.

As shown in Figure 12, a complete TOC removal is not reached, unlike the primary degradation of the aniline and benzothiazole mixture. This indicates that both compounds are easily transformed into more recalcitrant reaction by-products.

3.11. Energy Consumption

In order to compare and quantify the energy cost of the improvement introduced in this commercial photoreactor, the operating cost was estimated. The term electric energy per order (E_{EO}) is defined as the energy required to degrade a pollutant by an order of magnitude. E_{EO} values can be calculated from the following equation [55]:

$$E_{EO} = \frac{P \cdot t \cdot 1000}{V \cdot 60 \cdot \log\left(\frac{C_0}{C_t}\right)} \quad (31)$$

where P is the electrical power (kW), t is the irradiation time (min), V is the volume of treated effluent (L), C_0 and C_t are the initial at any time aniline or benzothiazole concentration in mg L⁻¹ respectively. Estimated energy costs for experiments with a mixture of aniline and benzothiazole are shown in Figure 13.

The price of electricity that was considered for industrial consumers in Spain was 0.1059 € per kWh [56]. Under optimal conditions the suspended-supported photoreactor with 60.0 mg L⁻¹ TiO₂ (variant C of Figure 13) gives the lowest treatment cost (2.19 € m⁻³ order⁻¹).

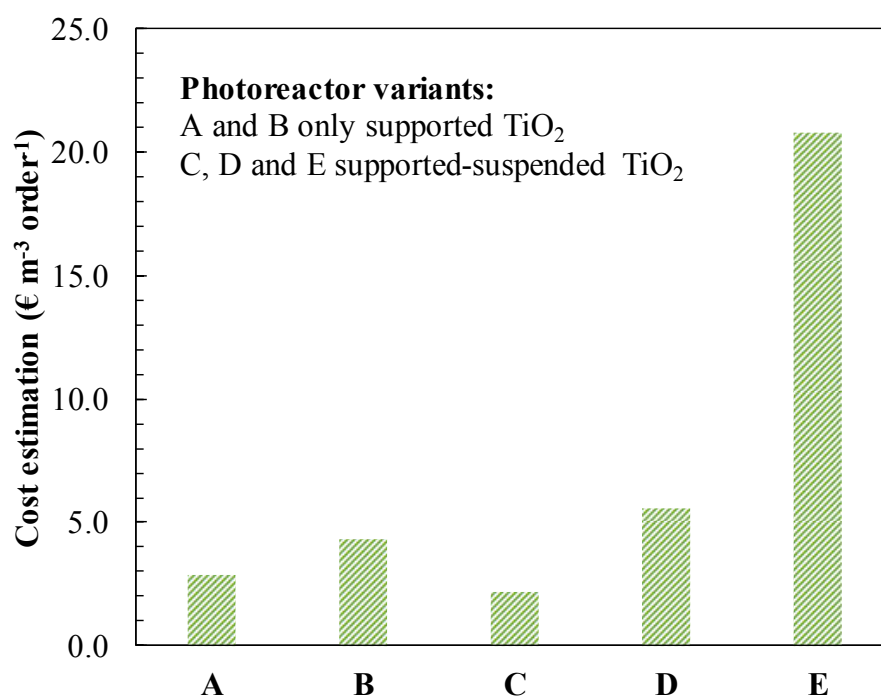


Figure 13. Electrical cost estimation for photocatalytic oxidation of mixtures of aniline and benzothiazole. Photoreactor variants: A and B, only supported TiO₂ (pH = 8.0); C, D and E, supported-suspended TiO₂ at pH = 12. Conditions: A (pH = 8.0), B (pH = 12.0), C ([TiO₂] = 60.0 mg L⁻¹), D ([TiO₂] = 80.0 mg L⁻¹), E ([TiO₂] = 100.0 mg L⁻¹).

4. Conclusions

In this work, the removal performance of aniline and benzothiazole has been improved in a commercial reactor, getting the most favourable operational conditions using a hybrid photoreactor based on the simultaneous use of supported and suspended TiO₂ catalyst. Different operational variants have been offered to enhance the photodegradation removal with small TiO₂ concentrations in suspension. The phenomenon of adsorption of aniline and benzothiazole on TiO₂ P25 was studied. The best adjustment was achieved to the Langmuir isotherm with parameter values of K_L at $T = 20$ °C of 0.138 and 0.419 L mg⁻¹ for aniline and benzothiazole, respectively. From the thermodynamic analysis, a chemisorption type adsorption mechanism on TiO₂ was deduced. Regarding the photocatalytic oxidation, from the individualized analysis of each compound, the most favourable conditions for aniline degradation was determined at pH = 12.0 ($k_{app} = 0.327$ h⁻¹). On the other hand, at pH = 2.5 the poorest degradation rate was obtained ($k_{app} = 0.112$ h⁻¹), because of darkening effect of formed polyaniline. In the case of benzothiazole, slower oxidation kinetics than for aniline were obtained due to the presence of several negatively charged by-products that difficult the chemisorption process on TiO₂.

A 100.0 mg L⁻¹ TiO₂ suspended dose was found to be the most convenient either for aniline ($k_{app} = 0.408$ h⁻¹) or benzothiazole ($k_{app} = 0.181$ h⁻¹) removal, in separate solutions. Higher concentrated suspensions prevented UV light to reach the TiO₂ on the reactor wall.

When treating samples with both compounds, pH = 12.0 was found the most convenient and a higher removal (23% of the total pollutant amount), respect to the only supported catalyst, was obtained. The optimal TiO₂ dose used was 60.0 mg L⁻¹, leading to the lowest energy cost: 2.19 € m⁻³ order⁻¹.

Author Contributions: V.Z. performed the conceptualization; M.J.R. and J.I.L. carried out the design of the methodology and analyses; C.F. and N.V. contributed to the model validation; C.F. carried out the formal analysis; C.F. performed the investigation; C.F. wrote the original draft preparation; C.F. and N.V. wrote the review & editing; V.Z. supervised the experimentation; J.I.L. and J.M.R. could acquire the funding.

Funding: This research was funded by the Basque Government for the financial support of the study through the AID PPG17/53 within the program to consolidate Groups (Basque University System), European funding (ERDF and ESF), and the University of the Basque Country for the C. Ferreiro's predoctoral PIF grant.

Acknowledgments: Authors are very grateful to General Química S.A.U. (Dynasol group) for the availability for experimenting with a pilot photoreactor of its own.

Conflicts of Interest: The authors declare no conflict of interest.

References

1. Harvey, P.J.; Campanella, B.F.; Castro, P.M.L.; Harms, H.; Lichtfouse, E.; Schaffner, A.R.; Smrcek, S.; Werck-Reichharts, D. Phytoremediation of polyaromatic hydrocarbons, anilines and phenols. *Environ. Sci. Pollut. Res.* **2002**, *9*, 29–47. [[CrossRef](#)]
2. Shahrezaei, F.; Mansouri, Y.; Zinatizadeh, A.A.L.; Akhbari, A. Photocatalytic degradation of aniline using TiO₂ nanoparticles in a vertical circulating photocatalytic reactor. *Int. J. Photoenergy* **2012**, *2012*, 430638. [[CrossRef](#)]
3. Herrero, P.; Borrull, F.; Pocurull, E.; Marcé, R.M. An overview of analytical methods and occurrence of benzotriazoles, benzothiazoles and benzenesulfonamides in the environment. *TrAC Trends Anal. Chem.* **2014**, *62*, 46–55. [[CrossRef](#)]
4. Mestankova, H.; Parker, A.M.; Bramaz, N.; Canonica, S.; Schirmer, K.; von Gunten, U.; Linden, K.G. Transformation of Contaminant Candidate List (CCL3) compounds during ozonation and advanced oxidation processes in drinking water: Assessment of biological effects. *Water Res.* **2016**, *93*, 110–120. [[CrossRef](#)]
5. Jin, X.; Peldszus, S.; Huck, P.M. Reaction kinetics of selected micropollutants in ozonation and advanced oxidation processes. *Water Res.* **2012**, *46*, 6519–6530. [[CrossRef](#)] [[PubMed](#)]
6. Anotai, J.; Jevprasesphant, A.; Lin, Y.-M.; Lu, M.-C. Oxidation of aniline by titanium dioxide activated with visible light. *Sep. Purif. Technol.* **2012**, *84*, 132–137. [[CrossRef](#)]
7. US EPA. Contaminant Candidate List 4-CCL 4. Available online: <https://www.epa.gov/ccl/contaminant-candidate-list-4-ccl-4-0> (accessed on 9 October 2018).
8. Felis, E.; Sochacki, A.; Magiera, S. Degradation of benzotriazole and benzothiazole in treatment wetlands and by artificial sunlight. *Water Res.* **2016**, *104*, 441–448. [[CrossRef](#)]
9. Wang, L.; Zhang, J.; Sun, H.; Zhou, Q. Widespread Occurrence of Benzotriazoles and Benzothiazoles in Tap Water: Influencing Factors and Contribution to Human Exposure. *Environ. Sci. Technol.* **2016**, *50*, 2709–2717. [[CrossRef](#)]
10. Ikehata, K.; Gamal El-Din, M.; Snyder, S.A. Ozonation and advanced oxidation treatment of emerging organic pollutants in water and wastewater. *Ozone-Sci. Eng.* **2008**, *30*, 21–26. [[CrossRef](#)]
11. Canle, L.M.; Santaballa, J.A.; Vulliet, E. On the mechanism of TiO₂-photocatalyzed degradation of aniline derivatives. *J. Photochem. Photobiol. A Chem.* **2005**, *175*, 192–200. [[CrossRef](#)]
12. Elfalleh, W.; Assadi, A.A.; Bouzaza, A.; Wolbert, D.; Kiwi, J.; Rtimi, S. Innovative and stable TiO₂ supported catalytic surfaces removing aldehydes under UV-light irradiation. *J. Photochem. Photobiol. A Chem.* **2017**, *343*, 96–102. [[CrossRef](#)]
13. Sánchez, L.; Peral, J.; Domènech, X. Photocatalyzed destruction of aniline in UV-illuminated aqueous TiO₂ suspensions. *Electrochim. Acta* **1997**, *42*, 1877–1882. [[CrossRef](#)]
14. Chen, H.Y.; Zahraa, O.; Bouchy, M. Inhibition of the adsorption and photocatalytic degradation of an organic contaminant in an aqueous suspension of TiO₂ by inorganic ions. *J. Photochem. Photobiol. A Chem.* **1997**, *108*, 37–44. [[CrossRef](#)]
15. Stafford, U.; Gray, K.A.; Kamat, P.V.; Varma, A. An in situ diffuse reflectance FTIR investigation of photocatalytic degradation of 4-chlorophenol on a TiO₂ powder surface. *Chem. Phys. Lett.* **1993**, *205*, 55–61. [[CrossRef](#)]
16. Murgolo, S.; Yargeau, V.; Gerbasi, R.; Visentin, F.; El Habra, N.; Ricco, G.; Lacchetti, I.; Carere, M.; Curri, M.L.; Mascolo, G. A new supported TiO₂ film deposited on stainless steel for the photocatalytic degradation of contaminants of emerging concern. *Chem. Eng. J.* **2017**, *318*, 103–111. [[CrossRef](#)]
17. Costa, A.R.; de Pinho, M.N. Performance and cost estimation of nanofiltration for surface water treatment in drinking water production. *Desalination* **2006**, *196*, 55–65. [[CrossRef](#)]

18. Bansal, P.; Verma, A.; Aggarwal, K.; Singh, A.; Gupta, S. Investigations on the degradation of an antibiotic Cephalexin using suspended and supported TiO₂: Mineralization and durability studies. *Can. J. Chem. Eng.* **2016**, *94*, 1269–1276. [[CrossRef](#)]
19. Verma, A.; Toor, A.P.; Prakash, N.T.; Bansal, P.; Sangal, V.K. Stability and durability studies of TiO₂ coated immobilized system for the degradation of imidacloprid. *New J. Chem.* **2017**, *41*, 6296–6304. [[CrossRef](#)]
20. Kete, M.; Pliekhova, O.; Matoh, L.; Štangar, U.L. Design and evaluation of a compact photocatalytic reactor for water treatment. *Environ. Sci. Pollut. Res. Int.* **2018**, *25*, 20453–20465. [[CrossRef](#)]
21. Santiago, D.E.; Espino-Estévez, M.R.; González, G.V.; Araña, J.; González-Díaz, O.; Doña-Rodríguez, J.M. Photocatalytic treatment of water containing imazalil using an immobilized TiO₂ photoreactor. *Appl. Catal. A Gen.* **2015**, *498*, 1–9. [[CrossRef](#)]
22. Ribao, P.; Rivero, M.J.; Ortiz, I. TiO₂ structures doped with noble metals and/or graphene oxide to improve the photocatalytic degradation of dichloroacetic acid. *Environ. Sci. Pollut. Res. Int.* **2017**, *24*, 12628–12637. [[CrossRef](#)] [[PubMed](#)]
23. Inwatech Környezetvédelmi Kft. Innováció és Technológiák a Környezetért. Available online: <http://www.inwatech.com/en/> (accessed on 18 January 2019).
24. Silva, T.L.; Ronix, A.; Pezoti, O.; Souza, L.S.; Leandro, P.K.T.; Bedin, K.C.; Beltrame, K.K.; Cazetta, A.L.; Almeida, V.C. Mesoporous activated carbon from industrial laundry sewage sludge: Adsorption studies of reactive dye Remazol Brilliant Blue R. *Chem. Eng. J.* **2016**, *303*, 467–476. [[CrossRef](#)]
25. Morrow, W.; McLean, L. Self-Cleaning UV Reflective Coating. U.S. Patent No. 2003/0059549, 27 March 2003.
26. Matthews, R.W.; McEvoy, S.R. A comparison of 254 nm and 350 nm excitation of TiO₂ in simple photocatalytic reactors. *J. Photochem. Photobiol. A Chem.* **1992**, *66*, 355–366. [[CrossRef](#)]
27. Sanchez, M.; Rivero, M.J.; Ortiz, I. Kinetics of dodecylbenzenesulphonate mineralisation by TiO₂ photocatalysis. *Appl. Catal. B Environ.* **2011**, *101*, 515–521. [[CrossRef](#)]
28. Zhou, D.; Ji, Z.; Jiang, X.; Dunphy, D.R.; Brinker, J.; Keller, A.A. Influence of Material Properties on TiO₂ Nanoparticle Agglomeration. *PLoS ONE* **2013**, *8*, e81239. [[CrossRef](#)]
29. Plieth, W. 12—Nanoelectrochemistry. In *Electrochemistry for Materials Science*; Plieth, W., Ed.; Elsevier: Amsterdam, The Netherlands, 2008; pp. 365–388. ISBN 978-0-444-52792-9.
30. Yousef, R.I.; El-Eswed, B. The effect of pH on the adsorption of phenol and chlorophenols onto natural zeolite. *Colloids Surf. A Physicochem. Eng. Asp.* **2009**, *334*, 92–99. [[CrossRef](#)]
31. Adam, O.E.-A.A. Removal of Resorcinol from Aqueous Solution by Activated Carbon: Isotherms, Thermodynamics and Kinetics. *Am. Chem. Sci. J.* **2016**, *16*, 1–13. [[CrossRef](#)]
32. Mack, E. Average cross-sectional areas of molecules by gaseous diffusion methods. *J. Am. Chem. Soc.* **1925**, *47*, 2468–2482. [[CrossRef](#)]
33. Sing, K.S.W.; Everett, D.H.; Haul, R.A.W.; Moscou, L.; Pierotti, R.A.; Rouquerol, J.; Siemieniewska, T. Reporting Physisorption Data for Gas/Solid Systems. In *Handbook of Heterogeneous Catalysis*; Ertl, G., Ed.; Wiley-VCH Verlag GmbH & Co. KGaA: Weinheim, Germany, 2008; ISBN 978-3-527-31241-2.
34. Lin, J.; Weng, X.; Jin, X.; Megharaj, M.; Naidu, R.; Chen, Z. Reactivity of iron-based nanoparticles by green synthesis under various atmospheres and their removal mechanism of methylene blue. *RSC Adv.* **2015**, *5*, 70874–70882. [[CrossRef](#)]
35. Meena, A.K.; Kadirvelu, K.; Mishra, G.K.; Rajagopal, C.; Nagar, P.N. Adsorption of Pb(II) and Cd(II) metal ions from aqueous solutions by mustard husk. *J. Hazard. Mater.* **2008**, *150*, 619–625. [[CrossRef](#)]
36. Kaur, S.; Rani, S.; Mahajan, R.K. Adsorption Kinetics for the Removal of Hazardous Dye Congo Red by Biowaste Materials as Adsorbents. *J. Chem.* **2013**, *2013*, 628582. [[CrossRef](#)]
37. Gupta, V.K.; Agarwal, S.; Sadegh, H.; Ali, G.A.M.; Bharti, A.K.; Hamdy Makhoulouf, A.S. Facile route synthesis of novel graphene oxide-β-cyclodextrin nanocomposite and its application as adsorbent for removal of toxic bisphenol A from the aqueous phase. *J. Mol. Liq.* **2017**, *237*, 466–472. [[CrossRef](#)]
38. Enniya, I.; Rghioui, L.; Jourani, A. Adsorption of hexavalent chromium in aqueous solution on activated carbon prepared from apple peels. *Sustain. Chem. Pharm.* **2018**, *7*, 9–16. [[CrossRef](#)]
39. Markandeya; Shukla, S.P.; Kisku, G.C. Linear and Non-Linear Kinetic Modeling for Adsorption of Disperse Dye in Batch Process. *Res. J. Environ. Toxicol.* **2015**, *9*, 320–331.
40. Banerjee, S.; Chattopadhyaya, M.C. Adsorption characteristics for the removal of a toxic dye, tartrazine from aqueous solutions by a low cost agricultural by-product. *Arab. J. Chem.* **2017**, *10*, S1629–S1638. [[CrossRef](#)]

41. Ayawei, N.; Ebelegi, A.N.; Wankasi, D. Modelling and Interpretation of Adsorption Isotherms. *J. Chem.* **2017**, *2017*, 3039817. [[CrossRef](#)]
42. Fil, B.A.; Yilmaz, M.T.; Bayar, S.; Elkoca, M.T. Investigation of adsorption of the dyestuff astrazon red violet 3RN (basic violet 16) on montmorillonite clay. *Braz. J. Chem. Eng.* **2014**, *31*, 171–182. [[CrossRef](#)]
43. Ho, Y.S.; McKay, G. A Comparison of Chemisorption Kinetic Models Applied to Pollutant Removal on Various Sorbents. *Process Saf. Environ. Prot.* **1998**, *76*, 332–340. [[CrossRef](#)]
44. Largette, L.; Pasquier, R. A review of the kinetics adsorption models and their application to the adsorption of lead by an activated carbon. *Chem. Eng. Res. Des.* **2016**, *109*, 495–504. [[CrossRef](#)]
45. Inyinbor, A.A.; Adekola, F.A.; Olatunji, G.A. Kinetics, isotherms and thermodynamic modeling of liquid phase adsorption of Rhodamine B dye onto Raphia hookerie fruit epicarp. *Water Resour. Ind.* **2016**, *15*, 14–27. [[CrossRef](#)]
46. Orha, C.; Pode, R.; Manea, F.; Lazau, C.; Bandas, C. Titanium dioxide-modified activated carbon for advanced drinking water treatment. *Process Saf. Environ. Prot.* **2017**, *108*, 26–33. [[CrossRef](#)]
47. O’Shea, K.E.; Dionysiou, D.D. Advanced Oxidation Processes for Water Treatment. *J. Phys. Chem. Lett.* **2012**, *3*, 2112–2113. [[CrossRef](#)]
48. Wols, B.A.; Hofman-Caris, C.H.M. Review of photochemical reaction constants of organic micropollutants required for UV advanced oxidation processes in water. *Water Res.* **2012**, *46*, 2815–2827. [[CrossRef](#)] [[PubMed](#)]
49. Yang, H.; Bard, A.J. The application of fast scan cyclic voltammetry. Mechanistic study of the initial stage of electropolymerization of aniline in aqueous solutions. *J. Electroanal. Chem.* **1992**, *339*, 423–449. [[CrossRef](#)]
50. Chong, M.N.; Jin, B.; Chow, C.W.K.; Saint, C. Recent developments in photocatalytic water treatment technology: A review. *Water Res.* **2010**, *44*, 2997–3027. [[CrossRef](#)] [[PubMed](#)]
51. Doña, J.M.; Garriga, C.; Araña, J.; Pérez, J.; Colon, G.; Macías, M.; Navio, J.A. The effect of dosage on the photocatalytic degradation of organic pollutants. *Res. Chem. Intermed.* **2007**, *33*, 351–358. [[CrossRef](#)]
52. Andreozzi, R.; Insola, A.; Caprio, V.; D’Amore, M.G. Ozonation of pyridine in aqueous solution: Mechanistic and kinetic aspects. *Water Res.* **1991**, *25*, 655–659. [[CrossRef](#)]
53. Valdés, H.; Zaror, C.A.; Jekel, M. Removal of Benzothiazole from Contaminated Waters by Ozonation: The Role of Direct and Indirect Ozone Reactions. *J. Adv. Oxid. Technol.* **2016**, *19*, 338–346. [[CrossRef](#)]
54. Velmurugan, R.; Subash, B.; Krishnakumar, B.; Selvam, K.; Swaminathan, M. Solar photocatalytic treatment of gelatin industry effluent: Performance of pilot scale reactor with suspended TiO₂ and supported TiO₂. *Indian J. Chem. Technol.* **2016**, *23*, 8.
55. Davididou, K.; McRitchie, C.; Antonopoulou, M.; Konstantinou, I.; Chatzisyneon, E. Photocatalytic degradation of saccharin under UV-LED and blacklight irradiation. *J. Chem. Technol. Biotechnol.* **2018**, *93*, 269–276. [[CrossRef](#)]
56. European Union. *Eurostat Regional Yearbook*, 2018 ed.; Statistical Books; Publications Office of the European Union: Luxembourg, 2018; ISBN 978-92-79-87876-3.




3.5. 5. argitalpena. Removal of aniline and benzothiazole wastewaters using an efficient MnO₂/GAC catalyst in a photocatalytic fluidised bed reactor

3.5 kapitulua artikulu honi dagokio:

C. Ferreiro, N. Villota, J.I. Lombraña, M.J. Rivero, V. Zúñiga, J.M. Rituerto. Removal of aniline and benzothiazole wastewaters using an efficient MnO₂/GAC catalyst in a photocatalytic fluidised bed reactor. *Materials*, 14, 18, 5207, 2021. DOI: 10.3390/ma14185207.

Article

Removal of Aniline and Benzothiazole Wastewaters Using an Efficient MnO₂/GAC Catalyst in a Photocatalytic Fluidised Bed Reactor

Cristian Ferreiro ^{1,*} , Natalia Villota ², José Ignacio Lombrana ¹ , María J. Rivero ³ , Verónica Zúñiga ⁴ and José Miguel Rituerto ⁴

¹ Department of Chemical Engineering, Faculty of Science and Technology, University of the Basque Country UPV/EHU, Barrio Sarriena s/n, 48940 Leioa, Spain; ji.lombrana@ehu.es

² Department of Chemical and Environmental Engineering, Faculty of Engineering Vitoria-Gasteiz, University of the Basque Country UPV/EHU, Nieves Cano 12, 01006 Vitoria-Gasteiz, Spain; natalia.villota@ehu.es

³ Department of Chemical and Biomolecular Engineering, University of Cantabria, 39005 Santander, Spain; riveromj@unican.es

⁴ General Química, S.A.U. (Grupo Dynasol), 01213 Lantaron, Spain; veronica.zuniga@repsol.com (V.Z.); jrituertol@repsol.com (J.M.R.)

* Correspondence: cristian.ferreiro@ehu.es; Tel.: +34-946-012-512

Abstract: This work presents an efficient method for treating industrial wastewater containing aniline and benzothiazole, which are refractory to conventional treatments. A combination of heterogeneous photocatalysis operating in a fluidised bed reactor is studied in order to increase mass transfer and reduce reaction times. This process uses a manganese dioxide catalyst supported on granular activated carbon with environmentally friendly characteristics. The manganese dioxide composite is prepared by hydrothermal synthesis on carbon Hydrodarco[®] 3000 with different active phase ratios. The support, the metal oxide, and the composite are characterised by performing Brunauer, Emmett, and Teller analysis, transmission electron microscopy, X-ray diffraction analysis, X-ray fluorescence analysis, UV–Vis spectroscopy by diffuse reflectance, and Fourier transform infrared spectroscopy in order to evaluate the influence of the metal oxide on the activated carbon. A composite of MnO₂/GAC (3.78% in phase α -MnO₂) is obtained, with a 9.4% increase in the specific surface of the initial GAC and a 12.79 nm crystal size. The effect of pH and catalyst load is studied. At a pH of 9.0 and a dose of 0.9 g L⁻¹, a high degradation of aniline and benzothiazole is obtained, with an 81.63% TOC mineralisation in 64.8 min.

Keywords: MnO₂/GAC composite; fluidised bed photoreactor; aniline; benzothiazole; sustainable photocatalysis; industrial wastewater



Citation: Ferreiro, C.; Villota, N.; Lombrana, J.I.; Rivero, M.J.; Zúñiga, V.; Rituerto, J.M. Removal of Aniline and Benzothiazole Wastewaters Using an Efficient MnO₂/GAC Catalyst in a Photocatalytic Fluidised Bed Reactor. *Materials* **2021**, *14*, 5207. <https://doi.org/10.3390/ma14185207>

Academic Editor: Dror Avisar

Received: 18 August 2021

Accepted: 8 September 2021

Published: 10 September 2021

Publisher's Note: MDPI stays neutral with regard to jurisdictional claims in published maps and institutional affiliations.



Copyright: © 2021 by the authors. Licensee MDPI, Basel, Switzerland. This article is an open access article distributed under the terms and conditions of the Creative Commons Attribution (CC BY) license (<https://creativecommons.org/licenses/by/4.0/>).

1. Introduction

One challenge associated with wastewater treatment is the presence of recalcitrant compounds, which are difficult to remove through conventional technologies [1]. Unfortunately, many of these pollutants play a key role in everyday-use products and are continuously added to aquatic environments through anthropogenic activities in sectors such as agriculture, industry, transport, and energy [2–4]. Recalcitrant contaminants broadly consist of high-molecular-weight hydrophobic molecules, including alcohols, phenols, and nitrogenous and sulphur compounds [5].

These emission sources without proper water treatments increase recalcitrant pollutants' concentration in water, consequently damaging the environment and human health [6]. Therefore, degrading these refractory pollutants has become one of the challenges listed in the Sustainable Development Goals (SDGs), more specifically in SDG 6, towards mitigating their environmental impact by 2030. For this purpose, cost-effective

treatment strategies should be developed to remove and mineralise these hazardous substances [7,8].

This study focuses on the removal of aniline (ANI) and benzothiazole (BTH) from industrial effluents. These two recalcitrant pollutants are commonly found in the leather and wood industry as well as in rubber chemicals production, specifically as raw materials for the synthesis of vulcanisation accelerators. In particular, these two pollutants have adverse effects on the health of organisms in aquatic environments and may also be tumour inducers and allergens [6,9]. In addition, BTH (included in Contaminant Candidate List 4) is not only found in industrial effluents but can also be detected in domestic wastewater and airport runoff water [10–12]. Bioremediation studies have reported uncertainty about the biodegradation of both compounds, especially aniline, owing to its genotoxic character. For this reason, conventional biological treatment systems or active sludge has failed to metabolise these pollutants [13,14].

Several technologies have been used to treat water containing ANI or BTH, such as coagulation [15], activated carbon adsorption [16–18], ozonation [9,19,20], photocatalysis [21–23], wet oxidation [24,25], and membrane separation [26]. However, the implementation of these technologies has some limitations, such as the adsorption capacity of the adsorbent, high disposal costs, high energy consumption, and low efficiency [27]. In membrane separation, zero-waste generation is unfeasible, because this process produces effluents with a high concentration of the target pollutants [26]. Moreover, adsorption processes only transfer the pollutant to a new phase (solid waste), which needs further treatment [28–30].

To overcome these major obstacles, photocatalytic degradation with new semiconductor materials has recently attracted worldwide attention as a green technology capable of degrading low-biodegradability organic and inorganic pollutants from industrial effluents [1,31,32]. Photocatalysis is a promising technology for degrading highly polluting compounds into other harmless by-products or even for mineralising them into CO₂ and H₂O. In addition, this low-cost technology can operate at room temperature [33–35].

Semiconductor photocatalytic materials are highly effective for treating wastewater containing recalcitrant pollutants when irradiated by ultraviolet (UV) or visible light. Some of the most widely used photocatalysts include TiO₂, ZnO, and SnO [36–38]. In addition to the aforementioned catalysts, transition metals, such as copper, vanadium, nickel, and manganese, are being studied for their specific characteristics, including their affordable cost, effectiveness, abundance, and sustainability [39]. Catalysts such as TiO₂ or ZnO, which could be widely used, are also associated with a series of drawbacks which affect the sustainability of their processes regarding the light source used to initiate the catalytic reaction. Their forbidden band (about 3.2 V) is so wide that they can only be activated under UV light, thus precluding visible light activation [40]. Consequently, establishing a photocatalytic process using clean and renewable solar energy would require the improvement of photocatalysts to enhance their visible light absorption. In this context, manganese oxides, whether supported or not on another material, could play a key role [41].

Manganese oxides have attracted attention in photocatalytic processes for the treatment of recalcitrant contaminants for their different morphologies and crystalline structures (α -, β -, γ - or δ -MnO₂), in addition to their high efficiency, abundance, affordability (approximately 75% less expensive than TiO₂) [29], high reproducibility during the manufacturing process, good adsorption properties, low toxicity, acid resistance, redox potential, and environmental friendliness [42–44]. The α -MnO₂ phase has demonstrated a higher potential for removing organic compounds than the phases β -, γ -, and δ -MnO₂, because α -MnO₂ has the lowest oxidation state of all phases, according to Nawaz et al. [45]. Therefore, the α -MnO₂ phase has the highest catalytic activity, owing to its high redox power. MnO₂ has, as a function of the structure resulting from the synthesis process, a forbidden band energy of approximately 1–2 eV, which enables its activation in the visible region and makes it a highly competitive catalyst among other classical oxides [46,47]. Furthermore, manganese oxides can improve their efficiency by supporting them on carbonaceous materials [48–50].

As a result, modifying materials such as granular activated carbon (GAC) with manganese oxides (see Table S1) could lead to a better photocatalysis performance for ANI and BTH removal. For more details see Supplementary Materials.

In recent studies comparing different types of reactors, the authors have concluded that integrating an AOP with packed-, fixed-, and fluidised-bed (FBR) reactors facilitates large-scale operations and requires less oxidant and catalyst loading to degrade pollutants [51]. Nevertheless, Tian et al. [52] and Bello et al. [1] concluded that packed- and fixed-bed reactors were not suitable for photocatalytic processes, because they cannot provide a great surface area and mass transfer, and only a small fraction of the catalyst is exposed to light. However, fluidised beds, which are widely used in other petrochemical, combustion, or gasification applications would overcome these disadvantages by providing a good mass transfer rate and uniform mixing of the liquid-solid (LS) contact, a robust design for alterations in the starting effluent, a large-volume water-processing capacity, and a low operating cost. Moreover, fluidised beds are easy to operate, scale up, and build [5,53].

Most published studies have demonstrated improvements in the performance of processes which apply FBRs. Kanki et al. [54] studied the photocatalytic degradation of phenol and bisphenol A in an FBR using TiO₂-coated ceramic particles, reporting that under the same oxidation conditions, the contaminant was removed four times faster in this FBR than in other reactor configurations. Huang and Huang [55] achieved 98% mineralisation of an aqueous stream containing phenol with an FBR-photocatalytic system using FeOOH on glass spheres. In both cases, they concluded that the FBR system adapted to a photocatalytic process improved light penetration and contaminant adsorption on the materials.

Therefore, using a α -MnO₂ catalyst supported on granular activated carbon (GAC) in a photocatalytic FBR could achieve high removal and mineralisation rates, as well as facilitate scaling up the process to the industrial level for treating industrial effluents containing recalcitrant contaminants such as ANI and BTH, using an inexpensive, energy-efficient, environmentally friendly, regenerative, and robust process with visible light.

In this work, we propose the implementation on a pilot scale of an efficient photocatalytic system with a novel MnO₂/GAC catalyst operating in an FBR in order to remove aniline and benzothiazole from an industrial effluent from the accelerator production for rubber manufacturing. Such a system requires the development of a new catalytic material supported on GAC, Hydrodarco[®] 3000 (HD 3000, Boston, MA, USA), using a hydrothermal technique with low environmental impact and high reproducibility to prepare the alpha crystalline phase, and adequately distributing α -MnO₂ on the GAC surface. The MnO₂/GAC catalyst in the FBR system will avoid any subsequent separation operation. In addition, we studied operational parameters, such as pH and catalyst loading, to show the potential of this global strategy based on the FBR-photocatalytic system for subsequent scaling-up to an industrial level and increasing mineralisation yields and recalcitrant compound degradation with the lowest environmental impact and economic and energy costs.

2. Materials and Methods

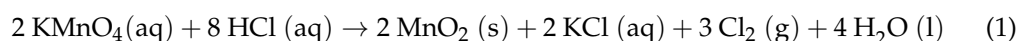
2.1. Chemicals

Hydrochloric acid (HCl, Merck, 37%, Darmstadt, Germany), sodium hydroxide (NaOH, Panreac, 50%, Barcelona, Spain), potassium permanganate (KMnO₄, Probus, >99%, Esparreguera, Spain), sulphuric acid (H₂SO₄, Sigma-Aldrich, 98%, St. Louis, MI, USA), hydrogen peroxide (H₂O₂, Labkem, 30%), sodium bicarbonate (NaHCO₃, Merck, >99.7%, Darmstadt, Germany), sodium carbonate (Na₂CO₃, Merck, \geq 99.5%, Darmstadt, Germany), sodium chloride (NaCl, VWR, 99.8%, Radnor, PA, USA), dichloromethane (CH₂Cl₂, Merck, >99.9%, Darmstadt, Germany), and diphenylamine (C₁₂H₁₁N, Merck, 99%, Darmstadt, Germany) were used. Deionised water was supplied by a Milli-Q[®] water purification unit. Hydrodarco[®] 3000 granular activated carbon was supplied by Cabot Corporation (Boston, MA, USA).

2.2. Catalyst Preparation

The MnO₂/GAC material was synthesised using a hydrothermal preparation technique. This method was selected due to its simplicity, good reproducibility, and high reliability. In addition, the size and morphology of the nanostructure could be easily adapted to the granular activated carbon support.

The activated carbon was pre-treated with a piranha solution consisting of a (70:30 v/v) mixture of H₂SO₄ and H₂O₂ for 24 h to remove any impurity derived from the GAC manufacturing process and to prepare the GAC surface for active phase deposition [56]; subsequently, washing with deionised water and drying in an oven at 80 °C were carried out. Then, 9.97 g of KMnO₄ was dissolved in 228.36 mL deionised water and shaken for 5 min. Then, 21.19 mL of concentrated HCl was poured on the permanganate solution dropwise for 15 min. The minimum amount of HCl required was used to prevent the potential loss of crystallinity in the final product and unwanted oxides such as hausmannite [57]. During the synthesis, at room temperature, the following reaction was performed:



where in the main reaction by-product is KCl. Then, 14.0 g of pre-treated GAC was added to this solution under slow stirring for 1.25 h. Then, the mixture was transferred to a Teflon[®] autoclave reactor and remained at 180 °C for 12 h in an oven. The resulting MnO₂/GAC-3 composite was washed several times with deionised water until the removal of the excess of MnO₂ and unwanted by-products and dried in an oven at 80 °C for 12 h. The MnO₂/GAC-1 and MnO₂/GAC-2 catalytic materials were prepared with 1.94 g and 18.41 g of KMnO₄, respectively, corresponding to the stoichiometric ratio between KMnO₄ and HCl, according to Equation (1). The MnO₂ nanoparticles (NPs) were synthesised following the procedures used to prepare the MnO₂/GAC-3 composite, without incorporating the activated carbon support.

2.3. Analyses

2.3.1. Chemical Analysis

ANI and BTH removal was quantified by gas chromatography (GC) using an Agilent 6890N gas chromatograph (Agilent, Santa Clara, CA, USA) coupled to an Agilent 5975 mass spectrometer (Agilent, Santa Clara, CA, USA). The chromatograph was equipped with a 30.0 cm non-polar phase column.

The aqueous samples were adjusted to pH = 11.0 for ANI and to pH = 3.0 for BTH. The samples were prepared by extraction with CH₂Cl₂ (using 0.1% C₁₂H₁₁N as an internal standard). A sample volume of 0.4 µL was injected using the method described by Ferreira et al. [21]. The degree of mineralisation was quantified by total organic carbon (TOC) analysis on a Shimadzu TOC-VCSH analyser with ASI-V autosampler (Izasa Scientific, Alcobendas, Spain). The colour was analysed using a PerkinElmer Lambda 10 UV-Vis spectrophotometer (PerkinElmer, Madrid, Spain) by directly measuring the absorbance at 455 nm, and the aromatic ring rupture was determined from the sample's absorbance at 254 nm [58]. The turbidity was analysed using the turbidimeter Eutech TN-100 (Thermo Scientific, Singapore), and the chemical oxygen demand (COD) concentration was measured using Merck Spectroquant[®] kits (Merck KGaA, Darmstadt, Germany). Conductivity, temperature, dissolved oxygen, and pH were measured using a PCE-PHD1 multiparameter meter (PCE Ibérica, Tobarra, Spain). Total ammonia was determined by YSI TruLine ion-selective electrode (Yellow Springs, OH, USA). The analytical methods used to characterise the industrial influent are detailed in the Supplementary Materials.

2.3.2. Catalytic Material Characterisation

The catalytic material composite was characterised using several techniques to analyse both its physical and chemical properties. The morphology and microstructure of the smallest particles in each sample were analysed by performing high-resolution transmis-

sion electron microscopy (HRTEM) on a Philips CM200 microscope (Philips, Eindhoven, The Netherlands), with a LaB₆ filament as an electron source operating at an acceleration voltage of 200 kV. The microscope was coupled to an EDAX Genesis 4000 energy dispersive X-ray (EDX) spectroscopy platform (AMETEK GmbH, Weiterstadt, Germany) with a Si(Li)-type detector with a Super Ultra-Thin window to analyse the chemical composition of both pristine GAC Hydrodarco[®] 3000 and MnO₂/GAC-3 composite. Spectra and images were acquired using the software EDAM IV (AMETEK GmbH, Weiterstadt, Germany). The samples were dispersed in an equimolar ethanol–water mixture and ultrasonicated. Observations of the surface morphology of the smallest particles of the composite and MnO₂ nanoparticles were carried out on a MULTIMODE 8 atomic-force microscope (AFM) Nanoscope V Bruker (Azbil Telstar Technologies, Terrassa, Spain). In addition, scanning electron microscopy (SEM) using a JEOL JSM-7000F electron microscope (JEOL B.V., Nieuw-Vennep, the Netherlands) was used.

MnO₂/GAC-3 was characterised in a Malvern Panalytical Mastersizer 3000 particle-size analyser (Malvern Panalytical, Malvern, UK). Other physical properties, such as the pore size or specific surface area, were determined through adsorption–desorption analysis with high-purity nitrogen (N₂) at boiling temperature (−196 °C), using the Micromeritics Surface Area and Porosimetry System (ASAP) 2010 high-performance gas adsorption analyser (Micromeritics France S.A., Verneuil Halatte, France). Prior to the adsorption experiments, the sample was degassed at 383 K for 3 h. The pore-size distribution of the new catalyst was obtained by the BJH method [6].

The crystalline phase and crystal size were determined by X-ray diffraction (XRD) on a Philips PW1710 diffractometer (Philips, Eindhoven, the Netherlands). The samples were finely ground and subjected to CuK α radiation in continuous scan from 5° to 70° and at a 2 θ angle sweep speed of 0.026° s^{−1}. The data were analysed using the software Winplot[®] (Institut des Sciences Chimiques de Rennes, Rennes, France). The phases of the catalyst were identified by matching each characteristic peak with the Joint Committee on Powder Diffraction Standards (JCPDS) files.

The MnO₂ content was measured by X-ray fluorescence (XRF) spectroscopy. From each sample, a borated glass bead was prepared by melting in an induction micro-furnace, the Spectromelt A12 flux (Merck KGaA, Darmstadt, Germany), with the sample using a 20:1 ratio. An oxidising agent was added to favour the elimination of all organic carbon and the fixation of the inorganic oxides. The chemical analysis of the beads was performed under a vacuum atmosphere using a Panalytical AXIOS wavelength-dispersion XRF sequential spectrometer (WDXRF). The fluorometer is equipped with an Rh tube and three detectors (gas flow, scintillation, and Xe seal) (Malvern Panalytical, Malvern, UK).

The dispersion of the deposited metallic active phase MnO₂ on GAC was determined by H₂ chemisorption in a Micromeritics ASAP 2020 Plus analyser (Micromeritics France S.A., Verneuil Halatte, France). The reduction was performed by degassing 0.35 g of catalyst at 300 °C for 60 min, followed by reduction at a 50 mL min^{−1} flow with a 5% H₂/Ar gas stream at 350 °C for 2 h. The adsorption isotherm was performed with H₂ at 35 °C. To assess the amount of chemisorbed H₂, the adsorption isotherm was repeated, gassing the sample again for 60 min, thereby determining the difference between the first and second isotherms.

Surface functional groups of pristine GAC and MnO₂/GAC composite samples were identified using Fourier transform infrared spectroscopy (FTIR). Samples were ground in an agate mortar, and the resulting powders were mixed with anhydrous KBr. A pressed disc of the mixed sample was placed in a disc holder in a JASCO 4200 spectrometer (JASCO Corporation, Tokyo, Japan) equipped with a deuterated L-alanine doped triglycine sulphate detector (DLATGS). Using Spectra Manager software V 2.14.02 (JASCO Corporation, Tokyo, Japan), spectra were acquired in transmittance mode in the range 4000–400 cm^{−1} with an average of 64 scans and at a resolution of 4 cm^{−1}. A pressed disc of pure KBr was used as a background for each measurement.

The chemical state of MnO₂ deposited on the GAC support was determined by X-ray photoelectron spectroscopy (XPS) on a Leybold-Heraeus LHS-10 spectrometer (Leybold GmbH, Munich, Germany), with a twin anode Al/Mg X-ray source and a hemispherical electron energy analyser (HSA). XPS measurements were performed with a 150 W X-ray source, taking the C_{1s} peak (284.8 eV) as reference with an uncertainty of 0.2 eV. The samples were prepared on double-sided adhesive tape, compatible with high vacuum, and the XPS data were fitted using the XPSPEAK41 program (Leybold GmbH, Munich, Germany). Samples were measured in duplicate. Peaks' deconvolution was performed using a nonlinear Shirley baseline to subtract the background, as well as a combination of Gaussian and Lorentzian type curves.

The point of zero charge (PZC) was determined using the method described by Ferreira et al. [6] on a NaCl solution with 0.100 g of composite, measuring the pH on a CRISON GLP 22 pH meter (Hach Lange Spain, L'Hospitalet de Llobregat, Spain).

The optical properties to calculate the band gap of the new materials were characterised by UV–Vis absorption spectroscopy (200–2200 nm) at 25 °C on the Agilent Cary 5000 UV–Vis–NIR spectrophotometer (Agilent, Santa Clara, CA, USA).

2.4. UV-A Pilot Plant Description and Experimental Procedure

Aniline and benzothiazole contained in industrial effluents were removed on an FBR-photoreactor at pilot scale AOP 1 of h₂o.TITANIUM[®] (patent US20030059549A1) [59], which was modified for fluidised bed operation (see Figure 1).

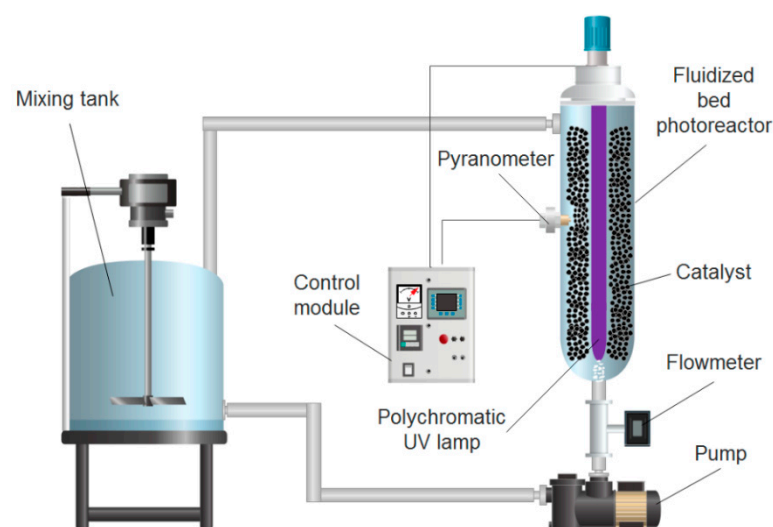


Figure 1. Schematic representation of the FBR-photoreactor at pilot scale used in the photocatalytic and adsorption experiments for aniline and benzothiazole removal from industrial effluents.

The pilot plant consisted of a 47.3 cm long, 2.15 L stainless steel tubular reactor with a 25 W polychromatic UV-A lamp (BL368/4-Eubizz Water, Eubizz Water, Høyanger, Norway) (see Figure S1), protected by a quartz tube ($\varnothing_{\text{int}} = 3.7$ cm) and positioned axially in a cylindrical stainless steel photoreactor ($\varnothing_{\text{int}} = 7.6$ cm). The pilot plant was operated in batch mode with a recirculation flow rate of $0.75 \text{ m}^3 \text{ h}^{-1}$ supplied by a 0.18 kW centrifugal pump (Pool Pump-72512, The Pool Shop, Tauranga, New Zealand) and a total volume of 10 L. The flow was controlled with a flow meter (GPI Electronic Digital Meter, Sparta, NJ, USA).

The irradiated surface of the FBR-photoreactor ($S_{\text{irradiated}}$, m²) and the irradiated liquid volume ($V_{\text{irradiated}}$, m³) were estimated using Equations (2) and (3):

$$S_{\text{irradiated}} = 2 \times \pi \times r_{\text{int, FBR}} \times L_{\text{lamp}} \quad (2)$$

$$V_{\text{irradiated}} = L_{\text{lamp}} \times \pi \times (r_{\text{int, FBR}}^2 - r_{\text{int, lamp}}^2), \quad (3)$$

where L_{lamp} is the length of the UV-A lamp (m), and $r_{\text{int, FBR}}$ and $r_{\text{int, lamp}}$ are the inner radius of the FBR and inner UV-A lamp (m), respectively. The irradiated area was 0.05 m², with an irradiated volume of 1.63 L. To compare the energy consumption with other reaction systems such as slurry reactors, the accumulated UV-A energy per unit of volume (Q_{UVA} , kJ L⁻¹) was calculated using Equation (4):

$$Q_{\text{UVA}} = \text{Irradiation dose} \times \frac{S_{\text{irradiated}}}{V}, \quad (4)$$

where the *Irradiation dose* (kJ m⁻²) is the product of the irradiance emitted by the UV-A lamp in W m⁻² multiplied by the exposure time in seconds. The irradiance emitted by the lamp was monitored throughout the experiment using a radiometer (PLS Systems AB, Sloga Ingenieros S.L., Puertollano, Spain). Under favourable operating conditions, a maximum irradiance of 155.8 W m⁻² was reached, which corresponds to a Q_{UVA} value of 13.04 kJ L⁻¹.

The photocatalytic experiments were performed at a constant temperature of 26 °C, a constant recirculation flow rate, and constant pH, with a variation of less than 3% in the averaged physicochemical characteristics of the industrial effluent outlined in Table 1.

Table 1. Average physical–chemical profile of the industrial effluent containing ANI and BTH.

Parameter	Value
Aniline (mg L ⁻¹)	12.0 ± 0.5
Benzothiazole (mg L ⁻¹)	12.0 ± 0.6
Dissolved oxygen (mg O ₂ L ⁻¹)	7.5 ± 0.37
pH	7.8 ± 0.1
Conductivity at 20 °C (μS cm ⁻¹)	605 ± 30
Chemical oxygen demand (mg O ₂ L ⁻¹)	45.46 ± 2.27
Total organic carbon (mg C L ⁻¹)	16.73 ± 0.53
Temperature (°C)	26 ± 0.1
Turbidity (NTU)	1.01 ± 0.05
Aromatic ring rupture (AU)	2.453 ± 0.122
Colour (AU)	0.717 ± 0.03
Nitrite (mg NO ₂ L ⁻¹)	0.041 ± 0.001
Nitrate (mg NO ₃ L ⁻¹)	1.6 ± 0.1
Chloride (mg Cl L ⁻¹)	31.7 ± 1.6
Total phosphorus (mg P L ⁻¹)	0.05 ± 0.01
Phosphates (mg PO ₄ L ⁻¹)	0.07 ± 0.01
Total ammonia (mg NH ₄ L ⁻¹)	0.14 ± 0.01

The effluents were introduced into a mixing tank equipped with a mechanical stirrer until complete homogenisation (10 min), adjusting the initial pH. An initial sample was taken to verify the ANI and BTH concentrations. Subsequently, the dose of catalyst was added, and the recirculation system was connected until it reached the adsorption equilibrium (0.12 h). Then, the UV-A lamp was turned on, and the photocatalytic experiment started. The samples were collected at regular intervals to analyse aniline and benzothiazole degradation, as well as other physicochemical parameters. All experiments were performed in triplicate, with an error lower than 5.3%. Similarly, all collected samples were filtered with a 0.45-μm MF Millipore filter (Merck KGaA, Darmstadt, Germany) prior to their analysis.

3. Results and Discussion

3.1. Catalyst Characterisation

The type of composite structure used in the photocatalysis process may determine the results. Figure 2 shows SEM and HRTEM images of powder MnO_2 , GAC Hydrodarco[®] 3000, and $\text{MnO}_2/\text{GAC-3}$ structures.

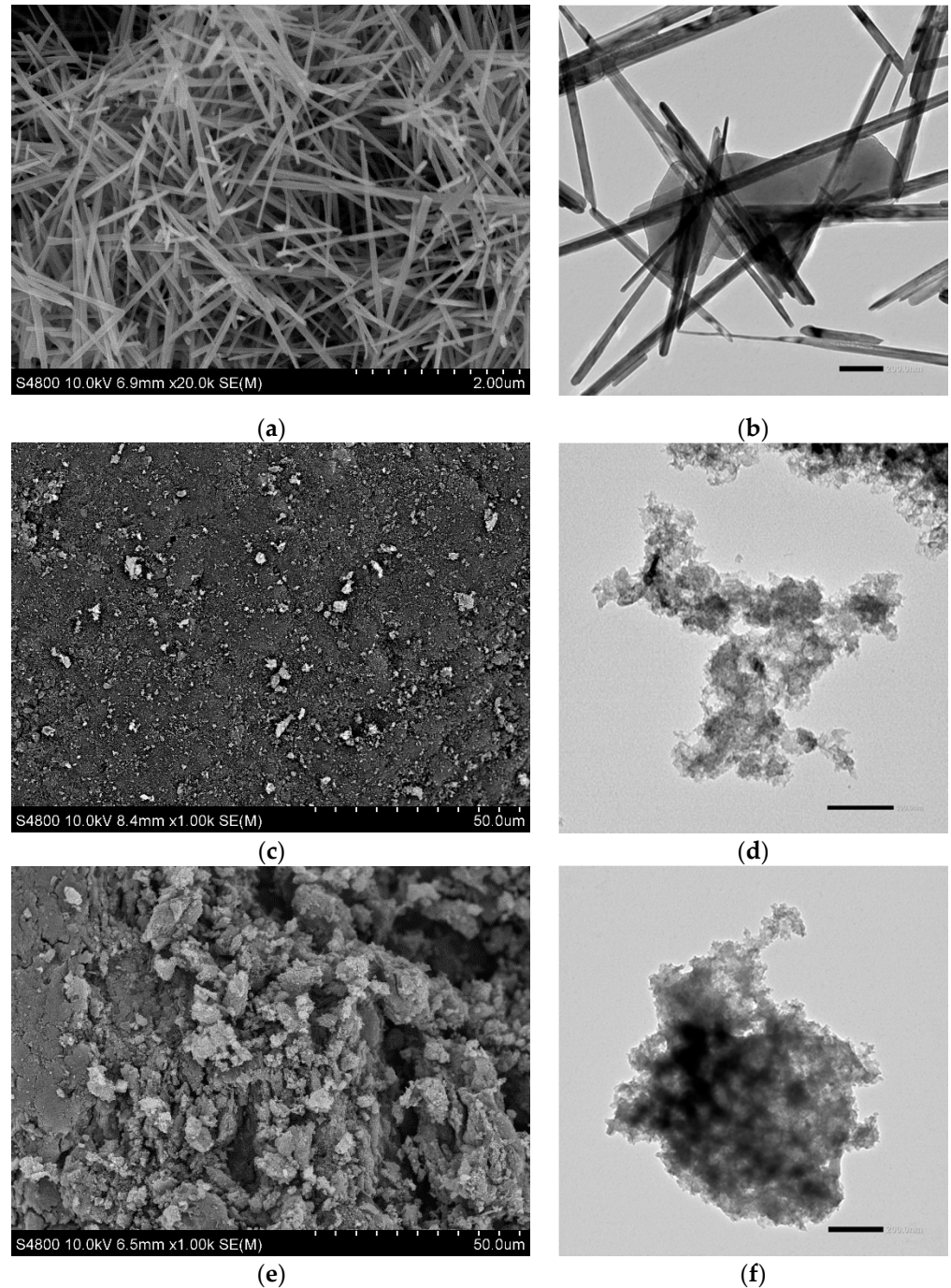


Figure 2. SEM (left) and HRTEM (right) micrographs of structures: (a,b) $\alpha\text{-MnO}_2$ nanoparticles; (c,d) commercial activated carbon Hydrodarco[®] 3000; (e,f) synthesised $\text{MnO}_2/\text{GAC-3}$ composite.

Figure 2a,b show that the $\alpha\text{-MnO}_2$ phase has a morphology typical of a basic octahedral structure in the shape of needles, which are approximately 3 μm long and 50 to 250 nm wide, with a smooth texture, similar to that observed by Nawaz et al. [45] in a comparative study conducted with different manganese oxide phases. As shown in Figure 2b, defects in

the amorphous structure could trap excited electrons, prolonging the separation of charge carriers, which some authors have related to an increase in the organic pollutant degradation efficiency [29]. However, the formation of particles agglomeration was observed, which could lead to a reduction in the number of catalyst active sites available for the photocatalytic reaction.

Figure 2c,d show the typical structure of microporous granular activated carbon with highly rough edges, irregular cavities, and fine open pores, similar to that observed by Alhamed et al. [60]. In contrast, the images in Figure 2e and f show spongy α -MnO₂ nanoparticles that are approximately 5 μ m in size and are responsible for increasing the external surface and the interior of the pores. In addition, the nanoparticles were well-dispersed, which increased the heterogeneity of the photocatalyst surface and helped to develop a porous structure without agglomerated particles, thus preventing the blockage of the pores and consequently reducing the catalytic and adsorptive properties of the new composite. Semi-quantitative elemental analysis of an EDX spectrum indicated the presence of Mn and C (see Figure S2).

Recently, Zhou et al. [50] doped ϵ -MnO₂ samples with graphene, preparing a non-homogeneous material with a specific surface 24.3% higher than that of the initial ϵ -MnO₂.

Figure 3 shows AFM images of α -MnO₂ nanoparticles, GAC Hydrodarco[®] 3000, and the MnO₂/GAC-3 composite. This technique revealed particles of 250 nm.

The morphological study of Figure 3a,b shows that α -MnO₂ nanoparticles were spherical, with a diameter of 30–40 nm, according to topographic images, forming large structures consisting of 200 nm agglomerates. This behaviour was similar to that observed by Khan et al. [61] after synthesizing α -MnO₂ nanoparticles using a precipitation method. In turn, Figure 3c,d show that commercial GAC had a rather uniform surface with small irregularities of approximately 0.5 nm, which were attributable to the porosity of the activated carbon. Finally, Figure 3e,f show that the particles were adequately dispersed on the surface of the GAC. Figure 3e shows changes in the 1 nm surface, thus confirming the MnO₂ nanocrystals observed in HRTEM images. In addition, the comparison of the image of phase changes in Figure 3d–f indicates that the synthesised composite material MnO₂/GAC-3 acquired significantly different properties. The MnO₂/GAC composite synthesis method proposed in this study represents a major development compared with other procedures, such as that of Ma et al. [41], because the MnO₂/GAC composites were prepared by adsorption from solution. As a result, MnO₂ homogeneously covered the surface of the activated carbon. According to the SEM images, the agglomerates practically blocked and rendered useless the internal porosity of activated carbon, thus decreasing the ability of the composite to adsorb organic compounds [4,20].

The size of the activated carbon particles modified with MnO₂ is a relevant property required for the operation of an FBR [54]. The Geldart classification is one of the most useful ways of classifying solids [1], and it is usually applied to an FBR in group B (with a size between 100 and 800 μ m) and group D (larger than 1 mm) particles [62]. Figure 4 shows the particle-size distribution assessed by laser diffraction spectrometry.

As shown in Figure 4, the average particle diameter was 1.3 mm, Geldart group D, with a mean standard deviation of 0.15. Fernández et al. [63] assessed particle-size effects on dissolved organic carbon (DOC) by comparing two size ranges of zeolitic supports (0.2–0.5 mm and 0.5–0.8 mm, respectively).

Figure 5 shows the adsorption–desorption isotherms as well as the hysteresis curve and pore-size distribution, which were calculated from the desorption data of the studied materials.

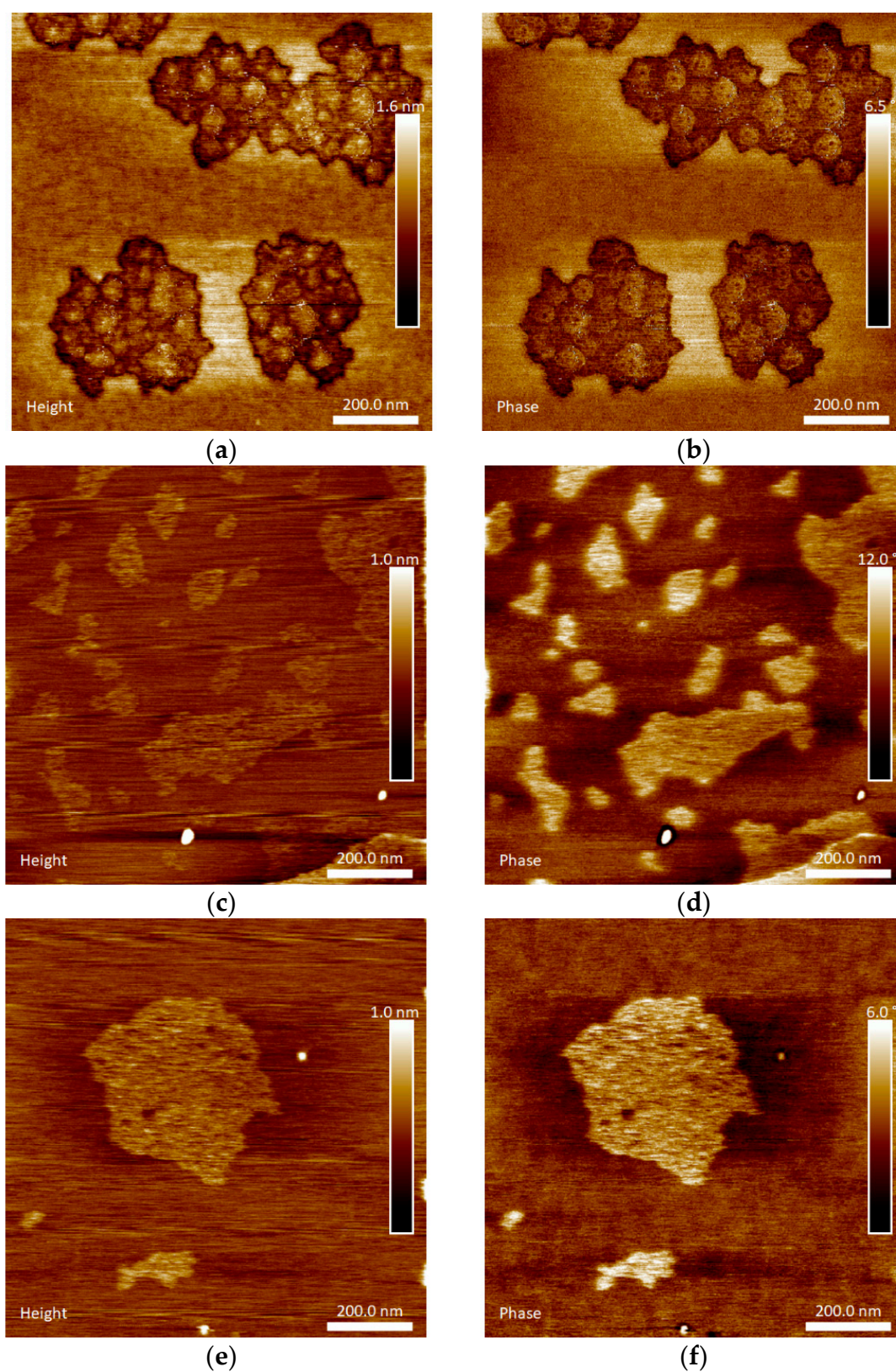


Figure 3. AFM topographic images of (a,b) α -MnO₂ nanoparticles; (c,d) commercial activated carbon Hydrodarco® 3000; (e,f) synthesised MnO₂/GAC-3 composite.

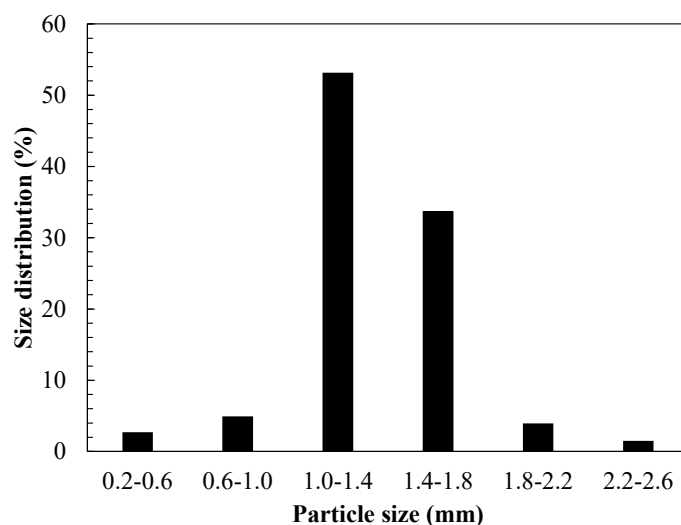


Figure 4. Particle-size distribution of the synthesised MnO₂/GAC-3 composite.

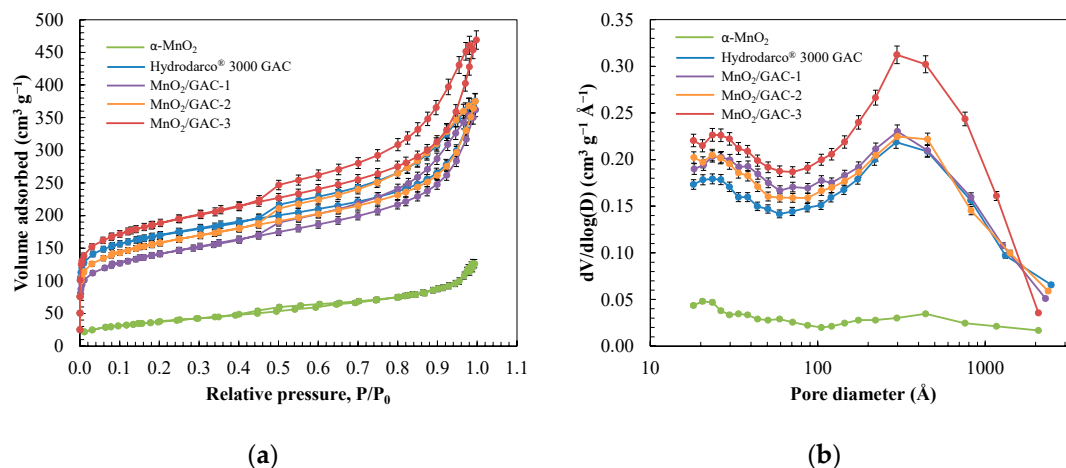


Figure 5. N₂ adsorption isotherm (a) and pore-size distribution (b) of synthesised α-MnO₂ nanoparticles, commercial activated carbon Hydrodarco® 3000, and three MnO₂/GAC composites synthesised in this study.

Figure 5a shows that the initial amount of adsorbed N₂ rapidly increased until it attained a relative pressure of $P/P_0 = 0.2$ before reaching GAC and MnO₂/GAC composite saturation. The isotherm of the composites, which was typical of microporous materials, was associated with a type IV isotherm in which adsorbed N₂ formed a monolayer, while the second branch formed multiple layers. All four cases showed an H3 hysteresis loop, which was associated with capillary condensation that occurs in the mesopores [64]. Conversely, α-MnO₂ nanoparticles showed a type II isotherm, which is commonly found in low-porosity or macroporous materials. The pore-size distribution of the composites and GAC ranged from 200 to 500 Å, while the α-MnO₂ nanoparticles ranged from 20 to 1000 Å. This wider range may have resulted from the temperature applied during the hydrothermal synthesis process, which was high enough to enable some degree of sintering and thus obtain a practically homogeneous distribution for a wide range of sizes [65].

Table 2 outlines the physical properties of the new composites, α-MnO₂ nanoparticles, and GAC Hydrodarco® 3000. The results of Table 2 showed an increase (9.47%) in the Brunauer, Emmett, and Teller (BET) specific surface area of the MnO₂/GAC-3 composite, which was 664.1 m² g⁻¹, in comparison to the value of 601.2 m² g⁻¹ for GAC Hydrodarco® 3000. The external surface area increased from the initial 276.4 m² g⁻¹ for GAC Hydrodarco® 3000 to 345.49 m² g⁻¹ for the MnO₂/GAC-3 composite. This in-

crease was in agreement with topographic AFM images showing that the roughness of the MnO₂/GAC-3 composite significantly increased, and thus matching the HRTEM and SEM images in which the MnO₂/GAC-3 composite displayed a good distribution of MnO₂ nanoparticles. In addition, the activation of the MnO₂/GAC-3 composite by mild calcination opened the pores, increasing the mean pore diameter (88.03 Å), as described by Ghasemi et al. [66] and Ferreiro et al. [6]. In turn, a major drawback was observed in the composites MnO₂/GAC-1 and MnO₂/GAC-2, because MnO₂ nanoparticles formed agglomerates and blocked the internal porosity of GAC.

Table 2. Results from N₂ physisorption of the synthesised α -MnO₂ nanoparticles, commercial active carbon Hydrodarco[®] 3000, and three MnO₂/GAC composites prepared in this study.

Sample	S _{BET} , m ² g ⁻¹	S _{ext} , m ² g ⁻¹	V _T , cm ³ g ⁻¹	V _μ , cm ³ g ⁻¹	V _M , cm ³ g ⁻¹	V _M /V _T ·100 %	V _μ /V _T ·100 %	D _P , Å
α -MnO ₂	23.5	10.5	0.07	0.05	0.02	28.6	71.4	127.7
Hydrodarco [®] 3000 GAC	601.2	276.4	0.51	0.14	0.35	68.6	27.5	83.98
MnO ₂ /GAC-1	496.1	294.1	0.49	0.09	0.38	77.6	18.0	81.28
MnO ₂ /GAC-2	556.3	305.8	0.51	0.1	0.38	74.5	19.6	80.50
MnO ₂ /GAC-3	664.1	345.49	0.62	0.13	0.48	77.4	21.0	88.03

The results of the MnO₂/GAC-3 composite represent an improvement over previously published preparation methods. For example, Liu et al. [67] synthesised MnO₂/GAC composites by electrodeposition to be used as an electrode with a smaller surface (625 m² g⁻¹) compared with the original activated carbon (724 m² g⁻¹). Choi et al. [68] synthesised composites with various MnO₂ proportions using a simple hydrothermal preparation technique, which led to a drastic decrease in specific surface area from the 1844 m² g⁻¹ of the original activated carbon to 1017 m² g⁻¹ of the MnO₂/GAC composite, with a 12.37% MnO₂ content. Yang et al. [69] managed to keep the physical properties of activated carbon unchanged. In both cases, the authors highlighted that MnO₂ deposition on GAC partly blocked the carbon pores, thereby decreasing the specific surface area, and consequently causing the loss of adsorptive properties of the activated carbon.

The crystallography of photocatalysts plays a key role in the optical, physical, and chemical properties of these materials. Reddy et al. [23] made considerable efforts to control the size of the synthesized nanoparticles, as well as the size of the crystalline phase, both related to minimising the recombination of electron-hole pairs, the energy band gap, and the surface area. Preparing a phase without impurities, such as α -MnO₂, may help to improve the interaction between the photocatalyst and the light source.

Figure 6 shows the XDR spectra of the MnO₂/GAC-3 composite and MnO₂ nanoparticles prepared by hydrothermal synthesis. Figure 6a shows the typical diffraction peaks at the positions 2 θ = 21.2, 25.5, 36.6, 43.7, 50.3, 60.2, and 68.4°, corresponding to an amorphous carbon structure (JCPDS file No. 75-1621) and a tetragonal structure of α -MnO₂ (JCPDS file No. 44-0141). Figure 6b shows diffraction peaks at the positions 2 θ = 12.8, 18.1, 25.5, 28.6, 36.6, 37.6, 38.9, 42.1, 50.3, 56.2, 60.2, 65.4, 69.5, and 73° corresponding to a tetragonal structure of α -MnO₂ (hollandite). According to Thackeray [70], this crystalline structure was made of double MnO₆ octahedra in which the α -MnO₂ structure tied at the edges to form 1 × 1 and 2 × 2 tunnels of 1.89 and 4.6 Å, respectively.

The spectra in Figure 6 show that introducing MnO₂ in the activated carbon structure had no effect on the catalyst structure with respect to the formation of α -MnO₂. However, the intensity of the characteristic peaks of α -MnO₂ was attenuated, which may be due to changes in crystallinity resulting from GAC incorporation.

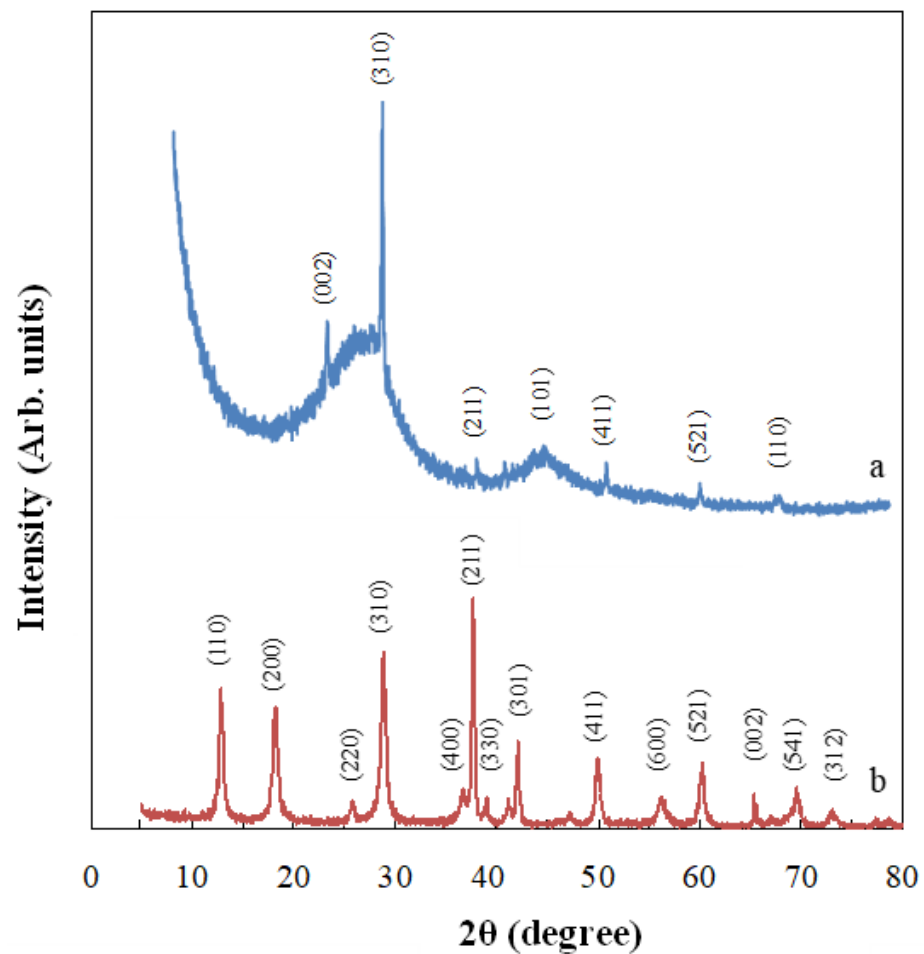


Figure 6. XRD spectra of the MnO₂/GAC-3 composite (a) and synthesised MnO₂ powder (b).

The average size of the crystals, D (nm), was determined from crystallographic data using the Debye–Scherer equation [71]:

$$D = \frac{k \times \lambda}{\beta \times \cos \theta'} \quad (5)$$

where in k is the Scherer constant (0.94), λ is the length of the X-ray source (for Cu K α , $\lambda = 0.15418$ nm), β is the angular width based on the full width at half maximum (FWHM) of the peak, and θ is the diffraction angle. According to Shen et al. [72], the crystal size may introduce some error in the determination of β owing to stress effects of the crystal and the instrument used to record the spectra. For this reason, the FWHM was corrected by widening the instrumental line, b , thus recalculating the β value using Equation (6):

$$\beta = \sqrt{FWHM^2 - b^2} \quad (6)$$

Equations (5) and (6) were used to estimate the theoretical average crystal size of α -MnO₂ nanoparticles (2.68 nm) and the MnO₂/GAC-3 composite (12.79 nm). The average sizes of the MnO₂/GAC-1 and MnO₂/GAC-2 composites were 18.06 and 14.30 nm, respectively, owing to the formation of agglomerates, as previously mentioned [71].

Another relevant aspect of the new composite was the range of light necessary for its photoactivation. Figure 7a shows the absorption spectra of α -MnO₂ nanoparticles and the three MnO₂/GAC composites prepared in this study. α -MnO₂ showed an intense absorption band in the UV region below 500 nm. This band may be due to charge transfer between the 2p orbital of oxygen and the 4d orbital of manganese [50].

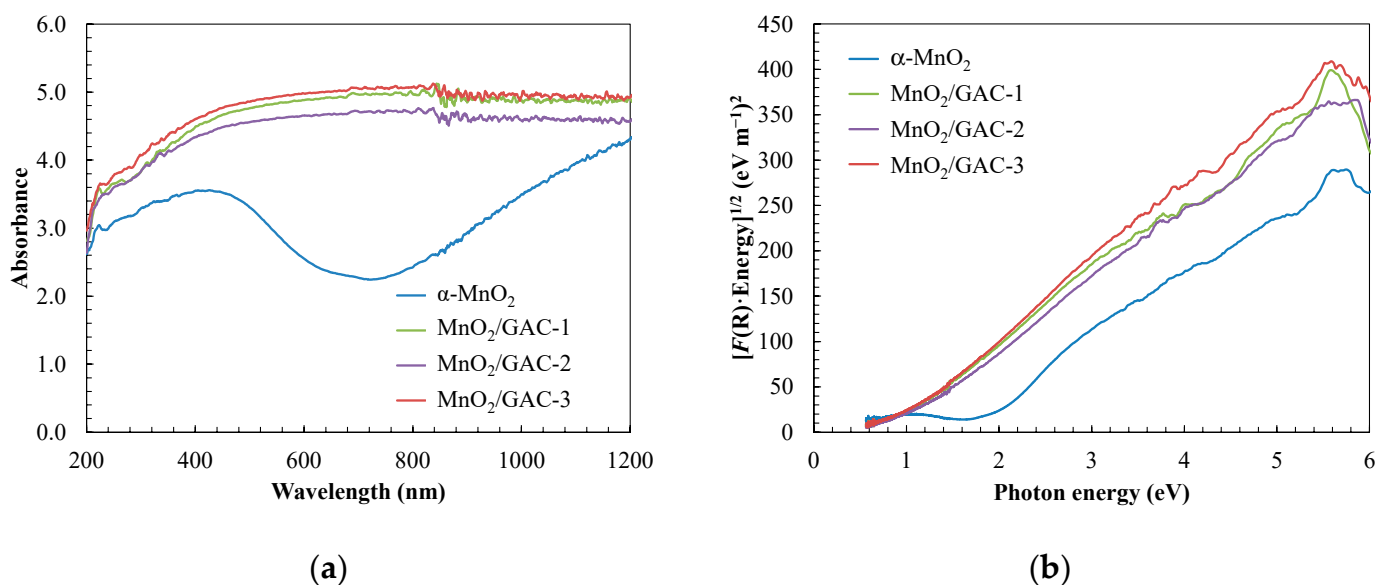


Figure 7. UV-Vis absorption spectra (a) and determination of the band gap values of the new catalysts (b).

The band gap was determined using the Tauc plot (Figure 7b) and the transformed Kubelka–Munk function [71,73]:

$$\alpha \times h \times \nu = A \times (h \times \nu - \text{Bandgap})^n \quad (7)$$

$$[F(R) \times h \times \nu]^n = A \times (h \times \nu - \text{Bandgap}) \quad (8)$$

$$F(R) = \frac{(1 - R)^2}{2 \times R}, \quad (9)$$

where ν is the vibration frequency (Hz), A is the absorbance (AU), h is the Planck constant (4.135×10^{-15} eV s), R is the diffuse reflectance (%), and n has a constant value of 0.5 for direct transitions. According to Figure 7b, the band gap of each photocatalyst was determined by representing Equation (8) as a function of the band gap and extrapolating to the abscissa axis in its linear region.

As shown in Figure 7b, the band gap decreased from 1.81 ± 0.03 eV in α -MnO₂ nanoparticles to 0.90 ± 0.03 eV in the MnO₂/GAC-1 composite, while the band gaps of MnO₂/GAC-2 and MnO₂/GAC-3 composites were 0.92 ± 0.03 and 0.95 ± 0.03 eV, respectively. Therefore, the composite material resulted in the nanoparticle absorption changing to longer wavelengths. Reducing the band gap made it possible to activate the new composites under visible light. Improving the absorbance of visible light of the new composites could improve photocatalytic activity, as more electron-hole pairs can be generated. Moreover, the addition of a carbonaceous material could inhibit the recombination of the photogenerated electron-hole pairs, as was previously reported in other oxides such as TiO₂ and Zn or Al oxides with carbonaceous structures [50,71,73].

The chemical elements and the oxidation state of the GAC Hydrodarco[®] 3000 and the MnO₂/GAC-3 composite were determined by X-Ray photoelectron spectroscopy (XPS). Figure 8 shows the resulting spectrum, confirming the presence of Mn, O, and C.

Figure 8c shows that the intensity of the peak corresponding to O 1s_{1/2} (530.3 eV) increased in the composite of GAC Hydrodarco[®] 3000 with MnO₂. This increase may be due to a possible change in the surface of the MnO₂/GAC-3 composite in relation to the original GAC, resulting from the formation of a new functional group associated with some type of Mn–O–Mn bond [74]. Another relevant result in Figure 8b shows Mn 2p_{1/2} and Mn 2p_{3/2} peaks with 654.0 eV and 642.2 eV bond energies, respectively. Choi et al. [68] associated the Mn 2p_{3/2} peak with the oxidation state of Mn (IV) through the binding energy at which the peak was detected. According to Xiong et al. [75], preparing a strongly

oxidising active phase of manganese in its oxidation state (IV) was crucial, because under this oxidation state, manganese deposited on GAC plays a key role in promoting the generation of hydroxyl radicals and therefore providing photocatalytic processes with a high performance of organic pollutant removal.

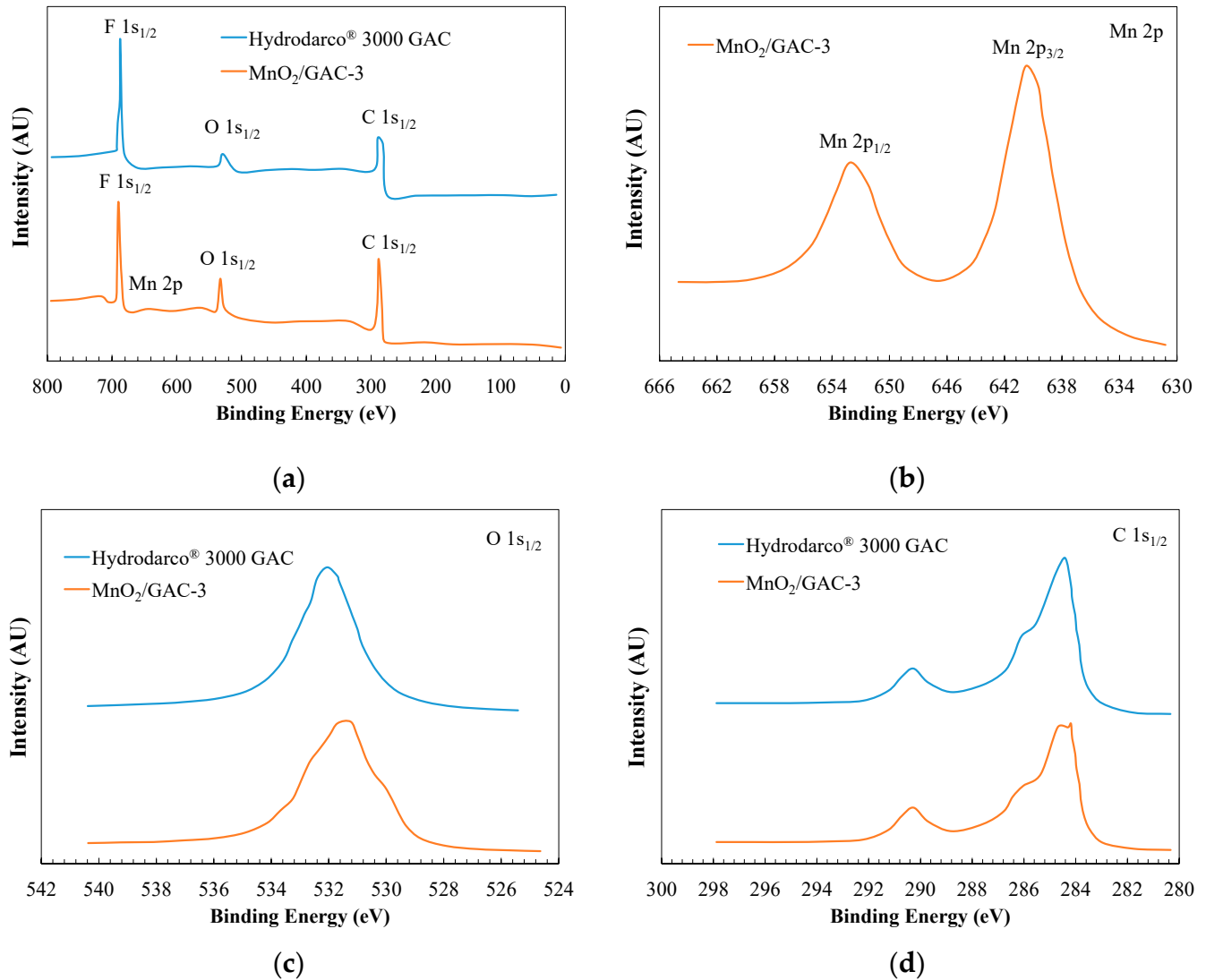


Figure 8. XPS spectra of the GAC Hydrodarco® 3000 and the MnO₂/GAC-3 composite (a) XPS; and enlarged spectra of the peaks: (b) Mn 2p; (c) O 1s_{1/2}; (d) C 1s_{1/2}.

Regarding the detection of C 1s_{1/2}, Figure 8d shows three types of bonds. At a 284.5 eV binding energy, the peak is associated with a C–C bond. The peak at 286.1 eV likely corresponds to a C–O bond, while the peak at 290.4 eV indicates a C=O bond. Therefore, no notable changes were observed between the original GAC and the MnO₂/GAC-3 composite.

Figure 9 shows the FTIR spectrum of the synthesised α -MnO₂ nanoparticles, the GAC Hydrodarco® 3000, and the MnO₂/GAC-3 composite.

The absorption band that was highlighted in Figure 9 in the 3100–3700 cm⁻¹ range was associated with a bending vibration of the O–H bond, which would correspond to the water used to prepare the potassium bromide pellet [6]. The 1500–1700 cm⁻¹ bands would be associated with stress vibrations of groups with double bonds such as C=O or their conjugated C–O bonds, as observed in the XPS spectra [76,77]. The band observed at 1118 cm⁻¹ could correspond to a stretching vibration of the C–O bond. Finally, MnO₂ was identified from the absorption band at 546 cm⁻¹, which would correspond to a stretching

vibration of the Mn–O bond. The comparison of the spectra of the GAC Hydrodarco® 3000 and the MnO₂/GAC-3 composite showed that during the process of MnO₂ deposition, the GAC surface changed significantly, as was found by other researchers such as Ma et al. [74]. These changes were shown by the disappearance of the bands at 1543 and 1662 cm⁻¹, which were replaced by a single peak red-shifted to 1551 cm⁻¹.

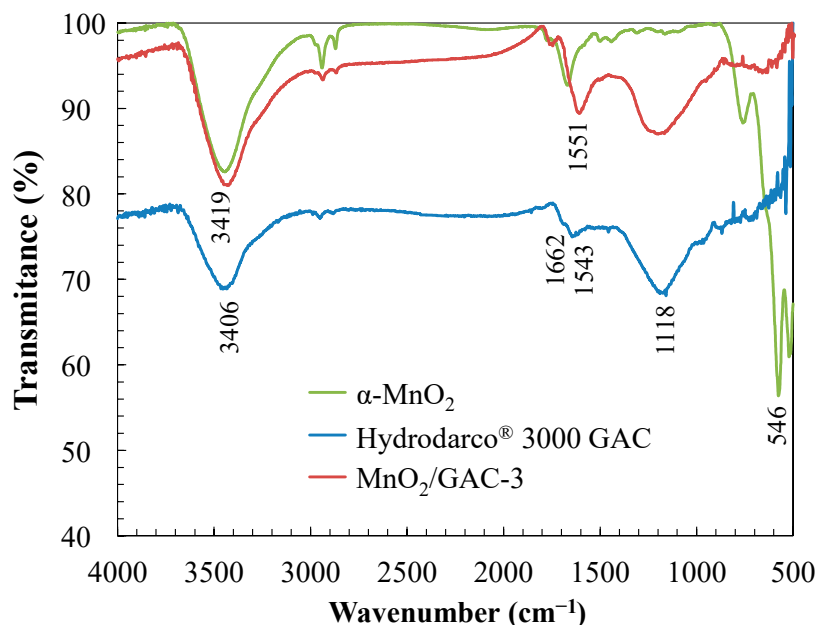


Figure 9. FTIR spectrum of the region between 4000 and 500 cm⁻¹ of α -MnO₂ nanoparticles, GAC Hydrodarco® 3000, and MnO₂/GAC-3 composite.

To better understand the chemical properties of the new MnO₂/GAC composite and their implications for the photocatalytic process, the point of zero charge (PZC), the degree of dispersion of the active phase MnO₂ on GAC, and the MnO₂ content were measured in the three MnO₂/GAC composites synthesised in this study. Metal dispersion (*Disp*) was calculated based on the coating of the H₂ chemisorption monolayer in MnO₂/GAC according to Equation (10):

$$Disp = \left(\frac{V_{\text{mon}}}{22414} \right) \times S \times M \times \frac{100}{\text{Metal content}}, \quad (10)$$

where V_{mon} is the volume of the H₂ monolayer in MnO₂/GAC in cm³ g⁻¹, S is the stoichiometric factor of H₂ to the Mn atom ($S = 2$) [78], M is the atomic weight of Mn in g mol⁻¹ ($M = 54.938$ g mol⁻¹), and *Metal content* (%) is the weight percentage of the deposited metal determined by XRF analysis. As shown in Figure S3, the amount of H₂ chemisorbed on the catalyst surface was calculated as the difference between the first and the second isotherms.

Table 3 outlines the chemical properties of each sample. The results indicate that the MnO₂/GAC-3 composite had the highest MnO₂ content (3.78%). Although this active phase content was modest when compared to the amount of MnO₂ deposited by Choi et al. [68] (MnO₂ content of 12.37%) or by Liu et al. [67] (MnO₂ content of 6.7%), the hydrothermal preparation method presented in this study was different, because the external surface of GAC was kept without obstructing its pores and channels and without compromising the amount of MnO₂ deposited on GAC. These findings were confirmed by metal dispersion, because dispersion increased with the MnO₂ content, with a 21.0% Mn dispersion in the MnO₂/GAC-3 composite. In turn, in the composites with low Mn content, dispersion decreased as the surface area decreased. In the MnO₂/GAC-1 and

MnO₂/GAC-2 composites, the decrease in Mn dispersion may have resulted from the formation of particle aggregates, which blocked carbon porosity [72].

Table 3. Analysis and chemical properties of the synthesised α -MnO₂ nanoparticles, commercial activated carbon Hydrodarco[®] 3000, and the three MnO₂/GAC composites prepared in this study.

Properties	Sample				
	α -MnO ₂	Hydrodarco [®] 3000 GAC	MnO ₂ /GAC-1	MnO ₂ /GAC-2	MnO ₂ /GAC-3
pH _{PZC}	2.60	7.25	7.10	6.85	6.61
Disp, %	—	—	15.5	17.3	21.0
MnO ₂ , %	N/A	N/A	1.34	2.07	3.78
Al ₂ O ₃ , %	—	0.66	0.41	0.57	0.77
Fe ₂ O ₃ , %	—	0.26	0.15	0.36	0.34
SiO ₂ , %	—	6.96	7.27	7.72	6.02
MgO, %	—	0.15	0.23	0.06	0.23
CaO, %	—	0.11	0.15	0.11	0.09
Na ₂ O, %	—	0.01	0.01	0.01	0.01
K ₂ O, %	—	0.21	0.18	0.30	0.16
TiO ₂ , %	—	0.17	0.14	0.38	0.10
P ₂ O ₅ , %	—	0.01	0.01	0.01	0.01
S, %	—	0.21	0.34	0.22	0.12

The PZC of the new composites decreased slightly as the amount of deposited MnO₂ increased, with a pH_{PZC} of 6.61 for MnO₂/GAC-3. The surface change could influence the adsorption step in the photocatalytic removal of aniline and benzothiazole, because they have dissociation constant (pK_a) values of 4.61 and 0.85, respectively [21].

Consequently, the MnO₂/GAC-3 composite would have the best properties for an efficient use in an FBR-photoreactor.

3.2. Reaction in the FBR-Photoreactor

The application of an FBR in a photocatalysis process requires the careful determination of building and operating parameters. The lack of a clear and robust design method could result in an ineffective FBR implementation in water treatment processes on an industrial scale [63]. During its implementation, researchers often face common problems, such as insufficient fluidisation or pneumatic entrainment of the catalyst, reactor failures, and poor treatment due to a high dose of catalyst [53]. Consequently, not only the appropriate photocatalyst but also the correct design parameters are critical steps in correctly configuring the photoreactor. Therefore, the reactor geometry and surface velocity of the fluid are discussed below.

3.2.1. FBR Sizing

Reactor size affects photocatalyst mixing and mass transfer. With regard to geometry, cylindrical reactors provide better mixing than those with rectangular geometry, because dead zones prevent reaction bulk homogenisation. To stabilise feed flow and to minimise eddies, backmixed zones, or sudden bed expansion due to highly turbulent flow, the fluid should enter through a uniform cross-sectional area in flat-bottom reactors [79]. Furthermore, a 5° angle in the fluid inlet mouth would ensure the minimisation of the problem of sudden bed expansion [54].

The aspect ratio between the height and the diameter of the FBR directly affects the flow velocity of the fluid and therefore the mixture between the liquid phase and the solid [5]. According to Bello et al. [1], a suitable aspect ratio for an FBR should be between 5 and 25 for a laboratory-scale installation and between 2 and 5 for a water treatment plant. Consequently, the FBR was built with an aspect ratio of 6.22, according to the optimisation by Ochieng et al. [80].

Furthermore, other elements, such as the UV-A lamp, acted as baffle elements to modify the flow and to improve the fluidisation of the MnO₂/GAC-3 catalyst particles, which promoted a more uniform mixture throughout the reactor. In this regard, authors such as Nam et al. [81] used a drag tube and other elements within the FBR to improve phenolic removal efficiency.

3.2.2. Catalytic Material and Surface Velocity of Fluid in the FBR

When assessing the catalyst particle-size effect on mass transfer and on fluid dynamic properties, the specific area of the catalyst bed after fluidisation (a_S) should be considered, because a high a_S leads to more satisfactory results [82]. The term a_S of the FBR system, which was 2.88 m⁻¹, was determined from Equation (11):

$$a_S = \frac{6 \times (1 - \varepsilon)}{d \times F_S} \quad (11)$$

where ε is the bed porosity, d is the mean particle diameter (mm), and F_S is a shape factor ($F_S = 1$, for spherical particles). Together with the surface area, the density of catalyst particles strongly influences the surface velocity of the fluid. In this regard, dense particles, which consist of non-porous materials, will require a higher velocity than porous materials such as activated carbon [79,83]. Hence, there are advantages of using activated carbon as MnO₂ catalytic support over denser α -MnO₂ nanoparticles. Moreover, the surface velocity is proportional to the energy needs of the process. Consequently, that velocity should be slightly higher than the minimum fluidisation to minimise operational costs as much as possible [1]. The minimum fluidisation velocity (U_{mf}) was determined according to Equation (12):

$$U_{mf} = 16.5 \times \frac{d^2 \times (\rho_S - \rho) \times g}{\mu} \quad (12)$$

where ρ_S and ρ are the specific gravity of the MnO₂/GAC-3 catalyst and water (g m⁻³), respectively, μ is the viscosity of water (g m⁻¹ h), and g is the gravitational constant (m h⁻²). In this study, a velocity of 165.3 m h⁻¹, which is similar to the minimum fluidisation velocity, was used in the FBR system. Delebarre et al. [84] also worked with a fluid velocity near the minimum fluidisation velocity. Working at a U_f much higher than the U_{mf} would lead to a shorter reaction time, albeit not offset by the higher operational cost.

3.3. MnO₂/GAC Composite Testing in Photocatalysis for Aniline and Benzothiazole Removal from Wastewater

Activated carbon is the adsorbent most commonly used in the wastewater treatment industry for the effective retention of a broad spectrum of pollutants [85]. The removal performances of adsorption and photocatalysis processes with MnO₂/GAC-3 composites were compared using an industrial effluent containing ANI and BTH. Figure 10 shows the evolution of the primary degradation of both contaminants and the total organic carbon (TOC) mineralisation.

Figure 10 shows that photocatalyst irradiation significantly improved ANI and BTH removal compared with the adsorption process, both in terms of primary degradation, completed after 5 h of irradiation, and in terms of mineralisation, which reached 86%, showing that MnO₂/GAC-3 had photocatalytic activity. To determine the contribution of α -MnO₂ deposited on GAC, the photocatalytic process and the adsorption capacity of the GAC Hydrodarco[®] 3000, which was used as support to prepare the MnO₂/GAC-3 composite, were compared. The results presented in Figure S4 indicate that UV-A irradiation of the GAC had no effect on aniline and benzothiazole removal or on the mineralisation, regardless of the pH of the solution. These findings confirm that GAC without α -MnO₂ did not exhibit photocatalytic activity when using the light source.

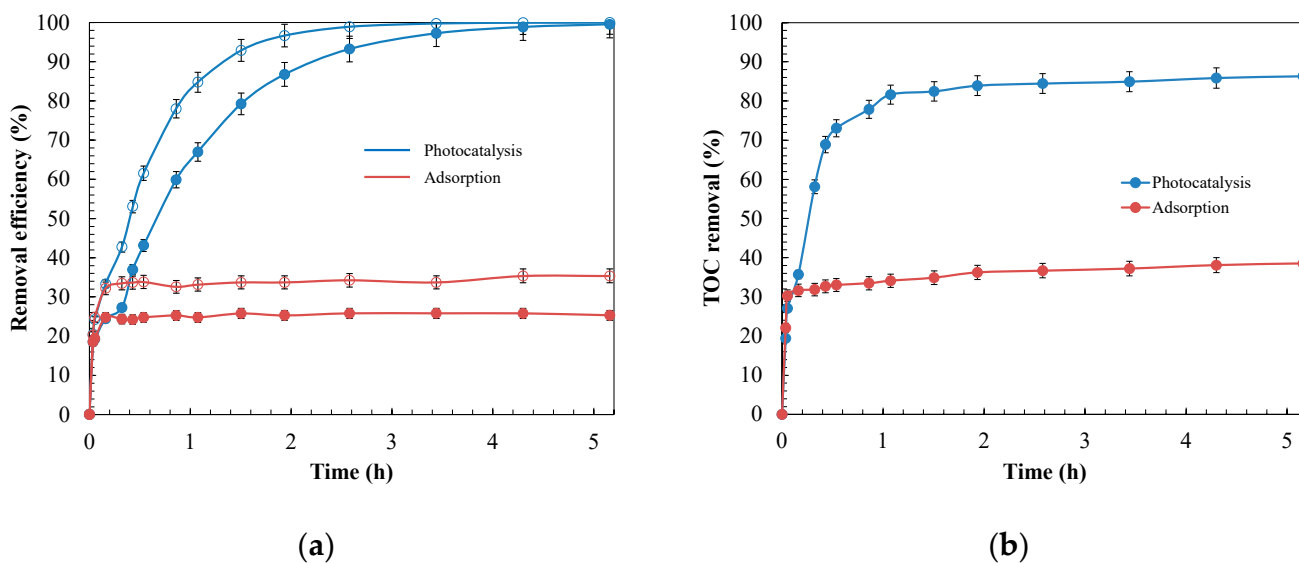


Figure 10. Removal efficiency of adsorption and photocatalysis processes for 12.0 mg L⁻¹ of ANI (○) and BTH (●) at pH = 9.0 with 0.9 g L⁻¹ composite MnO₂/GAC-3. Evolution: (a) primary degradation; (b) mineralisation.

The catalytic activity of the composites prepared in this study is compared in terms of primary degradation and mineralisation in Figure 11.

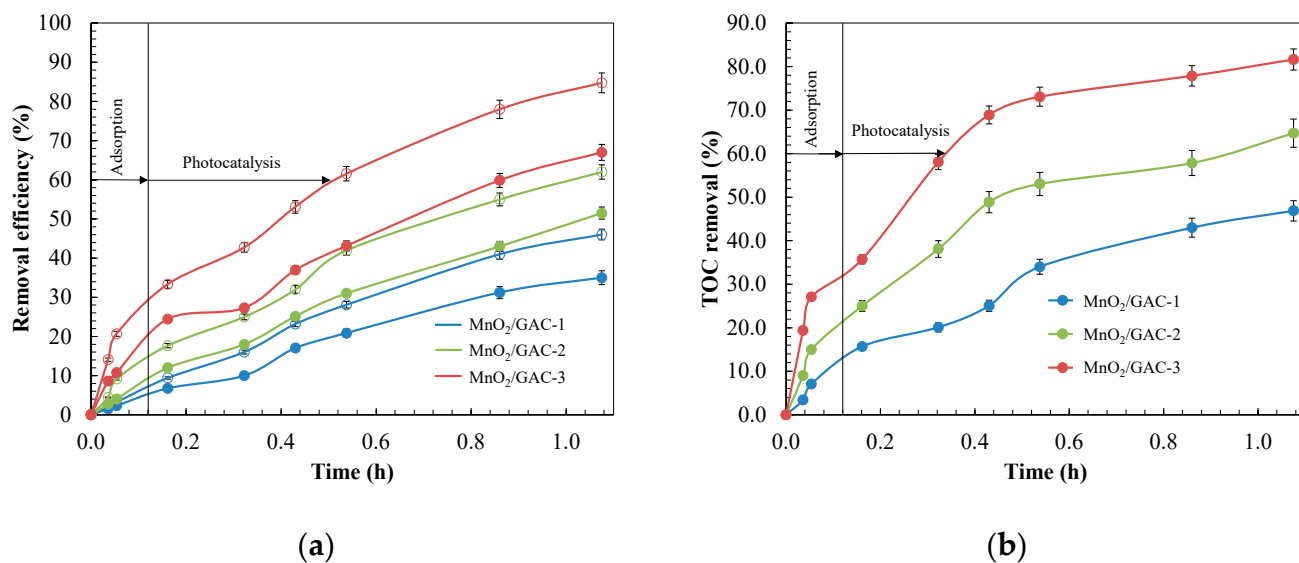


Figure 11. Comparison of the catalytic activity of MnO₂/GAC composites. Evolution of the: (a) primary degradation of ANI (○) and BTH (●); (b) mineralisation. Experimental conditions: C₀ = 12.0 mg L⁻¹; pH = 9.0; m_{CAT} = 0.9 g L⁻¹; Irradiation dose = 155.8 W m⁻².

As shown in Figure 11, the MnO₂/GAC-3 composite had the highest degree of mineralisation (81.6%) and degradation of both ANI (84.7%) and BTH (67.0%) after 1.08 h of reaction. The presence of a higher α -MnO₂ content (3.78%) in the MnO₂/GAC-3 composite and the increase in BET surface area led to better removal results [86]. Crystal size could also influence the electron-hole recombination [87], thus generally decreasing the photocatalytic activity as the crystal sizes increased. Therefore, the MnO₂/GAC-3 size of 12.79 nm was better than MnO₂/GAC-1 (18.06 nm) and MnO₂/GAC-2 (14.30 nm). The same trend was observed by Khlyustova et al. [86].

3.3.1. Kinetics of ANI and BTH Adsorption and Photodegradation with the MnO₂/GAC-3 Composite

To identify the controlling stage of the photocatalytic process, the degradation kinetics of ANI and BTH were modelled under both darkness (adsorption) and UV-A light (photocatalysis), fitting them to pseudo-first-order (Langmuir–Hinshelwood) [88] and pseudo-second-order (Lagergren) [89] kinetic models, using the following equations:

$$\frac{dq_t}{dt} = k_1 \times (q_e - q_t), \quad (13)$$

where q_e (mg g⁻¹) is the adsorption capacity at equilibrium, q_t (mg g⁻¹) is the amount of ANI or BTH adsorbed at a given time t , and k_1 (h⁻¹) is the pseudo-first-order kinetic constant; and

$$\frac{dq_t}{dt} = k_2 \times (q_e - q_t)^2 \quad (14)$$

where k_2 (g mg⁻¹ h⁻¹) is the pseudo-second-order constant. The kinetic parameters that fitted the data shown in Figure 10 are presented in Table 4. The correlation coefficients (R^2) of the pseudo-second-order model were higher than 0.90, but they were low for the pseudo-first-order model ($R^2 \approx 0.67$). Consequently, the pseudo-second-order model was the most appropriate to describe the evolution of both adsorption and photocatalysis. Assuming that the global photocatalysis process consists of a series combination of adsorption steps followed by the reaction, the kinetics of the slowest step will control the global process [21,30]. Therefore, the adsorption step controlled the global process, because its kinetic constant was lower than that of the photocatalytic reaction.

Table 4. Results from the kinetic modelling of the photocatalysis and adsorption process during ANI and BTH removal using the photocatalyst MnO₂/GAC-3. Experimental conditions: $C_0 = 12.0$ mg L⁻¹; pH = 9.0; $m_{CAT} = 0.9$ g L⁻¹; Irradiation dose = 155.8 W m⁻².

Kinetic Model	Parameters	Process			
		Adsorption		Photocatalysis	
		Aniline	Benzothiazole	Aniline	Benzothiazole
Pseudo-1st-order	q_e (mg g ⁻¹)	18.16	14.12	1.81	1.84
	k_1 (h ⁻¹)	0.479	0.509	1.208	0.914
	R^2	0.663	0.688	0.996	0.988
Pseudo-2nd-order	q_e (mg g ⁻¹)	45.25	30.03	2.14	1.90
	k_2 (g mg ⁻¹ h ⁻¹)	0.084	0.113	1.442	1.169
	R^2	0.995	0.988	0.950	0.844

Nevertheless, the process can be affected by other experimental variables, such as pH or catalyst dose [4], that will be studied in detail in the following sections.

3.3.2. Effects of pH and Catalyst Dose during the Photocatalysis Process for ANI and BTH Removal with the Composite MnO₂/GAC-3

The effects of the pH and catalyst dose on the photocatalytic activity of the process were compared by simplifying a Langmuir–Hinshelwood kinetic model to a pseudo-first-order kinetic model. This approach is widely used to describe photocatalytic processes with various organic pollutants [73,90,91]. The rate equation was:

$$r = \frac{dC}{dt} = k \times \frac{K \times C}{1 + K \times C + \sum_i K_i \times C_{int}} \approx k_{app} \times C, \quad (15)$$

where r is the oxidation rate of the pollutants to CO₂ (mg L⁻¹ h), C is the concentration of the reactants (mg L⁻¹), k_{app} is an apparent first-order kinetic constant (h⁻¹), t is the

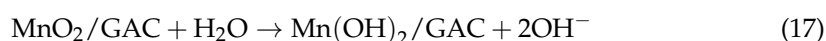
irradiation time (h), k is the kinetic constant of the reaction ($\text{mg L}^{-1} \text{h}$), K and K_i are the Langmuir adsorption constants for C and reaction intermediates (L mg^{-1}), and C_{int} is the concentration of the various intermediate products of ANI or BTH degradation (mg L^{-1}).

Another parameter which is frequently used to compare apparent first-order kinetics is the half-life time $t_{1/2}$ (h) (Equation (16)) [91]:

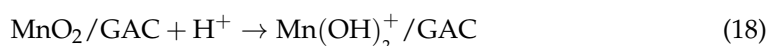
$$t_{\frac{1}{2}} = \frac{\ln 2}{k_{\text{app}}} \quad (16)$$

The pH can affect the overall photocatalytic process with the $\text{MnO}_2/\text{GAC-3}$ composite. For the highest photocatalytic activity, the most favourable pH will depend on the surface charge of the catalyst and on the oxidation potential of the reaction. Consequently, throughout the experiments, the pH was controlled to be kept constant. As a general rule, according to Equations (17)–(19), the surface of the $\text{MnO}_2/\text{GAC-3}$ catalyst would be positively charged when the pH of the dissolution was lower than the pH_{PZC} . Conversely, the surface would be negatively charged when the pH values were higher than the pH_{PZC} [92].

Under acid pH conditions ($\text{pH} < \text{pH}_{\text{PZC}}$):



Under neutral pH conditions ($\text{pH} \approx \text{pH}_{\text{PZC}}$):



Under alkaline pH conditions ($\text{pH} > \text{pH}_{\text{PZC}}$):



The experiments were performed at pH 3.0, 7.0 and 9.0 to assess the effect on ANI and BTH degradation (Figure 12). The values of the kinetic constants (k_{app}) and half-life time ($t_{1/2}$) are outlined in Table 5. The experiments were properly fitted to the apparent first-order kinetic model with a correlation coefficient R^2 higher than 0.98. For both mineralisation (81.6%) and degradation under UV-A light after 1 h of reaction, the most favourable conditions were found at a slightly basic pH ($\text{pH} = 9.0$) with half-life times of 0.39 h and 0.66 h for ANI and BTH, respectively. These conditions were favourable because the negatively charged $\text{MnO}_2/\text{GAC-3}$ catalyst in alkaline medium contributed to electrostatic interactions with ANI and BTH, which were positively charged. David and Vedhi [93] reported a similar response to an alkaline pH in the degradation of cationic dyes. In addition, they observed that the generation of radical species increased as a consequence of the reaction between the hydroxide ions and the photogenerated holes.

Table 5. Summary of the kinetic parameters and coefficients of determination (R^2) of the photocatalytic process using $\text{MnO}_2/\text{GAC-3}$ composites after reaction for 1 h.

Effect	$k_{\text{app, ANI}}$ (h^{-1})	$t_{1/2, \text{ANI}}$ (h)	R^2	$k_{\text{app, BTH}}$ (h^{-1})	$t_{1/2, \text{BTH}}$ (h)	R^2	Irradiation Dose (W m^{-2})
pH¹							
3.0	0.87	0.79	0.98	0.52	1.33	0.99	155.8
7.0	1.31	0.53	0.99	0.77	0.90	0.99	155.8
9.0	1.75	0.39	0.99	1.04	0.66	0.99	155.8
$\text{MnO}_2/\text{GAC-3}$ dosage² (g L^{-1})							
0.5	1.05	0.66	0.99	0.61	1.12	0.98	199.6
0.9	1.75	0.39	0.99	1.04	0.66	0.99	155.8
3.0	1.50	0.46	0.99	0.87	0.79	0.99	72.4

¹ Experiments performed with a catalyst mass of 0.9 g L^{-1} . ² Assessment of the catalyst loading effect at $\text{pH} = 9.0$.

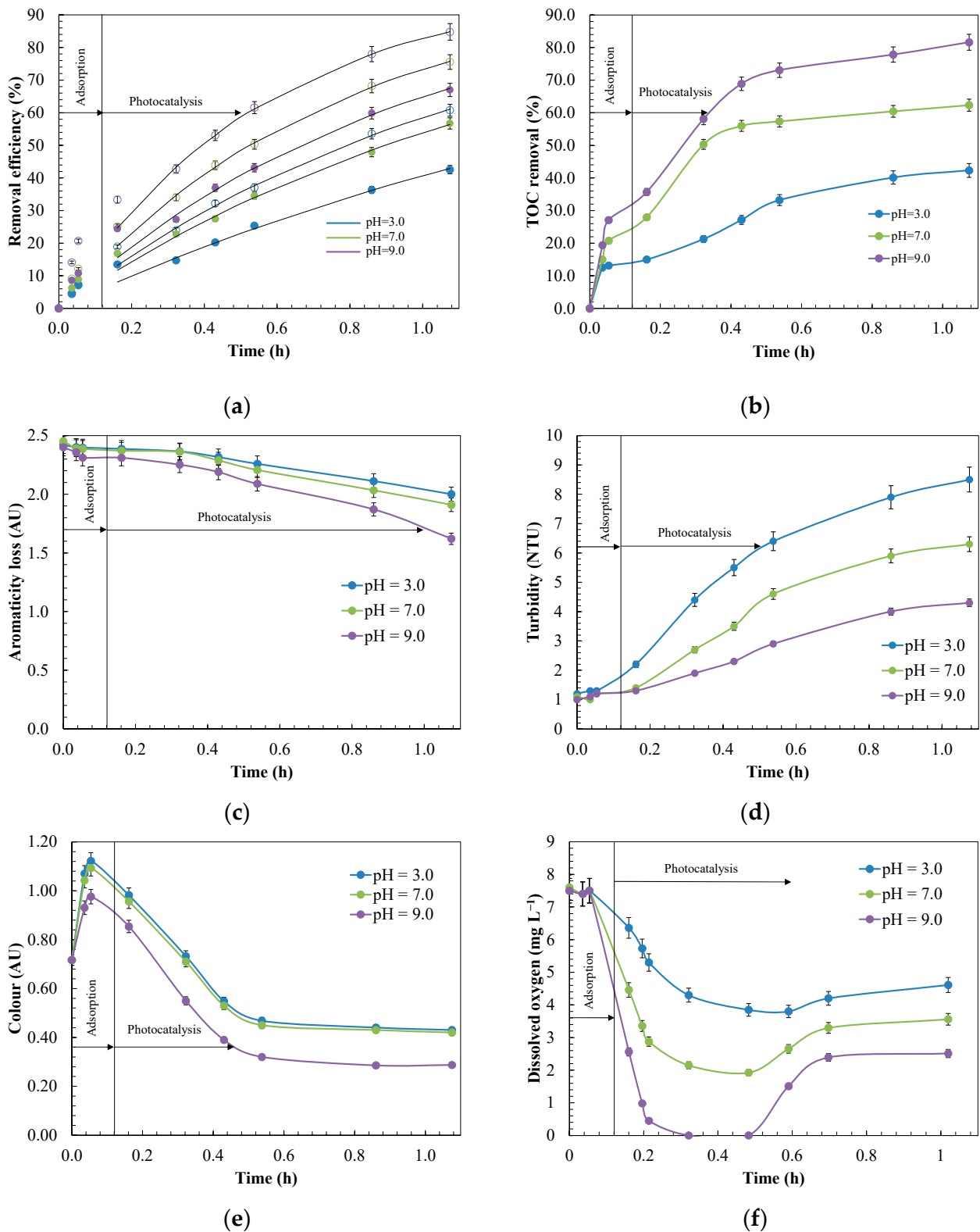


Figure 12. Study of the pH effect on the photocatalytic removal of ANI and BTH from industrial effluents with the MnO₂/GAC-3 photocatalyst. Evolution of the: (a) primary degradation of ANI (○) and BTH (●) fitted to the apparent first-order kinetic model; (b) total organic carbon (TOC) removal; (c) loss of aromaticity; (d) turbidity; (e) colour induction during aniline and benzothiazole oxidation; (f) dissolved oxygen. Experimental conditions: $C_0 = 12.0 \text{ mg L}^{-1}$; $m_{\text{CAT}} = 0.9 \text{ g L}^{-1}$; Irradiation dose = 155.8 W m^{-2} ; $T = 26 \text{ }^\circ\text{C}$.

In turn, at acid pH values (pH = 3.0), both the catalyst and ANI and BTH, which were positively charged, caused repulsion phenomena. Under these conditions, a more modest yield was assessed for both mineralisation (42.3%) and ANI (60.8%), as well as BTH (42.5%) removal. In addition, the half-life time of both ANI (0.79 h) and BTH (1.33 h) increased considerably, corresponding to $k_{app} = 0.87$ and 0.52 h^{-1} , respectively [50].

Other variables, such as the formation of condensation compounds, including polyaniline, compared to other more easily oxidisable degradation intermediates, could explain the worst results at alkaline pH conditions [20,21]. In addition, Zhou et al. [25] reported that during BTH oxidation, organic radicals could react with each other by C–C coupling to generate dimers. These dimers in turn would react with BTH radicals to form macromolecules, which were difficult to oxidise.

Parameters such as the loss of aromaticity (Figure 12c) or turbidity (Figure 12d) could explain the differences in behaviour. Thus, the loss of aromaticity, which was expressed as the decrease in absorbance at 254 nm, corresponded to a greater degradation, owing to the breakdown of the aromatic structure. According to Sanchez et al. [94] and De Wever and Verachtert [13], at pH = 9.0, absorbance decreased further, owing to the possible formation of hydroxylated ANI intermediates such as resorcinol, catechol, *p*-benzoquinone, and carboxylic acids, or 2-mercaptobenzothiazole and 2-hydroxibenzothiazole of BTH.

Similar to the aromaticity, the turbidity in this FBR-photoreactor indicated the presence of insoluble high-molecular-weight degradation products [30]. High turbidity levels further deteriorate the optical properties of the effluent and prevent light transmission to the photocatalyst. To ensure an adequate reaction rate and optimal UV light use, the turbidity should not exceed 5 NTU [36]. Figure 12d shows that the turbidity increased largely with the decrease in pH, and was appreciably higher at pH = 3.0, reaching a value of 8.5 NTU; this is in line with the most unfavourable conditions discussed above. Figure S5 compares the turbidity values with those obtained from a photocatalytic experiment performed with the GAC Hydrodarco® 3000 at different pH values. At acid pH, the turbidity was much higher, approximately 10.8 NTU, thus matching the turbidity reached by the MnO₂/GAC-3 composite, and this was most likely due to the formation of higher-molecular-weight condensation intermediates such as polyaniline, as reported by Bard and Yang [95], or macromolecules derived from BTH polymerisation [25]. In turn, at a pH of 9.0, the turbidity was 4.3 NTU and was thus lower than the threshold indicated by Bodzek and Rajca [36].

In addition, during the photocatalytic removal of ANI and BTH, the colour of the oxidised water also changed. Accordingly, these colour changes were observed by Jing et al. [19] during the oxidation of effluents containing ANI and by De Wever et al. [96] and Derco et al. [97] in effluents with BTH, with colours including pink, reddish orange, reddish brown, and light yellow. Coloured intermediates were also observed in this work during the removal of ANI and BTH, whose main intermediates could correspond to *p*-benzoquinone, phenol, nitrobenzene, 2-mercaptobenzothiazole and aminophenol. Thus, a higher colour intensity during the oxidation reaction represented lower pollutant mineralisation. Figure 12e shows that the colour intensity increased to extreme values at pH values of 3.0 and 7.0 (*Colour* = 1.12 AU), owing to the generation of a greater amount of oxidised chromophoric species. In turn, at pH = 9.0, both the maximum intensity (*Colour* = 0.97 AU) and the residual colour (*Colour* = 0.28 AU) were lower, owing to favourable oxidative conditions.

Dissolved oxygen was another factor that affects the photocatalytic process, given its key role during oxidation with MnO₂/GAC-3 photocatalysts in providing efficient electron scavenging to form O₂^{•−} and subsequently HO[•] radicals, thus improving the efficiency of the photocatalytic process [98,99].

As shown in Figure 12f, dissolved oxygen rapidly decreased throughout the pH range, which was in agreement with the ANI and BTH oxidation rates shown in Figure 12a. The absence of oxygen at pH = 9.0 for 10 min could explain the slowdown in the mineralisation and primary degradation. Velo-Gala et al. [100] reported that in the absence of dissolved oxygen, the process became inefficient, because only the positive holes of the photocatalyst

remained actively transforming water molecules into hydroxyl radicals, and the lack of an electron scavenger could not avoid the undesirable recombination phenomenon.

However, after 36 min of reaction, the oxygen concentration recovered slightly, albeit much more strongly at pH = 9.0, because the reaction system was fed from an open reservoir, which could explain this natural reoxygenation process [98].

In short, a pH of 9.0 provided the most satisfactory results in terms of oxidation, regeneration, and efficiency of the photocatalytic process, owing to its higher photocatalytic activity during the removal of ANI and BTH.

The dose of the catalyst used in the photocatalytic system was another key factor for guaranteeing a good performance of the system and avoiding wasting catalytic materials. The effect of the catalyst dose was assessed by varying the catalyst concentration in the 0.5–3.0 g L⁻¹ range. Figure 13 showed the catalyst loading effect on ANI and BTH removal, TOC conversion profiles, colour, turbidity, aromatic ring breakage, which was expressed as absorbance at 254 nm, and dissolved oxygen.

Generally, as the catalyst dose increased, so did the number of active sites available for adsorption and degradation processes on the catalyst surface [36]. This degradation rate increased until a maximum value, after which the rate gradually decreased, with the subsequent loss of photocatalytic activity. As shown in Figure 13a,b, the best ANI and BTH removal yield was reached with a dose of 0.9 g L⁻¹ and a constant of k_{app} of 1.75 h⁻¹ and 1.04 h⁻¹, respectively, with 81.6% mineralisation after 1 h of reaction was achieved. Increasing the dose favoured the generation of e⁻ and h⁺, which produced a greater amount of hydroxyl radicals, thus improving the performance of the photocatalytic process with the MnO₂/GAC-3 catalyst [21,101]. However, upon reaching a dose of 0.9 g L⁻¹, the catalytic activity worsened, with a k_{app} of 1.50 h⁻¹ for ANI and 0.87 h⁻¹ for BTH for a catalyst loading of 3.0 g L⁻¹. The decrease in degradation rate might be due to reactions of free radical species with each other when generated in excess, instead of degrading ANI and BTH [21,102]. Furthermore, excessive catalyst loading could help to form agglomerates and to increase the turbidity, reducing the photocatalytic activity. As a result, the light could be scattered, thereby decreasing the radiation dose received by the photocatalyst from 155.8 W m⁻² to 72.4 W m⁻² with doses of 0.9 and 3.0 g L⁻¹, respectively [36].

The removal yields were higher than those reported in previous studies [21] using other catalysts such as TiO₂ in suspension in a hybrid reactor for the removal of ANI and BTH from industrial effluents. In that study, a 22-h irradiation time was required for the primary degradation of both potential contaminants. Furthermore, mineralisation only reached 50%, which may be because it was more difficult to remove the reaction intermediates than those initially present. In the present study, higher removal and mineralisation yields were achieved with shorter irradiation times than in other cases [21]. The MnO₂/GAC-3 catalyst led to characteristics and interactions between ANI, BTH and the surface, which affected to a great extent the degradation rate, which was mostly determined by the increased generation of radical species [103].

Other parameters, such as colour, turbidity, or loss of aromaticity, which were determined by the absorbance at 254 nm (see Figure 13c–e), decreased with a dose of 0.9 g L⁻¹. In addition, the lowest absorbance value at 254 nm demonstrated a high level of aromatic ring breakage, which indicated a good oxidative action under these operational conditions.

To more practically evaluate the feasibility of the favourable operating conditions studied for the FBR-photoreactor system and its biodegradability, the average oxidation state (AOS) was estimated. This parameter is capable of indicating the degree of oxidation of complex solutions, and it is especially useful for oxidation stages at which the initial organic pollutant is a minor component compared to its degradation intermediates. In turn, the AOS indirectly provides information on biodegradability without requiring that the biological oxygen demand (BOD) be determined [104,105]. The AOS was calculated using Equation (20):

$$\text{AOS} = \frac{4 \times (\text{TOC} - \text{COD})}{\text{TOC}}, \quad (20)$$

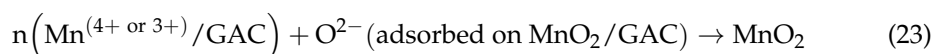
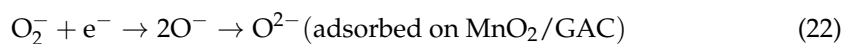
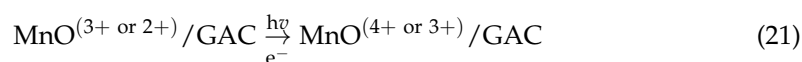
where TOC was the total organic carbon (mol C L^{-1}), and COD was the chemical oxygen demand ($\text{mol O}_2 \text{ L}^{-1}$). The parameter AOS can range from -4 at the most reduced state of C to $+4$ at the most oxidised state of C. AOS values from 0 to $+1$ would represent suitable conditions for biological organic removal [104]. Figure 14 shows the evolution of AOS over time under the best operating conditions.

As shown in Figure 14, AOS increased throughout the photocatalytic process, reaching a plateau after 1 h, with 84.7% and 67.4% primary degradation for ANI and BTH, respectively, and 81.6% mineralisation. The results indicate that a larger number of ANI and BT degradation intermediates were formed during the first 30 min of reaction, and from that time on, no relevant changes occurred in the chemical nature of the degradation intermediates, as the AOS value remained almost constant at 0.63 [106]. Consequently, the intermediates that remained in solution did not alter substantially the biodegradability of the treated effluent.

3.4. Stability of $\text{MnO}_2/\text{GAC-3}$ after Photocatalysis and Treatment Cost Estimation

The ability of a photocatalyst to continuously maintain its catalytic activity for ANI and BTH removal over successive cycles is crucial for its practical application. Consequently, the $\text{MnO}_2/\text{GAC-3}$ photocatalyst was subjected to six cycles of use. As shown in Figure 15, the photocatalyst showed a similar catalytic activity after six consecutive 1-h reaction cycles, maintaining an 84.7% ANI primary degradation and 67.0% BTH primary degradation, with an 81.6% mineralisation.

No changes in catalytic activity were observed. Nevertheless, Lekshemi et al. [107] observed that this could be due to a regeneration process of the $\text{MnO}_2/\text{GAC-3}$ photocatalyst taking place during the reaction, according to the following mechanism:



However, once the catalytic properties of the photocatalyst have been spent, it must be disposed of as a solid waste. Additionally, the amount of catalyst used is small, so the volume of waste generated would be low.

In addition, FTIR spectra of the photocatalyst were recorded before and after six reaction cycles. Infrared spectrum analysis (Figure 16) showed no new vibration bands.

However, the band at 3416 cm^{-1} associated with a bending vibration of the O–H bond qualitatively increased, owing to a higher water adsorption during the KBr pellet preparation process. The bands at 2915 , 2851 , and 546 cm^{-1} showed no difference from the fresh photocatalyst.

Nevertheless, the considerable increase in the absorption band corresponding to the peak at 1551 cm^{-1} could be related to the bending mode of the adsorbed water molecules when in contact with ANI [108]. Finally, the peak corresponding to the band at 1118 cm^{-1} also increased, most likely due to the adsorption and accumulation of compounds primarily formed by low-molecular-weight organic acids derived from ANI and BTH degradation [76].

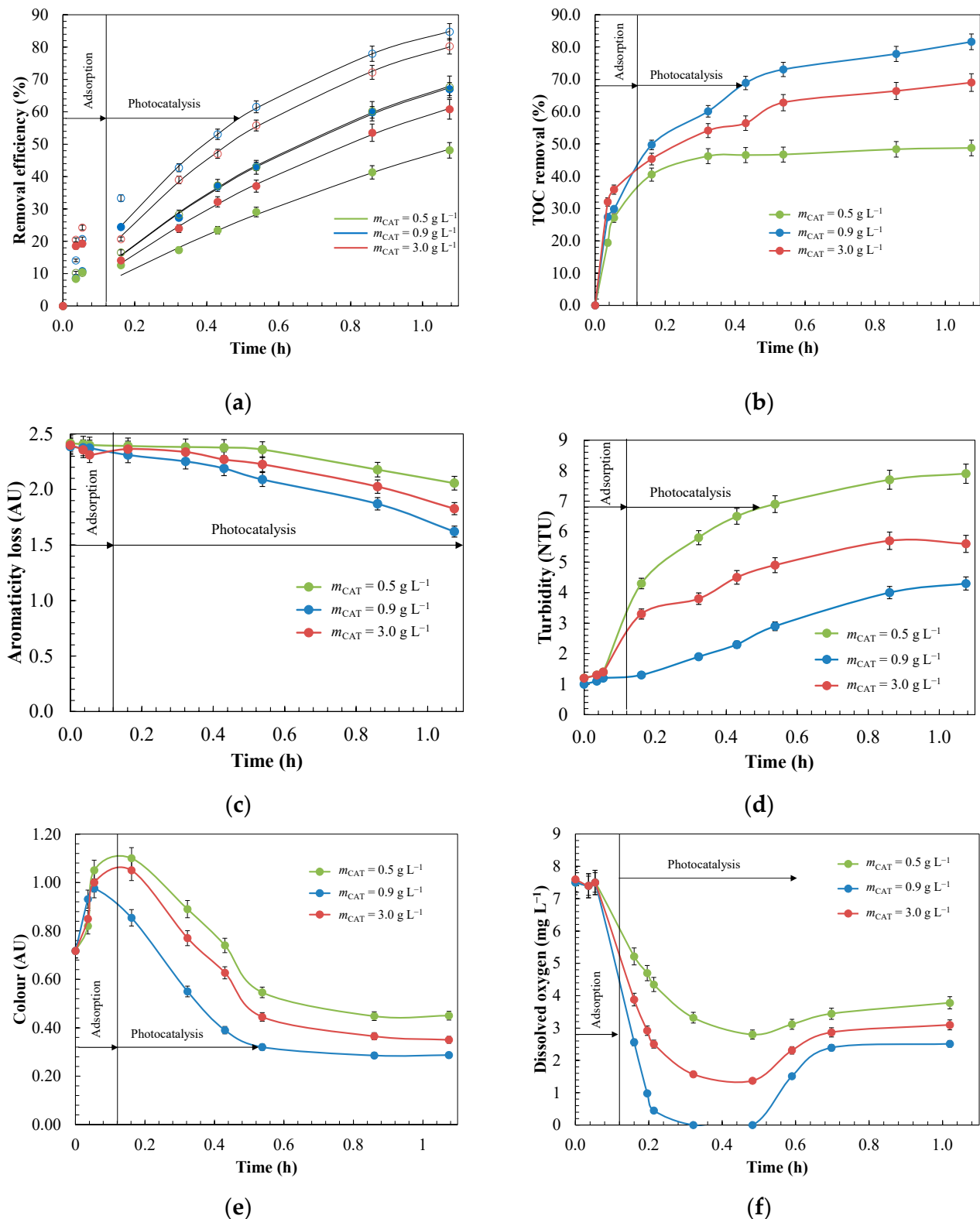


Figure 13. Plots showing the variation in the effect of the $\text{MnO}_2/\text{GAC-3}$ catalyst dose during the photocatalytic removal of ANI and BTH from industrial effluents. Evolution of the: (a) primary degradation of ANI (○) and BTH (●) fitted to the apparent first-order kinetic model; (b) total organic carbon (TOC) removal; (c) aromaticity loss; (d) turbidity; (e) colour induction during aniline and benzothiazole oxidation; (f) dissolved oxygen. Experimental conditions: $C_0 = 12.0 \text{ mg L}^{-1}$; $\text{pH} = 9.0$; $T = 26 \text{ }^\circ\text{C}$.

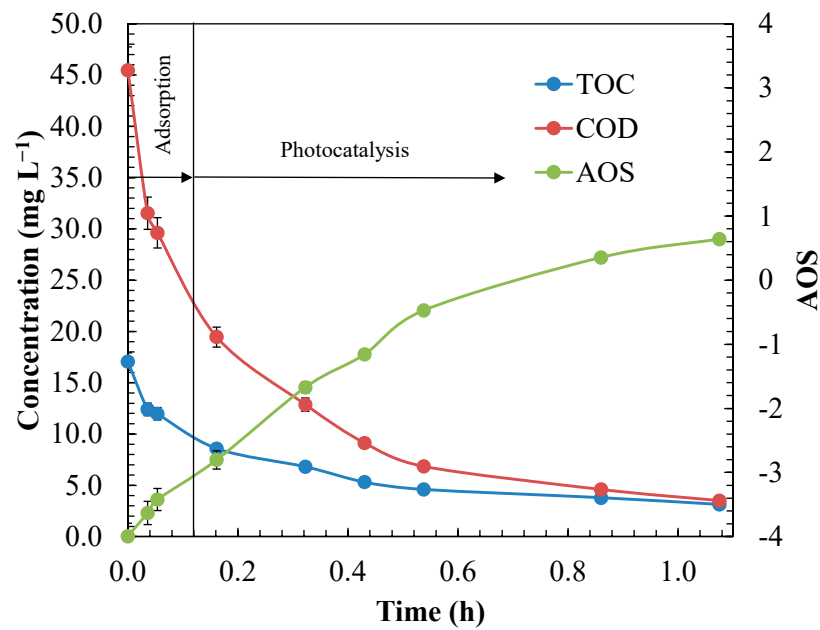


Figure 14. Evolution of the average oxidation state (AOS) and chemical oxygen demand (COD) during photocatalysis of ANI and BTH. Experimental conditions: $C_0 = 12.0 \text{ mg L}^{-1}$; $\text{pH} = 9.0$; $m_{\text{CAT}} = 0.9 \text{ g L}^{-1}$; *Irradiation dose* = 155.8 W m^{-2} ; $T = 26 \text{ }^\circ\text{C}$.

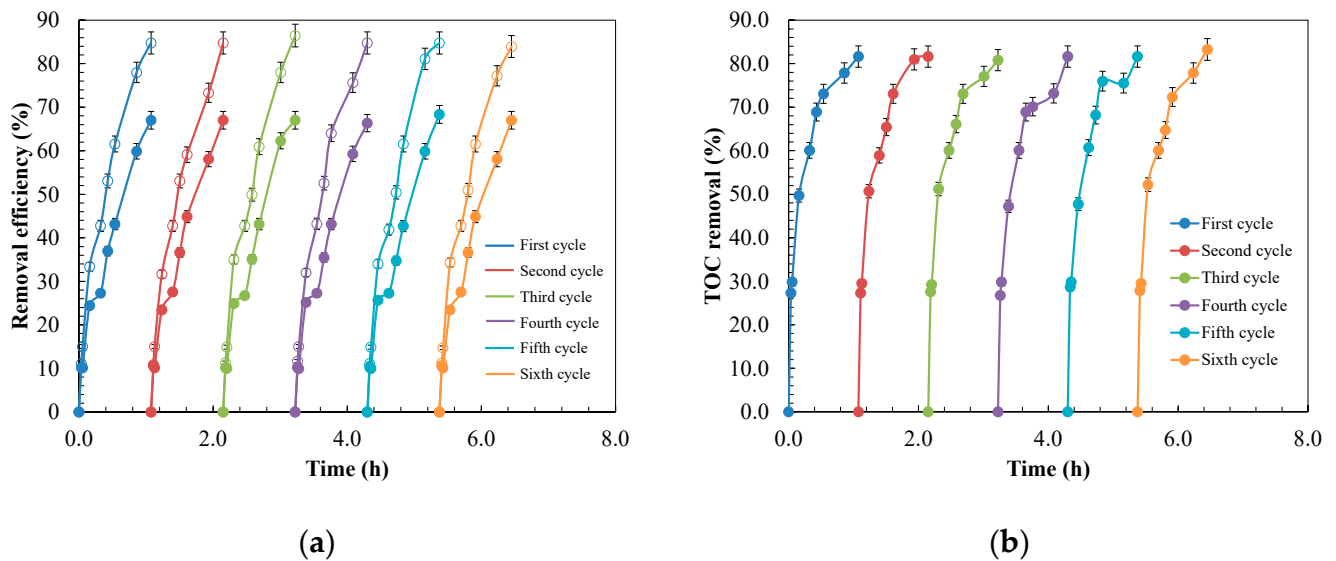


Figure 15. Reusability test for the photocatalytic degradation of ANI and BTH within six repeated cycles using $\text{MnO}_2/\text{GAC}-3$ catalyst. Evolution of: (a) primary degradation of ANI (\circ) and BTH (\bullet); (b) mineralisation. Experimental conditions: $C_0 = 12.0 \text{ mg L}^{-1}$; $\text{pH} = 9.0$; $m_{\text{CAT}} = 0.9 \text{ g L}^{-1}$; *Irradiation dose* = 155.8 W m^{-2} ; $T = 26 \text{ }^\circ\text{C}$.

The cost of an advanced oxidation process is very difficult to estimate, because factors such as mass transfer, operating conditions, and initial pollutant load can affect the degradation pathway and the oxidation kinetics, and therefore the oxidation efficiency [109]. For a direct comparison, equipment or maintenance costs were omitted, because they depend on the specific characteristics of each experimental system. Consequently, the cost of applying the FBR-photoreactor was estimated and compared to that of other systems reported in the literature that reach 90% of contaminant degradation. For this purpose, the previously

determined first-order kinetic constants (k, h^{-1}) were used to estimate the time required for 90% primary degradation of the contaminant (t_{90}, h) according to Equation (24):

$$t_{90} = \frac{2.3025851}{k} \quad (24)$$

Based on the t_{90} estimate as well as on the residence time of the reactor, the energy density ($\varepsilon, kW L^{-1}$) required for treatment was calculated according to Equation (25):

$$\varepsilon = \frac{E_A}{\text{Treated volume}}, \quad (25)$$

where E_A (kW) is the average energy required for a treatment cycle calculated according to Equation (26):

$$E_A = \frac{P_{\text{ele}} \times t \times 1000}{V \times 60 \times \log\left(\frac{C_0}{C_t}\right)}, \quad (26)$$

where P_{ele} is the electrical power (kW), t is the irradiation time (min), V is the total treated volume (L), and C_0 and C_t represent the ANI and BTH concentrations ($mg L^{-1}$) at the start and at time t , respectively. The cost of a treatment cycle was calculated considering the price of electricity for industrial customers in Spain, which was $0.0882 \text{ € kWh}^{-1}$ [110]. In Table 6, the cost of a treatment cycle is estimated and compared to others reported in the literature.

As outlined in Table 6, the FBR-photocatalytic system with the $MnO_2/GAC-3$ catalyst developed in this study for the removal of ANI and BTH from an industrial effluent costs 0.17 € m^{-3} in contrast to the value of 2.19 € m^{-3} [21] for a hybrid reactor or 0.29 € m^{-3} for the FBR-Fenton system [5]. This system achieved high efficiencies, which could facilitate its industrial implementation with $MnO_2/GAC-3$ catalysts.

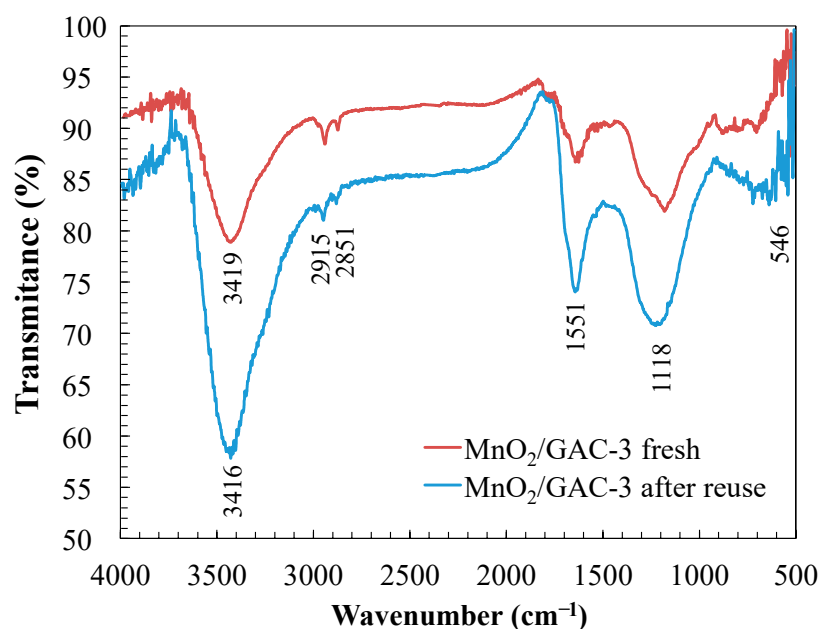


Figure 16. Infrared spectrum of $MnO_2/GAC-3$ before and after six cycles of reuse during the photocatalytic process for ANI and BTH degradation. Experimental conditions: $C_0 = 12.0 \text{ mg L}^{-1}$; $pH = 9.0$; $m_{\text{CAT}} = 0.9 \text{ g L}^{-1}$; Irradiation dose = 155.8 W m^{-2} ; $T = 26 \text{ °C}$.

Table 6. Procedure and comparison of ANI and BTH treatment cost estimates.

Process	Pollutant	k	Treated Volume (L)	P_{ele} (kW)	t_{90} (h)	ϵ (kW L ⁻¹)	V (L)	$V \times \epsilon$ (kW)	Cost (€ m ⁻³)	Ref.
FBR-Fenton	ANI	1.739 h ⁻¹	0.859	0.012	1.32	0.014	238.26	3.33	0.29	[5]
Ozone	ANI	2.003 h ⁻¹	1.0	0.200	1.14	235.43	1.0	235.43	0.81	[19]
Ozone	BTH	1.296 h ⁻¹	5.0	0.200	1.77	1.84	5.0	9.20	2.76	[9]
Photocatalysis	ANI and BTH mixture	0.341 h ⁻¹ (ANI) 0.091 h ⁻¹ (BTH)	2.15	0.026	6.75 (ANI) 25.30 (BTH)	4.97	16.0	79.59	2.19	[21]
FBR-Photocatalytic	ANI and BTH mixture	1.75 h ⁻¹ (ANI) 1.04 h ⁻¹ (BTH)	1.63	0.025	1.31 (ANI) 2.21 (BTH)	0.057	10.0	0.57	0.17 ¹	This work

¹ Considering the electric energy consumption of pumping.

4. Conclusions

A novel composite of granular activated carbon modified with MnO₂ (MnO₂/GAC) was prepared by hydrothermal synthesis with KMnO₄ solutions for its use in an FBR-photoreactor for the treatment of an industrial effluent containing aniline and benzothiazole. The study of the characteristics of the material highlighted the presence of the alpha-MnO₂ crystal in the composite by XRD analysis. Similarly, SEM, HRTEM, and AFM images showed an excellent dispersion of the MnO₂ particles on the surface of the GAC, which was confirmed by H₂ chemisorption (21.0%) and N₂ adsorption, showing a 9.47% increase in the specific surface relative to the initial surface of the GAC (601.2 m² g⁻¹). In particular, the band gap of this composite (MnO₂/GAC-3) was 0.95 eV, which enabled its use under visible light. XPS analysis confirmed the oxidation state (IV) of MnO₂ deposited on GAC. The catalytic activities of three MnO₂/GAC composites with different MnO₂ contents were compared when applied to an industrial effluent. The MnO₂/GAC-3 composite with 3.78% MnO₂ content, which was determined by XRF, showed the best performance in terms of primary degradation and mineralisation. The efficiency of the process could be attributed to the use of a suitable combination of photocatalyst and FBR-photoreactor. Parameters such as geometry, particle size, surface velocity of the fluid, pH and catalyst dose were considered when establishing the most favourable conditions: pH 9.0 and a dose of 0.9 g L⁻¹ for ANI and BTH removal from an industrial effluent containing 12.0 mg L⁻¹, achieving 84.7% and 67.0% removal for ANI and BTH, respectively, and 81.6% mineralisation after 1 h of reaction. The degradation kinetics were modelled by fitting them to a pseudo-first-order kinetic model, thus determining the following parameters for the most favourable conditions: $k_{app, ANI} = 1.75 \text{ h}^{-1}$ and $k_{app, BTH} = 1.04 \text{ h}^{-1}$. Other parameters, such as AOS (AOS = 0.63), indicated that the effluent treated in this study had optimal conditions for returning to the water environment. The novel MnO₂/GAC-3 photocatalyst showed excellent stability after six cycles, with an economic cost of treatment of 0.17 € m⁻³, thus showing a promising potential for practical applications. This study presents an efficient technology for treating industrial effluents containing organic pollutants that are not easily removed, using a novel catalytic and sustainable material.

Supplementary Materials: The following are available online at <https://www.mdpi.com/article/10.3390/ma14185207/s1>, Figure S1: Spectrum of the UV-A lamp used in the experimental equipment, Figure S2: EDX spectra of the materials used in the study, Figure S3: Determination of the H₂ monolayer chemisorbed on the surface of the three MnO₂/GAC composites synthesised in this study, Figure S4: pH effect on the efficiency of the ANI and BTH removal process using GAC Hydrodarco[®] 3000 during the adsorption and photocatalysis processes, Figure S5: pH effect on turbidity during the photocatalysis of industrial effluents containing ANI and BTH using the GAC Hydrodarco[®] 3000, Table S1: Previous studies of photocatalysis using manganese oxides supported on carbonaceous materials, Table S2: Limit of quantification values (LOQ) and limit of detection values (LOD) of different parameters, Table S3: Linearity values of different parameters, Table S4: Specificity values of different parameters, Table S5: Accuracy values of different parameters, Table S6: Precision values of different parameters.

Author Contributions: C.F., V.Z. and J.I.L. performed the conceptualisation; N.V. and M.J.R. carried out the design of the methodology and analyses; C.F., N.V. and V.Z. contributed to the model validation; C.F., J.M.R. and V.Z. performed the investigation; C.F., V.Z. and J.I.L. prepared the original draft; M.J.R., J.M.R. and N.V. reviewed and edited the manuscript; V.Z., M.J.R. and J.M.R. supervised the experimentation; J.M.R. and J.I.L. acquired the funding. All authors have read and agreed to the published version of the manuscript.

Funding: The authors are grateful to the University of the Basque Country (UPV/EHU) for their financial support of this study through the GIU20/56 project and C. Ferreiro's predoctoral PIF grant (PIF16/367).

Institutional Review Board Statement: Not applicable.

Informed Consent Statement: Not applicable.

Acknowledgments: The authors are thankful for the technical and human support provided by the Singular Coupled Multispectroscopy Laboratory (Raman-LASPEA), Analytical and High-Resolution Microscopy in Biomedicine, Macrobehaviour–Mesostructure–Nanotechnology Service, and the Central Analysis Service (Araba Unit), which is part of the General Research Services (SGIker) of the UPV/EHU; General Química S.A.U. (Dynasol group) for the ability to experiment with its own pilot photoreactor; and Cabot Corporation for supplying the sample of activated carbon used in this work.

Conflicts of Interest: The authors declare no conflict of interest.

References

1. Bello, M.M.; Abdul Raman, A.A.; Purushothaman, M. Applications of Fluidized Bed Reactors in Wastewater Treatment—A Review of the Major Design and Operational Parameters. *J. Clean. Prod.* **2017**, *141*, 1492–1514. [CrossRef]
2. Aitken, D.; Rivera, D.; Godoy-Faúndez, A.; Holzapfel, E. Water Scarcity and the Impact of the Mining and Agricultural Sectors in Chile. *Sustainability* **2016**, *8*, 128. [CrossRef]
3. Boczkaj, G.; Fernandes, A. Wastewater Treatment by Means of Advanced Oxidation Processes at Basic pH Conditions: A Review. *Chem. Eng. J.* **2017**, *320*, 608–633. [CrossRef]
4. Ferreiro, C.; Villota, N.; de Luis, A.; Lombrana, J.I. Analysis of the Effect of the Operational Variants in a Combined Adsorption-Ozonation Process with Granular Activated Carbon for the Treatment of Phenol Wastewater. *React. Chem. Eng.* **2020**, *5*, 760–778. [CrossRef]
5. Tisa, F.; Abdul Raman, A.A.; Wan Daud, W.M.A. Applicability of Fluidized Bed Reactor in Recalcitrant Compound Degradation through Advanced Oxidation Processes: A Review. *J. Environ. Manag.* **2014**, *146*, 260–275. [CrossRef] [PubMed]
6. Ferreiro, C.; Villota, N.; Lombrana, J.I.; Rivero, M.J. An Efficient Catalytic Process for the Treatment of Genotoxic Aniline Wastewater Using a New Granular Activated Carbon-Supported Titanium Dioxide Composite. *J. Clean. Prod.* **2019**, *228*, 1282–1295. [CrossRef]
7. Hering, J.G.; Maag, S.; Schnoor, J.L. A Call for Synthesis of Water Research to Achieve the Sustainable Development Goals by 2030. *Environ. Sci. Technol.* **2016**, *50*, 6122–6123. [CrossRef] [PubMed]
8. United Nations About the Sustainable Development Goals. Available online: <https://www.un.org/sustainabledevelopment/sustainable-development-goals/> (accessed on 7 February 2021).
9. Valdés, H.; Zaror, C.A.; Jekel, M. Removal of Benzothiazole from Contaminated Waters by Ozonation: The Role of Direct and Indirect Ozone Reactions. *J. Adv. Oxid. Technol.* **2016**, *19*, 338–346. [CrossRef]
10. Corsi, S.R.; Zitomer, D.H.; Field, J.A.; Cancilla, D.A. Nonylphenol Ethoxylates and Other Additives in Aircraft Deicers, Anticlers, and Waters Receiving Airport Runoff. *Environ. Sci. Technol.* **2003**, *37*, 4031–4037. [CrossRef]
11. Seitz, W.; Winzenbacher, R. A Survey on Trace Organic Chemicals in a German Water Protection Area and the Proposal of Relevant Indicators for Anthropogenic Influences. *Environ. Monit. Assess.* **2017**, *189*, 244. [CrossRef]
12. Ribeiro, A.R.; Nunes, O.C.; Pereira, M.F.R.; Silva, A.M.T. An Overview on the Advanced Oxidation Processes Applied for the Treatment of Water Pollutants Defined in the Recently Launched Directive 2013/39/EU. *Environ. Int.* **2015**, *75*, 33–51. [CrossRef]
13. De Wever, H.; Verachtert, H. Biodegradation and Toxicity of Benzothiazoles. *Water Res.* **1997**, *31*, 2673–2684. [CrossRef]
14. Felis, E.; Sochacki, A.; Magiera, S. Degradation of Benzotriazole and Benzothiazole in Treatment Wetlands and by Artificial Sunlight. *Water Res.* **2016**, *104*, 441–448. [CrossRef]
15. Mei-yan, X.; Can, D.; Godefroid, B.; Jian, Y. Treatment of Pharmaceutical Wastewater Containing Recalcitrant Compounds in a Fenton-Coagulation Process. *J. Environ. Sci.* **2006**, *18*, 459–463.
16. Suresh, S.; Srivastava, V.C.; Mishra, I.M. Adsorptive Removal of Aniline by Granular Activated Carbon from Aqueous Solutions with Catechol and Resorcinol. *Environ. Technol.* **2012**, *33*, 773–781. [CrossRef]
17. Liu, Q.; Zhang, L.; Hu, P.; Huang, R. Removal of Aniline from Aqueous Solutions by Activated Carbon Coated by Chitosan. *J. Water Reuse Desalin.* **2015**, *5*, 610–618. [CrossRef]

18. Sumegova, L.; Derco, J.; Melicher, M. Degradation of Benzothiazole by Ozonation and Adsorptive Ozonation. *Chem. Biochem. Eng. Q.* **2015**, *29*, 63–66. [[CrossRef](#)]
19. Jing, Z.; Cao, S.; Yu, T.; Hu, J. Degradation Characteristics of Aniline with Ozonation and Subsequent Treatment Analysis. *J. Chem.* **2015**, *2015*, 905921. [[CrossRef](#)]
20. Ferreira, C.; Villota, N.; Lombraña, J.I.; Rivero, M.J. Heterogeneous Catalytic Ozonation of Aniline-Contaminated Waters: A Three-Phase Modelling Approach Using TiO₂/GAC. *Water* **2020**, *12*, 3448. [[CrossRef](#)]
21. Ferreira, C.; Villota, N.; Lombraña, J.I.; Rivero, M.J.; Zúñiga, V.; Rituerto, J.M. Analysis of a Hybrid Suspended-Supported Photocatalytic Reactor for the Treatment of Wastewater Containing Benzothiazole and Aniline. *Water* **2019**, *11*, 337. [[CrossRef](#)]
22. Canle, L.M.; Santaballa, J.A.; Vulliet, E. On the Mechanism of TiO₂-Photocatalyzed Degradation of Aniline Derivatives. *J. Photochem. Photobiol. A Chem.* **2005**, *175*, 192–200. [[CrossRef](#)]
23. Reddy, P.A.K.; Reddy, P.V.L.; Kwon, E.; Kim, K.-H.; Akter, T.; Kalagara, S. Recent Advances in Photocatalytic Treatment of Pollutants in Aqueous Media. *Environ. Int.* **2016**, *91*, 94–103. [[CrossRef](#)] [[PubMed](#)]
24. Gomes, H.T.; Machado, B.F.; Ribeiro, A.; Moreira, I.; Rosário, M.; Silva, A.M.T.; Figueiredo, J.L.; Faria, J.L. Catalytic Properties of Carbon Materials for Wet Oxidation of Aniline. *J. Hazard. Mater.* **2008**, *159*, 420–426. [[CrossRef](#)]
25. Zhou, L.; Xie, Y.; Cao, H.; Guo, Z.; Wen, J.; Shi, Y. Enhanced Removal of Benzothiazole in Persulfate Promoted Wet Air Oxidation via Degradation and Synchronous Polymerization. *Chem. Eng. J.* **2019**, *370*, 208–217. [[CrossRef](#)]
26. Ferreira, C.; Gómez-Motos, I.; Lombraña, J.I.; de Luis, A.; Villota, N.; Ros, O.; Etxebarria, N. Contaminants of Emerging Concern Removal in an Effluent of Wastewater Treatment Plant under Biological and Continuous Mode Ultrafiltration Treatment. *Sustainability* **2020**, *12*, 725. [[CrossRef](#)]
27. Rahmat, M.; Rehman, A.; Rahmat, S.; Bhatti, H.N.; Iqbal, M.; Khan, W.S.; Bajwa, S.Z.; Rahmat, R.; Nazir, A. Highly Efficient Removal of Crystal Violet Dye from Water by MnO₂ Based Nanofibrous Mesh/Photocatalytic Process. *J. Mater. Res. Technol.* **2019**, *8*, 5149–5159. [[CrossRef](#)]
28. Shivaraju, H.P.; Midhun, G.; Anil Kumar, K.M.; Pallavi, S.; Pallavi, N.; Behzad, S. Degradation of Selected Industrial Dyes Using Mg-Doped TiO₂ Polyscales under Natural Sun Light as an Alternative Driving Energy. *Appl. Water Sci.* **2017**, *7*, 3937–3948. [[CrossRef](#)]
29. Chiam, S.-L.; Pung, S.-Y.; Yeoh, F.-Y. Recent Developments in MnO₂-Based Photocatalysts for Organic Dye Removal: A Review. *Environ. Sci. Pollut. Res.* **2020**, *27*, 5759–5778. [[CrossRef](#)]
30. Orha, C.; Pode, R.; Manea, F.; Lazau, C.; Bandas, C. Titanium Dioxide-Modified Activated Carbon for Advanced Drinking Water Treatment. *Process. Saf. Environ. Prot.* **2017**, *108*, 26–33. [[CrossRef](#)]
31. Ameta, S. *Advanced Oxidation Processes for Wastewater Treatment: Emerging Green Chemical Technology*; Academic Press: San Diego, CA, USA, 2018; ISBN 978-0-12-810499-6.
32. Gomez-Pastora, J.; Dominguez, S.; Bringas, E.; Rivero, M.J.; Ortiz, I.; Dionysiou, D.D. Review and Perspectives on the Use of Magnetic Nanophotocatalysts (MNPCs) in Water Treatment. *Chem. Eng. J.* **2017**, *310*, 407–427. [[CrossRef](#)]
33. Munir, S.; Dionysiou, D.D.; Khan, S.B.; Shah, S.M.; Adhikari, B.; Shah, A. Development of Photocatalysts for Selective and Efficient Organic Transformations. *J. Photochem. Photobiol. B Biol.* **2015**, *148*, 209–222. [[CrossRef](#)]
34. Ribao, P.; Rivero, M.J.; Ortiz, I. TiO₂ Structures Doped with Noble Metals and/or Graphene Oxide to Improve the Photocatalytic Degradation of Dichloroacetic Acid. *Environ. Sci. Pollut. Res. Int.* **2017**, *24*, 12628–12637. [[CrossRef](#)] [[PubMed](#)]
35. Sanchez, M.; Rivero, M.J.; Ortiz, I. Kinetics of Dodecylbenzenesulphonate Mineralisation by TiO₂ Photocatalysis. *Appl. Catal. B Environ.* **2011**, *101*, 515–521. [[CrossRef](#)]
36. Bodzek, M.; Rajca, M. Photocatalysis in the Treatment and Disinfection of Water. Part I. Theoretical Backgrounds. *Ecol. Chem. Eng.* **2012**, *19*, 489–512. [[CrossRef](#)]
37. Ramos-Delgado, N.A.; Gracia-Pinilla, M.A.; Mangalaraja, R.V.; O’Shea, K.; Dionysiou, D.D. Industrial Synthesis and Characterization of Nanophotocatalysts Materials: Titania. *Nanotechnol. Rev.* **2016**, *5*, 467–479. [[CrossRef](#)]
38. He, J.; Zhang, Y.; Guo, Y.; Rhodes, G.; Yeom, J.; Li, H.; Zhang, W. Photocatalytic Degradation of Cephalexin by ZnO Nanowires under Simulated Sunlight: Kinetics, Influencing Factors, and Mechanisms. *Environ. Int.* **2019**, *132*, 105105. [[CrossRef](#)] [[PubMed](#)]
39. Sui, X.; Wang, X.; Huang, H.; Peng, G.; Wang, S.; Fan, Z. A Novel Photocatalytic Material for Removing Microcystin-LR under Visible Light Irradiation: Degradation Characteristics and Mechanisms. *PLoS ONE* **2014**, *9*, e95798. [[CrossRef](#)] [[PubMed](#)]
40. Dette, C.; Pérez-Osorio, M.A.; Kley, C.S.; Punke, P.; Patrick, C.E.; Jacobson, P.; Giustino, F.; Jung, S.J.; Kern, K. TiO₂ Anatase with a Bandgap in the Visible Region. *Nano Lett.* **2014**, *14*, 6533–6538. [[CrossRef](#)] [[PubMed](#)]
41. Ma, J.; Sui, M.-H.; Chen, Z.-L.; Wang, L.-N. Degradation of Refractory Organic Pollutants by Catalytic Ozonation—Activated Carbon and Mn-Loaded Activated Carbon as Catalysts. *Ozone Sci. Eng.* **2004**, *26*, 3–10. [[CrossRef](#)]
42. Tang, N.; Tian, X.; Yang, C.; Pi, Z.; Han, Q. Facile Synthesis of α -MnO₂ Nanorods for High-Performance Alkaline Batteries. *J. Phys. Chem. Solids* **2010**, *71*, 258–262. [[CrossRef](#)]
43. Lin, H.; Chen, D.; Liu, H.; Zou, X.; Chen, T. Effect of MnO₂ Crystalline Structure on the Catalytic Oxidation of Formaldehyde. *Aerosol Air Qual. Res.* **2017**, *17*, 1011–1020. [[CrossRef](#)]
44. Wang, B.; Zhang, H.; Wang, F.; Xiong, X.; Tian, K.; Sun, Y.; Yu, T. Application of Heterogeneous Catalytic Ozonation for Refractory Organics in Wastewater. *Catalysts* **2019**, *9*, 241. [[CrossRef](#)]
45. Nawaz, F.; Cao, H.; Xie, Y.; Xiao, J.; Chen, Y.; Ghazi, Z.A. Selection of Active Phase of MnO₂ for Catalytic Ozonation of 4-Nitrophenol. *Chemosphere* **2017**, *168*, 1457–1466. [[CrossRef](#)] [[PubMed](#)]

46. Das, M.; Bhattacharyya, K.G. Oxidation of Rhodamine B in Aqueous Medium in Ambient Conditions with Raw and Acid-Activated MnO₂, NiO, ZnO as Catalysts. *J. Mol. Catal. A Chem.* **2014**, *391*, 121–129. [[CrossRef](#)]
47. Zhu, K.; Wang, C.; Camargo, P.H.C.; Wang, J. Investigating the Effect of MnO₂ Band Gap in Hybrid MnO₂–Au Materials over the SPR-Mediated Activities under Visible Light. *J. Mater. Chem. A* **2019**, *7*, 925–931. [[CrossRef](#)]
48. Warsi, M.F.; Bilal, M.; Zulfiqar, S.; Khalid, M.U.; Agboola, P.O.; Shakir, I. Enhanced Visible Light Driven Photocatalytic Activity of MnO₂ Nanomaterials and Their Hybrid Structure with Carbon Nanotubes. *Mater. Res. Express* **2020**, *7*, 105015. [[CrossRef](#)]
49. Wang, Y.; Zhu, L.; Yang, X.; Shao, E.; Deng, X.; Liu, N.; Wu, M. Facile Synthesis of Three-Dimensional Mn₃O₄ Hierarchical Microstructures and Their Application in the Degradation of Methylene Blue. *J. Mater. Chem. A* **2015**, *3*, 2934–2941. [[CrossRef](#)]
50. Zhou, J.; Wu, M.; Zhang, Y.; Zhu, C.; Fang, Y.; Li, Y.; Yu, L. 3D Hierarchical Structures MnO₂/C: A Highly Efficient Catalyst for Purification of Volatile Organic Compounds with Visible Light Irradiation. *Appl. Surf. Sci.* **2018**, *447*, 191–199. [[CrossRef](#)]
51. Shih, Y.-J.; Tsai, M.-T.; Huang, Y.-H. Mineralization and Defluoridation of 2,2,3,3-Tetrafluoro-1-Propanol (TFP) by UV Oxidation in a Novel Three-Phase Fluidized Bed Reactor (3P-FBR). *Water Res.* **2013**, *47*, 2325–2330. [[CrossRef](#)]
52. Tian, S.H.; Tu, Y.T.; Chen, D.S.; Chen, X.; Xiong, Y. Degradation of Acid Orange II at Neutral pH Using Fe₂(MoO₄)₃ as a Heterogeneous Fenton-like Catalyst. *Chem. Eng. J.* **2011**, *169*, 31–37. [[CrossRef](#)]
53. Moussavi, G.; Aghapour, A.A.; Yaghmaei, K. The Degradation and Mineralization of Catechol Using Ozonation Catalyzed with MgO/GAC Composite in a Fluidized Bed Reactor. *Chem. Eng. J.* **2014**, *249*, 302–310. [[CrossRef](#)]
54. Kanki, T.; Hamasaki, S.; Sano, N.; Toyoda, A.; Hirano, K. Water Purification in a Fluidized Bed Photocatalytic Reactor Using TiO₂-Coated Ceramic Particles. *Chem. Eng. J.* **2005**, *108*, 155–160. [[CrossRef](#)]
55. Huang, C.-P.; Huang, Y.-H. Application of an Active Immobilized Iron Oxide with Catalytic H₂O₂ for the Mineralization of Phenol in a Batch Photo-Fluidized Bed Reactor. *Appl. Catal. A Gen.* **2009**, *357*, 135–141. [[CrossRef](#)]
56. Al Mgheer, T.; Abdulrazzak, F.H. Oxidation of Multi-Walled Carbon Nanotubes in Acidic and Basic Piranha Mixture. *Front. Nanosci. Nanotechnol.* **2016**, *2*, 155–158. [[CrossRef](#)]
57. Feng, X.H.; Liu, F.; Tan, W.F.; Liu, X.W. Synthesis of Birnessite from the Oxidation of Mn²⁺ by O₂ in Alkali Medium: Effects of Synthesis Conditions. *Clays Clay Miner.* **2004**, *52*, 240–250. [[CrossRef](#)]
58. Mijangos, F.; Varona, F.; Villota, N. Changes in Solution Color During Phenol Oxidation by Fenton Reagent. *Environ. Sci. Technol.* **2006**, *40*, 5538–5543. [[CrossRef](#)] [[PubMed](#)]
59. Morrow, W.; McLean, L. Self-Cleaning UV Reflective Coating. U.S. Patent US20030059549A1, 30 October 2003.
60. Alhamed, Y.A. Adsorption Kinetics and Performance of Packed Bed Adsorber for Phenol Removal Using Activated Carbon from Dates' Stones. *J. Hazard. Mater.* **2009**, *170*, 763–770. [[CrossRef](#)] [[PubMed](#)]
61. Khan, I.; Sadiq, M.; Khan, I.; Saeed, K. Manganese Dioxide Nanoparticles/Activated Carbon Composite as Efficient UV and Visible-Light Photocatalyst. *Environ. Sci. Pollut. Res.* **2019**, *26*, 5140–5154. [[CrossRef](#)] [[PubMed](#)]
62. Begum, S.S.; Radha, K.V. Gas–Liquid Mass Transfer Studies in Inverse Fluidized Bed Biofilm Reactor for the Biodegradation of Industrial Effluent Rich in Phenolic Compounds. *Environ. Prog. Sustain. Energy* **2016**, *35*, 433–438. [[CrossRef](#)]
63. Fernández, N.; Montalvo, S.; Borja, R.; Guerrero, L.; Sánchez, E.; Cortés, I.; Colmenarejo, M.F.; Travieso, L.; Raposo, F. Performance Evaluation of an Anaerobic Fluidized Bed Reactor with Natural Zeolite as Support Material When Treating High-Strength Distillery Wastewater. *Renew. Energy* **2008**, *33*, 2458–2466. [[CrossRef](#)]
64. Silva, T.L.; Ronix, A.; Pezoti, O.; Souza, L.S.; Leandro, P.K.T.; Bedin, K.C.; Beltrame, K.K.; Cazetta, A.L.; Almeida, V.C. Mesoporous Activated Carbon from Industrial Laundry Sewage Sludge: Adsorption Studies of Reactive Dye Remazol Brilliant Blue R. *Chem. Eng. J.* **2016**, *303*, 467–476. [[CrossRef](#)]
65. Papirer, E.; Li, S.; Donnet, J.-B. Contribution to the Study of Basic Surface Groups on Carbons. *Carbon* **1987**, *25*, 243–247. [[CrossRef](#)]
66. Ghasemi, B.; Anvaripour, B.; Jorfi, S.; Jaafarzadeh, N. Enhanced Photocatalytic Degradation and Mineralization of Furfural Using UVC/TiO₂/GAC Composite in Aqueous Solution. *Int. J. Photoenergy* **2016**, *2016*, 2782607. [[CrossRef](#)]
67. Liu, Y.-H.; Hsi, H.-C.; Li, K.-C.; Hou, C.-H. Electrodeposited Manganese Dioxide/Activated Carbon Composite As a High-Performance Electrode Material for Capacitive Deionization. *ACS Sustain. Chem. Eng.* **2016**, *4*, 4762–4770. [[CrossRef](#)]
68. Choi, J.R.; Lee, J.W.; Yang, G.; Heo, Y.-J.; Park, S.-J. Activated Carbon/MnO₂ Composites as Electrode for High Performance Supercapacitors. *Catalysts* **2020**, *10*, 256. [[CrossRef](#)]
69. Yang, Y.; Zhang, H.; Jin, S. A New Method of Activated Carbon Loading MnO₂ to Formaldehyde Degradation. *Adv. Mater. Res.* **2011**, *332–334*, 1743–1746. [[CrossRef](#)]
70. Thackeray, M.M. Manganese Oxides for Lithium Batteries. *Prog. Solid State Chem.* **1997**, *25*, 1–71. [[CrossRef](#)]
71. Noorimotlagh, Z.; Kazeminezhad, I.; Jaafarzadeh, N.; Ahmadi, M.; Ramezani, Z.; Silva Martinez, S. The Visible-Light Photodegradation of Nonylphenol in the Presence of Carbon-Doped TiO₂ with Rutile/Anatase Ratio Coated on GAC: Effect of Parameters and Degradation Mechanism. *J. Hazard. Mater.* **2018**, *350*, 108–120. [[CrossRef](#)]
72. Shen, X.; Garces, L.-J.; Ding, Y.; Laubernds, K.; Zerger, R.P.; Aindow, M.; Neth, E.J.; Suib, S.L. Behavior of H₂ Chemisorption on Ru/TiO₂ Surface and Its Application in Evaluation of Ru Particle Sizes Compared with TEM and XRD Analyses. *Appl. Catal. A Gen.* **2008**, *335*, 187–195. [[CrossRef](#)]
73. Almeida, Â.; Calisto, V.; Domingues, M.R.M.; Esteves, V.I.; Schneider, R.J.; Soares, A.M.V.M.; Figueira, E.; Freitas, R. Comparison of the Toxicological Impacts of Carbamazepine and a Mixture of Its Photodegradation Products in Scrobicularia Plana. *J. Hazard. Mater.* **2017**, *323*, 220–232. [[CrossRef](#)] [[PubMed](#)]

74. Ma, Y.; Wang, S.-G.; Fan, M.; Gong, W.-X.; Gao, B.-Y. Characteristics and Defluoridation Performance of Granular Activated Carbons Coated with Manganese Oxides. *J. Hazard. Mater.* **2009**, *168*, 1140–1146. [[CrossRef](#)] [[PubMed](#)]
75. Xiong, W.; Chen, N.; Feng, C.; Liu, Y.; Ma, N.; Deng, J.; Xing, L.; Gao, Y. Ozonation Catalyzed by Iron- and/or Manganese-Supported Granular Activated Carbons for the Treatment of Phenol. *Environ. Sci. Pollut. Res. Int.* **2019**, *26*, 21022–21033. [[CrossRef](#)] [[PubMed](#)]
76. Rubinson, K.A.; Rubinson, J.F. *Contemporary Instrumental Analysis*; Prentice Hall: Upper Saddle River, NJ, USA, 2000; ISBN 978-0-13-790726-7.
77. Hu, E.; Wu, X.; Shang, S.; Tao, X.; Jiang, S.; Gan, L. Catalytic Ozonation of Simulated Textile Dyeing Wastewater Using Mesoporous Carbon Aerogel Supported Copper Oxide Catalyst. *J. Clean. Prod.* **2016**, *112*, 4710–4718. [[CrossRef](#)]
78. Spivey, J.J.; Agarwal, S.K.; Bartholemew, C.H. H₂ adsorption on supported noble metals and its use in determining metal dispersion. *Catalysis* **1994**, *11*, 93–126. [[CrossRef](#)]
79. Askaripour, H.; Molaei Dehkordi, A. Effects of Initial Static Bed Height on Fractional Conversion and Bed Pressure Drop in Tapered-in and Tapered-out Fluidized Bed Reactors. *Int. J. Multiph. Flow* **2016**, *79*, 50–61. [[CrossRef](#)]
80. Ochieng, A.; Odiyo, J.O.; Mutsago, M. Biological Treatment of Mixed Industrial Wastewaters in a Fluidised Bed Reactor. *J. Hazard. Mater.* **2003**, *96*, 79–90. [[CrossRef](#)]
81. Nam, W.; Woo, K.; Han, G. Photooxidation of Anionic Surfactant (Sodium Lauryl Sulfate) in a Three-Phase Fluidized Bed Reactor Using TiO₂/SiO₂ Photocatalyst. *J. Ind. Eng. Chem.* **2009**, *15*, 348–353. [[CrossRef](#)]
82. Shim, S.; Won, S.; Reza, A.; Kim, S.; Ahmed, N.; Ra, C. Design and Optimization of Fluidized Bed Reactor Operating Conditions for Struvite Recovery Process from Swine Wastewater. *Processes* **2020**, *8*, 422. [[CrossRef](#)]
83. Zarekar, S.; Bück, A.; Jacob, M.; Tsotsas, E. Numerical Study of the Hydrodynamics of Fluidized Beds Operated under Sub-Atmospheric Pressure. *Chem. Eng. J.* **2019**, *372*, 1134–1153. [[CrossRef](#)]
84. Delebarre, A.; Morales, J.-M.; Ramos, L. Influence of the Bed Mass on Its Fluidization Characteristics. *Chem. Eng. J.* **2004**, *98*, 81–88. [[CrossRef](#)]
85. Mojoudi, N.; Mirghaffari, N.; Soleimani, M.; Shariatmadari, H.; Belver, C.; Bedia, J. Phenol Adsorption on High Microporous Activated Carbons Prepared from Oily Sludge: Equilibrium, Kinetic and Thermodynamic Studies. *Sci. Rep.* **2019**, *9*, 19352. [[CrossRef](#)] [[PubMed](#)]
86. Khlyustova, A.; Sirotkin, N.; Kusova, T.; Kraev, A.; Titov, V.; Agafonov, A. Doped TiO₂: The Effect of Doping Elements on Photocatalytic Activity. *Mater. Adv.* **2020**, *1*, 1193–1201. [[CrossRef](#)]
87. Shang, M.; Wang, W.; Sun, S.; Zhou, L.; Zhang, L. Bi₂WO₆ Nanocrystals with High Photocatalytic Activities under Visible Light. *J. Phys. Chem. C* **2008**, *112*, 10407–10411. [[CrossRef](#)]
88. Largette, L.; Pasquier, R. A Review of the Kinetics Adsorption Models and Their Application to the Adsorption of Lead by an Activated Carbon. *Chem. Eng. Res. Des.* **2016**, *109*, 495–504. [[CrossRef](#)]
89. Ho, Y.S.; McKay, G. Pseudo-Second Order Model for Sorption Processes. *Process. Biochem.* **1999**, *34*, 451–465. [[CrossRef](#)]
90. Sampaio, M.J.; Silva, C.G.; Silva, A.M.T.; Faria, J.L. Kinetic Modelling for the Photocatalytic Degradation of Phenol by Using TiO₂-Coated Glass Raschig Rings under Simulated Solar Light. *J. Chem. Technol. Biotechnol.* **2016**, *91*, 346–352. [[CrossRef](#)]
91. Chen, P.H.; Jenq, C.H. Kinetics of Photocatalytic Oxidation of Trace Organic Compounds over Titanium Dioxide. *Environ. Int.* **1998**, *24*, 871–879. [[CrossRef](#)]
92. Saroyan, H.; Kyzas, G.Z.; Deliyanni, E.A. Effective Dye Degradation by Graphene Oxide Supported Manganese Oxide. *Processes* **2019**, *7*, 40. [[CrossRef](#)]
93. David, A.; Vedhi, C. Synthesis of Nano Co₃O₄-MnO₂-ZrO₂ Mixed Oxides for Visible-Light Photocatalytic Activity. *Int. J. Adv. Res. Sci. Eng. Technol.* **2017**, *6*, 613–623.
94. Sánchez, L.; Peral, J.; Domènech, X. Photocatalyzed Destruction of Aniline in UV-Illuminated Aqueous TiO₂ Suspensions. *Electrochim. Acta* **1997**, *42*, 1877–1882. [[CrossRef](#)]
95. Yang, H.; Bard, A.J. The Application of Fast Scan Cyclic Voltammetry. Mechanistic Study of the Initial Stage of Electropolymerization of Aniline in Aqueous Solutions. *J. Electroanal. Chem.* **1992**, *339*, 423–449. [[CrossRef](#)]
96. De Wever, H.; Vereecken, K.; Stolz, A.; Verachtert, H. Initial Transformations in the Biodegradation of Benzothiazoles by Rhodococcus Isolates. *Appl. Environ. Microbiol.* **1998**, *64*, 3270–3274. [[CrossRef](#)]
97. Derco, J.; Kassai, A.; Melicher, M.; Dudas, J. Removal of the 2-Mercaptobenotiazole from Model Wastewater by Ozonation. *Sci. World J.* **2014**, *2014*, e173010. [[CrossRef](#)] [[PubMed](#)]
98. Zhao, X.; Zhang, G.; Zhang, Z. TiO₂-Based Catalysts for Photocatalytic Reduction of Aqueous Oxyanions: State-of-the-Art and Future Prospects. *Environ. Int.* **2020**, *136*, 105453. [[CrossRef](#)]
99. Ma, J.; Minakata, D.; O'Shea, K.; Bai, L.; Dionysiou, D.D.; Spinney, R.; Xiao, R.; Wei, Z. Determination and Environmental Implications of Aqueous-Phase Rate Constants in Radical Reactions. *Water Res.* **2021**, *190*, 116746. [[CrossRef](#)]
100. Velo-Gala, I.; López-Peñalver, J.J.; Sánchez-Polo, M.; Rivera-Utrilla, J. Activated Carbon as Photocatalyst of Reactions in Aqueous Phase. *Appl. Catal. B Environ.* **2013**, *142–143*, 694–704. [[CrossRef](#)]
101. Chiam, S.-L.; Yeoh, F.Y.; Pung, S.-Y. *Heavy Metal Ions Removal Using Beta-MnO₂ Particles under UV Irradiation*; Amer Inst Physics: Melville, NY, USA, 2020; ISBN 978-0-7354-2030-4.
102. Chen, X.; Zhou, J.; Chen, Y.; Zhou, Y.; Ding, L.; Liang, H.; Li, X. Degradation of Tetracycline Hydrochloride by Coupling of Photocatalysis and Peroxymonosulfate Oxidation Processes Using CuO-BiVO₄ Heterogeneous Catalyst. *Process. Saf. Environ. Prot.* **2021**, *145*, 364–377. [[CrossRef](#)]

103. Hemmati Borji, S.; Nasser, S.; Mahvi, A.H.; Nabizadeh, R.; Javadi, A.H. Investigation of Photocatalytic Degradation of Phenol by Fe(III)-Doped TiO₂ and TiO₂ Nanoparticles. *J. Environ. Health Sci. Eng.* **2014**, *12*, 101. [[CrossRef](#)]
104. Méndez-Arriaga, F.; Maldonado, M.I.; Gimenez, J.; Esplugas, S.; Malato, S. Abatement of Ibuprofen by Solar Photocatalysis Process: Enhancement and Scale Up. *Catal. Today* **2009**, *144*, 112–116. [[CrossRef](#)]
105. Reyes, C.; Fernández, J.; Freer, J.; Mondaca, M.A.; Zaror, C.; Malato, S.; Mansilla, H.D. Degradation and Inactivation of Tetracycline by TiO₂ Photocatalysis. *J. Photochem. Photobiol. A Chem.* **2006**, *184*, 141–146. [[CrossRef](#)]
106. Zapata, A.; Oller, I.; Gallay, R.; Pulgarín, C.; Maldonado, M.I.; Malato, S.; Gernjak, W. Comparison of Photo-Fenton Treatment and Coupled Photo-Fenton and Biological Treatment for Detoxification of Pharmaceutical Industry Contaminants. *J. Adv. Oxid. Technol.* **2008**, *11*, 261–269. [[CrossRef](#)]
107. Lekshmi, K.P.V.; Yesodharan, S.; Yesodharan, E.P. MnO₂ and MnO₂/TiO₂ mediated, persulphate enhanced photocatalysis for the removal of indigo carmine dye pollutant from water. *Eur. Chem. Bull.* **2017**, *6*, 177–191. [[CrossRef](#)]
108. De Almeida, M.F.; Bellato, C.R.; Munteer, A.H.; Ferreira, S.O.; Milagres, J.L.; Miranda, L.D.L. Enhanced Photocatalytic Activity of TiO₂-Impregnated with MgZnAl Mixed Oxides Obtained from Layered Double Hydroxides for Phenol Degradation. *Appl. Surf. Sci.* **2015**, *357*, 1765–1775. [[CrossRef](#)]
109. Krichevskaya, M.; Klauson, D.; Portjanskaja, E.; Preis, S. The Cost Evaluation of Advanced Oxidation Processes in Laboratory and Pilot-Scale Experiments. *Ozone Sci. Eng.* **2011**, *33*, 211–223. [[CrossRef](#)]
110. European Commission. Eurostat Regional Yearbook 2020. *Stat. Books* **2020**, *1*, 1–196. [[CrossRef](#)]

3.6. 6. argitalpena. Analysis of the effect of the operational conditions in a combined adsorption-ozonation process with granular activated carbon for the treatment of phenol wastewater

3.6 kapitulua artikulu honi dagokio:

C. Ferreiro, N. Villota, A. de Luis, J.I. Lombraña. Analysis of the effect of the operational conditions in a combined adsorption-ozonation process with granular activated carbon for the treatment of phenol wastewater. *Reaction Chemistry & Engineering*, 5, 4, 760-778, 2020. DOI: 10.1039/c9re00424f.



Cite this: *React. Chem. Eng.*, 2020, 5, 760

Analysis of the effect of the operational conditions in a combined adsorption–ozonation process with granular activated carbon for the treatment of phenol wastewater

Cristian Ferreiro, ^{*a} Natalia Villota,^b
Ana de Luis ^c and Jose Ignacio Lombraña ^a

This work proposes a mathematical model as a basis for studying the combined adsorption–ozonation process (Ad/Ox) with the complexity involved in a three-phase system. The description of this operation involves several parameters that describe the system kinetics and adsorption phenomena. This paper analyses the Ad/Ox process compared with simple ozonation, investigating the benefits of activated carbon (AC) in ozonation, primary degradation and mineralization of phenol solutions. This study focuses on Ad/Ox with granular activated carbon (GAC) and analyses how the phenol degradation kinetics depend on the amount of AC. Thus, a priority order of relevance is established for the proposed mathematical model parameters. For example, the adsorption kinetic constant may vary meaningfully within the same process. Finally, this paper studies the GAC behaviour after a given number of cycles, followed by the regeneration process. The calculated kinetic coefficients relating to the liquid and solid media explain the changes in process efficiency.

Received 4th November 2019,
Accepted 12th February 2020

DOI: 10.1039/c9re00424f

rsc.li/reaction-engineering

1. Introduction

It is difficult to degrade certain organic compounds, such as phenol. Phenol is chosen in this work to study the ozonation process, which has been used as a possible alternative for several decades.^{1,2} Phenol is mainly used to produce phenolic resins, which are used in plywood manufacturing. It is also used in household appliance manufacturing, as well as in the production of caprolactam and bisphenol A, two intermediates used in manufacturing nylon and epoxy resins.^{3,4}

Phenol is highly irritating to the human skin, eyes and mucous membranes after prolonged exposure. Short-term inhalation may cause anorexia, diarrhoea, dizziness, and dark-coloured urine. Long-term effects on the blood and liver may occur. The lethal dose in humans may be as low as 14–214 mg phenol per kg.⁵ The United States Environmental Protection Agency (US EPA) has classified phenol as a Group D contaminant, not classifiable with respect to human carcinogenicity.⁶ However, the European Union (EU) through the European Chemicals Agency (ECHA) included this

pollutant in 2015 in the Community Rolling Action Plan (CoRAP), because it is considered a suspect mutagenic substance and a potential endocrine disruptor.⁷ In addition to the human health effects, it can cause considerable damage to the aquatic environment. For example, 1500 mg L⁻¹ phenol was lethal to *Chilomonas* and *Euglena gracilis*; at 2500 mg L⁻¹ it was lethal to *Peramena*. At a dose of 10–40 mg L⁻¹, phenol inhibited the photosynthesis of *Chlorella*. An exposure to 50 mg L⁻¹ phenol caused *Pimephales promelas* to lose balance and gasp at the surface, while a dose of 6.3 mg L⁻¹ caused hyperactivity and rapid operculum in *Salmo gairdneri*. The most critical sublethal effect of phenol is on the reproductive potential of the biota. For example, an exposure to 5 mg L⁻¹ phenol causes reduced fertility in *Daphnia longispina*.⁸

In this study, industrial wastewater with a representative phenol concentration of 1000 mg L⁻¹ was used. Phenols are present in the wastewater of various industries, such as coke oven industries (28–3900 mg L⁻¹), coal processing (9–6800 mg L⁻¹) and petrochemical plants (2.8–1220 mg L⁻¹). Other sources containing 0.1–1600 mg L⁻¹ phenols are pharmaceuticals, plastics, wood products, varnish and paper industries.^{9,10} Several authors noted in the bibliography studied the elimination of phenol from industrial wastewater, as shown in Table 1. The processes studied to date require complex treatment and reaction times long enough to achieve complete degradation and a sufficiently high degree of mineralization to avoid damage to the environment.

^a Department of Chemical Engineering, Faculty of Science and Technology, University of the Basque Country UPV/EHU, Leioa, Spain.

E-mail: cristian.ferreiro@ehu.eus

^b Department of Chemical and Environmental Engineering, Escuela de Ingeniería de Vitoria-Gasteiz, University of the Basque Country UPV/EHU, Vitoria-Gasteiz, Spain

^c Department of Chemical and Environmental Engineering, Faculty of Engineering, University of the Basque Country UPV/EHU, Bilbao, Spain

Therefore, the ozonisation process is proposed as a clear alternative for the elimination of phenol. Nevertheless, the unstable characteristic of ozone makes its effective application complicated, as demonstrated in several studies within recent decades.^{11–13} This disadvantage leads us to consider the convenience of combining ozonation with catalysts and adsorbent materials such as activated carbon (AC).

In early attempts to add active carbon in ozonation, the benefits were connected to the high adsorption capacity of AC.¹⁴ Subsequent studies^{15–17} have shown that AC catalyses the decomposition of ozone in the aqueous phase by accelerating the transformation of free hydroxyl radicals.

Generally, ozone is adsorbed on the surface of AC at acidic pH values, but the generation of hydroxyl radicals is minimal by this route, since the predominant mechanism is the molecular path. However, at a pH between 6 and 9, ozone decomposition occurs and is catalysed by hydroxyl groups adsorbed onto the AC surface.¹⁸ The mechanism of ozone decomposition and the subsequent phenol oxidation in the presence of activated carbon is shown below:²



Table 1 Previous studies on the treatment of industrial wastewater containing phenol

Treatment	Catalyst	Operation conditions	Comments	Ref.
Noncatalytic wet air oxidation	—	[T] = 125–320 °C [P] = 0.5–20 MPa [Time] = 120 min [% COD] = 75–90% acidic media	An extremely clean process because it neither uses any harmful chemical reagents nor produces any harmful final products (carbon dioxide and water are the products if a complete oxidation is achieved)	31
TiO ₂ /UV photocatalysis	TiO ₂	[Cat] = 1 g L ⁻¹ C ₀ = 50 mg L ⁻¹ [Time] = 90 min [UV power] = 400 W [%] = 100% intermediate pH	The oxidation of phenol under UV irradiation and the presence of photocatalysts lead to increased degradation. The immobilization of the photocatalyst led to a reduction in photoactive capacity compared to the use of the suspended catalyst	32
Microwave in UV/H ₂ O ₂ system	—	[MW irradiation] = 2.5 GHz [% TOC] = 50% C ₀ = 200 mg L ⁻¹ [H ₂ O ₂] = 1200 mg L ⁻¹ T = 50 °C [%] = 95% [Time] = 30 min	The introduction of microwave irradiation into the system reduces the reaction time, increases the reaction selectivity, reduces the activation energy, reduces the equipment size and makes the process easier to control	33
Fenton reaction	Fe/ZrO ₂ and 4% Fe-sulfonated-ZrO ₂	C ₀ = 0.1 g L ⁻¹ [H ₂ O ₂] = 0.5 g L ⁻¹ [Cat] = 2 g L ⁻¹ T = 25 °C P = 1 atm [time] = 6 h [%] = 100% [% TOC] = 64% Acidic media	Sulfonation of zirconia followed by Fe impregnation shows a positive effect on the oxidative degradation and mineralization of phenol. The catalyst maintains its activity even after four cycles of regeneration and reuse	34
O ₃ /Ca(OH) ₂	Ca(OH) ₂	C ₀ = 450 mg L ⁻¹ [Cat] = 2 g L ⁻¹ C _{O₃G} = 75 mg L ⁻¹ Q _G = 3 L min ⁻¹ T = 25 °C P = 0.25 MPa [Time] = 55 min [%] = 100% [% TOC] = 100%	It is necessary to treat the catalyst as a solid residue once spent. The mechanism for Ca(OH) ₂ intensified mineralization of phenol solution is the simultaneous removal of CO ₃ ²⁻ ions as hydroxyl radical scavengers, due to the presence of Ca ²⁺ ions	4
O ₃ /Cu-AC	Cu-AC	C ₀ = 200 mg L ⁻¹ [Cat] = 2.5 mg mL ⁻¹ C _{O₃G} = 11.2 mg L ⁻¹ pH ₀ = 4 T = 25 °C P = 1 atm [Time] = 30 min [%] = 70%	The presence of the Cu-AC catalyst enhances the decomposition of ozone into hydroxyl radicals. The CuO and surface oxygen groups in the activated carbon have a slight effect on the degradation of phenol	35



Later, Beltran *et al.* and Sanchez *et al.* concluded that with these processes, the complete mineralization of many pollutants is possible.^{19,20} These authors studied O₃/AC systems in detail and showed that the surface chemistry of activated carbon, along with its textural characteristics, plays a very important role in its behaviour as a promoter of ozone decomposition to hydroxyl radicals.

Ozonation combined with AC can operate in a batch process, but it is generally sequential, which presents disadvantages in application.²¹⁻²³ In this work, the simultaneous application of adsorption and ozonisation is proposed, analysing the elimination of phenol as a pollutant.²⁴ AC's application together with ozonation occupies a relevant place in recent works for its clear advantages in catalytic heterogeneous ozonation. The increasing development of new activated carbons^{25,26} and the advantages associated with their dual functions (adsorptive and catalytic) support the growth of this technology.^{27,28}

Despite the findings in this field,^{29,30} it is necessary to detail the combined action of ozone and activated carbon to predict and estimate the effects of the process and operational variants on the removal performance. In this respect, this work contributes with suitable modelling and estimation of the characteristic parameters of the combined system and their influence on the process efficiency.

This study analyses the results obtained when using granular activated carbon (GAC) during ozonation. Based on an adsorption study of active carbon with solutions containing phenol, the simultaneous mode of operation (Ad/Ox) was studied, using the advantages of the adsorptive-reactive function that occurs on the AC surface. The study objective is therefore to assess the extent of the adsorption and reaction effect in the efficiency of phenol removal, used here as a pollutant model, considering catalytic material regeneration.

2. Experimental methods

2.1. Materials and reagents

Phenol (C₆H₅OH, Sigma-Aldrich, ≥99.0%), sulfuric acid (H₂SO₄, Panreac, 1 M), sodium hydroxide (NaOH, Panreac, 1 M), hydrogen chloride (HCl, Labkem, 37%), sodium chloride (NaCl, VWR, 99.8%), powder activated carbon (PAC, Panreac, pure) and HPLC-grade methanol (CH₃OH, Merck, >99.99%) were used as received. Deionised water was supplied by a

Milli-Q® water purification unit supplied by Merck. Kemisorb® 530 GR 12x40 granular activated carbon was purchased from Kemira.

2.2. GAC characterization methods

Nitrogen adsorption measurements were performed using a Micromeritics ASAP 2010 instrument at 77 K with ultra-high purity nitrogen gas. All the samples were dried and degassed under high vacuum at 473 K for 24 h prior to measurements. The surface area was calculated using the BET equation, and the pore size distribution was determined by applying the BJH model.

The point of zero charge (PZC) was determined by the acid-base titration method.^{36,37} A total of 50 mL of 0.01 M NaCl solution was prepared in 100 mL flasks. The initial pH between 2 and 12 was then adjusted using 0.1 M NaOH or HCl, and then, 0.15 g of activated carbon was added to start the test at a certain pH. After a 24 h contact time, the final pH was measured. The final pH was plotted against the initial pH for all assays to obtain the pH_{pzc} value.

A Waters 2695 HPLC system with a Teknokroma Mediterranea SEA C18 threaded column (150 mm × 4.6 mm, 1.8 μm) with the guard column working at 20 °C under isocratic elution (60% buffered water at pH 3, 40% methanol) and a flow rate of 1 mL min⁻¹ was used for phenol quantification. A Waters 2487 UV/vis detector was used at a wavelength of 272 nm. The degree of mineralization was quantified by total organic carbon (TOC) analysis on a Shimadzu TOC-VSCH analyzer.

2.3. Adsorption experiments

Phenol adsorption experiments on activated carbon were performed at temperatures ranging from 15–35 °C and at pH = 6.5 for powdered active carbon and for granular activated carbon, Kemisorb® 530. The kinetics and adsorption isotherms were obtained by preparing 500.0 mL phenol solutions (C₀ = 1000 mg L⁻¹), in a 0.5 L jacketed reactor with a magnetic stirrer, in which 0.25 g of carbon active powder or granulate were added, after adjusting the pH according to the experiment.

The agitation was kept steady at 500 rpm, in order to maintain perfect mixing for at least 24 h, to ensure equilibrium. The temperature was controlled by a thermostatic bath, providing the reactor with necessary water flux at the desired temperature. To remove the catalyst particles, the solutions were filtered through a 0.45 μm membrane (MF-Millipore) before proceeding to the analysis of the concentration of phenol by HPLC. For the analysis of adsorption kinetic data, the amount of phenol adsorbed at time *t* was obtained from eqn (9):

$$q_t = \frac{(C_0 - C_t) \cdot V}{M} \quad (9)$$

where C₀ and C_t are the initial and phenol concentrations at any time, respectively; V is the volume of the solution and M

is the mass of activated carbon. All adsorption experiments were performed in triplicate, and the mean values were used for the adsorption study. The maximum standard deviation of measured concentrations was not greater than 0.1 mg L^{-1} .

2.4. Ozonation experiments

The removal of phenol in the Ad/Ox process was carried out in a gas–liquid contactor using powder activated carbon and, in other cases, granular activated carbon Kemisorb® 530. The experimental ozonation system consisted of a 30.41 L cylindrical column where the solution to treat was placed. Ozone gas is introduced into the reactor through a venturi installed in the recirculation stream, thus ensuring a perfect homogenization of the system. To improve the contact between the descending liquid and the ascending gas, the column has a sprayer on the top that atomizes the liquid (Fig. 1). Part of the solution that the system recirculates is pumped upward and returns to the reactor at the top, where it is sprayed, thus destroying the foam that is formed in some cases by the strong agitation of the system. The recirculation system provides enough stirring to ensure a good mixture in the system. As shown in Fig. 1, the reacting medium interacts with a certain load of GAC packed in a cartridge, through which the reacting stream passes.

The experiments were carried out at a constant temperature of $20.0 \text{ }^\circ\text{C}$, operated in batches with loads of approximately 10.0 L of phenol solutions with an initial concentration of 1000 mg L^{-1} . All assays were carried out under constant gas flow, $Q_G = 4.0 \text{ L min}^{-1}$, constant ozone

concentration in the gas phase at the inlet, $C_{O_3,G} = 19.0 \text{ mg L}^{-1}$, a pH of 6.5 and 250.0 or 500.0 g of activated carbon. Ozone was produced from extra pure oxygen in a TRIOGEN LAB2B generator. The temperature was controlled using a refrigerating bath. The ozone concentration in the gas phase was monitored with a BMT 964C ozone analyser. Liquid phase ozone concentration and temperature were measured with a Rosemount Analytical Model 499AOZ-54 probe inserted in the recirculation. The pH was controlled with a Rosemount Analytical model 399-09-62 probe, integrated with the ozone probe in a Rosemount Analytical Solu Comp II recorder. Gas-phase ozone leaving the reactor was removed with a Zonosistem thermocatalytic ozone destructor.

2.5. GAC regeneration

2.5.1. Regeneration with NaOH. The regeneration of granulated activated carbon was carried out according to the procedure described by Martin & Ng and Sun *et al.*,^{38,39} which consists of treating spent activated carbon with a 10% NaOH solution at a temperature of $105 \text{ }^\circ\text{C}$, circulating in the opposite direction to that during the reaction. The activated carbon was then washed with distilled water to neutralize its pH before drying in an oven at $90 \text{ }^\circ\text{C}$ for 24 hours.

2.5.2. Ozone regeneration procedure. In this case, spent granular activated carbon was treated according to the procedure described by Martin and Ng,³⁸ which consists of placing the spent GAC into a jacket glass reactor with 1500 mL of deionized water, similar to the process described by Ferreiro *et al.*²⁵ An ozone gas flow, $Q_G = 4.0 \text{ L min}^{-1}$, was then introduced, using an ozone concentration of 262.0 mg O_3 per g GAC treated.⁴¹ The GAC was treated with ozone for 60 min and then dried in an oven at $90 \text{ }^\circ\text{C}$ for 24 h before reuse.

3. Theory

3.1. Three-phase reaction model

As described in the introduction, a combined Ad/Ox process is postulated as a good option for the treatment of contaminants such as phenol. In this section, a mathematical model is proposed to describe the simultaneous ozonisation and adsorption process (Ad/Ox), in batch, based on the definition of the corresponding adsorption and phenol oxidation kinetic constants. The proposed model calculates the variation in the phenol concentration during the reaction, and analyses the oxidation that takes place in the liquid and the active carbon.

Phenol's primary degradation process can be described through ozone consumption. In this case, the stoichiometric coefficient, z , of the reaction between phenol and ozone is used, according to:

$$-\frac{dC_p}{dt} = z \cdot N_{O_3} \quad (10)$$

where N_{O_3} is the ozone consumption, coincident with the ozone transferred to the G–L–S system. The coefficient z can

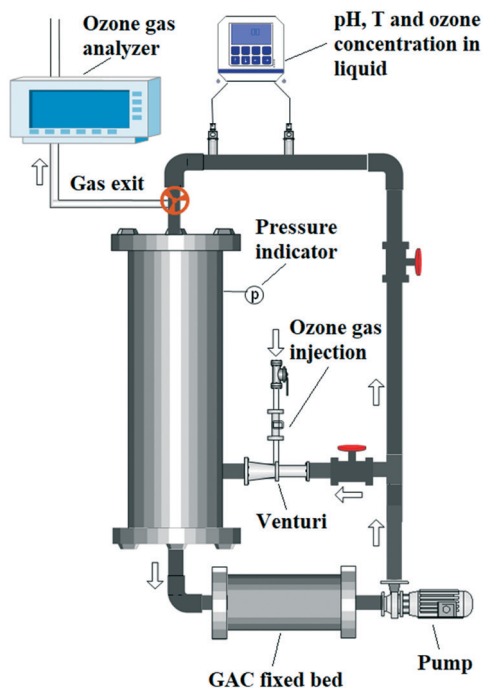


Fig. 1 Diagram of the Ad/Ox experimental equipment used to carry out ozonation assays with phenol.

also be thought of as the efficiency of the global ozonisation process, involving several stages of mass transfer and chemical reactions. Fig. 2 shows a resistance model of the mass transfer and chemical reaction stages involved in the global ozonisation process.

According to Fig. 2, in this case, reactions occur simultaneously in the liquid and inside the activated carbon, in many cases conditioned by the ozone transfer rate through the liquid and in the solid.⁴² The total consumption of ozone in the process, which occurs both in the liquid phase and within the active carbon (see the green dotted line in Fig. 2), is given by:

$$N_{O_3} = K_G^*(P_{O_3} - 0) = K_G a_1 (P_{O_3} - P_{O_3}^*) = K_L^*(C_{O_3} - 0) = \frac{K_L^*}{He} (P_{O_3}^* - 0) \quad (11)$$

where K_G^* is the overall ozonisation process coefficient, including the material transfer and chemical reaction stages in the total parallel-series system (Fig. 2), collected through the constants K_G and K_L^* . Consequently, the ozone transfer rate, N_{O_3} , is directly proportional to the driving force of the ozone partial pressure, P_{O_3} .

The overall gas-liquid mass transfer coefficient, $K_G a_1$, can be expressed in terms of the individual liquid and gas coefficients ($k_L a_1$ and $k_G a_1$; double film theory). Thus, taking into account Henry's constant, He , corresponding to the G-L equilibrium, we have the following equation:

$$K_G a_1 (P_{O_3} - P_{O_3}^*) = k_G a_1 (P_{O_3} - P_{O_3,i}) = k_L a_1 (C_{O_3,i} - C_{O_3}) = \frac{k_L}{He} a_1 (P_{O_3,i} - P_{O_3}^*) \quad (12)$$

where $P_{O_3,i}$ is the partial pressure of ozone at the G-L interface, in equilibrium with that of the liquid interface, $C_{O_3,i}$.

The ozone transferred to the liquid is consumed through the chemical reaction produced in the liquid, $N_{O_3}^I$ (see the discontinuous blue line in Fig. 2), and through the reaction in the active carbon, $N_{O_3}^{II}$, according to the equations:

$$N_{O_3}^I = k_{c,L} \cdot C_{O_3} \cdot C_P = \frac{k_{c,L} \cdot C_P}{He} (P_{O_3}^* - 0) \quad (13)$$

$$N_{O_3}^{II} = k_{c,S} Z_{O_3} Z_P w^2 = \frac{k_{c,S} Z_P}{m} (C_{O_3}^* - 0) = \frac{k_{c,S} Z_P}{m He} (P_{O_3}^* - 0) \quad (14)$$

Consequently, the overall ozone consumption rate, N_{O_3} (the sum of $N_{O_3}^I$ and $N_{O_3}^{II}$), depends on the kinetic constants indicated in eqn (13) and (14), equalizing the ozone transferred from the gas to the liquid. Thus, $N_{O_3}^I$ can be expressed as a function of the diffusional parameters of ozone, by combining eqn (11)–(13), to give:

$$N_{O_3}^I = \frac{(P_{O_3} - 0)}{\frac{1}{k_G a_1} + \frac{He}{k_L a_1} + \frac{He}{k_c C_P}} \quad (15)$$

The consumption of ozone in the solid, $N_{O_3}^{II}$, is described by the constant K_L^S , which includes the stages of ozone transfer and the chemical reaction inside the active carbon particles, according to:

$$K_L^S (C_{O_3,L} - 0) = k_L a_2 (C_{O_3} - C_{O_3,i}) = k_S a_2 (Z_{O_3,i} - Z_{O_3}) = k_{c,S} (Z_{O_3} - 0) \quad (16)$$

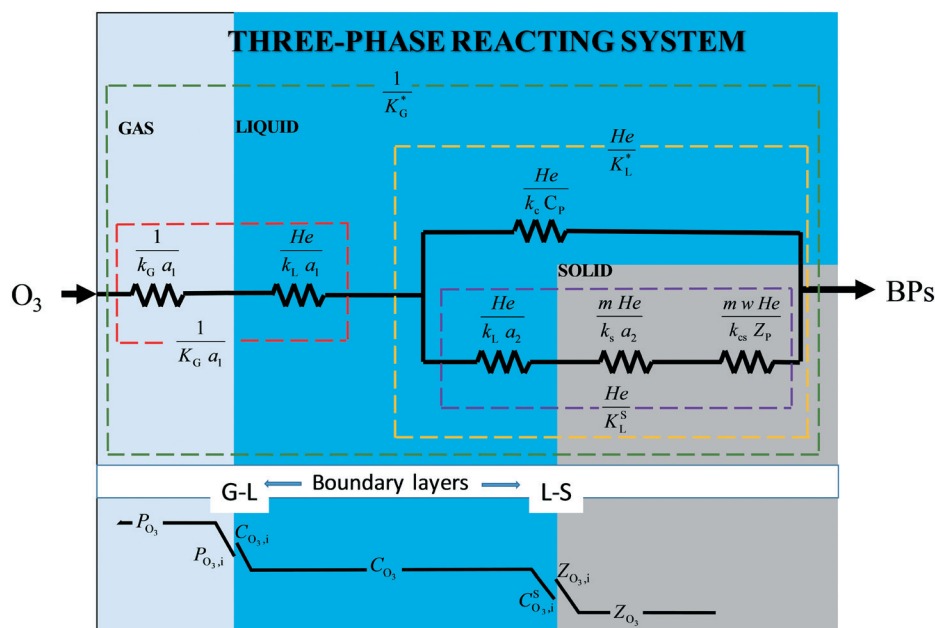


Fig. 2 Ozone transfer phenomena and chemical reaction resistances involved in the Ad/Ox process.

If Henry's constant, He , in the equilibrium G-L is considered together with the L-S equilibrium constant, m , according to:

$$He = P_{O_3}^*/C_{O_3} = P_{O_3,i}/C_{O_3,i} = P_{O_3}^{\wedge}/C_{O_3}^* \quad (17)$$

$$m = C_{O_3,i}^S/Z_{O_3,i} = C_{O_3}^*/Z_{O_3}, \quad (18)$$

Eqn (16) can be expressed as a function of the ozone partial pressure, according to:

$$\begin{aligned} \frac{K_L^S}{He} (P_{O_3}^* - 0) &= \frac{k_L a_2}{He} (P_{O_3}^* - P_{O_3,i}) = \frac{k_S a_2}{m He} (P_{O_3,i} - P_{O_3}^{\wedge}) \\ &= \frac{k_{c,S}}{m He} (P_{O_3}^{\wedge} - 0) \end{aligned} \quad (19)$$

Consequently, $N_{O_3}^{II}$ can also be expressed as a function of the ozone transport parameters, according to:

$$N_{O_3}^{II} = \frac{(P_{O_3} - 0)}{\frac{1}{k_G a_1} + \frac{He}{k_L a_1} + \frac{He}{k_L^S}} \quad (20)$$

Moreover, the variation of phenol concentration, considering the oxidation terms in the liquid and on the surface of the active carbon, together with the removal by adsorption, gives the following general expression:

$$\left(-\frac{dC_P}{dt}\right) = \left(-\frac{dC_P}{dt}\right)_{ox,L} + \left(-\frac{dC_P}{dt}\right)_{ox,S} + \left(-\frac{dC_P}{dt}\right)_{ads} \quad (21)$$

The proposed model is based on the following assumptions:

- The liquid and solid oxidation rates are considered to be pseudo-first order with respect to phenol.

- The pseudo-first order constants are affected by the ozone transport parameters, which leads to certain ozone concentrations: C_{O_3} (in the liquid) and Z_{O_3} (in the solid). Both C_{O_3} and Z_{O_3} are considered constants once they have reached steady state.

- Activated carbon consists of porous particles in which ozone and phenol diffusion mechanisms occur. Therefore, either for phenol or ozone, a concentration gradient is assumed to exist from the periphery to the inside of the particle.

- The adsorption kinetics are affected by the operational conditions even during the process.

Redefining the terms of eqn (13) and (14), according to eqn (10), through the term z , eqn (22) and (23) are obtained, which describe the variation of phenol concentration by oxidation in both the liquid phase and on the surface of the solid.

$$\left(-\frac{dC_P}{dt}\right)_{ox,L} = z k_{c,L} C_{O_3} C_P = k_{oxL} C_P \quad (22)$$

$$\left(-\frac{dC_P}{dt}\right)_{ox,S} = z k_{c,S} Z_{O_3} Z_P w^2 = k_{oxS} Z_P w \quad (23)$$

As can be seen, the above equations contain k_{oxL} and k_{oxS} constants, the factor z , the elemental kinetic constants $k_{c,L}$ and $k_{c,S}$, and the ozone concentrations C_{O_3} and Z_{O_3} . These ozone concentrations can be assumed constant after the initial transitory period.⁴² If the diffusional L-S resistances are negligible, the ozone concentration in the solid is in equilibrium with that of the liquid, according to eqn (18), to obtain:

$$C_{O_3}^* = m Z_{O_3} \approx C_{O_3} \quad (24)$$

The phenol concentration in the activated carbon, Z_P , depends on the adsorption process rate. In quick adsorption processes, Z_P is assumed to be in equilibrium with the phenol concentration in the liquid, C_P and is estimated from the Freundlich equation:⁴³

$$Z_P = Z_{P,\infty} = K_F (C_P)^{\frac{1}{n_F}} \quad (25)$$

where C_P is the phenol concentration in the liquid, in equilibrium with Z_P , or phenol adsorbed in the active carbon particle. The constant K_F indicates the AC adsorption capacity, and n_F is the heterogeneity factor. However, the phenol concentration in the solid, Z_P , usually depends on the adsorption kinetics of the process and does not reach equilibrium during the process. On the other hand, the AC adsorption kinetics with ozone change significantly compared to the adsorption process without it.⁴⁴ This will be demonstrated later in this work with the estimated reaction and adsorption kinetic constants.

To describe the phenol adsorption kinetics dependence on AC, a pseudo-second order model is chosen, which has been conveniently verified in previous works,⁴⁴ according to:

$$\left(-\frac{dC_P}{dt}\right)_{ads} = \left(-\frac{dZ_P}{dt}\right)_{ads} w = k_{ads} (Z_{P,\infty} - Z_P)^2 w \quad (26)$$

where k_{ads} ($g\ mg^{-1}\ min^{-1}$) is the pseudo-second order kinetic constant. From eqn (22), (23) and (26), eqn (27) is deduced to express the phenol removal in the Ad/Ox process.

$$-\frac{dC_P}{dt} = k_{oxL} C_P + k_{oxS} Z_P w + k_{ads} (Z_{P,\infty} - Z_P)^2 w \quad (27)$$

The adsorption phenomenon that occurs together with ozonisation may be quite different from that observed in its absence, so parameters k_{ads} and $Z_{P,\infty}$ should not be confused with those observed in eqn (32) and (36).

4. Results and discussion

4.1. Nitrogen adsorption studies

Fig. 3 shows the adsorption-desorption isotherms of Kemisorb® 530 GAC and PAC. According to the shape of the

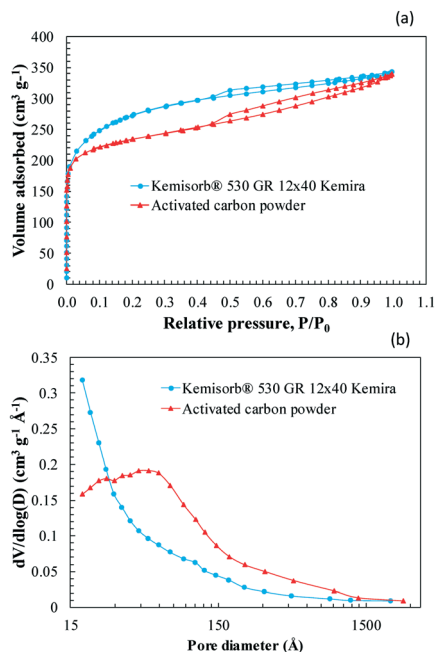


Fig. 3 Activated carbon characterization: (a) nitrogen adsorption-desorption isotherms and (b) pore size distribution of Kemisorb® 530 GAC and powder activated carbon calculated using the BJH model.

curves in Fig. 3a, a type I isotherm is observed, in which at low relative pressures the amount of adsorbed nitrogen increases with the relative pressure due to the high interaction between active carbon and nitrogen, but without reaching any plateau, *i.e.*, the solid does not clearly present the limit of its adsorption capacity. This is probably because thermodynamic equilibrium is not reached due to incomplete monolayer formation.⁴⁵

Moreover, a hysteresis cycle was observed, which reveals a capillary condensation effect on the pores of the activated carbons, associated with the mesoporous part of the solid.

The physical properties of the activated carbons used in this work are shown in Table 2. GAC Kemisorb® 530 presents a BET surface area of 961.5 m² g⁻¹, greater than that of PAC, which is 832.3 m² g⁻¹. However, PAC has a higher mesopore volume ($V_M = 0.20$ cm³ g⁻¹) and average pore diameter (35.0 Å), and should have greater adsorption capacity than GAC Kemisorb® 530 for higher molecular weight compound removal. The micropore volume value of PAC corresponds to the macroporous region.⁴⁶

4.2. Point-zero charge determination

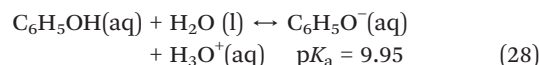
During the phenol adsorption processes, the AC characteristics, such as molecular size, solubility, pK_a and adsorbate nature (*i.e.*, aromatic or not), influence the adsorption process. As indicated in the previous section, the molecular size controls the contaminant accessibility to the AC pores together with solubility, a consequence of hydrophobic interactions. These are greatly conditioned by

the contaminant pK_a , and closely linked to the solution pH, as explained below.

Thus, the efficiency of the activated carbon in the Ad/Ox process can be affected by its point of zero charge (PZC). A surface charge is at its point of zero charge when the surface charge density equals zero. It is a negative logarithmic value for the activity of the charge-determining ions in the bulk phase.⁴⁷ According to Ferreiro *et al.*,²⁵ when the surface of the catalyst is positively charged, it favours interactions with anionic pollutants ($pH < pH_{pzc}$), whereas a negatively charged surface promotes interactions with cationic pollutants, due to the ionization of oxygenated functional groups ($pH > pH_{pzc}$).²⁶

The experimental curve obtained by Silva *et al.* describes the method for Kemisorb® 530 GAC and PAC, as shown in Fig. 4.³⁶ The point of zero charge, pH_{pzc} , of Kemisorb® 530 GAC was 9.69, whereas that of PAC was 10.19. The pH_{pzc} values obtained are the same as the typical values of fresh activated carbon (between 8 and 10), obtained by authors such as Valdés & Zaror and Adam.^{37,48} This high PZC value is beneficial, since an increase in the acidity of the AC surface results in a decrease in the amount of phenol adsorbed.⁴⁹

The point of zero charge together with the speciation of phenol, which is dependent on the solution pH, may influence the adsorptive behaviour of the activated carbon in terms of adsorption capacity. The acid ionization equation of phenol is shown in eqn (28):⁵⁰



According to the pK_a value shown in eqn (28), phenol is a very weak acid. For a pH lower than 9.95, the phenoxide ion concentration is negligible, while for a pH higher than 9.95, the phenol will be ionized and consequently the adsorption on the activated carbon will decrease due to electrostatic repulsion interactions. Thus, the overall reactivity of phenol towards ozone increases from 1300 M⁻¹ s⁻¹ at $pH < 9.9$ to 1.4×10^9 M⁻¹ s⁻¹ at $pH > 9.9$.^{51,52} Despite the favourable effect on ozonisation with alkaline pH, an industrial implementation

Table 2 Surface properties of the activated carbons studied

Property	Kemisorb® 530 GR 12x40 Kemira	Activated carbon powder
S_{BET} , m ² g ⁻¹	961.5	832.3
S_{ext} , m ² g ⁻¹	410.4	264.0
V_T , cm ³ g ⁻¹	0.38	0.44
V_{μ} , cm ³ g ⁻¹	0.24	0.24
V_M , cm ³ g ⁻¹	0.14	0.20
V_M/V_T , %	36.8	45.5
V_{μ}/V_T , %	63.2	54.5
D_P , Å	27.9	35.0

S_{BET} – BET surface area; S_{ext} – external surface area; V_T – total pore volume; V_{μ} – micropore volume; V_M – mesopore volume; V_M/V_T – mesopore percentage; V_{μ}/V_T – micropore percentage; D_P – average pore diameter.

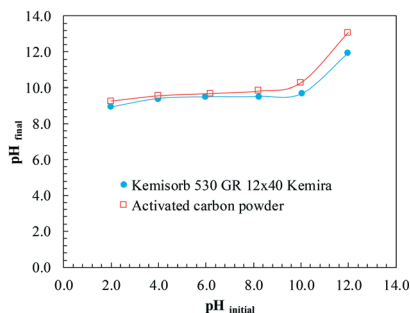


Fig. 4 Point of zero charge of Kemisorb® 530 and powder activated carbon determined by the acid-base titration method.

would be unviable for the following reasons: i) chemical operating costs would increase by 36.1%,⁵³ ii) the adsorption stage would not be favoured, iii) pH adjustment would require more contact or residence time to adjust a wide range of pH, iv) it would be environmentally unsustainable, as the discharge pH must be between 6.0 and 8.0.⁴⁴

4.3. Adsorption process of phenol on AC and thermodynamic aspects

Adsorption isotherms are used to evaluate the adsorption capacity of active carbons for a specific pollutant. This tool enables discrimination between different active carbons, evaluating the adsorption phenomenon, in order to select the most suitable AC for a desired application.⁴⁹ To analyse the adsorption phenomenon in the two activated carbons under study, the equilibrium data obtained were adjusted to widely used models such as the Langmuir, Freundlich and Dubinin-Radushkevich isotherms.⁵⁴ Fig. 5 shows the adsorption isotherms of phenol on Kemisorb® 530 and PAC at 15 °C, 25 °C and 35 °C at pH = 6.5.

As seen in Fig. 5a, PAC has an L-type isotherm without a plateau according to the classification made by Limousin *et al.*⁵⁵ This type of isotherm indicates that the ratio between the amount of adsorbed phenol and the solution concentration decreases with the increased concentration in the equilibrium. Furthermore, this isotherm does not clearly present the limit of its adsorption capacity. However, the granular activated carbon Kemisorb® 530 shows a C-type isotherm (Fig. 5b), characteristic of materials in which the ratio of q_e to C_e is almost constant at any concentration.

The mathematical representation of the three models mentioned is shown below. Dubinin-Radushkevich's isotherm (D-R's model) is characteristic of single solute systems,³⁷ and much more general than Langmuir's isotherm since it assumes the homogeneity of the surface according to:⁵⁶

$$q_{\infty} = q_s \exp(-\beta \varepsilon^2) \quad (29)$$

where β is the activity coefficient related to the adsorption free energy E , expressed by:

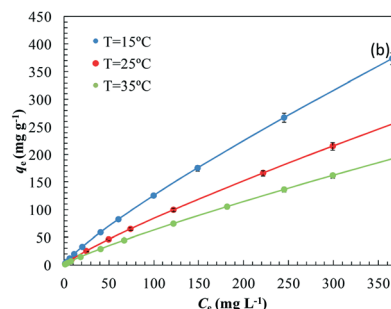
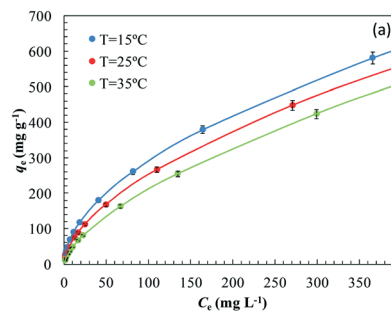


Fig. 5 Adsorption isotherms of phenol at pH = 6.5 on two types of activated carbons at different temperatures fitted to the Freundlich isotherm model: (a) powder activated carbon and (b) Kemisorb® 530.

$$E = \frac{1}{\sqrt{2\beta}} \quad (30)$$

where ε is the Polanyi potential, expressed as a function of temperature through:⁵⁷

$$\varepsilon = RT \ln \left(1 + \frac{1}{C_{\infty}} \right) \quad (31)$$

The Freundlich equation is given by:⁵⁸

$$q_{\infty} = K_F C_{\infty}^{\frac{1}{n_F}}, \quad (32)$$

in which n_F refers to the process irreversibility, so values clearly greater than one mean spontaneous adsorption.

Langmuir's model assumes the formation of a monolayer on the surface of activated carbon with minimal interaction among the adsorbate molecules (phenol), and the adsorption sites having the same adsorption energy. The Langmuir equation is given by Enniya *et al.*:⁵⁹

$$q_{\infty} = q_{\max} \frac{K_L C_{\infty}}{1 + K_L C_{\infty}} \quad (33)$$

where K_L is the equilibrium constant related to the affinity of the binding sites and adsorption nature, and q_{\max} is the monolayer adsorption capacity.

Table 3 shows the adjustment parameters obtained using the different adsorption models. Due to the inherent bias resulting from linearization, the isotherm and kinetics parameters were determined by the non-linear regression method. The method uses an optimization routine to maximize the coefficient of determination, between the experimental data and isotherm model.⁶⁰ Based on the non-

Table 3 Adsorption isotherm parameters for phenol adsorption on activated carbon powder and Kemisorb® 530 at different temperatures

Adsorbent	Activated carbon powder			Kemisorb® 530 GR 12x40 Kemira		
	Temperature, °C			Temperature, °C		
Isotherm model	15	25	35	15	25	35
Langmuir						
K_L , L mg ⁻¹	0.125	0.016	0.0060	0.029	0.007	0.001
q_{max} , mg g ⁻¹	582.34	404.10	365.37	401.02	248.71	113.93
R^2	0.981	0.982	0.984	0.995	0.993	0.987
Freundlich						
K_F , (mg g ⁻¹) (L mg ⁻¹) ^{1/n}	25.35	17.42	11.14	2.55	1.60	1.17
n_F	1.88	1.76	1.60	1.20	1.17	1.13
R^2	0.995	0.991	0.993	0.991	0.989	0.991
Dubinin–Radushkevich						
q_s , mg g ⁻¹	430.88	403.14	376.35	247.61	148.57	106.54
β , mol ² kJ ⁻²	194.38	320.83	347.25	170.71	235.45	415.51
E , kJ mol ⁻¹	0.050	0.039	0.037	0.054	0.046	0.034
R^2	0.763	0.796	0.879	0.934	0.969	0.971

linear regression analysis of the experimental data obtained from phenol adsorption, it may be inferred, with a determination coefficient of $R^2 \cong 0.98$, that the phenol adsorption on either PAC or GAC Kemisorb® 530 GR is fairly described with Freundlich's model for all studied temperatures. Moreover, n_F is greater than one for the two types of carbons used, proving a favourable adsorption process.⁵⁶

According to D–R's model parameters shown in Table 3, the adsorption energy value is much higher for GAC Kemisorb® 530 than for powdered activated carbon, proving that adsorption on PAC is more favoured than on Kemisorb® 530.

Finally, as far as the parameters obtained from Langmuir's model are concerned, the maximum adsorption capacity of phenol, q_{max} , increases as the temperature decreases from 365.37 mg g⁻¹ to 582.34 mg g⁻¹, on powdered activated carbon, and from 113.93 mg g⁻¹ to 401.02 mg g⁻¹ on GAC Kemisorb® 530, proving that adsorption on both carbons is exothermic. In addition, the low values of Langmuir's equilibrium constant suggest a weak interaction of phenol with the surface of the two types of carbons, as observed in Table 3. The separation factor obtained in both carbons indicates that the adsorption process is favourable, as predicted by Freundlich's model.

The maximum amounts of adsorbed phenol, q_{max} , of PAC and GAC are compared with others from the bibliography study by Ma *et al.*⁶¹ The carbons selected for this work have q_{max} values of 582.34 mg g⁻¹ for PAC and 401.02 mg g⁻¹ for GAC Kemisorb® 530, against those of other materials such as ACs from bamboo (with 59.62 mg g⁻¹) or from coconut shell (with 45.45 mg g⁻¹). Nevertheless, the latter two have larger specific surface areas (over 1000 m² g⁻¹ versus 900 m² g⁻¹ for the carbons studied here). Moreover, the ACs referred to by Ma *et al.*⁶¹ have an average pore diameter lower than 27 Å (microporosity), and consequently, the accessibility of molecules such as phenol is impeded. Therefore, carbons with high microporosity (unlike the ones studied in this

work) present a greater diffusion resistance and are not suitable for phenol removal.

PAC and GAC adsorption was analysed following three different kinetic models: pseudo-first order, pseudo-second order and intraparticle diffusion. Fig. 6 shows the evolution of the adsorption kinetics of phenol on PAC and GAC Kemisorb® 530 GR at 15 °C, 25 °C and 35 °C, maintaining pH = 6.5 in all cases.

The pseudo first-order kinetic model is given by eqn (34), according to Markandeya *et al.*⁴³

$$\frac{dq_t}{dt} = k_1(q_\infty - q_t) \quad (34)$$

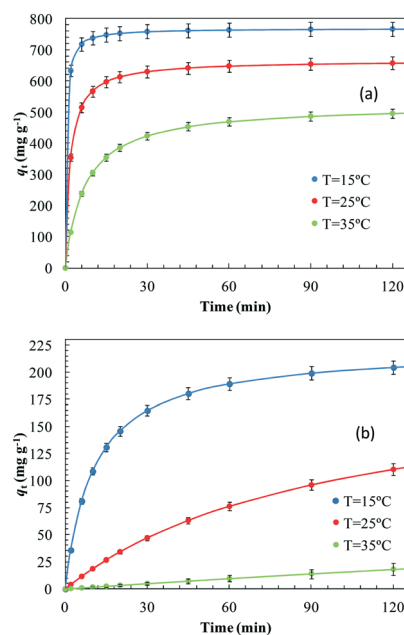


Fig. 6 Modelling of a pseudo-second-order kinetics of the adsorption process onto: (a) powdered activated carbon and (b) GAC Kemisorb® 530 GR.

where k_1 is the pseudo-first-order rate constant. Integrating and linearizing eqn (34) for the boundary conditions, $q_t = 0$ at $t = 0$, leads to the following expression:

$$\log(q_\infty - q_t) = \log q_\infty - \frac{k_1}{2.303} t \quad (35)$$

The pseudo-second-order model is represented as:⁶²

$$\frac{dq_t}{dt} = k_2(q_\infty - q_t)^2 \quad (36)$$

where k_2 is the pseudo-second-order rate constant. Integrating and rearranging eqn (36) for the initial conditions, $q_t = 0$ at $t = 0$, the following equation is obtained:

$$\frac{t}{q_t} = \frac{1}{k_2 q_\infty^2} + \frac{1}{q_\infty} t \quad (37)$$

Finally, the intraparticle diffusion model in a dimensionless form is given by:⁶³

$$\frac{\partial C_p}{\partial t} = \frac{1}{\eta^S} \frac{\partial}{\partial \eta} \left(\eta^S \frac{\partial C_p}{\partial \eta} \right) \quad (38)$$

where τ is the dimensionless time defined in eqn (39), η is the dimensionless spatial variable defined in eqn (40) and S is a particle geometry constant ($S = 2$ for a sphere).

$$\tau = \frac{D_{app}}{R_A^2} t \quad (39)$$

$$\eta = r_A/R_A \quad (40)$$

The defined the apparent diffusivity (D_{app}) in eqn (39) considers two diffusion coefficients, fluid and surface diffusivities. The resolution of eqn (38) was carried out using the FlexPDE® calculation tool. It was considered the initial solute concentration inside particle is equal to zero and that r_A or η equal to zero in the particle centre.

Table 4 shows the fit parameters obtained for the three kinetic models proposed for 15, 25 and 35 °C.

The regression analysis of experimental data obtained from phenol adsorption shows a determination coefficient of $R^2 \cong 0.99$, indicating that the pseudo-second-order model is

best at describing the phenol adsorption kinetics either for PAC or GAC Kemisorb® 530. According to Ho and McKay,⁶² adsorption cases following the second-order model demonstrate a chemical-step controlled adsorption process. The mechanism of the adsorption phenomenon that takes place consists of the following stages:⁴⁴ (i) external mass transfer from the aqueous medium to the boundary film, (ii) mass transfer from the boundary film to the activated carbon external surface, (iii) mass transfer in the pores, (iv) adsorption onto activated carbon active sites, and v) internal diffusion.

In the intraparticle diffusion model, values of apparent diffusivity around $10^{-6} \text{ cm}^2 \text{ s}^{-1}$ were obtained, similar to those obtained by Schwaab *et al.*⁶³ However, the determination coefficient obtained with the fitting to this model was not satisfactory.

The above results were confirmed by the evaluation of thermodynamic parameters. Enthalpy, entropy and free energy changes in the adsorption mechanism were determined through the following expressions:⁵⁸

$$\Delta G^\circ = -RT \ln K_L \quad (41)$$

where ΔG° is the standard Gibbs free energy, R is the universal gas constant, T is the absolute temperature and K_L is the equilibrium constant. Enthalpy and entropy values were determined through the van't Hoff equation:^{56,59,64}

$$\ln \frac{K_L}{\gamma} = \frac{\Delta S^\circ}{R} - \frac{\Delta H^\circ}{R T} \quad (42)$$

where ΔS° is the entropy change, ΔH° is the enthalpy change associated with the adsorption process and γ is the coefficient of activity of the adsorbate. The equilibrium constant used in van't Hoff's equation corresponds to the Langmuir isotherm model fitted at different temperatures.⁶⁴ The value of the equilibrium constant of the Langmuir model in L mol^{-1} units and the activity coefficient for water-phenol system (1.64) were used to estimate the thermodynamic parameters.⁶⁵ The thermodynamic parameters of phenol adsorption on both ACs are given in Table 5.

Table 5 shows the negative enthalpy values determined for GAC Kemisorb® 530 and PAC, characteristic of an exothermic process. According to Adam and Thue *et al.*,^{37,66} enthalpy

Table 4 Kinetic parameters for the adsorption of phenol on activated carbon powder and Kemisorb® 530 at different temperatures

Adsorbent	Powder activated carbon			Kemisorb® 530 GR 12x40 Kemira		
	Temperature, °C			Temperature, °C		
Kinetic model	15	25	35	15	25	35
Pseudo-1st order						
k_1, min^{-1}	0.0167	0.0086	0.0010	0.0021	0.0012	0.0003
R^2	0.989	0.981	0.924	0.801	0.797	0.724
Pseudo-2nd order						
$k_2, \text{g mg}^{-1} \text{min}^{-1}$	3.07×10^{-3}	8.43×10^{-4}	2.67×10^{-4}	4.20×10^{-4}	4.96×10^{-5}	6.85×10^{-6}
R^2	0.995	0.996	0.993	0.990	0.997	0.995
Intraparticle diffusion						
$D_{app}, \text{cm}^2 \text{s}^{-1}$	7.03×10^{-6}	7.40×10^{-6}	7.78×10^{-6}	3.82×10^{-6}	4.02×10^{-6}	4.22×10^{-6}
R^2	0.879	0.851	0.897	0.900	0.899	0.881

Table 5 Thermodynamic parameters of phenol adsorption on both ACs

Adsorbent	$T, ^\circ\text{C}$	$\ln(K_L/\gamma)$	$\Delta H, \text{kJ mol}^{-1}$	$\Delta S, \text{J mol}^{-1} \text{K}^{-1}$	$\Delta G, \text{kJ mol}^{-1}$	$E_a, \text{kJ mol}^{-1}$	k_0
Kemisorb® 530	15	7.41	-124.02	367.91	-18.95	151.9	1.24×10^{-31}
	25	5.99			-16.08		
	35	4.04			-11.64		
PAC	15	8.83	-110.95	312.86	-22.35	90.15	1.36×10^{-19}
	25	6.82			-18.13		
	35	5.84			-16.23		

changes in the range 0–84 kJ mol⁻¹ indicate a physisorption mechanism, while values between 84 and 420 kJ mol⁻¹ are typical of chemisorption mechanisms. In the studied activated carbons, an enthalpy value was obtained corresponding to a chemisorption mechanism. The entropy change (367.91 J mol⁻¹ K⁻¹ for Kemisorb® 530 and 312.86 J mol⁻¹ K⁻¹ for PAC) reflects the randomness increase between the solution and solid interface and, consequently, structural changes in the activated carbons and phenol.^{44,59}

The negative free energy change values indicate the feasibility and the spontaneous nature of phenol adsorption on both activated carbons. The observed free energy increment, from -18.95 to -11.64 kJ mol⁻¹ for GAC Kemisorb® 530 and from -22.35 to -16.23 kJ mol⁻¹ for PAC, when the temperature increases from 15 to 35 °C, proves that better adsorption occurs at low temperatures.

In addition, the activation energy was estimated from the kinetic data taken at 15, 25 and 35 °C. The activation energy value was estimated through the Arrhenius equation:⁶⁷

$$\ln k_2 = \ln k_0 - \frac{E_a}{R} \frac{1}{T}, \quad (43)$$

where k_0 is the frequency factor and E_a is the activation energy for the adsorption process. According to Ferreiro *et al.* and Fil *et al.*,^{44,68} E_a values are a consequence of the type of adsorption phenomenon. Values between 88 and 400 kJ mol⁻¹ correspond to a chemical adsorption. Thus, values of 151.9 kJ mol⁻¹ for GAC Kemisorb® 530 and 90.15 kJ mol⁻¹ for PAC correspond to chemisorption mechanisms.

4.4. Activated carbon activity comparison

This section discusses the results simultaneously obtained in an Ad/Ox process using a bed of activated carbon packed in a cartridge in the reactor, as seen in Fig. 1, compared with those from simple ozonation.

The operational conditions employed in the batch experiments were: $Q_G = 4.0 \text{ L min}^{-1}$, $C_{O_3,G} = 19.0 \text{ mg L}^{-1}$, $C_0 = 1000.0 \text{ mg L}^{-1}$, pH = 6.5 and $M = 500.0 \text{ g}$. First, the results obtained through a simple ozonation process were compared, and those obtained through an Ad/Ox process were analysed and are shown in Fig. 7.

Fig. 7 shows the phenol removal results with 100% removal in just 30 minutes for a 1000 mg L⁻¹ phenol concentration. Additionally, mineralization exceeding 80% was achieved (not shown in Fig. 7). Therefore, the results

indicate that the use of GAC in Ad/Ox processes gives superior results in phenol removal and mineralization, despite using a lower dose of ozone. The type of activated carbon (GAC or PAC) does not seem to influence the oxidation efficiency. The generation of radicals on the AC surface explains the higher speed of reaction in the liquid.^{15,30}

After the analysis of the first results about simple ozonation and the different types of sequential Ad/Ox processes, the appropriateness of the simultaneous Ad/Ox process with both GAC and PAC was postulated. Ad/Ox with GAC was selected for the remainder of the experiments because of the handling advantages of the granulated material. In addition, GAC Kemisorb® 530 is extensively used in water potabilization facilities due to, among other factors, its low cost, easy reuse and regeneration, and treatment unit, making it the most suitable type of activated carbon for fixed bed contact systems.⁶⁹ PAC is generally used in treatment plants with mixing units for coagulation purposes, where PAC is suspended in the water to be treated.⁷⁰

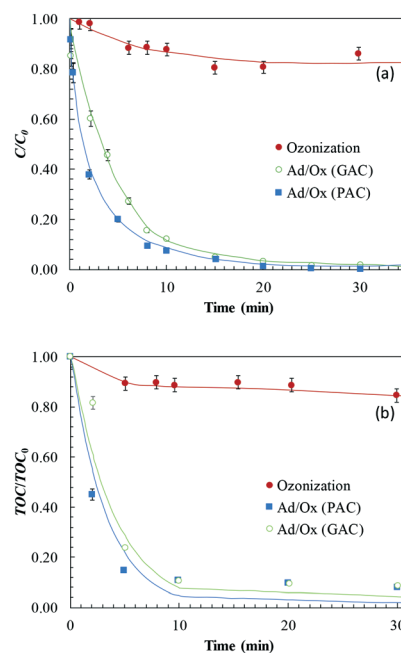


Fig. 7 Comparison of the degradation of phenol (a) and mineralisation (b) with ozonisation and Ad/Ox processes. Experimental conditions: $C_0 = 1000.0 \text{ mg L}^{-1}$, $Q_G = 4.0 \text{ L min}^{-1}$, $C_{O_3,G} = 19.0 \text{ mg L}^{-1}$, pH = 6.5, $V = 10.0 \text{ L}$, $T = 20 \text{ }^\circ\text{C}$, $m_{GAC} = 500.0 \text{ g}$.

4.5. Kinetic analysis of the Ad/Ox process

Ad/Ox ozonation experiments were performed under the ozone flow and concentration conditions indicated in the 'Experimental methods' section. The process was applied in all cases to a 1000.0 mg L⁻¹ phenol solution, varying the amount of GAC in the cartridge, using a mass of 250.0 g or 500.0 g according to the experiment.

The phenol degradation results for both primary degradation and mineralization were obtained by measuring the total organic carbon (TOC) in the treated solution. The degradation kinetics were adjusted to the proposed model in section 3, by solving eqn (19) and (21). The solution process for these equations involved the FlexPDE® calculation tool, a simulation programme used here to determine, through a corresponding fitting process, the kinetic constants of adsorption and ozonation and the modelled kinetics of phenol concentration and TOC during degradation. Because the fluid velocity is large enough to operate in a turbulent regime, it was assumed that the GAC load confined inside the cartridge (see Fig. 1) behaves as if it was perfectly distributed in the reactor, due to the vigorous agitation of the reaction medium through the recirculation system. Consequently, the kinetic parameters of oxidation in the liquid and solid and adsorption phenomena will be affected by the mixing conditions in the ozonator through G-L and L-S flows and the corresponding mass transfer parameters.

The initial conditions or values of the dependent variables involved in the differential equations at time zero (the starting time for the Ad/Ox phenol removal process) were defined before the calculus process. The concentration at any position within the reactor is $C_P = C_0 = 1000.0 \text{ mg L}^{-1}$ and therefore the load placed on the bed of activated carbon is zero, $Z_P = 0.0 \text{ mg g}^{-1}$. The programme simulates the degradation kinetics on the basis of the value of the initial variables, varying parameters to calculate k_{ads} , k_{oxL} and k_{oxS} to achieve the best fit to the experimental degradation kinetics.

Kinetics modelling of the experimental degradation was carried out for two different amounts of GAC, 250.0 and 500.0 g. In Fig. 8, fittings of the experimental data to the kinetic model proposed for the two different GAC quantities loaded in the reaction media are shown. Fig. 8 shows that an increase in catalyst dosage provides more active surface sites, thus facilitating the decomposition of ozone molecules into more hydroxyl radicals.⁷¹ The previously mentioned kinetic model was also employed in the analysis of mineralization. The TOC values were used in this case as the experimental results. Similar to the primary degradation, the TOC results were fitted to the proposed model; the results are shown in Fig. 8. The fitting result was good, yielding a determination coefficient of $R^2 = 0.95$ for primary degradation fitting and $R^2 = 0.99$ for mineralisation fitting. Similarly, Table 6 also shows the values of the obtained adsorption and oxidation kinetic constants to fit the experimental kinetics for a simultaneous Ad/Ox process.

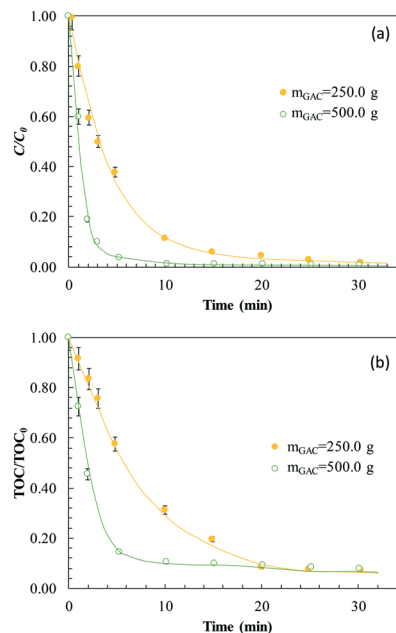


Fig. 8 Experimental and modelled kinetic profiles of phenol degradation in an Ad/Ox process for phenol degradation, varying the amount of GAC in the cartridge: (a) primary degradation of phenol and (b) evolution of mineralisation. Experimental conditions: $C_0 = 1000.0 \text{ mg L}^{-1}$, $Q_G = 4.0 \text{ L min}^{-1}$, $C_{O_3, G} = 19.0 \text{ mg L}^{-1}$, $\text{pH} = 6.5$, $V = 10.0 \text{ L}$, $T = 20 \text{ }^\circ\text{C}$.

Table 6 shows the constants obtained in the fitting process, which reveal that an increased GAC amount does not affect the constant of oxidation in the solid (which is similar in both cases), but contributes to an increased oxidation constant k_{oxL} in the liquid. This apparent constant includes the ozone concentration in the liquid and a coefficient z that depends strongly on the efficiency and concentration of OH^\cdot (see eqn (16)), clearly influenced by the catalytic activity of the GAC surface that competes with the adsorptive capacity. An equilibrium balance in GAC's dual role (adsorbent-reactive) is essential to develop a good Ad/Ox process efficiency.⁷²

Conversely, the value of the oxidation constant in the liquid, k_{oxL} , is halved in mineralization compared to the primary degradation value, because of the more refractory nature of degradation intermediates.⁷³ Another effect

Table 6 Summary of the kinetic constants of adsorption and oxidation related to the removal of phenol and mineralisation for 1 Ad/Ox cycle. Experimental conditions: $C_0 = 1000.0 \text{ mg L}^{-1}$, $Q_G = 4.0 \text{ L min}^{-1}$, $C_{O_3, G} = 19.0 \text{ mg L}^{-1}$, $\text{pH} = 6.5$, $V = 10.0 \text{ L}$, $T = 20 \text{ }^\circ\text{C}$

		GAC catalyst loading, g	
		250	500
Phenol removal	Kinetic parameter		
	$k_{\text{ads}} \times 10^5, \text{ min}^{-1}$	4.0	9.0
	$k_{\text{oxL}} \times 10^1, \text{ min}^{-1}$	2.5/1.0	7.0/1.0
	$k_{\text{oxS}} \times 10^1, (\text{mg L}^{-1})/(\text{mg min g}^{-1})$	0.1	0.1
Mineralisation	$k_{\text{ads}} \times 10^5, \text{ min}^{-1}$	4.0	9.0
	$k_{\text{oxL}} \times 10^1, \text{ min}^{-1}$	1.4/0.9	3.0/0.1
	$k_{\text{oxS}} \times 10^1, (\text{mg L}^{-1})/(\text{mg min g}^{-1})$	0.1	0.1

observed in k_{oxL} is a continuous decline as the process goes on, as a result of the progressive occupation of the GAC surface by the phenol and its derivatives.

4.6. Analysis of successive Ad/Ox cycles and regeneration

In view of the good results obtained with an Ad/Ox simultaneous process, the possibility of several consecutive cycles was assessed to see the extent of the changes in the GAC's adsorptive properties. It is interesting to quantify the number of consecutive cycles that can be performed using the same fixed bed of GAC, until it completely loses its adsorption capacity or deactivates. Initially, we performed two consecutive Ad/Ox cycles of 30 minutes each, with the same operational conditions as discussed above.

The same experimental conditions of the previous section were used, but with only 250.0 g of GAC for the consecutive cycle's experiments. The reactor was fed with 10 L of 1000.0 mg L⁻¹ phenol solution, covering 30 minutes of process to complete the first cycle (Ad/Ox 1). The solution was then extracted and a new 1000.0 mg L⁻¹ phenol solution was introduced, while keeping the previously loaded GAC.

According to Fig. 9, the fitting results were good, yielding a determination coefficient of $R^2 = 0.98$ for primary degradation fitting and $R^2 = 0.99$ for mineralization fitting. Fig. 9 shows that the results obtained for the primary degradation and for mineralization in cycles 1 and 2 are similar, above 95% in the first cycle and 80% in the second cycle. This result may have two possible causes. The first is that the amount of GAC in the cartridge is large with

respect to the phenol solution and does not reach saturation in the first cycle; there are active centres free to continue with the dissolution of phenol adsorption.²² The second effect is that ozone acts directly on the bed of GAC, cleaning active centres and allowing an additional quantity of phenol to be adsorbed.²⁹ In any case, the adsorption is altered by oxidation at the surface of the granular activated carbon.

After an analysis of the behaviour of two consecutive cycles to discover the advantages and disadvantages of a combined process compared with a simple process, the consecutive Ad/Ox cycles with the same activated carbon were analysed. The kinetic constants were also determined following the previously mentioned procedure for an Ad/Ox cycle, taking into account that the GAC in the cartridge was not changed from one cycle to another. Then, when an additional cycle starts, the amount of phenol adsorbed on the AC is nonzero; it was necessary to define a starting Z_p value, different and growing as the number of cycles increases. Thus, the Z_p to initiate the calculus process of the FlexPDE® software for the beginning of the second cycle is the final Z_p of the first cycle, and the value at the beginning of the third cycle will be the value at the end of the second cycle, and so on.

The adsorption and oxidation kinetic constants obtained for 6 consecutive Ad/Ox cycles with 250.0 and 500.0 g GAC amounts are presented in Tables 7 and 8, respectively.

In view of the results in Table 7, the oxidation occurs predominantly in the liquid since the kinetic constants in the liquid are considerably higher than those in the solid. This finding could be due to the contribution of the GAC to the reactions, only as free radical generators that are involved in the oxidation in the bulk liquid. However, the value of these constants decreases when the number of cycles increases, which can be explained by the decrease of free active centres, since the GAC deteriorates or becomes covered by phenol and other compounds by oxidation.^{26,44}

The kinetic adsorption constant on the solid surface k_{ads} and the corresponding oxidation constant k_{oxS} are fairly constant as the number of consecutive Ad/Ox cycles increases, since not enough phenol or intermediate compounds have been adsorbed to modify the surface of the activated carbon.⁷⁴ On the other hand, neither constant appears to be modified during mineralization. Accordingly, the reagent mechanisms on the GAC surface seem to be more significant for mineralization.⁷⁵

Using a fixed bed of 500.0 g of GAC, a considerable increase in the oxidation kinetic constant in the liquid was observed, nearly 100 times the kinetic constant of oxidation in the liquid in a non-catalytic ozonisation process, which is 0.09 min⁻¹, under the same operational conditions. This can be explained by a competition between the ozone and phenol flows at the GAC surface.⁷⁶ The dominance of the phenol flow involves the formation of layers of phenol on the GAC; the adsorption of this phenol will result in the deactivation of the GAC active centres and a decrease in its adsorptive and

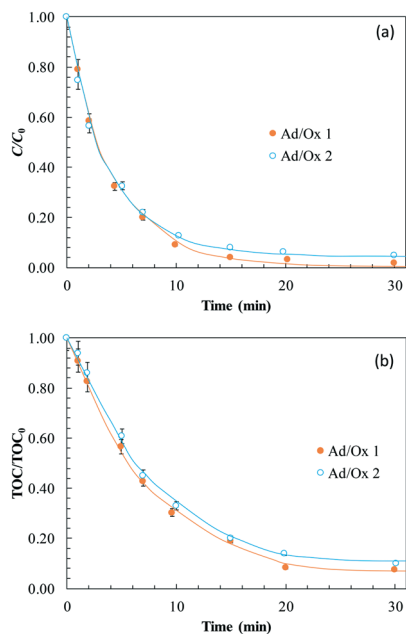


Fig. 9 Comparison of removal efficiencies in Ad/Ox consecutive cycles: (a) primary degradation of phenol and (b) mineralization or TOC removal. Experimental conditions: $C_0 = 1000.0$ mg L⁻¹, $Q_G = 4.0$ L min⁻¹, $C_{O_3,G} = 19.0$ mg L⁻¹, pH = 6.5, $V = 10.0$ L, $T = 20$ °C, $m_{\text{GAC}} = 250.0$ g.

Table 7 Summary of the adsorption and oxidation kinetic constants for the primary degradation of phenol solution and mineralisation, for 6 cycles with $m_{\text{GAC}} = 250.0$ g. Experimental conditions: $C_0 = 1000.0$ mg L⁻¹, $Q_G = 4.0$ L min⁻¹, $C_{\text{O}_3\text{G}} = 19.0$ mg L⁻¹, pH = 6.5, $V = 10.0$ L, $T = 20$ °C

Evolution	Kinetic parameter	Cycle no.					
		1	2	3	4	5	6
Phenol removal	$k_{\text{ads}} \times 10^5, \text{min}^{-1}$	4.0	4.0	4.0	4.0	4.0	4.0
	$k_{\text{oxL}} \times 10^4, \text{min}^{-1}$	2.5/1.0	2.2/1.0	1.6/0.8	1.1/0.6	1.0/0.4	0.8/0.2
	$k_{\text{oxS}} \times 10^1, (\text{mg L}^{-1})/(\text{mg min g}^{-1})$	0.1	0.1	0.1	0.1	0.1	0.1
Mineralisation	$k_{\text{ads}} \times 10^5, \text{min}^{-1}$	4.0	4.0	4.0	4.0	4.0	4.0
	$k_{\text{oxL}} \times 10^4, \text{min}^{-1}$	1.4/0.9	1.2/0.9	1.0/0.9	0.6/0.5	0.6/0.3	0.4/0.3
	$k_{\text{oxS}} \times 10^1, (\text{mg L}^{-1})/(\text{mg min g}^{-1})$	0.1	0.1	0.1	0.1	0.1	0.1

Table 8 Summary of adsorption and oxidation kinetic constants up to 6 cycles during oxidation of phenol solutions. Experimental conditions: $C_0 = 1000.0$ mg L⁻¹, $Q_G = 4.0$ L min⁻¹, $C_{\text{O}_3\text{G}} = 19.0$ mg L⁻¹, pH = 6.5, $V = 10.0$ L, $T = 20$ °C, $m_{\text{GAC}} = 500.0$ g

Evolution	Kinetic parameter	Cycle no.					
		1	2	3	4	5	6
Phenol removal	$k_{\text{ads}} \times 10^5, \text{min}^{-1}$	9.0	9.0	7.0/3.0	1.0	1.0	1.0
	$k_{\text{oxL}} \times 10^4, \text{min}^{-1}$	7.0/1.0	3.0/1.0	3.0/1.0	2.0/1.0	2.0/0.5	2.0/0.5
	$k_{\text{oxS}} \times 10^1, (\text{mg L}^{-1})/(\text{mg min g}^{-1})$	0.1	0.1	0.1	0.1	0.1	0.1
Mineralisation	$k_{\text{ads}} \times 10^5, \text{min}^{-1}$	9.0	9.0	7.0	1.0	1.0	1.0
	$k_{\text{oxL}} \times 10^4, \text{min}^{-1}$	3.0/0.1	2.5/0.1	2.0/0.1	1.8/0.1	1.6/0.1	1.4/0.1
	$k_{\text{oxS}} \times 10^1, (\text{mg L}^{-1})/(\text{mg min g}^{-1})$	0.1	0.1	0.1	0.1	0.1	0.1

reactive capacities.^{77,78} Otherwise, it would lead to an excess of radical activity, causing ineffective decomposition of ozone.¹⁵

The analysis of kinetic constants obtained for 250.0 and 500.0 g GAC shows that phenol oxidation is produced mostly in the liquid, although it should be noted that all of the constants shown in Tables 7 and 8 decrease as the number of cycles increases.

In the case of the adsorption kinetics, despite adsorption constants having the same order of magnitude, they also decrease when the number of cycles increases.⁷⁴ The only constant that holds a value independent of the number of cycles is k_{oxS} . Consequently, constant k_{oxL} includes both the oxidation occurring in the liquid and that as a result of the generation of radicals in the solid surface, and reflects most of the oxidative activity of the system as a whole. This constant decreases as the number of cycles increases; this relationship is a direct consequence of GAC deterioration. Thus, GAC active centres experience a continuous decrease in their catalyst activity and consequently a progressive decrease in radical generation.⁷²

Following the same procedure, mineralization was analysed and the corresponding constants were determined, using the same kinetic model as the primary degradation but replacing the phenol concentration with TOC values.

From Table 8, in the mineralization, as in the primary degradation, most secondary compounds oxidize in the liquid. The presence of GAC triggers a high quantity of radicals that cause a considerable increase the kinetic oxidation constant in the first cycles, when the active sites are free.⁷⁹ Nevertheless, the k_{oxL} values related to mineralisation in this case are lower, since the secondary compounds formed

in the reaction are much more refractory.⁸⁰ Remarkably, in the case of 250.0 g of GAC, both constant adsorption kinetics and the oxidation constant in the solid are constant and independent of the number of cycles. This behaviour is explained because the GAC reaches the complete development of its activity.⁴⁹

The increase in the kinetic oxidation constant in the liquid was twice that of the kinetic oxidation constant in the liquid in a non-catalytic ozonisation process, estimated to be 0.15 min^{-1} , while using a bed of 500.0 g of GAC, due to the greater radical activity of a GAC surface less occupied by adsorbed phenol. When comparing the kinetic constants obtained in the primary degradation with those in mineralization, for this last case, the constants are lower in all cases by the amount of intermediate products such as acetic acid,²⁰ which are increasingly refractory, as the reaction progresses.

A series of experiments of 9, 12 and 15 Ad/Ox cycles were performed, in which the phenol removal and the mineralization degree were observed and measured as the number of cycles increases (see Fig. 10). According to Fig. 10, the fitting results were good, presenting a determination coefficient of $R^2 = 0.97$ for primary degradation fitting and $R^2 = 0.99$ for mineralization fitting. Oxidation kinetics were slower as the GAC deteriorates to cycle number 15. The results seem to indicate that if the number of cycles continues to rise, the kinetics could approach the behaviour of non-catalytic ozonation. Consequently, the activated carbon would not have any reactive and catalytic activity, leading to a less efficient use of ozone.^{81,82}

Fig. 10 shows the progress of successive Ad/Ox 30 min cycles, which cause a gradual decrement in the phenol

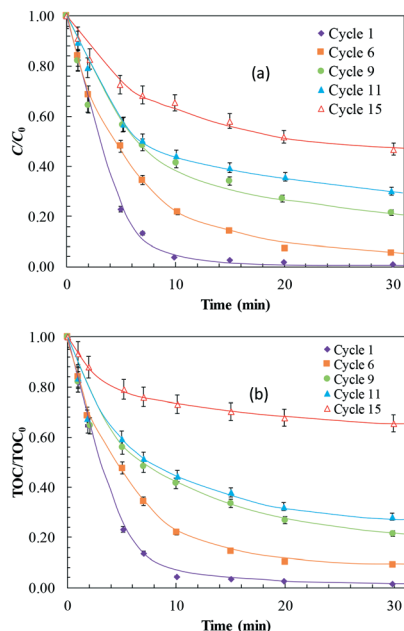


Fig. 10 Effect of the successive number of use cycles on an Ad/Ox process. (a) Phenol removal and (b) mineralisation. Experimental conditions: $C_0 = 1000.0 \text{ mg L}^{-1}$, $Q_G = 4.0 \text{ L min}^{-1}$, $C_{O_3,G} = 19.0 \text{ mg L}^{-1}$, $\text{pH} = 6.5$, $V = 10.0 \text{ L}$, $T = 20 \text{ }^\circ\text{C}$, $m_{\text{GAC}} = 500.0 \text{ g}$.

removal from the solution; *i.e.*, 100% phenol is eliminated in the first cycle, while in cycle number 9, it decreases to 70%, and after 15 cycles, Ad/Ox barely removes 40% of the initial phenol.

In addition to the phenol removal, the effect of increasing cycle number on mineralization was analysed. The mineralization degree is very similar to the primary degradation in the early cycles. The GAC characteristics do not change the very significant participation of the activated carbon surface in the degree of mineralization; it is about the same order as the early cycles (until cycle 9; see Fig. 10). Only when the number of cycles is high (>9) does the primary degradation become more intense than the mineralization as a result of a remarkable loss of GAC reactivity. Decreasing GAC reactivity significantly influences the mineralization and to a lesser extent the primary degradation, which is less dependent on the surface of the activated carbon.⁸³

Clearly, when the number of cycles increases, the Ad/Ox process tends to approach that of non-catalytic ozonation, either for primary degradation of phenol or for mineralization, which means that the GAC will deteriorate, losing efficiency and activity in the phenol degradation reaction system.

The surface area of the activated carbon is often coated by the adsorbate. Thus, when the GAC catalytic bed reaches the maximum phenol adsorption capacity, it must be regenerated to remove the phenol before reuse. In many occasions, the cost of the complete replacement of a fixed bed of GAC by another with pristine GAC is prohibitive.³⁸ The economics of a regeneration method could be a deciding factor when choosing the appropriate adsorbent for a given application.⁸⁴

Therefore, in order to design a more sustainable process, two chemical regeneration techniques were studied, regeneration with NaOH and with ozone. Among the advantages of a regenerative Ad/Ox processes over an Ad/Ox with AC replacement are the process robustness, waste reduction and a cost savings of up to 50%. The cost of replacing a virgin GAC is approximately between \$0.70 and \$1.20 per lb while the cost of regeneration ranges between \$0.50 and \$0.78 per lb. The operating costs of this operation depend on the wastewater effluent characteristics and the GAC adsorption capacity.⁸⁵

Fig. 11 compares the results of either phenol removal or mineralization degree, under the conditions described in this section for two Ad-Ox cycles with intermediate regeneration stages.

Even though NaOH regeneration is a widely used treatment,^{38,39} the post-regeneration mineralization obtained with this method was poor, losing 20% of the mineralizing capacity observed in the first cycle. This treatment is based on the modification of the surface polarity of the oxides in the carbon, since alkaline pH reduces the sorption forces. In addition, NaOH can promote decomposition or hydrolysis of phenol, reducing its sorption over GAC.⁸⁶ From the results shown in Fig. 11, this regeneration strategy does not appear to be suitable for recovering the initial properties of GAC.

Table 9 lists the physicochemical properties of the porous structure of virgin and regenerated GAC calculated from nitrogen adsorption data. It is clearly seen that the regeneration with NaOH produced a decrease of $37 \text{ m}^2 \text{ g}^{-1}$ in

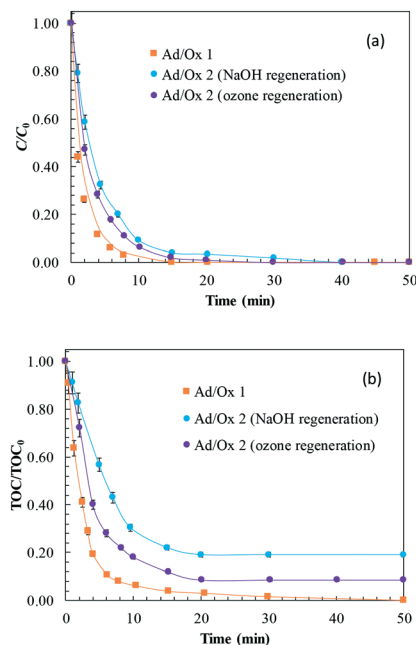


Fig. 11 Degradation kinetics of phenol: (a) primary and (b) mineralization, using the NaOH and ozone regeneration methods for GAC Chemisorb® 530. Experimental conditions: $C_0 = 1000.0 \text{ mg L}^{-1}$, $Q_G = 4.0 \text{ L min}^{-1}$, $C_{O_3,G} = 19.0 \text{ mg L}^{-1}$, $\text{pH} = 6.5$, $V = 10.0 \text{ L}$, $T = 20 \text{ }^\circ\text{C}$, $m_{\text{GAC}} = 500.0 \text{ g}$.

Table 9 Physicochemical properties of virgin GAC, after its use in phenol removal and after NaOH or ozone regeneration. Experimental conditions: $C_0 = 1000.0 \text{ mg L}^{-1}$, $Q_G = 4.0 \text{ L min}^{-1}$, $C_{O_3,G} = 19.0 \text{ mg L}^{-1}$, $\text{pH} = 6.5$, $V = 10.0 \text{ L}$, $T = 20 \text{ }^\circ\text{C}$, $m_{\text{GAC}} = 500.0 \text{ g}$

Property	Kemisorb® 530 GR 12x40 Kemira	Spent GAC	After NaOH regeneration	After O ₃ regeneration
S_{BET} , $\text{m}^2 \text{g}^{-1}$	961.5	830.5	924.5	955.5
S_{ext} , $\text{m}^2 \text{g}^{-1}$	410.4	289.2	358.1	407.1
V_{T} , $\text{cm}^3 \text{g}^{-1}$	0.38	0.26	0.30	0.37
V_{M} , $\text{cm}^3 \text{g}^{-1}$	0.24	0.15	0.17	0.21
V_{M} , $\text{cm}^3 \text{g}^{-1}$	0.14	0.11	0.13	0.16
$V_{\text{M}}/V_{\text{T}}$, %	36.8	42.3	43.3	43.0
$V_{\text{M}}/V_{\text{T}}$, %	63.2	57.7	56.7	56.8
D_{P} , Å	27.9	22.1	23.3	26.6
pH_{pzc}	9.69	7.61	8.18	9.35

the specific surface area and the volume of the micropore. The latest was also observed in ozone regeneration. A slight increase in the volume of mesopores was observed with ozone regeneration, as a consequence of the widening of micropores produced by ozone. Overall, some destruction of pores and a decrease of PZC from 9.69 to 8.18 for NaOH regeneration and 9.35 for ozone regeneration were observed. However, these changes are more pronounced in the NaOH regeneration. This can explain the lowering of the GAC adsorption properties. First, a lower specific surface area is available for adsorption. Second, according to Álvarez *et al.*,⁸⁷ the decrease of PZC is due to the increase in the polarity of the GAC external surface.

These structural changes in the GAC were also observed by Álvarez *et al.* and He *et al.*,^{40,41} where they observed a 15% decrease in the specific surface area and in the PZC. Conversely, regeneration with ozone resulted in a greater catalytic activity recovery, reaching a regeneration percentage of 91.5% due to degradation of phenol and phenol by-products. According to Álvarez *et al.* and Vega & Valdes,^{41,83} this result may be because the O₃/GAC ratio used during the regeneration stage leads to a lower formation of acidic oxygen groups on the surface (SOG), which are responsible for creating obstructions in the entrance of micropores, which may inhibit the adsorption of phenol during use after the regeneration stage.

Conclusions

The combination of adsorption and ozonation (an Ad/Ox process), simultaneously with PAC or GAC, produces an improvement in both the kinetics of phenol removal and the mineralization degree compared to a simple ozonation process, even when low ozone dosages are used. The elimination improvement is mainly related to the generation of radicals in the liquid phase.

GAC has a favourable effect, obtained through an Ad/Ox process, compared with a simple ozonation process. The improvement in the amount of phenol eliminated is evident with values exceeding 100% in all analysed cases. The kinetic constant of adsorption, k_{ads} , is a fundamental parameter to characterize the batch adsorption-ozonation

process. This, together with Freundlich adsorption parameters, is fundamental for adjusting the experimental data during the initial transient period. An appropriate combination of both, together with the ozonation kinetics concerning k_{oxL} in the liquid and k_{oxS} in the solid, determines not only the initial transient stage but also the time to reach a steady state.

The succession of consecutive cycles does not affect the oxidation constant observed in the solid, k_{oxS} , either for mineralization or for primary degradation, suggesting the decisive participation of surface phenomena in mineralization. In contrast, the value of the oxidation constant in the liquid, k_{oxL} , becomes halved during mineralization compared with phenol removal, because of the more refractory nature of degradation intermediates. Another observed effect involves the continuous decrease of k_{oxL} as a consequence of the progressive occupation of the GAC surface by the phenol and its derivatives during the process.

During simultaneous Ad/Ox, the predominant ozone action occurs in the liquid phase because of the greater oxidation constants than in the solid. The value of these liquid phase kinetic oxidation constants decreases as the number of cycles increases, likely due to the decrease in active centres in the GAC, causing the generation of radicals to decrease. Consequently, as the number of cycles increases, the removal efficiency approaches that obtained through simple ozonation, both for primary mineralization and phenol elimination, which indicates that the GAC has deteriorating adsorptive and reactive functions.

Nomenclature

a_1	Specific contact area G-L, m^{-1}
a_2	Specific contact area L-S, m^{-1}
β	Activity coefficient related to adsorption energy, $\text{mol}^2 \text{kJ}^{-2}$
C_0	Initial concentration of phenol, mg L^{-1}
C_∞	Equilibrium concentration of phenol, mg L^{-1}
C_{O_3}	Ozone concentration, mg L^{-1}
$C_{\text{O}_3,\text{L}}$	Ozone concentration in liquid, mg L^{-1}
$C_{\text{O}_3}^*$	Concentration of ozone in the equilibrium with the ozone adsorbed on the activated carbon, mg L^{-1}

$C_{O_3,i}$	Ozone concentration at the gas-liquid interface, mg L^{-1}	$P_{O_3}^*$	Partial pressure of the ozone in equilibrium with the adsorbed ozone on the solid, bar
C_t	Concentration of phenol at a given time t , mg L^{-1}	$P_{O_3,i}$	Partial ozone pressure at the gas-liquid interface, bar
C_P	Concentration of phenol in the liquid, mg L^{-1}	$P_{O_3}^\wedge$	Partial pressure of ozone in equilibrium with $C_{O_3}^*$, bar
$C_{O_3,G}$	Ozone concentration in the gas phase at the ozonator inlet, mg L^{-1}	q_t	Amount of phenol adsorbed at a time t , mg g^{-1}
$C_{O_3,i}^S$	Ozone concentration in the liquid-solid interface, mg L^{-1}	q_∞	Amount of phenol adsorbed on activated carbon, mg g^{-1}
D_{app}	Apparent diffusivity, $\text{cm}^2 \text{s}^{-1}$	q_s	Maximum amount of adsorbate that can be adsorbed on adsorbent, mg g^{-1}
ε	Polanyi potential	Q_G	Gas flow, L min^{-1}
E	Adsorption free energy per molecule, kJ mol^{-1}	R	Universal gas constant, $\text{J mol}^{-1} \text{K}^{-1}$
E_a	Activation energy, J mol^{-1}	r_A	Radius at a given distance, cm
γ	Activity coefficient, dimensionless	R_A	Radius of spherical particles, cm
ΔG	Free energy changes, J mol^{-1}	ΔS	Entropy change, $\text{J mol}^{-1} \text{K}^{-1}$
He	Henry's constant, bar L mg^{-1}	T	Temperature, K
ΔH	Enthalpy change, J mol^{-1}	t	Time, min
$k_{c,L}$	Elemental kinetic constant for the ozonation in the liquid, $\text{L mg}^{-1} \text{min}^{-1}$	τ	Dimensionless time, dimensionless
$k_{c,S}$	Elemental kinetic constant for the ozonation in the solid, $\text{L mg}^{-1} \text{min}^{-1}$	V	Volume of dissolution, L
K_G^*	Ozone transfer constant for the whole process, $\text{mg bar}^{-1} \text{L}^{-1} \text{min}^{-1}$	w	Activated carbon concentration, g L^{-1}
K_L^*	Global ozone transfer constant in the liquid including parallel reaction stages, $\text{mg bar}^{-1} \text{L}^{-1} \text{min}^{-1}$	z	Stoichiometric relation of the reaction between phenol and ozone
K_L^S	Global ozone transfer constant in the L-S interface, including the in-series reaction in the solid, $\text{mg bar}^{-1} \text{L}^{-1} \text{min}^{-1}$	Z_{O_3}	Ozone concentration onto activated carbon, mg L^{-1}
K_G	Global ozone transfer constant in the L-S interface, $\text{mg bar}^{-1} \text{L}^{-1} \text{min}^{-1}$	$Z_{O_3,i}$	Ozone concentration in the liquid-solid interface, mg g^{-1}
k_L	Liquid-layer ozone transfer constant in the L-S interface, $\text{mg bar}^{-1} \text{m}^{-2} \text{min}^{-1}$	Z_P	Concentration of phenol in the solid, mg g^{-1}
k_G	Ozone transfer constant in the G-L interface, $\text{mg bar}^{-1} \text{m}^{-2} \text{min}^{-1}$	$Z_{P,\infty}$	Amount of phenol adsorbed in the solid in equilibrium, mg g^{-1}
k_S	Solid-layer ozone transfer constant in the G-L interface, $\text{mg bar}^{-1} \text{m}^{-2} \text{min}^{-1}$		
k_{oxL}	Kinetic constant of phenol oxidation in the liquid, min^{-1}		
k_{oxS}	Kinetic constant of phenol oxidation in the solid, $(\text{mg L}^{-1})/(\text{mg min g}^{-1})$		
k_{ads}	Kinetic constant of phenol adsorption, min^{-1}		
K_F	Freundlich constant, $(\text{mg g}^{-1}) (\text{L mg}^{-1})^{1/n_F}$		
K_L	Langmuir equilibrium constant, L mg^{-1}		
k_1	Pseudo first order rate constant, min^{-1}		
k_2	Pseudo second order rate constant, $\text{g mg}^{-1} \text{min}^{-1}$		
k_0	Frequency factor		
m	Slope of the equilibrium line between the liquid and solid phase		
M	Adsorbent mass, g		
η	Dimensionless spatial variable, dimensionless		
N_{O_3}	Whole ozone consumption: $N_{O_3} = N_{O_3}^I + N_{O_3}^{II}$, $\text{mg L}^{-1} \text{min}^{-1}$		
$N_{O_3}^I, N_{O_3}^{II}$	Ozone consumption in the liquid, and in the solid, $\text{mg L}^{-1} \text{min}^{-1}$		
n_F	Heterogeneity factor, dimensionless		
P_{O_3}	Partial pressure of ozone in the gas phase, bar		

Conflicts of interest

There are no conflicts of interest to declare.

Acknowledgements

The authors are grateful to the University of the Basque Country for their financial support of this study through the PPGA19/63 project and C. Ferreiro's predoctoral PIF grant (PIF16/367).

References

- 1 S. Nakayama, K. Esaki, K. Namba, Y. Taniguchi and N. Tabata, *Ozone: Sci. Eng.*, 1979, **1**, 119–131.
- 2 B. Wang, H. Zhang, F. Wang, X. Xiong, K. Tian, Y. Sun and T. Yu, *Catalysts*, 2019, **9**, 241.
- 3 I. Bartalis, I. Siminiceanu and E. Arany, *Rev. Chim.*, 2011, **62**, 1047–1051.
- 4 W. Cheng, X. Quan, R. Li, J. Wu and Q. Zhao, *Ozone: Sci. Eng.*, 2018, **40**, 173–182.
- 5 S. Gupta, G. Ashrith, D. Chandra, A. K. Gupta, K. W. Finkel and J. S. Guntupalli, *Clin. Toxicol.*, 2008, **46**, 250–253.
- 6 O. US EPA, *Phenol CASRN 108-95-2 | IRIS | US EPA, ORD*, https://cfpub.epa.gov/ncea/iris2/chemicalLanding.cfm?substance_nmbr=88, (accessed July 2, 2019).

- 7 ECHA, *CoRAP list of substances*, <https://echa.europa.eu/information-on-chemicals/evaluation/community-rolling-action-plan/corap-list-of-substances>, (accessed July 2, 2019).
- 8 H. Babich and D. L. Davis, *Regul. Toxicol. Pharmacol.*, 1981, **1**, 90–109.
- 9 S. Mohammadi, A. Kargari, H. Sanaeepur, K. Abbassian, A. Najafi and E. Mofarrah, *Desalin. Water Treat.*, 2015, **53**, 2215–2234.
- 10 A. Hussain, S. K. Dubey and V. Kumar, *Water Resources and Industry*, 2015, **11**, 81–90.
- 11 Y.-P. Chiang, Y.-Y. Liang, C.-N. Chang and A. C. Chao, *Chemosphere*, 2006, **65**, 2395–2400.
- 12 Y. Z. Pi, J. Schumacher and M. Jekel, *Water Res.*, 2005, **39**, 83–88.
- 13 M. Sanchez-Polo, J. Rivera-Utrilla, G. Prados-Joya, M. A. Ferro-Garcia and I. Bautista-Toledo, *Water Res.*, 2008, **42**, 4163–4171.
- 14 M. A. Atieh, *APCBEE Proc.*, 2014, **10**, 136–141.
- 15 U. Jans and J. Hoigné, *Atmos. Environ.*, 2000, **34**, 1069–1085.
- 16 J. Rivera-Utrilla and M. Sanchez-Polo, *Appl. Catal., B*, 2002, **39**, 319–329.
- 17 C. A. Zaror, *J. Chem. Technol. Biotechnol.*, 1997, **70**, 21–28.
- 18 J. Nawrocki, *Appl. Catal., A*, 2013, **142–143**, 465–471.
- 19 F. J. Beltran, J. F. Garcia-Araya and I. Giraldez, *Appl. Catal., B*, 2006, **63**, 249–259.
- 20 I. Sanchez, F. Stuber, J. Font, A. Fortuny, A. Fabregat and C. Bengoa, *Chemosphere*, 2007, **68**, 338–344.
- 21 F. Lange, S. Cornelissen, D. Kubac, M. M. Sein, J. von Sonntag, C. B. Hannich, A. Golloch, H. J. Heipieper, M. Moeder and C. von Sonntag, *Chemosphere*, 2006, **65**, 17–23.
- 22 S. H. Lin and C. H. Wang, *Environ. Technol.*, 2003, **24**, 1031–1039.
- 23 X. Qu, J. Zheng and Y. Zhang, *J. Colloid Interface Sci.*, 2007, **309**, 429–434.
- 24 W. Pratarn, T. Pornsiri, S. Thanit, C. Tawatchai and T. Wiwut, *Chin. J. Chem. Eng.*, 2011, **19**, 76–82.
- 25 C. Ferreira, N. Villota, J. I. Lombraña and M. J. Rivero, *J. Cleaner Prod.*, 2019, **228**, 1282–1295.
- 26 H. Valdes, M. Sanchez-Polo, J. Rivera-Utrilla and C. A. Zaror, *Langmuir*, 2002, **18**, 2111–2116.
- 27 P. M. Alvarez, J. Pablo Pocostales and F. J. Beltran, *J. Hazard. Mater.*, 2011, **185**, 776–783.
- 28 L. Lei, L. Gu, X. Zhang and Y. Su, *Appl. Catal., A*, 2007, **327**, 287–294.
- 29 S. M. de Arruda Guelli Ulson de Souza, F. B. de Souza and A. A. Ulson de Souza, *Ozone: Sci. Eng.*, 2012, **34**, 259–268.
- 30 J. W. Choi and J. Chung, *J. Korean Soc. Environ. Eng.*, 2014, **36**, 311–316.
- 31 F. Luck, *Catal. Today*, 1999, **53**, 81–91.
- 32 M. C. Hidalgo, M. Maicu, J. A. Navío and G. Colón, *Catal. Today*, 2007, **129**, 43–49.
- 33 D.-H. Han, S.-Y. Cha and H.-Y. Yang, *Water Res.*, 2004, **38**, 2782–2790.
- 34 S. S. Sable, K. J. Shah, P.-C. Chiang and S.-L. Lo, *J. Taiwan Inst. Chem. Eng.*, 2018, **91**, 434–440.
- 35 R. Yi-fei, L. Han-jin, W. Chao-hai and L. Ling-feng, *J. Cent. South Univ. Technol.*, 2010, **17**, 300–306.
- 36 T. L. Silva, A. Ronix, O. Pezoti, L. S. Souza, P. K. T. Leandro, K. C. Bedin, K. K. Beltrame, A. L. Cazetta and V. C. Almeida, *Chem. Eng. J.*, 2016, **303**, 467–476.
- 37 O. E.-A. A. Adam, *Am. Chem. Sci. J.*, 2016, **16**, 1–13.
- 38 R. J. Martin and W. J. Ng, *Water Res.*, 1984, **18**, 59–73.
- 39 K. Sun, J. Jiang and J. Xu, *Iran. J. Chem. Chem. Eng.*, 2009, **28**, 79–83.
- 40 X. He, M. Elkouz, M. Inyang, E. Dickenson and E. C. Wert, *J. Hazard. Mater.*, 2017, **326**, 101–109.
- 41 P. M. Álvarez, F. J. Beltrán, V. Gómez-Serrano, J. Jaramillo and E. M. Rodríguez, *Water Res.*, 2004, **38**, 2155–2165.
- 42 C. Rodríguez, J. Ignacio Lombraña, A. de Luis and J. Sanz, *J. Chem. Technol. Biotechnol.*, 2017, **92**, 656–665.
- 43 S. P. Shukla Markandeya and G. C. Kisku, *Res. J. Environ. Toxicol.*, 2015, **9**, 320–331.
- 44 C. Ferreira, N. Villota, J. I. Lombraña, M. J. Rivero, V. Zúñiga and J. M. Rituerto, *Water*, 2019, **11**, 337.
- 45 K. S. W. Sing, D. H. Everett, R. A. W. Haul, L. Moscou, R. A. Pierotti, J. Rouquerol and T. Siemieniewska, in *Handbook of Heterogeneous Catalysis*, ed. G. Ertl, Wiley-VCH Verlag GmbH & Co. KGaA, Weinheim, Germany, 2008.
- 46 A. Omri and M. Benzina, *Journal de la Société Chimique de Tunisie*, 2012, **14**, 175–183.
- 47 J. Lyklema, *Pure Appl. Chem.*, 1991, **63**, 895–906.
- 48 H. Valdés and C. A. Zaror, *Ingeniare, Revista chilena de ingeniería*, 2010, vol. 18, pp. 38–43.
- 49 C. Moreno-Castilla, *Carbon*, 2004, **42**, 83–94.
- 50 W. H. Brown, C. S. Foote, B. L. Iverson and E. Anslyn, *Organic Chemistry*, Cengage Learning, 2011.
- 51 C. VonSonntag and U. VonGunten, *Chemistry of Ozone in Water and Wastewater Treatment: From Basic Principles to Applications*, Iwa Publishing, London, 2012.
- 52 F. J. Beltran, *Ozone Reaction Kinetics for Water and Wastewater Systems*, CRC Press, 2003.
- 53 D. G. Argo, *J. - Water Pollut. Control Fed.*, 1980, **52**, 750–759.
- 54 F. A. Banat, B. Al-Bashir, S. Al-Asheh and O. Hayajneh, *Environ. Pollut.*, 2000, **107**, 391–398.
- 55 G. Limousin, J.-P. Gaudet, L. Charlet, S. Szenknect, V. Barthès and M. Krimissa, *Appl. Geochem.*, 2007, **22**, 249–275.
- 56 S. Kaur, S. Rani and R. K. Mahajan, *J. Chem.*, 2013, 628582.
- 57 T. Allen, *Particle Size Measurement: Volume 2: Surface Area and Pore Size Determination.*, Springer Science & Business Media, 1996.
- 58 A. K. Meena, K. Kadirvelu, G. K. Mishra, C. Rajagopal and P. N. Nagar, *J. Hazard. Mater.*, 2008, **150**, 619–625.
- 59 I. Enniya, L. Rghioui and A. Jourani, *Sustainable Chem. Pharm.*, 2018, **7**, 9–16.
- 60 J. He, S. Hong, L. Zhang, F. Gan and Y.-S. Ho, *Fresenius Environ. Bull.*, 2010, **19**, 2651.
- 61 Y. Ma, N. Gao, W. Chu and C. Li, *Front. Environ. Sci. Eng.*, 2013, **7**, 158–165.
- 62 Y. S. Ho and G. McKay, *Process Biochem.*, 1999, **34**, 451–465.
- 63 M. Schwaab, E. Steffani, E. Barbosa-Coutinho and J. B. Severo Júnior, *Chem. Eng. Sci.*, 2017, **173**, 179–186.

- 64 E. C. Lima, A. Hosseini-Bandegharai, J. C. Moreno-Piraján and I. Anastopoulos, *J. Mol. Liq.*, 2019, **273**, 425–434.
- 65 K. Tochigi, T. Goto, S. Kurita and K. Kojima, *J. Chem. Eng. Jpn.*, 1997, **30**, 1116–1119.
- 66 P. S. Thue, A. C. Sophia, E. C. Lima, A. G. N. Wamba, W. S. de Alencar, G. S. dos Reis, F. S. Rodembusch and S. L. P. Dias, *J. Cleaner Prod.*, 2018, **171**, 30–44.
- 67 S. Banerjee and M. C. Chattopadhyaya, *Arabian J. Chem.*, 2017, **10**, S1629–S1638.
- 68 B. A. Fil, M. T. Yilmaz, S. Bayar and M. T. Elkoca, *Braz. J. Chem. Eng.*, 2014, **31**, 171–182.
- 69 J. García Prieto, P. Pérez Galende, J. M. Cachaza Silverio and M. Roig, *Water Sci. Technol.: Water Supply*, 2012, **13**, 74.
- 70 N. R. C. (US) S. D. W. Committee, An Evaluation of Activated Carbon for Drinking Water Treatment, National Academies Press (US), 1980.
- 71 S. P. Ghuge and A. K. Saroha, *J. Environ. Manage.*, 2018, **211**, 83–102.
- 72 T. Nunoura, G. H. Lee, Y. Matsumura and K. Yamamoto, *Chem. Eng. Sci.*, 2002, **57**, 3061–3071.
- 73 C. Huang and H. Shu, *J. Hazard. Mater.*, 1995, **41**, 47–64.
- 74 H. Valdes, M. Sanchez-Polo and C. A. Zaror, *Lat. Am. Appl. Res.*, 2003, **33**, 219–223.
- 75 M. E. Suarez-Ojeda, F. Stuber, A. Fortuny, A. Fabregat, J. Carrera and J. Font, *Appl. Catal., B*, 2005, **58**, 105–114.
- 76 Y. Guo, L. Yang and X. Wang, *J. Environ. Anal. Toxicol.*, 2012, **2**, 7.
- 77 A. Fortuny, J. Font and A. Fabregat, *Appl. Catal., B*, 1998, **19**, 165–173.
- 78 H. Delmas, C. Creanga, C. Julcour-Lebigue and A.-M. Wilhelm, *Chem. Eng. J.*, 2009, **152**, 189–194.
- 79 A. Rodríguez, R. Rosal, J. A. Perdigón-Melón, M. Mezcua, A. Agüera, M. D. Hernando, P. Letón, A. R. Fernández-Alba and E. García-Calvo, in *Emerging Contaminants from Industrial and Municipal Waste*, ed. D. Barceló and M. Petrovic, Springer Berlin Heidelberg, Berlin, Heidelberg, 2008, vol. 5S/2, pp. 127–175.
- 80 W. Xiong, N. Chen, C. Feng, Y. Liu, N. Ma, J. Deng, L. Xing and Y. Gao, *Environ. Sci. Pollut. Res.*, 2019, **26**, 21022–21033.
- 81 I. Quesada-Penate, C. Julcour-Lebigue, U. J. Jauregui-Haza, A. M. Wilhelm and H. Delmas, *J. Hazard. Mater.*, 2012, **221**, 131–138.
- 82 A. Eftaxias, J. Font, A. Fortuny, J. Giralt, A. Fabregat and F. Stuber, *Appl. Catal., B*, 2001, **33**, 175–190.
- 83 E. Vega and H. Valdes, *Microporous Mesoporous Mater.*, 2018, **259**, 1–8.
- 84 T. Dutta, T. Kim, K. Vellingiri, D. C. W. Tsang, J. R. Shon, K.-H. Kim and S. Kumar, *Chem. Eng. J.*, 2019, **364**, 514–529.
- 85 EPA, *United States Environmental Protection Agency*, https://cfpub.epa.gov/ncea/iris2/chemicalLanding.cfm?substance_nmbr=88, (accessed July 2, 2019).
- 86 P.-J. Lu, H.-C. Lin, W.-T. Yu and J.-M. Chern, *J. Taiwan Inst. Chem. Eng.*, 2011, **42**, 305–311.
- 87 P. M. Álvarez, F. J. Beltrán, F. J. Masa and J. P. Pocostales, *Appl. Catal., B*, 2009, **92**, 393–400.

3.7. 7. argitalpena. Application of a combined adsorption–ozonation process for phenolic wastewater treatment in a continuous fixed-bed reactor

3.7 kapitulua artikulu honi dagokio:

C. Ferreiro, A. de Luis, N. Villota, J.M. Lomas, J.I. Lombraña, L.M. Camarero. Application of a combined adsorption–ozonation process for phenolic wastewater treatment in a continuous fixed-bed reactor. *Catalysts*, 11, 8, 1014, 2021. DOI: 10.3390/catal11081014.

Article

Application of a Combined Adsorption–Ozonation Process for Phenolic Wastewater Treatment in a Continuous Fixed-Bed Reactor

Cristian Ferreiro ^{1,*} , Ana de Luis ² , Natalia Villota ³, Jose María Lomas ³, José Ignacio Lombrana ¹ 
and Luis Miguel Camarero ³

¹ Department of Chemical Engineering, Faculty of Science and Technology, University of the Basque Country UPV/EHU, Barrio Sarriena s/n, 48940 Leioa, Spain; ji.lombrana@ehu.eu

² Department of Chemical and Environmental Engineering, Faculty of Engineering in Bilbao, University of the Basque Country UPV/EHU, Plaza Ingeniero Torres Quevedo, 1, 48013 Bilbao, Spain; ana.deluis@ehu.eu

³ Department of Environmental and Chemical Engineering, Faculty of Engineering of Vitoria-Gasteiz, University of the Basque Country UPV/EHU, 01006 Vitoria-Gasteiz, Spain; natalia.villota@ehu.eu (N.V.); josemaria.lomas@ehu.eu (J.M.L.); luismiguel.camarero@ehu.eu (L.M.C.)

* Correspondence: cristian.ferreiro@ehu.eu; Tel.: +34-946-012-512

Abstract: This work studied the removal of phenol from industrial effluents through catalytic ozonation in the presence of granular activated carbon in a continuous fixed-bed reactor. Phenol was chosen as model pollutant because of its environmental impact and high toxicity. Based on the evolution of total organic carbon (TOC) and phenol concentration, a kinetic model was proposed to study the effect of the operational variables on the combined adsorption–oxidation (Ad/Ox) process. The proposed three-phase model expressed the oxidation phenomena in the liquid and the adsorption and oxidation on the surface of the granular activated carbon in the form of two kinetic constants, k_1 and k_2 respectively. The interpretation of the constants allow to study the benefits and behaviour of the use of activated carbon during the ozonisation process under different conditions affecting adsorption, oxidation, and mass transfer. Additionally, the calculated kinetic parameters helped to explain the observed changes in treatment efficiency. The results showed that phenol would be completely removed at an effective contact time of 3.71 min, operating at an alkaline pH of 11.0 and an ozone gas concentration of 19.0 mg L⁻¹. Under these conditions, a 97.0% decrease in the initial total organic carbon was observed.

Keywords: catalytic ozonation; three-phase modelling; fixed-bed reactor; wastewater treatment; phenol; granular activated carbon; Ad/Ox



Citation: Ferreiro, C.; de Luis, A.; Villota, N.; Lomas, J.M.; Lombrana, J.I.; Camarero, L.M. Application of a Combined Adsorption–Ozonation Process for Phenolic Wastewater Treatment in a Continuous Fixed-Bed Reactor. *Catalysts* **2021**, *11*, 1014. <https://doi.org/10.3390/catal11081014>

Academic Editor: Pedro B. Tavares

Received: 26 July 2021

Accepted: 21 August 2021

Published: 22 August 2021

Publisher's Note: MDPI stays neutral with regard to jurisdictional claims in published maps and institutional affiliations.



Copyright: © 2021 by the authors. Licensee MDPI, Basel, Switzerland. This article is an open access article distributed under the terms and conditions of the Creative Commons Attribution (CC BY) license (<https://creativecommons.org/licenses/by/4.0/>).

1. Introduction

Increases in the world population and the industrial revolution have brought many advantages to humanity. However, the intensive use and pollution of natural resources is leading many developed countries on the European and American continents towards an ecological deficit by the first third of the 21st century [1]. For this reason, national governments are encouraging the improvement of manufacturing production processes to increase the efficiency of water resources, as well as raw materials, in order to minimise the environmental impact of goods produced. In the context of water scarcity, the responsible use and management of wastewater is a desirable objective [2].

To safeguard the environment and public health, it is necessary the development and implementation of effective wastewater treatment that allow us to exceed the quality standards regulated by the U.S. Environmental Protection Agency's (EPA) Water Quality Standards Regulation (WQSR) [3] or the Water Framework Directive (Directive 2000/60/EC) of the European Union [4]. This is one of the highest-priority challenges that society must solve in the next decade. In fact, in 2015, the United Nations (UN) included SDG 6 on Clean

Water and Sanitation in the Sustainable Development Goals (SDGs) for the safe treatment of wastewater, to ensure the availability of water and its sustainable management for future generations [5].

A common example of this type of pollution is phenolic wastewater from the cellulose, oil refining, metallurgical, and plastics industries [6]. Phenol is an EPA priority compound listed on the Contaminant Candidate List 4 (CCL4) [7] of substances that are of high toxicity to humans and aquatic life. In humans, phenol has been reported as a potential source of skin irritation and kidney problems, and it has been associated with leukaemia and other mutagenic diseases [8]. Toxicity levels harmful to humans and aquatic life are between 9 and 25 mg L⁻¹ [9]. In many countries, such as Brazil, its discharge into the environment is limited to a concentration of 0.5 mg L⁻¹ and in the USA, to a concentration of less than 0.001 mg L⁻¹.

Different treatment methods have been proposed for the removal of phenols from wastewater, the most traditional being chemical oxidation by Fenton reaction (100%) [10], adsorption (26%) [6], extraction by liquid membrane emulsion (72%) [11], coagulation and precipitation (36.8%) [12], or activated sludge (87%) [9]. Other biological treatments [13], especially enzymatic treatments, using peroxidases (98%) [14] or tyrosinase (25%) [15] reduced the phenol concentration after 30 and 2 h respectively. Activated sludge is one of the most widely used treatments due to its low cost and ease of handling, but it is limited in applicability because the microorganisms, despite prior acclimatisation, are incapable of treating phenol concentrations of more than 100 mg L⁻¹. This is due to the low biodegradability of these effluents and the inhibitory effects that these concentrations of phenol have on the microorganisms [16]. Unfortunately, many wastewaters from chemical and petrochemical industries far exceed these concentrations. For example, in the coke industry and petrochemical plants concentrations in the range of 28–3900 mg L⁻¹ are common [17]. Other treatments based on adsorption on activated carbons could be a feasible alternative. Adsorption is considered one of the most efficient and effective methods to separate emerging pollutants such as diclofenac [18] and petrochemical effluents containing benzene and toluene [19], due to its simplicity and flexibility of use, its high porosity, large specific surface area and, the high degree of surface interactions [20]. However, the presence of organic content in the wastewater could be a potential limitation because it could interfere in pollutants removal efficiency by competing for adsorption active sites on activated carbon [21]. Consequently, given the complexity of typical aqueous effluents in the industry, adsorption alone would not be the most suitable method.

In order to provide efficient solution for the treatment of these effluents, advanced oxidation processes (AOPs) have attracted the interest of many researchers due to their advantages [22,23]. Among the many existing AOPs, ozonation is a process with a high oxidation potential, which can lead to efficient removal of organic compounds, such as pharmaceuticals, personal care products, pesticides, solvents and surfactants, even at low ozone concentrations [24–26]. However, certain groups of organic compounds are particularly refractory to oxidation by ozone, such as carboxylic, oxalic, and pyruvic acids [27].

A combination of ozonisation and adsorption processes with activated carbon (AC) could be more efficient and sustainable treatment for wastewaters containing refractory organic pollutants. Some of the previous studies in which catalytic ozonisation processes with activated carbons were used for the removal of different organic compounds are listed in Table S1. According with Table S1, catalytic ozonation with granular activated carbons (GAC) could overcome the limitations of ozonation due to the adsorption capacity, high surface area, and the catalytic activity.

The catalytic mechanism of ozonisation in the presence of GAC is still unclear, but recent results suggest that the carbon essentially promotes the decomposition of ozone with a consequent increase in the production of radicals. These hydroxyl radicals would not be bound to the surface, remaining free to react in the aqueous phase. Therefore, the activated

carbon would behave as an initiator of the radical-like chain reaction that transforms ozone into hydroxyl radicals, which in turn react with the organic compounds in the bulk [28].

On the other hand, other authors, such as Nawrocki and Kasprzyk-Hordern [29] and Guo et al. [30], have postulated that the activated carbon initiates the decomposition of ozone into hydroxyl radicals, and then the ozone reacts with the superficial oxygenated groups to generate H_2O_2 , which in turn reacts with the ozone in the bulk to produce hydroxyl radicals. In other words, in this model, the catalyst plays a dual role during the catalytic ozonisation process. First, it adsorbs and decomposes the ozone, leading to the formation of active species, and then the active species reacts with the non-chemisorbed organic compounds. In addition, the activated carbon adsorbs organic compounds, and then reacts with the oxidising species generated on the catalyst's surface via the Criegee mechanism [31].

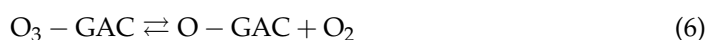
These mechanistic reactions of ozone decomposition and radical reactions, depending on the pH of the medium, can be summarised, according to Beltrán et al. [26]:

- Homogeneous reaction (at the liquid level):

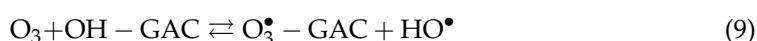
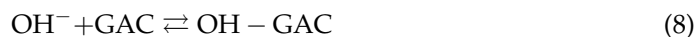


- Heterogeneous reactions (at the level of the solid):

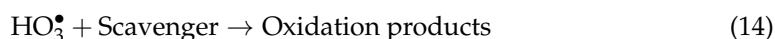
For an acid pH:



For an alkaline pH:



- Homogeneous propagation and termination reactions:



According with this, the integration of a GAC catalyst into a continuous adsorption-ozonisation (Ad/Ox) process would lead to a complete removal and mineralisation of phenol containing waters. Ad/Ox process is a complex system involving different aspects, such as mass transfer and radical generation or adsorption equilibria, among others. Few studies deepened the kinetics of the process with the prospect of implementation of this catalytic technology on an industrial scale. Thus, a study of the behaviour of the system operating in a fixed-bed under different operating conditions through a kinetic model could provide the necessary information to achieve the desired final scale-up.

Given the excessive number of variables involved in Ad/Ox process, some of which are unknown, it is impossible to develop a rigorous model, let alone propose a detailed reaction mechanism. Consequently, from a practical point of view, a model employing experimental data derived under different operational conditions can serve as a basis for real applications, as long as the model adequately simulates the experimental data.

Therefore, this study aimed to develop a three-phase kinetic model of a continuous process in a fixed-bed catalytic ozonation (Ad/Ox) treatment with granular activated carbon (GAC). Phenol was chosen as a model organic pollutant because of its environmental impact, high toxicity, and occurrence in the industry. It has been proposed a kinetic model that includes mass transfer parameters, adsorption equilibria, and reaction rate constants at the solid and liquid surface, to analyze the effect of operating conditions and to identify the operational strategies that will lead to increased degradation and mineralisation rates.

2. Results and Discussion

2.1. Removal of Phenol and Mineralisation

In order to study the influence of GAC on phenol removal, a preliminary experiment was performed with ozone alone in a fixed-bed reactor, with an inert material (glass spheres) and adsorption or ozonation only in the presence of GAC, in order to evaluate the improvement achieved by activated carbon. The transitory profiles of the primary degradation and mineralisation of the three systems are compared in Figure 1.

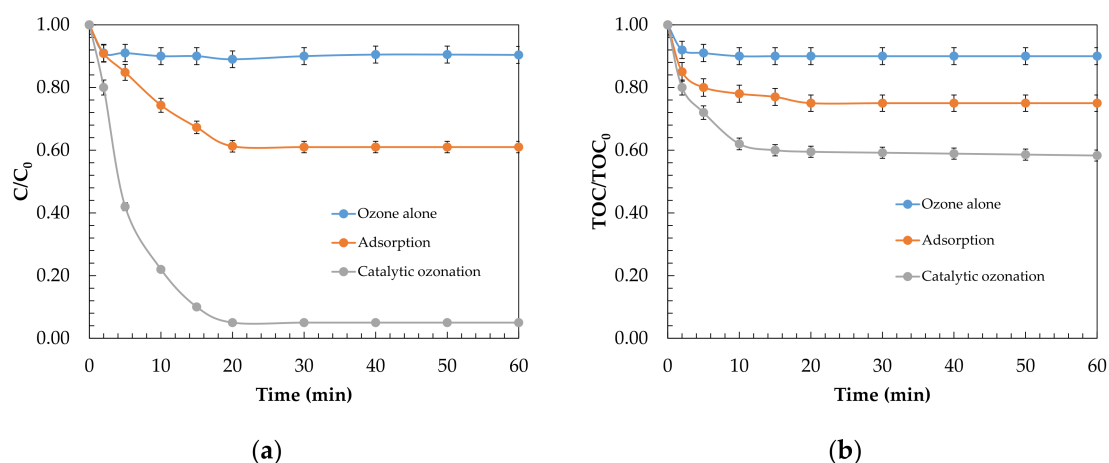


Figure 1. Comparison of ozonation alone, adsorption, and catalytic ozonation processes with GAC in a fixed-bed reactor for phenol removal. Evolution of (a) primary degradation and (b) mineralisation in terms of TOC. Experimental conditions: $C_0 = 250 \text{ mg L}^{-1}$; $Q_G = 0.05 \text{ L h}^{-1}$; $C_{O_3, G} = 12.0 \text{ mg L}^{-1}$; $Q_L = 12 \text{ mL min}^{-1}$; $\text{pH} = 6.5$; $M_{\text{CAT}} = 70.8 \text{ g L}^{-1}$; $P = 1.0 \text{ atm}$; $T = 20 \text{ }^\circ\text{C}$; $V = 0.14 \text{ L}$.

Ozonation alone achieved a primary degradation of only 10% (see Figure 1). This low degradation could be due to the oxidation potential of ozone being lower ($E^\circ = 2.07 \text{ V}$) than that of the hydroxyl radicals ($E^\circ = 2.80 \text{ V}$) generated by the indirect reactions associated with the decomposition of ozone in the presence of GAC [22]. The mineralisation of phenol in the catalytic system was more efficient compared with ozonation alone or adsorption, with a 41.7% mineralisation achieved 20 min after reaching the steady state.

As can be seen in Figure 1b, the mineralisation obtained by catalytic ozonisation with GAC does not match the sum (35.0%) of the efficiencies obtained by ozonisation or adsorption with GAC. According to Lin et al. [32], this could be because during the catalytic ozonisation adsorption, reaction, and desorption processes of oxidised pollutants were involved, in contrast to the ozonisation. In overall, the results indicate that GAC had some catalytic activity to increase the generation of oxidative species responsible for the degradation of phenol. This same effect was observed by Xiong et al. [33], who obtained 26.1% additional mineralisation using the catalytic system with GAC in a basket reactor, compared with adsorption or ozonisation alone. According with their research, the lower molecular weight of the oxidation by-products adsorbed onto the GAC could explain the higher removal obtained in comparison with ozone alone.

2.2. Kinetic Model of the Ad/Ox Process Operated in a Continuous Fixed-Bed Reactor

The implementation of this system on an industrial scale requires predictions of the system's behaviour. Therefore, the development of the three-phase model was based on the considerations made by Ferreiro et al. [17], in which the G–L–S ozone mass transfer, the adsorption process of both ozone and phenol, and the parallel chemical reaction occurring at both the liquid and solid levels were taken into account. The application of the Ad/Ox model in a continuous system was based on the following considerations:

- The overall oxidation rate of the process is represented by the ozone consumption in the parallel reaction process (both at the liquid and solid level);
- The oxidation rate of the parallel stages, in the liquid phase and on the GAC, were represented by pseudo-first-order kinetics with respect to phenol;
- The GAC was considered a sufficiently porous material, where the diffusion of ozone and phenol into the catalyst particles took place;
- The adsorption kinetics during the Ad/Ox process are represented by a pseudo-second-order kinetic equation (Equation (20));
- The kinetic constant of phenol removal in the solid incorporates the degradation and desorption of organic compounds;
- The degradation kinetics in both liquids and solids, as well as the adsorption, are influenced by the operational conditions of the ozonisation process.

Taking into account the above, the combined process of the physical adsorption and oxidation of phenol must be described through its correlation with ozone consumption. Therefore, the following expression was defined, which relates the rate of phenol oxidation, $-r_P$, to the ozone consumed:

$$-r_P = -\frac{dF_P}{dV} = z \times N_{O_3}, \quad (15)$$

where z is the stoichiometric coefficient of the reaction between transferred ozone and oxidised phenol, V is the bed volume, F_P is the phenol mass flow and N_{O_3} is the total ozone consumption. From the ozone consumption in the liquid ($N_{O_3}^I$) and the production of ozone at the GAC's surface ($N_{O_3}^{II}$), the following expressions (Equations (16)–(18)) were obtained:

$$N_{O_3} = N_{O_3}^I + N_{O_3}^{II} = K_L a \times (C_{O_3,L}^* - C_{O_3,L}) \quad (16)$$

$$N_{O_3}^I = k_{c,L} \times C_{O_3,L} \times C_P = k_{c,L} \times C_P \times (C_{O_3,L} - 0) = k_{c,L} \times C_P \times \left(\frac{P_{O_3}^*}{He} - 0 \right) \quad (17)$$

$$N_{O_3}^{II} = k_{c,S} \times \frac{C_{O_3,L}}{m} \times Z_P \times M_{CAT}, \quad (18)$$

where $K_L a$ is the volumetric ozone mass transfer coefficient, $C_{O_3,L}^*$ is the concentration of dissolved ozone in the liquid phase at saturation conditions, $k_{c,L}$ is the kinetic constant of the reaction between phenol and ozone at the liquid level, $C_{O_3,L}$ is the ozone concentration in the liquid phase, C_P is the phenol concentration, $P_{O_3}^*$ is the partial pressure of ozone in equilibrium with the ozone concentration in the liquid phase, He is Henry's constant, Z_P is the concentration of phenol adsorbed on the GAC, and M_{CAT} is the GAC concentration. Equation (18) assumes that the ozone adsorbed on the solid phase catalyst is in equilibrium with the ozone concentration in the liquid, which can be expressed as $C_{O_3,L} = m \times C_{O_3,S}^*$, where m is the slope of the equilibrium line between the liquid and solid phases.

After the description of the phenol degradation process through ozone consumption, the adsorption equilibrium must have been taken into account in the kinetic model of the Ad/Ox process, because the catalytically functional adsorbent used in this system was GAC, a material with high porosity and large available specific surface area. The equilibrium was assumed to be a Freundlich isotherm, in accordance with the adsorption experiments carried out in previous studies of the same GAC [17]. Freundlich equation

was used because the adsorption step in these systems is usually a quick process [34]. Freundlich's equation is given by the following expression [24]:

$$Z_{P,\infty} = K_F \times C_P^{1/n_F} \quad (19)$$

where $Z_{P,\infty}$ is the concentration of phenol in equilibrium with the concentration of the liquid phase, K_F is the Freundlich constant and n_F is a factor describing the adsorption intensity. Consequently, the kinetics corresponding to the adsorption process could be described through pseudo-second-order kinetics, according to the following equation [35]:

$$\left(-\frac{dZ_P}{dt}\right)_{\text{ads}} = k_{\text{ads}} \times (Z_{P,\infty} - Z_P)^2 \times M_{\text{CAT}} \quad (20)$$

To describe the evolution of the phenol concentration over time at each longitudinal position of the fixed-bed tubular system, it has been used the axial dispersion model of Alhemed et al. [36]. The measurement of axial dispersion considers the possible deviation from ideal flow due to turbulence, as well as changes in bed characteristics and gas presence. For a tubular system, with one-dimensional flow and first-order kinetics, the axial dispersion is given by the following Equation (21):

$$v \times \frac{dC_P}{dL} - D_L \times \frac{d^2C_P}{dL^2} = 0 \quad (21)$$

where D_L is the axial dispersion coefficient, L is the length of tubular reactor (GAC bed height), and v is the linear flow velocity of the fluid. Through Equations (19)–(21), the overall velocity, incorporating the kinetic terms of adsorption, chemical reaction and dispersion, can be inferred from the following general expression:

$$\left(-\frac{dC_P}{dt}\right) = \left(-\frac{dC_P}{dt}\right)_{\text{disp}} + \left(-\frac{dC_P}{dt}\right)_{\text{ads}} + \left(-\frac{dF_P}{dV}\right)_{\text{ox}}, \quad (22)$$

To determine the evolution of phenol oxidation with reaction time and reactor position during a continuous catalytic ozonation process (Ad/Ox) on a GAC bed, for a dL volume it was obtained the following Equation (23):

$$v \times \frac{\partial C_P}{\partial L} - D_L \times \frac{\partial^2 C_P}{\partial L^2} + \frac{\partial C_P}{\partial t} + \left(\frac{1-\varepsilon}{\varepsilon}\right) \times \frac{\partial Z_P}{\partial t} + k_P \times C_P^n = 0, \quad (23)$$

where ε is the bed porosity, k_P is the kinetic constant that relates the reaction of ozone to the phenol in both the liquid and the solid, and n is the kinetic order reaction. Considering that the chemical reaction takes place both in the liquid and at the surface of the GAC, it has been obtained the following Equation (24) from Equations (17) and (18):

$$-r_{O_3} = k_{c,L} \times C_{O_3,L} \times C_P + k_{c,S} \times \frac{C_{O_3,L}}{m} \times Z_P = k_{c,L} \times C_{O_3,L} \times C_P + k_{c,S} \times \frac{C_{O_3,L}}{m} \times M_{\text{CAT}}^2 \times K_F \times C_P^{1/n_F} \quad (24)$$

Assuming that the ozone concentration is constant after an initial transitory period, and that the ozone distribution in the liquid and solid is proportional to its consumption [17,37], the following global kinetic constants, k_1 and k_2 , were defined, which incorporated the chemical reaction and mass transfer, leading to the following expression:

$$v \times \frac{\partial C_{O_3,L}}{\partial L} - D_L \times \frac{\partial^2 C_P}{\partial L^2} + \frac{\partial C_{O_3,L}}{\partial t} + k_1 \times C_P + k_2 \times C_P^{1/n_F} = 0, \quad (25)$$

where k_1 and k_2 are the kinetic constants of phenol removal, referring to the liquid and solid phases, respectively. The combination of Equations (19)–(21) and (25) offers a description of the evolution of the phenol concentration in the system through the determination of the kinetic, fluidynamic, and equilibrium parameters.

2.3. Determination of the Characteristic Parameters of the Continuous Ad/Ox System

Due to the high complexity of the three-phase Ad/Ox model, before solving the equations describing the process, it was necessary to determine the characteristic parameters of the system. The characteristic parameters it have been considered the interstitial velocity, dispersion coefficient, kinetic constants of adsorption and equilibrium parameters.

The interstitial velocity was determined from the velocity at which the liquid flows through the voids in the bed, according to Equation (26):

$$v = \frac{Q_L}{A \times \varepsilon} \quad (26)$$

where Q_L is the liquid flow rate through the bed voids and A is the cross-sectional area of the reactor. With the studied flow rate ($Q_L = 12 \text{ mL min}^{-1}$) and void fraction ($\varepsilon = 0.32$), an interstitial velocity of 5.8 cm min^{-1} was obtained. Another characteristic parameter was the axial dispersion coefficient, which characterises the degree of back-mixing of the flow. For a flow rate $Q_G = 0.2 \text{ mL min}^{-1}$, a dispersion coefficient $D_L = 12.8 \text{ cm}^2 \text{ min}^{-1}$ was obtained.

Regarding the residence time, the ratio of liquid and gas volumes was considered to be proportional to their respective flow rates. Consequently, both liquid and gas take the same time to circulate through the GAC fixed-bed column. For the studied flow rate, an empty bed contact time (EBCT) of 11.6 min was estimated. This value coincided with the time commonly used (10–30 min) in industrial water treatment processes in real plants [38].

With respect to the determination of the mass transfer coefficient of the reaction system ($K_L a$) was estimated from ozone concentration in the gas (see Figure S1) for each pressure and ozone flow rate with a determination coefficient of $R^2 \cong 0.99$ (see Figures S2 and S3). It was observed that with increasing gas flow rate, the mass transfer coefficient increased slightly from 0.130 to 0.183 min^{-1} at a flow rate of 0.05 and 0.4 L h^{-1} respectively. Regarding the pressure it was observed an increased from 0.110 to 0.125 min^{-1} at a pressure of 1.0 and 2.5 atm respectively. Obtained $K_L a$ values were according with other ozonation systems of literature [24,27].

Finally, it have been discussed the equilibrium and kinetic adsorption parameters necessary for the resolution of Equations (19)–(21) and (25). The adsorptive characteristics of the GAC at different pH conditions between 3.0 and 11.0 are shown in Figure 2.

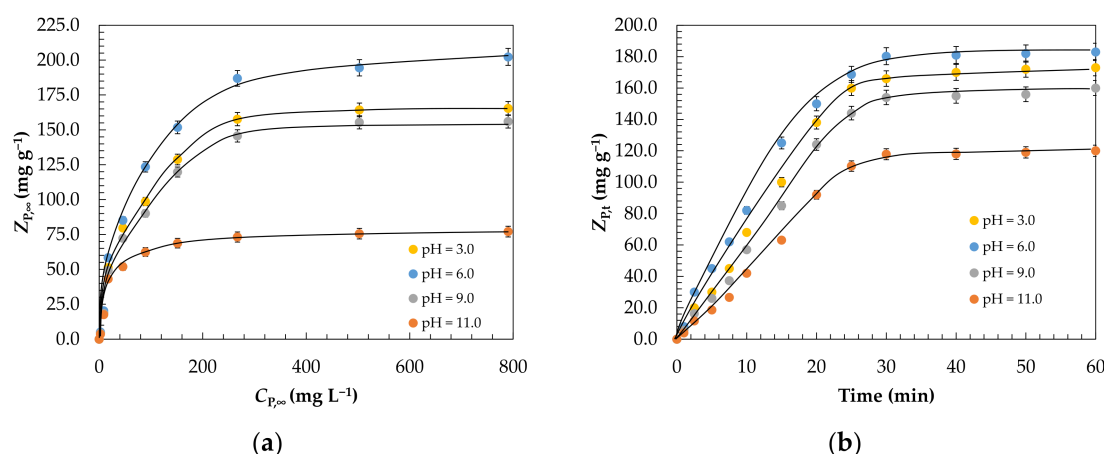


Figure 2. Determination of the adsorption parameters for the different pH values studied and at a temperature of $20 \text{ }^\circ\text{C}$. (a) Adsorption isotherms of phenol on GAC; (b) evolution of adsorption kinetics fitted to a pseudo-second order model for different hydraulic retention times.

All phenol adsorption isotherms in Figure 2a were fitted by the empirical Freundlich multilayer adsorption model, which assumes the existence of interactions between the adsorbed molecules on the adsorbent [39]. Figure 2b shows the adsorption kinetic profiles

fitted to a pseudo-second order model, which assumes that the chemical reaction is significant. The adsorption parameters necessary to the Ad/Ox kinetic model were listed in Table 1. A regression analysis of the experimental data showed a coefficient of determination $R^2 > 0.98$, indicating that both the Freundlich isotherm and the pseudo-second-order kinetic model adequately described the adsorption phenomena. The amount of phenol adsorbed on the GAC surface was greater ($K_F = 2.01 \text{ (mg g}^{-1}) \text{ (L mg}^{-1})^{1/n_F}$) at neutral pH than that at an alkaline pH ($K_F = 1.49 \text{ (mg g}^{-1}) \text{ (L mg}^{-1})^{1/n_F}$). This could be because when the pH of the solution is higher, the electrostatic interactions of attraction between the phenol and the GAC are lower [40].

Table 1. Summary of the kinetic parameters obtained from the pseudo-second-order and equilibrium model determined via the Freundlich isotherm model for the adsorption of phenol on the GAC's surface at a temperature of 20 °C and different pH values.

	pH = 3.0	pH = 6.0	pH = 9.0	pH = 11.0
Equilibrium				
$K_F, \text{ (mg g}^{-1}) \text{ (L mg}^{-1})^{1/n_F}$	1.89	2.01	1.82	1.49
n_F	1.12	1.19	1.10	1.06
R^2	0.981	0.995	0.984	0.991
Kinetic				
$k_{\text{ads}}, \text{ g mg}^{-1} \text{ min}^{-1}$	2.77×10^{-4}	3.10×10^{-4}	2.52×10^{-4}	4.85×10^{-5}
R^2	0.992	0.987	0.996	0.993

In order to explain the effect of pH on the adsorption phenomenon in more detail, the zeta potential was determined over a wide range of pH (2.5–11.5) (Figure 3). Based on obtained zeta potential values, at pH = 7.0, it was observed that the attraction due to electrostatic charge was greater than at other acidic or alkaline pH values. This is because their potential value (32.2 mV) was higher than that observed at pH = 3.0 (30.53 mV) or pH = 9.0 (10.47 mV). In contrast, at pH = 11.0, a lower adsorption capacity was achieved because of the repulsive forces between the negative charges of the phenol and the GAC surface difficult the adsorption of phenol. For this reason, the zeta potential value was −2.2 mV. Although higher adsorption of phenol would be achieved at neutral or acidic pH, oxidation by catalytic ozonation will be more effective at alkaline pH values because the generation of more hydroxyl radicals is promoted. Consequently, it will be necessary to work at higher pH values even if the adsorptive properties of the GAC are lost.

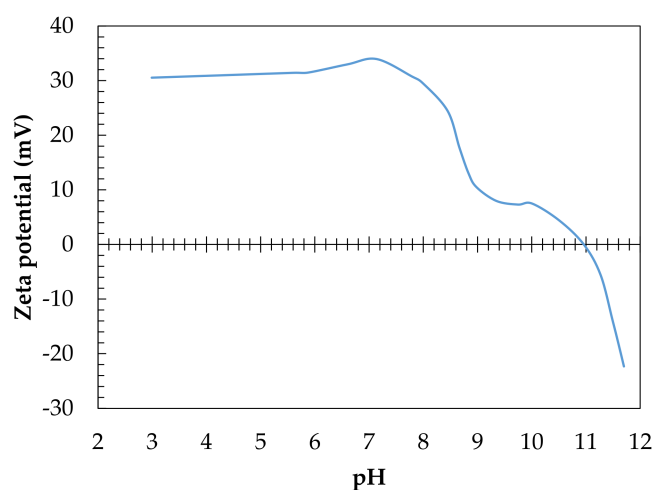


Figure 3. Evolution of the GAC's zeta potential at different pH values.

2.4. Effect of Operational Conditions and Kinetic Model Validation

In order to establish the most favourable operational conditions leading to higher mineralisation and primary degradation, the effects of system pressure, ozone dose, ozone flow rate, initial phenol concentration, and pH on the fixed-bed reaction system with GAC were analysed. Figure 4 shows the transient profiles of the obtained primary degradation and mineralization, fitted to the proposed Ad/Ox model.

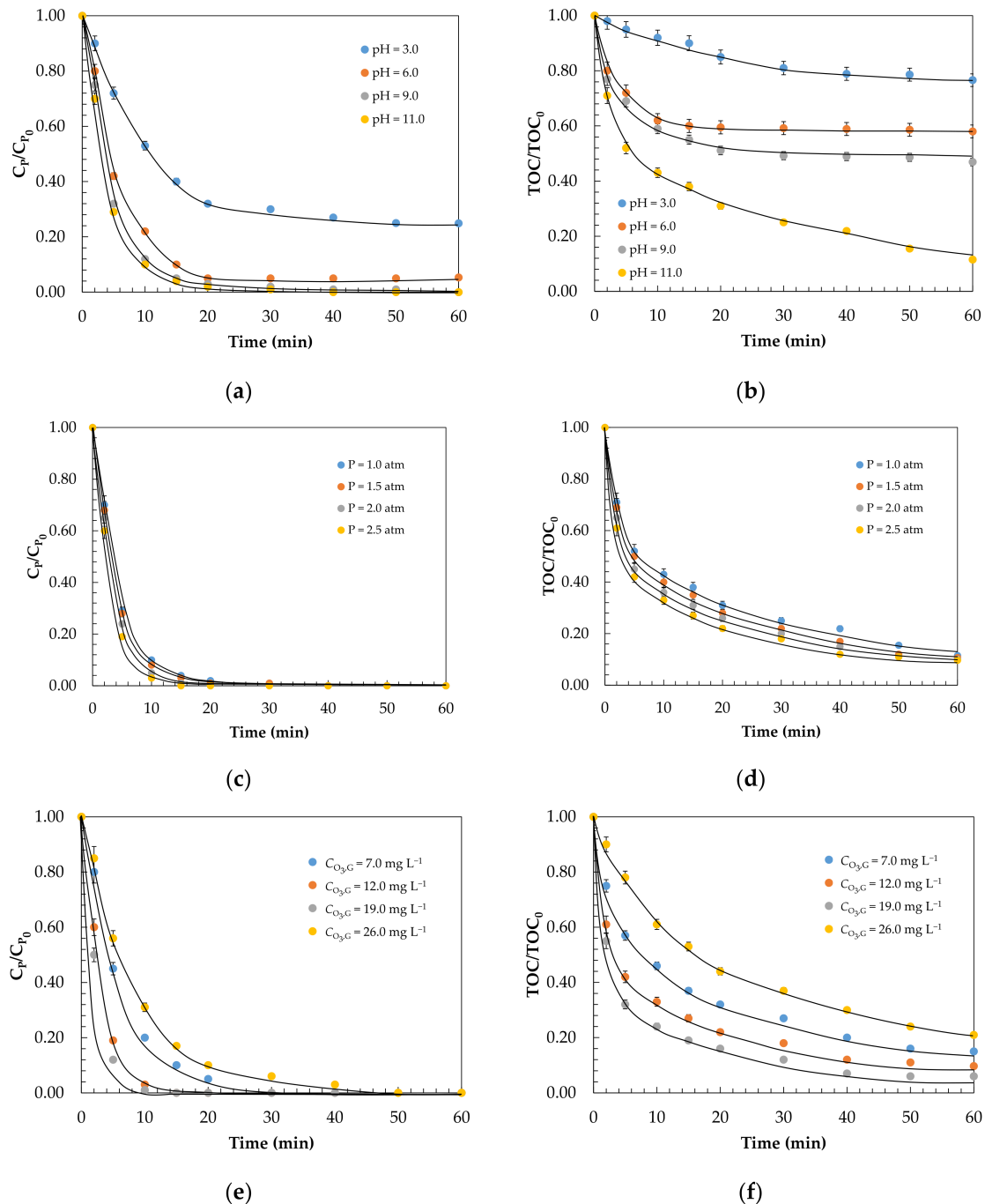
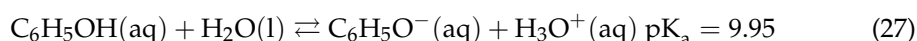


Figure 4. Effect of operational conditions on the primary degradation and mineralisation of phenol-containing waters during a catalytic ozonation process with GAC: (a,b) pH¹, (c,d) pressure², and (e,f) ozone concentration at inlet³, showing the experimental profiles and fitted to the Ad/Ox kinetic model. Experimental conditions: ¹ $C_{P_0} = 250.0 \text{ mg L}^{-1}$, $P = 1.0 \text{ atm}$, $C_{O_3,G} = 12.0 \text{ mg L}^{-1}$, $Q_L = 12 \text{ mL min}^{-1}$, $Q_G = 0.05 \text{ L h}^{-1}$, $V = 0.14 \text{ L}$; ² $C_{P_0} = 250.0 \text{ mg L}^{-1}$, $\text{pH} = 11.0$, $C_{O_3,G} = 12.0 \text{ mg L}^{-1}$, $Q_L = 12 \text{ mL min}^{-1}$, $Q_G = 0.05 \text{ L h}^{-1}$, $V = 0.14 \text{ L}$; ³ $C_{P_0} = 250.0 \text{ mg L}^{-1}$, $P = 2.5 \text{ atm}$, $\text{pH} = 11.0$, $Q_L = 12 \text{ mL min}^{-1}$, $Q_G = 0.05 \text{ L h}^{-1}$, $V = 0.14 \text{ L}$.

According to Figure 4a,b, the pH of the solution plays an important role in the catalytic ozonation of phenol, as well as in the mass transfer and its subsequent decomposition [24]. As the pH of the solution increased, the rate of degradation and mineralisation increased, becoming higher than at more acidic pH. This is because at more alkaline pH, the oxidation mechanism involved is predominantly radicalary and generates more HO• due to the higher concentration of hydroxide anions, and, consequently, a higher oxidation potential ($E^\circ = 2.80$ V) [41] as shown in Figure S4a. In contrast, at weakly acidic pH levels, the predominant mechanism is the direct reaction of ozone, as this pathway is more selective [27]. This statement could lead to an error, given that at pH = 11.0, the participation of the direct reaction of ozone with phenol is insignificant. This is because depending on the pH, phenol can dissociate, according to the equilibrium shown in Equation (27) [17]:



According to Equation (27), the nature of these species could affect the reactivity with ozone. At acidic pH, electrophilic substitution reactions with ozone (direct reaction) would be promoted due to the character of the substituent groups. However, since the $-\text{O}-$ group of phenolate ion is more reactive group ($k = 1.4 \times 10^9 \text{ M}^{-1} \text{ s}^{-1}$) than $-\text{OH}$ ($k = 1300 \text{ M}^{-1} \text{ s}^{-1}$) of phenol [22], the reactivity of ozone increases with pH to attack the pollutant. Consequently, at pH = 11.0, complete primary degradation and mineralisation was achieved, with a total organic carbon reduction of 88.5%.

This same behaviour was observed by Xiong et al. [33]—in a slurry-type reactor. A mineralisation of 70.2% was achieved operating at an alkaline pH. Other authors such as, Chand et al. [42] observed an increase of 7.2% in phenol mineralisation operating at a slightly alkaline pH (pH = 9.0). The difference in efficiency observed could be due to the pH plays a determining role in the charge of the surface hydroxyl groups on the catalyst. In this respect, the adsorptive properties of the GAC could contribute to the greater adsorption of the degradation by-products, and, consequently, to a greater reduction in TOC. In any case, the contribution of adsorption during the catalytic ozonisation of phenol-containing waters did not comprise more than 5–23% of the TOC removal [43].

In order to validate the Ad/Ox kinetic model for the proposed continuous catalytic ozonisation process, the dynamics were adjusted for the different operational conditions. In Table 2, the values of the kinetic constants obtained after adjusting the profiles for the analyses of both primary degradation and mineralisation are shown. According to the relative standard error values, in general terms, the fit was good, showing an *RSE* of approximately 5% for the primary degradation and mineralisation profiles. According to the kinetic constant k_2 , referring to the solid, slight increases were observed at neutral ($4.6 \times 10^{-3} (\text{mg L}^{-1}) (\text{mg g}^{-1} \text{ GAC min})^{-1}$) and acidic ($3.8 \times 10^{-3} (\text{mg L}^{-1}) (\text{mg g}^{-1} \text{ GAC min})^{-1}$) pH values, agreeing with the adsorption phenomenon described above. Respect the kinetic constant of the liquid (k_1), at alkaline pH ($k_1 = 0.20 \text{ min}^{-1}$), it was observed in Figure S4a, an increased production of radical species capable of degrading a phenol-containing effluent. The kinetic constants obtained from the evolution of the mineralisation were lower due to the more refractory nature of the degradation products such as p-benzoquinone ($k = 2.5 \times 10^3 \text{ M}^{-1} \text{ s}^{-1}$) or catechol ($k = 5.2 \times 10^5 \text{ M}^{-1} \text{ s}^{-1}$) according with Figure S5 [22].

Table 2. Summary of the adsorption and oxidation kinetic constants of the Ad/Ox kinetic model related to the removal and mineralisation of phenol during catalytic ozonation with GAC.

Parameter/Evolution	Effect of pH ¹			
	pH = 3.0	pH = 6.0	pH = 9.0	pH = 11.0
Phenol removal				
k_1 (min ⁻¹)	0.05	0.09	0.12	0.20
$k_2 \times 10^3$ (mg L ⁻¹)(mg g ⁻¹ GAC min) ⁻¹	3.8	4.6	3.7	2.1
RSE (%)	4.5	5.3	5.0	4.8
Mineralisation				
$k_1 \times 10^1$ (min ⁻¹)	0.009	0.017	0.022	0.038
$k_2 \times 10^4$ (mg L ⁻¹)(mg g ⁻¹ GAC min) ⁻¹	0.71	0.86	0.69	0.39
RSE (%)	3.7	4.1	3.9	4.4
	Effect of pressure ²			
	P = 1.0 atm	P = 1.5 atm	P = 2.0 atm	P = 2.5 atm
Phenol removal				
k_1 (min ⁻¹)	0.20	0.21	0.22	0.23
$k_2 \times 10^3$ (mg L ⁻¹)(mg g ⁻¹ GAC min) ⁻¹	2.1	2.1	2.1	2.2
RSE (%)	4.1	4.6	4.0	5.2
Mineralisation				
$k_1 \times 10^1$ (min ⁻¹)	0.038	0.039	0.041	0.044
$k_2 \times 10^4$ (mg L ⁻¹)(mg g ⁻¹ GAC min) ⁻¹	0.39	0.39	0.39	0.42
RSE (%)	4.5	4.2	4.7	4.3
	Effect of ozone gas concentration ³			
	CO _{3,G} = 7.0 mg L ⁻¹	CO _{3,G} = 12.0 mg L ⁻¹	CO _{3,G} = 19.0 mg L ⁻¹	CO _{3,G} = 26.0 mg L ⁻¹
Phenol removal				
k_1 (min ⁻¹)	0.19	0.23	0.24	0.15
$k_2 \times 10^3$ (mg L ⁻¹)(mg g ⁻¹ GAC min) ⁻¹	2.0	2.2	2.4	1.8
RSE (%)	5.3	4.9	4.9	5.1
Mineralisation				
$k_1 \times 10^1$ (min ⁻¹)	0.036	0.044	0.045	0.028
$k_2 \times 10^4$ (mg L ⁻¹)(mg g ⁻¹ GAC min) ⁻¹	0.37	0.42	0.45	0.34
RSE (%)	4.8	4.2	4.6	4.7
	Effect of ozone flow rate ⁴			
	Q _G = 0.05 L h ⁻¹	Q _G = 0.1 L h ⁻¹	Q _G = 0.2 L h ⁻¹	Q _G = 0.4 L h ⁻¹
Phenol removal				
k_1 (min ⁻¹)	0.24	0.25	0.26	0.27
$k_2 \times 10^3$ (mg L ⁻¹)(mg g ⁻¹ GAC min) ⁻¹	2.4	2.4	2.5	2.5
RSE (%)	4.7	4.9	4.4	4.2
Mineralisation				
$k_1 \times 10^1$ (min ⁻¹)	0.045	0.047	0.049	0.051
$k_2 \times 10^4$ (mg L ⁻¹)(mg g ⁻¹ GAC min) ⁻¹	0.45	0.45	0.47	0.47
RSE (%)	5.0	4.4	4.8	4.3
	Effect of initial phenol concentration ⁵			
	C _{P0} = 250.0 mg L ⁻¹	C _{P0} = 500.0 mg L ⁻¹	C _{P0} = 750.0 mg L ⁻¹	C _{P0} = 1000.0 mg L ⁻¹
Phenol removal				
k_1 (min ⁻¹)	0.27	0.19	0.17	0.16
$k_2 \times 10^3$ (mg L ⁻¹)(mg g ⁻¹ GAC min) ⁻¹	2.5	2.7	3.0	3.2
RSE (%)	4.0	4.3	4.8	4.5
Mineralisation				
$k_1 \times 10^1$ (min ⁻¹)	0.051	0.036	0.031	0.030
$k_2 \times 10^4$ (mg L ⁻¹)(mg g ⁻¹ GAC min) ⁻¹	0.47	0.51	0.56	0.60
RSE (%)	4.2	4.6	3.9	4.4

Experimental conditions: ¹ C_{P0} = 250.0 mg L⁻¹, P = 1.0 atm, CO_{3,G} = 12.0 mg L⁻¹, Q_L = 12 mL min⁻¹, Q_G = 0.05 L h⁻¹, V = 0.14 L.

² C_{P0} = 250.0 mg L⁻¹, pH = 11.0, CO_{3,G} = 12.0 mg L⁻¹, Q_L = 12 mL min⁻¹, Q_G = 0.05 L h⁻¹, V = 0.14 L. ³ C_{P0} = 250.0 mg L⁻¹, P = 2.5 atm,

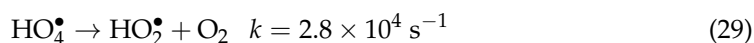
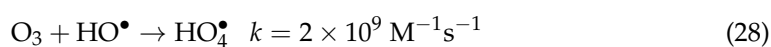
pH = 11.0, Q_L = 12 mL min⁻¹, Q_G = 0.05 L h⁻¹, V = 0.14 L. ⁴ C_{P0} = 250.0 mg L⁻¹, P = 2.5 atm, pH = 11.0; CO_{3,G} = 19.0 mg L⁻¹,

Q_L = 12 mL min⁻¹, V = 0.14 L. ⁵ pH = 11.0, P = 2.5 atm; CO_{3,G} = 19.0 mg L⁻¹, Q_L = 12 mL min⁻¹, Q_G = 0.4 L h⁻¹, V = 0.14 L.

The effect of system pressure on the enhancement of degradation and mineralisation was studied in the range of 1 to 2.5 atm. Pressure is a operational variable that could affect mass transfer and, consequently, improve the contact amongst the ozone molecules in the gaseous and liquid phases [44,45] (see Figure S2). As shown in Figure 4c,d, the increase in pressure to 2.5 atm had a slightly positive effect, but not as evident as the effect of pH,

because it only improved mineralisation by 1.8%, which was within the experimental error. The observed improvement could be due to the generation of slightly smaller bubbles, which could lead to an increase in the specific contact surface area between the liquid and gas phases. The same effect was observed for the kinetic constants of the Ad/Ox model. This could be due to the internal pressure in the gas microbubbles being much higher than the external pressure applied to them.

Figure 4e,f show the effects of ozone dose. Increasing the ozone dose from 7.0 to 19.0 mg L⁻¹ increased the force gradient, thus improving the mass transfer and ultimately significantly increasing the rate of phenol removal until complete degradation; subsequently, mineralisation improved from 85.0% to 94.0% after reaching a steady state at 60 min. However, higher ozone doses led to a decrease in mineralisation from 94.0% to 79.0% at 26.0 mg L⁻¹. This can be explained via the mechanism proposed by Buhler et al. [46], as shown in Equations (28) and (29):



According to Equations (27) and (28), when there is an ozone dose above the critical value of 19.0 mg L⁻¹, ozone reacts with the generated hydroxyl radicals, producing radicals with a lower oxidative capacity (HO₂[•] and O₂) than hydroxyl radical, according with Figure S4b. On the other hand, according to Rekhate and Srivastava [41], another feasible explanation could be that, when applying an excessive ozone dose, its utilisation is limited by the number of active sites available on the GAC catalyst's surface. Consequently, the resulting excess of ozone would react only through the direct pathway.

This same effect was observed by Nawaz et al. [47] who reported TOC removal rates of 50.6, 85.2, and 79.5% at ozone doses of 10, 20 and 50 mg L⁻¹, respectively. However, increasing the ozone dose did not lead to total phenol mineralisation.

After analysing the kinetic constants of the degradation and mineralisation profiles, the use of dose of 19.0 mg L⁻¹ enhanced the kinetics at the solid level ($k_2 = 2.4 \times 10^{-3}$ (mg L⁻¹) (mg g⁻¹ GAC min)⁻¹) compared with lower doses ($C_{\text{O}_3,\text{G}} = 7.0$ mg L⁻¹), where a constant of 2.0×10^{-3} (mg L⁻¹) (mg g⁻¹ GAC min)⁻¹ was obtained. This could have been because the pore structure of the activated carbon may have been affected by the ozonisation treatment, as described by Guelli Ulson de Souza et al. [6] and confirmed in previous studies with pristine and TiO₂-doped GACs [17,24].

Another operational variable that could have an effect on phenol removal is the ozone flow rate. Different flow rates between 0.05 and 0.4 L h⁻¹ were evaluated (Figure 5a,b). Increasing the ozone flow rate led to an increase in phenol degradation rate and mineralisation efficiency (97.0%) at a flow rate of 0.4 L h⁻¹. This increase could be due to the influence of the flow rate on the ozone mass transfer from the gas to the liquid phase (see Figure S3), and therefore on the effective ozone utilisation. This effect was negligible; a better explanation might be that the quantity of ozone transferred to the liquid phase was higher than that used for oxidation and subsequent decomposition. As was the case with pressure, the improvement in the kinetic constants was not clearly evident here, except the one for the oxidation in the liquid (k_1), which increased from 0.045 to 0.051 min⁻¹ in the mineralisation.

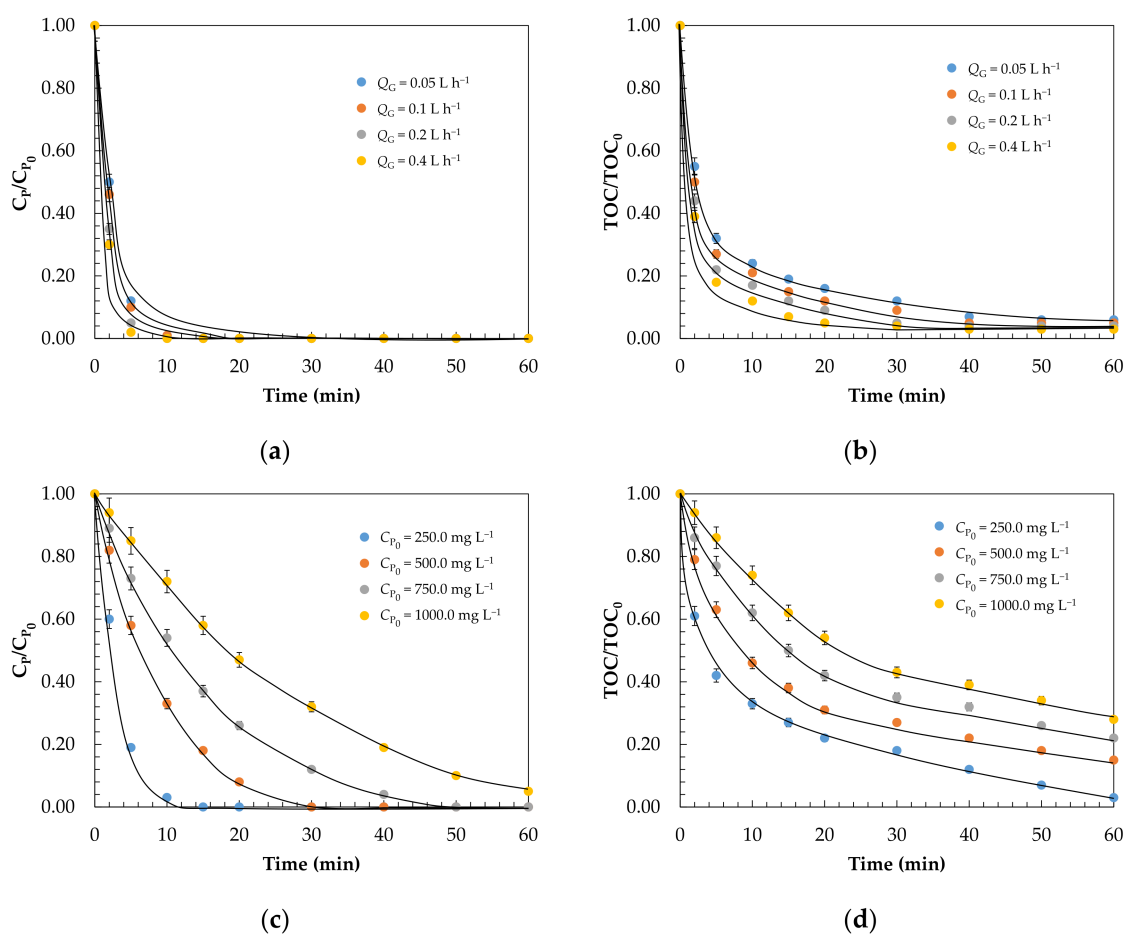


Figure 5. Analysis of C_P and TOC concentration profiles during the initial transitory period ($t < 70$ min) and adjustment to the Ad/Ox kinetic model. Effect of (a,b) ozone flow rate¹ and (c,d) concentration of the pollutant load². Experimental conditions: ¹ $C_{P_0} = 250.0 \text{ mg L}^{-1}$, $P = 2.5 \text{ atm}$, $\text{pH} = 11.0$; $C_{O_3,G} = 19.0 \text{ mg L}^{-1}$, $Q_L = 12 \text{ mL min}^{-1}$, $V = 0.14 \text{ L}$; ² $\text{pH} = 11.0$, $P = 2.5 \text{ atm}$; $C_{O_3,G} = 19.0 \text{ mg L}^{-1}$, $Q_L = 12 \text{ mL min}^{-1}$, $Q_G = 0.05 \text{ L h}^{-1}$, $V = 0.14 \text{ L}$.

This same effect was observed by Yang et al. [48] during the treatment of an industrial effluent. A significant reduction in COD was initially observed up to a critical value of 2.0 L min^{-1} . After that, a negative effect was seen.

In order to study the feasibility of the catalytic ozonation treatment in this continuous system, a wider range of initial phenol concentrations that are common in industrial effluents (up to 1000.0 mg L^{-1}) was evaluated [17]. As shown in Figure 5c,d, the time required for complete degradation and TOC removal was greater at higher initial phenol concentrations [49]. Evaluating the transitory profiles, it can be seen that after 70 min of reaction, the same levels of complete degradation and 97.0% mineralisation were reached, and kinetic constants for the initial concentration of 1000.0 mg L^{-1} of 0.27 min^{-1} and $2.5 \times 10^{-3} (\text{mg L}^{-1}) (\text{mg g}^{-1} \text{ GAC min})^{-1}$ were obtained.

As a comparison of the obtained efficiencies, Lin and Wang [50] studied the removal of phenol through a catalytic ozonation process in a basket reactor with AC as the catalyst. At a temperature of $30 \text{ }^\circ\text{C}$ and after 2 h of reaction, they achieved complete phenol removal and a COD reduction rate of 85%. Beltrán et al. [43] evaluated the use of AC catalysts with other oxides, such as Fe, Co, and alumina, to treat a phenol-containing effluent via catalytic ozonation in a slurry reactor. However, no significant improvement was observed in the catalytic activities of the AC and the other three composites in terms of TOC reduction, which was about 90% after 5 h of reaction. Chaichanawong et al. [39] degraded an aqueous solution containing phenol in a slurry-type reactor, via a catalytic ozonisation process with three ACs with different physico-chemical properties. With a mesoporous carbon, the

complete degradation of phenol and a mineralisation of 85.7% were obtained during the ozonisation and simultaneous adsorption process over 2 h. Guelli Ulson de Souza et al. [6] studied the simultaneous application of ozonation and adsorption processes in a packed bed of AC for the removal of phenol from an industrial stream. With a catalyst loading of 592.22 g L^{-1} , it achieved complete degradation and a COD reduction of 60.67%.

Finally, the toxicity of the effluent was determined in order to evaluate the feasibility of the discharge of the treated effluent into the river. According to De Luis et al. [16], a toxicity value less than 1 TU indicates that an effluent is non-toxic or exhibits low toxicity. Thus, the effluent before treatment showed a value of 18.02 TU, while after treatment carried out under favourable operational conditions its toxicity decreased to 0.09 TU.

In overall terms, taking into account that complete degradation, a mineralisation of 97.0% and a toxicity-free effluent were obtained with an empty bed contact time of 11.6 min and a catalyst load of 432.14 g L^{-1} . The adequately combine adsorption and ozonisation processes shows that the proposed continuous Ad/Ox system would be viable for scaling up into a real process in accordance with the technical criteria.

3. Materials and Methods

3.1. Materials

The granular activated carbon Kemisorb[®] 530 GR 12×40 (Kemira Ibérica, Barcelona, Spain) was used as the catalytic material, with an average particle size of 1.0 mm. The activated carbon used throughout the experiments was characterised in a previous work [17]. Table 3 summarises the main physical properties of the GAC Kemisorb[®] 530.

Table 3. Textural and chemical surface properties of GAC Kemisorb[®] 530.

Property	Kemisorb [®] 530
S_{BET} ($\text{m}^2 \text{ g}^{-1}$)	961.5
S_{ext} ($\text{m}^2 \text{ g}^{-1}$)	410.4
V_{T} ($\text{cm}^3 \text{ g}^{-1}$)	0.38
V_{micro} ($\text{cm}^3 \text{ g}^{-1}$)	0.24
V_{meso} ($\text{cm}^3 \text{ g}^{-1}$)	0.14
$V_{\text{meso}}/V_{\text{T}}$ (%)	36.8
$V_{\text{micro}}/V_{\text{T}}$ (%)	63.2
D_{p} (Å)	27.9
pH_{pzc}	10.95
Ash (%)	11.99
Apparent density (kg m^{-3})	432.1

S_{BET} —BET surface area; S_{ext} —external surface area; V_{T} —total pore volume; V_{micro} —micropore volume; V_{meso} —mesopore volume; $V_{\text{meso}}/V_{\text{T}} \times 100$ —mesopore percentage; $V_{\text{micro}}/V_{\text{T}} \times 100$ —micropore percentage; D_{p} —average pore diameter.

The specific surface area (S_{BET}), total (V_{T}), mesopore (V_{meso}) and micropore (V_{micro}) volumes, and the average pore diameter (D_{p}) were obtained using the BJH model by observing N_2 adsorption–desorption isotherms at 77 K [51]. The point of zero charge (pH_{pzc}) was determined via electrokinetic zeta potential (ζ) measurements [52]. The composition of GAC Kemisorb[®] 530 was measured using X-ray fluorescence (XRF) [24]. The XRF results indicate that GAC is mainly composed of SiO_2 (7.72%) and Al_2O_3 (2.64%), followed by Fe_2O_3 (0.40%), CaO (0.33%), SO_3 (0.19%), MgO (0.07%), Na_2O (0.06%), K_2O (0.04%), P_2O_5 (0.09%), TiO_2 (0.11%), and MnO (0.001%).

3.2. Analytical Methods

Phenol concentration and primary intermediates was measured using a Waters Alliance 2695 high-performance liquid chromatograph system (Waters, Milford, CT, USA) equipped with a Teknokroma Mediterranea SEA C18 threaded column (150 mm \times 4.6 mm, 1.8 μm , Teknokroma Analitica, Sant Cugat del Vallès, Barcelona, Spain) and a guard column working at 20 °C under isocratic elution of a water/methanol mixture (60:40 *v/v*) containing acetic acid (1%), and a flow rate of 1 mL min^{-1} was used. A Waters 2487 UV/Vis

detector was used at a wavelength of 220 nm for phenol, hydroquinone, catechol, oxalic acid, formic acid and at 254 nm for *p*-benzoquinone [53].

The degree of mineralisation was quantified by total organic carbon (TOC) analysis on a Shimadzu TOC-VSCH analyser (Izasa Scientific, Alcobendas, Spain). Toxicity was evaluated in duplicate using the Microtox[®] bioassay in a Microtox[®] toxicity analyser, Azur 500 model (Microbics Corp., New Castle, DE, USA). The measurements were carried out according to ISO 11348-3 (1998), "Water Quality—Determination of the inhibitory effect of water samples on the light emission of *Aliivibrio fischeri* (Luminescent bacteria test)—Part 3: Method using freeze-dried bacteria" [54]. The concentration of I_3^- , proportional to the concentration of oxidising agents such as hydroxyl radicals was measured following the KI dosimetry method described by Alfonso-Muniozgueren et al. [55].

Zeta potential measurements were carried out with a ZetaSizer Ultra (Malvern Panalytical, Malvern, UK) for suspensions of 1 g L^{-1} GAC in distilled water at different pHs.

The composition of the GAC was determined by X-ray fluorescence spectroscopy (XRF). From the pulverised sample, a borate glass bead was prepared by melting in an induction micro furnace, and mixing the flux Spectromelt A12 (Merck KGaA, Darmstadt, Germany) and the sample to a ratio of 20:1. An oxidising agent was added to promote the removal (in the oxidation phase of the process) of all the organic parts of the carbon and the fixation of the inorganic oxides. The chemical analysis of the beads was carried out in a vacuum atmosphere, using an AXIOS model sequential wavelength dispersive X-ray fluorescence spectrometer (WDXRF—Panalytical). The fluorometer was equipped with an Rh and three detectors (gaseous flux, scintillation, and Xe) (Malvern Panalytical) [24].

3.3. Experimental Setup in the Continuous Fixed-Bed Catalytic System

Phenol removal via a continuous Ad/Ox process was carried out in a polyvinyl chloride (PVC) column filled with GAC with a 25 mm outer diameter, 21.2 mm inner diameter and 40 cm length (Figure 6). The single ozonation and Ad/Ox experiments were performed at a constant ozone flow rate ($Q_G = 0.05\text{ L h}^{-1}$) and a temperature of $20\text{ }^\circ\text{C}$, with a fresh GAC bed of 60.5 g for each experiment and a dissolution pumping rate of $Q_L = 12\text{ mL min}^{-1}$. The pH was measured at different initial values (between 3.0 and 11.0), initial phenol concentrations (250, 500, 750, and 1000 mg L^{-1}), and a pressure between 1.0 and 2.5 atm (depending on the experiment).

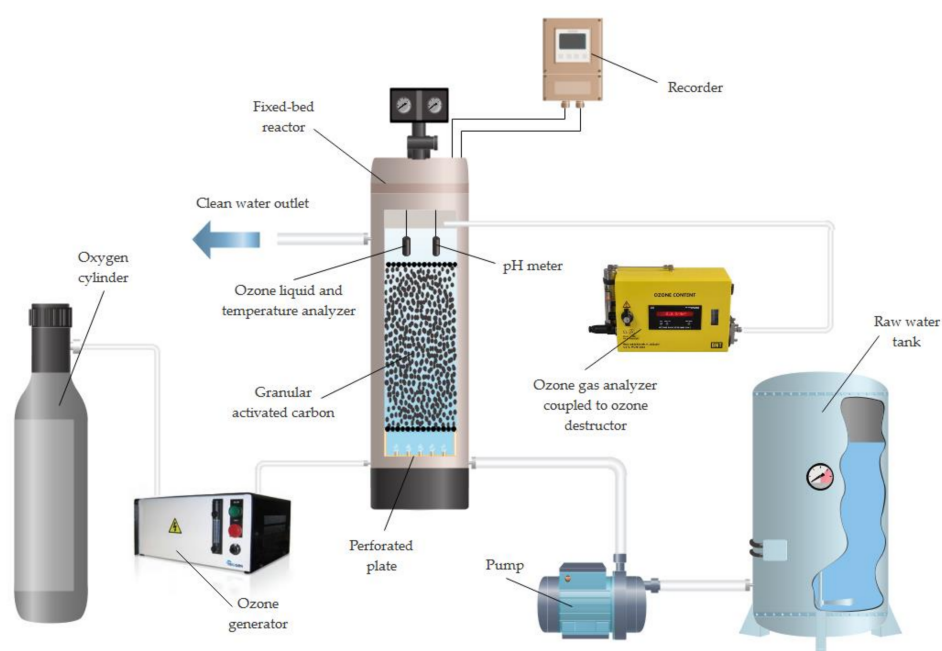


Figure 6. Experimental setup used to carry out ozonation and Ad/Ox tests.

A typical Ad/Ox or simple ozonisation experiment consisted of a continuous introduction of ozone generated in situ from ultrapure oxygen using a TRIOGEN LAB2B ozone generator (BIO UV, Lunel, France) through a porous plate placed at the bottom of the bed column. Here, the liquid flow of the phenol-containing solution was introduced through a PRECIFLOW peristaltic pump (LAMBDA Laboratory Instruments, Baar, Switzerland), through the lower inlet port on the side of the column. After ascending through the column, the gas and liquid flows passed through the granular activated carbon bed. Afterwards, the liquid flow was collected through one of the outlets downstream of the GAC packed bed.

The ozone concentration in the gas phase was measured with a BMT 964C ozone analyser (BMT MESSTECHNIK GMBH, Stahnsdorf, Germany) located on the side of the column. Dissolved ozone concentration and temperature were measured with a Rosemount 499AOZ-54 dissolved sensor (Emerson, Alcobendas, Spain). The pH value was recorded with a Rosemount Analytical model 399 sensor integrated into a Rosemount Analytical Solu Comp II recorder (Emerson). Residual ozone gas was removed using a Zonosistem thermocatalytic ozone destructor (Ingeniería del Ozono S.L.U, Cádiz, Spain).

Mass transfer characterization of the reactor was performed using deionized water in the presence of GAC, following a procedure previously described by Rodríguez et al. [37]. Operating conditions were kept similar to those used in the presence of phenol.

3.4. Statistical Analysis

The data were analysed with the SPSS software (IBM SPSS Statistics 27, SPSS Inc., Armonk, NY, USA). In each set of experiments, each experiment was performed in triplicate. Then, the relative standard deviation (*RSE*,%) of the data corresponding to conversions between 5 and 95% was calculated for the operational conditions established by Equation (30) [56]. Each measurement was replicated at least six times, and further replicates were carried out when the variation between each measurement exceeded 5%:

$$RSE = \sqrt{\frac{\sum_{i=1}^N \left(\frac{C_{\text{exp}} - C_{\text{mod}}}{C_{\text{exp}}} \right)^2}{N - 1}} \times 100 \quad (30)$$

4. Conclusions

A three-phase reaction kinetic model (Ad/Ox) for the description of G–L transfer within the liquid and on the catalyst's surface during the adsorption and ozonisation steps has been proposed. The model allows us to analyse catalytic ozonation, in the presence of GAC, for the removal of phenolic waters in a continuous process.

The combination of the simultaneous adsorption and ozonation processes with GAC resulted in an improvement of both phenol degradation kinetics and mineralisation efficiency, compared with an ozonation or adsorption process alone. The Ad/Ox kinetic model was verified via the experimental results of the catalytic ozonation process under a wide variety of operating conditions affecting the adsorption phenomena, the mass transfer, and the chemical reaction itself, providing a good fit with the experimental data, with a residual standard error of no more than 5% in most cases.

The estimation of the oxidation constants allowed us to study the role of GAC in the ozonisation process and its interaction with phenol. Depending on the degree of phenol dissociation, as a function of pH, the reactivity of ozone was different. At an alkaline pH (values over 11.0), greater degradation and mineralisation were obtained, with kinetic constants of 0.20 min^{-1} and $2.1 \times 10^{-3} (\text{mg L}^{-1})(\text{mg g}^{-1} \text{ GAC min})^{-1}$ for the liquid and solid, respectively. The use of an ozone dose above a critical value of 19.0 mg L^{-1} limited the kinetics and adsorption capacity of phenol, and its oxidation products by extension, leading to a decrease in mineralisation efficiency. On the other hand, at moderated ozone doses, a stronger influence of GAC adsorption mechanisms was observed, as the kinetic constant of the solid increased slightly to $k_2 = 2.4 \times 10^{-3} (\text{mg L}^{-1})(\text{mg g}^{-1} \text{ GAC min})^{-1}$.

Increases in the pressure and gas flow rate did not lead to significant improvements, due to the insufficiency of the excess ozone transferred.

The most favourable operating conditions for the enhancement of the catalytic and adsorptive action of GAC were pH = 11.0, ozone dose = 19.0 mg L⁻¹, gas flow rate = 0.4 L h⁻¹ and pressure = 2.5 atm. The GAC adsorbed the pollutant, subsequently exposing the phenol to attacks by ozone through the hydroxyl radicals generated on its surface. Consequently, the most favourable phenol removal conditions may involve a balance between the radical-generating and adsorptive functions of GAC.

The proposed model could be applied for the prediction of the operating behaviour of a continuous fixed-bed system under different working conditions, making it easily scalable to the industrial level.

Supplementary Materials: The following are available online at <https://www.mdpi.com/article/10.3390/catal11081014/s1>. Table S1: Previous studies on the treatment of wastewater through catalytic ozonation processes in the presence of activated carbon. Figure S1: Evolution of ozone concentration at the reactor outlet gas stream. Figure S2: Determination of mass transfer coefficient of the experimental system for various pressures. Figure S3: Determination of mass transfer coefficient of the experimental system for various ozone flow rates. Figure S4: I₃⁻ concentration as a function of time for 0.1 M KI. Figure S5: Analysis of the main degradation by-products during catalytic ozonation of phenol.

Author Contributions: J.I.L., A.d.L. and C.F. performed the conceptualisation; A.d.L., N.V. and J.I.L. carried out the design of the methodology and analyses; C.F. and N.V. contributed to the model validation; C.F., N.V. and L.M.C. carried out the formal analysis; C.F. and A.d.L. performed the investigation; C.F., J.I.L. and L.M.C. prepared the original draft; J.M.L., C.F. and N.V. reviewed and edited the manuscript; J.I.L. and A.d.L. supervised the experimentation; J.I.L., N.V. and J.M.L. acquired the funding. All authors have read and agreed to the published version of the manuscript.

Funding: The authors are grateful to the University of the Basque Country for their financial support of this study through the GIU20/56 project and C. Ferreiro's predoctoral PIF grant (PIF16/367).

Acknowledgments: The authors are thankful for the technical and human support provided by General X-ray Service and Macrobehaviour–Mesostructure–Nanotechnology Service of the General Research Services (SGIker) of the UPV/EHU.

Conflicts of Interest: The authors declare no conflict of interest.

Nomenclature

ϵ	Bed porosity, m ³ m ⁻³
v	Linear velocity of fluid flow, cm min ⁻¹
A	Reactor cross-sectional area, cm ²
$C_{O_3,L}^*$	Concentration of ozone in the equilibrium with the ozone adsorbed on the activated carbon, mg L ⁻¹
$C_{O_3,s}^*$	Concentration of ozone on the catalyst in equilibrium with the liquid ozone concentration, mg L ⁻¹
C_p^*	Calculated pollutant concentration in the liquid in terms of total organic carbon, mg L ⁻¹
C_{exp}	Experimental pollutant concentration in the liquid, mg L ⁻¹
C_{mod}	Modelled pollutant concentration in the liquid, mg L ⁻¹
$C_{O_3,G}$	Concentrations of ozone in the gas phase, mg L ⁻¹
$C_{O_3,L}$	Ozone concentration in liquid, mg L ⁻¹
C_p	Pollutant concentration in the liquid, mg L ⁻¹
D_L	Axial dispersion coefficient, cm ² min ⁻¹
F_G	Ozone mass flow, g O ₃ h ⁻¹
F_P	Phenol mass flow, g h ⁻¹
He	Henry's constant, bar L mg ⁻¹
k_1	Kinetic oxidation constant of phenol in the liquid, min ⁻¹
k_2	Kinetic oxidation constant of phenol in the solid, (mg L ⁻¹) (mg g ⁻¹ GAC min) ⁻¹

k_{ads}	Kinetic constant of phenol adsorption, $\text{g mg}^{-1} \text{min}^{-1}$
$k_{\text{c,L}}$	Elemental kinetic constant for the ozonation in the liquid, $\text{L mg}^{-1} \text{min}^{-1}$
$k_{\text{c,S}}$	Elemental kinetic constant for the ozonation in the solid, $\text{L mg}^{-1} \text{min}^{-1}$
K_{F}	Freundlich constant, $(\text{mg g}^{-1}) (\text{L mg}^{-1})^{1/n}$
$K_{\text{L}a}$	Volumetric ozone mass transfer coefficient, min^{-1}
k_{P}	Overall kinetic reaction constant referring to the removal of phenol in both the liquid and the solid, min^{-1}
L	Length of tubular reactor, cm
m	Slope of the equilibrium line between the liquid and solid phase
m_{CAT}	Catalyst's mass, g
M_{CAT}	Concentration of catalyst, g L^{-1}
n	Kinetic reaction order
N	Number of experimental values
n_{F}	Heterogeneity factor, dimensionless
$N^{\text{II}}_{\text{O}_3}$	Ozone consumption in the solid, $\text{mg L}^{-1} \text{min}^{-1}$
$N^{\text{I}}_{\text{O}_3}$	Ozone consumption in the liquid, $\text{mg L}^{-1} \text{min}^{-1}$
N_{O_3}	Whole ozone consumption, $\text{mg L}^{-1} \text{min}^{-1}$
P	Pressure, atm
$P^*_{\text{O}_3}$	Partial pressure of the ozone in equilibrium with the adsorbed ozone on the solid, bar
P_{O_3}	Partial pressure of ozone in the gas phase, bar
Q_{G}	Ozone gas flow, L min^{-1}
Q_{L}	Flow rate of liquid through the bed, mL min^{-1}
r_{O_3}	Chemical reaction rate of phenol removal reaction by catalytic ozonation, $\text{mg L}^{-1} \text{min}^{-1}$
r_{p}	Degradation of the pollutant in the liquid, $\text{mg L}^{-1} \text{min}^{-1}$
RSE	Relative standard deviation, %
t	Time, min
V	Reactor volume, L
z	Stoichiometric coefficient of the reaction between phenol and ozone
Z_{p}	Concentration of pollutant in the solid, mg g^{-1}
$Z_{\text{p},\infty}$	Amount of pollutant adsorbed in the solid in equilibrium, mg g^{-1}

References

- Akadiri, S.S.; Alola, A.A.; Alola, U.V.; Nwambe, C.S. The role of ecological footprint and the changes in degree days on environmental sustainability in the USA. *Environ. Sci. Pollut. Res.* **2020**, *27*, 24929–24938. [CrossRef]
- Aitken, D.; Rivera, D.; Godoy-Faúndez, A.; Holzapfel, E. Water Scarcity and the Impact of the Mining and Agricultural Sectors in Chile. *Sustainability* **2016**, *8*, 128. [CrossRef]
- Electronic Code of Federal Regulations (eCFR). Available online: <https://www.ecfr.gov/> (accessed on 27 April 2021).
- European Commission. Directive 2000/60/EC of the European Parliament and of the Council of 23 October 2000 Establishing a Framework for Community Action in the Field of Water Policy. *Official Journal* **2000**, *327*, 00001–0073. Available online: data.europa.eu/eli/dir/2000/60/oj (accessed on 22 December 2000).
- United Nations About the Sustainable Development Goals. Available online: <https://www.un.org/sustainabledevelopment/sustainable-development-goals/> (accessed on 7 February 2020).
- de Arruda Guelli Ulson de Souza, S.M.; de Souza, F.B.; Ulson de Souza, A.A. Application of Individual and Simultaneous Ozonation and Adsorption Processes in Batch and Fixed-Bed Reactors for Phenol Removal. *Ozone Sci. Eng.* **2012**, *34*, 259–268. [CrossRef]
- US EPA. Contaminant Candidate List 4-CCL 4. Available online: <https://www.epa.gov/ccl/contaminant-candidate-list-4-ccl-4-0> (accessed on 9 October 2018).
- Babich, H.; Davis, D.L. Phenol: A review of environmental and health risks. *Regul. Toxicol. Pharmacol.* **1981**, *1*, 90–109. [CrossRef]
- Ribeiro, H.B.; Bampi, J.; da Silva, T.C.; Dervanoski, A.; Milanese, P.M.; Fuzinato, C.F.; de Mello, J.M.M.; da Luz, C.; Vargas, G.D.L.P. Study of phenol biodegradation in different agitation systems and fixed bed column: Experimental, mathematical modeling, and numerical simulation. *Environ. Sci. Pollut. Res.* **2020**, *27*, 45250–45269. [CrossRef]
- Esplugas, S.; Giménez, J.; Contreras, S.; Pascual, E.; Rodríguez, M. Comparison of different advanced oxidation processes for phenol degradation. *Water Res.* **2002**, *36*, 1034–1042. [CrossRef]
- Sumalatha, B.; Narayana, A.V.; Kumar, K.K.; Babu, D.J.; Venkateswarulu, T.C. Phenol Removal from Industrial Effluent Using Emulsion Liquid Membranes. *J. Pharm. Sci. Res.* **2016**, *8*, 307–312.
- Chen, L.; Xu, Y.; Sun, Y. Combination of Coagulation and Ozone Catalytic Oxidation for Pretreating Coking Wastewater. *Int. J. Environ. Res. Public Health* **2019**, *16*, 1705. [CrossRef]
- Pradeep, N.V.; Anupama, S.; Navya, K.; Shalini, H.N.; Idris, M.; Hampannavar, U.S. Biological removal of phenol from wastewaters: A mini review. *Appl. Water Sci.* **2015**, *5*, 105–112. [CrossRef]

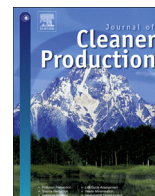
14. Klibanov, A.M.; Tu, T.M.; Scott, K.P. Peroxidase-catalyzed removal of phenols from coal-conversion waste waters. *Science* **1983**, *221*, 259–261. [[CrossRef](#)]
15. Bevilaqua, J.V.; Cammarota, M.C.; Freire, D.M.G.; Sant'Anna Jr., G.L. Phenol removal through combined biological and enzymatic treatments. *Braz. J. Chem. Eng.* **2002**, *19*, 151–158. [[CrossRef](#)]
16. De Luis, A.M.; Lombraña, J.I.; Menéndez, A.; Sanz, J. Analysis of the Toxicity of Phenol Solutions Treated with H₂O₂/UV and H₂O₂/Fe Oxidative Systems. *Ind. Eng. Chem. Res.* **2011**, *50*, 1928–1937. [[CrossRef](#)]
17. Ferreiro, C.; Villota, N.; de Luis, A.; Lombrana, J.I. Analysis of the effect of the operational variants in a combined adsorption-ozonation process with granular activated carbon for the treatment of phenol wastewater. *React. Chem. Eng.* **2020**, *5*, 760–778. [[CrossRef](#)]
18. Salvestrini, S.; Fenti, A.; Chianese, S.; Iovino, P.; Musmarra, D. Diclofenac sorption from synthetic water: Kinetic and thermodynamic analysis. *J. Environ. Chem. Eng.* **2020**, *8*, 104105. [[CrossRef](#)]
19. Erto, A.; Chianese, S.; Lancia, A.; Musmarra, D. On the mechanism of benzene and toluene adsorption in single-compound and binary systems: Energetic interactions and competitive effects. *Desalin. Water Treat.* **2017**, *86*, 259–265. [[CrossRef](#)]
20. Rout, P.R.; Zhang, T.C.; Bhunia, P.; Surampalli, R.Y. Treatment technologies for emerging contaminants in wastewater treatment plants: A review. *Sci. Total Environ.* **2021**, *753*, 141990. [[CrossRef](#)] [[PubMed](#)]
21. Rathi, B.S.; Kumar, P.S.; Show, P.-L. A review on effective removal of emerging contaminants from aquatic systems: Current trends and scope for further research. *J. Hazard. Mater.* **2021**, *409*, 124413. [[CrossRef](#)]
22. Von Sonntag, C.; Von Gunten, U. *Chemistry of Ozone in Water and Wastewater Treatment: From Basic Principles to Applications*; Iwa Publishing: London, UK, 2012; ISBN 978-1-84339-313-9.
23. Jamshidi, N.; Torabian, A.; Azimi, A.; Ghadimkhani, A. Degradation of Phenol in Aqueous Solution by Advanced Oxidation Process. *Asian J. Chem.* **2009**, *21*, 673–681.
24. Ferreiro, C.; Villota, N.; Lombraña, J.I.; Rivero, M.J. Heterogeneous Catalytic Ozonation of Aniline-Contaminated Waters: A Three-Phase Modelling Approach Using TiO₂/GAC. *Water* **2020**, *12*, 3448. [[CrossRef](#)]
25. Ameta, S. *Advanced Oxidation Processes for Wastewater Treatment: Emerging Green Chemical Technology*; Elsevier Science: San Diego, CA, USA, 2018; ISBN 978-0-12-810499-6.
26. Beltran, F.J. *Ozone Reaction Kinetics for Water and Wastewater Systems*; CRC Press: Boca Raton, FL, USA, 2003; ISBN 978-0-203-50917-3.
27. Rodríguez, A.; Rosal, R.; Perdigón-Melón, J.A.; Mezcuca, M.; Agüera, A.; Hernando, M.D.; Letón, P.; Fernández-Alba, A.R.; García-Calvo, E. Ozone-Based Technologies in Water and Wastewater Treatment. In *Emerging Contaminants from Industrial and Municipal Waste*; Barceló, D., Petrovic, M., Eds.; Springer: Berlin/Heidelberg, Germany, 2008; Volume 55/2, pp. 127–175, ISBN 978-3-540-79209-3.
28. Nawrocki, J. Catalytic ozonation in water: Controversies and questions. Discussion paper. *Appl. Catal. B Environ.* **2013**, *142–143*, 465–471. [[CrossRef](#)]
29. Nawrocki, J.; Kasprzyk-Hordern, B. The efficiency and mechanisms of catalytic ozonation. *Appl. Catal. B Environ.* **2010**, *99*, 27–42. [[CrossRef](#)]
30. Guo, Y.; Yang, L.; Wang, X. The Application and Reaction Mechanism of Catalytic Ozonation in Water Treatment. *J. Environ. Anal. Toxicol.* **2012**, *2*, 2161–0525. [[CrossRef](#)]
31. Criegee, R. Mechanism of Ozonolysis. *Angew. Chem. Int. Ed. Engl.* **1975**, *14*, 745–752. [[CrossRef](#)]
32. Lin, S.H.; Wang, C.H. Ozonation of phenolic wastewater in a gas-induced reactor with a fixed granular activated carbon bed. *Ind. Eng. Chem. Res.* **2003**, *42*, 1648–1653. [[CrossRef](#)]
33. Xiong, W.; Chen, N.; Feng, C.; Liu, Y.; Ma, N.; Deng, J.; Xing, L.; Gao, Y. Ozonation catalyzed by iron—and/or manganese—supported granular activated carbons for the treatment of phenol. *Environ. Sci. Pollut. Res. Int.* **2019**, *26*, 21022–21033. [[CrossRef](#)]
34. Shukla, S.; Kisku, G. Linear and Non-Linear Kinetic Modeling for Adsorption of Disperse Dye in Batch Process. *Res. J. Environ. Toxicol.* **2015**, *9*, 320–331. [[CrossRef](#)]
35. Ferreiro, C.; Gómez-Motos, I.; Lombraña, J.I.; de Luis, A.; Villota, N.; Ros, O.; Etxebarria, N. Contaminants of Emerging Concern Removal in an Effluent of Wastewater Treatment Plant under Biological and Continuous Mode Ultrafiltration Treatment. *Sustainability* **2020**, *12*, 725. [[CrossRef](#)]
36. Alhamed, Y.A. Adsorption kinetics and performance of packed bed adsorber for phenol removal using activated carbon from dates' stones. *J. Hazard. Mater.* **2009**, *170*, 763–770. [[CrossRef](#)]
37. Rodríguez, C.; Lombrana, J.I.; de Luis, A.; Sanz, J. Oxidizing efficiency analysis of an ozonation process to degrade the dye rhodamine 6G. *J. Chem. Technol. Biotechnol.* **2017**, *92*, 656–665. [[CrossRef](#)]
38. Gottschalk, C.; Saupe, A.; Libra, J.A. *Ozonation of Water and Waste Water: A practical Guide to Understanding Ozone and Its Application*; Wiley-VCH: Weinheim, Germany, 2010. [[CrossRef](#)]
39. Chaichanawong, J.; Yamamoto, T.; Ohmori, T. Enhancement effect of carbon adsorbent on ozonation of aqueous phenol. *J. Hazard. Mater.* **2010**, *175*, 673–679. [[CrossRef](#)] [[PubMed](#)]
40. Ferreiro, C.; Villota, N.; Lombraña, J.I.; Rivero, M.J.; Zúñiga, V.; Rituerto, J.M. Analysis of a Hybrid Suspended-Supported Photocatalytic Reactor for the Treatment of Wastewater Containing Benzothiazole and Aniline. *Water* **2019**, *11*, 337. [[CrossRef](#)]

41. Rekhate, C.V.; Srivastava, J.K. Recent advances in ozone-based advanced oxidation processes for treatment of wastewater—A review. *Chem. Eng. J. Adv.* **2020**, *3*, 100031. [[CrossRef](#)]
42. Chand, R.; Molina, R.; Johnson, I.; Hans, A.; Bremner, D.H. Activated carbon cloth: A potential adsorbing/oxidizing catalyst for phenolic wastewater. *Water Sci. Technol. J. Int. Assoc. Water Pollut. Res.* **2010**, *61*, 2817–2823. [[CrossRef](#)]
43. Beltrán, F.J.; Rivas, F.J.; Montero-de-Espinosa, R. Mineralization improvement of phenol aqueous solutions through heterogeneous catalytic ozonation. *J. Chem. Technol. Biotechnol.* **2003**, *78*, 1225–1233. [[CrossRef](#)]
44. Byun, S.; Cho, S.H.; Yoon, J.; Geissen, S.U.; Vogelpohl, A.; Kim, S.M. Influence of mass transfer on the ozonation of wastewater from the glass fiber industry. *Water Sci. Technol. J. Int. Assoc. Water Pollut. Res.* **2004**, *49*, 31–36. [[CrossRef](#)]
45. Rosen, H.M. Use of Ozone and Oxygen in Advanced Wastewater Treatment. *J. Water Pollut. Control Fed.* **1973**, *45*, 2521–2536.
46. Buhler, R.; Staehelin, J.; Hoigne, J. Ozone Decomposition in Water Studied by Pulse-Radiolysis 1. HO_2/O_2^- and HO_3/O_3^- as Intermediates. *J. Phys. Chem.* **1984**, *88*, 2560–2564. [[CrossRef](#)]
47. Nawaz, F.; Cao, H.; Xie, Y.; Xiao, J.; Chen, Y.; Ghazi, Z.A. Selection of active phase of MnO_2 for catalytic ozonation of 4-nitrophenol. *Chemosphere* **2017**, *168*, 1457–1466. [[CrossRef](#)]
48. Yang, L.; Sheng, M.; Li, Y.; Xue, W.; Li, K.; Cao, G. A hybrid process of Fe-based catalytic ozonation and biodegradation for the treatment of industrial wastewater reverse osmosis concentrate. *Chemosphere* **2020**, *238*, 124639. [[CrossRef](#)] [[PubMed](#)]
49. Hu, E.; Wu, X.; Shang, S.; Tao, X.; Jiang, S.; Gan, L. Catalytic ozonation of simulated textile dyeing wastewater using mesoporous carbon aerogel supported copper oxide catalyst. *J. Clean. Prod.* **2016**, *112*, 4710–4718. [[CrossRef](#)]
50. Lin, S.H.; Wang, C.H. Adsorption and catalytic oxidation of phenol in a new ozone reactor. *Environ. Technol.* **2003**, *24*, 1031–1039. [[CrossRef](#)] [[PubMed](#)]
51. Ribao, P.; Rivero, M.J.; Ortiz, I. TiO_2 structures doped with noble metals and/or graphene oxide to improve the photocatalytic degradation of dichloroacetic acid. *Environ. Sci. Pollut. Res. Int.* **2017**, *24*, 12628–12637. [[CrossRef](#)]
52. Kaledin, L.A.; Tepper, F.; Kaledin, T.G. Pristine point of zero charge (p.p.z.c.) and zeta potentials of boehmite's nanolayer and nanofiber surfaces. *Int. J. Smart Nano Mater.* **2016**, *7*, 1–21. [[CrossRef](#)]
53. Wu, C.; Liu, X.; Wei, D.; Fan, J.; Wang, L. Photosonochemical degradation of Phenol in water. *Water Res.* **2001**, *35*, 3927–3933. [[CrossRef](#)]
54. Association, A.P.H. *Standard Methods for the Examination of Water and Wastewater*; American Public Health Association: Washington, DC, USA, 2005; ISBN 978-0-87553-047-5.
55. Alfonso-Muniozguren, P.; Ferreira, C.; Richard, E.; Bussemaker, M.; Lombrana, J.I.; Lee, J. Analysis of Ultrasonic Pre-treatment for the Ozonation of Humic Acids. *Ultrason. Sonochem.* **2020**, *71*, 105359. [[CrossRef](#)]
56. Sanchez, M.; Rivero, M.J.; Ortiz, I. Kinetics of dodecylbenzenesulphonate mineralisation by TiO_2 photocatalysis. *Appl. Catal. B Environ.* **2011**, *101*, 515–521. [[CrossRef](#)]

3.8. 8. argitalpena. An efficient catalytic process for the treatment of genotoxic aniline wastewater using a new granular activated carbon-supported titanium dioxide composite

3.8 kapitulua artikulu honi dagokio:

C. Ferreiro, N. Villota, J.I. Lombraña, M.J. Rivero. An efficient catalytic process for the treatment of genotoxic aniline wastewater using a new granular activated carbon-supported titanium dioxide composite. *Journal of Cleaner Production*, 228, 1282-1295, 2019. DOI: 10.1016/j.jclepro.2019.04.198.



An efficient catalytic process for the treatment of genotoxic aniline wastewater using a new granular activated carbon-supported titanium dioxide composite

C. Ferreiro ^a, N. Villota ^b, J.I. Lombrana ^a, María J. Rivero ^{c,*}

^a Department of Chemical Engineering, Faculty of Science and Technology, University of the Basque Country UPV/EHU, 48940, Leioa, Spain

^b Department of Chemical and Environmental Engineering, Escuela de Ingeniería de Vitoria-Gasteiz, University of the Basque Country UPV/EHU, 01006, Vitoria-Gasteiz, Spain

^c Department of Chemical and Biomolecular Engineering, University of Cantabria, 39005, Santander, Spain

ARTICLE INFO

Article history:

Received 26 November 2018

Received in revised form

12 April 2019

Accepted 16 April 2019

Available online 19 April 2019

Keywords:

Waste elimination

Water management

Catalytic ozonation

TiO₂/GAC

Aniline

ABSTRACT

This work presents an efficient catalytic ozonation process for the treatment of aniline wastewater as a model pollutant. The process uses a granular activated carbon-supported titanium dioxide catalyst with environmentally-friendly and sustainable characteristics. Titanium dioxide composites were prepared by precipitation of alcoholic titanium tetrachloride solutions on two different carbon supports: Norit® GAC 1240 Plus and Norit® ROX 0.8. This method is an improvement on other composite preparation methods such as hydrothermal and impregnation by immersion techniques, which were also carried out for comparison. It characterised our composites by Brunauer–Emmett–Teller analysis, scanning electron microscopy–energy dispersive X-ray spectroscopy and Fourier-transform infrared spectroscopy to assess the influence of the carbon support. Composites synthesised via this novel precipitation method presented a 25% increase in their initial specific surface area and a 9.1% increase in titanium dioxide loading. It compared the catalytic activity of the different titanium dioxide composites on different aniline solutions, and studied the optimal pH and ozone dose. Norit® GAC 1240 Plus-supported titanium dioxide composite prepared by the precipitation method gave the highest removal yield with 80.24% mineralisation of total organic carbon in 45 min. With respect to the costs associated with the treatment, the composite achieved a removal yield of 26.8 mg ozone/mg total organic carbon.

© 2019 Elsevier Ltd. All rights reserved.

1. Introduction

Aniline (ANI) can be found in effluents derived from the production of vulcanisation accelerators, textiles, pesticides and dyes, among others, and it is known to have a negative impact on the environment (Chen et al., 2014; Mestankova et al., 2016; Zhang et al., 2015). Aniline is currently included on the first list of priority substances published by the European Chemicals Agency (European Commission, 2004; Lichtfouse et al., 2015), who have classified it as a skin sensitizer (Official Journal of the European Union, 2008). This pollutant has also been included in the US EPA's Contaminant Candidate List (US EPA, 2014), which indexes pollutants that are not currently subject to any national drinking

water regulations but are known or believed to exist in public water systems. According to the latest European Union Risk Assessment Report, the main effect of exposure to aniline by any route, whether via the skin, lungs or the gastrointestinal tract, is a change in the blood that affects oxygen transport to tissues. This alteration can have mild or severe consequences depending on the duration and magnitude of the exposure. Ingesting 1 g of aniline can be fatal to humans. The mean lethal dose of aniline is 5–30 g and the minimum lethal dose for a 68 kg human is 10 g (Harbison et al., 2015).

Lubash (1964) and Sihtmäe et al. (2010) studied the effects of aniline in different organisms. For example, aniline inhibited embryonic development in *Xenopus laevis* (African clawed frog), wherein body size was reduced and pigmentation inhibited at concentrations of 1–40 mg/L (DumPERT, 1987). Exposing ova from *Micropterus salmoides* (bass) and *Carassius auratus* (goldfish) to concentrations of aniline as high as 100 mg/L produced teratogenic effects and reduced hatching and survival in offspring (Birge et al.,

* Corresponding author.

E-mail addresses: cristian.ferreiro@ehu.es (C. Ferreiro), natalia.villota@ehu.es (N. Villota), ji.lombrana@ehu.es (J.I. Lombrana), riveromj@unican.es (M.J. Rivero).

1979). Baird et al. (1977) noted that exposure to aniline at concentrations of 20 mg/L had inhibitory effects on the respiration of bacteria that were degrading activated sludge, which suggests that a metabolite or metabolites may be responsible for the observed toxicity. Exposing *Daphnia magna* (planktonic crustacean) to aniline at concentrations of 43.2 µg/L caused mortality, while a concentration of 22 µg/L damaged its reproduction and growth (Gersich and Milazzo, 1990). In plants, aniline is absorbed via the roots then rapidly and irreversibly binds to plant constituents, causing perturbations in cellular DNA replication (Lyons et al., 1984). Moreover, a recent study has evidenced aniline-induced genotoxicity and growth inhibition in wheat crops (Tao et al., 2017).

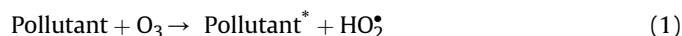
A remarkable case highlighting how aniline spills can cause serious damage to human health is that of Aguascalientes, Mexico, more precisely on the San Pedro river, where textile industries, wheat crops and Mexico's fourteenth largest metropolitan area coexist (Guzman-Colis et al., 2011; Spring 2011). Dye industries often generate aniline wastewater. In certain locations, such as the Mexican State of Aguascalientes, where there is a concentration of these industries, aniline has been detected in the San Pedro river at levels as high as 20 mg/L (Spring 2011; Vizcaíno et al., 2018). Based on the study by Tao et al. (2017), wheat crops lining the river may be seriously affected by aniline, causing genotoxicity in wheat root tip cells (Guzman-Colis et al., 2011). Significant chromosomal aberrations, even at aniline concentrations of just 5 mg/L, could lead to considerable damage to wheat crops (Eskola et al., 2018). Therefore, the implementation of an efficient wastewater treatment to remove aniline from water resources is essential to prevent perturbations in cellular DNA replication on growth of wheat and any risk to human health (Tao et al., 2017).

Sánchez et al. (1997) studied the photocatalytic oxidation of aniline in aqueous suspensions of TiO₂ using UV light. Shahrezaei et al. (2012) studied the possibility of applying UV/TiO₂ photocatalysis to treat aqueous effluents containing aniline. Anotai et al. (2012) investigated aniline oxidation using titanium dioxide activated with visible light. However, the high reaction time required and the low mineralisation precluded its industrial implantation. Aniline cannot be removed by biological treatments due to its low biodegradability and high toxicity. So alternative treatments that can reuse wastewater containing refractory contaminants must be considered (Sepehri and Sarrafzadeh, 2018). Some studies have proposed the use of diatomaceous chemical adsorbents (Aguedal et al., 2017, 2019; Bensalah et al., 2018). Catalytic ozonation therefore represents an alternative technology to achieve their complete mineralisation of refractory contaminants because more hydroxyl radical may be generated in the presence of both a catalyst and ozone (Boczka and Fernandes, 2017; Ghuge and Saroha, 2018; Kermani et al., 2018). Despite the availability of several catalysts, authors such as Beltran et al. (2004) and Song et al. (2010) have catalogued titanium oxide as an active material that can accelerate the ozonation process for different pollutants when used alone, or when combined with photocatalysis (Rivas et al., 2012). Beltran (2003) obtained conversions rates that were 40 times greater compared to non-catalytic ozonation.

The improvement in the removal yields can be attributed to the ozonation mechanisms that take place on catalytic surfaces. These mechanisms have not yet been fully defined (Rosal et al., 2008). According to Guo et al. (2012) and Rodríguez et al. (2008), the catalyst acts as an adsorbent where organic contaminants are first adsorbed on the catalyst surface and then removed. In this case the active adsorption sites combine with the organic molecules to form active complexes with a lower activation energy. The pollutants are oxidised by the molecular ozone and hydroxyl radicals available in the solution. Subsequently, the reaction intermediates are further oxidised on the catalyst surface or desorbed to the aqueous solution

where they are oxidised by the ozone or radical species in the medium. Another mechanism proposed by Legube and Leitner (1999) suggests that the metal oxide of the catalyst favours ozone mass transport and initiates its decomposition. This mechanism assumes that the hydroxyl groups on the catalytic surface play an important role in the generation of the radical species. The dissolved ozone is adsorbed on the catalyst surface, thus leading to a series of radical reactions that conclude with the formation of highly reactive hydroxyl radicals capable of oxidising the organic molecules in the wastewater. Beltran (2003) proposed a Langmuir–Hinshelwood (LH) mechanism to describe the catalytic gas-phase decomposition of ozone:

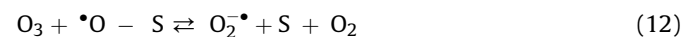
Homogeneous decomposition of ozone:



where *Pollutant*^{*} represents a destabilised state of the molecule due to polarisation. Surface reaction for the heterogeneous decomposition of ozone on the granular activated carbon-supported titanium dioxide catalyst (TiO₂/GAC) it represented for a pH of between 2 and 6 by:



where S represents one active site on the TiO₂/GAC catalyst surface. For a pH higher than 6:



Homogeneous propagation and termination reactions:



In recent years, TiO₂/GAC catalysts have attracted the attention of many researchers due to the synergistic effect obtained when used in combination with photocatalysis (MiarAlipour et al., 2018; Noorimotlagh et al., 2018; Xing et al., 2016) or ozonation (Ghuge and Saroha, 2018; Orge et al., 2017; Ratnawalti, 2017). However, a slow reaction rate and low mineralisation yields have impeded

their industrial implementation. Low removals can be attributed to: a) the choice of support, which should be able to provide enough surface area and a suitable pore structure; b) the catalyst's active components; and c) the catalyst preparation method (Guo et al., 2012). The structure and distribution of the catalysts are affected by the preparation method, so a good catalyst preparation process can significantly improve the catalytic activity. Table 1 shows the results from previous studies of aniline ozonation.

Considering the limitations of non-catalytic ozonation and the possibilities of catalytic ozonation combined with activated carbon for aniline degradation, this paper proposes a more efficient TiO₂/GAC catalytic ozonation process that focuses on reducing ozone consumption thanks to a new TiO₂/GAC material. Aniline was selected as a model compound due to its environmental impact, but other contaminants present in polluted waters could also be degraded by these catalysts. Therefore, this work contributes to solve a food safety problem with implications for human health and environmental protection. Given the importance of the synthesis method on the properties and effectiveness of the catalysts, we aimed to develop a new catalytic material from two GAC supports, Norit® GAC 1240 Plus and Norit® ROX 0.8, based on precipitation, hydrothermal or immersion-impregnation techniques, resulting in the deposition of perfectly distributed TiO₂ nanocrystals on the GAC support. Furthermore, we studied the effect of pH and O₃ dose with the best catalytic material in an attempt to reduce ozone consumption.

The above aims will contribute to the final implementation of the proposed technology. On an industrial scale, the process would be carried out in a fluidised bed reactor (FBR) considering their straightforward construction and operation, low operating costs and high flexibility in terms of liquid and solid-phase residence times. The use of TiO₂ nanoparticles supported on large pore size GAC would result in advantages such as greater mass and heat transfer in the FBR system (Tisa et al., 2014). In addition, the process would not require a catalytic material recovery stage and since the TiO₂ nanoparticles are bound to the GAC they would be less likely to cause any environmentally detrimental effects (Martins et al., 2017). Nor would this composite would require a regeneration stage because TiO₂ effectively destroys the pollutants adsorbed on the GAC (Colmenares et al., 2016). At the end of its useful life, the TiO₂/GAC catalyst can be disposed of as solid waste.

2. Experimental

2.1. Materials and reagents

Aniline (C₆H₅NH₂, Acros Organics, 99.5%), nitric acid (HNO₃, Acros Organics, 69%), titanium (IV) chloride (TiCl₄, Merck, synthesis quality), absolute ethanol (C₂H₆O, Panreac, 100%), hydrogen chloride (HCl, Merck, 37%), sulfuric acid (H₂SO₄, Sigma-Aldrich, 98%), sodium hydroxide (NaOH, Panreac, 50%) and HPLC-grade methanol

(CH₃OH, Merck, >99.99%) were used as received. Deionised water was supplied by a Milli-Q® water purification unit supplied by Merck. The TiO₂ Aeroxide® P90 catalyst was obtained from Evonik Industries. Granular activated carbons Norit® GAC 1240 Plus and Norit® ROX 0.8 were purchased from Cabot Corporation.

2.2. Synthesis of TiO₂/GAC composites

2.2.1. Precipitation method

The carbon was pretreated with 37% HCl for 30 min, then washed with deionised water. 440 mL of absolute ethanol with 10 mL of TiCl₄ were mixed for 30 min at 23 °C until a yellow solution was obtained. 2.0 mg of TiO₂ Aeroxide® P90 was dissolved in 50 mL of ethanol under sonication for 15 min and added to TiCl₄-EtOH solution in order to control the diameter and size distribution of the crystals. Then, 14.0 g of pretreated GAC was added and stirred slowly for 45 min. Finally, 19.2 mL of 50% NaOH was poured into the reactor for 2 h. The composite was washed with 10% HNO₃ and deionised water, then dried in an oven at 90 °C for 12 h and finally, it was calcined in an air atmosphere at 400 °C for 1 h.

2.2.2. Immersion impregnation

The carbon was pretreated with 37% HCl for 30 min, then washed with deionised water. 1.0 g of TiO₂ Aeroxide® P90 was dissolved in 400 mL of deionised water under sonication for 15 min. Aeroxide® P90 was selected over Aeroxide® P25 because it has a smaller particle size, thus facilitating its entry into the pores. The solution was transferred to a spherical reactor, 14.0 g of pretreated GAC was added and the pH adjusted to 12.0 with the addition of 50% NaOH. The activated carbon was left for 1 h in the TiO₂ solution under continuous agitation at room temperature. The resulting solution was subsequently heated in a thermostatic bath at 100 °C until 264 mL of solution had evaporated. The TiO₂/GAC composite was washed with deionised water and dried in an oven at 90 °C for 12 h before being calcined in an air atmosphere at 400 °C for 1 h.

2.2.3. Hydrothermal method

Again, the carbon was pretreated with 37% HCl for 30 min, washed with deionised water and dried in an oven at 80 °C for 24 h. 1.0 g of TiO₂ Aeroxide® P90 was dispersed in 400 mL of deionised water under sonication for 15 min, then transferred to a Teflon® recipient. 14.0 g of pretreated GAC was added and the mixture stirred constantly for 2 h at 20 °C. The Teflon recipient was then closed and placed in an oven at 120 °C for 3 h. Afterwards, the supernatant was removed and the solid washed with deionised water and dried in an oven at 50 °C for 12 h.

2.3. Characterisation methods

Nitrogen adsorption measurements were performed using the Micromeritics ASAP 2010 instrument at 77 K with ultra-high purity

Table 1

Previous studies on aniline ozonation at 25 °C. Removal efficiencies in Chemical Oxygen Demand (% COD) and Total Organic Carbon (% TOC).

Treatment	O ₃ time, min	C _{ANIL} , mg/L	O ₃ flow rate, g/h	O ₃ inlet concentration, mg/L	pH	V _{reac} , L	Catalyst	Catalyst mass, mg	Removal efficiency, %	Reference
O ₃	120	103.81	2.5	22.0	7.0	1.0	–	–	93.56% Aniline 31.03% COD	Jing et al. (2015)
O ₃ /GAC	30	102.44	0.0049	50.0	7.0	0.7	Norit 1240 Plus granular activated carbon	350.0	100% Aniline 56% TOC	Faria et al. (2007)
O ₃ /TiO ₂ -GAC	60	93.13	0.0049	50.0	5.6	0.25	Nanocyl 3100 activated carbon doped with TiO ₂ by hydration-dehydration method	125.0	100% Aniline 57% TOC	Orge et al. (2017)

nitrogen gas. All samples were dried and degassed under high vacuum at 473 K for 24 h prior to measurement. The surface area was calculated using the BET equation and the pore size distribution was determined by applying the BJH model. Morphology was obtained through scanning electron microscopy with energy dispersive X-ray spectroscopy (SEM-EDX) using a JEOL JSM-7000F electron microscope. TiO₂ composite loading was determined by micro X-ray fluorescence (micro-XRF) on all 17 spherule layers (SLs) with a Bruker Nano Analytics M4 Tornado 2D-micro-XRF spectrometer with polycapillary X-ray optics, using a Rh anode operating at 50 kV and 600 μA. Data was analysed using the M4 TORNADO software (Bruker Nano Analytics). Fourier-transform infrared spectroscopy (FTIR) was conducted with a Jasco 4200 model to determine FTIR spectres in medium infrared (4000–400 cm⁻¹) using KBr pellets for sample preparation. A Waters 2695 HPLC system with an Agilent ZORBAX Rapid Resolution High Definition Eclipse PAH threaded column (150 mm × 4.6 mm, 5 μm), with the guard column working at 20 °C under isocratic elution (10% methanol, 90% water), a flow rate of 1 mL/min and an injection volume of 1.0 μL, was used for aniline quantification. The Waters 996 photodiode array (PDA) detector was used at a wavelength of 230 nm. The degree of mineralisation was quantified by total organic carbon (TOC) analysis in a Shimadzu TOC-VCSH Analyzer. Colour was analysed using a PerkinElmer Lambda 10 UV/Vis spectrophotometer by directly measuring absorbance at 455 nm (Mijangos et al., 2006) and aromatic ring rupture was determined from the sample's absorbance at 254 nm.

2.4. Ozonation experiments

Aniline was removed from aqueous solutions using three TiO₂/GAC composites prepared by precipitation, impregnation by immersion and hydrothermal methods. Each composite was prepared with two types of activated carbon (Norit® GAC 1240 Plus and Norit® ROX 0.8). Experiments were carried out at an initial pH of 7.5, an ozone dose of 11.3 mg/L and a gas flow of 2.5 g O₃/h. Operational variables were analysed at different ozonation pHs (3.0, 5.0, 7.0 and 9.0) and ozone doses (3.7, 5.4, 11.3 and 20.1 mg/L) keeping both parameters constant throughout the experiment. Ozonation

experiments were performed in a 2 L jacketed reactor equipped with a stirrer and several ozone diffusers (see Fig. 1).

For each experiment, the reactor was filled with 1.5 L of 20.0 mg/L aniline solution at the desired pH and 5.0 g of the catalyst. The experiments were carried out under a constant flow of gas, constant ozone concentration at the inlet, 18 °C and at 1 atm. The agitation was maintained constant at 60 rpm to ensure a homogeneous mixture. Ozone was produced from extra pure oxygen in the TRIOGEN LAB2B generator. The temperature was controlled using a refrigerating bath. The ozone concentration in the gas phase was monitored with a BMT 964C ozone analyser. Dissolved ozone concentration in the liquid phase and temperature were measured with a Rosemount Analytical model 499AOZ-54 probe. The pH was controlled with a Rosemount Analytical model 399-09-62 probe, integrated with the ozone probe in a Rosemount Analytical Solu Comp II recorder. Gas-phase ozone leaving the reactor was removed with a Zonosistem thermocatalytic ozone destructor. TiO₂/GAC composites were analysed after each experiment via FTIR. Neither aniline nor any oxidation intermediates were detected adsorbed on the surface of the catalytic material.

3. Results and discussion

3.1. Experimental system characterisation

The experimental system was characterised by determining the volumetric mass transfer coefficient ($k_L a$) under the optimal operating conditions obtained from the study. The ozone mass balance in a volume element of aqueous phase during an isothermal ozonation process controlled by a chemical step is shown in Eq. (17):

$$\frac{dC_{O_3}}{dt} = k_L a (C_{O_3}^* - C_{O_3,s}) - k_d C_{O_3,s}^n \quad (17)$$

where k_L is the liquid phase individual mass transfer coefficient in m/s, a is the specific gas–liquid interfacial surface inside the ozonation reactor in m⁻¹, $C_{O_3}^*$ is the equilibrium concentration of ozone dissolved in water in mol/L, $C_{O_3,s}$ is the concentration of

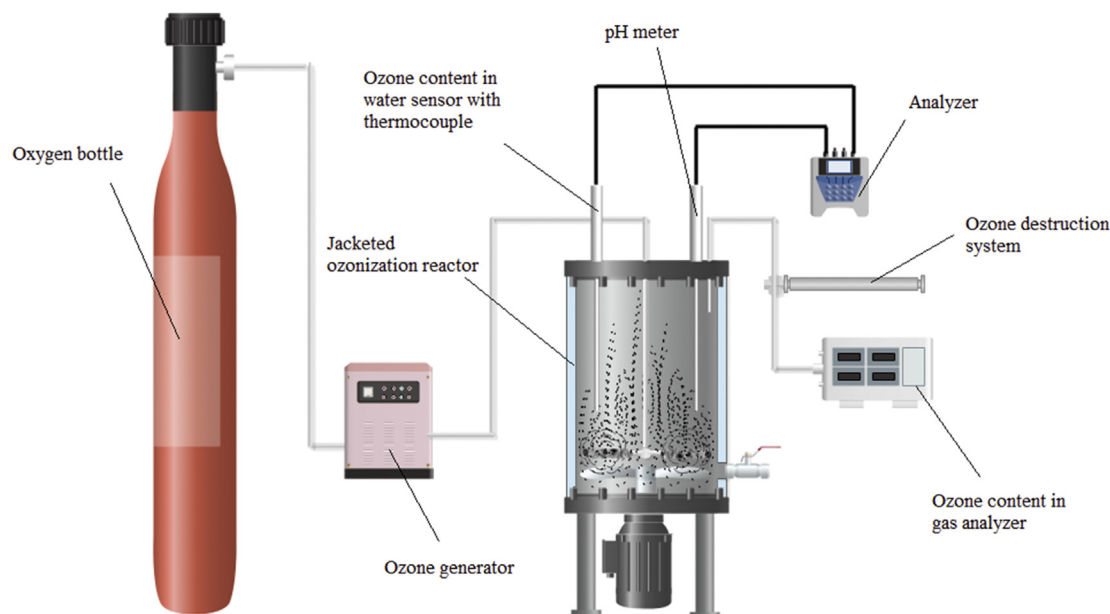


Fig. 1. Diagram of the experimental equipment used to carry out the catalytic ozonation assays with aniline.

ozone dissolved in water after reaching a stationary value in mol/L, n is the kinetic order and k_d is the ozone decomposition kinetic constant. The value of k_d depends on: temperature, dissolved organic and inorganic matter, pH, alkalinity and ionic strength (Beltran, 2003; Rodríguez et al., 2017).

The experimental conditions used to calculate $k_L a$ were: a gas flow of 2.5 g O₃/h, ozone concentration of 5.4 mg/L, pH = 7.0, reaction volume of 1.5 L of deionised water, 60 rpm, 1 atm and a temperature of 18.0 °C. After 10 min, the system reached a fluid-dynamic steady state. Fig. S1 shows the concentration of dissolved ozone, $C_{L O_3}$, during the ozonation of deionised water where catalytic ozonation takes place. In Fig. S1a, three different regions can be distinguished. According to Rodríguez et al. (2008) zone I is characterised by a strong increase in dissolved ozone, followed by zone II, where the ozone saturation concentration is reached at a stationary value $C_{O_3, s}$ and finally in zone III ozone decomposition takes place after stopping ozone generation.

Applying Eq. (17) to zones II and III produced the following expression:

$$0 = k_L a (C_{O_3}^* - C_{O_3, s}) - k_d C_{O_3, s}^n \quad (18)$$

$$-r_d = k_d C_{O_3}^n \quad (19)$$

where r_d is the rate of ozone decomposition. $C_{O_3}^*$ was calculated from Henry's law:

$$P_{O_3} = C_{O_3}^* H_e \quad (20)$$

where the Henry's law solubility constant H_e (atm mole fraction⁻¹) was calculated from the Roth and Sullivan (1981) correlation:

$$H_e = 3.84 \times 10^7 C_{OH}^{0.035} \exp\left(-\frac{2428}{T}\right) \quad (21)$$

The estimated value of the ozone decomposition kinetic constant (k_d) was 0.239 L^{0.1} mg^{-0.1} min⁻¹ and the kinetic order (n) was 1.1. The mass transfer constant value was estimated to be 0.32 min⁻¹ with a standard deviation of 0.017 (Fig. S1b). This $k_L a$ value was similar to the one obtained for other ozonation systems (Rodríguez et al., 2008; Rodríguez et al., 2017).

3.2. Morphology studies

SEM composite images of samples prepared with TiO₂ impregnated by immersion (Fig. 2c and f) or hydrothermal treatment (Fig. 2b and e) show a significant agglomeration and irregular distribution of particles with diameters over 4 μm. These particles are bigger than those obtained by the precipitation method (Fig. 2a and d). These conventional techniques present a limited capacity for ensuring TiO₂ enters inside the pores, leading to a merely superficial TiO₂ deposition. Such particles could block the internal porosity of the activated carbon and therefore reduce its catalytic activity. In Fig. 2a and d, the TiO₂ crystals deposited via the precipitation method present a better distribution, regardless of the particular porosity of each type of activated carbon. Thus, TiO₂/GAC composites prepared by this method are expected to provide better catalytic activity.

A SEM/EDAX analysis was performed on two composite materials synthesised using the precipitation method (see Fig. 3). Fig. 3a and b shows SEM images of pristine activated carbons. EDAX analysis shows the presence of Si and Al, both typical of lignocellulosic carbons (Daud et al., 2017). Fig. 3c and d are useful for analysing the cross-section and also reveal the presence of TiO₂

particles adsorbed on all the internal cavities of the activated carbon. In addition, Fig. 3c shows a perfectly developed porous structure free of agglomerated particles. The EDAX images confirm that TiO₂ was definitely deposited.

3.3. FTIR studies

FTIR spectra for the commercially available activated carbon Norit[®] GAC 1240 Plus, TiO₂ and the TiO₂/GAC composite prepared by the precipitation method are shown in Fig. 4. The absorption band from 3100 to 3700 cm⁻¹ is associated with an -OH stretch corresponds to the water used to prepare the samples during the potassium bromide pellet technique (Rubinson and Rubinson, 2000). This is confirmed by the band at 1715–1720 cm⁻¹, which can be assigned to a vibrational -OH group (Nakamoto, 1997). In the region between 400 and 800 cm⁻¹, the peak in the composite spectrum is much more pronounced than the one observed in the spectrum for Norit[®] GAC 1240 Plus active carbon. According to Bagheri et al. (2016) and Orha et al. (2017), this absorption band corresponds to a Ti-O stretching group. These results confirm the presence of TiO₂ in the composite synthesised by the precipitation method.

3.4. Nitrogen sorption studies

The nitrogen adsorption–desorption isotherms for the TiO₂/GAC composite samples are shown in Fig. 5. The initial amount of nitrogen adsorbed by each sample increases rapidly as the relative pressure increases to $P/P_0 \approx 0.3$, before it reaches an almost horizontal saturation plateau. This behaviour is associated with a type I isotherm and a H4 hysteresis cycle.

These experiments confirmed that composites prepared with Norit[®] ROX 0.8 carbon have a microporous configuration because Norit[®] ROX 0.8 contains pores with a diameter of less than 30 Å. Nevertheless, the mesoporous carbon Norit[®] GAC 1240 Plus has pore diameters of between 100 and 1000 Å. The increased pore size in composites prepared from Norit[®] ROX 0.8 could be due to the calcination stage at 400 °C (Ghasemi et al., 2016).

The physical properties of our TiO₂/GAC composites are shown in Table 2. SEM images confirmed that composites prepared by hydrothermal or immersion-impregnation methods present a reduced surface area. This could be attributed to porous blocking. However, the specific surface area of TiO₂/Norit[®] GAC 1240 Plus prepared by precipitation is higher, 985.0 m²/g, than the original value of 967.0 m²/g. Even the total pore volume and average pore diameter did not vary significantly, the deposition of TiO₂ results in a 25% increase of the external surface area. These are promising results given that the synthesis methods published to date (Andriantsiferana et al., 2015; Noorimotlagh et al., 2018; Orge et al., 2017) produce composites with a reduction of 70–80% of the initial specific surface area. In such cases, poor dispersion of TiO₂ due to the formation of agglomerates would block the pores and obstruct access to the internal porosity of the activated carbon.

Compared to other synthesis methods, Yao et al. (2012) developed a TiO₂/GAC composite using tetrabutyltitanate and the sol-gel method at low temperatures resulting in a significantly altered porous structure. The specific surface area was reduced by 54%, from 837.6 to 383.5 m²/g. Regarding total pore volume, they reported a decrease from 0.46 to 0.31 cm³/g, representing a reduction of 33%. This was attributed to the pores being blocked by TiO₂.

3.5. Micro-X-ray fluorescence analysis and pH_{pzc} determination

Table 2 shows the weight percent of TiO₂ deposited in the different TiO₂/GAC composites. Each sample was analysed 15 times.

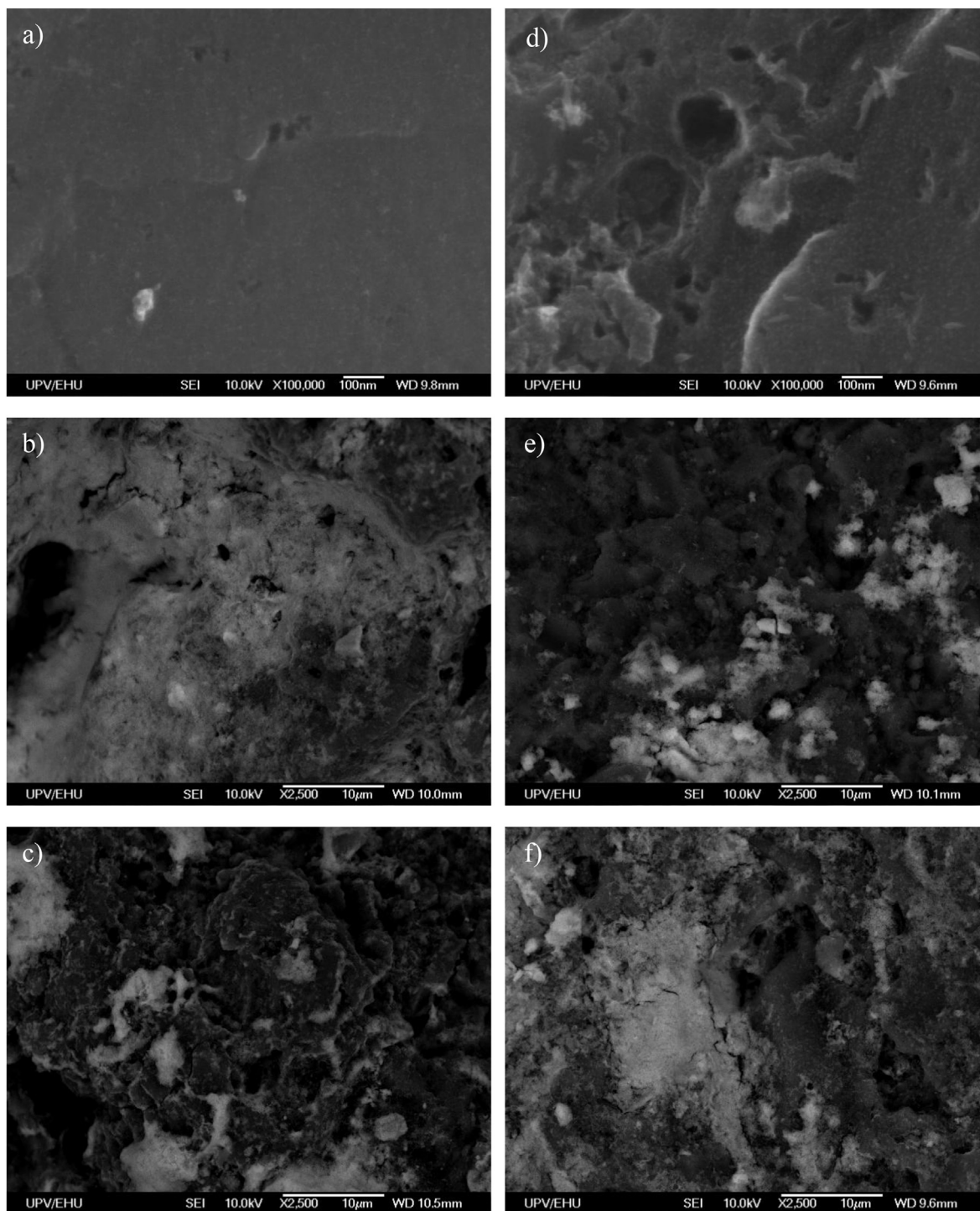


Fig. 2. SEM images of the TiO₂/Norit[®] GAC 1240 Plus prepared by: a) precipitation; b) hydrothermal; and c) impregnation by immersion; and TiO₂/Norit[®] ROX 0.8 prepared by: d) precipitation; e) hydrothermal; and f) impregnation by immersion.

A relative standard deviation of 2.1% was obtained. The highest TiO₂ loadings were obtained with the precipitation method for the TiO₂/Norit[®] GAC 1240 Plus composite with a deposition of 9.1% of TiO₂. Orge et al. (2017) synthesised similar materials but they did not quantify the TiO₂ loading. Other authors, such as Noorimotlagh et al. (2018) only managed to deposit 0.7% of TiO₂.

Andriantsiferana et al. (2014), using the metal-organic chemical vapor deposition technique (MOCVD), obtained a TiO₂/GAC catalytic material with a specific surface area of 962 m²/g starting from

a surface area of activated carbon of 1100 m²/g; however, the pore size (12 Å), volume of mesopores (0.041 cm³/g) and amount of TiO₂ deposited (7.9%) is less suitable in comparison with the TiO₂/Norit[®] GAC 1240 Plus composite prepared in this work. Moreover, their methodology is more complicated and requires special equipment.

The efficiency of the catalyst could be affected by its point of zero charge (PZC). When the surface of the catalyst is positively charged it favours interactions with anionic pollutants, whereas a negatively charged surface promotes interactions with cationic

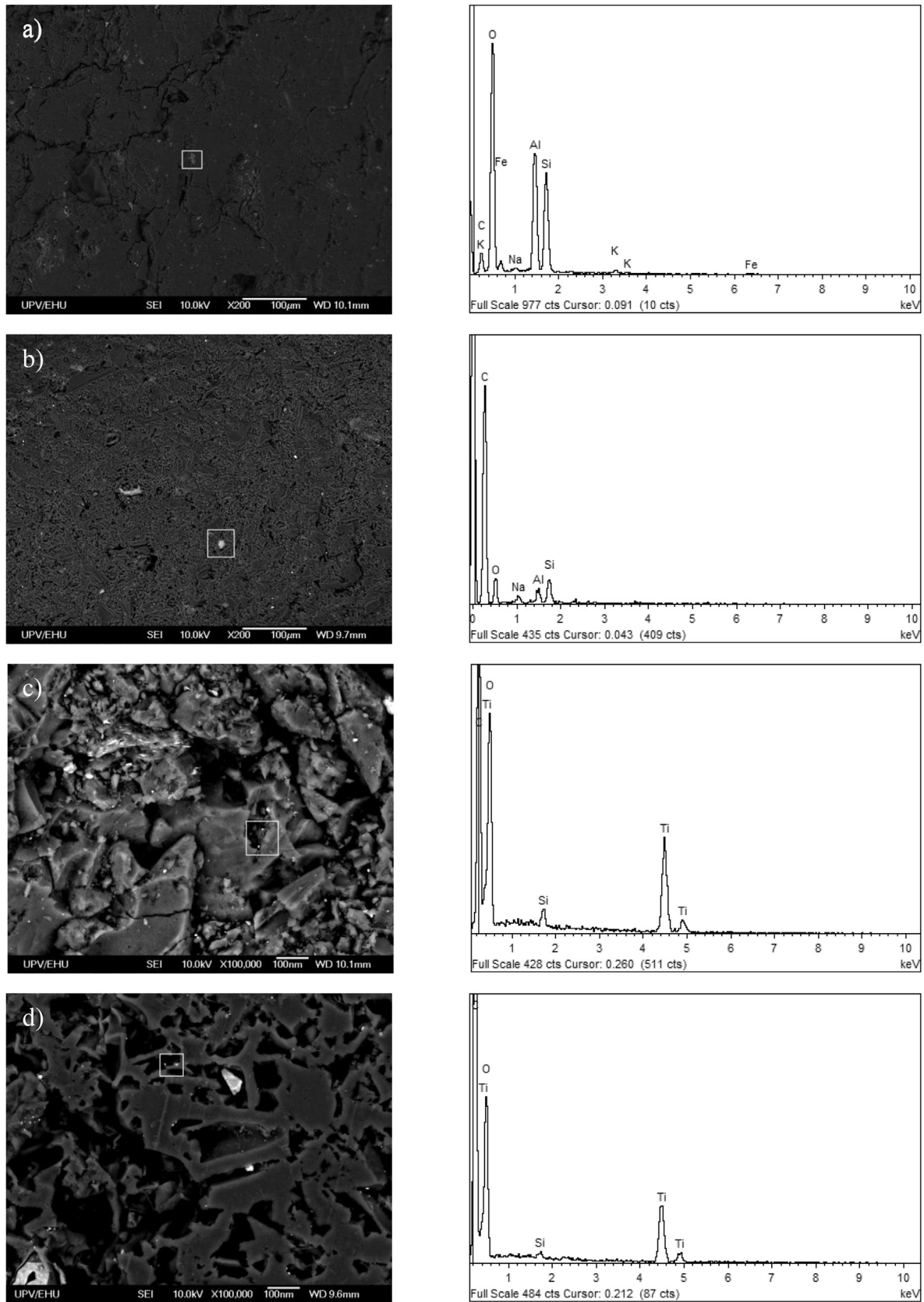


Fig. 3. SEM micrographs and EDAX composition of pristine activated carbons: a) original Norit[®] GAC 1240 Plus; and b) original Norit[®] ROX 0.8 external surface; cross-section of: c) TiO₂/GAC composite prepared with Norit[®] GAC 1240 Plus by the precipitation method; and d) TiO₂/GAC composite prepared with Norit[®] ROX 0.8 by the precipitation method.

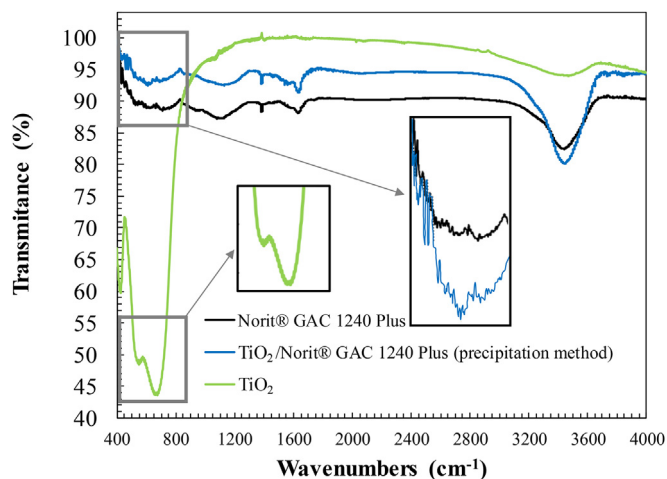


Fig. 4. FTIR spectra in the region between 4000 and 400 cm^{-1} for the Norit® GAC 1240 Plus catalyst, TiO_2 and the $\text{TiO}_2/\text{Norit}^\circledast$ GAC 1240 Plus composite prepared by the precipitation method.

pollutants. The point of zero charge was determined according to the method described by Silva et al. (2016). A surface charge is at its point of zero charge when the surface charge density equals zero. It

is a negative logarithm value for the activity of the charge-determining ions in the bulk phase (Lyklima, 1991). On porous materials, such as TiO_2/GAC composites, a point of zero charge value represents the net total (external and internal) of the particle's surface charges (Menéndez et al., 1995). As shown in Table 2, different PZC values were obtained for the different composites in this study. The differences can be attributed to three reasons. Firstly, in function of the synthesis method, the proportion of groups on the TiO_2 surface (singly coordinated Ti_3O^0 , doubly coordinated $\text{Ti}_2\text{O}^{2/3-}$ and triply coordinated $\text{TiO}^{4/3-}$) can modify the PZC. Secondly, the increase in the size of agglomerates can displace the point of zero charge to lower pH values. Finally, the presence of large TiO_2 particles that obstruct part of the GAC pores (Ferreiro et al., 2019; Skwarek et al., 2016). According to Table 2, the PZC was 6.4 for the $\text{TiO}_2/\text{Norit}^\circledast$ GAC 1240 Plus composite prepared by the precipitation method. This value is similar to the one obtained for commercial Aerioxide® P25 catalysts (Song et al., 2010; Zheng et al., 2018). Therefore, the $\text{TiO}_2/\text{Norit}^\circledast$ GAC 1240 Plus composite's PZC has a very limited influence on the removal of aniline because of the low dissociation constant ($\text{pK}_a = 4.61$) and high PZC of the catalyst ($\text{pH}_{\text{pzc}} = 6.4$).

3.6. Catalyst activity comparison

To compare the catalytic activity of the composites obtained in

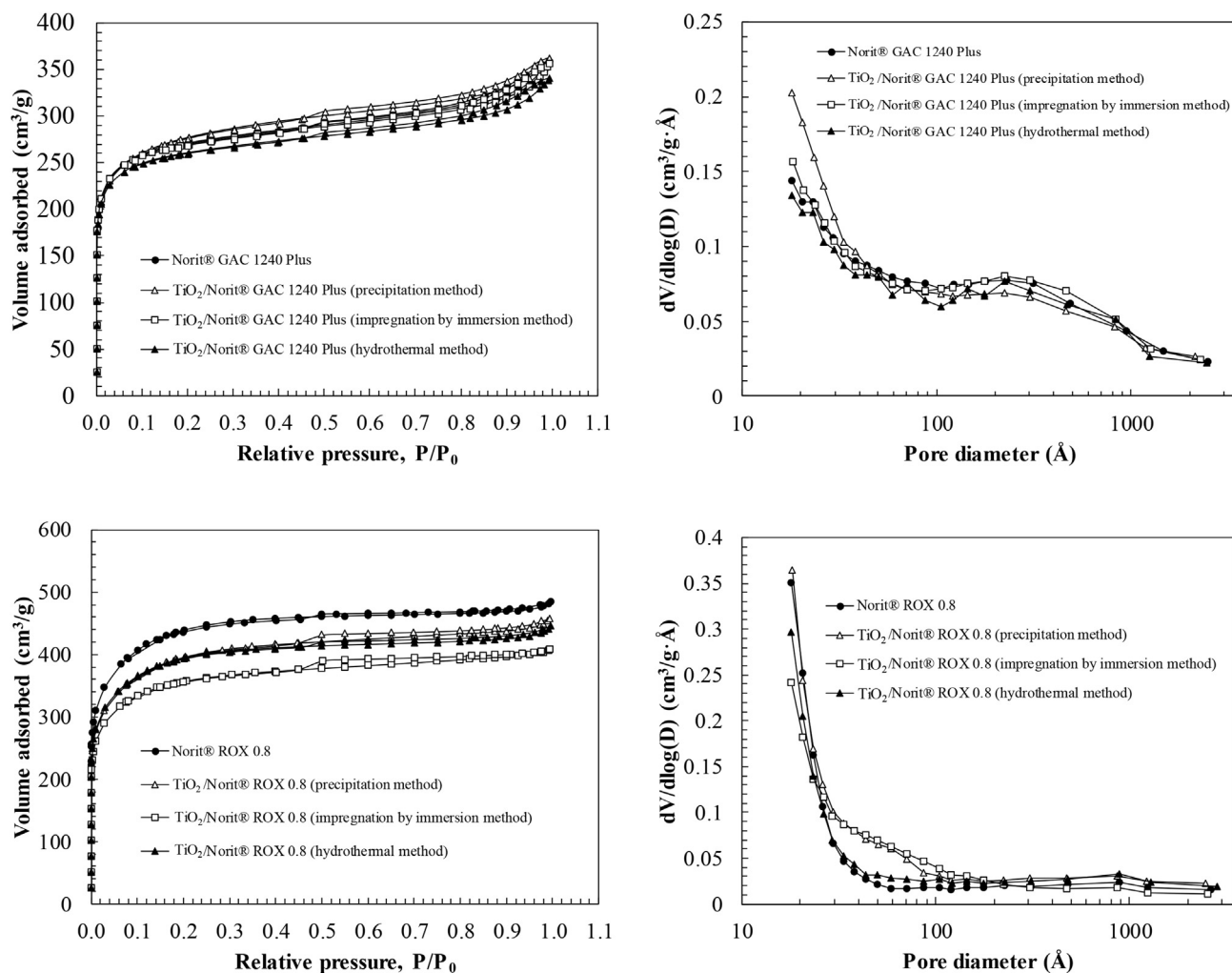


Fig. 5. Nitrogen adsorption–desorption isotherms and pore size distribution of GACs and TiO_2/GAC composites calculated using the BJH model.

Table 2
Surface properties of synthesised TiO₂/GAC composites.

Sample	S _{BET} , m ² /g	S _{ext} , m ² /g	V _T , cm ³ /g	V _μ , cm ³ /g	V _M , cm ³ /g	V _M /V _T , %	V _μ /V _T , %	D _p , Å	pH _{pzc}	TiO ₂ loading, wt %
Norit® GAC 1240 Plus	967.0	224.4	0.48	0.32	0.16	33.3	66.7	36.8	7.4	0.0
TiO ₂ /Norit® GAC 1240 Plus (precipitation method)	985.0	298.9	0.45	0.29	0.16	35.2	64.8	33.9	6.4	9.1
TiO ₂ /Norit® GAC 1240 Plus (hydrothermal method)	931.3	208.6	0.46	0.31	0.15	32.0	68.0	36.3	3.6	2.1
TiO ₂ /Norit® GAC 1240 Plus (impregnation by immersion method)	963.7	223.2	0.48	0.32	0.16	33.3	66.7	36.8	5.5	2.9
Norit® ROX 0.8	1558.9	494.7	0.54	0.45	0.09	16.7	83.3	25.2	8.9	0.0
TiO ₂ /Norit® ROX 0.8 (precipitation method)	1400.9	446.8	0.53	0.41	0.12	23.3	76.7	27.5	6.0	5.5
TiO ₂ /Norit® ROX 0.8 (hydrothermal method)	1395.4	376.2	0.54	0.44	0.10	18.6	81.4	27.7	4.4	2.8
TiO ₂ /Norit® ROX 0.8 (impregnation by immersion method)	1266.4	320.6	0.51	0.41	0.10	20.2	79.8	27.5	7.4	3.8

S_{BET} – BET surface area; S_{ext} – external surface area; V_T – total pore volume; V_μ – micropore volume; V_M – mesopore volume; V_M/V_T – mesopore percentage; V_μ/V_T – micropore percentage; D_p – average pore diameter.

this work, the primary degradation of solutions containing 20.0 mg/L of aniline at pH₀ = 7.5 and C_{CO₂, in} = 11.3 mg/L using 5.0 g of catalyst (see Fig. 6). Eq. (22) may describe the kinetic model for aniline degradation considering a parallel second-order reaction mechanism.

$$-r_{\text{ANI}} = -\frac{dC_{\text{ANI}}}{dt} = k_{\text{hom}}C_{\text{ANI}}C_{\text{O}_3} + k_{\text{het}}C_{\text{ANI}}C_{\text{OH}} \quad (22)$$

where k_{hom} and k_{het} are the kinetic constants associated with the molecular and radical ozonation pathways. According to several authors (Beltran, 2003; Orge et al., 2017), Eq. (22) can be simplified for an overall analysis of the ozonation process, leading to Eq. (23).

$$-r_{\text{ANI}} = -\frac{dC_{\text{ANI}}}{dt} = k' C_{\text{ANI}} \quad (23)$$

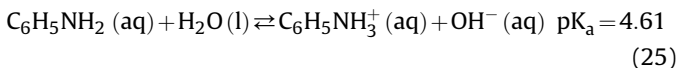
where k' (min⁻¹) is an apparent first-order constant. To assess the reaction rate, another option is to calculate the half-life of the reaction ($t_{1/2}$), as in Eq. (24).

$$t_{1/2} = \frac{\ln 2}{k'} \quad (24)$$

Table 3 summarises the corresponding rate constants. The standard deviation was less than 3% in all cases. The TiO₂/Norit® GAC 1240 Plus composite synthesised by the precipitation method showed the highest degree of mineralisation and oxidation rate. Complete aniline removal took 5 min with this composite (Fig. 6a). The same material produced a mineralisation of 61.73% after 45 min (Fig. 6b), $t_{1/2} = 0.65$ min and a kinetic constant of $k' = 1.07$ min⁻¹.

3.7. Effect of pH

The effect of pH on the O₃/TiO₂/GAC process was studied from 3.0 to 9.0 (Fig. 7) because this range is closely related to the ionic species in solution considering the aniline dissociation pK_a (see Eq. (25)).



According to the pK_a value in Eq. (25), the concentration of anilinium cations is negligible at pH > 4.61. Consequently, the reaction rate is expected to increase under basic conditions, which is also enhanced by a parallel increase in hydroxyl radical generation. Conversely, at acidic pH below 4.61, the greater presence of anilinium cations and a positively charged catalyst surface would justify a significant reduction in the degradation rate. Thus, the overall

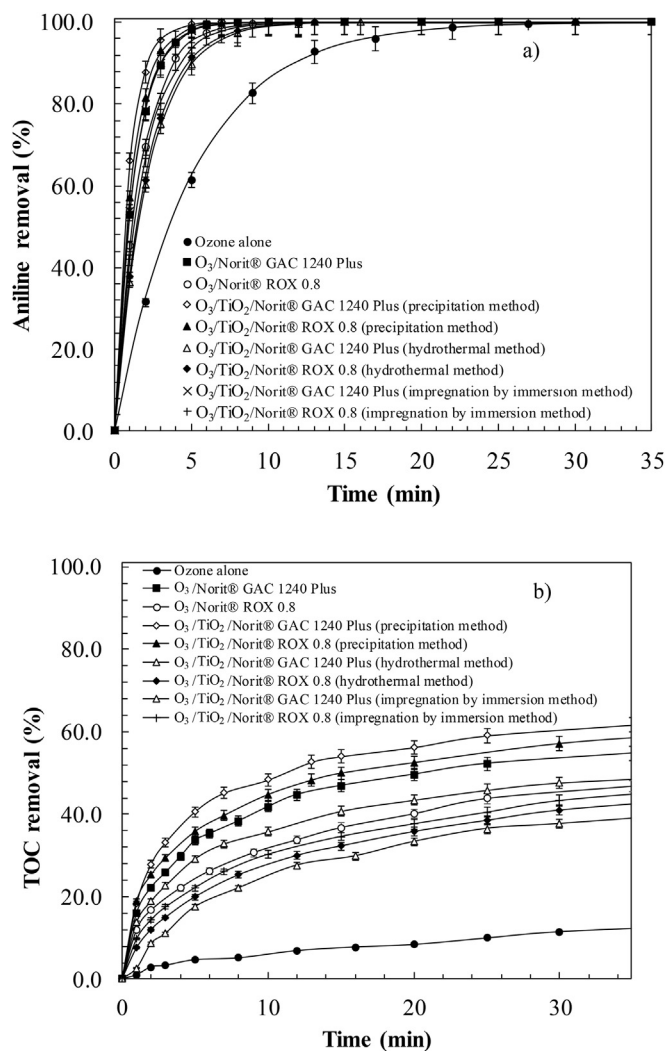


Fig. 6. Comparison of the activity of the synthesised catalysts. a) Predictions of the proposed first-order kinetics model for aniline degradation. b) Mineralisation of degraded aniline samples using direct and catalytic ozonation treatments combined with composites prepared by: precipitation, immersion-impregnation and hydrothermal methods. Experimental conditions: C₀ = 20.0 mg/L; pH₀ = 7.5; T = 18.0 °C; P = 1 atm; F_{O₃} = 2.5 g O₃/h; C_{CO₂, in} = 11.3 mg/L; m_{cat} = 5.0 g; V_{reac} = 1.5 L.

reactivity of aniline towards ozone (k_{hom}) in Eq. (22) increases from $5.9 \cdot 10^4 \text{ M}^{-1} \text{ s}^{-1}$ at pH = 1.5 to $1.4 \cdot 10^7 \text{ M}^{-1} \text{ s}^{-1}$ at pH = 6.5 (VonSonntag and VonGunten, 2012). According to Table 3, a higher oxidation rate was achieved at pH = 7.0. Furthermore, the kinetic

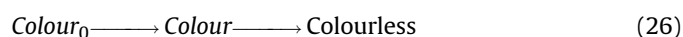
Table 3Summary of kinetic parameters and process performance of the catalytic ozonation treatment using TiO₂/GAC composites for aniline degradation after 45 min of reaction.

Ozonation Conditions ^a	TOC removal, %	ANI removal, %	η_{O_3} , mg O ₃ /mg TOC	k' , min ⁻¹	$t_{1/2}$, min	k_1 , AU ⁻¹ min ⁻¹	k_2 , AU ⁻¹ min ⁻¹
Ozone alone	12.96	99.9		0.2	3.54		
O ₃ /Norit® ROX 0.8	46.85	100.0		0.61	1.14		
O ₃ /TiO ₂ /Norit® ROX 0.8 (hydrothermal method)	43.84	99.9		0.47	1.47		
O ₃ /TiO ₂ /Norit® ROX 0.8 (impregnation by immersion method)	46.25	99.9		0.52	1.32		
O ₃ /TiO ₂ /Norit® ROX 0.8 (precipitation method)	59.71	100.0		0.87	0.8		
O ₃ /Norit® GAC 1240 Plus	54.77	99.9		0.76	0.92		
O ₃ /TiO ₂ /Norit® GAC 1240 Plus (hydrothermal method)	40.26	99.9		0.47	1.49		
O ₃ /TiO ₂ /Norit® GAC 1240 Plus (impregnation by immersion method)	49.36	100.0		0.75	0.92		
O ₃ /TiO ₂ /Norit® GAC 1240 Plus (precipitation method).	61.73	100.0		1.07	0.65		
Variants ^b : pH=3.0 (constant)	53.47	100.0	839.1	0.80	0.87	401.94	29.47
pH=5.0 (constant)	63.46	100.0	689.8	1.15	0.60	397.04	41.91
pH=7.0 (constant)	70.72	100.0	552.5	1.26	0.55	382.50	53.82
pH=9.0 (constant)	61.58	100.0	703.3	1.11	0.62	399.20	35.65
C _{GO3} =3.7 mg/L	71.75	100.0	399.5	1.34	0.52	377.63	59.14
C _{GO3} =5.4 mg/L	80.24	100.0	26.8	1.65	0.42	372.50	66.37
C _{GO3} =11.3 mg/L	70.72	100.0	552.5	1.26	0.55	382.50	53.82
C _{GO3} =20.1 mg/L	47.45	100.0	1522.2	0.74	0.94	403.91	27.60

^a In all the cases pH₀=7 (initial) and C_{GO3}=11.3 mg/L.^b For the last item (precipitation method), effects of several constant pHs (C_{GO3}=11.3 mg/L) and C_{GO3} values (constant pH=7.0).

constant had a value of $k' = 1.26 \text{ min}^{-1}$ and a mineralisation of 70.72% was obtained within 45 min. The considerable improvement of the process in terms of TOC reduction suggests that the byproducts are better degraded at a neutral pH.

During the degradation of aniline, we observed colour changes in oxidised water. Other studies have also reported these colour changes, with aniline solutions presenting colours such as pink, purplish red, reddish orange, orange, yellow, reddish brown and light yellow (Jing et al., 2015). The colour changes probably correspond to the appearance of various intermediate products generated during aniline's transformation, where the main intermediates would be benzoquinone (245 nm), nitrobenzene (252 nm) and nitroaniline (375 nm). Based on this phenomenon, we have proposed a colour kinetic model that considers a second-order kinetic reaction scheme (Eq. (26)), similar to that applied by Villota et al. (2018):



In the proposed reaction model, Colour_0 is the initial level and Colour is the corresponding level at time t . The initial coloration was attributed to the aniline in solution with a value of 0.004 AU. k_1 expresses the kinetic constant for the colour appearance due to aniline removal, whereas k_2 represents colour disappearance due to the degradation of aniline intermediates during the reaction. As shown in Table 3, the constant k_1 is about 10 times greater than k_2 . So, this scheme can be considered as consecutive reactions and the kinetics of colour formation ($t < t_{\max}$) and colour disappearance ($t > t_{\max}$) can be described using the following second-order equations:

$$\frac{d\text{Colour}}{dt} = k_1 \text{Colour}^2 \quad (27)$$

$$\frac{d\text{Colour}}{dt} = -k_2 \text{Colour}^2 \quad (28)$$

The evolution of colour formation with time can be obtained by integrating Eq. (27), up to t_{\max} , as shown in Eq. (29). The colour disappearance is represented by Eqs. (28) and (30) respectively.

$$\frac{1}{\text{Colour}} - \frac{1}{\text{Colour}_0} = -k_1 t \quad (29)$$

$$\frac{1}{\text{Colour}} - \frac{1}{\text{Colour}_{\max}} = k_2 (t - t_{\text{colour}}) \quad (30)$$

The estimated constants k_1 and k_2 (in AU⁻¹min⁻¹) are shown in Table 3. The standard deviation was less than 2% in all cases. A greater colour intensity during the oxidation reaction represents less mineralisation of the contaminants present in the solution, so it is important that the value of the constant k_2 is as high as possible, and is indicative of further degradation of aniline intermediates, leading to the complete removal of coloured compounds. Fig. 7c shows that colour intensity increased at extreme values of pH, 3.0 and 9.0, due to the generation of a higher concentration of chromophore oxidised species. Contrastingly, at neutral pH, both the maximum colour intensity and the residual colour at the end of catalytic ozonation were clearly lower. There is a clear improvement in the oxidative reactivity at pH=7.0 because it coincides with the highest value for the colour disappearance constant ($k_2 = 53.82 \text{ AU}^{-1} \text{ min}^{-1}$). This favours oxidation of the chromophore species leading to colourless degradation products; the colour decreases to the initial value ($\text{Colour} = 0.004 \text{ AU}$) in just 10 min.

The decrease of absorbance at 254 nm (Fig. 7b) represents greater degradation due to rupture of the aromatic structure and, consequently, minimum absorbance values are found (Chen et al., 2019). The greatest decrease in absorbance at 254 nm was recorded at pH=7.0. This behaviour is similar to that observed for the colour reduction. Therefore, pH=7.0 seems to promote both aromatic ring rupture and the destruction of the chromophore's groups, thus leading to favourable oxidation conditions.

3.8. Effect of inlet O₃ concentration

The effect of ozone dose was studied by varying the inlet ozone concentration in the range of 3.7–20.1 mg O₃/L. Fig. 7 shows the influence on aniline removal, TOC conversion profiles, colour and aromatic ring rupture expressed as absorbance at 254 nm. In general, the catalytic activity improves as the concentration of ozone increases. But, when there is an excess of ozone, above a dose of 5.4 mg/L, it can react with the hydroxyl radicals producing

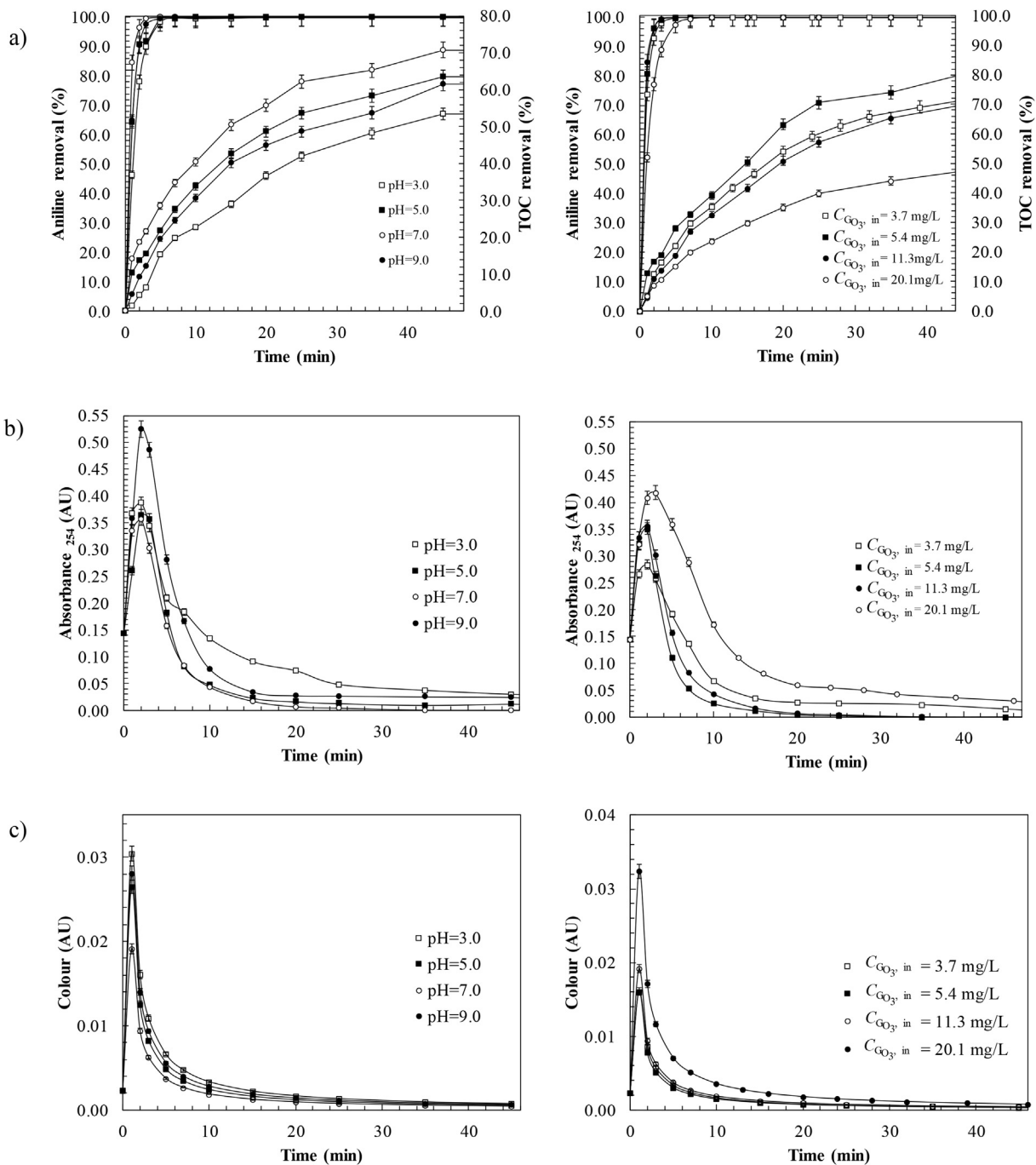


Fig. 7. Study of the effect of pH and ozone dose during the catalytic ozonation of aniline with TiO_2/GAC composites. Evolution of: a) primary aniline degradation fitted to a first-order kinetic model and TOC removal; b) aromatic ring rupture; c) colour induction in the oxidation of aniline solutions fitted to a second-order kinetic model. Experimental conditions: 1) effect of pH: $C_0 = 20.0 \text{ mg/L}$; $T = 18.0^\circ\text{C}$; $P = 1 \text{ atm}$; $C_{\text{O}_3, \text{ in}} = 11.3 \text{ mg/L}$; $m_{\text{cat}} = 5.0 \text{ g}$; $V_{\text{react}} = 1.5 \text{ L}$; and 2) effect of ozone dose: $C_0 = 20.0 \text{ mg/L}$; $\text{pH} = 7.0$; $T = 18.0^\circ\text{C}$; $P = 1 \text{ atm}$; $m_{\text{cat}} = 5.0 \text{ g}$; $V_{\text{react}} = 1.5 \text{ L}$.

hydroperoxyl radicals (HO_2^\bullet) of lower oxidative capacity, thus reducing the treatment's efficacy. This can be explained through the mechanism proposed by Buhler et al. (1984) and Staehelin et al. (1984) as shown in Eqs. (31) and (32):

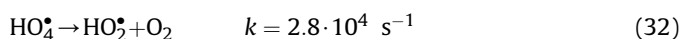
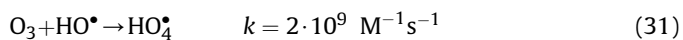


Figure S2 shows the evolution of the concentration of ozone in

the liquid phase (Fig. S2a) and its concentration in the gas phase at the outlet (Fig. S2b). The ozone concentration in the liquid phase at a dose of 5.4 mg/L can be split into three stages: i) between 0 and 2 min – the absence of ozone in the liquid phase can be associated with the primary removal of aniline; ii) between 6 and 8 min – a strong increase in the ozone would be associated with the elimination of intermediate degradation products; and iii) after 10 min – the concentration of ozone in the liquid phase slowly increases, so the process loses efficiency.

With an optimal ozone dose of 5.4 mg/L, we observed a

Table 4
Treatment costs in aniline ozonation.

Treatment	C ₀ , mg/L	TOC removed, mg	Overall O ₃ consumption, mg	Energy consumption, kWh/kg TOC	Treatment cost, €/kg TOC	References
O ₃	103.81	71.37 ^a	56.01	7.84 ^a	0.83 ^a	Jing et al. (2015)
O ₃ /GAC	102.44	26.60	225.00	84.59	8.96	Faria et al. (2007)
O ₃ /TiO ₂ -GAC	93.13	24.62	450.00	182.78	19.35	Orge et al. (2017)
This work	20.0	8.46	5.15	6.08	0.64	-

^a Calculated from COD reduction

mineralisation of 80.24% and a very high oxidation rate ($k' = 1.65 \text{ min}^{-1}$) in just 45 min. Other works achieved 70% TOC removal in 180 min (Faria et al., 2007; Orge et al., 2017). Consequently, this new composite together with the optimal operating conditions proposed here far exceeded published results for catalytic ozonation of aniline wastewaters. Other parameters such as colour tended to diminish at the optimal ozone dose of 5.4 mg/L with a colour disappearance constant of $k_2 = 66.37 \text{ AU}^{-1} \text{ min}^{-1}$ due to the oxidation of aniline to low molecular weight colourless compounds. Conversely, at the higher ozone dose of 20.1 mg/L, we recorded a greater colour intensity and lower colour disappearance constant ($k_2 = 27.60 \text{ AU}^{-1} \text{ min}^{-1}$).

An excess of ozone lead to (see Eqs. (31) and (32)) the production of inefficient hydroperoxyl radicals, decreasing the system's oxidizing capacity as evidenced by a greater amount of coloured products. Moreover, the lowest absorbance value at 254 nm compared to the other doses studied was also observed with the optimal ozone dose of 5.4 mg/L. This demonstrates the high level of aromatic ring rupture and the favourable oxidative efficiency of the radicals formed under these conditions.

An important aspect of catalytic ozonation processes is the amount of ozone consumed since this is the most important factor when determining the treatment cost. The efficiency of the process was evaluated through the parameter η_{O_3} , as defined in Eq. (33) proposed by Alvarez et al. (2011):

$$\eta_{O_3} = \frac{F_G \int_0^{t_f} (C_{G_{O_3},in} - C_{G_{O_3},out}) dt}{V(TOC_0 - TOC_f)} \quad (33)$$

where F_G is the gas flow rate (mg/min); $C_{G_{O_3},in}$ and $C_{G_{O_3},out}$ are the concentrations of ozone at the reactor inlet and outlet gas streams (mg/L), respectively; and V is the reaction volume (L). According to Eq. (33), with an ozone dose of 5.4 mg/L, the process is much more efficient in terms of ozone usage than other experimental conditions. The consumption was drastically reduced to $\eta_{O_3} = 26.8 \text{ mg O}_3/\text{mg TOC}$ when operated under optimal conditions (see Table 3). This is very noteworthy for the implementation of a catalytic ozonation system because the cost of ozone is the key economic factor (Alvarez et al., 2011; Carbajo et al., 2006). The cost of any ozonation treatment is very hard to estimate because factors such as mass transfer and ozone gas-phase concentration can influence the reaction route and kinetics and therefore oxidation efficiency (Krichevskaya et al., 2011). Equipment or maintenance costs were omitted for the estimations since they depend on the particular conditions of each system. The TOC or COD were used to compare costs between the different technologies since in many cases the byproducts of the degradation of pollutants pose a significant threat to the environment and their disposal may be as significant as that of the parent compound. Therefore, we estimated that ozone generation requires 10 kWh/kg O₃ and the price of electricity for industrial consumers in Spain is 0.1059 €/kWh (European Union, 2018). The costs associated with ozone consumption are summarised in Table 4.

According to Table 4, the catalytic ozonation of aniline with the TiO₂/GAC composite developed in this study has a cost of 0.64 €/kg TOC compared to 8.96 €/kg TOC (Faria et al., 2007) or the 19.35 €/kg TOC calculated by Orge et al. (2017). This system has achieved high efficiencies which could lead to its industrial implementation with the new materials proposed in this work.

4. Conclusions

An efficient catalytic ozonation process has been tested for the treatment of water containing aniline as an alternative to the use of activated sludge. With the aim of preventing the inhibitory effects of aniline on enzyme activity and sludge respiration, we have proposed several methods for the synthesis of new materials based on TiO₂ and activated carbon. It has been analysed aniline degradation and mineralisation for all the new composites. The best results were obtained with a new TiO₂/GAC catalyst based on "in situ" formation of TiO₂ using alcoholic TiCl₄ precursor solutions on granular activated carbon Norit® GAC 1240 Plus. This method has achieved high TiO₂ dispersions with a homogeneous distribution of nanocrystals (10 nm) on both the external surface and the internal pores of the activated carbon support. It was observed a 25% increase in the composite's external surface, as well as a BET surface of 985 m²/g with 9.1% TiO₂ loading. It was tested our TiO₂/GAC composites in the ozonation of aniline solutions and optimised variables such as pH and ozone dose. As a result, a pH = 7.0 and ozone dose of 5.4 mg/L were the best working conditions producing complete aniline degradation in only 5 min ($k' = 1.65 \text{ min}^{-1}$). Under these optimum conditions, in 45 min the system achieved 80.24% mineralisation and total colour loss, with only 26.8 mg O₃/mg TOC removed and at a cost of ozone treatment of 0.64 €/kg TOC.

Acknowledgements

The authors are grateful to the Basque Government for their financial support of this study through the project PPG17/53 through the programme to consolidate Groups (Basque University System) and Spanish Ministry of Economy and Competitiveness and from FEDER funds through the project CTM 2015-69845-R (MINECO/FEDER, UE). The authors also wish to thank the University of Basque Country for C. Ferreiro's predoctoral PIF grant (PIF16/367) and to SGIker of UPV/EHU for the analytical support provided in the characterisation of the composites. Finally, thanks to Cabot Corporation for supplying the samples of activated carbon used in this work.

Appendix A. Supplementary data

Supplementary data to this article can be found online at <https://doi.org/10.1016/j.jclepro.2019.04.198>.

References

- Aguedal, H., Hentit, H., Merouani, D.R., Iddou, A., Shishkin, A., Jumas, J.C., 2017. Improvement of the sorption characteristics of diatomite by heat treatment.

- Key Eng. Mater. <https://doi.org/10.4028/www.scientific.net/KEM.721.111>.
- Aguedal, H., Iddou, A., Aziz, A., Shishkin, A., Ločs, J., Juhna, T., 2019. Effect of thermal regeneration of diatomite adsorbent on its efficacy for removal of dye from water. *Int. J. Environ. Sci. Technol.* 16, 113–124. <https://doi.org/10.1007/s13762-018-1647-5>.
- Alvarez, P.M., Pablo Pocostales, J., Beltran, F.J., 2011. Granular activated carbon promoted ozonation of a food-processing secondary effluent. *J. Hazard Mater.* 185, 776–783. <https://doi.org/10.1016/j.jhazmat.2010.09.088>.
- Andriantsiferana, C., Mohamed, E.F., Delmas, H., 2015. Sequential adsorption - photocatalytic oxidation process for wastewater treatment using a composite material TiO₂/activated carbon. *Environ. Eng. Res.* 20, 181–189. <https://doi.org/10.1515/2015.20.2.181>.
- Andriantsiferana, C., Mohamed, E.F., Delmas, H., 2014. Photocatalytic degradation of an azo-dye on TiO₂/activated carbon composite material. *Environ. Technol.* 35, 355–363. <https://doi.org/10.1080/09593330.2013.828094>.
- Anotai, J., Jevprasesphant, A., Lin, Y.-M., Lu, M.-C., 2012. Oxidation of aniline by titanium dioxide activated with visible light. *Sep. Purif. Technol., Technol. Sustain. Water Environ.* 84, 132–137. <https://doi.org/10.1016/j.seppur.2011.09.035>.
- Bagheri, S., Mohd Hir, Z.A., Termeh Yousefi, A., Abd Hamid, S.B., 2016. Photocatalytic performance of activated carbon-supported mesoporous titanium dioxide. *Desalination Water Treat.* 57, 10859–10865. <https://doi.org/10.1080/19443994.2015.1038593>.
- Baird, R., Carmona, L., Jenkins, R., 1977. Behavior of benzidine and other aromatic-amines in aerobic wastewater-treatment. *J. Water Pollut. Control Fed.* 49, 1609–1615.
- Beltran, F.J., 2003. Ozone Reaction Kinetics for Water and Wastewater Systems. CRC Press. <https://doi.org/10.1201/9780203509173>.
- Beltran, F.J., Rivas, F.J., Montero-de-Espinoza, R., 2004. A TiO₂/Al₂O₃ catalyst to improve the ozonation of oxalic acid in water. *Appl. Catal. B Environ.* 47, 101–109. <https://doi.org/10.1016/j.apcatb.2003.07.007>.
- Bensalah, F., Iddou, A., Hentit, H., Aziz, A., Shishkin, A., 2018. Activated carbon design from sludge to remove red scarlet nilyosan “F3GL” in aqueous solution. *Key Eng. Mater.* <https://doi.org/10.4028/www.scientific.net/KEM.762.87>.
- Birge, W.J., Black, J.A., Hudson, J.E., Bruser, D.M., 1979. Embryo-larval toxicity tests with organic compounds. *Aquat. Toxicol. Proc. Second Annu. Symp. Aquat. Toxicol.* <https://doi.org/10.1520/STP34883S>.
- Boczkaj, G., Fernandes, A., 2017. Wastewater treatment by means of advanced oxidation processes at basic pH conditions: a review. *Chem. Eng. J.* 320, 608–633. <https://doi.org/10.1016/j.cej.2017.03.084>.
- Buhler, R., Staehelin, J., Hoigne, J., 1984. Ozone decomposition in water studied by pulse-radiolysis. I. HO₂/O₂⁻ and HO₃/O₃⁻ as intermediates. *J. Phys. Chem.* 88, 2560–2564.
- Carbajo, M., Beltran, F.J., Medina, F., Gimeno, O., Rivas, F.J., 2006. Catalytic ozonation of phenolic compounds - the case of gallic acid. *Appl. Catal. B Environ.* 67, 177–186. <https://doi.org/10.1016/j.apcatb.2006.04.019>.
- Chen, H., Zhuang, R., Yao, J., Wang, F., Qian, Y., Masakorala, K., Cai, M., Liu, H., 2014. Short-term effect of aniline on soil microbial activity: a combined study by isothermal microcalorimetry, glucose analysis, and enzyme assay techniques. *Environ. Sci. Pollut. Res.* 21, 674–683. <https://doi.org/10.1007/s11356-013-1955-8>.
- Chen, W., Gu, Z., Wen, P., Li, Q., 2019. Degradation of refractory organic contaminants in membrane concentrates from landfill leachate by a combined coagulation-ozonation process. *Chemosphere* 217, 411–422. <https://doi.org/10.1016/j.chemosphere.2018.11.002>.
- Colmenares, J.C., Varma, R.S., Lisowski, P., 2016. Sustainable hybrid photocatalysts: titania immobilized on carbon materials derived from renewable and biodegradable resources. *Green Chem.* 18, 5736–5750. <https://doi.org/10.1039/C6GC02477G>.
- Daud, Z., Abubakar, M.H., Kadir, A.A., Latif, A.A.A., Awang, H., Halim, A.A., Marto, A., 2017. Batch study on COD and ammonia nitrogen removal using granular activated carbon and cockle shells. *Int. J. Eng.* 30, 937–944. <https://doi.org/10.5829/ije.2017.30.07a.02>.
- Dumpert, K., 1987. Embryotoxic effects of environmental chemicals - tests with the south-african clawed toad (*Xenopus laevis*). *Ecotoxicol. Environ. Saf.* 13, 324–338. [https://doi.org/10.1016/0147-6513\(87\)90031-5](https://doi.org/10.1016/0147-6513(87)90031-5).
- Eskola, M., Altieri, A., Galobart, J., 2018. Overview of the activities of the European food safety authority on mycotoxins in food and feed. *World Mycotoxin J.* 11, 277–289. <https://doi.org/10.3920/WMJ2017.2270>.
- European Commission, 2004. European Union Risk Assessment Report Aniline. Office for Official Publications of the European Communities, Luxembourg.
- European Union, 2018. Eurostat Regional Yearbook, 2018 edition. Statistical books Publications Office of the European Union, Luxembourg.
- Faria, P.C.C., Orfao, J.J.M., Pereira, M.F.R., 2007. Ozonation of aniline promoted by activated carbon. *Chemosphere* 67, 809–815. <https://doi.org/10.1016/j.chemosphere.2006.10.020>.
- Ferreiro, C., Villota, N., Lombrana, J.I., Rivero, M.J., Zúñiga, V., Rituerto, J.M., 2019. Analysis of a hybrid suspended-supported photocatalytic reactor for the treatment of wastewater containing benzothiazole and aniline. *Water* 11, 337. <https://doi.org/10.3390/w11020337>.
- Gersich, F., Milazzo, D., 1990. Evaluation of a 14-day static renewal toxicity test with daphnia-magna straus. *Arch. Environ. Contam. Toxicol.* 19, 72–76. <https://doi.org/10.1007/BF01059814>.
- Ghasemi, B., Anvaripour, B., Jorfi, S., Jaafarzadeh, N., 2016. Enhanced photocatalytic degradation and mineralization of furfural using UVC/TiO₂/GAC composite in aqueous solution. *Int. J. Photoenergy*, 2782607. <https://doi.org/10.1155/2016/2782607>.
- Ghuge, S.P., Saroha, A.K., 2018. Catalytic ozonation for the treatment of synthetic and industrial effluents - application of mesoporous materials: a review. *J. Environ. Manag.* 211, 83–102. <https://doi.org/10.1016/j.jenvman.2018.01.052>.
- Guo, Y., Yang, L., Wang, X., 2012. The application and reaction mechanism of catalytic ozonation in water treatment. *J. Environ. Anal. Toxicol.* 02. <https://doi.org/10.4172/2161-0525.1000150>.
- Guzman-Colis, G., Thalasso, F., Marcela Ramirez-Lopez, E., Rodriguez-Narciso, S., Lilian Guerrero-Barrera, A., Javier Avelar-Gonzalez, F., 2011. Spatial-temporal evaluation of the water quality of the san Pedro river. *Rev. Int. Contam. Ambient.* 27, 89–102.
- Harbison, R.D., Bourgeois, M.M., Johnson, G.T., 2015. Hamilton and Hardy's Industrial Toxicology. John Wiley & Sons.
- Jing, Z., Cao, S., Yu, T., Hu, J., 2015. Degradation characteristics of aniline with ozonation and subsequent treatment analysis. *J. Chem.* 905921. <https://doi.org/10.1155/2015/905921>.
- Kermani, M., Kakavandi, B., Farzadkia, M., Esrafil, A., Jokandan, S.F., Shahsavani, A., 2018. Catalytic ozonation of high concentrations of catechol over TiO₂/Fe₃O₄ magnetic core-shell nanocatalyst: optimization, toxicity and degradation pathway studies. *J. Clean. Prod.* 192, 597–607. <https://doi.org/10.1016/j.jclepro.2018.04.274>.
- Krichevskaya, M., Klauson, D., Portjanskaja, E., Preis, S., 2011. The cost evaluation of advanced oxidation processes in laboratory and pilot-scale experiments. *Ozone Sci. Eng.* 33, 211–223. <https://doi.org/10.1080/01919512.2011.554141>.
- Legube, B., Leitner, N.K.V., 1999. Catalytic ozonation: a promising advanced oxidation technology for water treatment. *Catal. Today* 53, 61–72. [https://doi.org/10.1016/S0920-5861\(99\)00103-0](https://doi.org/10.1016/S0920-5861(99)00103-0).
- Lichtfouse, E., Schwarzbauer, J., Robert, D., 2015. Pollutants in Buildings, Water and Living Organisms. Springer.
- Lubash, G.D., 1964. Acute aniline poisoning treated by hemodialysis: Report of a case. *Arch. Intern. Med.* 114, 530. <https://doi.org/10.1001/archinte.1964.03860100112013>.
- Lyklema, J., 1991. Nomenclature, symbols, definitions and measurements for electrified interfaces in aqueous dispersions of solids (Recommendations 1991). *Pure Appl. Chem.* 63, 895–906. <https://doi.org/10.1016/j.pac.199163060895>.
- Lyons, C., Katz, S., Bartha, R., 1984. Mechanisms and pathways of aniline elimination from aquatic environments. *Appl. Environ. Microbiol.* 48, 491–496.
- Martins, A.C., Cazetta, A.L., Pezoti, O., Souza, J.R.B., Zhang, T., Pilau, E.J., Asefa, T., Almeida, V.C., 2017. Sol-gel synthesis of new TiO₂/activated carbon photocatalyst and its application for degradation of tetracycline. *Ceram. Int.* 43, 4411–4418. <https://doi.org/10.1016/j.ceramint.2016.12.088>.
- Menéndez, J.A., Illán-Gómez, M.J., y León, C.A.L., Radovic, L.R., 1995. On the difference between the isoelectric point and the point of zero charge of carbons. *Carbon* 33, 1655–1657. [https://doi.org/10.1016/0008-6223\(95\)96817-R](https://doi.org/10.1016/0008-6223(95)96817-R).
- Mestankova, H., Parker, A.M., Bramaz, N., Canonica, S., Schirmer, K., von Gunten, U., Linden, K.G., 2016. Transformation of Contaminant Candidate List (CCL3) compounds during ozonation and advanced oxidation processes in drinking water: Assessment of biological effects. *Water Res.* 93, 110–120. <https://doi.org/10.1016/j.watres.2015.12.048>.
- MiarAlipour, S., Friedmann, D., Scott, J., Amal, R., 2018. TiO₂/porous adsorbents: recent advances and novel applications. *J. Hazard Mater.* 341, 404–423. <https://doi.org/10.1016/j.jhazmat.2017.07.070>.
- Mijangos, F., Varona, F., Villota, N., 2006. Changes in solution color during phenol oxidation by fenton reagent. *Environ. Sci. Technol.* 40, 5538–5543. <https://doi.org/10.1021/es060866q>.
- Nakamoto, K., 1997. Infrared and Raman Spectra of Inorganic and Coordination Compounds, fifth ed. John Wiley & Sons, New York.
- Noorimotlagh, Z., Kazeminezhad, I., Jaafarzadeh, N., Ahmadi, M., Ramezani, Z., Silva Martinez, S., 2018. The visible-light photodegradation of nonylphenol in the presence of carbon-doped TiO₂ with rutile/anatase ratio coated on GAC: effect of parameters and degradation mechanism. *J. Hazard Mater.* 350, 108–120. <https://doi.org/10.1016/j.jhazmat.2018.02.022>.
- Official Journal of the European Union, 2008. Regulation (EC) No 1272/2008 of the European Parliament and of the Council of 16 December 2008 on Classification, Labelling and Packaging of Substances and Mixtures, Amending and Repealing Directives 67/548/EEC and 1999/45/EC, and Amending Regulation (EC) No 1907/2006 (Text with EEA Relevance). L 353.
- Orge, C.A., Faria, J.L., Pereira, M.F.R., 2017. Photocatalytic ozonation of aniline with TiO₂-carbon composite materials. *J. Environ. Manag.* 195, 208–215. <https://doi.org/10.1016/j.jenvman.2016.07.091>.
- Orha, C., Póde, R., Manea, F., Lazau, C., Bândas, C., 2017. Titanium dioxide-modified activated carbon for advanced drinking water treatment. *Process Saf. Environ. Protect.* 108, 26–33. <https://doi.org/10.1016/j.psep.2016.07.013>.
- Ratnawalti, Enjarlis, Slamet, 2017. Combination of ozonation and photocatalysis for pharmaceutical wastewater treatment. In: Tursiloadi, S., Rinaldi, N. (Eds.), Proceedings of the 3rd International Symposium on Applied Chemistry (Isac) 2017. Amer Inst Physics, Melville, UNSP 020019.
- Rivas, F.J., Beltran, F.J., Encinas, A., 2012. Removal of emergent contaminants: integration of ozone and photocatalysis. *J. Environ. Manag.* 100, 10–15. <https://doi.org/10.1016/j.jenvman.2012.01.025>.
- Rodríguez, A., Rosal, R., Perdigón-Melón, J.A., Mezcuca, M., Agüera, A., Hernando, M.D., Letón, P., Fernández-Alba, A.R., García-Calvo, E., 2008. Ozone-based technologies in water and wastewater treatment. In: Barceló, D., Petrovic, M. (Eds.), Emerging Contaminants from Industrial and Municipal Waste. Springer Berlin Heidelberg, Berlin, Heidelberg, pp. 127–175. https://doi.org/10.1007/978-3-540-78888-8_10.

- [org/10.1007/698_5_103](https://doi.org/10.1007/698_5_103).
- Rodríguez, C., Ignacio Lombrana, J., de Luis, A., Sanz, J., 2017. Oxidizing efficiency analysis of an ozonation process to degrade the dye rhodamine 6G. *J. Chem. Technol. Biotechnol.* 92, 656–665. <https://doi.org/10.1002/jctb.5051>.
- Rosal, R., Rodríguez, A., Gonzalo, M.S., García-Calvo, E., 2008. Catalytic ozonation of naproxen and carbamazepine on titanium dioxide. *Appl. Catal. B Environ.* 84, 48–57. <https://doi.org/10.1016/j.apcatb.2008.03.003>.
- Roth, J., Sullivan, D., 1981. Solubility of ozone in water. *Ind. Eng. Chem. Fundam.* 20, 137–140. <https://doi.org/10.1021/i100002a004>.
- Rubinson, K.A., Rubinson, J.F., 2000. *Contemporary Instrumental Analysis*. Prentice Hall, Upper Saddle River, New Jersey.
- Sánchez, L., Peral, J., Domènech, X., 1997. Photocatalyzed destruction of aniline in UV-illuminated aqueous TiO₂ suspensions. *Electrochim. Acta* 42, 1877–1882. [https://doi.org/10.1016/S0013-4686\(96\)00400-8](https://doi.org/10.1016/S0013-4686(96)00400-8).
- Sepehri, A., Sarrafzadeh, M.-H., 2018. Effect of nitrifiers community on fouling mitigation and nitrification efficiency in a membrane bioreactor. *Chem. Eng. Process. - Process Intensif.* 128, 10–18. <https://doi.org/10.1016/j.cep.2018.04.006>.
- Shahrezaei, F., Mansouri, Y., Zinatizadeh, A. a. L., Akhbari, A., 2012. Photocatalytic degradation of aniline using TiO₂ nanoparticles in a vertical circulating photocatalytic reactor. *Int. J. Photoenergy*, 430638. <https://doi.org/10.1155/2012/430638>.
- Sihtmäe, M., Mortimer, M., Kahru, A., Blinova, I., 2010. Toxicity of five anilines to crustaceans, protozoa and bacteria. *J. Serb. Chem. Soc.* 75, 1291–1302. <https://doi.org/10.2298/JSC091219103S>.
- Silva, T.L., Ronix, A., Pezoti, O., Souza, L.S., Leandro, P.K.T., Bedin, K.C., Beltrame, K.K., Cazetta, A.L., Almeida, V.C., 2016. Mesoporous activated carbon from industrial laundry sewage sludge: adsorption studies of reactive dye Remazol Brilliant Blue. *Rev. Chem. Eng. J.* 303, 467–476. <https://doi.org/10.1016/j.cej.2016.06.009>.
- Skwarek, E., Janusz, W., Gun'ko, V.M., Pakhlov, E.M., Zarko, V.I., Gdula, K., 2016. Characteristics of surface and electrochemical properties of composites with fumed metal oxides and hydroxyapatite. *Adsorption* 22, 725–734. <https://doi.org/10.1007/s10450-016-9770-4>.
- Song, S., Liu, Z., He, Z., Zhang, A., Chen, J., 2010. Impacts of morphology and crystallite phases of titanium oxide on the catalytic ozonation of phenol. *Environ. Sci. Technol.* 44, 3913–3918. <https://doi.org/10.1021/es100456n>.
- Spring, Ú.O., 2011. *Water Resources in Mexico: Scarcity, Degradation, Stress, Conflicts, Management, and Policy*. Springer Science & Business Media.
- Staehelein, J., Buhler, R., Hoigne, J., 1984. Ozone decomposition in water studied by pulse-radiolysis 2 OH and HO₄. *J. Phys. Chem.* 88, 5999–6004. <https://doi.org/10.1021/j150668a051>.
- Tao, N., Liu, G., Bai, L., Tang, L., Guo, C., 2017. Genotoxicity and growth inhibition effects of aniline on wheat. *Chemosphere* 169, 467–473. <https://doi.org/10.1016/j.chemosphere.2016.11.063>.
- Tisa, F., Abdul Raman, A.A., Wan Daud, W.M.A., 2014. Applicability of fluidized bed reactor in recalcitrant compound degradation through advanced oxidation processes: a review. *J. Environ. Manag.* 146, 260–275. <https://doi.org/10.1016/j.jenvman.2014.07.032>.
- US EPA, O., 2014. Contaminant Candidate List 4-CCL 4. US EPA accessed 10.9.18. <https://www.epa.gov/ccl/contaminant-candidate-list-4-ccl-4-0>.
- Villota, N., Lomas, J.M., Camarero, L.M., 2018. Kinetic modelling of water-color changes in a photo-Fenton system applied to oxidate paracetamol. *J. Photochem. Photobiol. A Chem.* 356, 573–579. <https://doi.org/10.1016/j.jpchem.2018.01.040>.
- Vizcaíno, I., Carrera, E., Muñoz-Romero, S., Cumbal, L., Rojo-Álvarez, J., Vizcaíno, I.P., Carrera, E.V., Muñoz-Romero, S., Cumbal, L.H., Rojo-Álvarez, J.L., 2018. Spatio-temporal river contamination measurements with electrochemical probes and mobile sensor networks. *Sustainability* 10, 1449. <https://doi.org/10.3390/su10051449>.
- VonSonntag, C., VonGunten, U., 2012. *Chemistry of Ozone in Water and Wastewater Treatment: from Basic Principles to Applications*. Iwa Publishing, London.
- Xing, B., Shi, C., Zhang, C., Yi, G., Chen, L., Guo, H., Huang, G., Cao, J., 2016. Preparation of TiO₂/activated carbon composites for photocatalytic degradation of RhB under UV light irradiation. *J. Nanomater.* 1–10, 2016. <https://doi.org/10.1155/2016/8393648>.
- Yao, S.H., Jia, Y.F., Zhao, S.L., 2012. Photocatalytic oxidation and removal of arsenite by titanium dioxide supported on granular activated carbon. *Environ. Technol.* 33, 983–988. <https://doi.org/10.1080/09593330.2011.604857>.
- Zhang, Xin, Song, J., Ji, W., Xu, N., Gao, N., Zhang, Xuhong, Yu, H., 2015. Phase-selective gelators based on closed-chain glucose derivatives: their applications in the removal of dissolved aniline/nitrobenzene, and toxic dyes from contaminated water. *J. Mater. Chem.* 3, 18953–18962. <https://doi.org/10.1039/C5TA01232E>.
- Zheng, X., Yu, N., Wang, X., Wang, Y., Wang, L., Li, X., Hu, X., 2018. Adsorption properties of granular activated carbon-supported titanium dioxide particles for dyes and copper ions. *Sci. Rep.* 8, 6463. <https://doi.org/10.1038/s41598-018-24891-1>.

3.9. 9. argitalpena. Heterogeneous catalytic ozonation of aniline-contaminated waters: a three-phase modelling approach using TiO₂/GAC

3.9 kapituluua artikulu honi dagokio:

C. Ferreiro, N. Villota, J.I. Lombraña, M.J. Rivero. Heterogeneous catalytic ozonation of aniline-contaminated waters: a three-phase modelling approach using TiO₂/GAC. *Water*, 12, 12, 3448, 2020. DOI: 10.3390/w12123448.

Article

Heterogeneous Catalytic Ozonation of Aniline-Contaminated Waters: A Three-Phase Modelling Approach Using TiO₂/GAC

Cristian Ferreiro ^{1,*} , Natalia Villota ², José Ignacio Lombraña ¹  and María J. Rivero ³

¹ Department of Chemical Engineering, Faculty of Science and Technology, University of the Basque Country UPV/EHU, Barrio Sarriena s/n, 48940 Leioa, Spain; ji.lombrana@ehu.eus

² Department of Chemical and Environmental Engineering, Faculty of Engineering Vitoria-Gasteiz, University of the Basque Country UPV/EHU, Nieves Cano 12, 01006 Vitoria-Gasteiz, Spain; natalia.villota@ehu.eus

³ Department of Chemical and Biomolecular Engineering, University of Cantabria, 39005 Santander, Spain; riveromj@unican.es

* Correspondence: cristian.ferreiro@ehu.eus; Tel.: +34-946-012-512

Received: 30 October 2020; Accepted: 3 December 2020; Published: 8 December 2020



Abstract: This work aims to study the sustainable catalytic ozonation of aniline promoted by granular active carbon (GAC) doped with TiO₂. Aniline was selected as a model compound for the accelerator manufacturing industries used in the manufacture of rubber due to its environmental impact, low biodegradability, and harmful genotoxic effects on human health. Based on the evolution of total organic carbon (TOC), aniline concentration measured using high performance liquid chromatography (HPLC), pH and ozone concentration in liquid and gas phase, and catalyst loading, a three-phase reaction system has been modelled. The proposed three-phase model related the ozone transfer parameters and the pseudo-first order kinetic constants through three coefficients that involve the adsorption process, oxidation in the liquid, and the solid catalyst. The interpretation of the kinetic constants of the process allowed the predominance of the mechanism of Langmuir–Hinshelwood or modified Eley–Rideal to be elucidated. Seven intermediate aromatic reaction products, representative of the direct action of ozone and the radical pathway, were identified and quantified, as well as precursors of the appearance of turbidity, with which two possible routes of degradation of aniline being proposed.

Keywords: aniline; catalytic ozonation; degradation routes; industrial wastewater; three-phase system; TiO₂/GAC

1. Introduction

At present, as part of corporate social responsibility, manufacturing industries must compromise in the short-term in order to carry out environmental protection actions. A report from the United Nations has indicated that, in 2015, more than 80% of the wastewaters of worldwide human activities were being discharged into rivers and sea without the removal of polluting substances [1]. Despite the fact that manufacturing companies have been opting for environmentally sustainable processes, the Sustainable Development Goals (SDGs) are unfortunately far from being met in 2030 [2]. In this work, the removal of aniline, as a model pollutant of environmental concern, is studied. Aniline (ANI) is mainly used in the synthesis of methylene diphenyl isocyanate to produce polyurethane foams, antioxidants, activators, and accelerators in the rubber industry, as well as in the synthesis of indigo and other dyes [3]. It is also employed as a raw material in the manufacturing of different types of fungicides in the agricultural and pharmaceutical industries [4,5].

The uncontrolled discharge of industrial effluents containing aniline is harmful to both humans and the environment. In humans, it has been well-documented to induce carcinogenic, teratogenic, and mutagenic effects [6]. Acute exposure to high amounts of aniline (>1 g) for a 75 kg person could lead to coma or even death [7]. In addition, uncontrolled discharges containing aniline could disturb the aquatic environment, causing mortality in aquatic animals and plants [4]. High concentrations of aniline in rivers and groundwater could affect crop safety and, consequently, human health. Studies of aniline genotoxicity in plants have also been carried out, which concluded that it significantly inhibits the growth of wheat crops irrigated with water contaminated with aniline at a concentration of 25 mg L⁻¹ [8]. Therefore, aniline has garnered great attention and has been classified as a persistent organic pollutant by the U.S. Environmental Protection Agency [9]. Conventional treatment systems based on biological processes are not suitable for the treatment of wastewater contaminated with aniline, due to micro-organism deactivation. Hence, new treatment technologies are needed, in order to transform aniline into biodegradable substances of lower toxicity before conducting biological treatment [6,8].

The removal of aniline from contaminated water has been a topic of concern for several research groups, as shown in Table 1. According to Table 1, in most studies a high degree of mineralization and degradation of the aniline was not achieved. Additionally, most of the treatment technologies for aniline removal require complex equipment, which are costly and have limited potential for full-scale implementation in wastewater treatment plants. Among such technologies, heterogeneous catalytic ozonation based on the use of TiO₂/granular active carbons (GAC) has emerged as a sustainable and cost-effective (0.64 Euro per kg of total organic carbon (TOC) eliminated) treatment alternative for the removal of aniline from contaminated waters [4]. An increase in the number of scientific reports has indicated the successful development of new activated carbon types modified through the incorporation of metal oxides with enhanced catalytic activity, thus endorsing the application of this catalytic technology at industrial scale [10,11]. The improvement in the removal yields can be attributed to the ozonation mechanisms that take place on catalytic surfaces. These mechanisms have not yet been fully defined [12]. One mechanism postulated is that the catalyst acts as an adsorbent where organic contaminants are first adsorbed on the catalyst surface and then removed [13]. The other mechanism proposed suggests that the titanium oxides favours ozone mass transport and initiates its decomposition. This mechanism assumes that the hydroxyl groups on the catalytic surface play an important role in the generation of the radical species [14].

In order to fulfil the industrial implementation requirements of this new catalytic technology, the prediction of operating behaviour under different working conditions becomes a critical point, which is yet to be solved. Delmas et al. [15] modelled a sequential process based on adsorption onto activated carbon followed by a wet catalytic oxidation with ozone. However, only a few studies have focused on the prediction and estimation of the effects of the main operational variables (e.g., pH, ozone dose, and catalyst load), as well as the contribution of chemical surface properties of TiO₂/GAC composite during the heterogeneous catalytic ozonation of wastewater containing aniline [16–19]. The study presented here addresses such challenges. In particular, we aim to develop a three-phase modelling approach that includes mass transfer parameters and rate constants from both surface and liquid bulk reactions which allow for the establishment of operating conditions that: (i) enhance radical generation due to ozone decomposition promoted by the TiO₂/GAC composite and (ii) avoid both catalyst deactivation and deterioration of the physical–chemical properties of the GAC.

Table 1. Previous studies regarding the treatment of industrial wastewater containing aniline.

Treatment	Catalyst	Operating Conditions	Comments	References
Ozone	—	(Time) = 120 min; $C_0 = 103.81 \text{ mg L}^{-1}$; pH = 7.0; $T = 20 \text{ }^\circ\text{C}$; $F_G = 2.5 \text{ g h}^{-1}$; $C_{O_3,G} = 22.0 \text{ mg L}^{-1}$; (%) = 93.56%; (% COD) = 31.03%	Studied the effect of operational variables on the biodegradability of aniline oxidation by-products, highlighting among them diacid butane, oxalic acid, and formic acid.	[6]
US/O ₃	—	(Time) = 30 min; $C_0 = 100 \text{ mg L}^{-1}$; pH ₀ = 7.0; $T = 25 \text{ }^\circ\text{C}$; $F_G = 12 \text{ mg min}^{-1}$; $US_{\text{density}} = 0.1 \text{ W mL}^{-1}$; (%) = 99%; (% TOC) = 51%	The synergistic effect improved the degradation and mineralization of aniline by 64% and 110% respectively in terms of total organic carbon (TOC) compared to simple ozonation.	[20]
O ₃ /GAC	GAC (Norit® 1240 Plus granular activated carbon (Cabot Norit Americas, Inc., Marshall, TX, USA))	(Time) = 30 min; $C_0 = 102.44 \text{ mg L}^{-1}$; pH = 7.0; $T = 25 \text{ }^\circ\text{C}$; $F_G = 150 \text{ cm}^3 \text{ min}^{-1}$; $C_{O_3,G} = 50.0 \text{ mg L}^{-1}$; (%) = 100%; (% TOC) = 56%; $M_{\text{CAT}} = 500 \text{ mg L}^{-1}$	Studied the catalytic effect of GAC on the ozonisation process. Basic GACs had a higher capacity for decomposition of O ₃ and organics adsorption.	[21]
O ₃ /TiO ₂ -GAC	TiO ₂ /GAC (Nanocyl® 3100 activated carbon doped with TiO ₂ by hydration–dehydration method (Nanocyl SA, Sambreville, Belgium))	(Time) = 60 min; $C_0 = 93.13 \text{ mg L}^{-1}$; pH = 5.6; $T = 25 \text{ }^\circ\text{C}$; $F_G = 150 \text{ cm}^3 \text{ min}^{-1}$; $C_{O_3,G} = 50.0 \text{ mg L}^{-1}$; (%) = 100%; (% TOC) = 57%; $M_{\text{CAT}} = 500 \text{ mg L}^{-1}$	A higher mineralization was observed when doping the GAC with TiO ₂ oxides. The absence of NH ₄ ⁺ promoted a different oxidation mechanism compared to pristine GAC.	[22]
	TiO ₂ /GAC (Norit® 1240 Plus granular activated carbon doped with TiO ₂ by precipitation method (Cabot Norit Americas, Inc., Marshall, TX, USA))	(Time) = 45 min; $C_0 = 20.0 \text{ mg L}^{-1}$; pH = 7.0; $T = 18 \text{ }^\circ\text{C}$; $F_G = 2.5 \text{ g h}^{-1}$; $C_{O_3,G} = 5.4 \text{ mg L}^{-1}$; (%) = 100%; (% TOC) = 80.24%; $M_{\text{CAT}} = 3.33 \text{ g L}^{-1}$	Through a novel method of synthesis by precipitation, a high yield was obtained in terms of degradation and mineralization.	[4]
TiO ₂ /UV	Hybrid Suspended-Supported TiO ₂	(Time) = 4.73 h; $C_0 = 22 \text{ mg L}^{-1}$; $M_{\text{CAT}} = 60 \text{ mg L}^{-1}$; (Supp. Cat.) = 2.3 mg cm^{-2} ; pH = 12.0; $T = 25 \text{ }^\circ\text{C}$; (%) = 99%	Under favourable operating conditions, using a hybrid system with suspended TiO ₂ catalyst, a 23% improvement in the elimination of aniline was observed compared to supported catalyst.	[5]

2. Materials and Methods

2.1. Materials

The granular activated carbon Norit[®] GAC 1240 Plus was used as a parent material (provided by the Cabot Corporation, Marshall, TX, USA) with an average particle size of 1.4 mm. The GAC was chemically modified and TiO₂ was introduced using a wet precipitation method already described elsewhere [4]; this combination is denoted as TiO₂/GAC. Both activated carbon samples have been previously characterized [4]; Table 2 summarizes their key textural and chemical surface properties. Textural characteristics, such as specific surface area (S_{BET}), micropore (V_{micro}) and mesopore (V_{meso}) volumes, and average pore diameter (D_p), were obtained by observing N₂ adsorption–desorption isotherms at 77 K [4]. The pH of the point of zero charge (pH_{pzc}) was determined using an acidimetric–alkalimetric titration method [5]. The bulk chemical composition of GAC samples was measured using X-ray fluorescence (XRF), as described previously [4]. The XRF results indicate that the parent GAC is mainly composed of SiO₂ (5.61%) and Al₂O₃ (0.45%), followed by Fe₂O₃ (0.28%), CaO (0.12%), S (0.08%), MgO (0.05%), Na₂O (0.04%), TiO₂ (0.03%), and MnO (0.01%). After the applied modification treatment to the parent GAC, the TiO₂/GAC sample was principally comprised of TiO₂ (9.33%) and SiO₂ (7.01%), followed by Al₂O₃ (1.00%), Fe₂O₃ (0.25%), CaO (0.11%), S (0.19%), Cl (2.53%), MgO (0.22%), Na₂O (0.04%), and MnO (0.01%), as determined using XRF.

Table 2. Textural and chemical surface properties of the parent and modified GAC samples [4].

Samples	S_{BET} ($\text{m}^2 \text{g}^{-1}$)	V_{micro} ($\text{cm}^3 \text{g}^{-1}$)	V_{meso} ($\text{cm}^3 \text{g}^{-1}$)	D_p (Å)	pH_{pzc}
Norit [®] GAC 1240 Plus	967.0	0.32	0.16	36.8	7.4
TiO ₂ /GAC	985.0	0.29	0.16	33.9	6.4

2.2. Analytical Methods

Aniline concentration was measured using HPLC with a Waters Alliance 2695 liquid chromatograph (Waters, Milford, CT, USA) equipped with an Agilent ZORBAX[®] Rapid Resolution High Definition (RRHD) Eclipse PAH threaded column (150 mm × 4.6 mm, 5 μm) (Agilent Technologies, Palo Alto, CA, USA) with a guard column and kept at 20 °C. A volume of 20.0 μL of sample was injected. A water:methanol (80:20 *v/v*) solution was used as a mobile phase with a flow-rate of 1.0 mL min^{−1}. Aniline was detected using a Waters 996 UV-DAD detector (Waters, Milford, CT, USA) at 230 nm.

Aniline oxidation by-products were identified using liquid chromatography coupled to mass spectrometry (MS) in an Agilent 6530 Q-TOF LC/MS (Agilent Technologies, Palo Alto, CA, USA). The separation was carried out using a Kinetex EVO[®] C18 column (100 mm × 3 mm, 2.6 μm) (Phenomenex, Torrance, CA, USA) kept at 35 °C. A 5.0 μL volume of sample was injected using a flow of 0.3 mL min^{−1}. A mobile phase A consisting of water and a mobile phase B of acetonitrile both containing 0.1% (*v/v*) HCOOH were used. The elution started with 20% of B and was maintained for 2 min. Then, the concentration of B was increased until it reached 100% at 22 min. The concentration was kept stable for 4 min and a new separation started after 2 min. MS detection was carried out in the positive voltages, following the optimization of electrospray ionization (ESI) parameters. A nitrogen flow of 10 L min^{−1}, a capillary voltage of 3500 V, a nebulizer pressure of 20 psi, and a source temperature of 350 °C were applied. Calibration curves were formed using aqueous solutions of external standards of known composition.

The degree of mineralization was quantified following the total organic carbon (TOC) concentration using a Shimadzu TOC-VCSH analyzer (Izasa Scientific, Alcobendas, Spain). Turbidity was determined using a turbidimeter EUTECH TN-100 from Thermo Scientific (Thermo Scientific, Singapore).

Chemical surface functionalities of pristine and spent GAC samples were identified using Fourier-transform infrared spectroscopy (FTIR). GAC samples were ground in an agate mortar and the

resulting powders were mixed with anhydrous KBr to yield a mix with 0.5 % *w/w* of GAC. A pressed disc of the mixed sample was placed in a disc holder in a JASCO 4200 spectrometer (JASCO Corporation, Tokyo, Japan) equipped with a DLaTGS detector. Spectra were acquired in transmittance mode in the range 4000–400 cm^{-1} with an average of 64 scans and at a resolution of 4 cm^{-1} , using Spectra Manager software V 2.14.02 (JASCO Corporation, Tokyo, Japan). A pressed disc of pure KBr was used as a background for each measurement.

2.3. Experimental Set Up of The Catalytic Ozonation System

Catalytic ozonation experiments were conducted in a 2 L semi-batch jacketed slurry reactor equipped with a magnetic stirrer and several ozone gas diffusers (see Figure 1). The experiments were carried out using a fixed volumetric flow of ozone ($Q_G = 4 \text{ L min}^{-1}$) at different pH conditions (3.0, 5.0, 7.0, and 9.0), with varying ozone doses in the gas phase (3.7, 5.4, 11.3, and 20.1 mg L^{-1}) and catalyst load (1.6, 3.3, 6.6, and 13.3 g L^{-1}).

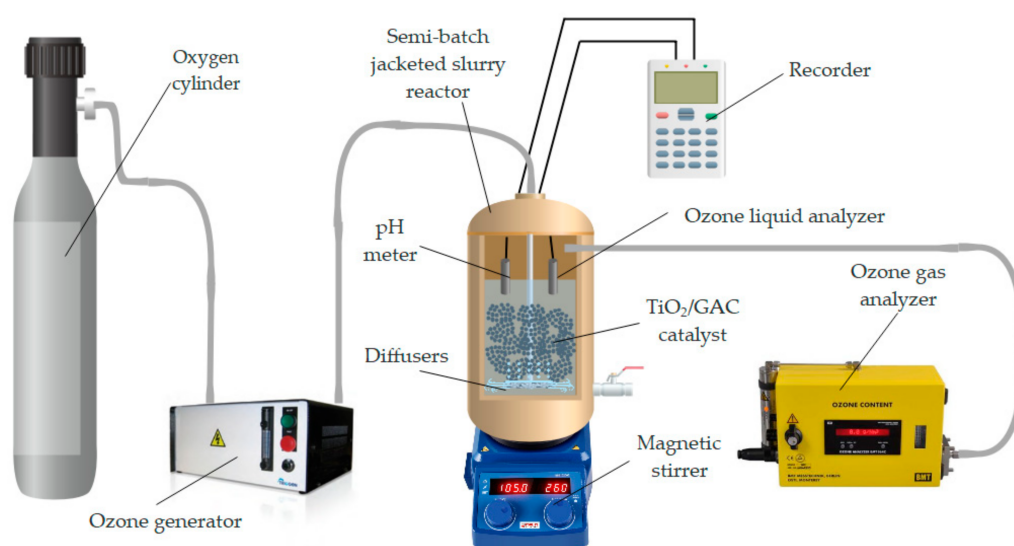


Figure 1. Experimental set-up used to carry out catalytic ozonation tests.

In this study, a concentration of 20.0 mg L^{-1} of aniline—a typical value found in industrial effluent discharges—was used [10,11]. In a typical experiment, the reactor was charged with a 1.5 L solution of aniline at a selected pH value and catalyst load. All experiments were carried out at an authorised discharged temperature of 18 °C and 60 rpm. Ozone was generated in situ from ultra-pure oxygen using a TRIOGEN LAB2B ozone generator (BIO UV, Lunel, France). Ozone concentration in the gas phase was monitored using a BMT 964C ozone analyzer (BMT MESSTECHNIK GMBH, Stahnsdorf, Germany). Dissolved ozone concentration and temperature were measured using a Rosemount 499AOZ-54 dissolved sensor (Emerson, Alcobendas, Spain). The pH value was registered with a Rosemount Analytical model 399 sensor integrated into a Rosemount Analytical Solu Comp II recorder (Emerson, Alcobendas, Spain).

Mass-transfer characterization of the reactor was performed using deionized water in the presence of TiO₂/GAC catalyst, following a procedure previously described by Rodríguez et al. [23]. Operating conditions were kept similar to those used in the presence of aniline. Ozone concentrations in the gas and liquid phases were monitored as described above. All experiments were conducted in duplicate with a maximum standard deviation in concentration measurements not exceeding 0.1 mg L^{-1} .

3. Results and Discussion

3.1. Mathematical Modelling Approach Using TiO₂/GAC Catalysts

3.1.1. Ozone Kinetic Mass Transfer Modelling

In catalytic ozonation processes, mass transfer is considered to be one of the most important stages in the elimination of organic compounds from industrial wastewater. The transfer of ozone from the gas phase to the aqueous phase is often a controlling step in the process [24]. Therefore, effective ozonation is necessary to improve the oxidation of those compounds that are not highly biodegradable and refractory. Thus, the effect of operational variables involved in the transfer of ozone to the liquid (N_{O_3} , mg L⁻¹ min⁻¹) through the overall mass transfer coefficient of ozone gas to water ($K_G a$) or $K_L a$ is expressed as follows:

$$N_{O_3} = K_G a \times (P_{O_3} - P_{O_3}^*) = K_L a \times (C_{O_3,L}^* - C_{O_3,L}) = \frac{Q_G}{V_{\text{reac}}} \times (C_{O_3,\text{in}} - C_{O_3,\text{out}}) \quad (1)$$

For calculation of the mass transfer coefficient ($K_L a$) through the second equality, the contactor was considered to be a perfectly mixed semi-continuous reactor. Equation (1) describes the transfer of ozone from the gas to the aqueous phase during the isothermal catalytic ozonation process, where $K_L a$ is the volumetric ozone mass transfer coefficient (min⁻¹), $C_{O_3,L}^*$ is the concentration of dissolved ozone in the liquid phase at saturation conditions (mg L⁻¹), V_{reac} is the volume of reaction solution (L), Q_G is the flow rate of ozone gas at the inlet (L min⁻¹), and $C_{O_3,\text{in}}$ and $C_{O_3,\text{out}}$ are the concentrations of ozone in the gas phase at the inlet and outlet, respectively (mg L⁻¹).

According to Rodriguez et al. and Schulz and Prendiville [23,25], in this study, the mass transfer resistance in the gas phase was considered negligible compared to that of the liquid. Consequently, the mass transfer coefficient $K_L a$ can be influenced by the volumetric gas flow, the pH of the solution, the bubble size, and mixing regime, among others. A correctly designed ozone contactor should have a good ozone transfer, avoiding mass transfer control in order to achieve a high mineralization

For determination of the $K_L a$ coefficient, the ozone concentration in the liquid at equilibrium was determined through Henry's law, according to Equation (2):

$$C_{O_3,L}^* = P_{O_3} / \text{He} \quad (2)$$

where Henry's solubility constant (atm mole fraction⁻¹) was estimated through Roth and Sullivan's correlation [26]:

$$\text{He} = 3.84 \times 10^7 \times C_{\text{OH}^-}^{0.035} \times \exp\left(-\frac{2428}{T}\right), \quad (3)$$

where C_{OH^-} is the concentration of hydroxyl ions (mol L⁻¹) and T is the system temperature (K). Through the execution of a calculation program with Scilab[®] software version 6.1.0 (Scilab Enterprises, Rungis, France), the $K_L a$ values (with a determination coefficient of $R^2 \cong 0.99$) were determined for different pH values and ozone doses at the reactor input. Figure 2 shows the estimated values of the mass transfer constant as a function of pH maintaining a constant ozone dose (11.3 mg L⁻¹) and as a function of ozone dose maintaining a constant neutral pH of 7.0 for an ozonation system with TiO₂/GAC catalyst in the absence of a pollutant.

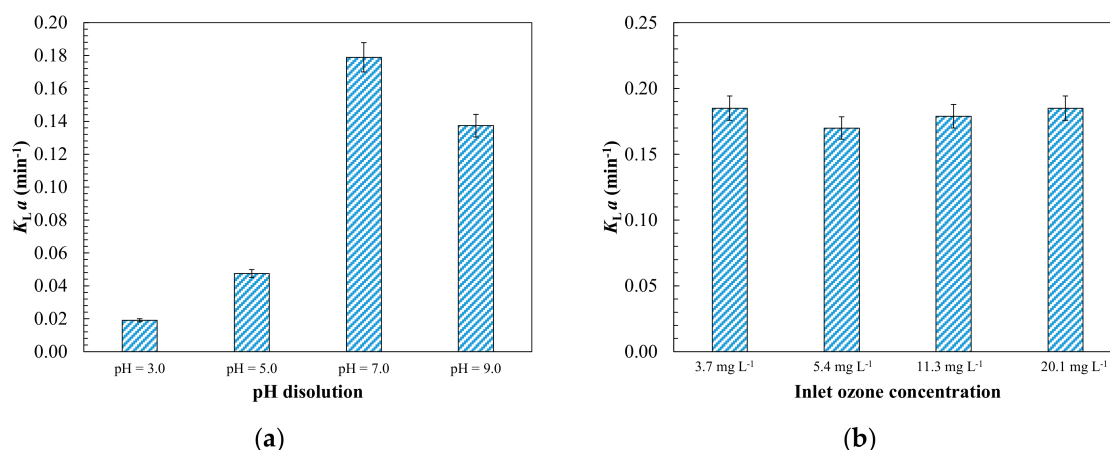


Figure 2. Comparison of volumetric mass transfer coefficient: (a) influence of pH on K_La^1 and (b) effect of inlet ozone concentration on K_La^2 . Experimental conditions: $Q_G = 4 \text{ L min}^{-1}$; $M_{\text{CAT}} = 3.3 \text{ g L}^{-1}$; $T = 18.0 \text{ }^\circ\text{C}$; $P = 1 \text{ atm}$; $V_{\text{reac}} = 1.5 \text{ L}$; (Agitation) = 60 rpm. ¹ $\text{CO}_{3,\text{in}} = 11.3 \text{ mg L}^{-1}$; ² pH = 7.0.

According to Figure 2a, an increase in the mass transfer coefficient was obtained by increasing the pH of the solution. This is due to the fact that the solubility of ozone in water decreases in acid (pH \cong 2–3) and alkaline (pH \cong 8–12) solutions [27]. Under acidic conditions, the decrease in solubility is due to the formation of protonated ozone. This is because the protonation of ozone by the hydronium ion (H_3O^+) is thermodynamically unfavourable and the reverse reaction leads to a lower activation energy, which consequently leads to a decrease in solubility [28,29]. On the other hand, under alkaline conditions (pH > 8), the decrease in ozone solubility in water is associated with the self-decomposition of ozone due to the catalytic action of hydroxyl radicals.

The mass transfer coefficients obtained were of the same order of magnitude as those found by other authors [23,30,31], emphasizing the significant increase at pH = 7.0, where Rodríguez et al. [23] obtained a coefficient of 0.073 min^{-1} .

In Figure 2b, the mass transfer coefficients obtained at different ozone doses compared while maintaining a pH of 7.0 are shown. It was found that the dose of ozone had no significant effect on the obtained K_La values. As can be seen, the mass transfer coefficient was independent of the input gas concentration, which was 0.182 min^{-1} . The same K_La obtained at different inlet ozone concentrations is due to the fact that an increase in the ozone concentration in the gas simultaneously produces an increase in the amount adsorbed and in the driving gradient ($C_{\text{O}_3,\text{L}}^* - C_{\text{O}_3,\text{L}}$). This confirms that ozone transfer is controlled by the liquid phase, as reported by Berry et al. [32] in a study using membranes and different doses of ozone injected into the reaction system.

According to the results obtained, it is suggested that these transfer coefficients depend mainly on other external factors, such as the system through which the gas is introduced into the contactor or the fluid dynamic conditions of the agitation of the ozonized solution. For better comprehension, Figure S1 shows the evolution of the utilization coefficient as a function of the pH and dose of ozone. The utilization coefficient (%) is defined as follows:

$$U_{\text{O}_3} = \frac{C_{\text{O}_3,\text{in}} - C_{\text{O}_3,\text{out}}}{C_{\text{O}_3,\text{in}}} \times 100 \quad (4)$$

In both cases, two consecutive and distinct steps were observed. In the first step, up to approximately 5 min, it was observed that ozone transferred from the gas phase to the liquid phase, in which ozone becomes a molecular compound in water that previously did not exist. After that, a transitory step occurred, in which the ozone transferred from the gas to the liquid phase is greater than that consumed through self-decomposition and reaction with TiO_2/GAC catalyst. Finally, a stationary

state was reached, in which ozone accumulated in the system reached saturation and a constant value, resulting in an equilibrium between the transferred and consumed ozone.

In Figure S1a, it can be observed that, after reaching saturation, a utilization coefficient of 32% was obtained at pH = 7.0, compared to 19.5% obtained at pH = 3.0. This difference was due to the different solubility that ozone has in water at different pH values, as explained above. The utilization value of 24.8% obtained at pH = 9.0 may be due to the fact that the transferred ozone instead contributes to the accumulation of ozone in the liquid phase; in this case, it would undergo self-decomposition [12]. In the study of the ozone dose effect (Figure S1b), it can be observed that an increase in the ozone dose reduces the efficiency of ozone use. This can be justified largely by the study carried out by Rodriguez et al. [23]. In their study, the degradation of a dye such as rhodamine 6G was evaluated at different pH values and doses of ozone in the presence of activated carbon. The ozone transfer and subsequent consumption was conditioned by parameters, such as pH, which indirectly affect the reactivity of the compound to be oxidized but not the concentration of ozone dose applied.

Von Sonntag and Von Gunten [33] studied the reactivity of aniline oxidation in an ozonation process at different pH values. It was found that, at pH = 6.5, an oxidation kinetic constant of $1.4 \times 10^7 \text{ M}^{-1} \text{ s}^{-1}$ was obtained versus pH = 1.5, where a constant of $5.9 \times 10^4 \text{ M}^{-1} \text{ s}^{-1}$ was obtained. All of this indicates that, at pH = 7.0, the best operating conditions will be obtained (with regards to the chemical reaction of oxidation and transfer of ozone from the gas phase to the liquid).

3.1.2. Aniline Degradation Kinetic Modelling

Modelling of the catalytic ozonation process was carried out to describe the combined action of ozone and TiO₂/GAC composite and to predict and estimate the overall parameters affecting the process of degradation (and, in particular, the mineralization) of aniline. In this section, we propose applying the adaptation of the three-phase mathematical model described by Ferreiro et al. [19], which considers G-L ozone mass transfer, the adsorption process as well as the parallel oxidation that takes place in the liquid phase and the oxidation at the surface of the catalytic material (TiO₂/GAC). The model proposed allows the evolution of the monitored pollutant or total organic carbon (TOC) during the simultaneous oxidation reaction and adsorption process to be calculated. For application of this simultaneous adsorption–oxidation (Ad/Ox) model, it was assumed that:

- The rate of the global ozonation process, or G-L mass transfer rate, coincides with the consumption of ozone in the parallel (liquid and solid) reactive process.
- The oxidation kinetics of aniline in the liquid and in the solid, in terms of TOC, is considered as pseudo-first order.
- For the TiO₂/GAC composite, it was considered a sufficiently porous material for ozone and aniline diffusion mechanisms to take place also in the internal surface of particle.
- The kinetic constant of the aniline oxidation on the solid, also in terms of TOC, includes desorption of degradation compounds.
- The adsorption process is simultaneous to the reaction process on the solid so that its kinetics are strongly affected by the ozonation conditions.

Based on these considerations, Ferreiro et al. [19], for an Ad/Ox process, deduced Equation (5) to express the decrease in contaminant concentration in the liquid in terms of total organic carbon (C_p). The degradation of the pollutant, r_p , should be explained at two levels: in the liquid (r_p^I) and on the activated carbon (r_p^{II}), as a consequence of the oxidative action of the ozone transferred and consumed in the liquid ($N_{O_3}^I$) and on the solid ($N_{O_3}^{II}$), respectively. In addition to the degradation of the pollutant, the elimination due to adsorption is important in the first stages of the process.

$$-\frac{dC_p}{dt} = r_p^I + r_p^{II} + \left(\frac{dC_p}{dt}\right)_{\text{ads}} \quad (5)$$

The kinetic parameters of oxidation and adsorption can be expressed as a function of the respective kinetic constants ($k_{c,L}$, $k_{c,S}$, and k_{ads}), ozone concentration, and pollutant, according to the following:

$$r_p^I + r_p^{II} = (z^I N_{O_3}^I + z^{II} N_{O_3}^{II}) = k_{c,L} \times C_{O_3,L} \times C_p + k_{c,S} \times \frac{C_{O_3,L}}{m} \times M_{CAT} \times Z_p \quad (6)$$

$$\left(\frac{dC_p}{dt}\right)_{ads} = k_{ads} \times (Z_{p,\infty} - Z_p)^2 \times M_{CAT} \quad (7)$$

In Equation (6), the stoichiometric coefficients z^I and z^{II} express the amount of pollutant (mg TOC per mg of ozone) consumed in the liquid and on the catalyst, respectively. The above equation assumes that the concentration of ozone on the catalyst, $C_{O_3,S}^*$ is in equilibrium with the liquid ozone concentration, $C_{O_3,L}$, and can be expressed as a function of this, according to $C_{O_3,L} = m \times C_{O_3,S}^*$, where m (mg L⁻¹)/(mg g⁻¹ catalyst) is the slope of the corresponding L-S balance. On the other hand, Z_p is the concentration of total organic carbon adsorbed in the catalyst (mg g⁻¹), M_{CAT} is the concentration of catalyst (g L⁻¹), and $Z_{p,\infty}$ is the amount of total organic carbon adsorbed in the catalytic material at equilibrium (mg g⁻¹), according to the Freundlich equation:

$$Z_{p,\infty} = K_F \times C_p^{1/n} \quad (8)$$

where K_F is a Freundlich constant that indicates the adsorption capacity of the adsorbent (mg g⁻¹) (L mg⁻¹)^{1/n} and n describes the adsorption intensity. Values of n between 2 and 10 indicate good adsorption intensity [34].

In a semi-continuous process in which an ozone flow is continuously injected, the concentration of ozone in the liquid, C_{O_3} , is assumed to be constant during the reaction [23]. This assumption can be used to define the apparent first-order kinetic constants— k_{oxL} in the liquid and k_{oxS} over the catalyst—to describe the degradation of the aniline, in terms of TOC (min⁻¹). Consequently, the overall pollutant concentration variation (Equation (5)) can be written as follows:

$$-\frac{dC_p}{dt} = k_{oxL} \times C_p + k_{oxS} \times M_{CAT} \times Z_p + k_{ads} \times (Z_{p,\infty} - Z_p)^2 \times M_{CAT}, \quad (9)$$

where C_p is the concentration of the pollutant (TOC) at a given time t (mg L⁻¹), Z_p is the concentration of total organic carbon adsorbed onto the catalyst (mg g⁻¹), M_{CAT} is the concentration of catalyst (g L⁻¹), $Z_{p,\infty}$ is the amount of total organic carbon adsorbed in the composite at equilibrium (mg g⁻¹), k_{oxL} is the first-order kinetic constant due to the oxidation of aniline in the liquid (min⁻¹), k_{oxS} is the pseudo-first-order kinetic constant due to oxidation on the catalytic material (min⁻¹), and k_{ads} is the aniline adsorption constant (g mg⁻¹ min⁻¹). The combination of Equations (8) and (9) provides a description of the variation in the pollutant concentration in the system from the determination of the kinetic parameters (k_{oxL} , k_{oxS} , and k_{ads}) and the equilibrium parameters (K_F and n).

3.1.3. Evaluation of Operating Conditions for Model Validation

Operational parameters such as pH, ozone concentration, or the dose of catalyst used have a considerable effect on the efficiency of the removal of aniline using catalytic ozonation processes with TiO₂/GAC catalyst. Using the Ad/Ox model described above, it is possible to explain the effects of the different parameters, such as the behaviour of the ozone or the catalyst dosage. In Figure 3, the evolution of aniline degradation is shown, as well as the mineralization under various pH values (3.0, 5.0, 7.0, and 9.0), ozone concentrations at the inlet (3.7, 5.4, 11.3, and 20.1 mg L⁻¹), and catalyst doses (1.6, 3.3, 6.6, and 13.3 g L⁻¹).

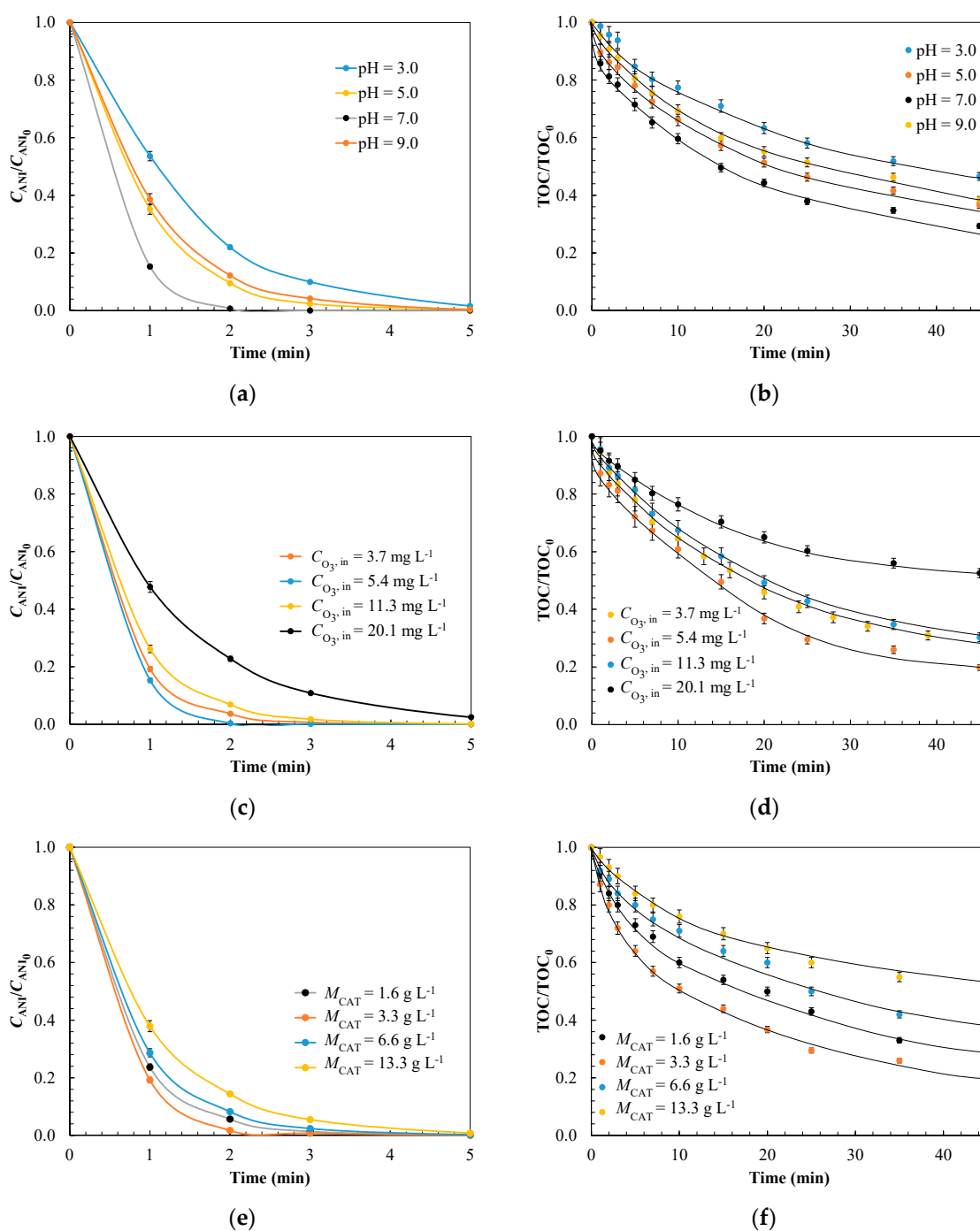


Figure 3. Effect of operating conditions on catalytic ozonation with TiO_2/GAC : (a) pH¹, (c) inlet ozone concentration², and (e) mass of TiO_2/GAC catalyst in the aniline removal³ and (b)¹, (d)² and (f)³ in TOC (mineralization), showing experimental and modelled profiles fitted to the Ad/Ox process³. Experimental conditions: $Q_G = 4 \text{ L min}^{-1}$; $T = 18.0 \text{ }^\circ\text{C}$; $P = 1 \text{ atm}$; $V_{\text{reac}} = 1.5 \text{ L}$; (Agitation) = 60 rpm. ¹ $C_{\text{O}_3,\text{in}} = 5.4 \text{ mg L}^{-1}$, $M_{\text{CAT}} = 3.3 \text{ g L}^{-1}$; ² pH = 7.0, $M_{\text{CAT}} = 3.3 \text{ g L}^{-1}$; ³ pH = 7.0, $C_{\text{O}_3,\text{in}} = 5.4 \text{ mg L}^{-1}$.

The pH has a significant effect on the catalyst, as it directly affects the pathway through which the ozone acts on the organic compound. Figure 3a,b shows that the best conditions for the effective removal of aniline are present at a neutral pH of 7.0. The change in basicity associated with pollutant removal at that pH, or specific basicity loss, is optimal [35]. In addition, it was observed that those experiments conducted at slightly alkaline pH (pH = 9.0) obtained a higher oxidation rate because, under these conditions, the indirect pathway for hydroxyl radical generation is promoted by the

interaction between ozone and the TiO₂/GAC catalyst. On the other hand, at acidic pH (pH = 3.0), a more limited oxidation and mineralization rate was observed because, at this pH value, the attack through the molecular pathway between ozone and aniline is mostly promoted [36,37]. Although this pathway is more selective than the radical one, the oxidation power of molecular ozone (2.07 V) is lower than that of the hydroxyl radicals (2.80 V) [28].

On the other hand, the dose of ozone in the catalytic ozonation reaction system is a critical parameter for the degradation and mineralization of aniline. In Figure 3c,d, it is shown that, with an ozone dose of 5.4 mg L⁻¹, the highest aniline mineralization was achieved, with a value of 80.2%. However, upon increasing the ozone dose considerably (to 20.1 mg L⁻¹), a negative effect was obtained as opposed to the generation of a larger amount of hydroxyl radicals. This was due to the fact that, on the surface of the TiO₂/GAC catalyst, instead of generating hydroxyl radicals for the degradation of the organic compound, other species were generated, such as hydroperoxyl radicals—which have a lower oxidation potential (1.70 V) than hydroxyl radicals (2.80 V) or ozone (2.07 V) [38]. Moreover, a very high ozone dose (20.1 mg L⁻¹) could transform the basic sites into acidic sites, as the oxidation of the carbonaceous support can generate acidic groups such as lactones or carboxylic acid, which could negatively influence the adsorptive properties of the TiO₂/GAC composite itself [39]. This last aspect will be analysed in detail later on.

In Figure 3e,f, the effect of the catalyst dose on the aniline removal rate is shown, providing information on the optimal use of the TiO₂/GAC material. An increase in catalyst dosage led to increased degradation and mineralization of the aniline, with a favourable dosage of 3.3 g L⁻¹, where mineralization was close to 80% and complete degradation of the aniline was achieved in less than 10 min. In general, a higher catalyst dose increases the number of active sites on the surface of the composite, thus facilitating the further decomposition of ozone into hydroxyl radicals [40]. However, above a certain critical value, a decrease in TOC removal was observed, which may be due to the adsorption of a higher proportion of pollutant on the catalyst, thus reducing the catalytic effect [38] in favour of the adsorption. This indicates that a small amount of catalyst is sufficient to induce a radical chain reaction that appears to be more effective on the dissolved than adsorbed pollutant. Moussavi and Khavanin [41] studied the effect of the dose of activated carbon in a catalytic ozonation process for the removal of phenol. It was observed that, from the optimal dose of catalyst, no further improvement in mineralization was observed, as with the TiO₂/GAC composite. Consequently, it was concluded that there is an optimal dose of catalyst, which changes depending on the type of catalyst, the organic compound to be eliminated, the operational conditions of the reaction, and the desired cost-effectiveness.

The TOC removal kinetics was fitted to the model proposed in Section 3.1.2 by solving Equations (8) and (9). Before analysing the results obtained from the Ad/Ox model, it was verified that under the operating conditions studied the assumption of control of the chemical reaction during catalytic ozonation was satisfied.

The control regime was verified through the U_{O_3} profiles shown in Figure S2. It can be seen at the lowest ozone doses ($C_{O_3,in} = 3.7 \text{ mg L}^{-1}$), in the initial instants, the ozone concentration in the gaseous phase is practically zero ($U_{O_3} = 100\%$). This indicates that the process is controlled by the mass transfer. However, after 4 min it changes to be controlled by the chemical reaction, once $C_{O_3,L}$ starts rising. For resolution of the TOC removal kinetics, the calculation tool Scilab[®] was used, with which the corresponding adjustment to the experimental data was simulated to obtain the adsorption and ozonation kinetics constants during the removal of aniline with the previous determination of equilibrium adsorption constants. As for the initial conditions of the dependent variables involved in the differential equation, at the initial time, an aniline concentration of 20.0 mg L⁻¹ was considered, corresponding to an initial TOC concentration of $C_{p,0} = 12.50 \text{ mg L}^{-1}$ and the TiO₂/GAC free of aniline or other organics ($Z_{p,0} = 0.0 \text{ mg g}^{-1}$). C_p^* vs. t modelled profiles were fitted to the experimental ones

(of N values), in order to minimize the weighted standard deviation, σ , given by Equation (10). Thus, the estimated values of k_{ads} , k_{oxL} , and k_{oxS} are listed in Table 3 [42]:

$$\sigma = \sqrt{\frac{\sum_{i=1}^N \left(\frac{C_p - C_p^*}{C_p} \right)^2}{N - 1}} \quad (10)$$

Table 3. Summary of the adsorption and oxidation kinetic constants for the mineralization of wastewater containing aniline using Norit® GAC 1240 Plus and TiO₂/GAC composite by catalytic ozonation.

Catalyst Comparison				
Kinetic Parameter	Norit® GAC 1240 Plus ^{1,2}	TiO ₂ /GAC ^{1,2}		
$k_{\text{ads}} \times 10^{-4}$, g mg ⁻¹ min ⁻¹	2.4	3.5		
$k_{\text{oxL}} \times 10^1$, min ⁻¹	8.1	5.9		
$k_{\text{oxS}} \times 10^1$, min ⁻¹	0.0030	2.3		
σ	0.050	0.046		
TiO ₂ /GAC Composite Analysis				
Kinetic Parameter	Effect of pH			
	3.0	5.0	7.0	9.0
$k_{\text{ads}} \times 10^{-4}$, g mg ⁻¹ min ⁻¹	3.6	3.1	2.9	2.5
$k_{\text{oxL}} \times 10^1$, min ⁻¹	3.4	6.5	8.3	8.6
$k_{\text{oxS}} \times 10^1$, min ⁻¹	0.20	1.1	1.2	0.90
σ	0.061	0.053	0.059	0.048
Kinetic Parameter	Effect of Ozone Inlet Concentration, mg L ⁻¹			
	3.7	5.4	11.3	20.1
$k_{\text{ads}} \times 10^{-4}$, g mg ⁻¹ min ⁻¹	3.2	3.5	2.9	1.8
$k_{\text{oxL}} \times 10^1$, min ⁻¹	4.2	5.9	8.3	11.5
$k_{\text{oxS}} \times 10^1$, min ⁻¹	1.5	2.3	1.2	0.50
σ	0.052	0.046	0.057	0.045
Kinetic Parameter	Effect of Catalyst Dose, g L ⁻¹			
	1.6	3.3	6.6	13.3
$k_{\text{ads}} \times 10^{-4}$, g mg ⁻¹ min ⁻¹	1.8	3.5	4.4	8.4
$k_{\text{oxL}} \times 10^1$, min ⁻¹	3.8	5.9	2.2	1.0
$k_{\text{oxS}} \times 10^1$, min ⁻¹	1.9	2.3	1.5	0.90
σ	0.054	0.046	0.055	0.052

¹ Experimental conditions: $Q_G = 4 \text{ L min}^{-1}$; $C_{O_3, \text{in}} = 5.4 \text{ mg L}^{-1}$; $\text{pH}_0 = 7.0$; $M_{\text{CAT}} = 3.3 \text{ g L}^{-1}$; $T = 18.0 \text{ }^\circ\text{C}$; $P = 1 \text{ atm}$; $V_{\text{reac}} = 1.5 \text{ L}$; (Agitation) = 60 rpm. ² Freundlich equilibrium parameters: $K_F = 33.07 \text{ (mg g}^{-1}\text{)(L mg}^{-1}\text{)}^{1/n}$, $n = 2.39$ for Norit® GAC 1240 Plus and $K_F = 44.02 \text{ (mg g}^{-1}\text{)(L mg}^{-1}\text{)}^{1/n}$, $n = 3.97$ for TiO₂/GAC composite.

The Freundlich parameters of the catalytic materials tested are given in Table 3, which were obtained experimentally in the previous adsorption tests. The C_p values had an acceptable fit to the Ad/Ox model with a weighted standard deviation of $\sigma \cong 0.05$ for the mineralization kinetics.

In Table 3 it was observed that the k_{oxS} constant was lower than k_{oxL} . This is because in the solid involved an oxidation reaction in conjunction with the adsorption phenomena in parallel. From the comparison of the catalytic ozonation with Norit® GAC 1240 Plus activated carbon and TiO₂/GAC composite, it can be seen that the TiO₂/GAC catalysts kinetically favour adsorption, with $k_{\text{ads}} = 3.5 \times 10^{-4} \text{ g mg}^{-1} \text{ min}^{-1}$, compared to commercial carbon ($k_{\text{ads}} = 2.4 \times 10^{-4} \text{ g mg}^{-1} \text{ min}^{-1}$). Its higher adsorption capacity, rather than the specific surface ($S_{\text{EXT}} = 298.9 \text{ m}^2 \text{ g}^{-1}$)—which is very similar to that of commercial activated carbon ($S_{\text{EXT}} = 224.4 \text{ m}^2 \text{ g}^{-1}$)—explains this behaviour, despite the fact that TiO₂/GAC has a 25% larger external surface, as seen in the Material and Methods

section [43]. The adsorption properties of metal oxides, such as TiO_2 , deposited onto GAC, appear to also enhance the catalytic activity. Other authors [37,44] have highlighted that metal oxides have a high adsorption capacity, which is due to ligand exchange reactions that provide strong bonds between the ionized species and the active site of the metal oxide surface. The increase in the oxidation kinetic constant in the solid, from a value of $k_{\text{oxS}} = 0.003 \times 10^1$ to $2.3 \times 10^1 \text{ min}^{-1}$, in the TiO_2/GAC composite is remarkable. This increase is due to the contribution of TiO_2 in the activated carbon, improving its reactivity and the number of active sites on the catalyst. The deposited TiO_2 is responsible for efficiently decomposing the ozone, producing HO^\bullet radicals. Other properties, such as pore volume, porosity, pore size distribution, and, particularly, the presence of active sites on the surface (e.g., Lewis acid sites, which are responsible for the catalytic reactions), may be responsible for this increase in k_{oxS} [45]. Acidity or basicity, for example, is key to surface properties. Furthermore, the hydroxyl groups, which are present on all surfaces of the metal oxides, are dependent on the deposited metal oxide [39]. Valdés and Vega [45] studied the effect of the chemical structure of various active carbons on the catalytic activity for the generation of hydroxyl radicals, where they suggested that the presence of iron metal ions played an important role in the decomposition of ozone and hydrogen peroxide towards the generation of radicals. Those carbons with more basic surface functionalities led to a higher radical generation and, consequently, to a higher catalytic activity.

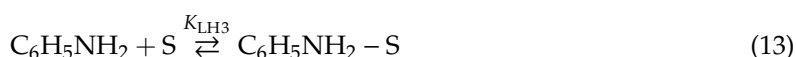
Authors such as Orge et al. [46] and Kasprzyk-Hordern et al. [38] have suggested that the variability of surface properties and interactions between the catalyst and ozone with organic pollutants results in different reaction mechanisms, derived from two main types: Langmuir–Hinshelwood (LH) or modified Eley–Rideal (ER).

The LH stage consists of adsorption, surface reaction, and subsequent desorption [28]:

Adsorption of ozone onto every site, S , of GAC surface:



Adsorption of aniline:

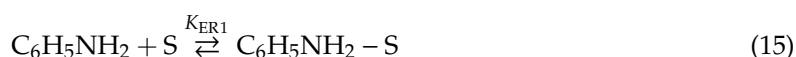


Surface reaction and desorption of oxidation products:

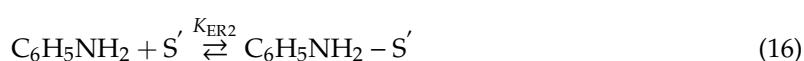


The other mechanism (modified ER), proposed by Beltran et al. [44], is specific for metal oxides supported on activated carbon materials and consists of an adsorption stage on the GAC, together with the assumptions of the modified ER mechanism. In this case, these stages are: (i) the adsorption of aniline onto the TiO_2/GAC composite, (ii) the reaction stage between the adsorbed aniline and the ozone, and (iii) the irreversible ozonation reaction of adsorbed pollutant.

Adsorption of aniline on the GAC active sites:

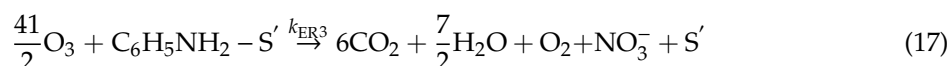


Adsorption of aniline on the TiO_2 active sites:



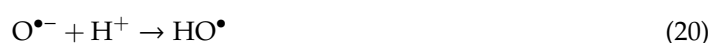
where S' represents any active site on the TiO_2 .

Reaction between ozone and adsorbed aniline on TiO₂ active sites:



In this last mechanism, it was assumed that the CO₂ generated corresponds to that resulting from complete mineralization. Overall, it can be concluded that the removal of aniline is due to an adsorption process on the GAC and to the catalytic ozonation itself, which takes place in the active centres of the TiO₂ metal oxide. Based on the values of the k_{oxS} and k_{oxL} constants obtained from the three-phase model, it is possible to qualitatively determine the predominant mechanism (LH or modified ER). An intensification of the k_{oxS} constant due to the presence of TiO₂ metal oxide against the k_{oxL} constant indicates the predominance of the modified ER mechanism. In contrast, negligible values of the k_{oxS} constant compared to the k_{oxL} constant indicate the predominance of the LH mechanism. Taking into account the mechanical aspects of the reaction system, the effect of operational variables, such as pH, ozone dosage, and TiO₂/GAC catalyst loading were analysed.

Regarding the effect of pH, due to the surface properties of the composite, it was observed that the adsorption constant increased under more acidic pH values, while under alkaline pH values, the quantity of aniline removed decreased. This is due to the speciation of the aniline, with $\text{pK}_a = 4.61$ [47], and the character of the surface of the composite through the zero loading point ($\text{pH}_{\text{pzc}} = 6.4$). The TiO₂/GAC composite, at a pH below 6.4, develops a negative charge on its surface; below $\text{pH} = 4.61$, it will mostly be in ionic form, favouring adsorption. On the other hand, under alkaline pH, the affinity between the aniline and the surface of the material is weak and adsorption is limited. Similarly, Shahamat et al. [48], in a catalytic ozonation process in which a carbon nanocomposite was used for the removal of phenol, observed the same behaviour at a pH between pH_{pzc} and pK_a . The oxidation constant in the liquid, k_{oxL} , increased from a value of 3.4×10^1 to $8.6 \times 10^1 \text{ min}^{-1}$, due to the fact that, under alkaline conditions, the radical pathway in which ozone directly attacks the OH⁻ generating radicals HO[•] is favoured, according to [49]:



As for k_{oxS} , the maximum value observed was $1.2 \times 10^1 \text{ min}^{-1}$ at $\text{pH} = 7.0$. This increase was due to the contribution that TiO₂ metal oxide provides to the GAC, thus improving the capacity of transforming ozone into hydroxyl radicals. According to Roshani et al. [50], the surface charge and the capacity of the TiO₂/GAC composite to transfer electrons to the ozone are factors that affect the elimination of TOC. Operating at a pH of 7.0, favourable conditions allow for a positive interaction between the ozone and TiO₂ metal oxide, which allows for the decomposition of ozone and, thus, the generation of a greater number of HO[•] radicals in sufficient quantity to oxidize the organic compounds adsorbed on the surface of the GAC. According to Nawrocki and Kasprzyk-Hordernb [51], considering the type of radicals formed on TiO₂ nanoparticles in the presence of ozone, it was concluded that catalytic ozonation was more effective at a pH close to pH_{pzc} . Under these conditions, the presence of neutral hydroxyls are responsible for the formation of the hydroxyl radical.

For the effect of the ozone dose, it was observed that the use of a low ozone dose ($C_{\text{O}_3, \text{in}} = 3.7 \text{ mg L}^{-1}$) led to a mineralization yield of 69%, as the amount of hydroxyl radicals generated was low. Taking into account the distribution of the kinetic constants obtained (Table 3), when the dose is insufficient, the adsorbent effect is enhanced but not the oxidation of the organic pollutant. On the other hand, with a high dose ($C_{\text{O}_3, \text{in}} = 20.1 \text{ mg L}^{-1}$), ozone accumulates in the system, favouring the generation of the less reactive perhydroxyl radical (HO₂[•]), according to [49]:



It seems evident that moderate concentrations favour the adsorption kinetics and result in a sufficient generation of hydroxyl radicals on the surface of the catalyst. A dose of 5.4 mg L^{-1} ensures that the aniline is adsorbed rapidly over the GAC ($k_{\text{ads}} = 3.5 \times 10^{-4} \text{ g mg}^{-1} \text{ min}^{-1}$) and, at the same time, maximizes oxidation at the solid level ($k_{\text{oxS}} = 2.3 \times 10^1 \text{ min}^{-1}$), where TiO_2 plays an important role. The action of ozone on the adsorbed aniline, according to the modified ER mechanism (see Equation (17)), appears to be the dominant mechanism in this case and responsible for the high k_{oxS} value.

Concerning the effect of catalyst loading, it was observed that, by increasing the dose from 1.6 to 13.3 g, the adsorption constant increased from 1.8×10^{-4} to $8.4 \times 10^{-4} \text{ g mg}^{-1} \text{ min}^{-1}$. A higher quantity of adsorbed organics and ozone is to be expected when increasing the amount of catalyst but does not result in further destruction of the aniline. It can be observed that high doses of catalyst lead to a predominance of surface oxidation reactions, as a result of increased TiO_2/GAC active sites and an increased amount of adsorbed contaminant [36]. However, the most favourable values were produced with an intermediate amount of catalyst ($k_{\text{oxS}} = 2.3 \times 10^1 \text{ min}^{-1}$). The negative effect became increasingly evident as the amount of catalyst increased, which was related to a change in the mechanism of the oxidation processes at the solid level. According to the assumption made in Section 3.1.3, a transition from the modified ER to the LH mechanism should take place. In effect, with small amounts of catalyst, a moderate amount of contaminants was adsorbed—preferably on TiO_2 —through non-associated hydroxyl groups [52] or S' sites (Equation (17)) with favourable incidence in the increase of k_{oxS} and consequently in the degradation of the contaminant. An increase in the amount of catalyst led to a greater proportion of the contaminant being adsorbed, resulting in the occupation of S sites and participation of slow rate reactions (such as that shown in Equation (14)), with a subsequent decrease in k_{oxS} . A decrease in the degradation of the aniline at the liquid phase as $k_{\text{oxL}} = 1.0 \times 10^1 \text{ min}^{-1}$ decreased and the lower proportion of contaminant in the liquid were other negative effects associated with an increase in the amount of catalyst [38]. Moderate amounts of catalyst (3.3 g L^{-1}) favoured oxidation at the solid and liquid level, obtaining the highest mineralization (80% TOC removal) in 45 min.

3.2. Physicochemical Surface Characterization of Spent-Granular Activated Carbon

In order to verify the lower generation of hydroxyl radicals when a high catalyst dose was used and that the aniline would be oxidized under very poor oxidation conditions, an analysis of the physicochemical properties of the TiO_2/GAC composite used was carried out, as shown in Table 4.

Table 4 shows a decrease of the specific surface of the TiO_2/GAC composite of the experiment performed with a catalyst load of 13.3 g L^{-1} from 985.0 to $901.2 \text{ m}^2 \text{ g}^{-1}$. The pore volume was also reduced, but the physical properties were practically unchanged with a catalyst dose of 3.3 g L^{-1} . Considering the importance of the adsorption stages contemplated in the Ad/Ox model, the necessary equilibrium of reactions at the liquid and solid level should not be broken. This balance is broken when the catalyst dose is increased, with negative effects on the degradation of the contaminant being key in the optimization of the process.

Concerning the chemical properties (e.g., the point of zero charge), ozone appeared to affect them by a small amount. The carbonaceous support lost active basic sites while the concentration of the acidic functional groups increased, leading to a reduction in adsorption capacity over long periods [53].

Table 4. Physicochemical properties of pristine and spent TiO₂/GAC in aniline ozonation with different catalyst doses. Experimental conditions: $Q_G = 4 \text{ L min}^{-1}$; $C_{O_3, \text{in}} = 5.4 \text{ mg L}^{-1}$; $\text{pH} = 7.0$; $T = 18.0 \text{ }^\circ\text{C}$; $P = 1 \text{ atm}$; $V_{\text{reac}} = 1.5 \text{ L}$; (*Agitation*) = 60 rpm.

Property	Pristine TiO ₂ /GAC	Spent TiO ₂ /GAC	
		$M_{\text{CAT}} = 3.3 \text{ g L}^{-1}$	$M_{\text{CAT}} = 13.3 \text{ g L}^{-1}$
$S_{\text{BET}}, \text{m}^2 \text{ g}^{-1}$	985.0	980.4	901.2
$S_{\text{ext}}, \text{m}^2 \text{ g}^{-1}$	298.9	289.1	267.5
$V_T, \text{cm}^3 \text{ g}^{-1}$	0.45	0.39	0.32
$V_\mu, \text{cm}^3 \text{ g}^{-1}$	0.29	0.25	0.20
$V_M, \text{cm}^3 \text{ g}^{-1}$	0.16	0.14	0.12
$V_M/V_T, \%$	35.2	35.9	37.5
$V_\mu/V_T, \%$	64.8	64.1	62.5
$D_p, \text{Å}$	33.9	33.0	29.3
pH_{pzc}	6.4	6.2	6.3

Moreover, Figure 4 shows FTIR spectra of the non-ozonized and ozonized TiO₂/GAC catalyst using a 13.3 g L^{-1} load, in order to confirm the presence of compounds that verify the previous hypothesis. According to Figure 4, it was observed that most of the spectral bands corresponded to organic compounds, highlighting the band from 3300 to 3500 cm^{-1} (–OH stretching), which is due to the presence of water in the sample during preparation. The 500 cm^{-1} spectral band (Ti–O stretching) corresponded to the presence of TiO₂ deposited on the GAC [54]. The main spectral modifications, when comparing the sample of the non-ozonized composite and the ozonized one, were detected in the emergence of the 790 cm^{-1} band. The accumulation of intermediate species, such as oxamic acid, and subsequent sorption in the solid explain this FTIR sorption band [55]. The peak near to 2800 cm^{-1} would correspond to aldehyde groups, such as formaldehyde or acetaldehyde, and strongly depended on the ozone dose, adsorbed on the catalyst due to the opening of the aromatic ring [56], while another band at 1102 cm^{-1} was due to the superoxide radical [57].

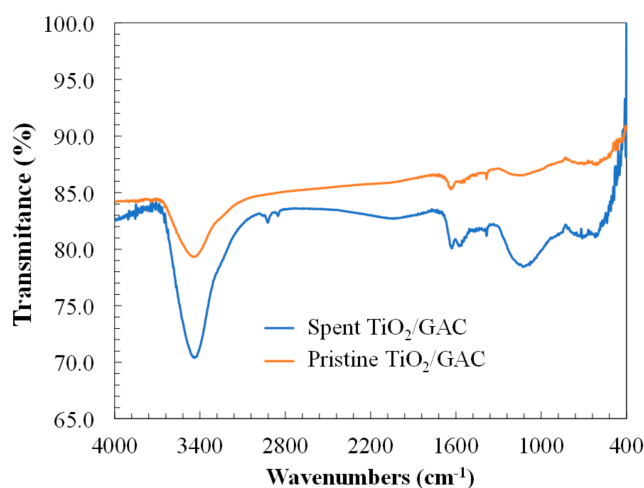


Figure 4. FTIR spectra of pristine and spent TiO₂/GAC composite in the aniline catalytic ozonation. Experimental conditions: $Q_G = 4 \text{ L min}^{-1}$; $C_{O_3, \text{in}} = 5.4 \text{ mg L}^{-1}$; $\text{pH} = 7.0$; $M_{\text{CAT}} = 13.3 \text{ g L}^{-1}$; $T = 18.0 \text{ }^\circ\text{C}$; $P = 1 \text{ atm}$; $V_{\text{reac}} = 1.5 \text{ L}$; (*Agitation*) = 60 rpm.

3.3. Degradation Pathway Approach

In order to provide more detail on the types of intermediates formed when increasing the dose of catalyst, other physical–chemical parameters, such as turbidity, were analysed. In Figure 5, the effect of the catalyst dose on turbidity is shown. Solid particles or high molecular weight insoluble degradation products usually cause turbidity [58]. The experiment with the highest amount of catalyst

(13.3 g L⁻¹ TiO₂/GAC catalyst), with an ozone dose of 5.4 mg L⁻¹ and a neutral pH, led to the highest turbidity, with a turbidity of 17 NTU after a reaction time of 45 min. However, with a catalyst dose of 3.3 g L⁻¹, the lowest turbidity was produced, corresponding to the highest mineralization observed. Consequently, the higher turbidity could be associated with the formation of more recalcitrant intermediate products.

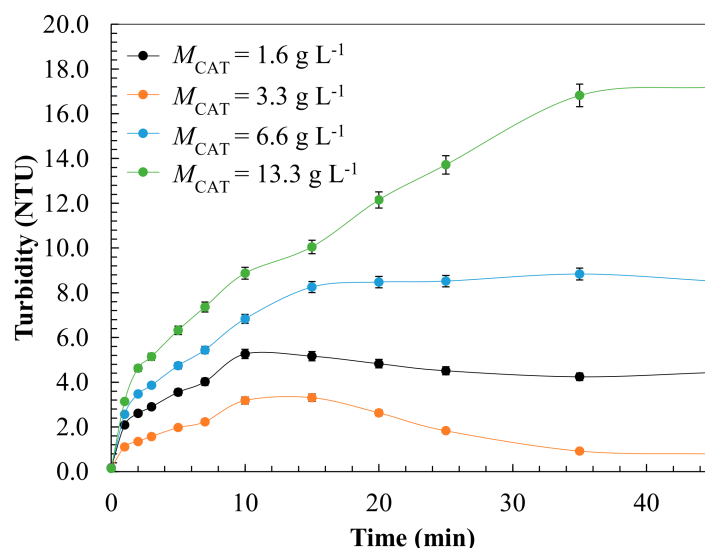


Figure 5. Effect of TiO₂/GAC catalyst dosage on turbidity during catalytic ozonation of aniline containing wastewater. Experimental conditions: $Q_G = 4 \text{ L min}^{-1}$; $C_{O_3, \text{in}} = 5.4 \text{ mg L}^{-1}$; $\text{pH} = 7.0$; $T = 18.0 \text{ }^\circ\text{C}$; $P = 1 \text{ atm}$; $V_{\text{reac}} = 1.5 \text{ L}$; (*Agitation*) = 60 rpm.

Orge et al. [22] have highlighted oxalic and oxamic acid among the reaction products of aniline with the highest resistance to degradation. Figure 6 shows the results obtained from the identification of aniline, oxamic acid, and oxalic acid at the initial time, after decomposition of the aniline (≈ 5 min), and after a sufficiently long reaction time. Figure 6d shows the chromatogram obtained at zero time (peak 1) with a retention time of 8.21 min, which was assigned to aniline. After the catalytic ozonation reaction had progressed for 5 min, the peak of the aniline (1) decreased but others appeared, which persisted until sufficiently long reaction times (30–40 min). The mass spectra of the identified peaks are shown in Figure 6a–c. These peaks were assigned to oxalic (2, 1.80 min) and oxamic acid (3, 2.65 min), corresponding to two degradation intermediates formed during the ozonation of the ozone aniline [59].

Oxalic acid under conditions of low hydroxyl radical generation as well as its conjugate base are stable degradation intermediates for a wide variety of organic contaminants, such as pesticides. The accumulation of this refractory compound in the reaction system is due to its very low oxidation constant ($k < 0.04 \text{ M}^{-1} \text{ s}^{-1}$ at pH values above 5.0), compared to that of other aniline oxidation products such as hydroquinone ($k = 2.3 \times 10^6 \text{ M}^{-1} \text{ s}^{-1}$ at $\text{pH} = 7.0$) [33,60]. On the other hand, oxamic acid is another compound present in the degradation of aniline that, under poor oxidation conditions, shows high refractoriness to ozonation [61].

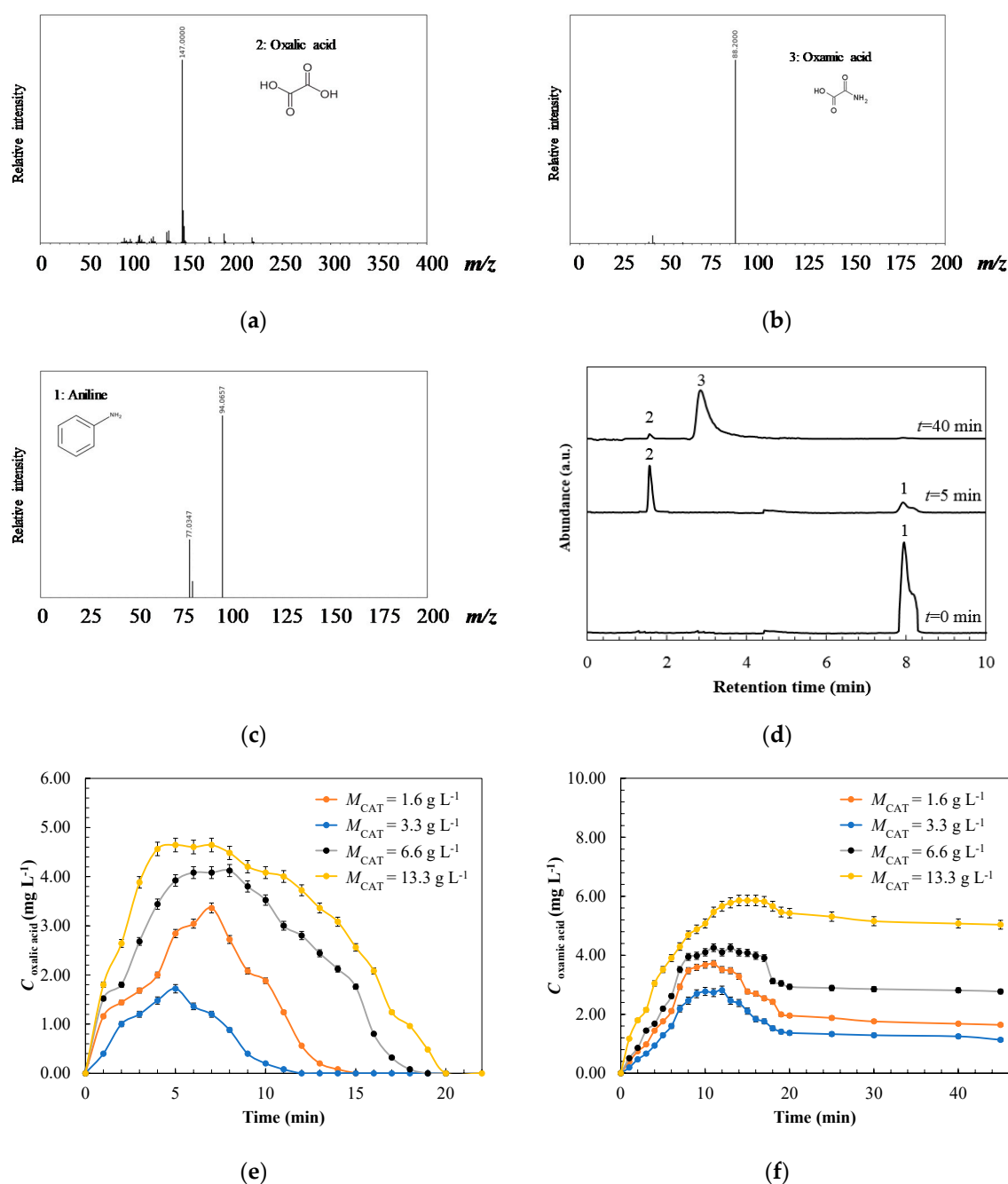


Figure 6. Analysis of some by-products formed during the TiO₂/GAC ozonation of aniline: (a–c) mass spectrometry (MS) of the aniline at different ozonation times, (d) liquid chromatography (LC) of the aniline and representative ozonation by-products, and (e,f) effect of catalyst dosage on the evolution of oxalic and oxamic acid during ozonation. Experimental conditions: $Q_G = 4 \text{ L min}^{-1}$; $C_{O_3, \text{in}} = 5.4 \text{ mg L}^{-1}$; $\text{pH} = 7.0$; $T = 18.0 \text{ }^\circ\text{C}$; $P = 1 \text{ atm}$; $V_{\text{reac}} = 1.5 \text{ L}$; $(\text{Agitation}) = 60 \text{ rpm}$.

Figure 6e,f show the evolution of the concentration of oxamic and oxalic acid for different doses of catalyst. For both acids and for all doses of catalyst studied, a continuous increase corresponding to the accumulation phenomenon was observed during the first 5 min. Then, coinciding with the primary degradation of the aniline (Figure 3e), a maximum was reached, which was higher with an increased catalyst dose. The increase in turbidity observed in Figure 5 at any catalyst dose studied is coincident with that of both acids. The relationship between oxalic acid and turbidity is evident, as well as the amount associated with the mechanism change from modified ER to LH. A Langmuir–Hinshelwood

(LH) type oxidative mechanism was dominant, with high amounts of TiO_2/GAC (6.6 or 13.3 g L^{-1}), promoting oxidation products such as oxalic acid [22]. Concerning the evolution of oxamic acid, the initial accumulation was slower, reaching its maximum 7 min later than that observed for oxalic acid. Unlike oxalic acid, oxamic acid could not be removed, explaining the flat tailing observed in the TOC profiles in Figure 3f. In these cases, the hypothesis of a dominant reactive mechanism of type LH at the surface with very low reaction rate (k_{oxS}) seems evident. This situation also led to the high occupation of active centres with a decrease in the radical concentration in the liquid and subsequent decrease in k_{oxL} . Authors such as Faria et al. [61] have reported a similar result during the removal of oxalic and oxamic acid via catalytic ozonation using active carbon. Furthermore, it has been reported that, at neutral pH, oxamic acid is mainly present as a zwitterion ($^-\text{OOC}-\text{CONH}^{3+}$), which is highly hydrophilic and stable in water. The C–H bonds explain its low reactivity towards hydroxyl radicals, and although it is possible to mineralize it completely (according to Legube and Leitner [14]), it requires a hydroxyl radical concentration approximately 100 times higher than that needed for other organic compounds with the same functional group. Thus, the persistence of oxamic acid in the liquid phase can explain the observed turbidity increase.

Due to the catalytic ozonation process in which the aniline was degraded, some degradation intermediates were formed. Using liquid chromatography (LC), higher concentration degradation products, such as nitrobenzene, phenol, catechol, o-benzoquinone, 1,2,3-benzenetriol, p-benzoquinone, and muconic acid, were detected excluding oxamic and oxalic acid. Other organic compounds, which were detected at lower concentrations, could not be identified. In this section, only the first intermediates (C_6) are included, in an attempt to determine the beginning of the first degradation routes. Many of these degradation products showed up in the solution within the first 5 min, through the change from a non-coloured solution to another with reddish, brown, and yellow colouring [6,62,63]. In Figure 7, three cases with the same mass of TiO_2/GAC (3.3 g L^{-1}) were selected, representative of the different experimental conditions studied. Among them, an adverse situation was selected with a low generation of hydroxyl radicals at $\text{pH} = 3.0$, as well as another with an excess of oxidant of 20.1 mg L^{-1} —which was ineffective due to the low mineralization achieved—and, finally, with the favourable conditions indicated in the previous section. For additional information, Figures S3 and S4 show the concentrations of each intermediate in terms of TOC. In Figure S4c, it can be observed that the amount of unknown TOC after 5 min of reaction was 5.9 mg L^{-1} .

According to Figure 7, the two possible degradation routes can be differentiated, according to the involvement of the direct and radical ozone pathways. In addition, it was observed that the rupture of the aniline molecule occurred in the bond between the benzene ring and the amino group ($-\text{NH}_2$). Other authors, such as Villota et al. [64] and Von Sonntag and Von Gunten [33], have also observed this same rupture.

In Figure 7a, it can be observed that the direct attack of ozone could be responsible for the high selectivity towards the formation of dihydroxy aromatic rings, such as catechol or 1,2,4-benzenetriol, through ortho-, meta-, and para-substituted oxidation pathways and electrophilic substitutions [65]. However, the carboxylic acids or muconic acid detected later (after about 10 min of reaction) were more refractory to direct ozone attack, which explains the 40% mineralization observed after a reaction time of 20 min [66].

However, the results in Figure 7b show a different behaviour, in which the aniline was degraded by another mechanism—attributed to the radical pathway. In this case, we note the presence of nitrobenzene. According to Brillas et al. and Tolosana-Moranchel et al. [67,68], the presence of nitrobenzene could be due to the high selectivity of the hydroperoxyl radical, compared with the hydroxyl radical, to the amino group, which strongly favours its conversion to a nitro group. Despite the last point, considering the radical species generated from direct interaction with TiO_2/GAC , Sanchez et al. [69] suggested that the hydroxyl radical is responsible for abstracting hydrogen from the amino group and then substituting it with an iminium radical, thus generating nitrobenzene. The generation of nitrobenzene could explain the low reactivity and inefficiency observed when using

a high dose of ozone. With respect to the presence of phenol or p-benzoquinone, Commninellis and Pulgarin [70] attributed it to hydroxylation reactions of these benzene structures with hydroxyl groups.

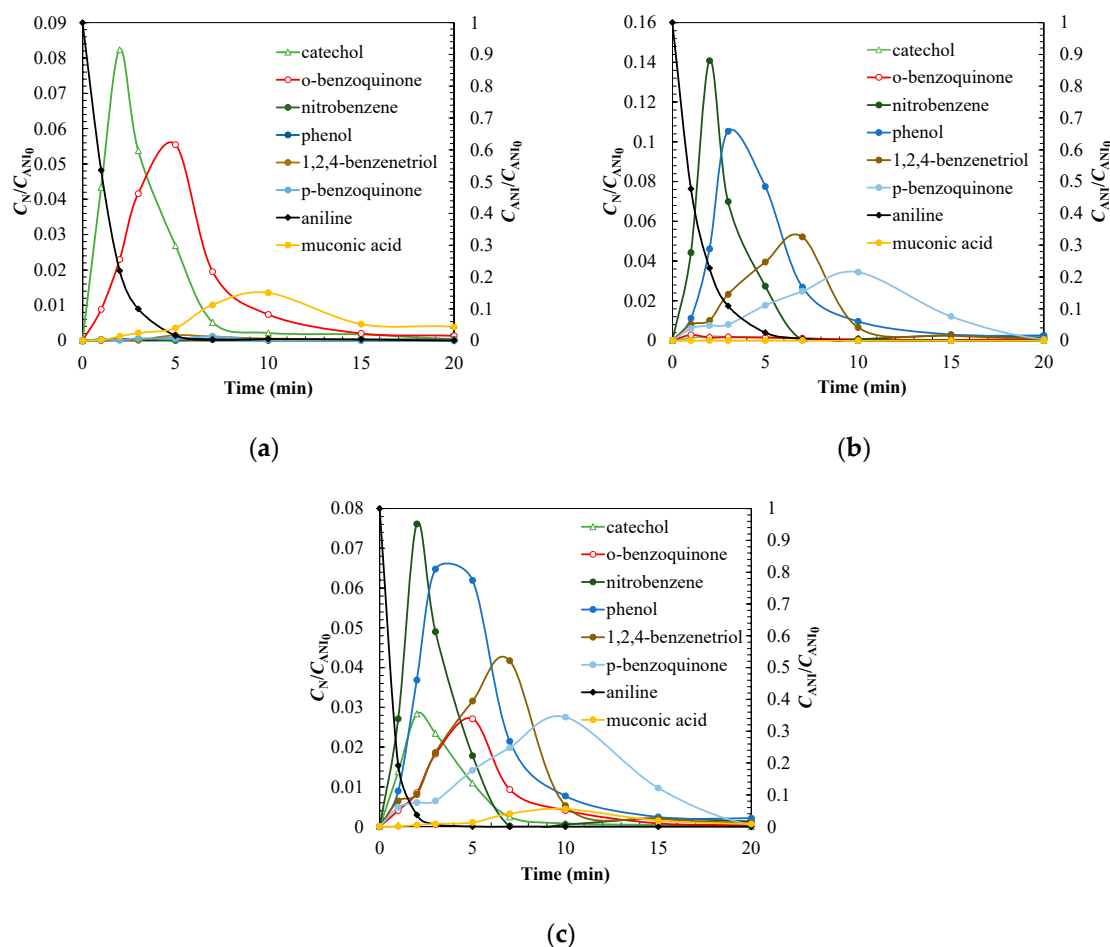


Figure 7. Analysis of the main intermediates in the aniline catalytic ozonation with TiO₂/GAC excluding oxalic and oxamic acid in different cases: (a) molecular attack of ozone at pH = 3.0, (b) ozone in excess and dominance of radicalary attack (pH = 7.0 and ozone dose of 20.1 mg L⁻¹), and (c) most favourable conditions (pH = 7.0, 5.4 mg L⁻¹ ozone concentration) or combined molecular radicalary attack. Experimental conditions: $Q_G = 4 \text{ L min}^{-1}$; $M_{CAT} = 3.3 \text{ g L}^{-1}$; $T = 18.0 \text{ }^\circ\text{C}$; $P = 1 \text{ atm}$; $V_{\text{reac}} = 1.5 \text{ L}$; (Agitation) = 60 rpm.

In Figure 7c, an overlap of both radical and molecular pathways can be observed, which is consistent with the kinetic parameters obtained from the Ad/Ox model, where an equilibrium situation was observed between oxidation in the liquid and on the surface of the solid through adsorption. The results obtained in the analyses carried out allow us to propose the mechanism of aniline degradation shown in Figure 8.

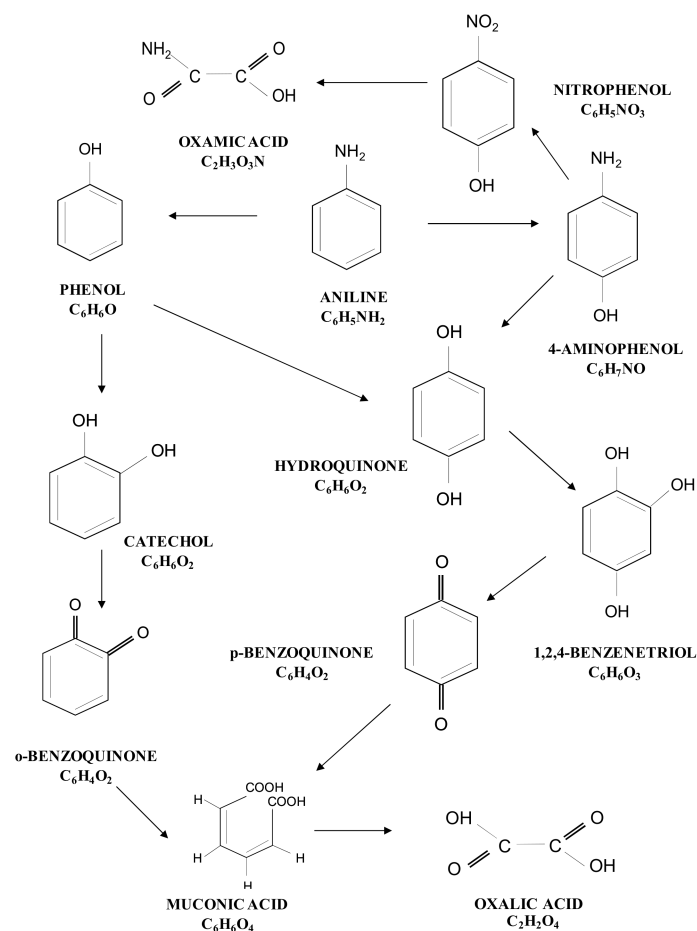


Figure 8. Oxidation pathway proposed for aniline oxidation via catalytic ozonation with TiO₂/GAC composites.

4. Conclusions

A three-phase mathematical model reaction (Ad/Ox) was proposed that describes the stages of G–L transfer, adsorption, and oxidation in the liquid and on the surface of the catalyst, in order to study catalytic ozonation using TiO₂/GAC composites. The model was verified using experimental aniline ozonation results. Despite the wide variety of conditions studied, the model provided a good fit to the experimental data, obtaining a weighted standard deviation lower than 0.05 in all cases. The model has been applied to evaluate the effect of the main operational variables on the G–L mass transfer. The analysis resulted in $K_L a$ values of 0.18 min⁻¹ at neutral pH, with no significance of other process conditions and no effect on the overall process rate (chemical reaction control).

Catalytic oxidation using commercial activated carbons, such as Norit® GAC 1240 Plus, was proved to occur through a Langmuir–Hinshelwood mechanism with preferential oxidation in the liquid phase. With the TiO₂/GAC composite, the estimated oxidation constants—in the liquid and in the solid—suggest a modified Eley–Rideal type mechanism, obtaining 80.2% mineralization in the most favourable conditions. Estimation of the oxidation constants allowed us to deduce that ozone acts mainly in the liquid at acidic pH, whereas under basic pH values, oxidation happens either on the solid or in the liquid. The use of high doses of ozone limits the kinetics and adsorption capacity of aniline and its degradation oxidation products, with oxidation in the liquid being the principal route of degradation. On the other hand, at moderate ozone doses, a greater role of the adsorption and oxidation mechanisms of the TiO₂ deposited in the GAC was observed. An excess in the catalyst load was ineffective and led to an increase in turbidity by inducing degradation pathways that ended with oxidation products such as oxalic acid and, especially, oxamic acid. Finally, the model allowed us

to analyse the significance of the different stages involved in the catalytic ozonation. Additionally, the most favourable operating conditions for the potentiation of the TiO₂ deposited on the GAC were found (pH = 7.0, 5.4 mg L⁻¹ ozone dose, and 3.3 g L⁻¹ catalyst load). TiO₂ contributed to a greater capacity of the material to adsorb the pollutant and subsequent predisposition to be attacked by the ozone through the hydroxyl radicals generated on its surface. From the identification and analysis of the degradation intermediates, two possible routes—which occur simultaneously under the most favourable conditions mentioned above—were proposed. This model could be applied at an industrial level with new catalysts for the prediction of operating behaviour under different working conditions.

Supplementary Materials: The following are available online at <http://www.mdpi.com/2073-4441/12/12/3448/s1>, Figure S1: Utilization efficiencies of ozone in a TiO₂/GAC catalytic system at different pHs, Figure S2: Effect of the ozone dose on the control stage during catalytic ozonation of aniline with the TiO₂/GAC catalyst, Figure S3: Analysis of some by-products formed during the TiO₂/GAC ozonation of aniline in terms of TOC, Figure S4: Analysis of the main intermediates in the aniline catalytic ozonation with TiO₂/GAC in terms of TOC, excluding oxalic and oxamic acid in different cases.

Author Contributions: J.I.L. and C.F. performed the conceptualization; M.J.R. and J.I.L. carried out the design of the methodology and analyses; C.F. and N.V. contributed to the model validation; C.F. carried out the formal analysis; C.F. performed the investigation; C.F. and J.I.L. prepared the original draft; M.J.R., C.F. and N.V. reviewed and edited the manuscript; J.I.L. and M.J.R. supervised the experimentation; M.J.R., N.V., and J.I.L. acquired the funding. All authors have read and agreed to the published version of the manuscript.

Funding: The authors are grateful to the University of the Basque Country for their financial support of this study through the PPGA19/63 project and C. Ferreiro's predoctoral PIF grant (PIF16/367).

Acknowledgments: The authors are thankful for the technical and human support provided by The Singular Coupled Multispectroscopy Laboratory (Raman-LASPEA) and Central Analysis Service (Araba Unit), part of the General Research Services (SGIker) of the UPV/EHU, and Cabot Corporation for supplying the sample of activated carbon used in this work.

Conflicts of Interest: The authors declare no conflict of interest.

Nomenclature

σ	Weighted standard deviation
$C_{O_3,L}^*$	Concentration of ozone in the equilibrium with the ozone adsorbed on the activated carbon, mg L ⁻¹
$C_{O_3,S}^*$	Concentration of ozone on the catalyst in equilibrium with the liquid ozone concentration, mg L ⁻¹
C_p^*	Calculate pollutant concentration in the liquid in terms of total organic carbon, mg L ⁻¹
C_N	Concentration degradation products, mg L ⁻¹
$C_{O_3,in}$	Concentrations of ozone in the gas phase at the inlet, mg L ⁻¹
$C_{O_3,L}$	Ozone concentration in liquid, mg L ⁻¹
$C_{O_3,out}$	Concentration of ozone in the gas phase at the outlet, mg L ⁻¹
C_{OH^-}	Concentration of hydroxyl ions, mol L ⁻¹
C_p	Pollutant concentration in the liquid in terms of total organic carbon, mg L ⁻¹
He	Henry's constant, bar L mg ⁻¹
k_{ads}	Kinetic constant of aniline adsorption, g mg ⁻¹ min ⁻¹
$k_{c,L}$	Elemental kinetic constant for the ozonation in the liquid, L mg ⁻¹ min ⁻¹
$k_{c,S}$	Elemental kinetic constant for the ozonation in the solid, L mg ⁻¹ min ⁻¹
K_F	Freundlich constant, (mg g ⁻¹) (L mg ⁻¹) ^{1/n_F}
K_{Ga}	Overall mass transfer coefficient of ozone gas to water, min ⁻¹
K_{La}	Volumetric ozone mass transfer coefficient, min ⁻¹
k_{oxL}	Apparent first-order kinetic constant in the liquid in terms of TOC, min ⁻¹
k_{oxS}	Apparent first-order kinetic constant over the catalyst in terms of TOC, min ⁻¹
m	Slope of the equilibrium line between the liquid and solid phase
M_{CAT}	Concentration of catalyst, g L ⁻¹
n	Heterogeneity factor, dimensionless
N	Number of experimental values
$N_{O_3}^{II}$	Ozone consumption in the solid, mg L ⁻¹ min ⁻¹
$N_{O_3}^I$	Ozone consumption in the liquid, mg L ⁻¹ min ⁻¹

N_{O_3}	Whole ozone consumption, $\text{mg L}^{-1} \text{min}^{-1}$
$P_{O_3}^*$	Partial pressure of the ozone in equilibrium with the adsorbed ozone on the solid, bar
P_{O_3}	Partial pressure of ozone in the gas phase, bar
Q_G	Ozone gas flow, L min^{-1}
r_p^{II}	Degradation of the pollutant on the activated carbon, $\text{mg L}^{-1} \text{min}^{-1}$
r_p^{I}	Degradation of the pollutant in the liquid, $\text{mg L}^{-1} \text{min}^{-1}$
T	Temperature, K
t	Time, min
U_{O_3}	Utilization coefficient, %
V_{reac}	Volume of dissolution, L
z^{I}	Amount of pollutant consumed in the liquid, $\text{mg TOC mg}^{-1} O_3$
z^{II}	Amount of pollutant consumed on the catalyst, $\text{mg TOC mg}^{-1} O_3$
Z_p	Concentration of pollutant in the solid, mg g^{-1}
$Z_{p,\infty}$	Amount of pollutant adsorbed in the solid in equilibrium, mg g^{-1}

References

1. United Nations. About the Sustainable Development Goals. Available online: <https://www.un.org/sustainabledevelopment/sustainable-development-goals/> (accessed on 27 November 2020).
2. Zouboulis, A.I.; Katsoyiannis, I.A. Recent Advances in Water and Wastewater Treatment with Emphasis in Membrane Treatment Operations. *Water* **2019**, *11*, 45. [CrossRef]
3. Anotai, J.; Jevprasesphant, A.; Lin, Y.-M.; Lu, M.-C. Oxidation of aniline by titanium dioxide activated with visible light. *Sep. Purif. Technol.* **2012**, *84*, 132–137. [CrossRef]
4. Ferreiro, C.; Villota, N.; Lombraña, J.I.; Rivero, M.J. An efficient catalytic process for the treatment of genotoxic aniline wastewater using a new granular activated carbon-supported titanium dioxide composite. *J. Clean. Prod.* **2019**, *228*, 1282–1295. [CrossRef]
5. Ferreiro, C.; Villota, N.; Lombraña, J.I.; Rivero, M.J.; Zúñiga, V.; Rituerto, J.M. Analysis of a Hybrid Suspended-Supported Photocatalytic Reactor for the Treatment of Wastewater Containing Benzothiazole and Aniline. *Water* **2019**, *11*, 337. [CrossRef]
6. Jing, Z.; Cao, S.; Yu, T.; Hu, J. Degradation Characteristics of Aniline with Ozonation and Subsequent Treatment Analysis. *J. Chem.* **2015**, 905921. [CrossRef]
7. European Commission. *European Union Risk Assessment Report aniline*; Office for Official Publications of the European Communities: Luxembourg, 2004; Volume 50.
8. Tao, N.; Liu, G.; Bai, L.; Tang, L.; Guo, C. Genotoxicity and growth inhibition effects of aniline on wheat. *Chemosphere* **2017**, *169*, 467–473. [CrossRef]
9. United State Environmental Protection Agency. Contaminant Candidate List 4-CCL 4. Available online: <https://www.epa.gov/ccl/contaminant-candidate-list-4-ccl-4-0> (accessed on 9 October 2020).
10. Álvarez, P.M.; Beltrán, F.J.; Masa, F.J.; Pocostales, J.P. A comparison between catalytic ozonation and activated carbon adsorption/ozone-regeneration processes for wastewater treatment. *Appl. Catal. B Environ.* **2009**, *92*, 393–400. [CrossRef]
11. Cheng, W.; Quan, X.; Li, R.; Wu, J.; Zhao, Q. Ozonation of Phenol-Containing Wastewater Using $O_3/Ca(OH)_2$ System in a Micro Bubble Gas-Liquid Reactor. *Ozone-Sci. Eng.* **2018**, *40*, 173–182. [CrossRef]
12. Rodríguez, A.; Rosal, R.; Perdígón-Melón, J.A.; Mezcuca, M.; Agüera, A.; Hernando, M.D.; Letón, P.; Fernández-Alba, A.R.; García-Calvo, E. Ozone-Based Technologies in Water and Wastewater Treatment. In *Emerging Contaminants from Industrial and Municipal Waste. Removal Technologies*; Barceló, D., Petrovic, M., Eds.; Springer-Verlag: Heidelberg, Germany, 2008; Volume 5S/2, pp. 127–175. ISBN 978-3-540-79209-3.
13. Guo, Y.; Yang, L.; Wang, X. The Application and Reaction Mechanism of Catalytic Ozonation in Water Treatment. *J. Environ. Anal. Toxicol.* **2012**, *2*. [CrossRef]
14. Legube, B.; Karpel Vel Leitner, N. Catalytic ozonation: A promising advanced oxidation technology for water treatment. *Catal. Today* **1999**, *53*, 61–72. [CrossRef]
15. Delmas, H.; Creanga, C.; Julcour-Lebigue, C.; Wilhelm, A.-M. AD-OX: A sequential oxidative process for water treatment-Adsorption and batch CWAO regeneration of activated carbon. *Chem. Eng. J.* **2009**, *152*, 189–194. [CrossRef]

16. Erol, F.; Ozbelge, T.A.; Ozbelge, H.O. Modeling of catalytic ozonation process in a three-phase reactor. *J. Environ. Sci. Health A Tox. Hazard Subst. Environ. Eng.* **2009**, *44*, 295–306. [[CrossRef](#)] [[PubMed](#)]
17. Cheng, J.; Yang, Z.R.; Chen, H.Q.; Kuo, C.H.; Zappi, E.M. Modeling of organic pollutant destruction in a stirred-tank reactor by ozonation. *J. Environ. Sci. (China)* **2001**, *13*, 449–452.
18. Guelli Ulson de Souza, S.M.d.A.; de Souza, F.B.; Ulson de Souza, A.A. Application of Individual and Simultaneous Ozonation and Adsorption Processes in Batch and Fixed-Bed Reactors for Phenol Removal. *Ozone-Sci. Eng.* **2012**, *34*, 259–268. [[CrossRef](#)]
19. Ferreira, C.; Villota, N.; de Luis, A.; Lombrana, J.I. Analysis of the effect of the operational variants in a combined adsorption-ozonation process with granular activated carbon for the treatment of phenol wastewater. *React. Chem. Eng.* **2020**, *5*, 760–778. [[CrossRef](#)]
20. Song, S.; He, Z.; Chen, J. US/O₃ combination degradation of aniline in aqueous solution. *Ultrason. Sonochem.* **2007**, *14*, 84–88. [[CrossRef](#)]
21. Faria, P.C.C.; Orfao, J.J.M.; Pereira, M.F.R. Ozonation of aniline promoted by activated carbon. *Chemosphere* **2007**, *67*, 809–815. [[CrossRef](#)]
22. Orge, C.A.; Faria, J.L.; Pereira, M.F.R. Photocatalytic ozonation of aniline with TiO₂-carbon composite materials. *J. Environ. Manag.* **2017**, *195*, 208–215. [[CrossRef](#)]
23. Rodriguez, C.; Ignacio Lombrana, J.; de Luis, A.; Sanz, J. Oxidizing efficiency analysis of an ozonation process to degrade the dye rhodamine 6G. *J. Chem. Technol. Biotechnol.* **2017**, *92*, 656–665. [[CrossRef](#)]
24. Byun, S.; Cho, S.H.; Yoon, J.; Geissen, S.U.; Vogelpohl, A.; Kim, S.M. Influence of mass transfer on the ozonation of wastewater from the glass fiber industry. *Water Sci. Technol.* **2004**, *49*, 31–36. [[CrossRef](#)]
25. Christopher, R.; Schulz, P.E.; Paul, W. Prendiville P.E. Designing High Concentration Ozone Contactors for Drinking Water Treatment Plants. *Ozone Sci. Eng.* **1993**, *15*, 245–266. [[CrossRef](#)]
26. Roth, J.; Sullivan, D. Solubility of Ozone in Water. *Ind. Eng. Chem. Fundam.* **1981**, *20*, 137–140. [[CrossRef](#)]
27. Egorova, G.V.; Voblikova, V.A.; Sabitova, L.V.; Tkachenko, I.S.; Tkachenko, S.N.; Lunin, V.V. Ozone Solubility in Water. *Moscow Univ. Chem. Bull.* **2015**, *70*, 207–210. [[CrossRef](#)]
28. Beltran, F.J. *Ozone Reaction Kinetics for Water and Wastewater Systems*; CRC Press: Boca Raton, FL, USA, 2003; ISBN 978-0-203-50917-3.
29. Cacace, F.; Speranza, M. Protonated Ozone: Experimental Detection of O₃H⁺ and Evaluation of the Proton Affinity of Ozone. *Science* **1994**, *265*, 208–209. [[CrossRef](#)] [[PubMed](#)]
30. Flores-Payán, V.; Herrera-López, E.J.; Navarro-Laboulais, J.; López-López, A. Parametric sensitivity analysis and ozone mass transfer modeling in a gas-liquid reactor for advanced water treatment. *J. Ind. Eng. Chem.* **2015**, *21*, 1270–1276. [[CrossRef](#)]
31. Ratnawati, R.; Kusumaningtyas, D.; Suseno, P.; Prasetyaningrum, A. Mass Transfer Coefficient of Ozone in a Bubble Column. *MATEC Web Conf.* **2018**, *156*, 02015. [[CrossRef](#)]
32. Berry, M.J.; Taylor, C.M.; King, W.; Chew, Y.M.J.; Wenk, J. Modelling of Ozone Mass-Transfer through Non-Porous Membranes for Water Treatment. *Water* **2017**, *9*, 452. [[CrossRef](#)]
33. VonSonntag, C.; VonGunten, U. *Chemistry of Ozone in Water and Wastewater Treatment: From Basic Principles to Applications*; Iwa Publishing: London, UK, 2012; ISBN 978-1-84339-313-9.
34. Masel, R.I. *Principles of Adsorption and Reaction on Solid Surfaces*, 1st ed.; Wiley: Oak Brook, IL, USA, 1996.
35. De Luis, A.; Lombraña, J.I. pH-Based Strategies for an Efficient Addition of H₂O₂ During Ozonation to Improve the Mineralisation of Two Contaminants with Different Degradation Resistances. *Water Air Soil Pollut.* **2018**, *229*, 372. [[CrossRef](#)]
36. Wang, B.; Zhang, H.; Wang, F.; Xiong, X.; Tian, K.; Sun, Y.; Yu, T. Application of Heterogeneous Catalytic Ozonation for Refractory Organics in Wastewater. *Catalysts* **2019**, *9*, 241. [[CrossRef](#)]
37. Zheng, X.; Yu, N.; Wang, X.; Wang, Y.; Wang, L.; Li, X.; Hu, X. Adsorption Properties of Granular Activated Carbon-Supported Titanium Dioxide Particles for Dyes and Copper Ions. *Sci. Rep.* **2018**, *8*, 6463. [[CrossRef](#)]
38. Kasprzyk-Hordern, B.; Ziótek, M.; Nawrocki, J. Catalytic ozonation and methods of enhancing molecular ozone reactions in water treatment. *Appl. Catal. B Environ.* **2003**, *46*, 639–669. [[CrossRef](#)]
39. Valdes, H.; Sanchez-Polo, M.; Rivera-Utrilla, J.; Zaror, C.A. Effect of ozone treatment on surface properties of activated carbon. *Langmuir* **2002**, *18*, 2111–2116. [[CrossRef](#)]
40. Ghuge, S.P.; Saroha, A.K. Catalytic ozonation for the treatment of synthetic and industrial effluents—Application of mesoporous materials: A review. *J. Environ. Manag.* **2018**, *211*, 83–102. [[CrossRef](#)] [[PubMed](#)]

41. Moussavi, G.; Khavanin, A.; Alizadeh, R. The investigation of catalytic ozonation and integrated catalytic ozonation/biological processes for the removal of phenol from saline wastewaters. *J. Hazard. Mater.* **2009**, *171*, 175–181. [[CrossRef](#)] [[PubMed](#)]
42. Sanchez, M.; Rivero, M.J.; Ortiz, I. Kinetics of dodecylbenzenesulphonate mineralisation by TiO₂ photocatalysis. *Appl. Catal. B Environ.* **2011**, *101*, 515–521. [[CrossRef](#)]
43. MiarAlipour, S.; Friedmann, D.; Scott, J.; Amal, R. TiO₂/porous adsorbents: Recent advances and novel applications. *J. Hazard. Mater.* **2018**, *341*, 404–423. [[CrossRef](#)] [[PubMed](#)]
44. Beltran, F.J.; Rivas, F.J.; Montero-de-Espinosa, R. A TiO₂/Al₂O₃ catalyst to improve the ozonation of oxalic acid in water. *Appl. Catal. B-Environ.* **2004**, *47*, 101–109. [[CrossRef](#)]
45. Vega, E.; Valdes, H. New evidence of the effect of the chemical structure of activated carbon on the activity to promote radical generation in an advanced oxidation process using hydrogen peroxide. *Microporous Mesoporous Mat.* **2018**, *259*, 1–8. [[CrossRef](#)]
46. Orge, C.A.; Sousa, J.P.S.; Gonçalves, F.; Freire, C.; Órfão, J.J.M.; Pereira, M.F.R. Development of Novel Mesoporous Carbon Materials for the Catalytic Ozonation of Organic Pollutants. *Catal. Lett.* **2009**, *132*, 1–9. [[CrossRef](#)]
47. Turhan, K.; Uzman, S. The degradation products of aniline in the solutions with ozone and kinetic investigations. *Ann. Chim.* **2007**, *97*, 1129–1138. [[CrossRef](#)]
48. Shahamat, Y.D.; Farzadkia, M.; Nasseri, S.; Mahvi, A.H.; Gholami, M.; Esrafil, A. Magnetic heterogeneous catalytic ozonation: A new removal method for phenol in industrial wastewater. *J. Environ. Health Sci. Eng.* **2014**, *12*, 50. [[CrossRef](#)] [[PubMed](#)]
49. Boczkaj, G.; Fernandes, A. Wastewater treatment by means of advanced oxidation processes at basic pH conditions: A review. *Chem. Eng. J.* **2017**, *320*, 608–633. [[CrossRef](#)]
50. Roshani, B.; McMaster, I.; Rezaei, E.; Soltan, J. Catalytic ozonation of benzotriazole over alumina supported transition metal oxide catalysts in water. *Sep. Purif. Technol.* **2014**, *135*, 158–164. [[CrossRef](#)]
51. Nawrocki, J.; Kasprzyk-Hordern, B. The efficiency and mechanisms of catalytic ozonation. *Appl. Catalysis B Environ.* **2010**, *99*, 27–42. [[CrossRef](#)]
52. Tamura, H.; Mita, K.; Tanaka, A.; Ito, M. Mechanism of Hydroxylation of Metal Oxide Surfaces. *J. Colloid Interface Sci.* **2001**, *243*, 202–207. [[CrossRef](#)]
53. Valdés, H.; Sánchez-Polo, M.; Zaror, C.A. Role of oxygen-containing functional surface groups of activated carbons on the elimination of 2-hydroxybenzothiazole from waters in A hybrid heterogeneous ozonation system. *J. Adv. Oxid. Technol.* **2017**, *20*. [[CrossRef](#)]
54. Orha, C.; Pode, R.; Manea, F.; Lazau, C.; Bandas, C. Titanium dioxide-modified activated carbon for advanced drinking water treatment. *Process Saf. Environ. Protect.* **2017**, *108*, 26–33. [[CrossRef](#)]
55. Beltrán, F.J.; Rivas, J.; Álvarez, P.; Montero-de-Espinosa, R. Kinetics of Heterogeneous Catalytic Ozone Decomposition in Water on an Activated Carbon. *Ozone Sci. Eng.* **2002**, *24*, 227–237. [[CrossRef](#)]
56. Leyva, E.; Moctezuma, E.; Noriega, S. Photocatalytic degradation of omeprazole. Intermediates and total reaction mechanism. *J. Chem. Technol. Biotechnol.* **2017**, *92*, 1511–1520. [[CrossRef](#)]
57. Bulanin, K.M.; Lavalley, J.C.; Tsyganenko, A.A. Infrared Study of Ozone Adsorption on TiO₂ (Anatase). *J. Phys. Chem.* **1995**, *99*, 10294–10298. [[CrossRef](#)]
58. Bodzek, M.; Rajca, M. Photocatalysis in the treatment and disinfection of water. Part I. Theoretical backgrounds. *Ecol. Chem. Eng. S* **2012**, *19*, 489–512. [[CrossRef](#)]
59. Orge, C.A.; Faria, J.L.; Pereira, M.F.R. Removal of oxalic acid, oxamic acid and aniline by a combined photolysis and ozonation process. *Environ. Technol.* **2015**, *36*, 1075–1083. [[CrossRef](#)] [[PubMed](#)]
60. Zazo, J.A.; Casas, J.A.; Mohedano, A.F.; Gilarranz, M.A.; Rodríguez, J.J. Chemical Pathway and Kinetics of Phenol Oxidation by Fenton's Reagent. *Environ. Sci. Technol.* **2005**, *39*, 9295–9302. [[CrossRef](#)] [[PubMed](#)]
61. Faria, P.C.C.; Órfão, J.J.M.; Pereira, M.F.R. Activated carbon catalytic ozonation of oxamic and oxalic acids. *Appl. Catal. B Environ.* **2008**, *79*, 237–243. [[CrossRef](#)]
62. Villota, N.; Lombraña, J.I.; Cruz-Alcalde, A.; Marcé, M.; Esplugas, S. Kinetic study of colored species formation during paracetamol removal from water in a semicontinuous ozonation contactor. *Sci. Total Environ.* **2019**, *649*, 1434–1442. [[CrossRef](#)] [[PubMed](#)]
63. Mijangos, F.; Varona, F.; Villota, N. Changes in Solution Color During Phenol Oxidation by Fenton Reagent. *Environ. Sci. Technol.* **2006**, *40*, 5538–5543. [[CrossRef](#)] [[PubMed](#)]

64. Villota, N.; Lomas, J.M.; Camarero, L.M. Study of the paracetamol degradation pathway that generates color and turbidity in oxidized wastewaters by photo-Fenton technology. *J. Photochem. Photobiol. A Chem.* **2016**, *329*, 113–119. [[CrossRef](#)]
65. Rasalingam, S.; Kibombo, H.S.; Wu, C.-M.; Peng, R.; Baltrusaitis, J.; Koodali, R.T. Competitive role of structural properties of titania–silica mixed oxides and a mechanistic study of the photocatalytic degradation of phenol. *Appl. Catal. B Environ.* **2014**, *148–149*, 394–405. [[CrossRef](#)]
66. Anpo, M.; Kamat, P.V. (Eds.) *Environmentally Benign Photocatalysts: Applications of Titanium Oxide-based Materials; Nanostructure Science and Technology*; Springer: New York, NY, USA, 2010; ISBN 978-0-387-48441-9.
67. Brillas, E.; Bastida, R.M.; Llosa, E.; Casado, J. Electrochemical Destruction of Aniline and 4-Chloroaniline for Wastewater Treatment Using a Carbon-PTFE O₂—Fed Cathode. *J. Electrochem. Soc.* **1995**, *142*, 1733. [[CrossRef](#)]
68. Tolosana-Moranchel, A.; Montejano, A.; Casas, J.A.; Bahamonde, A. Elucidation of the photocatalytic-mechanism of phenolic compounds. *J. Environ. Chem. Eng.* **2018**, *6*, 5712–5719. [[CrossRef](#)]
69. Sánchez, L.; Peral, J.; Domènech, X. Photocatalyzed destruction of aniline in UV-illuminated aqueous TiO₂ suspensions. *Electrochim. Acta* **1997**, *42*, 1877–1882. [[CrossRef](#)]
70. Comninellis, C.; Pulgarin, C. Anodic oxidation of phenol for waste water treatment. *J. Appl. Electrochem.* **1991**, *21*, 703–708. [[CrossRef](#)]

Publisher’s Note: MDPI stays neutral with regard to jurisdictional claims in published maps and institutional affiliations.

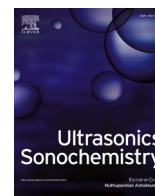


© 2020 by the authors. Licensee MDPI, Basel, Switzerland. This article is an open access article distributed under the terms and conditions of the Creative Commons Attribution (CC BY) license (<http://creativecommons.org/licenses/by/4.0/>).

3.10. 10. argitalpena. Analysis of ultrasonic pre-treatment for the ozonation of humic acids

3.10 kapitulua artikulu honi dagokio:

P. Alfonso-Muniozguren, C. Ferreiro, E. Richard, M. Bussemaker, J.I. Lombraña, J. Lee. Analysis of ultrasonic pre-treatment for the ozonation of humic acids. *Ultrasonics Sonochemistry*, 71, 105359, 2021. DOI: 10.1016/j.ultsonch.2020.105359.



Analysis of ultrasonic pre-treatment for the ozonation of humic acids

Pello Alfonso-Muniozguren^{a,b}, Cristian Ferreiro^b, Elodie Richard^{a,c}, Madeleine Bussemaker^a, José Ignacio Lombrana^{b,*}, Judy Lee^{a,*}

^a Chemical and Process Engineering, University of Surrey, Guildford GU27XH, United Kingdom

^b Department of Chemical Engineering, Faculty of Science and Technology, University of the Basque Country UPV/EHU, 48940 Leioa, Spain

^c Department of Chemistry, IUT Besançon-Vesoul, University of Franche-Comté, 25000 Besançon, France

ARTICLE INFO

Keywords:

Advanced oxidation processes
Fluorescence
Sonication
Water treatment
Humic substances

ABSTRACT

This paper presents an intensification study of an ozonation process through an ultrasonic pre-treatment for the elimination of humic substances in water and thus, improve the quality of water treatment systems for human consumption. Humic acids were used as representative of natural organic matter in real waters which present low biodegradability and a high potential for trihalomethane formation. Ultrasonic frequency (98 kHz, 300 kHz and 1 MHz), power (10–40 W) and sonicated volume (150–400 mL) was varied to assess the efficiency of the ultrasonic pre-treatment in the subsequent ozonation process. A direct link between hydroxyl radical (HO[•]) formation and fluorescence reduction was observed during sonication pre-treatment, peaking at 300 kHz and maximum power density. Ultrasound, however, did not reduce total organic carbon (TOC). Injected ozone (O₃) dose and reaction time were also evaluated during the ozonation treatment. With 300 kHz and 40 W ultrasonic pre-treatment and the subsequent ozonation step (7.4 mg O₃/L_{gas}), TOC was reduced from 21 mg/L to 13.5 mg/L (36% reduction). HO[•] attack seems to be the main degradation mechanism during ozonation. A strong reduction in colour (85%) and SUVA₂₅₄ (70%) was also measured. Moreover, changes in the chemical structure of the macromolecule were observed that led to the formation of oxidation by-products of lower molecular weight.

1. Introduction

Humic acids (HAs) are naturally occurring high molecular weight compounds easily found in natural water bodies. They are the main component of organic matter in natural waters and responsible for colour (yellow to black). These compounds are difficult to mineralise completely as HAs tend to be refractory and possess low biodegradability. Additionally, HAs can act as trihalomethane precursors [1]. The effects of ultrasonication on HAs have been studied in the literature, showing a potential for humic acid (HA) degradation (change in molecular structure), as well as an increase in biodegradability.

At low frequencies (20 kHz), changes in UV absorption of HA samples have been reported [2]. According to the authors, sonication could have induced alterations in the molecular structure of HAs. With an initial TOC concentration of 18.6 mg/L (equivalent to 50 mg HA/L) and 50 mg NaOCl/L, a TOC removal of 26.5% was reported after 120 min of treatment at 20 kHz [3]. Similar reactions have been measured at higher frequencies (200 kHz), e.g. a change in UV absorption and a reduction in the molecular weight of HAs [4]. Chen et al. [5] employed two different

ultrasonic reactors for the treatment of synthetic HA solutions (22.5 mg/L initial TOC): a 20 kHz horn and a 354 kHz transducer. 354 kHz reactor performed better in the reduction of TOC, achieving a TOC of 20.4 mg/L after 4 h of treatment. No TOC removal was observed with 20 kHz. The authors mentioned that even though TOC was not significantly reduced, the reduction in colour, as well as in SUVA₂₅₄ (specific ultraviolet absorbance at 254 nm where the aromatic nature of the solution is normalised over the total organic load [6]) would be translated into a change in molecular structure (destruction of aromatic rings, conjugated double bonds, etc.). Although different applied frequencies and power densities have been reported, variations in sonication equipment and reactor design makes it difficult to compare different studies to obtain a reliable conclusion on the best parameters for HA removal with ultrasound. Considering chemical and physical effects produced by ultrasound vary significantly depending on the applied frequency, power and sonication system [7–9], there is a need for a thorough study on the influence of these parameters on the degradation of HAs.

Ozone (O₃) has also been employed for the treatment of HAs. With an initial TOC concentration of 100 mg/L and an O₃ saturated solution at

* Corresponding authors.

E-mail addresses: ji.lombrana@ehu.eus (J.I. Lombrana), j.y.lee@surrey.ac.uk (J. Lee).

<https://doi.org/10.1016/j.ultsonch.2020.105359>

Received 3 June 2020; Received in revised form 19 September 2020; Accepted 2 October 2020

Available online 7 October 2020

1350-4177/© 2020 Elsevier B.V. This is an open access article under the CC BY-NC-ND license (<http://creativecommons.org/licenses/by-nc-nd/4.0/>).

0.46 mol/m³, TOC removal increased from 50% to 80% when treatment time was increased from 30 min to 5 h [10]. A complete mineralisation was difficult to reach considering refractory compounds were formed during ozonation. Besides TOC, O₃ can significantly reduce the molecular size distribution, colour₄₃₆ and UV₂₅₄ of HAs [11,12], as well as increase its biodegradability [11,13]. The authors, however, concluded that ozonation alone is insufficient to treat humic water [13].

The combination of O₃ and ultrasound to effectively treat HA has also been studied in the literature. Olson and Barbier [14] coupled ultrasound (20 kHz horn) and O₃ to treat a purified fulvic acid fraction of synthetic HA solution (10 mg/L initial TOC). Ultrasound alone had no effect on the absorbance of fulvic acid at 200 and 340 nm, whereas combined with O₃ the rate of decolouration (230 nm) increased. In regards to TOC, ultrasound alone did not mineralise carbon. When O₃ was applied and during the first 10 min of treatment, the same oxidation rate of TOC was observed between O₃ alone and the combined setup. Increasing treatment time in the coupled system induced a significant enhancement in TOC removal. According to the authors, pyrolysis mechanisms would explain the increase in O₃ decomposition rate due to ultrasound. Weavers et al. [15,16] stated that when O₃ is combined with ultrasound, an increase in O₃ mass transfer is observed due to the turbulence produced by acoustic streaming. Stepniak et al. [17] also used ultrasound and O₃ to treat synthetic HA solutions of 10, 15 and 20 mg HA/L. A 24 kHz ultrasonic horn with a maximum effective power of 300 W was used for sonication experiments. Two different configurations were employed when combining O₃ and ultrasound. In the first configuration, O₃ was first applied to the HA solution (3 mg O₃/L for 3 min) and sonicated later on in a subsequent step (10 min) reaching a TOC removal of 25.3%. The second configuration combined O₃ and ultrasound simultaneously for 10 min. The study reported no synergy when ultrasound and O₃ were applied simultaneously (second configuration), showing a slight increase in TOC removal to 28.8% with the coupled system. Chemical modification of aromatic structures of HAs were reported in the combined configurations. An increase in treatment time and increasing injected O₃ dose from 1 to 3 and 5 mg/L led to a higher removal of TOC for the coupled system.

Considering the above, the potential impact from the pre-treatment using ultrasound in a subsequent treatment process (i.e. ozonation) has not been investigated in the literature. Therefore, this research article presents a thorough study on the effect of an ultrasonic pre-treatment in a subsequent ozonation step for the treatment of HAs in waters intended for human consumption.

2. Materials and methods

2.1. Chemicals

HA (CASRN: 1415-93-6, Sigma-Aldrich, technical), sulfuric acid (H₂SO₄, Sigma-Aldrich, 98%), sodium hydroxide (NaOH, Panreac, 0.25 M), potassium iodide (KI, Panreac, 99%), sodium phosphate monobasic (H₂O₄PNa·H₂O, Fisher, 98%) and sodium phosphate dibasic heptahydrate (HNa₂O₄P·H₂O, Fisher, 99%) were used as received. Deionised water was supplied by a Milli-Q® water purification unit supplied by Merck.

2.2. Experimental procedure

HA sample preparation was carried out as follows: 100 mg HA were mixed with 2 L deionised water (50 mg HA/L) and dissolved by increasing the pH to 11 with 0.25 M NaOH. The dissolution was then stirred for 30 min at 400 rpm. Prior to sonication experiments, pH was reduced to 7 with 0.1 M H₂SO₄. Elemental analysis (CHONS), fluorescence, ¹³C NMR, FTIR and HPSEC spectrum of the employed HAs are shown in [supplementary information \(Fig. S1\)](#).

Sonication pre-treatment experiments (Fig. 1a) were carried out in a jacketed cylindrical glass vessel (15 cm height and 6.7 cm inner

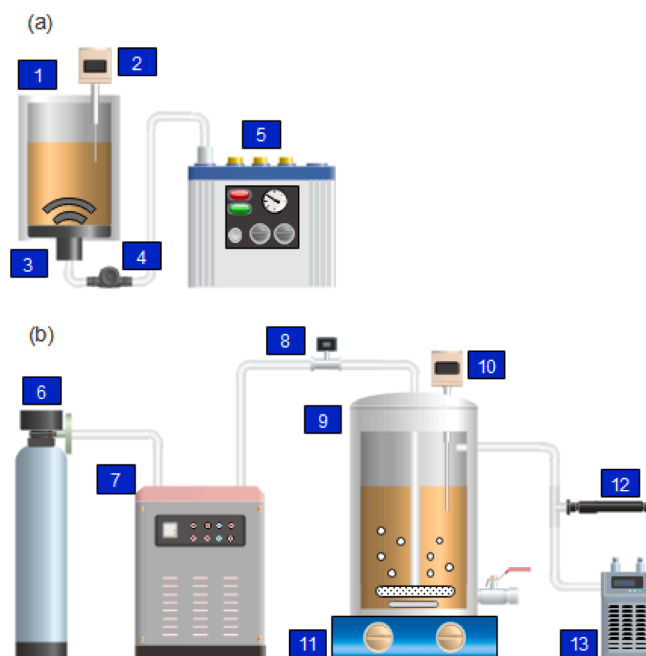


Fig. 1. Schematic of the experimental setup. (a) Pre-sonication setup; (1) Sonication vessel, (2) pH meter and thermometer, (3) Plate transducer, (4) Fuse, (5) Power amplifier. (b) Ozonation setup, (6) O₂ bottle, (7) O₃ generator, (8) Flow metre, (9) O₃ reactor, (10) pH meter and thermometer, (11) Magnetic stirrer, (12) O₃ destroyer, (13) O₃ analyser.

diameter). The ultrasonic transducer (Honda Electronics Co. LTD) was placed at the bottom of the vessel and powered by a power amplifier (T&C Power Conversion AG1006). Three different frequencies (98 kHz, 300 kHz and 1 MHz) at four different applied powers (10, 20, 30 and 40 W) were employed, varying sample volume from 150 mL to 400 mL. HA samples (50 mg HA/L) were sonicated for 10, 20 and 30 min. pH and temperature were continuously monitored (model GLP 22 from Crison) before and after pre-sonication experiments. When needed, pH was adjusted to 7 prior to ozonation.

Sonicated effluent was further treated with O₃ (Fig. 1b) in a 2 L cylindrical glass reactor previously described [18]. Two O₃ diffusers and a magnetic stirrer were placed at the bottom of the reactor, maintaining a constant injection gas flowrate (4.76 L/min) and mixing speed (60 rpm). O₃ was generated in-situ by the Triogen Lab2B generator from extra pure oxygen. 1 L pre-sonicated HA solution was ozonated for 30 and 120 min with O₃ injection at four different dosages: 5.4, 7.4, 11.3 and 19.7 mg O₃/L_{gas}. Dissolved O₃ (Rosemount Analytical model 499AOZ-54 probe) and exhaust O₃ (MT 964C ozone analyser) were continuously monitored, as well as dissolved O₂ (Rosemount Analytical Solu Comp II recorder), pH and temperature (Rosemount Analytical model 399-09-62 probe). Exhaust O₃ was destroyed by a Zonosistem thermocatalytic ozone destructor. All experiments were run at least in duplicates.

2.3. Analytical methods

Carbon, hydrogen, nitrogen and sulphur content present in the HA were determined by Euro EA Elemental Analyzer (CHNS). 10 mg of HA was completely oxidised by combustion with oxygen at a temperature of 1020 °C and combustion products identified with a thermal conductivity detector. Fourier-transform infrared spectroscopy (FTIR) was conducted with a Jasco 4200 model to determine FTIR values in infrared medium (4000–400 cm⁻¹) using KBr pellets for solid sample preparation. Pellet preparation was carried out by mixing 1.5 mg HA with 300 mg KBr. The mixture was then subjected to high vacuum compression until a 10 mm diameter and 1.5 mm thick pellet was obtained. Liquid sample analyses were carried out by evaporating 240 µL of sample at 80 °C and

atmospheric pressure in a 13×2 mm ZnSe tablet (Pika Technologies) placed inside an oven. ^{13}C NMR spectra were measured with a Bruker Avance III 400 MHz NMR spectrometer configured with the following characteristics: resonance frequency 100.62 MHz; $\pi/2$ pulse length 13.1 μs ; acquisition time 0.15 s; relaxation delay 1.5 s, $^1\text{J}_{\text{H-C}} = 7.5$ Hz and 120 scans. The pKa (acid dissociation constant) of the HA sample was calculated using UV–Visible spectrophotometry (PerkinElmer Lamda 10 UV/Vis spectrophotometer) and according to the method described by Reijenga et al. [19]. The determination of the E_3/E_5 ratio (ratio between UV absorbance at 350 and 550 nm and related to the molecular weight of humic substances) was carried out by dissolving 2 mg of HA in 10 mL of 0.05 M NaHCO_3 and a subsequent absorbance measurement by Perkin Elmer Lamda 10 UV/Vis spectrophotometer at wavelengths of 350 and 550 nm [20].

A Water 2695 HPSEC system with an Agilent ZORBAX GF-250 column (4.6×250 mm, 4 μm) was used for HPSEC analyses. A phosphate buffer (100% at pH 7) was injected at a flowrate of 1 mL/min with an ionic strength of 0.2 M and an injection volume of 20 μL . The Waters 2487 absorbance detector was used at a wavelength of 254 nm. The HPSEC system was calibrated with protein standards (Sigma-Aldrich) of known molecular weight between 14 and 600 kDa. A semi-exponential curve was obtained and used ($\text{MW} = 3 \times 10^8 \times t_{\text{R}}^{-9.691}$ with an $R^2 = 0.999$ for $\text{MW} > 47$ kDa and $\text{MW} = 21233 \times t_{\text{R}}^2 - 171755 \times t_{\text{R}} + 343352$ with an $R^2 = 1$ for $\text{MW} \leq 47$ kDa) for the determination of molecular weights at different retention times. Shimadzu TOC-VCSH Analyser was used for TOC measurements. Perkin Elmer LS-50B luminescence spectrophotometer (pre-sonication experiments) and Jasco FP-8200 fluorimeter (ozonation experiments) were used for fluorescence analyses, running a synchronous spectrum with an excitation spectra between 250 and 550 nm, a displacement of 20 nm and a scanning speed of 100 nm/min. Colour (PerkinElmer Lamda 10 UV/Vis spectrophotometer at 455 nm [21]) and SUVA_{254} (PerkinElmer Lamda 10 UV/Vis spectrophotometer at 254 nm) were also monitored. The concentration of I_3^- (proportional to the concentration of oxidising agents such as hydroxyl radicals) was measured following the KI dosimetry method [22,23].

3. Results and discussion

3.1. Ultrasonic pre-treatment

No significant TOC removal was measured after 30 min ultrasonic pre-treatment (300 kHz and 40 W). Therefore, impact of ultrasonic pre-treatment on the fluorescence spectra were investigated for any change at molecular level.

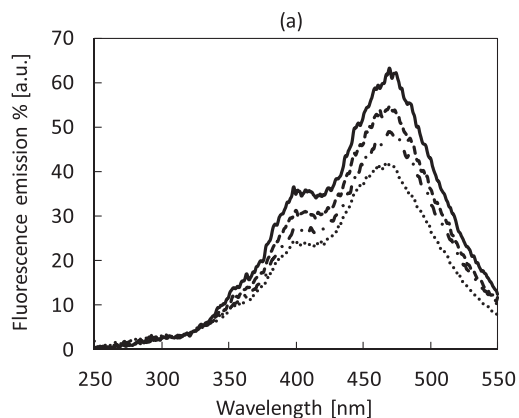


Fig. 2. Effect of ultrasound (40 W) on fluorescence emission of 50 mg HA/L samples. (a) Fluorescence emission percentage after 30 min and 400 mL sample. Initial sample with no sonication (—), 98 kHz (---), 1 MHz (· · ·) and 300 kHz (— · — ·). (b) Fluorescence emission intensity reduction percentage at 470 nm as a function of I_3^- concentration at 10, 20 and 30 min. 98 kHz (empty symbols), 300 kHz (black filled symbols), 1 MHz (grey filled symbols) and 150 mL (\circ), 200 mL (Δ), 300 mL (\diamond), 400 mL (\square) samples.

3.1.1. Fluorescence spectra and degradation mechanisms

Fluorescence emission intensity was monitored during ultrasonic pre-treatment in order to evaluate the impact of different frequencies and power densities on the fluorescence emission intensity band. Changes to the fluorescence emission indicates a change in the molecular structure of HAs [24], although this was not translated into carbon mineralisation (TOC removal).

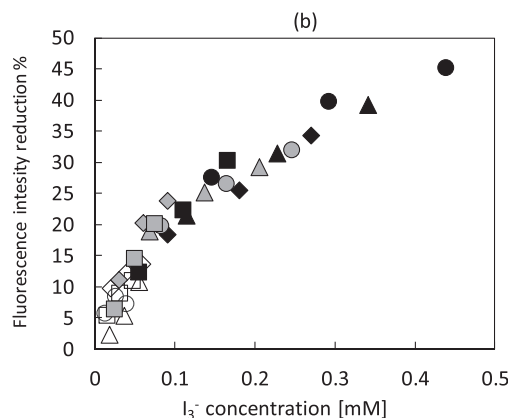
Fig. 2a shows the reduction in fluorescence intensity after 30 min of treatment at an applied power of 40 W for 98 kHz, 300 kHz and 1 MHz in 400 mL samples. Fluorescence intensity at λ_{max} was reduced the most at 300 kHz (31%), followed by 1 MHz (20%) and 98 kHz (11%). At 300 kHz, the reduction in fluorescence intensity was proportional to the applied power density (Fig. S2a). Reducing sample volume at a given applied power (increase in power density) also leads to a higher production of HO^\bullet [25] and has a similar effect on the fluorescence intensity reduction as decreasing applied power (Fig. S2 b). It is well known that ultrasound can produce HO^\bullet through the dissociation of water vapour when a cavitating bubble collapses [26,27], also leading to the formation of localised microjets when bubbles collapse asymmetrically near a surface [28,29]. These chemical (HO^\bullet) and physical (shear forces produced by microjets) processes are the principal mechanisms taking part in the degradation of compounds when ultrasound is applied. At low frequencies (98 kHz) physical effects are predominant due to a stronger collapse of the bubbles, while the highest HO^\bullet production is observed at medium–high frequencies (300 kHz) [26].

To evaluate whether the HO^\bullet production is the mechanism behind the reduction in fluorescence emission intensity of HAs, the concentration of HO^\bullet was evaluated in terms of concentration of I_3^- formed for each of the frequencies and different sample volumes. This was plotted against the fluorescence intensity reduction (Fig. 2b) to investigate its correlation that is independent of the applied frequency, increasing treatment time, applied power and sample volume. The strong correlation shown in Fig. 2b confirms that the reduction in fluorescence intensity could be mainly attributed to the attack of oxidising agents (HO^\bullet primarily) produced by ultrasound, and not to the mechanical (physical) effects.

3.2. Ozonation treatment

3.2.1. Effect of ozone injection dose on TOC

O_3 injection dose was varied (5.4, 11.3 and 19.7 $\text{mg O}_3/\text{L}_{\text{gas}}$) to maximise O_3 injection efficiency relative to TOC removal. Fig. 3 shows that increasing injected O_3 dose, TOC removal rate increased within the first ten minutes of the experiment. However, further increase in ozonation time up to 30 min, led to a similar TOC removal percentage for the



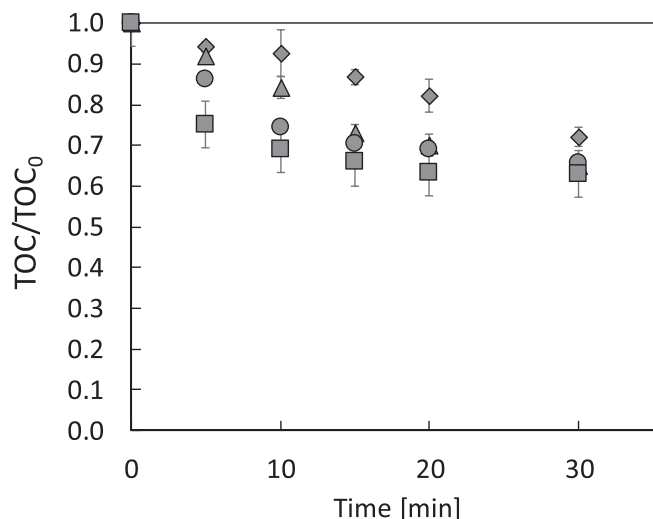


Fig. 3. TOC concentration as a function of treatment time for O_3 alone for different injected O_3 dosages of 5.4 mg O_3/L_{gas} (◆), 7.4 mg O_3/L_{gas} (▲), 11.3 mg O_3/L_{gas} (○), 19.7 mg O_3/L_{gas} (□), 19.7 mg O_3/L_{gas} (●).

three highest applied O_3 dosages (~36% reduction) and 27.8% reduction was measured for the lowest applied O_3 dosage of 5.4 mg O_3/L_{gas} . The difference in TOC removal rates between the aforementioned O_3 dosages (mainly 7.4 mg O_3/L_{gas} and 11.3 mg O_3/L_{gas}) would come from the action of molecular O_3 , considering a similar concentration of HO^\bullet would be expected from the two injection dosages (Fig. S3). Increasing O_3 injection dose increased dissolved O_3 concentration (Fig. S4a) in the HA solution, leading to a higher TOC removal rate within the first minutes of the treatment. This is supported by a strong correlation between TOC removal and dissolved O_3 concentration (Fig. S4b).

Once O_3 was transferred to the aqueous phase, a decrease in TOC was measured during the first stages of degradation probably due to decarboxylation reactions that can strongly oxidise the humic structure [30]. However, given the nature of the HA used, after the first degradation stages, the rate of oxidation decreased. The appearance of degradation by-products such as acids and esters could be responsible for the reduction in the oxidation rate, which have a lower reactivity ($k = 0.0019 \text{ mg TOC}^{-1} \text{ s}^{-1}$) than the aromatic groups, alcohols and phenols ($k = 0.071 \text{ mg TOC}^{-1} \text{ s}^{-1}$) that initially predominate in the first oxidation states of the HA structure [31]. The identification of these by-products was carried out using the FTIR spectra in Fig. 8, where an increase in 1260 cm^{-1} and 1720 cm^{-1} bands was observed, indicative of the formation of carboxylic acids. In addition to these organic compounds that are formed during ozonation, there are other inorganic compounds that are difficult to remove, such as bromate ions. Therefore, the increase in the TOC elimination rate in the initial stages of the treatment could be also related to the characteristics of the HA at that specific time [32].

3.3. Ultrasonic pre-treatment and ozonation

3.3.1. Effect on TOC

With 30 min ultrasonic pre-treatment (300 kHz and 40 W) and a subsequent ozonation (Fig. 4), a similar behaviour in TOC removal was observed. It is important to highlight, however, that the TOC reduction rate between 7.4 mg O_3/L_{gas} and 11.3 mg O_3/L_{gas} seemed to be similar, contrary to non-sonicated values (Fig. 3). This could be related to the change in the molecular structure of HAs during sonication pre-treatment stated earlier, leading to a lower demand in O_3 (reduction from 11.3 mg O_3/L_{gas} to 7.4 mg O_3/L_{gas}) to obtain a similar TOC removal rate. Similarly, Ma and Lin [3] showed that ultrasound pre-treatment (combined with O_2) decreased the consumption of chlorine

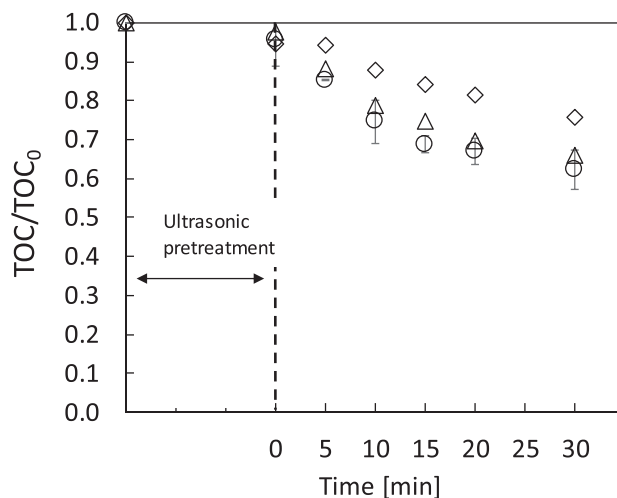


Fig. 4. TOC concentration as a function of treatment time for injected O_3 dosages of 5.4 mg O_3/L_{gas} (◇), 7.4 mg O_3/L_{gas} (△), 11.3 mg O_3/L_{gas} (○), 19.7 mg O_3/L_{gas} (□). 30 min ultrasound (300 kHz and 40 W) pre-treatment applied 400 mL sample and 50 mg HA/L.

in a subsequent chlorination process. Ultrasonic pre-treatment, nonetheless, did not increase the final TOC removal of O_3 treatment for the two abovementioned applied O_3 dosages. As it happened with non-sonication experiments, the lowest TOC removal percentage (24.3%) was once again obtained with 5.4 mg O_3/L_{gas} . For a given O_3 treatment (mg O_3/L_{gas}), pre-sonication at different frequencies had no notable impact on the TOC reduction rate. (Fig. 5).

3.3.2. Effect on colour and SUVA₂₅₄

For both ozonation alone and pre-sonication/ozonation experiments, a significant reduction in colour was observed. However, 30 min of sonication (300 kHz and 40 W) showed no significant reduction in colour, compared to 85% colour removal with ozonation treatment (Fig. 6a). Therefore, the colour reduction can be attributed to the breaking of polymers of humic material in water and the reactivity of O_3 with chromophore groups [33]. Although the final colour removal percentage was similar for the three O_3 dosages used (5.4, 7.4 and 11.3 mg O_3/L_{gas}), a difference in colour removal rates between 5.4 and 7.4 mg O_3/L_{gas} was evident (e.g. compared to 7.4 mg O_3/L_{gas} , colour values

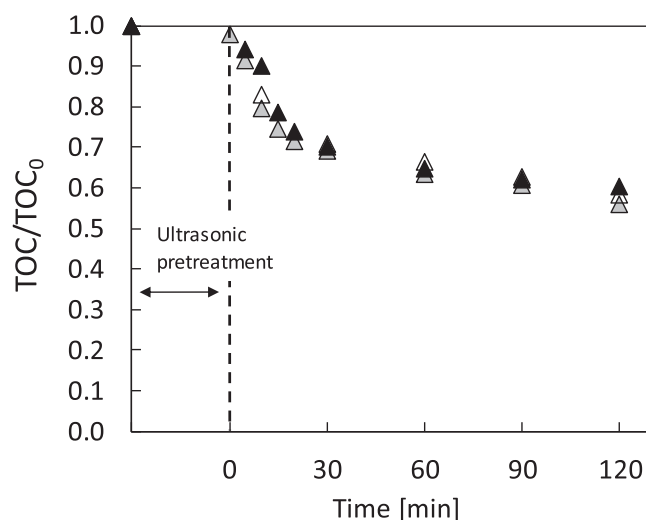


Fig. 5. TOC concentration as a function of treatment time for 30 min ultrasonic pre-treatment (40 W) and 120 min O_3 treatment (7.4 mg O_3/L). 98 kHz (▲); 300 kHz (▲); 1 MHz (△). 400 mL sample and 50 mg HA/L.

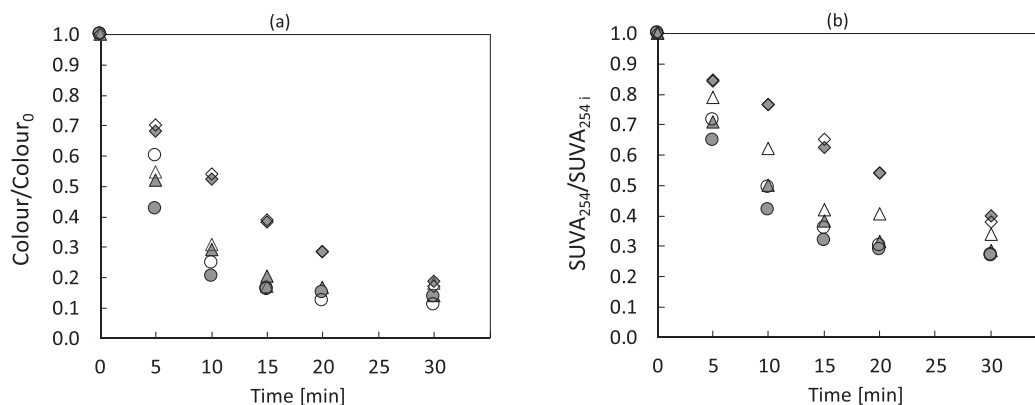


Fig. 6. HA degradation analysis through: (a) Colour as a function of time. (b) $SUVA_{254}$ as a function of time. 5.4 mg O_3/L_{gas} (\diamond), 7.4 mg O_3/L_{gas} (Δ) and 11.3 mg O_3/L_{gas} (\circ). O_3 alone (grey symbols), and 30 min ultrasound + O_3 (empty symbols). 300 kHz and 40 W for ultrasound experiments. 400 mL sample and 50 mg HA/L.

at 10 and 15 min were double for 5.4 mg O_3/L_{gas} .

Similarly, ultrasonic pre-treatment had negligible effect on the $SUVA_{254}$ (Fig. 6b) and a reduction of 70% was measured for the two highest O_3 dosages, reducing slightly the removal percentage to 62% with 5.4 mg O_3/L_{gas} . The difference during ozonation in $SUVA_{254}$ removal rates between 5.4 and 7.4 mg O_3/L_{gas} was also maintained in this case (e.g. $SUVA_{254}$ values at 10 and 15 min).

3.4. Degradation mechanisms

3.4.1. HO^\bullet yield

As indicated in Fig. 2b there is a strong correlation between HO^\bullet (quantified by measuring concentration of I_3^-) and the degradation of HAs. Fig. S3 shows that the concentration of I_3^- achieved with O_3 (7.4 and 11.3 mg O_3/L_{gas} injected) is approximately 10 times higher than the

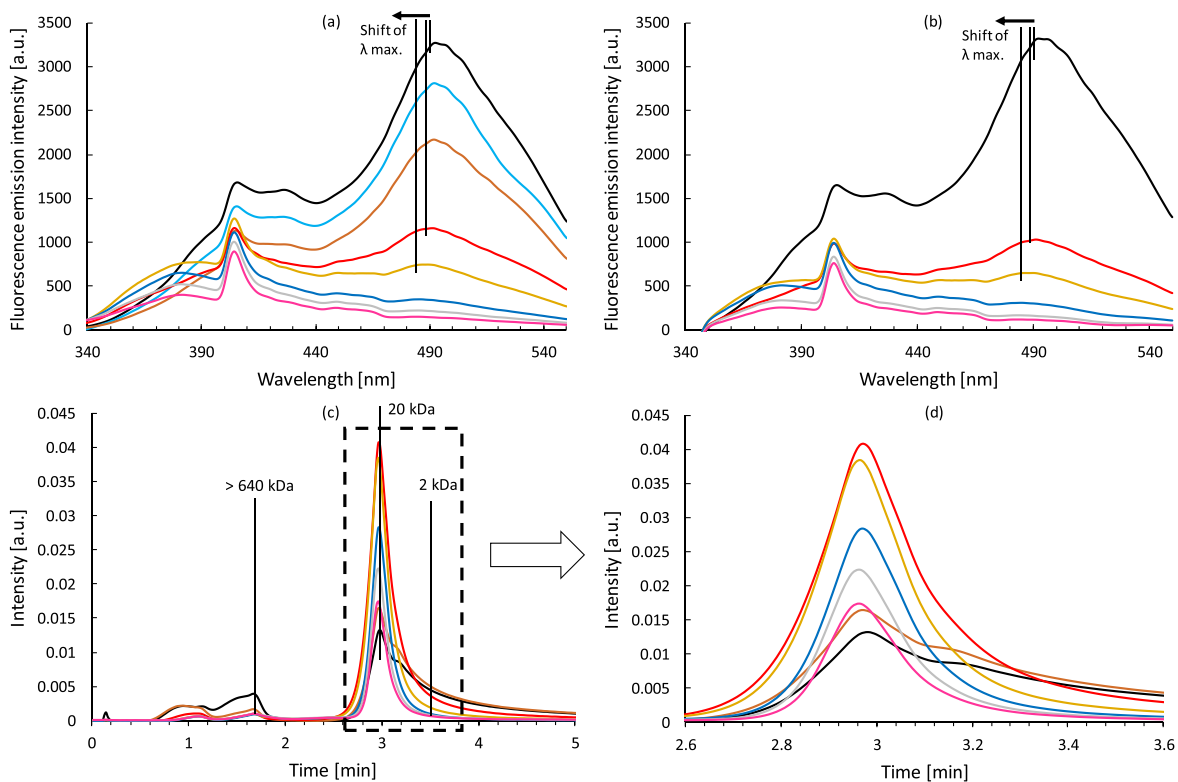


Fig. 7. HA degradation analysis through: (a) Fluorescence emission intensity US + O_3 ; (b) Fluorescence emission intensity O_3 alone; (c) HPSEC analysis US + O_3 ; (d) Zoomed in plot of (c) at 2.6–3.6 min time interval. (a, c, d) Initial sample (—), 10 min ultrasound (US, —), 30 min US (—), 30 min US + 5 min O_3 (—), 30 min US + 10 min O_3 (—), 30 min US + 15 min O_3 (—), 30 min US + 20 min O_3 (—) and 30 min US + 30 min O_3 (—); (b) Initial sample (—), 5 min O_3 (—), 10 min O_3 (—), 15 min O_3 (—), 20 min O_3 (—) and 30 min O_3 (—). Ultrasound pre-treatment: 300 kHz and 40 W. O_3 injection: 7.4 mg O_3/L_{gas} . 50 mg HA/L initial sample.

concentration obtained with ultrasound. This could explain the difference in TOC removal of HA solutions between ultrasound pre-treatment (<5%) and O₃ treatment (>40%) shown in Fig. 5, where the effect of a 30 min sonication pre-treatment is shown to have negligible effect on the subsequent ozonation process. During the first 25 min of ozonation, a sharp decrease in TOC is accompanied by a fast reduction in pH from 7 to 4. At pH between 7 and 4, both HO• and molecular O₃ would take part in the oxidation process of compounds due to a fast decomposition of O₃ [34,35]. When the pH reached 4 or below, a considerable reduction in TOC removal rate was observed, where oxidation and mineralisation of HAs would come primarily from the action of molecular O₃ (significantly lower oxidation potential compared to HO• [36]).

All this indicates that O₃ would have played a minor role in the reduction of TOC compared to HO•. That would explain why after approximately 25 min of ozonation TOC removal rate decreased significantly with only a 12% additional removal between 30 min and 2 h with 7.4 mg O₃/L_{gas} injected compared to a 30% reduction in the first 30 min (Fig. 5). The formation of refractory compounds during ozonation could have also reduced further mineralisation of HAs [10]. Therefore, ozonation time was set at 30 min for further experiments.

3.4.2. Effect on fluorescence spectra

The evolution of fluorescence is compared in Fig. 7a (ultrasound pre-treatment without and with post O₃ treatment) and 7b (O₃ treatment alone). In both cases, a significant decrease in 460–550 nm emission band was observed (Fig. S5) indicating decomposition of HAs which are composed of aromatic groups, alcohols and phenols, as well as ketone and aldehyde groups [37]. However, there was as negligible impact from US pre-treatment and ozone dosage. There is a second region consisting of proteins with a maximum emission peak at 405 nm. In this region, the fluorescence intensity for ozonation alone resulted in a consistently lower intensity compared to ozonation with ultrasonic pre-treatment, indicating higher degradation of proteins by ozone (Fig. S6).

In the fluorescence emission region between 340 and 410 nm, there is a notable increase in the intensity when ultrasound pre-treatment is applied compared to only ozonation. This could indicate that ozonation after ultrasonic pre-treatment led to an increase in the more biodegradable part of the humic structure (340–410 nm) [38], increasing: (i) the protein-like group that consists of xenobiotic compounds, (ii) the tryptophan-like group constituted by low molecular weight compounds and (iii) the tyrosine-like group composed of free molecules or molecules bound to higher molecular weight proteins, as well as peptides [39]. On the other hand, with O₃ treatment alone, although the humic region decreased its intensity in the same way as with the ultrasonic pre-

treatment, an increase in the 340–390 nm band (Fig. S7) that could indicate a greater oxidation of the humic structure into other by-products with more biodegradable characteristics was not observed.

3.4.3. HPSEC analysis

Fig. 7c and d correspond to HPSEC chromatography of the ultrasonic pre-treatment followed by the ozonation process. In general terms, a gradual reduction in humic substances up to 80% was observed along with the generation of lower molecular weight oxidation compounds such as carboxylic acids and esters. HAs were broken down into lower molecular weight compounds (from >640 kDa to ~20 kDa) during the treatment process as shown by Fig. 7d. No major difference was found in the formation of lower molecular weight compounds during ozonation with and without ultrasonic pre-treatment (Fig. S8).

3.4.4. FTIR analysis

With regards to the FTIR analysis, Fig. 8 shows the infrared spectra obtained during the ozonation process with ultrasonic pre-treatment. A decrease in the transmittance intensity at 1620–1630 cm⁻¹ indicates a decrease in aromatic groups after 30 min O₃ injection [40,41], likely due to O₃ being highly selective towards complex aromatic compounds [30]. The decrease in aromaticity is consistent with the decrease in SUVA₂₅₄ and fluorophore concentration in the emission band of 405–461 nm observed in fluorescence analyses [42,43]. After the hydroxylation and opening of aromatic rings, a slow oxidation of oxygenated saturated compounds likely took place [44] as observed in the decrease of the corresponding to aromatic ethers [45]. Along with the 1260 cm⁻¹ band functional group, a decrease of the 1030 cm⁻¹ band (alcohols) was also observed, that together with the phenolic groups slowly decreased with increasing reaction time [41]. It is also highlighted the decrease in transmittance in the 1720 cm⁻¹ band (corresponding to the C=O vibration tension) attributable to ketone groups and carboxylic acids. Above this wavelength there is a progressive decrease in compounds capable of absorbing in FTIR, which leads to a convergence of the spectra whatever the treatment. Finally, after the decrease in aromatic groups, alcohols, phenols, ketones and aldehydes, a greater abundance of the C-O tension bands (1220 cm⁻¹) was observed, corresponding to carboxylic acids [40,44]. These carboxylic groups increased during the reaction, being results in line with those observed in fluorescence analyses. In contrast, the 805 cm⁻¹ band would be attributable to tri- and tetrasubstituted aromatic rings which remained unchanged throughout the treatment [46]. This fraction could correspond to the residual humic structure observed in the fluorescence and which by its nature has a recalcitrant character that is difficult to eliminate (more aliphatic and polar) [41]. Finally, the intensity at 1540 and 1384 cm⁻¹ would correspond to the formation of nitrogen groups caused by O₃ injection [47].

4. Conclusions

Ultrasonic pre-treatment significantly lowered fluorescence emission intensity from HA samples with all the frequencies under study. 31% fluorescence reduction in λ max (470 nm) was obtained applying 300 kHz and 40 W (50 mg HA/L) for 30 min, measuring also changes in molecular structure. The subsequent 30 min ozonation reduced TOC down to 13.5 mg/L (36%) after applying 7.4 mg O₃/L_{gas}. O₃ injection also led to the production of oxidation by-products of lower molecular weight, reducing colour (85%) and SUVA₂₅₄ (70%) significantly. However, ultrasonic pre-treatment did not substantially improve the performance of ozonation treatment. Thus, similar results for TOC, colour and SUVA₂₅₄ were obtained with ozonation-alone experiments. In contrast, significant variations in the fluorescence emission of the samples were detected, despite reaching the same degree of mineralisation either with or without ultrasonic pre-treatment. In such a way, the use of ultrasound would be more advantageous if adequately combined with simple or biological adsorption processes.

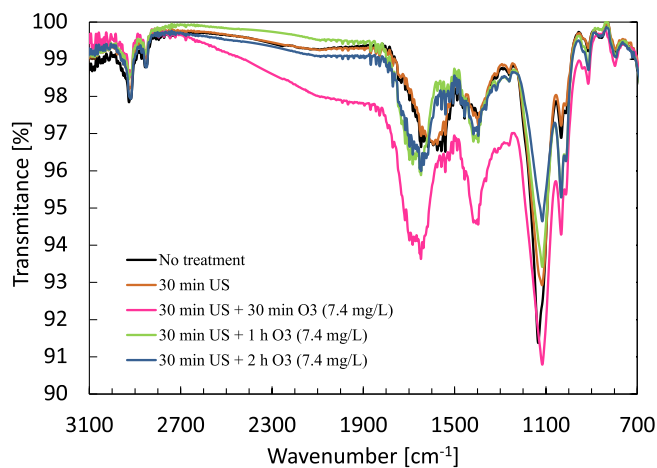


Fig. 8. FTIR spectra in the region between 3100 and 700 cm⁻¹ of initial sample (50 mg HA/L and 400 mL), 30 min ultrasound (US, 300 kHz and 40 W), 30 min US + 30 min O₃ (7.4 mg O₃/L_{gas}), 30 min US + 1 h O₃ and 30 min US + 2 h O₃.

CRediT authorship contribution statement

Pello Alfonso-Muniozguren: Conceptualization, Methodology, Validation, Formal analysis, Investigation, Data curation, Writing - original draft, Writing - review & editing, Visualization. **Cristian Ferreira:** Conceptualization, Methodology, Validation, Formal analysis, Investigation, Data curation, Writing - original draft, Writing - review & editing, Visualization. **Elodie Richard:** Investigation, Data curation. **Madeleine Bussemaker:** Resources, Writing - review & editing, Supervision, Funding acquisition. **José Ignacio Lombrana:** Conceptualization, Methodology, Resources, Writing - review & editing, Visualization, Supervision, Project administration, Funding acquisition. **Judy Lee:** Conceptualization, Methodology, Resources, Writing - review & editing, Visualization, Project administration, Funding acquisition.

Declaration of Competing Interest

The authors declare that they have no known competing financial interests or personal relationships that could have appeared to influence the work reported in this paper.

Acknowledgements

The authors are grateful to the University of the Basque Country for their financial support of this study through the PPGA19/63 project and C. Ferreira's predoctoral PIF grant (PIF16/367). Erasmus + programme is also acknowledged by P. Alfonso-Muniozguren.

Appendix A. Supplementary data

Supplementary data to this article can be found online at <https://doi.org/10.1016/j.ultsonch.2020.105359>.

References

- G.R. Aiken, D.M. McKnight, R.L. Wershaw, P. MacCarthy, An introduction to humic substances in soil, sediments and water, in: A.W.I. Publication (Ed.)1985, pp. 1–9.
- V. Naddeo, V. Belgiorno, R.M.A. Napoli, Behaviour of natural organic matter during ultrasonic irradiation, *Desalination* 210 (2007) 175–182.
- Y.-S. Ma, J.-G. Lin, Effect of pre-sonication on removal of organic matters resulting from chlorinated humic acids, *Water Sci. Technol.* 38 (1998) 253–260.
- Y. Nagata, K. Hirai, H. Bandow, Y. Maeda, Decomposition of hydroxybenzoic and humic acids in water by ultrasonic irradiation, *Environ. Sci. Technol.* 30 (1996) 1133–1138.
- D. Chen, Z. He, L. Weavers, C. Yu-ping, W. Harold, P. Hatcher, Sonochemical reactions of dissolved organic matter, *Res. Chem. Intermed* 30 (2004) 735–753.
- Y. Liu, Q. Wang, S. Zhang, J. Lu, S. Yue, NOM reactivity with chlorine in low SUVA water, *J. Water Supply: Res. Technol.-Aqua* 60 (2011) 231–239.
- R.J. Wood, J. Lee, M.J. Bussemaker, A parametric review of sonochemistry: control and augmentation of sonochemical activity in aqueous solutions, *Ultrason Sonochem.* 38 (2017) 351–370.
- S. Manickam, N. Abidin, S. Parthasarathy, I. Alzorqi, E.H. Ng, T.J. Tiong, R. L. Gomes, A. Ali, Role of H₂O₂ in the fluctuating patterns of COD (chemical oxygen demand) during the treatment of palm oil mill effluent (POME) using pilot scale triple frequency ultrasound cavitation reactor, *Ultrason Sonochem* 21 (2014) 1519–1526.
- E. Villaroel, J. Silva-Agrede, C. Petrier, G. Tabora, R.A. Torres-Palma, Ultrasonic degradation of acetaminophen in water: Effect of sonochemical parameters and water matrix, *Ultrason. Sonochem.* 21 (2014) 1763–1769.
- K. Kusakabe, S. Aso, J.-I. Hayashi, K. Isomura, S. Morooka, Decomposition of humic acid and reduction of trihalomethane formation potential in water by ozone with U.V. irradiation, *Water Research*, 24 (1990) 781–1.
- H. Miao, W. Tao, Ozonation of humic acid in water, *J. Chem. Technol. Biotechnol.* 83 (2008) 336–344.
- G.L. Amy, C.J. Kuo, R.A. Sierka, Ozonation of humic substances: Effects on molecular weight distributions of organic carbon and trihalomethane formation potential, *Ozone Sci. Eng.* 10 (1988) 39–54.
- J. Larose, A. Grasmick, P. Blondeau, S. Elmaleh, J.P. Legeron, Elimination of humic materials, *Ozone Sci. Eng.* 4 (1982) 79–89.
- T.M. Olson, P.F. Barbier, Oxidation kinetics of natural organic matter by sonolysis and ozone, *Water Res.* 28 (1994) 1383–1391.
- L.K. Weavers, M.R. Hoffmann, Sonolytic decomposition of ozone in aqueous solution: mass transfer effects, *Environ. Sci. Technol.* 32 (1998) 3941–3947.
- L.K. Weavers, F.H. Ling, M.R. Hoffmann, Aromatic compound degradation in water using a combination of sonolysis and ozonolysis, *Environ. Sci. Technol.* 32 (1998) 2727–2733.
- L. Stepniak, E. Stanczyk-Mazanek, M. Kusiak, Ultrasounds and ozone in removal of humic substances from water, *Inżynieria i Ochrona Środowiska* 15 (2012) 143–154.
- C. Ferreira, N. Villota, J.I. Lombrana, M.J. Riveiro, An efficient catalytic process for the treatment of genotoxic aniline wastewater using a new granular activated carbon-supported titanium dioxide composite, *J. Cleaner Prod.* 228 (2019) 1282–1295.
- J. Reijenga, A. van Hoof, A. van Loon, B. Teunissen, Development of Methods for the Determination of pKa Values, *Anal. Chem. Insights* 8 (2013) 53–71.
- A.A. Helal, G.A. Murad, A.A. Helal, Characterization of different humic materials by various analytical techniques, *Arabian J. Chem.* 4 (2011) 51–54.
- F. Mijangos, F. Varona, N. Villota, Changes in solution color during phenol oxidation by fenton reagent, *Environ. Sci. Technol.* 40 (2006) 5538–5543.
- E.J. Hart, A. Henglein, Free radical and free atom reactions in the sonolysis of aqueous iodide and formate solutions, *J. Phys. Chem.* 89 (1985) 4342–4347.
- A. Weissler, H.W. Cooper, S. Snyder, Chemical effect of ultrasonic waves: oxidation of potassium iodide solution by carbon tetrachloride, *J. Am. Chem. Soc.* 72 (1950) 1769–1775.
- E. Naffrechoux, S. Chanoux, P.J. Suptil, Sonochemical and photochemical oxidation of organic matter, *Ultrason. Sonochem.* 7 (2000) 255–259.
- P. Kanthale, M. Ashokkumar, F. Grieser, Sonoluminescence, sonochemistry (H₂O₂ yield) and bubble dynamics: frequency and power effects, *Ultrason Sonochem.* 15 (2008) 143–150.
- J. Lee, Importance of Sonication and Solution Conditions on the Acoustic Cavitation Activity, in: M. Ashokkumar (Ed.), *Handbook of Ultrasonics and Sonochemistry*, Springer Science + Business Media, Singapore, 2016, pp. 137–175.
- S. Parthasarathy, R.R. Mohammed, C.M. Fong, R.L. Gomes, S. Manickam, A novel hybrid approach of activated carbon and ultrasound cavitation for the intensification of palm oil mill effluent (POME) polishing, *J. Cleaner Prod.* 112 (2016) 1218–1226.
- P.R. Gogate, Application of cavitation reactors for water disinfection: current status and path forward, *J. Environ. Manage* 85 (2007) 801–815.
- R.A. Torres-Palma, J. Gibson, I.G. Droppo, P. Seto, R. Farnood, Surfactant-assisted sono-breakage of wastewater particles for improved UV disinfection, *Water Air Soil Pollut.* 228 (2017) 106.
- C. von Sonntag, U. von Gunten, *Chemistry of Ozone in Water and Wastewater Treatment: From Basic Principles to Applications*, IWA Publishing, 2012.
- T. Nöthe, H. Fahlenkamp, C.V. Sonntag, Ozonation of Wastewater: Rate of Ozone Consumption and Hydroxyl Radical Yield, *Environmental Science & Technology*, 43 (2009) 5990–5995.
- R.M. Hozalski, E.J. Bouwer, S. Goel, Removal of natural organic matter (NOM) from drinking water supplies by ozone-biofiltration, *Water Sci. Technol.* 40 (1999) 157–163.
- E.S. Melin, H. Ødegaard, The effect of biofilter loading rate on the removal of organic ozonation by-products, *Water Res.* 34 (2000) 4464–4476.
- M.-O. Buffle, J. Schumacher, S. Meylan, M. Jekel, U. von Gunten, Ozonation and advanced oxidation of wastewater: effect of O₃ dose, pH, DOM and HO• scavengers on ozone decomposition and HO• generation, *Ozone Sci. Eng.* 28 (2006) 247–259.
- P. Alfonso-Muniozguren, M. Hazzwan Bohari, A. Sicilia, C. Avignone-Rossa, M. Bussemaker, D. Saroj, J. Lee, Tertiary treatment of real abattoir wastewater using combined acoustic cavitation and ozonation, *Ultrason. Sonochem.* 64 (2020), 104986.
- S.C. Ameta, P.B. Punjabi, A. Kumar, R. Ameta, *Advanced Oxidation Processes: Basics and Applications*, in: D.G. Rao, R. Senthilkumar, J.A. Byrne, S. Feroz (Eds.) *Wastewater Treatment: Advanced Processes and Technologies*, IWA publishing 2012, pp. 46.
- N.P. Sanchez, A.T. Skeriotis, C.M. Miller, Assessment of dissolved organic matter fluorescence PARAFAC components before and after coagulation–filtration in a full scale water treatment plant, *Water Res.* 47 (2013) 1679–1690.
- N. Hudson, A. Baker, D. Ward, D.M. Reynolds, C. Brunson, C. Carliell-Marquet, S. Browning, Can fluorescence spectrometry be used as a surrogate for the Biochemical Oxygen Demand (BOD) test in water quality assessment? An example from South West England, *Sci. Total Environ.* 391 (2008) 149–158.
- S.A. Baghoth, S.K. Sharma, G.L. Amy, Tracking natural organic matter (NOM) in a drinking water treatment plant using fluorescence excitation–emission matrices and PARAFAC, *Water Res.* 45 (2011) 797–809.
- R. Gracia, J.L. Aragües, J.L. Ovelleiro, Study of the catalytic ozonation of humic substances in water and their ozonation byproducts, *Ozone Sci. Eng.* 18 (1996) 195–208.
- F.J. Rodríguez, P. Schlenger, M. García-Valverde, Monitoring changes in the structure and properties of humic substances following ozonation using UV–Vis, FTIR and 1H NMR techniques, *Sci. Total Environ.* 541 (2016) 623–637.
- M. Sillanpää, A. Matilainen, T. Lahtinen, Chapter 2 – Characterization of NOM, in: M. Sillanpää (Ed.) *Natural Organic Matter in Water*, Butterworth-Heinemann2015, pp. 17–53.
- X. Zhong, C. Cui, S. Yu, Identification of oxidation intermediates in humic acid oxidation, *Ozone Sci. Eng.* 40 (2018) 93–104.
- R. Gracia, S. Cortés, J. Sarasa, P. Ormad, J.L. Ovelleiro, Heterogeneous catalytic ozonation with supported titanium dioxide in model and natural waters, *Ozone Sci. Eng.* 22 (2000) 461–471.

- [45] H.-C. Kim, M.-J. Yu, Characterization of aquatic humic substances to DBPs formation in advanced treatment processes for conventionally treated water, *J. Hazard. Mater.* 143 (2007) 486–493.
- [46] M. Derrien, S.R. Brogi, R. Goncalves-Araujo, Characterization of aquatic organic matter: assessment, perspectives and research priorities, *Water Res* 163 (2019), 114908.
- [47] S. Preis, I. Panorel, S. Llauger Coll, I. Kornev, Formation of nitrates in aqueous solutions treated with pulsed corona discharge: the impact of organic pollutants, *Ozone Sci. Eng.* 36 (2014) 94–99.




3.11. 11. argitalpena. Contaminants of emerging concern removal in an effluent of wastewater treatment plant under biological and continuous mode ultrafiltration treatment

3.11 kapitulua artikulu honi dagokio:

C. Ferreiro, I. Gómez-Motos, J.I. Lombraña, A. de Luis, N. Villota, O. Ros, N. Etxebarria. Contaminants of emerging concern removal in an effluent of wastewater treatment plant under biological and continuous mode ultrafiltration treatment. *Sustainability*, 12, 2, 725, 2020. DOI: 10.3390/su12020725.

Article

Contaminants of Emerging Concern Removal in an Effluent of Wastewater Treatment Plant under Biological and Continuous Mode Ultrafiltration Treatment

Cristian Ferreiro ^{1,*}, Iker Gómez-Motos ¹, José Ignacio Lombrana ¹, Ana de Luis ², Natalia Villota ³, Oihana Ros ⁴ and Nestor Etxebarria ⁴

¹ Department of Chemical Engineering, Faculty of Science and Technology, University of the Basque Country UPV/EHU, Barrio Sarriena s/n, 48940 Bizkaia, Spain; igomez107@ikasle.ehu.eus (I.G.-M.); ji.lombrana@ehu.eus (J.I.L.)

² Department of Chemical and Environmental Engineering, Faculty of Engineering in Bilbao, University of the Basque Country UPV/EHU, Plaza Ingeniero Torres Quevedo, 1, 48013 Bilbao, Spain; ana.deluis@ehu.eus

³ Department of Chemical and Environmental Engineering, Faculty of Engineering Vitoria-Gasteiz, University of the Basque Country UPV/EHU, Nieves Cano 12, 01006 Vitoria-Gasteiz, Araba, Spain; natalia.villota@ehu.eus

⁴ Department of Analytical Chemistry, Faculty of Science and Technology, University of the Basque Country UPV/EHU, Barrio Sarriena s/n, 48940 Bizkaia, Spain; oihana.ros@ehu.eus (O.R.); nestor.etxebarria@ehu.eus (N.E.)

* Correspondence: cristian.ferreiro@ehu.eus; Tel.: +34-9460-153-88

Received: 26 December 2019; Accepted: 16 January 2020; Published: 19 January 2020



Abstract: This work presents a case study of a wastewater treatment plant (WWTP), located in Biscay (Spain), in which the removal of high-occurrence contaminants of emerging concern (CEC) was studied. The existing biological treatment in the WWTP was complemented with a continuous ultrafiltration (c-UF) pilot plant, as a tertiary treatment. Thus, the effect on CEC removal of both treatments could be analyzed globally and after each operation. A total of 39 CEC were monitored, including pharmaceutical products, industrial additives, food additives, herbicides and personal care products. For evaluation of the efficiencies, the removal rates of the biological and of the c-UF treatments, including their variability over a day and a week in relation to the ammonium content, were examined in the influent of the WWTP. In the biological treatment, a wide range of different removal rates was obtained due to the different CEC's biodegradability and concentration. In UF, lower, but more constant removal rates, were achieved. In addition, the reduction of the general toxicity by the UF treatment in terms of the Microtox[®] toxicity assay was also evaluated. After UF, all of the samples yielded values of TU₅₀ lower than 1, confirming this result the UF effectiveness for toxicity removal.

Keywords: emerging contaminants; ultrafiltration; wastewater treatment plant; ammonium; toxicity; Microtox

1. Introduction

The presence of contaminants of emerging concern (CEC) in the effluents of wastewater treatment plants (WWTPs) is a matter of growing concern [1]. Emerging contaminants are chemical compounds that, though they are still unregulated, could be candidates for future regulation, depending on the research results on their potential health effects and occurrence. These include pesticides, pharmaceuticals, drugs of abuse, hormones, other endocrine disruptors, surfactants,

surfactant metabolites, perfluorinated compounds, industrial additives and agents, and personal care products [2–4].

The occurrence of many CEC is often related to discharges from WWTPs, as a consequence of the widespread use of many of these compounds and the lack of technologies with sufficient removal efficiency, like ozonation or adsorption and their combinations [5]. In fact, the current legislation related to wastewater treatment (Directive 2000/60/EC, Directive 2008/56/EC, Directive 2013/39/EU) does not yet include most of these compounds and, therefore, WWTPs are not specifically designed to eliminate them. As a consequence, it has been found that WWTPs only a partial removal of several CEC, such as carbamazepine or diclofenac (< 25%) [6] continuous discharges give many aquatic environments at sublethal levels that could achieve chronic levels (low $\mu\text{g/L}$ range) of many CEC [7,8]. Moreover, these CEC have even been found in water designated for human consumption [9,10]. Consequently, recent research focused on avoiding the presence of certain CEC in drinking water [3].

In this sense, appropriate water treatment is fundamental for human and environmental health protection. As noted above, the efficiency of the treatments before discharge of water determines its impact on the aquatic ecosystems. Shelley et al. [11] reported that sublethal concentrations of herbicides such as atrazine alter spontaneous swimming activity, feeding behavior, and vulnerability to predation in *Oncorhynchus mykiss* (rainbow trout) after 96 hours of exposure. De Wever and Verachtert [12] studied the toxic effects of the industrial additive 2-hydroxybenzothiazole on *Candida albicans*. This CEC produced alterations in the cell membrane, causing vulnerability to attacks. In this context, the general trend in Europe during recent decades has been to raise the percentage of the population connected to WWTPs with tertiary treatments. This is particularly the case for countries such as the Netherlands, Germany, and Austria, where currently more than 90% of urban wastewater receives tertiary treatment [13]. The development of advanced treatments to be used as tertiary treatments is necessary to adequately avoid address the potential hazards.

Currently, membrane filtration technologies and the use of advanced oxidation processes (AOPs) are widely studied for the removal of micropollutants, either in wastewater or in drinking water [14–17]. Among these treatments, the most relevant processes are: ozonation [18,19], UV/H₂O₂/Fe³⁺ photocatalysis [20], electrochemical reactions [20,21], membrane bioreactors [22], nanofiltration or ultrafiltration, reverse osmosis [23–25] and adsorption [26]. Technologies based on hydrogen peroxide oxidation, such as Fenton, or others activated by UV [21,27,28] and ultrasound [29], have also proved significant. However, fundamental questions about the technical viability, cost-effectiveness ratio or the sustainability of the industrial implantation of different techniques are still under discussion. [30,31].

The well-known advantages of membrane filtration technologies over other technologies, such as their small process footprint, simplicity, easy maintenance, or high separation efficiency, make them an outstanding option for wastewater treatment, operating either alone or inside a hybrid process [32]. Among the different membrane technologies, that of ultrafiltration (UF) has been chosen in this work because of its characteristics: pore size and operability, with a good adaptation to the effluent treatment of a WWTP.

Within the available UF technologies, the continuous mode (c-UF) has been. The c-UF system used in this work has been patented in Spain under patent number ES201431341A. This technology has the following benefits when compared to current UF systems:

- Constant product flow even during cleanings
- Up to 30% cost reduction
- 50% footprint reduction
- 5% higher net production
- Large reduction of occupied space (suitable for modular plants)

The objective of this work is to study the in-situ removal ratio of a panel of 39 emerging compounds (see Table 1) by a c-UF pilot plant connected to the secondary (biological) effluent of a working WWTP. The target contaminants have been selected based on their frequency of appearance and concentration

in WWTPs [33] and the removal efficiency of the biological and UF processes has been quantified and compared, analyzing, in both cases, the influence of CEC concentration and in the case of the biological treatment the influence of biodegradability. In the UF treatment, we studied the specific behavior associated to adsorption phenomena. This factor, together with the complexity of the filtering mechanisms, requires global parameter for a complete valorisation of the UF effect, beyond the CEC reduction. Consequently, the effect of the UF treatment in the reduction of toxicity (Microtox[®]) has also been evaluated in order to obtain an estimation of the effectiveness of the treatment and the quality of the resulting effluent.

2. Materials and Methods

2.1. Equipment for UF and Operation Procedure

A pilot UF plant made by Fluytec S.A. (Bilbao, Spain) was used to treat the effluent from the biological process (BIO) of the WWTP of Galindo. This WWTP treats the urban and industrial water of the area of Bilbao (43°18'35.38'' N and 3°0'25.92'' W, Biscay, north of Spain), with an equivalent population of 1,500,000 inhabitants, using a conventional activated sludge process after various pretreatments (roughing, degreasing, sedimentation, and primary decantation).

The added UF plant has a treatment capacity of 5 m³/h and operates in continuous mode (c-UF) and without recirculation (dead end). The UF technology used works in dead-end mode, with a recovery factor of 98%. Then the retentate (2% of the feed water) corresponds to the wash water. This little stream could be recirculated to the biologic entrance to get further removal by biological degradation, and adsorption mechanism, or treated by ozonization. Its four hollow-fiber filtration modules are made of polyether sulfone (PES) with molecular weight cut off (MWCO) of 100 kDa, corresponding to a 20 nm pore size. The permeate stream presents a perpendicular direction across the membrane and a constant flow (3.3 m³/h) throughout the process. The estimated filtration rate through the membrane was 41.25 L/m²h taking into account that the effective membrane area was 80.0 m². The operation procedure includes the sequential washing of each filtration module, such that the other three modules are working meanwhile. A 9 min. washing was programmed after each filtration period of 47 min, when the transmembrane pressure reaches the value of 0.6 bar, and consists of three phases: flushing, backwashing, and rinsing. The feed pressure starts at 1.5 bar and rises to 2.3 bar at the end of the filtering period, just before the washing period starts.

2.2. Sampling Method

Analyzed samples were collected after primary, secondary, and tertiary treatments. Figure 1 schematically shows the entire water treatment process in the WWTP and the different sampling points selected. Different samples (BIO influent, UF influent, and UF effluent samples) used in this work were named according to this figure.

Composite grab samples of 1.5L were collected, on three randomly selected days (in triplicate) of October 2018. Each day, samples at 4 different hours (9:00, 10:00, 11:00, and 12:00am) were taken, and each 1.5 L hour sample was formed by three 500 mL subsamples taken every 5 min around the corresponding hour. Figure 1 shows the treatment units of the WWTP with the sampling points.

Corresponding UF influent samples were taken considering the hydraulic retention times in the aeration ponds and in the secondary settlers of the WWTP. Retention times fluctuated between 28 and 38 h, depending on the flow rate of treated wastewater. All samples were immediately frozen to preserve them until the analysis was performed. Samples were collected in prewashed amber glass bottles and transported to the laboratory in cooled boxes (4 °C). Samples were filtered through a 1.2 µm glass microfiber filter (GE Whatman, Maidstone, UK), and kept in the fridge at −4 °C before analysis. The analyses were performed within 24 h of sampling.

The ammonium concentration was obtained from the online monitoring system of the facility at the entrance of the biological process influent with measurements every 15 minutes, according to

ISO 7 150-2 (1986), Water quality—Determination of ammonium—Part 2: Automated spectrometric method [34]. Ammonia is related to human activities and oxygen present in wastewater and, therefore lead to an increase in CEC, mostly pharmaceuticals, excreted by people. Bicudo et al. analyzed the presence of pharmaceutical CEC, such as acetaminophen or valsartan, to human activity through monitoring of ammonia in the influent of a WWTP in Grand River watershed. As in this study, they found no relationship between ammonium concentrations and CEC [35].

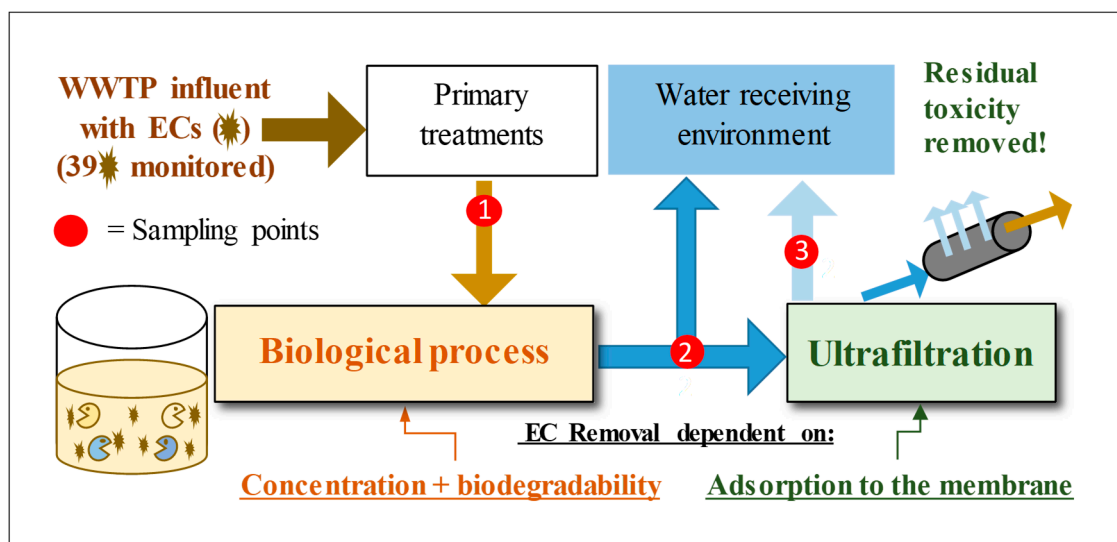


Figure 1. Scheme of the assembly of the different treatments in this work with specification of sampling points: biological process (BIO) influent (1), ultrafiltration (UF) influent (2) and UF effluent (3).

2.3. Analytical Method and Method Assurance

Water samples were analyzed in triplicate as one of the methods described by Mijangos et al. [36]. In this case, attending to the frequency at which compounds appeared and their concentration, 39 of the 41 compounds determined in that work were selected, which are listed in Table 1.

The applied method's quality parameters, including extraction recoveries and method limits of quantification, were evaluated elsewhere [33]. The analysis of the samples is briefly described, as follows. First, 100 mL of each sample was filtered through 1.2 μm glass fiber filters (GE Whatman, Maidstone, UK), and then 4.25 mL of Na_2EDTA (0.2 M) and 0.8 mL of a solution containing formic acid were added ($\text{pH} = 2$).

The compounds were loaded at a constant flow of 5 mL/min into a solid phase extraction (SPE) cartridge (OASIS-HLB, hydrophilic-lipophilic-balanced, 200 mg, Waters, Milford, USA) previously conditioned with 5 mL of methanol (MeOH), 5 mL of Milli-Q (MQ), and 5 mL of acidified MQ ($\text{pH} = 2$). After the samples were loaded, the cartridges were rinsed with 6 mL of MQ to remove the impurities, and the cartridges were vacuum dried for an hour. Methanol (6 mL) was used to elute the target analytes from the cartridges, and the extract was evaporated at 35 $^\circ\text{C}$ under a gentle stream of N_2 . Finally, samples were reconstituted in 200 μL of MeOH:MQ (30:70, v:v) and filtered using 0.22 μm polypropylene filters (PP, 0.22 μm , 13 mm, Phenomenex, Torrance, CA, USA), before liquid chromatography–tandem mass spectrometry (LC–MS/MS) analysis was performed [33].

Table 1. Name, CAS Registry Number and principal use of the 39 contaminants of emerging concern (CEC) studied [37].

Application	Micropollutant	CAS Registry Number	Properties of Concern (European Chemicals Agency, ECHA)
<i>Food additives</i>	Acesulfame	55589-62-3	—
	Caffeine	58-08-2	—
	Methylparaben	99-76-3	Possibly endocrine disrupting
	Sucralose	56038-13-2	—
<i>Herbicides</i>	Atrazine	1912-24-9	Skin sensitizing
	Diuron	330-54-1	Possibly carcinogenic Possibly endocrine disrupting Substance included in the Community Rolling Action Plan (CoRAP)
	Isoproturon	34123-59-6	Possibly carcinogenic
	Simasine	122-34-9	Possibly carcinogenic
<i>Industrial additives</i>	2-hydroxybenzothiazole	934-34-9	—
	Perfluorooctanesulfonamide (PFOSA)	754-91-6	—
	Perfluoro-n-nonanoic acid (PFNA)	375-95-1	Possibly carcinogenic Toxic to reproduction Persistent, bioaccumulative and toxic Substance of very high concern (SVHC) and included in the candidate list
	Potassium nonafluoro-1-butanefulfonate	29420-49-3	—
	Potassium perfluoro-1-octanesulfonate (PFOS)	2795-39-3	Possibly carcinogenic Toxic to reproduction

Table 1. Cont.

Application	Micropollutant	CAS Registry Number	Properties of Concern (European Chemicals Agency, ECHA)
<i>Medicaments</i>			
	Acetaminophen	103-90-2	—
	Amitriptyline hydrochloride	549-18-8	Skin sensitizing Respiratory sensitizing
	Bezafibrate	41859-67-0	—
	Carbamazepine	298-46-4	Skin sensitizing Respiratory sensitizing
	Ciprofloxacin	85721-33-1	—
	Clofibric acid	882-09-7	—
	Diclofenac	15307-86-5	—
	Eprosartan mesylate	144143-96-4	—
	Genistein	446-72-0	—
	Genistin	529-59-9	—
	Glycitin	40246-10-4	—
	Imipramine	50-49-7	—
	Irbesartan	138402-11-6	Toxic to reproduction
	Ketoprofen	22071-15-4	—
	Losartan Free Acid	114798-26-4	Toxic to reproduction Skin sensitizing
	Norfloxacin	70458-96-7	—
	Phenytoin	57-41-0	—
	Progesterone	57-83-0	Carcinogenic Toxic to reproduction
	Propranolol	525-66-6	—
	Sulfadiazine	68-35-9	Skin sensitizing Respiratory sensitising
	Sulfamethoxazole	723-46-6	Carcinogenic Skin sensitizing
	Telmisartan	144701-48-4	—
	Testosterone	58-22-0	—
	Trimethoprim	738-70-5	—
	Valsartan	137862-53-4	—
<i>Personal Care</i>			
	Butylparaben	94-26-8	—

The LC–MS/MS analysis was performed using an Agilent 1260 series HPLC chromatograph equipped with a degasser, binary pump, autosampler, and column oven, and coupled to an Agilent 6430 triple quadrupole (QqQ) mass spectrometer equipped with an electrospray ionization (ESI) source (Agilent Technologies, Palo Alto, CA, USA). The separation of the target analytes was carried out using a Kinetex F5 100 Å core-shell 2.1 mm × 100 mm, with a 2.6 µm column coupled to a Kinetex F5 pre-column 2.1 mm × 4.6 mm, 2.6 µm (Phenomenex, Torrance, 235 CA, USA). Then, 10 µL of sample was injected into the system and the column was maintained at 35 °C during the chromatographic run.

The separation was performed at a constant flow of 0.3 mL/min. under gradient elution with a binary mixture consisting of: water:MeOH (95:5, v:v) (mobile phase A) and MeOH:water (95:5, v:v) (mobile phase B), both containing 0.1% formic acid. The gradient profile started with 30% B, which was increased to 50% after 4 min and maintained for 12 min. Then, it was increased to 90% B, where it was maintained for 10 min. Initial gradient conditions (30% B) were then achieved in 6 min., where it was finally held for another 10 min (post-run step).

Electrospray ionization was carried out using a N₂ flow rate of 12 L/min, a capillary voltage of 3500 V, a nebulizer pressure of 45 psi, and a source temperature of 350 °C.

Quantification was performed in the selected reaction monitoring (SRM) acquisition mode by recording the three most intense transitions for each analyte (the most sensitive transition was chosen as the quantifier and the second and third ones as qualifiers) where possible. Both voltages, according to the target analytes, were simultaneously applied in a single injection.

In order to assess the toxicity levels of UF influent and effluent samples Microtox[®] toxicity bioassays were performed. The measurements were carried out according to ISO 11348-3 (1998), Water Quality—Determination of the inhibitory effect of water samples on the light emission of *Vibrio fischeri* (Luminescent bacteria test)—Part 3: Method using freeze-dried bacteria [34]. The results of this assay are usually expressed as EC₅₀, which represents the percentage of sample dilution (% v/v) that causes a 50% reduction in bacteria luminescence after 15 min of exposure. Consequently, the toxicity units (TU₅₀ = 100/EC₅₀) were used in this study to express the toxicity [38]. All the tests were carried out in duplicate in a Microtox[®] toxicity analyzer, Azur 500 model (Microbics Corp., New Castle, Delaware, USA).

3. Results and Discussion

3.1. Relationship Between Ammonium Concentration and Emerging Contaminants Concentration

In the first step of the study, time profiles of ammonium and CEC concentrations arriving at the WWTP were studied and compared. The concentration of the major CEC (those above 1 ng/L) in the influent of the biological treatment is shown in Table 2. As has been reported by Luo et al. [9], most emergent contaminants are typically found between 0.1 and 10 µg/L, and some, such as acetaminophen and caffeine, show much higher levels. On the contrary, concentrations below 1 ng/L were found for the following microcontaminants: atrazine, butylparaben, clofibric acid, genistin, glycitin, imipramine, perfluoro-n-nonanoic acid, potassium perfluoro-1-octanesulfonate, potassium nonafluoro-1-butanesulfonate, simasine, sucralose and sulfadiazine. Therefore, these minor components were not taken into account in the study.

Table 2. CEC analyzed at different hours in the influent of the biological treatment.

Micropollutant	Concentration (ng/L)			
	H1	H2	H3	H4
Acetaminophen	50,421 ± 3460	48,352 ± 1919	54,557 ± 1040	112,762 ± 4788
Caffeine	21,493 ± 1350	18,835 ± 382	16,047 ± 655	31,704 ± 1309
Valsartan	17,340 ± 245	10,072 ± 1220	12,143 ± 120	30,979 ± 1499
Sulfamethoxazole	8828 ± 119	2189 ± 62	135 ± 1	283 ± 4
Trimethoprim	5581 ± 116	851 ± 2	76 ± 1	82 ± 1
Methylparaben	5139 ± 119	2937 ± 100	2094 ± 67	8400 ± 250
Acesulfame	5041 ± 581	4102 ± 181	5851 ± 332	25,092 ± 1808
Losartan free acid	1267 ± 38	917 ± 168	1056 ± 4	1723 ± 125
Genistein	1191 ± 33	1198 ± 208	739 ± 97	1184 ± 131
Eprosartan mesylate	1049 ± 10	799 ± 108	874 ± 29	1588 ± 94
Ketoprofen	865 ± 99	643 ± 27	579 ± 42	1117 ± 86
Irbesartan	829 ± 4	714 ± 61	822 ± 24	1070 ± 42
Diclofenac	766 ± 18	692 ± 10	582 ± 17	458 ± 10
Telmisartan	593 ± 1	704 ± 30	1386 ± 129	1476 ± 67
Norfloxacin	452 ± 3	363 ± 5	233 ± 15	365 ± 10
2-hydroxybenzothiazole	422 ± 9	240 ± 3	219 ± 27	271 ± 14
Progesterone	243 ± 8	205 ± 1	—	276 ± 33
Bezafibrate	207 ± 5	199 ± 10	272 ± 18	474 ± 22
Perfluorosulfonamide	203 ± 11	148 ± 22	196 ± 12	302 ± 27
Diuron	174 ± 1	147 ± 8	57 ± 1	76 ± 2
Carbamazepine	116 ± 1	86 ± 2	90 ± 2	120 ± 2
Testosterone	107 ± 4	74 ± 7	61 ± 2	101 ± 6
Ciprofloxacin	79 ± 5	63 ± 2	51 ± 1	69 ± 3
Amitriptyline	68 ± 1	68 ± 2	71 ± 3	112 ± 3
Phenytoin	45 ± 2	41 ± 1	36 ± 6	49 ± 4
Propranolol	24 ± 1	23 ± 5	23 ± 2	17 ± 2
Isoproturon	3 ± 1	2 ± 1	2 ± 1	2 ± 1

Sampling hour at H1—(9:00 am); H2—(10:00 am); H3—(11:00 am); and, H4—(12:00 am).

Ammonium concentration levels varied between 27.6 and 55.2 g/m³ in the different analysis days. As can be seen in Figure 2a, the ammonium content steadily increased with increasing sampling time, probably because of the increasing levels of human activities throughout the morning.

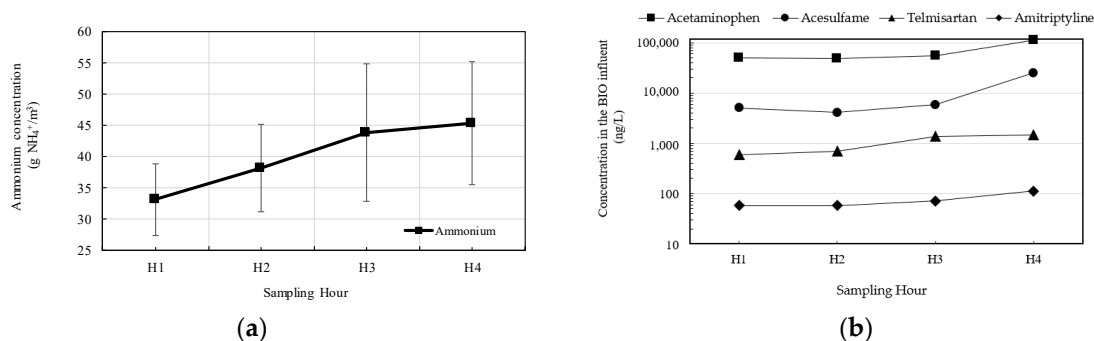


Figure 2. Concentration in the influent of the biological treatment at the different sampling hours of: (a) Ammonium; (b) certain representative emerging pollutants.

In the case of CEC (as shown in Table 2), some of them, such as acetaminophen, acesulfame, telmisartan, and amitriptyline, followed a pattern close to that of ammonium (Figure 2b—increasing their concentration as noon approached). This was also the case for other CEC, such as bezafibrate, eprosartan mesylate, and valsartan. Nevertheless, other CEC, such as diclofenac and diuron, showed the opposite tendency. However, most of them, such as testosterone and ciprofloxacin, showed a

random pattern. Therefore, according to our results, CEC concentration variation in wastewaters cannot be related to ammonium concentration.

3.2. Removal Yields of Emerging Contaminants with the Biological Treatment

Removal rates achieved with the biological treatment for each of the CEC were calculated taking into account the concentration (mean and standard deviation) at the influent and the effluent of the treatment. From all the CEC, 2-hydroxybenzothiazole, ketoprofen, telmisartan, and valsartan have been chosen as representatives of the different behaviors, and the variation of their removal rates for each sampling hour is shown in Figure 3a. As can be seen, ketoprofen and valsartan showed high removal ratios in all hour samples. However, 2-hydroxybenzothiazole and telmisartan, showed lower values of removal efficiency with higher variability.

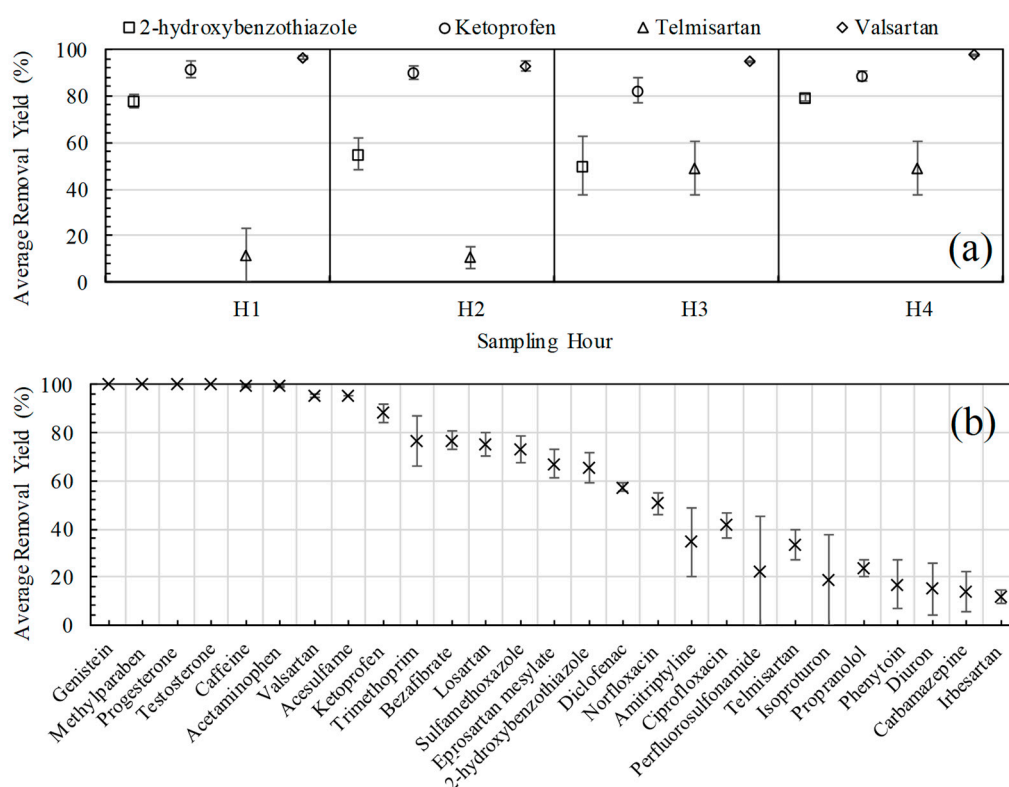


Figure 3. Average removal rates in the biological treatment for: (a) Four representative emerging pollutants at different hours; and (b) every emerging pollutant (with all samples).

As Figure 3b shows, in general, compounds showing a removal higher than 80% maintained approximately constant values in all hour samples. On the contrary, those having intermediate and low removal percentages displayed higher variability. These results seem to indicate a certain variability in removal rates, which could be explained by taking into account factors such as CEC concentration and biodegradability.

When removal rates are analysed in relation to the concentration values at the influent of the biological treatment (Table 2), a partial dependence can be observed, probably for kinetic reasons. In fact, solutions with concentrations higher than 1500 ng/L yielded, in all cases, efficiencies above 80.0%, except for the case of sulfamethoxazole in H2. This was the case of acesulfame, acetaminophen, caffeine, methylparaben, and valsartan at all hours, and of eprosartan mesylate, sulfamethoxazole, and trimethoprim only at the hours with a proper concentration. Higher variation of efficiency was observed for most compounds.

Mean removal efficiencies for all CEC under biological treatment are shown in Figure 3b. As can be seen in this treatment, genistein, methylparaben, progesterone, and testosterone were completely removed, and caffeine and acetaminophen showed removal percentages higher than 99.5%. Contrarily, irbesartan and carbamazepine presented the lowest removal ratios, with maximum values of 15.0% and 22.0%, respectively. Two special cases were perfluorosulfonamide and isoproturon, which, in some cases, were not eliminated at all.

It can also be observed that the efficiency of some CEC is higher depending on the targeted compound, their biodegradation, and adsorption onto activated sludge [39]. In fact, acesulfame, acetaminophen, caffeine, genistein, methylparaben, progesterone, testosterone, and valsartan showed efficiencies higher than 93.0% at all the hours, and ketoprofen had an efficiency that was higher than 82.0%. Of them, genistein, progesterone, testosterone, and ketoprofen are remarkable, as their concentration was lower than 1500 ng/L. In the rest of the analytes, in general, displayed efficiencies lower than 84.0%, and the variation in the removal rate with the sampling hour was much higher. This higher variability of the rates with lower efficiencies could be due to the higher difficulty for the degradation of compounds with less biodegradability and at lower concentrations.

These results are generally in agreement with those obtained in the literature. For example, poor removal levels of carbamazepine (23.1%) in combination with high removal of acetaminophen (99.9%), caffeine (99.2%), and ketoprofen (94.2%), medium–high of diclofenac (81.4%) and trimethoprim (69.0%), and medium–low of sulfamethoxazole have been found in different biological-based WWTPs [40], as in this study. Similarly, in other works, evidence of the poor removal rate of carbamazepine [3,41] and the high degradability of acetaminophen [42,43] and caffeine or medium–high degradability of trimethoprim has been found [44].

3.3. Removal Yields of Emerging Contaminants with UF Treatment

After biological treatment, effluent was submitted to c-ultrafiltration. Figure 4a shows removal rates with this treatment for the same emerging contaminants depicted in Figure 3a. Figure 4b shows the average efficiencies obtained with ultrafiltration for all the CEC.

As can be seen, the efficiencies achieved with ultrafiltration treatment were below 50.0% in almost all cases, except for amitriptyline (63.0%), and were systematically lower than those obtained with biological treatment. In addition to this, it is worth noting that the efficiencies were more stable throughout the day, though higher deviations were observed in the replicated measurements, probably due to the low removal rates achieved (high difficulty of the removal).

According to the literature, the predominant driving mechanism in UF is adsorption [45,46], and not size-exclusion due to the relatively large pore size. Therefore, the extent of the retention of the different compounds is related to the higher or lower affinity of each compound for the membrane. Nevertheless, it should be emphasized that, in general, ultrafiltration retention efficiency is not very high. For example, according to a reporting study [45], retention coefficients by different UF membranes were tested—obtaining average values below 50.0%. In addition, in other works, most of the compounds showed retention lower than 30.0% in the UF membrane [46].

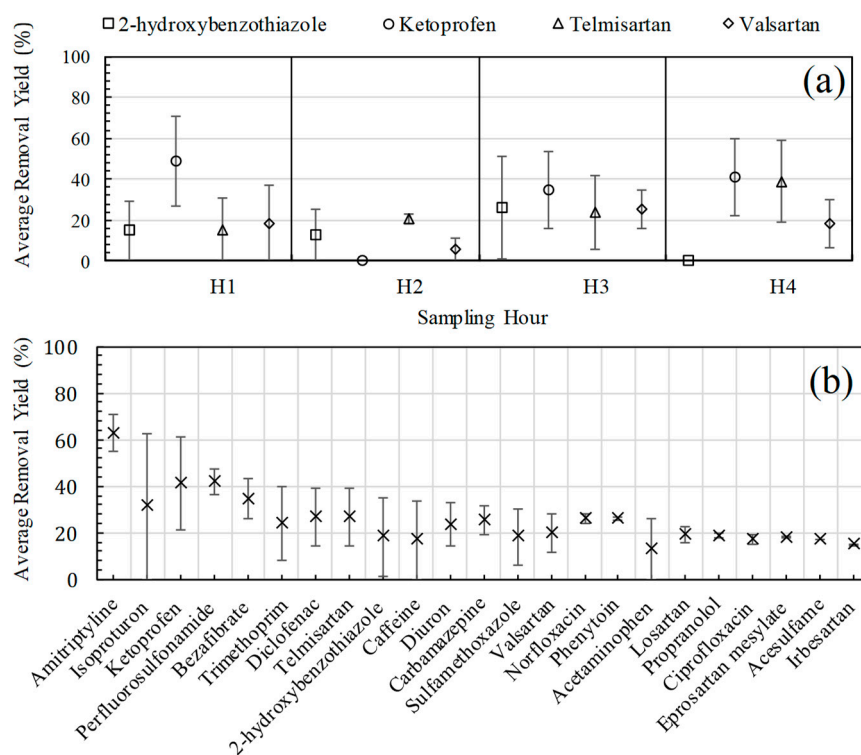


Figure 4. Average removal rates in continuous ultrafiltration (c-UF) treatment for: (a) Four selected emerging pollutants at different hours; (b) every emerging pollutant (with all samples).

3.4. Removal Yields and Adsorption Phenomena in UF Treatment

Figure 5 shows the removal rates of the 18 CEC detected versus permeate concentration during c-UF in the treated effluent, showing a specific behaviour that could be associated to adsorption phenomena. The concentration variability observed for each contaminant at the ultrafiltration inlet depends not only on the concentration, but also on its biodegradability and the adsorption equilibrium on the surface of the membrane, as will be studied below in detail. Thus, many of those contaminants that are emerging in Figure 5a are contaminants with high biodegradability; those in Figure 5c presented high concentration variability in the biological entrance; those in Figure 5b presented intermediate values of concentration and biodegradability. Examples of CEC with extreme variation in concentration are caffeine, with a low concentration (≈ 50 ng/L), and trimethoprim, with a high concentration (≈ 500 ng/L). Both compounds presented removal rates of about 30.0%, but a sharp decrease of the average yields, beneath 0.1%, was observed at extreme concentration values. This was an extended behavior in many of the emerging contaminants shown in Figure 5. Thus, one can mention, among those of great variability—ketoprofen, 2-hydroxybenzothiazole, bezafibrate, carbamazepine and phenytoin—and those with medium concentration—valsartan, perfluorosulfonamide, eprosartan mesylate and losartan. Although showing different removal yields at their respective medium–high concentrations, at low concentrations, all these contaminants presented removal rates below 0.1%. On the other hand, in all compounds with high concentration variability—shown in Figure 5c—removal rates below 0.1% were found both at high and low concentrations (extreme values).

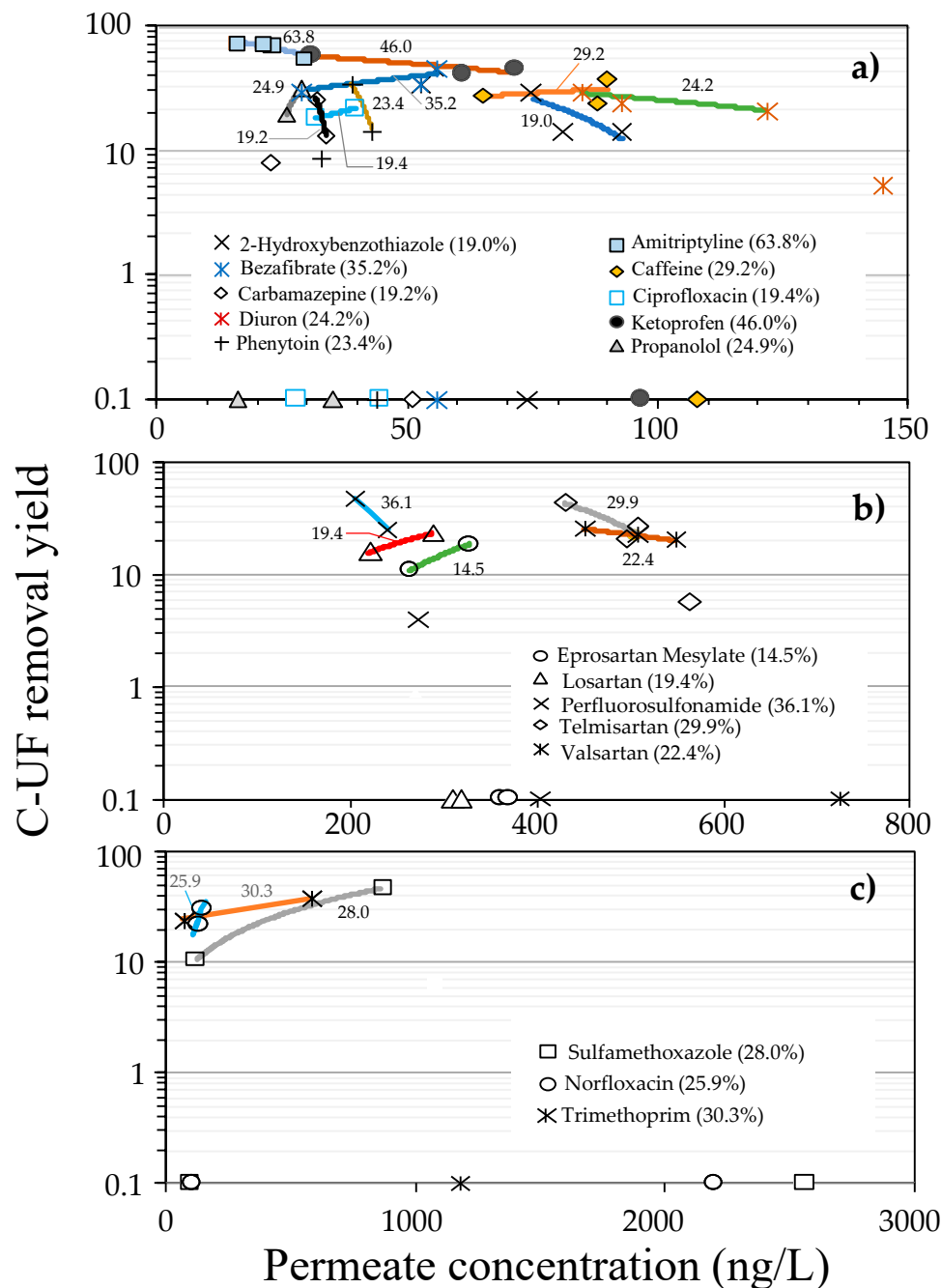


Figure 5. c-UF removal yields as a function of the permeate concentration for the emerging contaminants studied at: (a) low-, (b) medium-, and (c) high-concentration variability. Percentage average yields (values higher 10%) of each pollutant are given in brackets in the insets of the graphs. Values in the lower part of the graph correspond to yields below 0.1%.

This special behavior, observed in most emerging contaminants analyzed in c-UF, seems to be explained by adsorption phenomena [47]. Corresponding equilibria of different compounds could be affected by the organic matter present at the entrance of the UF. Nevertheless, the buffering effect of the biological process leads to similar organic matter content concentration and characteristics of organic matter at the outlet. Consequently, the effect on the balance of different CEC is negligible.

After analyzing the removal yields, it is deduced that the maximum removal rate, once filtered, lies within the middle values, within the variability of each contaminant. In such cases, a good recovery of the filter material after washing is deduced. The retention capacity for a contaminant can be defined

by the corresponding equilibrium adsorbed amount, q_{∞} (ng/g f.m.), which depends on the contaminant concentration in contact with the filter material, according to the Freundlich adsorption isotherm:

$$K_F = \frac{q_{\infty}}{C_e^{1/n_F}} \quad (1)$$

where C_e (ng/L) is the equilibrium concentration and K_F (ng/g) (L/ng) n_F is the Freundlich constant corresponding to a given contaminant and adsorbent material, when $n_F = 1$. For many compounds at low concentrations, as in the emerging compounds, the heterogeneity factor, n_F , is one [48].

Moreover, the duration of the filtration stage in the tests reported here was 47 min. For these times, it can be assumed that the retained load, q_{tf} , at the end of the filtration period, is in equilibrium with the contaminant concentration at the c-UF output (permeate). Consequently, $q_{tf} \approx q_{\infty}$, and is, therefore, in equilibrium with the output concentration, $C_p = C_e$. In this way, the K_F constant can be derived from:

$$q_{tf} = \frac{\eta \times C_0 \times Q \times t_f}{M_F} \quad (2)$$

$$K_F = \frac{q_{\infty}}{C_e}; \frac{q_{tf}}{C_p} \quad (3)$$

Equation (2) relates the removal yield (η) to q_{tf} , with M_F (g) being the ultrafiltration membrane mass used to treat a flow Q (L/min), in which C_0 (ng/L) is the input concentration for a certain CEC. Under certain conditions, also serves to estimate the retention capacity in equilibrium, q_{∞} . In other words, Equation (3) is assumable, as long as the adsorption capacity is maintained at the maximum value; that is, q_{∞} does not decrease and the adsorption kinetics, k_{ads} (g(ng min) $^{-1}$), are sufficiently fast. In principle, these circumstances would occur for the highest removal rate observed in each contaminant. In this case, the corresponding q_{tf} is assimilable to q_{∞} .

An estimation of the adsorption constant can be made by considering a pseudo-second order kinetics:

$$\frac{dq_{tf}}{dt_f} = k_{ads} \times (q_{\infty} - q_{tf})^2 \quad (4)$$

$$\frac{t_f}{q_{tf}} = \frac{1}{k_{ads} \times q_{\infty}^2} + \frac{t_f}{q_{\infty}} \quad (5)$$

Equation (5) enables the amount of contaminant retained during filtration to be determined. Solving for a time $t_f = 47$ min (filtration period), the q_{tf} value is obtained that should coincide with the experimental one from Equation (2). In the case of a low removal yield, the experimental q_{tf} values can be explained through Equation (5), because of the q_{∞} reduction to a lower effective value, q_{∞}^* ($= q_{\infty} - q_{irr}$), depending on the filtration conditions. This value tends to be zero at the extreme concentration values, within the variation range of each CEC. Table 3 shows the values of the adsorption parameters estimated from the retention observed for each compound. Diuron and caffeine were selected among the low-concentration CEC, telmisartan and losartan among those of medium concentration, and sulfamethoxazole and trimethoprim among those of high concentration. The q_{irr} value represents the amount irreversibly retained in the filtration membrane and not removed during washing, causing fouling [25]. In general, q_{irr} approaches q_{∞} at extreme values (high and/or low), leading to a low removal yield.

Table 3. Adsorption parameters of the c-UF filtration membrane, depending on the concentration, for selected pollutants.

Micropollutant	C_0 , ng/L	η , %	C_P , ng/L	K_F , (ng/g) (L/ng) ^{n_F}	q_{∞} , ng/g	k_{ads} , g (ng min) ⁻¹	q_{irr} , ng/g	q_{∞}^* , ng/g	F_q
<i>Amitriptyline</i>									
	51	68.6	16	2.40×10^{-1}	3.8	11.9	0.0	3.8	0.000
	68	67.6	22	2.40×10^{-1}	5.3	11.9	0.2	5.0	0.044
	69	66.7	23	2.40×10^{-1}	5.5	11.9	0.5	5.0	0.086
	63	52.4	30	2.40×10^{-1}	7.2	11.9	3.6	3.6	0.497
<i>Caffeine</i>									
	90	27.0	65.5	6.80×10^{-2}	4.5	0.295	1.7	2.8	0.385
	116	24.0	88	6.80×10^{-2}	6.0	0.295	2.9	3.2	0.476
	107	0.1	107	6.80×10^{-2}	7.3	0.295	7.3	0.0	0.996
	145	38.0	90	6.80×10^{-2}	6.2	0.295	0.0	6.1	0.006
<i>Telmisartan</i>									
	597	5.7	563	8.15×10^{-2}	45.9	0.350	42.1	3.8	0.917
	627	20.7	497	8.15×10^{-2}	40.5	0.350	26.2	14.3	0.647
	690	26.2	509	8.15×10^{-2}	41.5	0.350	21.6	19.9	0.520
	749	42.6	430	8.15×10^{-2}	35.0	0.350	0.0	35.0	0.000
<i>Losartan</i>									
	262	15.6	221	3.40×10^{-2}	7.5	0.085	2.8	4.7	0.370
	375	23.2	288	3.40×10^{-2}	9.8	0.085	0.0	9.8	0.001
	309	0.1	309	3.40×10^{-2}	10.5	0.085	10.4	0.1	0.989
	320	0.1	320	3.40×10^{-2}	10.9	0.085	10.8	0.1	0.990
<i>Norfloxacin</i>									
	106	0.1	106	4.90×10^{-2}	5.2	0.056	5.1	0.1	0.986
	163	22.1	127	4.90×10^{-2}	6.2	0.056	1.9	4.3	0.309
	205	29.8	144	4.90×10^{-2}	7.1	0.056	0.0	7.1	0.001
	2203	0.1	2201	4.90×10^{-2}	107.8	0.056	107.4	0.4	0.996
<i>Sulfamethoxazole</i>									
	92	0.1	92	9.30×10^{-2}	8.6	0.056	8.5	0.1	0.992
	137	10.2	123	9.30×10^{-2}	11.4	0.056	9.6	1.9	0.838
	1608	45.8	872	9.30×10^{-2}	81.1	0.056	0.0	81.1	0.000
	2573	0.1	2570	9.30×10^{-2}	239.0	0.056	238.5	0.5	0.998

C_0 —pollutant initial concentration; η —removal yield; C_P —pollutant output concentration; K_F —Freundlich constant; q_{∞} —equilibrium adsorbed amount; k_{ads} —pseudo-second-order rate constant of adsorption; q_{irr} —amount of adsorbed contaminant not eliminable; F_q —fouling factor.

A fouling factor, F_q , was defined for each component by the ratio of adsorbed contaminant, not eliminable or irreversible, q_{irr} , to the original adsorption capacity, q_{∞} , according to Equation (6):

$$F_q = \frac{q_{irr}}{q_{\infty}} \quad (6)$$

In Table 3, the variability of the removal yields with the concentration for some selected compounds are shown.

The highest removal yields correspond to situations with a fouling factor, F_q , close to zero. Thus, for each compound, the greatest removal yields correspond to situations, with a fouling factor, F_q , close to zero. In Figure 6, the retention capacity in equilibrium has been represented, according to Equation (3), for three representative compounds, of low (amitriptyline), medium (losartan), and high concentration (sulfamethoxazole). As explained above, q_{∞} is composed of a reversible part q_{∞}^* (white area below q_{∞} profile in Figure 6) which is removed by washing, after each filtration period, and another irreversible part or fouling, q_{irr} (shaded area). As q_{irr} approaches q_{∞} , it will be more difficult to recover the adsorption capacity after each cycle.

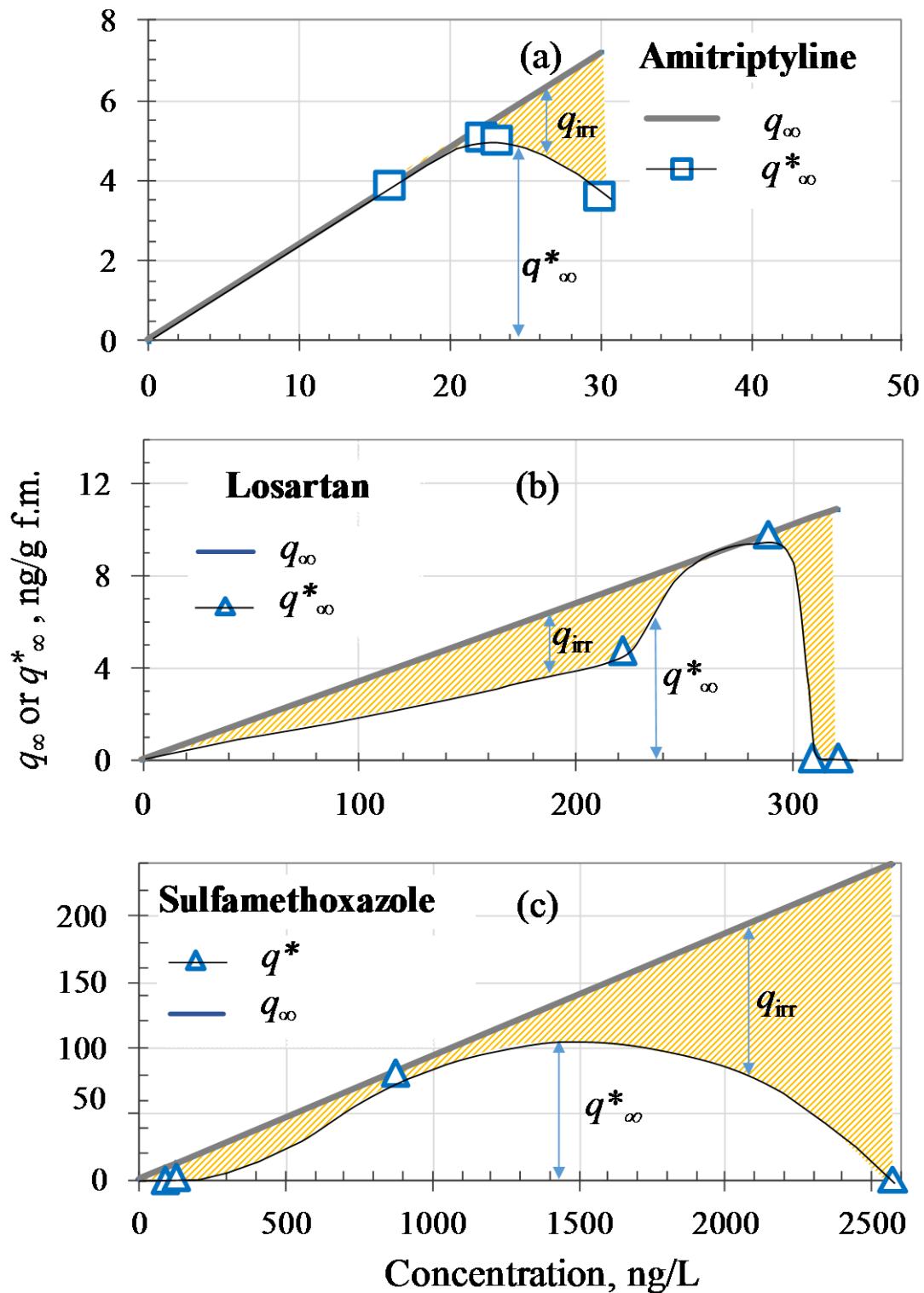


Figure 6. Variation of the equilibrium adsorption capacity: original (q_{∞}) and effective (q_{∞}^*), depending on the concentration for three selected CEC: (a) amitriptyline, (b) losartan, and (c) sulfamethoxazole.

Consequently, highest removal yields will occur as q_{∞}^* approaches q_{∞} . These favourable situations correspond to intermediate concentrations represented in Figure 6 by a large white area beneath the q_{∞} line, whereas q_{irr} (shaded area) is negligible. This concentration range of high removal yields can be more or less centred depending on the compound. Thus, losartan and sulfamethoxazole present

similar situations, whereas in the case of amitriptyline, the highest elimination yields correspond to the lowest concentrations.

3.5. Toxicity Test

The results (mean and standard deviation of three replicates) of the Microtox[®] assay in both the input and output of the c-UF plant, at each hour, are summarized in Table 4.

Table 4. Results of the Microtox[®] toxicity assays obtained in the influent and in the effluent of the c-UF treatment.

UF Influent		UF Effluent	
Sampling Hour	TU ₅₀	Sampling Hour	TU ₅₀
H1	27.0 (± 5.2)	H1	< 1 (Not Toxic)
H2	51.7 (± 12.8)	H2	< 1 (Not Toxic)
H3	11.1 (± 4.5)	H3	< 1 (Not Toxic)
H4	38.2 (± 7.4)	H4	< 1 (Not Toxic)

It is well known that UF removes mainly suspended solids and bacteria but also has significant efficiency in terms of toxicity removal, because it removes the low toxicity of the biological effluent (see Table 4); local discharge legislation establishes nontoxic effluents when TU₅₀ values are below 50. Moreover, part of CEC, as seen before, are also removed although this is not clearly related to the decrease of toxicity. Consequently, most of the toxicity may be due to non-measured contaminants or to only a part of the measured ones. Deeper experiments beyond the scope of this work would be necessary to clarify this aspect.

4. Conclusions

In this work, the removal of 39 high-occurrence CEC by the biological treatment of a WWTP and by a c-UF plant installed in its effluent was studied.

First, the time profile of the CEC concentration in the influent of the biological treatment was compared to the profile of ammonium and no significant relationships were obtained for most (75.0%) of the CEC.

In the case of the biological treatment, the removal rate of the CEC was dependent on the concentration and nature of each compound due to specific degradation biokinetics and biodegradability of the different compounds, respectively. Related to this, genistein, methylparaben, progesterone, testosterone, caffeine, and acetaminophen showed removal efficiencies above 99.5%. In contrast, irbesartan, carbamazepine, diuron, and phenytoin showed average removal rates below 20.0%. In addition, solutions with a higher concentration of CEC (above 1500 ng/L) presented high efficiencies above 80.0% in almost all cases.

In the case of ultrafiltration, removal rates were not higher than 30.0% in most cases, except for the case of amitriptyline, which reached 63.0%. In general, a strong variability of the removal rate with concentration was observed in all CEC. Low removal yields observed at low and/or high concentrations could be explained by fouling, or irreversibly adsorbed material on the filtration membrane.

Moreover, the Microtox[®] toxicity tests revealed that c-UF efficiently reduces the toxicity of the secondary effluent (biological). However, because of the complexity of this matter, beyond the scope of this work, the identification of responsible CEC for toxicity could not be found.

As a general conclusion, biological treatment complemented with c-UF allows a higher efficiency in removing CEC than the biological process alone. Nevertheless, ultrafiltration can be satisfactorily used as a tertiary treatment in order to help remove the small residual toxicity in the last WWTP stream.

5. Patents

The c-UF system used in this work has been patented in Spain under patent number ES201431341A.

Author Contributions: Conceptualization, J.I.L.; methodology and analyses, J.I.L. and O.R.; model validation, A.d.L. and N.V.; formal analysis, I.G.-M.; investigation, I.G.-M.; original draft preparation, A.d.L. and C.F.; review and editing, C.F. and N.V.; supervised the experimentation, N.E.; acquired the funding, J.I.L. and N.E. All authors have read and agreed to the published version of the manuscript

Funding: The authors are grateful to the University of the Basque Country for their financial support of this study through the PPGA19/63 and UFI 11/39 projects, and C. Ferreiro's predoctoral PIF grant (PIF16/367).

Acknowledgments: The authors also wish to acknowledge the assistance of Fluytec S.A. with a c-UF unit of its own for this study.

Conflicts of Interest: The authors declare no conflict of interest.

References

1. Chávez, A.M.; Ribeiro, A.R.; Moreira, N.F.F.; Silva, A.M.T.; Rey, A.; Álvarez, P.M.; Beltrán, F.J. Removal of Organic Micropollutants from a Municipal Wastewater Secondary Effluent by UVA-LED Photocatalytic Ozonation. *Catalysts* **2019**, *9*, 472. [CrossRef]
2. Lopera, A.E.C.; Ruiz, S.G.; Alonso, J.M.Q. Removal of emerging contaminants from wastewater using reverse osmosis for its subsequent reuse: Pilot plant. *J. Water Process. Eng.* **2019**, *29*, 100800. [CrossRef]
3. Gros, M.; Petrovic, M.; Barceló, D. Analysis of Emerging Contaminants of Municipal and Industrial Origin. In *Emerging Contaminants from Industrial and Municipal Waste: Occurrence, Analysis and Effects*; Barceló, D., Petrovic, M., Eds.; The Handbook of Environmental Chemistry; Springer: Berlin/Heidelberg, Germany, 2008; pp. 37–104. ISBN 978-3-540-74795-6.
4. Quiñones, D.H.; Álvarez, P.M.; Rey, A.; Beltrán, F.J. Removal of emerging contaminants from municipal WWTP secondary effluents by solar photocatalytic ozonation—A pilot-scale study. *Sep. Purif. Technol.* **2015**, *149*, 132–139. [CrossRef]
5. Tran, N.H.; Reinhard, M.; Gin, K.Y.H. Occurrence and fate of emerging contaminants in municipal wastewater treatment plants from different geographical regions—A review. *Water Res.* **2018**, *133*, 182–207. [CrossRef] [PubMed]
6. Prasse, C.; Stalter, D.; Schulte-Oehlmann, U.; Oehlmann, J.; Ternes, T.A. Spoilt for choice: A critical review on the chemical and biological assessment of current wastewater treatment technologies. *Water Res.* **2015**, *87*, 237–270. [CrossRef] [PubMed]
7. Montes-Grajales, D.; Fennix-Agudelo, M.; Miranda-Castro, W. Occurrence of personal care products as emerging chemicals of concern in water resources: A review. *Sci. Total Environ.* **2017**, *595*, 601–614. [CrossRef]
8. Pereira, L.C.; De Souza, A.O.; Bernardes, M.F.F.; Pazin, M.; Tasso, M.J.; Pereira, P.H.; Dorta, D.J. A perspective on the potential risks of emerging contaminants to human and environmental health. *Environ. Sci. Pollut. Res.* **2015**, *22*, 13800–13823. [CrossRef]
9. Luo, Y.L.; Guo, W.S.; Ngo, H.H.; Nghiem, L.D.; Hai, F.I.; Zhang, J.; Liang, S.; Wang, X.C. A review on the occurrence of micropollutants in the aquatic environment and their fate and removal during wastewater treatment. *Sci. Total Environ.* **2014**, *473*, 619–641. [CrossRef]
10. Vulliet, E.; Cren-Olive, C.; Grenier-Loustalot, M.F. Occurrence of pharmaceuticals and hormones in drinking water treated from surface waters. *Environ. Chem. Lett.* **2011**, *9*, 103–114. [CrossRef]
11. Shelley, L.K.; Ross, P.S.; Miller, K.M.; Kaukinen, K.H.; Kennedy, C.J. Toxicity of atrazine and nonylphenol in juvenile rainbow trout (*Oncorhynchus mykiss*): Effects on general health, disease susceptibility and gene expression. *Aquat. Toxicol.* **2012**, *124*, 217–226. [CrossRef]
12. De Wever, H.; Verachtert, H. Biodegradation and toxicity of benzothiazoles. *Water Res.* **1997**, *31*, 2673–2684. [CrossRef]
13. European Environment Agency. Urban Waste Water Treatment. Available online: <https://www.eea.europa.eu/data-and-maps/indicators/urban-waste-water-treatment/urban-waste-water-treatment-assessment-4> (accessed on 16 December 2019).
14. Oturan, M.A.; Aaron, J.J. Advanced Oxidation Processes in Water/Wastewater Treatment: Principles and Applications. A Review. *Crit. Rev. Environ. Sci. Technol.* **2014**, *44*, 2577–2641. [CrossRef]
15. Nasirabadi, P.S.; Saljoughi, E.; Mousavi, S.M. Membrane processes used for removal of pharmaceuticals, hormones, endocrine disruptors and their metabolites from wastewaters: A review. *Desalin. Water Treat.* **2016**, *57*, 24146–24175. [CrossRef]

16. Van Der Bruggen, B.; Vandecasteele, C.; Van Gestel, T.; Doyen, W.; Leysen, R. A review of pressure-driven membrane processes in wastewater treatment and drinking water production. *Environ. Prog.* **2003**, *22*, 46–56. [[CrossRef](#)]
17. Wang, J.; Tian, Z.; Huo, Y.B.; Yang, M.; Zheng, X.C.; Zhang, Y. Monitoring of 943 organic micropollutants in wastewater from municipal wastewater treatment plants with secondary and advanced treatment processes. *J. Environ. Sci.* **2018**, *67*, 309–317. [[CrossRef](#)]
18. Kudlek, E. Decomposition of Contaminants of Emerging Concern in Advanced Oxidation Processes. *Water* **2018**, *10*, 955. [[CrossRef](#)]
19. Márquez, G.; Rodríguez, E.M.; Beltrán, F.J.; Álvarez, P.M. Solar photocatalytic ozonation of a mixture of pharmaceutical compounds in water. *Chemosphere* **2014**, *113*, 71–78. [[CrossRef](#)]
20. De La Cruz, N.; Esquius, L.; Grandjean, D.; Magnet, A.; Tungler, A.; De Alencastro, L.; Pulgarin, C. Degradation of emergent contaminants by UV, UV/H₂O₂ and neutral photo-Fenton at pilot scale in a domestic wastewater treatment plant. *Water Res.* **2013**, *47*, 5836–5845. [[CrossRef](#)]
21. Serna-Galvis, E.A.; Silva-Agredo, J.; Giraldo, A.L.; Flórez-Acosta, O.A.; Torres-Palma, R.A.; Torres, R. Comparative study of the effect of pharmaceutical additives on the elimination of antibiotic activity during the treatment of oxacillin in water by the photo-Fenton, TiO₂-photocatalysis and electrochemical processes. *Sci. Total Environ.* **2016**, *541*, 1431–1438. [[CrossRef](#)]
22. Shi, B.J.; Wang, Y.; Geng, Y.K.; Liu, R.D.; Pan, X.R.; Li, W.W.; Sheng, G.P. Application of membrane bioreactor for sulfamethazine-contained wastewater treatment. *Chemosphere* **2018**, *193*, 840–846. [[CrossRef](#)]
23. Acero, J.L.; Benitez, F.J.; Leal, A.I.; Real, F.J.; Teva, F. Membrane filtration technologies applied to municipal secondary effluents for potential reuse. *J. Hazard. Mater.* **2010**, *177*, 390–398. [[CrossRef](#)] [[PubMed](#)]
24. Dolar, D.; Vuković, A.; Asperger, D.; Kosutić, K. Effect of water matrices on removal of veterinary pharmaceuticals by nanofiltration and reverse osmosis membranes. *J. Environ. Sci.* **2011**, *23*, 1299–1307. [[CrossRef](#)]
25. Ferrer-Polonio, E.; McCabe, M.; Mendoza-Roca, J.A.; Vincent-Vela, M.C. Fractionation of secondary effluents of wastewater treatment plants in view of the evaluation of membrane fouling in a further ultrafiltration step. *J. Chem. Technol. Biotechnol.* **2018**, *93*, 1495–1501. [[CrossRef](#)]
26. Gupta, V.K.; Carrott, P.J.M.; Carrott, M.M.L.R.; Suhas. Low-Cost Adsorbents: Growing Approach to Wastewater Treatment—A Review. *Crit. Rev. Environ. Sci. Technol.* **2009**, *39*, 783–842. [[CrossRef](#)]
27. Sanz, J.; Lombraña, J.I.; De Luis, A. Temperature-assisted UV/H₂O₂ oxidation of concentrated linear alkylbenzene sulphonate (LAS) solutions. *Chem. Eng. J.* **2013**, *533*–541. [[CrossRef](#)]
28. Ferreira, C.; Villota, N.; Lombraña, J.I.; Rivero, M.J.; Zúñiga, V.; Rituerto, J.M. Analysis of a Hybrid Suspended-Supported Photocatalytic Reactor for the Treatment of Wastewater Containing Benzothiazole and Aniline. *Water* **2019**, *11*, 337. [[CrossRef](#)]
29. Villota, N.; Lomas, J.M.; Camarero, L.M. Effect of ultrasonic waves on the water turbidity during the oxidation of phenol. Formation of (hydro) peroxo complexes. *Ultrason. Sonochem.* **2017**, *39*, 439–445. [[CrossRef](#)]
30. Benner, J.; Helbling, D.E.; Kohler, H.P.E.; Wittebol, J.; Kaiser, E.; Prasse, C.; Ternes, T.A.; Albers, C.N.; Aamand, J.; Horemans, B.; et al. Is biological treatment a viable alternative for micropollutant removal in drinking water treatment processes? *Water Res.* **2013**, *47*, 5955–5976. [[CrossRef](#)]
31. Oller, I.; Malato, S.; Sánchez-Pérez, J. Combination of Advanced Oxidation Processes and biological treatments for wastewater decontamination—A review. *Sci. Total Environ.* **2011**, *409*, 4141–4166. [[CrossRef](#)]
32. Uribe, I.O.; Mosquera-Corral, A.; Rodicio, J.L.; Esplugas, S. Advanced technologies for water treatment and reuse. *AIChE J.* **2015**, *61*, 3146–3158. [[CrossRef](#)]
33. Mijangos, L.; Ziarrusta, H.; Olivares, M.; Zuloaga, O.; Moeder, M.; Etxebarria, N.; Prieto, A. Simultaneous determination of 41 multiclass organic pollutants in environmental waters by means of polyethersulfone microextraction followed by liquid chromatography-tandem mass spectrometry. *Anal. Bioanal. Chem.* **2018**, *410*, 615–632. [[CrossRef](#)] [[PubMed](#)]
34. Association, A.P.H. *Standard Methods for the Examination of Water & Wastewater*; American Public Health Association: Washington, DC, USA, 2005; ISBN 978-0-87553-047-5.
35. Bicudo, J.R.; Brown, T.; Waller, M.; Saint, W.; Summach, D. Addressing ammonia levels in the Grand River through nitrification upgrades at the Kitchener WWTP. *Influents* **2016**, *11*, 54–57.

36. Mijangos, L.; Ziarrusta, H.; Ros, O.; Kortazar, L.; Fernández, L.A.; Olivares, M.; Zuloaga, O.; Prieto, A.; Etxebarria, N. Occurrence of emerging pollutants in estuaries of the Basque Country: Analysis of sources and distribution, and assessment of the environmental risk. *Water Res.* **2018**, *147*, 152–163. [[CrossRef](#)] [[PubMed](#)]
37. ECHA. CoRAP List of Substances. Available online: <https://echa.europa.eu/information-on-chemicals/evaluation/community-rolling-action-plan/corap-list-of-substances> (accessed on 2 July 2019).
38. De Luis, A.M.; Lombraña, J.I.; Menéndez, A.; Sanz, J. Analysis of the Toxicity of Phenol Solutions Treated with H₂O₂/UV and H₂O₂/Fe Oxidative Systems. *Ind. Eng. Chem. Res.* **2011**, *50*, 1928–1937. [[CrossRef](#)]
39. García-Becerra, F.Y.; Ortiz, I. Biodegradation of Emerging Organic Micropollutants in Nonconventional Biological Wastewater Treatment: A Critical Review. *Environ. Eng. Sci.* **2018**, *35*, 1012–1036. [[CrossRef](#)]
40. Behera, S.K.; Kim, H.W.; Oh, J.E.; Park, H.S. Occurrence and removal of antibiotics, hormones and several other pharmaceuticals in wastewater treatment plants of the largest industrial city of Korea. *Sci. Total Environ.* **2011**, *409*, 4351–4360. [[CrossRef](#)]
41. Zhang, Y.; Geißen, S.U.; Gal, C. Carbamazepine and diclofenac: Removal in wastewater treatment plants and occurrence in water bodies. *Chemosphere* **2008**, *73*, 1151–1161. [[CrossRef](#)]
42. Gómez, M.; Bueno, M.M.; Lacorte, S.; Fernández-Alba, A.; Agüera, A. Pilot survey monitoring pharmaceuticals and related compounds in a sewage treatment plant located on the Mediterranean coast. *Chemosphere* **2007**, *66*, 993–1002. [[CrossRef](#)]
43. Kasprzyk-Hordern, B.; Dinsdale, R.M.; Guwy, A.J. The removal of pharmaceuticals, personal care products, endocrine disruptors and illicit drugs during wastewater treatment and its impact on the quality of receiving waters. *Water Res.* **2009**, *43*, 363–380. [[CrossRef](#)]
44. Sui, Q.; Huang, J.; Deng, S.; Yu, G.; Fan, Q. Occurrence and removal of pharmaceuticals, caffeine and DEET in wastewater treatment plants of Beijing, China. *Water Res.* **2010**, *44*, 417–426. [[CrossRef](#)]
45. Acero, J.L.; Benitez, F.J.; Teva, F.; Leal, A.I. Retention of emerging micropollutants from UP water and a municipal secondary effluent by ultrafiltration and nanofiltration. *Chem. Eng. J.* **2010**, *163*, 264–272. [[CrossRef](#)]
46. Yoon, Y.; Westerhoff, P.; Snyder, S.A.; Wert, E.C.; Yoon, J. Removal of endocrine disrupting compounds and pharmaceuticals by nanofiltration and ultrafiltration membranes. *Desalination* **2007**, *202*, 16–23. [[CrossRef](#)]
47. Hendricks, D. *Fundamentals of Water Treatment Unit Processes: Physical, Chemical, and Biological*, 1st ed.; CRC Press: Boca Raton, FL, USA, 2010.
48. Kimura, K.; Amy, G.; Drewes, J.; Watanabe, Y. Adsorption of hydrophobic compounds onto NF/RO membranes: An artifact leading to overestimation of rejection. *J. Membr. Sci.* **2003**, *221*, 89–101. [[CrossRef](#)]



© 2020 by the authors. Licensee MDPI, Basel, Switzerland. This article is an open access article distributed under the terms and conditions of the Creative Commons Attribution (CC BY) license (<http://creativecommons.org/licenses/by/4.0/>).

3.12. 12. argitalpena. Water reuse study from urban WWTPs via c-ultrafiltration and ozonation technologies: basis for resilient cities and agriculture

3.12 kapitulua artikulu honi dagokio:

C. Ferreiro, N. Villota, A. de Luis, J.I. Lombraña, N. Etxebarria, J.M. Lomas. Water reuse study from urban WWTPs via c-ultrafiltration and ozonation technologies: basis for resilient cities and agriculture. *Agronomy*, 11, 2, 322, 2021. DOI: 10.3390/agronomy11020322.

Article

Water Reuse Study from Urban WWTPs via c-Ultrafiltration and Ozonation Technologies: Basis for Resilient Cities and Agriculture

Cristian Ferreiro ^{1,*}, Natalia Villota ², Ana de Luis ³, José Ignacio Lombrana ¹, Nestor Etxebarria ⁴ and Jose María Lomas ²

¹ Department of Chemical Engineering, Faculty of Science and Technology, University of the Basque Country UPV/EHU, Barrio Sarriena s/n, 48940 Leioa, Spain; ji.lombrana@ehu.eus

² Department of Chemical and Environmental Engineering, Faculty of Engineering Vitoria-Gasteiz, University of the Basque Country UPV/EHU, Nieves Cano 12, 01006 Vitoria-Gasteiz, Spain; natalia.villota@ehu.eus (N.V.); josemaria.lomas@ehu.eus (J.M.L.)

³ Department of Chemical and Environmental Engineering, Faculty of Engineering in Bilbao, University of the Basque Country UPV/EHU, Plaza Ingeniero Torres Quevedo, 1, 48013 Bilbao, Spain; ana.deluis@ehu.eus

⁴ Department of Analytical Chemistry, Faculty of Science and Technology, University of the Basque Country UPV/EHU, Barrio Sarriena s/n, 48940 Leioa, Spain; nestor.etxebarria@ehu.eus

* Correspondence: cristian.ferreiro@ehu.eus; Tel.: +34-9460-153-88



Citation: Ferreiro, C.; Villota, N.; de Luis, A.; Lombrana, J.I.; Etxebarria, N.; Lomas, J.M. Water Reuse Study from Urban WWTPs via c-Ultrafiltration and Ozonation Technologies: Basis for Resilient Cities and Agriculture. *Agronomy* **2021**, *11*, 322. <https://doi.org/10.3390/agronomy11020322>

Academic Editor: Youssef Rouphael

Received: 14 December 2020

Accepted: 9 February 2021

Published: 12 February 2021

Publisher's Note: MDPI stays neutral with regard to jurisdictional claims in published maps and institutional affiliations.



Copyright: © 2021 by the authors. Licensee MDPI, Basel, Switzerland. This article is an open access article distributed under the terms and conditions of the Creative Commons Attribution (CC BY) license (<https://creativecommons.org/licenses/by/4.0/>).

Abstract: The water–development nexus is essential for the advancement and progress of cities in the face of problems such as climate change, water security and increasing environmental stress in the agricultural sector. Aiming for a circular economy and, at the same time, improving the resilience of water supply alternatives and achieving a goal of zero waste, this work presents a technical–economic study of a novel continuous ultrafiltration (c-UF) system with self-cleaning capacity coupled to an ozonation process, for the treatment of urban WWTP effluent. The removal efficiencies achieved were analysed both through macroscopic parameters (suspended solids, turbidity) and for the most frequently occurring contaminants of emerging concern (CECs). Consequently, an effluent suitable for irrigation was obtained, with a total recovery factor of 97.92%, a concentration of suspended solids (SS) below 1 mg L⁻¹, 0.06 NTU turbidity and toxicity free, complying with the new European Regulation on Water Reuse (EU 2020/741). A comparative analysis of the proposed process with regard to conventional tertiary treatment revealed that the proposed process was 39.1% more economic, with a cost of 0.0325 € m⁻³. This alternative treatment will be of great interest because of its favourable technical–economic characteristics, being postulated as a basic process for implementation in modern water reuse plants.

Keywords: urban wastewater treatment; water reuse; sustainable agriculture; ozonation; continuous ultrafiltration; compounds of emerging concern; safety food; sustainable process; new water resources; sustainable city

1. Introduction

Urbanization is one of the most significant trends of the 21st century. By 2050, it is expected that more than 68% of the world's population will reside in large cities, which will mean a movement of more than 4000 million people migrating from rural areas to large population centres [1]. Currently, many of these cities are experiencing rapid and uncontrolled growth, largely by people with low per capita income to which the government is not able to provide infrastructures consistent with those of a developed city. Authors such as Luthy et al. [2] concluded in their study of cities in California that most people living in newly developed residential areas were living in areas with limited water availability, and more than 68% of these new settlements in large cities lacked an adequate sanitation

system. Many of these untreated or conventional primary treatment wastewaters end up in ditches or urban rivers with consequent risks to public health [3].

Water pollution is one of the largest threats to health, human development and the environment. The composition of these wastewaters generally varies depending on the different polluting sources [4]. Domestic wastewater is characterized by a high concentration of nutrients (N, P, K, Ca and Mg) and by high bacterial loads, such as pathogenic bacteria, viruses, common protozoa (*Giardia* and *Cryptosporidium*) and helminths, which can pose a direct threat to human health. Therefore, given the epidemiological health hazard, eliminating pathogens is one of the objectives of wastewater treatment systems [5]. In addition, these urban wastewaters can also contain contaminants of emerging concern (CECs). This category includes any synthetic or naturally occurring chemical or any microorganism that is not commonly controlled and that can cause adverse effects on both human health and the environment [6]. Among the main categories of CECs are Pharmaceuticals and Personal Care Products (PPCPs) and endocrine disruptors (EDCs). In 2013, the European Parliament expanded the classification by Directive 2013/39/EU to include steroid hormones, surfactants, perfluorinated compounds, flame retardants, industrial additives, drugs and UV filters. Many of these contaminants, due to their low concentration of approximately 3 ng L^{-1} [7], are only regulated to a certain extent in the European Union (EU) and USA. In the EU, the implementation of this regulation is collected through a list of priority substances listed as CECs in Decision 2015/495/EU and Decision 2018/840/EU. The European Commission, as it became aware of the adverse effects of other substances not included in this list, has expanded the number of substances to be monitored through the Registration, Evaluation, Authorization and Restriction of Chemicals (REACH). In the USA, the CECs are regulated from the Contaminants Candidate List of unregulated contaminants [8]. The long-term impacts of CECs are unknown since they can bioaccumulate in aquatic species. Regulatory authorities, such as the European Environmental Agency (EEA)—integrated by 32 Member States and seven cooperating countries—the International Chemical Safety Program (IPCS), the World Health Organization (WHO) and the U.S. Environmental Protection Agency (EPA) [9], are responsible for developing regulations and directives that improve the protection and sanitary safety of these freshwater resources.

The effects of water pollution also directly or indirectly influence the economic activity of large cities, such as industrial production, fishing, aquaculture and tourism [10]. In short, poor water quality hinders economic development. For this reason, large cities must adapt to this new reality and improve wastewater management by properly treating it and its subsequent reuse to minimize the negative impact of discharge and at the same time maximize the economic benefits it can bring without harming the environment and human health. This will change the way in which wastewater is viewed, becoming a point on which to obtain an economic benefit instead of a burden to deal with [1]. One of the potential sectors that could benefit from this new concept is horticulture. Reusing urban wastewater in peri-urban horticultural facilities in addition to securing continuous water resources would provide ecological services [11]. The produce obtained through this approach would reduce the carbon footprint of the food that people eat, in addition to modifying favourably the surrounding landscape. This solution would be most effective in arid or semiarid areas, whose population are notably increasing. In addition, in many countries where certain political and social conflicts makes it difficult to transport water from one region to another, the reuse of properly treated urban wastewater would provide a solution to this problem. Furthermore, having to construct expensive transfer pipelines, dams, etc., would be avoided. In short, proper water management and subsequent reuse in peri-urban agriculture would protect and optimize the use of natural resources [4,12].

For example, in Spain, one of the countries in Europe with the highest water consumption per capita ($800.9 \text{ m}^3 \text{ inhabitant}^{-1}$) and with an agricultural consumption of $25.47 \times 10^9 \text{ m}^3 \text{ year}^{-1}$ (68.19% of total use) is the first European country with reuse capacity and one of the few that has its own legislation that regulates it through Royal

Decree 1620/2007 [13]. In addition, the European Union, aware of a regulatory gap, has released a new regulation on the minimum requirements that reused water must meet (EU 2020/741) [14], with mandatory compliance within a period of 3 years, from 26 June 2023, for all countries of the European Union that will use this unconventional water source. This new regulation aims to ensure that the quality of reclaimed water for agricultural irrigation reaches the same levels of quality and control in all countries of the European Union. This community regulation defines the types of crops where reclaimed waters can be used, the minimum water quality requirements and stipulates the quality control that these waters must comply with. The reuse of urban waters in peri-urban agriculture would considerably reduce the environmental impact of this important economic activity and its dependence on weather effects, freeing up resources that could be used for domestic consumption. In turn, this approach would directly connect with the new paradigm of a circular economy in the new cities of the 21st century [15].

Today's purification technology generates effluents of reclaimed water of varying quality, even up to drinking water standards. To apply them for any agricultural use, advanced tertiary treatments are required in waste water treatment plants (WWTPs) [16,17]. However, reuse is not without risks, both in terms of its possible lack of agronomic suitability for irrigation as well as its sanitary suitability, due to the possible presence of pathogenic microorganisms in inadequately reclaimed waters [18]. The microbiological health risks associated with irrigating with purified water depend on several factors, which can be grouped into (i) factors associated with the characteristics of the water and the treatment received, among which include the microbial load and the purification system used; and (ii) the factors derived from the manipulation of water in irrigation. To avoid any risk due to misuse and to ensure adequate water quality for reuse, from a health and environmental point of view, it is necessary to implement robust purification processes together with an analytical control or self-control program.

For compliance and obtaining an effluent that meets the legal requirements for subsequent reuse in agriculture [5], different conventional and advanced physical and biological treatment options have been investigated for eliminating pathogenic microorganisms and CECs [19].

Table 1 shows the treatments that have performed best for eliminating CECs as well as other pathogens based on the use of physical, biological or chemical treatments. Biological processes have been one of the options that have most attracted researchers due to their low cost of implementation, ease of scaling and sustainability with the environment [20]. Among the most researched options are the active sludge process [21]. However, these biological treatment processes are inefficient, especially with regard to pharmaceutical products and are not sufficient for effectively eliminating several nonbiodegradable CECs [22].

For physical processes, these alternatives involve the use of adsorption processes [23], membranes, such as microfiltration [24], or ultrafiltration (UF) [4], despite the problem of surface fouling [25]. It is noteworthy that the removal of CECs by conventional physical treatments is unfeasible due to the low octanol/water partition coefficients [26]. According to Table 1, UF-based processes have greater advantages in terms of longevity and sustainability of the process [27], unlike processes such as adsorption, which presents difficulties once the adsorbent is saturated and involves high reclamation costs, with the only alternative being landfill management or energy recovery [28]. In the case of UF, separation is achieved mainly by the adsorption of contaminants on the surface of the membrane and electrostatic repulsion. In any case, the retention capacity depends on the specific matrix of the water to be treated and the presence of organic matter. Therefore, UF has application potential for obtaining high-quality effluents since it reduces parameters such as turbidity, suspended solids, bacteria (such as *E. coli*), coliforms and a wide range of CECs; it also has a low capital investment, versatility, no generation of sludge, no odours and ease of scaling that guarantees consistent quality of the treated water, regardless of the changes in the influent [29]. One of the drawbacks highlighted by authors such as Kim et al. [25] is the

appearance of fouling, which significantly influences the membrane properties, such as porosity and hydrophobicity, in addition to operating conditions, such as pressure. Therefore, a system that counteracts the negative effects of fouling and allows normal operation is something that would facilitate the large-scale implementation of this technology in urban WWTPs.

Table 1. Technologies for eliminating a wide range of contaminants of emerging concern (CECs) and mitigation of pathogenic organisms of effluents from secondary treatment.

Type of Treatment	Process	Notes	Ref.
Physical	Adsorption	Used carbon nanotubes (CNTs) as adsorbents for the selective removal of CECs. Excellent removal potential of CECs such as tetracycline (92%), amoxicillin ($\cong 90\%$) and 100% for ibuprofen, triclosan and norfloxacin. They were not able to eliminate a wide range of CECs due to the high selectivity of the adsorbent.	[30–32]
	Membranes	Studied several membranes with different pore sizes, hydrophobicity and surface charge. They found that ultrafiltration (UF) membranes made of polysulfone and polyvinylidene offered a good removal-pressure ratio applied for the removal of CECs. The UF showed a high efficiency for certain hormonal compounds and drugs such as diclofenac, caffeine, bisphenol A or ketoprofen but showed a lower separation yield for phthalate esters, due to its lower polarity. They highlighted the problems of fouling and the final removal from the reject and backwash stream. It proved to be an effective barrier for the removal of viruses and bacteria, suspended solids, parasites and microorganisms.	[31,33–37]
Biological	Conventional	Active sludge systems, despite being the most widely used in WWTP, were the least efficient for removing complex mixtures of CECs due to the specific biodegradability of each contaminant. In a WWTP in Finland, they obtained a CEC removal efficiency of 26% for diclofenac while for naproxen an efficiency close to 97–100%.	[38–41]
Chemical	Advanced Oxidation Processes (AOPs)	Among the most used processes is chlorination. It is effective for less reactive species such as triclosan or ibuprofen. The increase in the chlorine dose leads to the formation of oxidation products that are more difficult to remove. In contrast, ozonation is capable of eliminating most CECs with yields of 90–100%. However, the low concentrations of CECs and the operational costs of ozone production do not make it very attractive.	[42–44]

Another issue that the application of UF in the WWTP must resolve is the treatment of the concentrates from the reject stream. This stream is composed of organic contaminants, refractory products (such as PPCPs) and pathogenic microorganisms. Although the discharge to the water medium in many cases is not sufficiently regulated, the uncontrolled discharge of these streams into the environment is not acceptable. Here, AOPs can play a fundamental role in treating this stream. According to Table 1, ozonation processes demonstrate a high CEC removal yield between 90 and 100% with a high oxidation rate due to the high reactivity of ozone and hydroxyl radicals towards many of the organic compounds present, such as carbamazepine, diclofenac or bisphenol A, among others. However, this requires specific reaction conditions, such as pH. In this case, a pH = 9, which is usual for ozonation of this kind of effluent, was used [45,46]. In addition, it is a powerful disinfecting agent capable of inactivating a wide range of pathogens, such as bacteria, viruses, protozoa and prion proteins, without leaving a toxic residue [47]. Added to the outstanding advantages is that it does not generate sludge and it makes it possible to generate ozone using renewable energy sources.

In short, this new problem of this century constitutes one of the great priority challenges society must solve. Such is the importance that the United Nations in 2015 included it in the Sustainable Development Goals (SDGs) adopted by most countries, through SDG

6 for Clean Water and Sanitation, which addresses the problem of water scarcity, sanitation and hygiene, treatment and reuse of wastewater. Linked to this problem, SDG 3 for good health and well-being, SDG 11 for sustainable cities and communities and SDG 12 for responsible production and consumption promote the economic development of new cities together with sustainable agriculture and proximity to population centres. In this context, the nexus between the development of sustainable cities contributes through the appropriate reuse of their wastewater for local, sustainable and safe agriculture. Therefore, based on the background described, the use of a continuous ultrafiltration (c-UF) process that mitigates the effects of dreaded fouling through a self-cleaning system together with the treatment of the reject stream through an ozonation process is a real and low-cost alternative to conventional tertiary treatment based on coagulation–flocculation followed by a disinfection process using UV light or sodium hypochlorite for the efficient treatment of CECs and pathogenic microorganisms present in the urban waters of a WWTP.

This study aims to study the reuse of effluent from a secondary treatment of a real urban WWTP for use in agricultural irrigation through a c-UF pilot plant with a self-cleaning system coupled to an ozonation system for treating the reject stream. For this, the main parameters related to the quality of the treated water obtained (suspended solids, turbidity, total organic carbon and microbiology) will be analysed for both the UF and ozonation processes in addition to the removal yields of the most frequent CECs. Additionally, a study will be carried out in which the operational cost of the proposed technology and configuration will be evaluated and compared with the cost of tertiary treatment in a conventional WWTP.

2. Materials and Methods

2.1. Reagents and Chemical Used

Acetaminophen ($C_8H_9NO_2$), atrazine ($C_8H_{14}ClN_5$), diuron ($C_9H_{10}Cl_2N_2O$), ciprofloxacin hydrochloride ($C_{17}H_{19}ClFN_3O_3$), norfloxacin hydrochloride ($C_{16}H_{19}ClFN_3O_3$), isoproturon ($C_{12}H_{18}N_2O$), simazine ($C_7H_{12}ClN_5$), sulfamethoxazole ($C_{10}H_{11}N_3O_3S$) and trimethoprim ($C_{14}H_{18}N_4O_3$) were acquired from Fluka (Buchs, Switzerland). Amitriptyline hydrochloride ($C_{20}H_{23}N$), butylparaben ($C_{11}H_{14}O_3$), 2-hydroxybenzothiazole (C_7H_5NOS), caffeine ($C_8H_{10}N_4O_2$), clomipramine hydrochloride ($C_{19}H_{24}Cl_2N_2$), carbamazepine ($C_{15}H_{12}N_2O$), potassium perfluoro-1-octanesulfonate ($C_8F_{17}KO_3S$), diclofenac sodium salt ($C_{14}H_{10}Cl_2NNaO_2$), methylparaben ($C_8H_8O_3$), imipramine hydrochloride ($C_{19}H_{24}N_2$), nortriptyline hydrochloride ($C_{19}H_{21}N$), perfluoro-n-octanoic acid ($C_8HF_{15}O_2$), phenytoin ($C_{15}H_{12}N_2O_2$), potassium perfluoro-1-butanefluorobutanesulfonate ($C_4F_9KO_3S$), progesterone ($C_{21}H_{30}O_2$), sulfadiazine ($C_{10}H_{10}N_4O_2S$) and testosterone ($C_{19}H_{28}O_2$) were purchased from Sigma-Aldrich (St. Louis, MO, USA). Clofibric acid ($C_{10}H_{11}ClO_3$), ketoprofen ($C_{16}H_{14}O_3$), bezafibrate ($C_{19}H_{20}ClNO_4$) and propranolol hydrochloride ($C_{16}H_{21}NO_2$) were acquired from MP Biomedicals (Illkirch-Graffenstaden, France). Genistein ($C_{15}H_{10}O_5$), genistin ($C_{21}H_{20}O_{10}$) and glycitin ($C_{22}H_{22}O_{10}$) were purchased from Extrasynthese (Lyon, France), perfluorooctane sulfonamide ($C_8H_2F_{17}NO_2S$) from Dr. Ehrenstorfer (Augsburg, Germany), losartan potassium ($C_{22}H_{22}ClKN_6O$) from Merck (Darmstadt, Germany), valsartan ($C_{24}H_{29}N_5O_3$) and telmisartan ($C_{33}H_{30}N_4O_2$) from Boehringer (Ingelheim am Rhein, Germany), irbesartan ($C_{25}H_{28}N_6O$) from Sanofi (Paris, France) and eprosartan mesylate ($C_{24}H_{28}N_2O_7S_2$) from Solvay Pharmaceuticals (Brussels, Belgium). Acesulfame potassium ($C_4H_4KNO_4S$) and sucralose ($C_{12}H_{19}Cl_3O_8$) were supplied by Supelco (Bellefonte, PA, USA). The purity of all the target analytes was >95%. Methanol (CH_3OH , HPLC grade, 99.9%), ethyl acetate ($C_4H_8O_2$, 99.8%) and n-hexane (C_6H_{14} , HPLC grade, 95%) were supplied by Labscan (Dublin, Ireland); ethylenediaminetetraacetic sodium salt (Na_2EDTA , 99.0–101.1%) and ammonia solution (25% as NH_3) by Panreac (Barcelona, Spain); formic acid ($HCOOH \geq 98\%$) by Scharlau (Barcelona, Spain); and sodium chloride ($NaCl$, >99.8%), sodium sulfite (Na_2SO_3 , >100%) and acetic acid (CH_3COOH , 100%) by Merck (Darmstadt, Germany).

2.2. Equipment Used

2.2.1. Galindo WWTP

The experiments were carried out in the Galindo WWTP, located in the municipality of Sestao, in the historical territory of Bizkaia, Basque Country (43°18′35.38″ N and 3°0′25.92″ W, north of Spain). The WWTP of Galindo serves the entire area of influence of Greater Bilbao, with a population equivalent to 1,200,000 inhabitants and is capable of treating in secondary treatment an average daily flow of 6.0 L s⁻¹ with a maximum allowable in the primary treatment flow of 12 L s⁻¹. The treatment line of this WWTP consists of a primary, secondary and tertiary treatment, according to the following units:

- The primary treatment consists of a fine grinding unit followed by a degreasing and grit removal system. The water from the sandblasting passes through a distribution channel subjected to agitation where the installed rectangular decanters are sent. In this operation, approximately 75% of the suspended solids (SS) and 50% of the organic matter are removed.
- The secondary treatment consists of extended aeration in a biological reactor and secondary decantation. Approximately 10 t day⁻¹ of sludge accumulates in the decanters, which is treated and energetically recovered to supply part of the needs of the WWTP facilities.
- The tertiary treatment consists of a coagulation process with Al₂(SO₄)₃ and sodium hypochlorite (NaClO) followed by a flocculation system and subsequent lamellar decantation. The sludge produced is sent to the water line. The clarified water is directed to sand filters with an average filtration rate of 7.0 m³ m⁻² h⁻¹, adopting a filtration surface of 21.0 m². Subsequently, the water is disinfected in a chamber consisting of 80 lamps with a nominal consumption of 250 W lamp⁻¹ and a maximum power consumption of 12 kW.

The effluent obtained from the Galindo plant complies with Directive 91/271/EEC for urban wastewater treatment. The objective of this study is to propose an alternative treatment technology that is cheaper than the existing conventional tertiary treatment and that complies with the new regulation of the European Commission [14] in terms of water reuse for agricultural use so that the treated effluent currently discharged into the Ballonti River can be adequately treated with the technology described in the following section and reused for irrigation in peri-urban agricultural facilities of Greater Bilbao.

2.2.2. Membrane Technology Coupled to Ozonisation Treatment

A part of the effluent from the secondary treatment is diverted to the c-UF pilot plant at a flow rate of 3.3 m³ h⁻¹. The system consists of two independent frames. In the first frame, there are 4 UF modules (c-UF4XS, FLUYTEC, Erandio, Spain), containing a bundle of ultrafiltration membranes inside. In this same frame is the set of valves, pipes and instrumentation for the supply, drainage and permeate outlet. The second frame is composed of a main water tank intended for washing, a feed and washing pump, a compressed air system, roughing filtration (prefilter) and the corresponding valves, pipes and instrumentation.

In this ultrafiltration unit, hollow fibre membranes made from polyethersulfone (PES) are used, which are best suited for the operation and operate with an inside–outside configuration. The properties of this membrane are shown in Table 2.

The c-UF plant has a self-cleaning device that extends the filtration operating time, decreasing the number of cleaning cycles that must be performed to maintain the membrane properties over time. This system consists of a filter that is placed prior to the c-UF equipment, which has a self-cleaning system through a rotating purge arm, as shown in Figure 1.

According to Figure 1, when the pressure difference between the inlet, untreated water and outlet of the drainage pipe reaches a predetermined value, this arm goes into operation and starts the backwashing process automatically. The arm is connected to the filter element to be cleaned, opening a solenoid valve, which produces vacuum pressure

inside this element. Thus, part of the filtered water is forced to pass in the opposite direction, dragging the solids and encrustations that block the filter. This process is repeated with each of the filter elements until the washing cycle is completed.

Table 2. Characteristics of the ultrafiltration (UF) membranes.

Membrane Type	Polyethersulfone
Housing material	Polyvinylchloride (PVC)
Fibre material	Polyethersulfone (PES)
Active area	80.0 m ²
Fibre diameter	4.0 mm
Nominal diameter of the membrane pore	20 nm
Molecular weight cut off	100 kDa
Treatment capacity	5 m ³ h ⁻¹
Maximum operating temperature	40 °C
Recommended transmembrane pressure	<1 bar
Maximum transmembrane pressure	2.5 bar
pH Range	2–11
Maximum feed silt density index	SDI 5
Free chlorine tolerance	<0.1 mg L ⁻¹

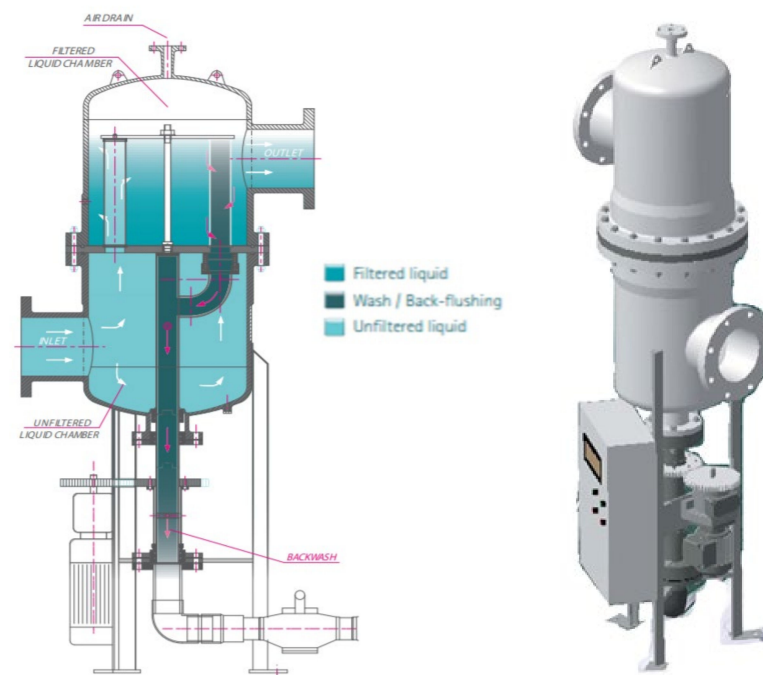


Figure 1. Diagram of the self-cleaning device of the c-UF pilot plant [48].

The reject stream and the wash waters were treated by an ozonation process in a pilot-scale gas-liquid contactor connected to the c-UF equipment. The ozonisation pilot system consisted of a 33.03 L stainless steel cylindrical contactor (with dimensions 795 mm × 230 mm), where the wastewater to be treated was introduced. Ozone was produced from extra pure oxygen in the ozone generator (TRIOGEN LAB2B, Triogen, De Goor, The Netherlands) and introduced into the reactor through a gas diffuser installed at the bottom of contactor, thus ensuring a perfect homogenization of the system. To improve the contact between the descending liquid and ascending gas, the column is provided on the top by a spray that atomizes the liquid. Part of the dissolution that the centrifugal pump (TMP04.08 S GF VN2BEN3, Argal Pumps, Brescia, Italy) recirculates is thrown up and returns to the reactor at the top where it is sprayed, which can also destroy the foams

that are often formed due to the strong agitation of the system. The recirculation system provides enough stirring to get a good mixture in the system.

2.3. Experimental Setup and Procedures

2.3.1. Operation of Pilot Plant

The method of operating the c-UF equipment was differentiated into two modes: filtration mode and washing mode. During the filtration mode, dead-end filtration was performed with an inside–outside configuration. In this way, all the water was forced to cross the membrane from the inside out, retaining the suspended solids and solutes (CECs, pathogenic microorganisms) on the inner surface of the fibres.

The c-UF equipment was fed through a feeding branch connected to the secondary treatment at a rate of $3.3 \text{ m}^3 \text{ h}^{-1}$ with a centrifugal pump (ZMR02.30 S GF V BS8 B EN3, Argal Pumps, Brescia, Italy), installed at the bottom of the equipment. The permeate obtained with each module, with a flow rate of $41.5 \text{ L m}^{-2} \text{ h}^{-1}$, was collected in the same branch of the filtered product. This parameter was continuously recorded through flow metres (FLS F3.80, Aliaxis, Okondo-Araba, Spain) (see Figure 2) to control membrane fouling and keep the production of treated water constant. Each filter operating cycle lasted 47 min. At the end of each cycle, the transmembrane pressure increased from the initial 0.6 bar to 2.3 bar.

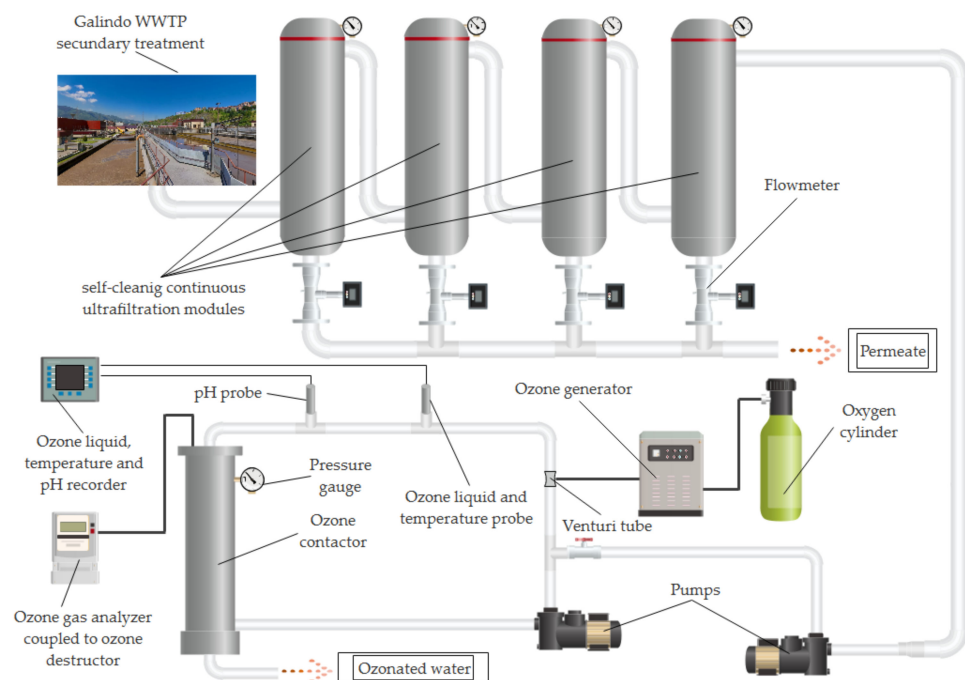


Figure 2. Diagram of the continuous ultrafiltration process coupled to the ozonation system for the treatment of the reject stream.

The second mode corresponded to washing. This mode consisted of a sequence of washes (flushing, backwashing and rinsing composed of Chemical Enhanced Flushing (CEF) and Cleaning In Place (CIP)), whose main objective was to recover the initial state of the membrane. This mode of operation effectively removed the solids and encrustations deposited on the inner surface of the fibres. This sequence of washes was performed module by module or in pairs, with the intention of keeping the permeate flow constant. This process lasted 9 min, at which time the transmembrane pressure reached a pressure of 0.6 bar. The ozonation experiments of the reject stream consisted of a batch treatment. For this, the ozonation contactor was filled with 30.0 L of water from the reject stream. Subsequently, ozone was introduced into the contactor through a venturi tube placed in

the recirculation loop followed by a static mixer. In addition, the contactor was provided with a liquid atomizer at the top to improve the gas–liquid (G-L) contact (see Figure 2). The experiments were carried out at a temperature of 15.0 °C, an initial pH of 9.0, a pressure of 1.5 bar, under constant flow of ozone (4 L min⁻¹) and constant ozone concentration at the inlet of 6.4 mg L⁻¹ during 180 min. The system pressure was controlled with a manometer (111.10, Wika Instruments, Barcelona, Spain) and the ozone concentration in the gas phase was monitored with an ozone analyser (BMT 964C, BMT MESSTECHNIK GMBH, Stahnsdorf, Germany). The dissolved ozone concentration in the liquid phase and temperature were measured with a probe (Rosemount 499AOZ-54, Emerson, Alcobendas, Spain). The pH was controlled with a probe (Rosemount 399-09-62, Emerson, Alcobendas, Spain), integrated with an ozone probe in a recorder (Rosemount Solu Comp II, Emerson, Alcobendas, Spain). Gas-phase residual ozone was removed with a thermocatalytic ozone destructor (KVM 20-2, ZonoSistem, El Puerto de Santa María, Spain). All experiments were conducted in duplicate.

2.3.2. Sampling Method

The analysed samples of the influent and effluent of the c-UF process and the ozonation of the reject stream were collected according to the procedure established by the EPA [49] for composite samples. Samples composed of 2.0 L were collected in triplicate over four selected days in May 2019. On each day, the samples were collected at 4 different hours that were sufficiently representative, taking into account the variable wastewater stream and contaminant concentration (8:00, 12:00, 15:00 and 20:00 h). Each 2.0 L sample in turn consisted of 4 subsamples taken every 5 min around the sampling time. For the feed influent of the c-UF plant, the hydraulic retention times of the secondary treatment were considered, which fluctuated between 28 and 38 h, depending on the organic load of the raw wastewater.

The samples were collected from authorized sampling points. Once collected they were transported to the laboratory in a portable cooler (4 °C). The collected samples were filtered with a 0.45 µm MF-Millipore membrane (Merck KGaA, Darmstadt, Germany) for the subsequent identification and quantification of CECs. In the case of the samples taken from the ozonator, sodium bisulphite was used as a reducing agent to stop the ozone reaction at a rate of 2.2 g Na₂SO₃ g of O₃⁻¹ [50].

2.4. Analytical Techniques

The identification and determination of the concentration of the CECs present in the water samples were analysed in triplicate according to the analysis method described by Mijangos et al. [51]. The method consisted of taking 100.0 mL of each sample to which 4.25 mL of Na₂EDTA (0.2 M) and 0.8 mL of an HCOOH solution were added to acidify the sample to pH = 2.0. The CECs were subjected to solid-phase extraction (SPE) (OASIS-HLB, hydrophilic–lipophilic-balanced, 200 mg, Waters, Milford, USA). The cartridge was previously conditioned with 5.0 mL of methanol (CH₃OH), 5.0 mL of Milli-Q water (MQ) and 5 mL of acidified Milli-Q water at pH = 2.0. Subsequently, the cartridges were rinsed with 6 mL of Milli-Q water to remove any impurities that could interfere with the analysis. Then, the SPE cartridges were vacuum-dried for 1 h. The sample was loaded into the cartridge at a constant flow of 5.0 mL min⁻¹. Methanol (6.0 mL) was used to elute the analytes to subsequently evaporate the extract at 35.0 °C under a nitrogen stream. Finally, before introducing the samples into the liquid chromatography with tandem mass spectrometry (LC-MS-MS) equipment, they were reconstituted in 200.0 µL of a CH₃OH:H₂O phase (30:70, *v:v*) and filtered with a 0.22 µm polypropylene filter (Phenomenex, Torrance, CA, USA).

The LC-MS-MS analysis was performed using an Agilent 1260 series HPLC chromatograph coupled to an Agilent 6430 triple quadrupole (QqQ) mass spectrometer equipped with an electrospray ionization source (ESI) (Agilent Technologies, Palo Alto, CA, USA). The separation of the target analytes was carried out using a Kinetex F5 100 Å core-shell 2.1 mm × 100 mm, 2.6 µm column coupled to a Kinetex F5 pre-column 2.1 mm × 4.6 mm,

2.6 μm (Phenomenex, Torrance, CA, USA). Then, 10 μL of sample was injected into the system and the column was maintained at 35 $^{\circ}\text{C}$ during the chromatographic run. The separation was performed at a constant flow of 0.3 mL min^{-1} under gradient elution with a binary mixture of: $\text{H}_2\text{O}:\text{CH}_3\text{OH}$ (95:5, $v:v$) (mobile phase A) and $\text{CH}_3\text{OH}:\text{H}_2\text{O}$ (95:5, $v:v$) (mobile phase B), both containing 0.1% formic acid. The gradient profile started with 30% B, which was increased to 50% after 4 min and maintained for 12 min. Then, it was increased to 90% B, where it was maintained for 10 min. Initial gradient conditions (30% B) were then achieved in 6 min, where it was finally held for another 10 min (post-run step). Electrospray ionization was carried out using a N_2 flow rate of 12 L min^{-1} , a capillary voltage of 3500 V, a nebulizer pressure of 3.0 bar and a source temperature of 350 $^{\circ}\text{C}$. Quantification was performed recording the three most intense transitions for each analyte. Both voltages, according to the target analytes, were simultaneously applied in a single injection.

The determination of suspended solids (SS) was carried out according to the procedure described in ISO 11923:1997, "Water quality—Determination of suspended solids by filtration through glass-fibre filters". Turbidity was analysed using the turbidimeter Eutech TN-100 (Thermo Scientific, Singapore). The degree of mineralization was quantified by dissolved organic carbon (DOC) analysis on a Shimadzu TOC-VSCH analyser with ASI-V autosampler (Izasa Scientific, Alcobendas, Spain). Toxicity was evaluated in duplicate using the Microtox[®] bioassay in a Microtox[®] toxicity analyser, Azur 500 model (Microbics Corp., New Castle, Delaware, USA). The measurements were carried out according to ISO 11348-3 (1998), "Water Quality—Determination of the inhibitory effect of water samples on the light emission of *Aliivibrio fischeri* (Luminescent bacteria test)—Part 3: Method using freeze-dried bacteria" [52]. The results of this assay are usually expressed as EC_{50} , which represents the percentage of sample dilution (% $v:v$) that causes a 50% reduction in bacteria luminescence after 15 min of exposure. The Toxicity (TU) parameter used was defined according to Equation (1) [46]:

$$\text{Toxicity} = \frac{C_0}{EC_{50}} \quad (1)$$

where C_0 corresponds to the concentration of the compound used to obtain its EC_{50} value. Total coliforms and *Escherichia coli* (*E. coli*) measurements were analysed according with the Standard Methods for the Examination of Water and Wastewater, 9222 B and 9221 B, in a laboratory incubator Culture Model 153 (Hach Lange GmbH, Düsseldorf, Germany) [52].

3. Results and Discussion

3.1. Application of c-UIF for the Removal of CECs from a Secondary Treatment

3.1.1. Characterization of the Influent and Effluent at Galindo WWTP

The influent and effluent of the Galindo WWTP during May 2019 were characterized. Table 3 shows the maximum, minimum and mean values of the different parameters analysed, as well as the standard deviation. The values of the different parameters observed indicate that the WWTP treats medium pollution loads [53].

The variability observed between the maximum and minimum values is due to the different lifestyle habits of the population served by the Galindo WWTP. Regarding CECs in these waters, concentrations similar or lower than those detected in other WWTPs around the world were identified. For example, in Greece, they detected ciprofloxacin concentrations of 460 ng L^{-1} [54], and in Rome, caffeine concentrations of 20 $\mu\text{g L}^{-1}$ [55].

The removal of parameters such as dissolved organic carbon (85.2%) and toxicity (<1 TU) shows that the WWTP of Galindo achieves a quality effluent in accordance with Spanish regulations (Royal Decree Law 11/1995). However, certain CECs, such as 2-hydroxybenzothiazole or carbamazepine, yielded 64.6% and 14.1%, respectively. According to Machado et al. [56] or Egea-Corbacho et al. [55], not completely eliminating CECs could create problems in human health for reuse applications in agricultural activities and the environment due to their low biodegradability.

Table 3. Physicochemical characterization of the treated wastewater at Galindo WWTP (May 2019).

	INFLUENT				EFFLUENT			
	MIN	MAX	AVERAGE	S.D.	MIN	MAX	AVERAGE	S.D.
Suspended Solids (mg L ⁻¹)	145	322	233.5	102.19	1.2	5.6	3.4	2.54
Turbidity (NTU)	67	385.8	226.4	184.06	8.0	11.0	9.5	1.73
pH	5.6	8.9	7.32	1.82	8.1	8.5	8.3	0.23
DOC (mg C L ⁻¹)	37.4	87.7	62.55	29.04	6.82	11.75	9.28	2.85
BOD ₅ (mg O ₂ L ⁻¹)	201	324	262.5	71.01	3	5	4	1.15
<i>E. coli</i> (CFU 100 mL ⁻¹)	1.66 × 10 ⁵	5.35 × 10 ⁵	3.51 × 10 ⁵	2.13 × 10 ⁵	236	2400	793	1071.76
Total coliforms (CFU 100 mL ⁻¹)	4.3 × 10 ⁶	7.1 × 10 ⁹	5.0 × 10 ⁸	1.71 × 10 ⁹	1.1 × 10 ⁵	3.20 × 10 ⁸	2.95 × 10 ⁷	8.06 × 10 ⁷
Toxicity (TU)	11.1	51.7	32	17.21	<1	<1	<1	0.0
Ammonium (mg NH ₄ ⁺ L ⁻¹)	28.1	52.3	41.35	12.15	0.10	0.75	0.425	1.38
Temperature (°C)	11.6	14.6	13.1	1.73	12.7	15.2	13.95	1.44
2-Hydroxybenzothiazole (ng L ⁻¹)	219	422	288	91.85	98.55	105.5	102.025	4.91
Acesulfame potassium (ng L ⁻¹)	4102	5851	5021.5	716.22	205.1	58.51	131.805	103.65
Amitriptyline hydrochloride (ng L ⁻¹)	68	112	79.75	21.55	54.4	56	55.2	1.13
Bezafibrate (ng L ⁻¹)	199	474	288	128.24	59.7	94.8	77.25	24.82
Caffeine (ng L ⁻¹)	16,047	31,704	22,019.75	6828.34	160.47	317.04	238.755	110.71
Carbamazepine (ng L ⁻¹)	86	120	103	17.47	81.7	96	88.85	10.11
Ciprofloxacin hydrochloride (ng L ⁻¹)	51	79	65.5	11.70	33.15	39.5	36.325	4.49
Diclofenac sodium salt (ng L ⁻¹)	458	766	624.5	134.30	206.1	306.4	256.25	70.92
Diuron (ng L ⁻¹)	57	174	113.5	55.92	54.15	130.5	92.325	53.99
Eprosartan mesylate (ng L ⁻¹)	799	1588	1077.5	356.09	319.6	397	358.3	54.73
Phenytoin (ng L ⁻¹)	36	49	42.75	5.56	32.4	34.3	33.35	1.34
Genistein (ng L ⁻¹)	739	1198	1078	226.07	0.0	0.0	0.0	0.0
Irbesartan (ng L ⁻¹)	714	1070	858.75	150.35	642.6	909.5	776.05	188.73
Isoproturon (ng L ⁻¹)	2	3	2.25	0.50	2.0	1.8	1.9	0.14
Ketoprofen (ng L ⁻¹)	579	1117	801	243.72	86.85	111.7	99.275	17.57
Losartan potassium (ng L ⁻¹)	917	1723	1240.75	352.23	275.1	344.6	309.85	49.14
Methylparaben (ng L ⁻¹)	2094	8400	4642.5	2814.78	0.0	0.0	0.0	0.0
Norfloxacin hydrochloride (ng L ⁻¹)	233	452	353.25	90.27	128.15	203.4	165.775	53.21
Acetaminophen (ng L ⁻¹)	48,352	112,762	66,523	30,933.75	483.52	1127.62	805.57	455.45
Perfluorooctane sulfonamide (ng L ⁻¹)	148	302	212.25	64.63	148	166.1	157.05	12.80
Progesterone (ng L ⁻¹)	205	276	241	29.02	0.0	0.0	0.0	0.0
Propranolol hydrochloride (ng L ⁻¹)	17	24	21.75	3.20	13.6	16.8	15.2	2.26
Sulfamethoxazole (ng L ⁻¹)	1350	8828	3799.25	3406.83	472.5	1765.6	1119.05	914.36

Table 3. Cont.

	INFLUENT				EFFLUENT			
	MIN	MAX	AVERAGE	S.D.	MIN	MAX	AVERAGE	S.D.
Telmisartan (ng L ⁻¹)	593	1476	1039.75	455.53	415.1	885.6	650.35	332.69
Testosterone (ng L ⁻¹)	61	107	85.75	21.87	0.0	0.0	0.0	0.0
Trimethoprim (ng L ⁻¹)	558	851	747.25	131.70	195.3	85.1	140.2	77.92
Valsartan (ng L ⁻¹)	10,072	30,979	17,633.5	9407.63	503.6	309.79	406.695	137.04

3.1.2. Removal Yields of CECs in the c-UF Pilot Plant

In Table 4, the removal yields of the CECs detected in the Galindo WWTP were analysed, both for the biological treatment and for the c-UF plant following this process.

Table 4. Removal yields of the different CECs in the secondary treatment and through the c-UF pilot plant with a self-cleaning system.

Compound (ng L ⁻¹)	Removal in Secondary Treatment (%)			Removal in c-UF Plant (%)		
	MIN	MAX	AVERAGE	MIN	MAX	AVERAGE
2-hydroxybenzothiazole	59.5	71.4	68.6	1.1	35.2	27.3
Acesulfame potassium	94.9	96.4	95.4	17.0	21.7	19.8
Amitriptyline hydrochloride	20.5	48.6	13.5	54.6	71.1	63.9
Bezafibrate	72.9	80.7	77.6	25.7	43.2	34.3
Caffeine	99.8	99.8	99.8	0.0	33.5	25.6
Carbamazepine	5.2	21.9	8.7	19.0	31.2	28.4
Ciprofloxacin hydrochloride	36.3	46.9	40.2	14.9	19.2	16.7
Diclofenac sodium salt	56.0	58.9	54.0	14.4	39.4	29.0
Diuron	4.0	25.8	20.0	14.3	32.8	29.5
Eprosartan mesylate	61.0	73.0	70.6	17.5	18.6	18.2
Phenytoin	7.0	26.9	24.4	25.4	39.0	26.8
Genistein	100.0	100.0	100.0	—	—	—
Irbesartan	9.0	14.6	7.2	12.9	29.0	15.3
Isoproturon	0.0	50.0	33.3	0.0	75.0	62.5
Ketoprofen	84.6	91.7	87.8	21.5	61.3	40.4
Losartan potassium	70.5	79.9	78.1	16.0	22.8	22.7
Methylparaben	100.0	100.0	100.0	—	—	—
Norfloxacin hydrochloride	46.1	55.3	53.2	21.0	32.9	24.8
Acetaminophen	99.5	99.8	99.6	0.0	45.7	43.5
Perfluorooctane sulfonamide	0.0	72.9	31.3	36.3	55.3	48.4
Progesterone	100.0	100.0	100.0	—	—	—
Propranolol hydrochloride	7.1	47.4	20.0	12.9	34.9	18.5
Sulfamethoxazole	67.3	95.4	83.7	1.2	75.2	10.2
Telmisartan	6.2	60.5	37.3	5.5	59.1	23.3
Testosterone	100.0	100.0	100.0	—	—	—
Trimethoprim	66.3	87.4	72.3	35.3	64.4	27.0
Valsartan	91.0	97.0	95.3	7.7	79.7	23.0

The variability of the observed yields for the different CECs is due to the strong dependence of the water stream treated in the WWTP with the precipitations [57]. It was observed that CECs such as genistein or progesterone were completely removed in the secondary treatment, in line with what was observed by Gros et al. [58], due to removal mechanisms based on adsorption and biodegradation. According to the study by Yu et al. [59], of the two possible pathways, biodegradation under aerobic conditions would be the main pathway removing both compounds.

However, drugs such as phenytoin (24.4%), irbesartan (7.2%) or carbamazepine (8.7%) were observed to be completely refractory to biological treatment [60]. Guedes-Alonso et al. [61] obtained carbamazepine removal yields of 5.7%, which are similar to those obtained in the Galindo WWTP. This low removal yield of carbamazepine is due to its molecular structure and hydrophilicity. For irbesartan or phenytoin, removal yields were similar to those observed by Das et al. [62] (with 21.1% and 6.5%, respectively) because these antibiotics induce an inhibition process of biocenosis [63].

Regarding the removal of CECs by ultrafiltration, it was observed that compounds such as amitriptyline (63.9%) and perfluorooctanesulfonamide (48.4%) performed better than others such as ciprofloxacin (16.7%) or sulfamethoxazole (10.2%). The difference in performance is due to the changing adsorption capacity of the filter membrane according to the CEC. Ferreira et al. [9] studied the adsorption mechanism that occurred in an ultrafiltration process at certain concentrations of CECs, such as amitriptyline or sulfamethoxazole. According to the adsorption equilibria of such compounds [9], the high concentration of both CECs at the c-UF inlet favours retention during filtration.

To evaluate the efficiency of this c-UF unit, it is necessary to evaluate and determine a recovery factor, Y (%), that takes into account the overall performance of this operation, as defined in Equation (2):

$$Y = \frac{Q_P}{Q_A} \cdot 100 = \left(1 - \frac{Q_R}{Q_A}\right) \cdot 100 \quad (2)$$

where Q_P is the permeate stream, Q_A is the feed stream and Q_R is the reject stream in $\text{m}^3 \text{h}^{-1}$. According to Equation (2), the recovery rate associated with the c-UF unit was 97.9% for 425.67 min, in which a complete cycle of ultrafiltration followed by washing occurred. The recovery obtained from this c-UF system is slightly higher than that obtained by other ultrafiltration systems studied in the literature. Fan et al. [64] studied the influence that materials had on the operation of ultrafiltration modules on a pilot scale. According to this study, they obtained recoveries of 93.5%, 95.3% and 95.9% for the modules built in PES, polyvinylidene fluoride (PVDF) and polyacrylonitrile (PAN), respectively. The slight increase in the recovery factor of 4.4% is largely due to the c-UF self-cleaning system, which is explained in the following subsection.

3.1.3. Effect of the Self-Cleaning System on the Water Quality

To evaluate the effect of self-cleaning, the suspended solids (SS), turbidity and dissolved organic carbon (DOC) were followed both in the permeate and in the flushing and backwashing operations (see Figure 3). A significant reduction of 87.5% in SS was observed in the permeate stream. In contrast, the streams corresponding to washing the membranes presented a much higher SS concentration compared to the feed stream. It should be noted that within the washing cycle, flushing had the highest SS removal (71 mg L^{-1}), while for backwashing, only 30 mg L^{-1} was removed. This indicates that the washing cycles are not nearly effective enough to partially recover the yield at the beginning of the filtration operation. According to Bourgeois et al. [65], this inefficiency is due to progressive fouling over time, either by solid material encrusting on the membrane surface or deposition and accumulation of particles in the form of gel inside the pores. The differences observed in the degree of SS removal between the four selected days explain the variability of the characteristics of the effluent from the secondary treatment.

Regarding the experiments performed with the self-cleaning system, a reduction in SS of 90.1–100% in the permeate stream was observed (see Figure 3b). This is because this novel system prevents the formation of a cake and the accumulation of a number of particles that block the membrane surface. Installing a self-cleaning system reduces the concentration of solids between 38 and 60%. This improvement is also noticeable in the wash streams, in which there was a lower concentration of solids in the flushing streams of 32.0 mg L^{-1} .

With respect to turbidity, Figure 3c illustrates that, without using the self-cleaning system, the reduction in turbidity was between 63 and 83%. On the other hand, with respect to the washing streams, a very high turbidity of 26.2 NTU was observed in flushing. These yields are in line with those obtained by authors such as Chen et al. [66] with a PVDF membrane, in which they achieved a reduction of 60% with an initial turbidity of 20 NTU. This decrease in yield may be because a large number of particles distributed along the membrane surface were able to form a layer in the form of a cake so thick that it contributed to the fouling of the membrane [67].

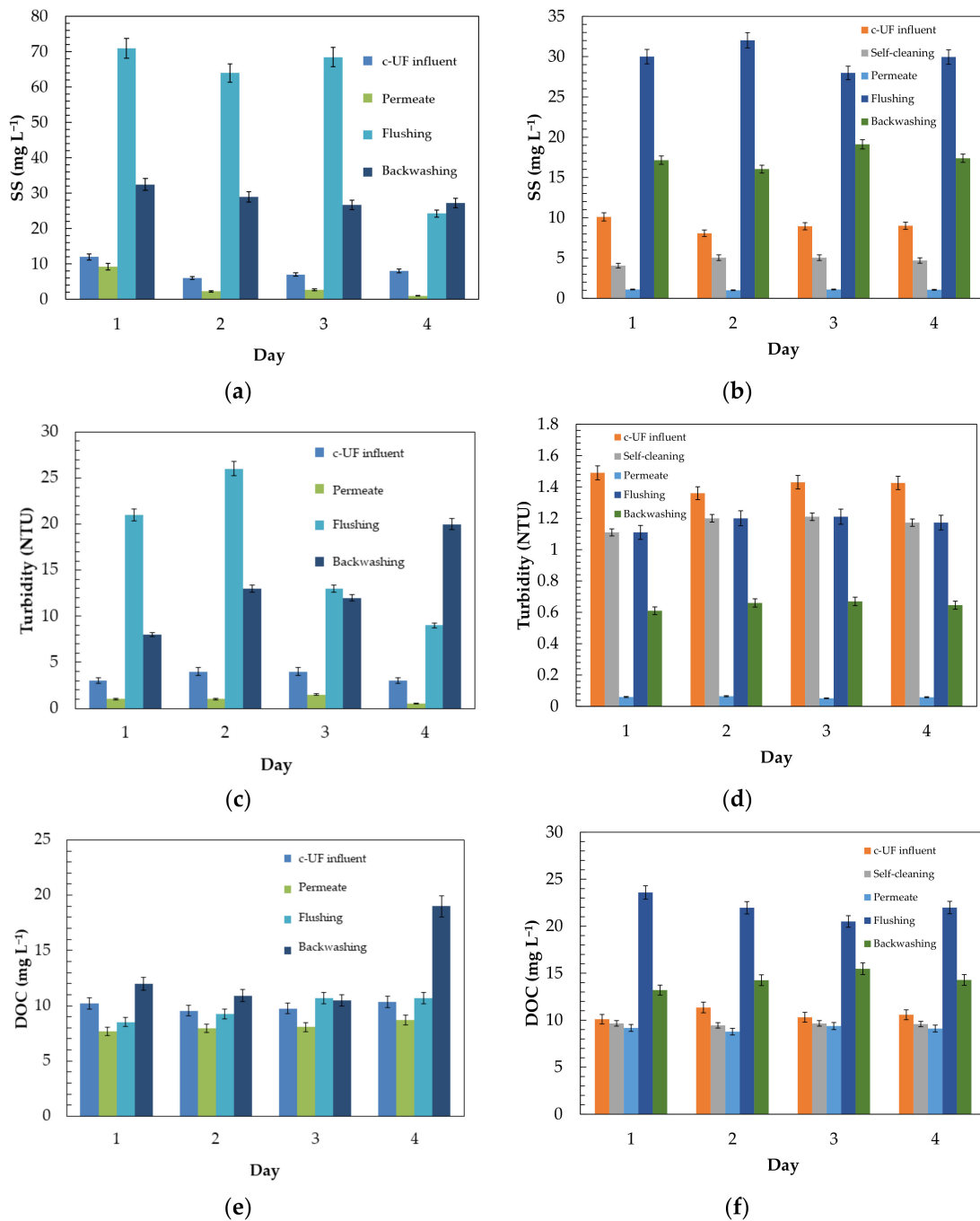


Figure 3. Comparison of the traditional c-UF system and self-cleaning c-UF on an effluent from the secondary treatment. Evaluation of macroscopic parameters of water quality: (a) suspended solids (SS); (c) turbidity; and (e) dissolved organic carbon (DOC); (b,d,f) with self-cleaning system.

Regarding the use of the self-cleaning system with the c-UF unit, Figure 3d shows a greater reduction in turbidity than that achieved without it, obtaining a reduction of between 95 and 96% in the permeate. On the other hand, according to Figure 3d, with the self-cleaning system alone, it was possible to reduce de facto by 12–25% the turbidity of the effluent from the secondary treatment. In addition, the wash stream corresponding to flushing showed a very high turbidity, somewhat indicative of a more efficient operation of the system, unlike a conventional UF system. From the SS and turbidity analyses, it was observed that similar trends followed in terms of greater production efficiency in the presence of the self-cleaning system. Likewise, there is a relationship between SS and

turbidity, as studied by Oliveira et al. [68], in which they observed that a decrease in solids necessarily implied a decrease in turbidity in the water.

In addition to SS and turbidity, the removal of dissolved organic carbon (DOC) was studied, as shown in Figure 3e,f. It was observed that the yields achieved in the c-UF system without the self-cleaning system did not exceed 15–25%. This is mainly because ultrafiltration processes are not the most effective for removing dissolved organic material [37,69]. When the self-cleaning system is included, it did not bring with it a significant reduction since the small observed improvement of 2.6% was within the range of experimental error. For the effective removal of dissolved organic matter, a nanofiltration membrane would be required, which would be totally inadvisable because of the fouling problem, causing a rapid blockage of the membrane pores that would prevent maintaining an adequate permeate stream for the process [70]. Another aspect that would contraindicate its use would be the high energy cost involved since an operating pressure of at least 5–20 bar is necessary [71].

In addition to the presence of CECs, another risk involved in the reuse of these resources of water is the presence of harmful microorganisms, which frequently produce toxic compounds once they come into contact with humans [72]. Therefore, the presence of *E. coli* bacteria, total coliforms and toxicity were studied as macroparameters indicative of the quality of the water intended for reuse, as shown in Table 5.

Table 5. Evaluation of the removal of toxicity and microbial density using c-UF technology with and without a self-cleaning system.

Process	Value	Parameter		
		Toxicity (TU)	<i>E. coli</i> (CFU 100 mL ⁻¹)	Total Coliforms (CFU 100 mL ⁻¹)
c-UF inlet	MIN	11.1	1.66×10^5	4.30×10^6
	MAX	51.7	5.35×10^5	7.10×10^9
	AVERAGE	32	3.51×10^5	5.00×10^5
	S.D.	17.21	2.13×10^5	1.71×10^9
Permeate	MIN	<1	0	0
	MAX	<1	2	10
	AVERAGE	<1	0.7	6
	S.D.	0.0	1.01	5.03
c-UF outlet without self-cleaning system	MIN	20.5	3.07×10^5	7.96×10^6
	MAX	95.6	9.90×10^5	1.31×10^{10}
	AVERAGE	44.3	5.51×10^5	3.23×10^8
	S.D.	38.4	3.46×10^5	7.49×10^9
Backwashing	MIN	18.4	2.74×10^5	6.88×10^6
	MAX	85.8	8.83×10^5	1.14×10^{10}
	AVERAGE	39.8	4.92×10^5	2.80×10^8
	S.D.	34.4	3.09×10^5	6.48×10^9
Permeate	MIN	<1	0	0
	MAX	<1	0	0
	AVERAGE	<1	0	0
	S.D.	0.0	0	0
c-UF outlet with self-cleaning system	MIN	18.3	2.74×10^5	7.10×10^6
	MAX	85.3	8.83×10^5	1.17×10^{10}
	AVERAGE	39.5	4.92×10^5	2.88×10^8
	S.D.	34.2	3.09×10^5	6.68×10^9
Backwashing	MIN	15.8	2.36×10^5	6.11×10^6
	MAX	73.4	7.60×10^5	1.01×10^{10}
	AVERAGE	34.0	4.23×10^5	2.48×10^8
	S.D.	29.5	2.66×10^5	5.75×10^9

According to Table 5, regardless of whether the self-cleaning system was used in the c-UF module, both *E. coli* and total coliforms were completely removed in the permeate stream. The pathogen removal yield of this system is in line with that observed by other researchers in which they inactivated *E. coli* in ranges ranging between 80 and 99% and between 95 and 100% [73,74]. The complete removal of pathogenic microorganisms together with the low levels of turbidity observed in the permeate stream below 1 NTU for both situations indicates that when the large particles are completely removed, this tends to eradicate the pathogens since they are not able to adhere to or remain embedded in the particles where they can reproduce more effectively [73]. In addition, this is because the pore size of the membrane (20 nm) is small enough to retain and block the passage of coliform species [75]. The results observed in the wash streams, both flushing and backwashing, indicate that the functioning of the c-UF wash cycles is adequate to notably increase the presence of coliforms and *E. coli*. However, when the self-cleaning system is included, it was observed that this would increase the operating times of water production by eliminating a lower volume of pathogens that would have been retained on the surface of the membrane. The same was observed by Slavik et al. [76] in a study that evaluated the impact of washing procedures on filtration productivity. According to this study, the backwashing mode had no impact on the efficiency of water production but did on the length of each cycle, which can be prolonged by optimizing the washing operations or introducing some type of additional system cleansing that avoids the irreversible adhesion of the retained compounds and particles.

Although UF technology is highly efficient at removing SS and pathogenic microorganisms, it is important to demonstrate that it is also effective in removing other compounds that could not be detected, either due to their low frequency of appearance or the low concentrations presented, below the limits of detection of the analytical techniques [9]. According to Table 5, it was observed that, in both systems, the toxicity decreased sharply until reaching a value less than 1. This indicates that the effluent produced was not toxic and that the UF operation was efficient enough to also retain the compounds identified as unknown.

3.2. Reject Stream Treatment via Ozonation Technologies

3.2.1. Analysis of Ozonation Removal Yields

To reduce the environmental impact of the UF operation and increase water production, the reject streams were treated in an ozonation process. In Table 6, the removal yields obtained from the identified CECs and the overall yield are shown. For this, the part removed during secondary treatment and the c-UF operation itself were taken into account.

In general, the high oxidation selectivity of ozone was observed due to its particular electronic structure. Molecular ozone was more effective with CECs that contained functional groups such as amines, phenols and double bonds [45,77,78]. This is because these CECs can be more easily degraded into degradation byproducts and acids by redox reactions and electrophilic substitution reactions. According to Table 6, in general, all identified CECs were completely removed with the exception of 2-hydroxybenzothiazole and caffeine, with 39.7% and 38.1%, respectively. This is because they are two of the CECs most refractory to ozonation. In the case of 2-hydroxybenzothiazole, the low yield is due to the low selectivity and reactivity of the hydroxyl radicals towards this compound. This was observed by Valdés et al. [79] in a study where they determined that the direct reaction with ozone was more selective and reactive ($k = 2.3 \text{ M}^{-1} \text{ s}^{-1}$) than the indirect reaction at an alkaline pH ($k = 5.6 \times 10^{-9} \text{ M}^{-1} \text{ s}^{-1}$). Regarding the yield of caffeine, at pH = 7.02, the degradation kinetic constant ($k = 0.92 \text{ M}^{-1} \text{ s}^{-1}$) was significantly lower than that corresponding to 2-hydroxybenzothiazole. Rosal et al. [80] observed that the presence of an intermediate reaction during the ozonation of caffeine could promote a stronger ozone decomposition. For other compounds, such as trimethoprim, with a higher removal percentage (97.8%), authors such as Kuang et al. [81] observed that the major contributors to the oxidation reaction were hydroxyl radicals, while the molecular ozone

pathway played a minor role. Regarding the overall removal yield, those CECs removed via biological treatment, such as valsartan (96.4%) or acetaminophen (99.7%), had better removal yields than the less biodegradable and more recalcitrant compounds, such as carbamazepine (45.2%) or irbesartan (35.3%). This would partly explain the importance of secondary treatment in the removal of CECs, apart from a significant improvement of the c-UF system itself through the incorporation of a self-cleaning system. The improvement resulting from secondary treatment implies a mitigation of problematic fouling on the membrane surface and a greater rejection of hydrophobic drugs [82].

Table 6. Removal yields obtained after ozonation of the CECs identified in the reject stream from the self-cleaning c-UF system. Experimental conditions: $F_G = 1.6 \text{ mg min}^{-1}$, $P = 1.5 \text{ bar}$, $C_{O_3} = 6.4 \text{ mg L}^{-1}$, $pH_0 = 9.0$, $T = 15.0 \text{ }^\circ\text{C}$ and $V = 30.0 \text{ L}$.

Compound	INFLUENT		EFFLUENT		Removal by Ozonation (%)	Overall Removal (%) ¹
	Average (ng L ⁻¹)	S.D.	Average (ng L ⁻¹)	S.D.		
2-hydroxybenzothiazole	235.5	43.97	142.0	40.81	39.7	77.0
Acesulfame potassium	242	40.81	23.25	4.35	90.4	96.5
Amitriptyline hydrochloride	46.25	5.85	0.0	0.00	100.0	85.7
Bezafibrate	48.25	12.82	0	0.00	100.0	84.8
Caffeine	67	26.44	41.5	14.20	38.1	99.8
Carbamazepine	117.75	28.91	0.0	0.00	100.0	45.2
Ciprofloxacin hydrochloride	25.5	5.80	0.0	0.00	100.0	61.6
Diclofenac sodium salt	276	82.58	12.5	2.38	95.5	78.3
Diuron	107.5	17.33	0.0	0.00	100.0	45.0
Eprosartan mesylate	207.5	49.68	0.0	0.00	100.0	73.0
Phenytoin	43.5	8.10	0.0	0.00	100.0	48.6
Irbesartan	609.5	194.94	0.0	0.00	100.0	35.3
Ketoprofen	98.5	10.41	0.0	0.00	100.0	93.0
Losartan potassium	215.5	46.22	0.0	0.00	100.0	80.0
Norfloxacin hydrochloride	74	14.54	0.0	0.00	100.0	83.5
Acetaminophen	186	23.01	0.0	0.00	100.0	99.7
Perfluorooctane sulfonamide	796	202.24	0.0	0.00	100.0	85.0
Propranolol hydrochloride	17	4.40	0.0	0.00	100.0	47.9
Sulfamethoxazole	119.75	14.97	0.0	0.00	100.0	77.8
Telmisartan	393.5	125.82	0.0	0.00	100.0	71.1
Trimethoprim	178.5	25.49	4.0	4.62	97.8	82.2
Valsartan	452.75	62.54	0.0	0.00	100.0	96.4

¹ This yield considers the part removed via secondary treatment, as well as the c-UF process and the ozonation of the reject stream.

As in the permeate stream, in the monitoring of the c-UF-treated reject stream, the microbiological parameters were evaluated. Figure 4 summarizes the toxicity and microbial density measured, such as *E. coli* and total coliforms, during the ozonation process of the reject stream.

According to Figure 4, the waters from the reject stream of the c-UF operation contained 2.9×10^5 colonies in 100 mL of faecal coliforms. However, as expected, the analysis of pathogenic microorganisms after ozonation revealed the absence of bacteria such as *E. coli* with an ozone dose of 6.4 mg L^{-1} and a contact time of 180 min. On the other hand, total coliforms were completely removed from all samples and days analysed. This result is in line with that observed by Iakovides et al. [83] in a bubble reactor in which a WWTP effluent from a secondary treatment was ozonized. With a hydraulic retention time of 20 min, a dose of $0.75 \text{ g O}_3 \text{ g DOC}^{-1}$ was able to completely inactivate *E. coli*. Ostoich et al. [84] completely inactivated faecal coliforms below the detection limit of $<0.01 \text{ CFU mL}^{-1}$ by ozonation in a WWTP, using ozone doses ranging from 10 to 15 mg L^{-1} and a contact time of 30 min. Another study focused on the inactivation of pathogenic microorganisms by ozonation with different contact times and ozone doses up to 50 mg L^{-1} and showed that more than 99% of heterotrophs, enterococci and total coliforms were removed in just 30 min [85].

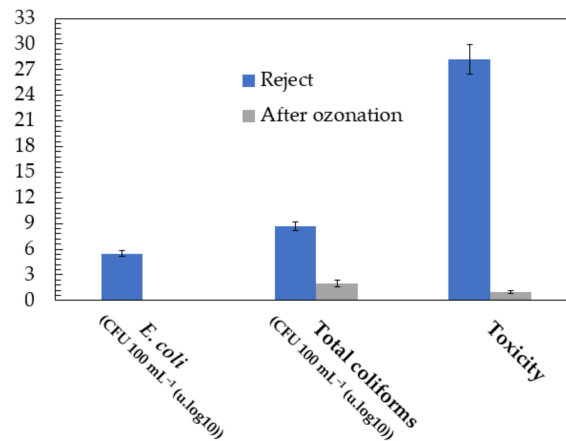


Figure 4. Reduction in toxicity and pathogenic microorganisms averaged over the 4 days analysed by applying an ozonation treatment. Experimental conditions: $F_G = 1.6 \text{ mg min}^{-1}$, $P = 1.5 \text{ bar}$, $\text{CO}_3 = 6.4 \text{ mg L}^{-1}$, $\text{pH}_0 = 9.0$, $T = 15.0 \text{ }^\circ\text{C}$ and $V = 30.0 \text{ L}$.

Regarding the toxicity of the ozonated effluent, it was observed that after 180 min of reaction, the toxicity was $<1 \text{ TU}$. This result is similar to that observed in the permeate stream of the c-UF. This corroborates the complete removal and mineralization of the identified CECs towards more biodegradable and lower molecular weight compounds [17].

3.2.2. Kinetic Analysis of the Ozonation Process

During the treatment of wastewater, SS is a crucial parameter for the analysis of the quality of water intended for reuse in agriculture. SS is a parameter that indicated the degradation of pollutants present in wastewater. In addition, they can act as a reservoir for pathogenic microorganisms due to their ease of adhering to particle surfaces [68]. Consequently, determining the relationship that SS could have with other global parameters, as other authors have done by associating suspended solids with turbidity, is necessary. According to Serajuddin et al. [86], SS are essentially constituted by organic matter. Currently, there is no correlation that relates SS with total organic carbon (TOC), unlike turbidity, for which there are already a few studies [68,87] concerning the waters of the Elbe River [86], despite finding significant seasonal variability. In this sense, considering dissolved organic carbon (DOC) could yield more reliable and accessible information for the monitoring of SS, which would include pathogenic microorganisms.

Considering that SS (mg L^{-1}) is constituted by an oxidizable part (oxidizable suspended solid, OSS) and a non oxidizable part (NOSS), which persist at the end of oxidation, the initial concentration of the OSS (OSS_0 , mg L^{-1}) can be quantified in terms of TOC according to the following expression:

$$\text{OSS}_0 = \text{SS}_0 - \text{NOSS} \quad (3)$$

Ozonation was monitored through the soluble organic matter (SOM) from the SS along with the existing SOM. The solubilization and subsequent degradation of OSS can be described through the following serial process:



In addition, taking into account the existence of an initial concentration of soluble organic matter (SOM_0 , mg L^{-1}) and assuming first-order reactions in Equation (4), the variation in SOM throughout ozonation can be described according to Equation (5) [88].

$$\text{SOM} = \frac{\text{OSS}_0 \cdot k_1}{k_2 - k_1} \cdot [\exp(-k_1 \cdot t) - \exp(-k_2 \cdot t)] + \text{SOM}_0 \cdot \exp(-k_2 \cdot t) \quad (5)$$

The first-order constant k_1 (min^{-1}) of this model represents the appearance of SOM as a consequence of the dissolution of SS. On the other hand, a first-order constant k_2 (min^{-1}) corresponds to the degradation of the SOM due to the action of the NOSS until reaching the residual value. Figure 5 shows the evolutions of SS and SOM for the ozonized reject stream fitted to the first-order serial kinetic model previously proposed.

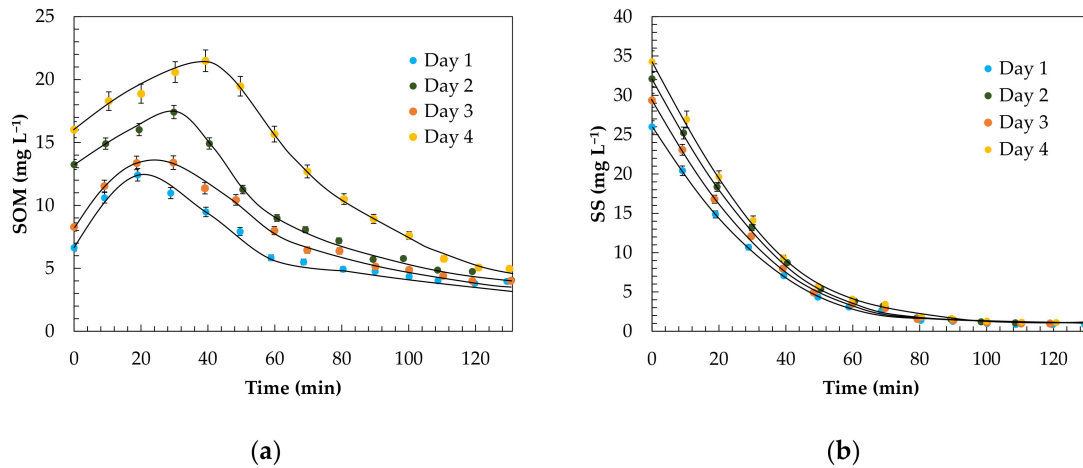


Figure 5. Evolution of the kinetics of SOM removal (a) and SS removal (b) fit to the first-order serial model. Experimental conditions: $F_G = 1.6 \text{ mg min}^{-1}$, $P = 1.5 \text{ bar}$, $C_{O_3} = 6.4 \text{ mg L}^{-1}$, $\text{pH}_0 = 9.0$, $T = 15.0 \text{ }^\circ\text{C}$ and $V = 30.0 \text{ L}$.

The k_1 and k_2 (min^{-1}) kinetic constants modelled in Table 7 were fit to the experimental values, minimizing the value of the mean standard deviation (σ), as shown in Equation (6) [89]:

$$\sigma = \sqrt{\frac{\sum_{i=1}^n \left(\frac{C_{\text{exp}} - C_{\text{sim}}}{C_{\text{exp}}} \right)^2}{N - 1}} \quad (6)$$

where N is the number of experimental points and C_{exp} and C_{sim} in mg L^{-1} are the experimental and simulated values obtained from simulating the first-order serial model, respectively. The mean standard deviation was less than 5.5% in all cases and demonstrates that through SOM monitoring, the removal of SS during an ozonation process can be extrapolated for WWTP streams.

Table 7. Kinetic parameters determined from the serial kinetic model proposed for predicting the SS from the SOM.

Parameters	Experiment			
	Day 1	Day 2	Day 3	Day 4
k_1 (min^{-1})	0.0438	0.0279	0.0308	0.0212
k_2 (min^{-1})	0.0525	0.0334	0.0369	0.0254
σ	0.0430	0.0520	0.0550	0.0310
η_{O_3} (mg O_3 (mg SOM^{-1}))	31.20	21.44	23.70	15.08

According to the proposed model, the higher the constants k_1 and k_2 are, the greater the SS and SOM removal rates. Consequently, a better ozonation behaviour was found in the experiment corresponding to Day 1, with a constant $k_1 = 0.0438 \text{ min}^{-1}$ and $k_2 = 0.0525 \text{ min}^{-1}$. According to Table 7 and the evolutions shown in Figure 5, the observed divergences could be due to the variability in the nature of the pollutant load of the reject stream, typical of systems highly influenced by the habits of the population [17]. However, the proposed model showed its robustness under different scenarios.

To estimate the efficiency of the ozonation treatment, Table 7 shows the parameter η_{O_3}

(mg O₃ mg SOM⁻¹) proposed by Álvarez et al. [90], through Equation (7), which relates the ozone consumed per mg of SOM removed:

$$\eta_{O_3} = \frac{F_G \cdot \int_0^t C_{O_3} - C_{O_3, \text{out}} \cdot dt}{V \cdot (SOM_0 - SOM)} \quad (7)$$

where F_G is the gas stream (mg min⁻¹), $C_{O_3, \text{out}}$ (mg L⁻¹) are the concentrations of ozone in the gas phase at the outlet of the reactor and V is the volume of treated water (L).

Ozone consumption was on the order of $\cong 20.0$ mg O₃ (mg SOM)⁻¹, similar to that observed by other authors, such as Álvarez et al. [90], with 19 mg O₃ (mg SOM)⁻¹, or Ferreiro et al. [91], with 26.8 mg O₃ (mg SOM)⁻¹, for the treatment of wastewater streams. In view of the results shown in Table 7, the ozone dose used on Day 1 could be reduced given the lower organic load (Figure 5) of the waters of that experiment and the high η_{O_3} value. However, for Days 2, 3 and 4, it would not be appropriate in any case to increase the ozone dose used, since an increase in the dose above 6.4 mg L⁻¹ would make the reuse proposal unfeasible by increasing the costs of ozonation in exchange for increasing the mineralization of practically negligible organic matter [13]. On the other hand, according to Beltran et al. [78], an excess of oxidant could lead to the generation of hydroperoxyl radicals (HO₂•) of lower oxidative capacity when the excess ozone reacts with the hydroxyl radicals produced.

3.3. Agriculture Reuse Aspects and Economic Estimation of the c-UF Process Coupled to Ozonation

3.3.1. Regulatory Aspects

In the reuse of water for direct use in agriculture, treatment with c-UF coupled to an ozonation system is proposed here to convert it into recycled water. The application of these reused waters is regulated by different criteria according to the country of destination. However, in the European Union (EU), to harmonize the regulation of each of the member states, a new regulation on water reuse has recently been proposed (EU 2020/741) [14]. This new regulation defines (i) types of crops, (ii) minimum quality requirements and (iii) quality control of the reclaimed water. In Table 8, the minimum criteria that the reclaimed waters must meet are detailed in the regulations of different governments for their use in all food crops, including tubers that could be consumed raw and food crops in which the edible part is in direct contact with the reclaimed waters, using any irrigation methods. Likewise, the average values obtained in this work were collected taking into account the c-UF process with a self-cleaning system and the coupled ozonation system for treating the reject stream.

According to Table 8, the new regulation incorporates stricter and more demanding parameters than other regulations adopted to date. For example, in comparison with the Royal Law 1620/2007 of Spain for *E. coli*, it is set at 100 CFU 100 mL⁻¹, while in the European Regulation (EU 2020/741), it is set at 10 CFU 100 mL⁻¹. The SS were set at 20 mg L⁻¹, compared to 10 mg L⁻¹. Finally, turbidity changed from 10 to 5 NTU with the new regulation.

In view of the results obtained, the reclaimed water obtained from the c-UF technology coupled to the ozonation system met the criteria established in the new European regulation in each and every one of the parameters specified by the regulations. By meeting these new limitations, it was ensured that the reclaimed waters were safe for irrigation in agricultural activities and that the environment was protected. In addition, a circular economy is promoted, since it would allow the reuse of more than half of the water flow of the WWTP effluent, avoiding the direct extraction of water from surface and underground sources. Additionally, this proposal would combat climate change and contribute to the fulfilling the SDG and Directive 2000/60/EC by promoting water savings.

Table 8. Minimum quality requirements of recycled water from WWTPs established by different state regulations for use in irrigated agricultural activities [5,14,92].

Parameter	This Work	EU 2020/741	Spain (Royal Law 1620/2007)	Italy (Regulation No. 8 of 18 April 2012)	Portugal (2006 Portuguese Standard NP 4434)	US EPA (EPA 600-R-12-618/2012)	Australia (ARMCANZ-ANZECC-NHMRC/2000)	Saudi Arabia (2009)
pH	8.20	n.a.	n.a.	6.00–9.50	6.50–8.40	6.00–9.00	5.00–8.50	6.00–8.50
Suspended solids (mg L ⁻¹)	0.06	≤10.0	20.0	10.0	60.0	n.a.	n.a.	n.a.
Turbidity (NTU)	0.95	≤5.0	10.0	n.a.	n.a.	≤2.0	n.a.	n.a.
BOD ₅ (mg L ⁻¹)	2.90 ¹	≤10.0	n.a.	n.a.	n.a.	≤10.0	n.a.	n.a.
<i>E. coli</i> (CFU 100 mL ⁻¹)	0.0	≤10.0	100.0	10.0	100.0	n.a.	n.a.	n.a.
Total coliforms (CFU 100 mL ⁻¹)	2.0	≤6.0	n.a.	n.a.	n.a.	null	n.a.	n.a.
Toxicity (TU)	<1.0	n.a.	n.a.	n.a.	n.a.	n.a.	n.a.	n.a.

¹ Calculated by Nutt et al. [93], the correlation between 5 day biochemical oxygen demand (BOD₅) and total organic carbon (TOC) for wastewater treatment plants (WWTPs).

3.3.2. Economic Comparison of c-UF Coupled to Ozonation Systems and a Conventional Tertiary Treatment

The costs related to reclaiming water through a conventional tertiary treatment and c-UF with ozonation are comparatively analysed. In both cases, the most representative costs were associated with the energy consumption of the different equipment used and the consumption of chemical reagents during some of the processes of the global operation.

Figure 6 shows the consumption derived from energy, as well as the reagents that were used in the tertiary treatment of the Galindo WWTP. Regarding the tertiary treatment (Figure 6a,b), the energy consumption was mainly attributed to the pumps (pumping raw water, pumps for the lamellar decanter for purging sludge, pumping for washing sand filters, bilge pumps for washing and treated water and chemical metering pumps), agitators (mixing tank, flocculation chamber and lamellar decanter), air blowers for washing the filters, helical fans and lamps for UV disinfection. It was estimated that the energy consumption of the Galindo WWTP was 161,110 kWh year⁻¹.

Regarding the cost attributed to the consumption of chemical reagents (Figure 6c), the use of sodium hypochlorite (NaClO) as an oxidizing agent and alumina sulphate (Al₂(SO₄)₃) as a coagulant were taken into account. In addition, the consumption of anionic polyelectrolyte as a flocculating agent was considered.

The energy consumption for the tertiary treatment plant estimated by the volume of the treated water was 0.1890 kWh m⁻³. Considering that the cost of energy for the industry in Spain is 0.0758 € kWh⁻¹ [94], the energy cost per cubic metre of treated water obtained by tertiary treatment was 0.0143 € m⁻³.

For the estimation of the treatment cost with c-UF coupled to the ozonation system, the FLUKE 434/435 True Phase Power Quality Analysers (Fluke Ibérica S.L, Alcobendas, Spain) tool was used. This equipment monitors and records the energy consumption in the different stages of a filtration cycle.

The energy consumption required in the filtration stage was estimated at 0.6322 kWh. Additionally, it is necessary to consider the washing phase (flushing, backwashing and rinsing), which was 0.1191 kWh. Apart from the wash per cycle, it is necessary to consider the Cleaning-In-Place (CIP) and Chemical Enhanced Flushing (CEF) operations over an operating period of 30 days with a volume of treated water of 2300 m³. With all this, it was estimated that the energy consumption for a 30-day supercycle was 725 kWh, including the energy consumption associated with the self-cleaning system. Another aspect that was considered was the costs of consumption of chemical reagents for the CEF and CIP in the c-UF unit, in which 25% NaOH, 33% HCl and 13% NaClO were used. This estimation

was made on the basis of the consumption of the reagents spent during both types of chemical cleaning.

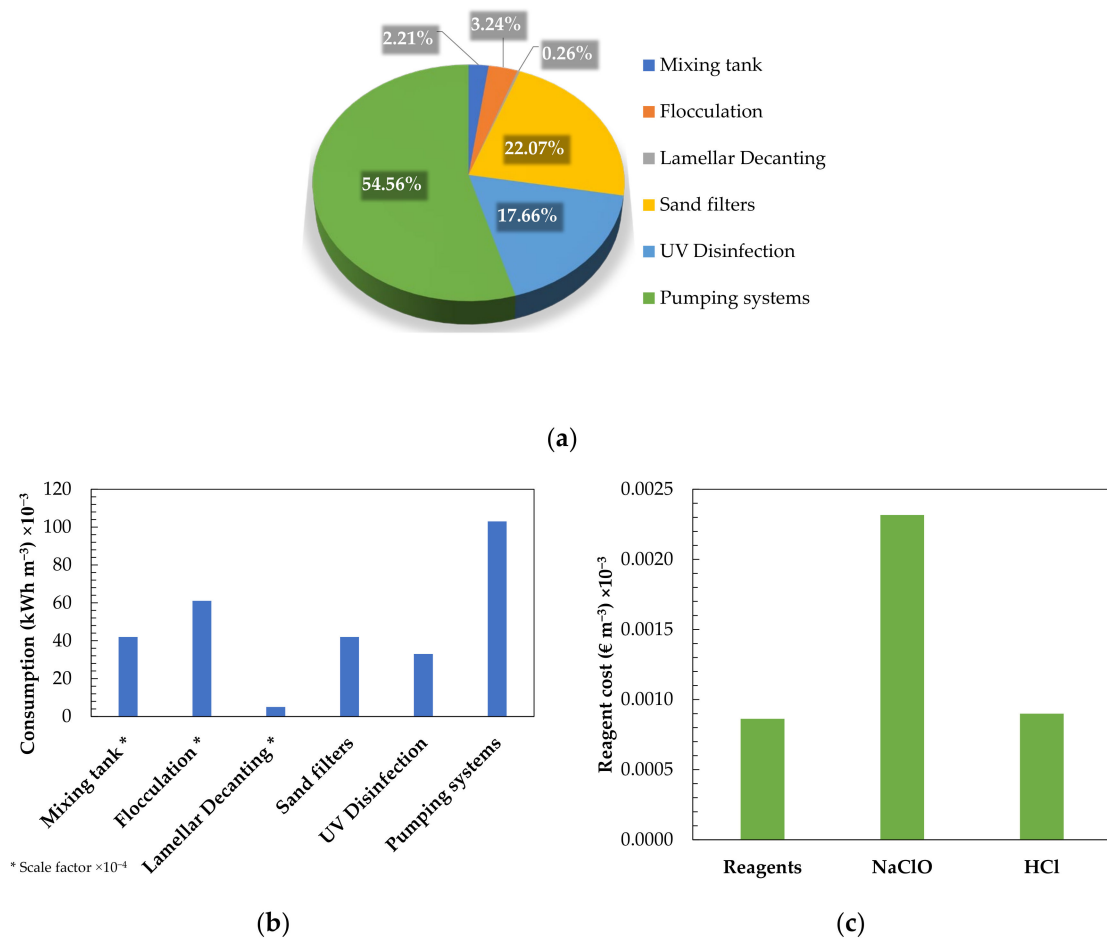


Figure 6. Electrical consumption and cost of the chemical reagents used in the conventional tertiary treatment of the Galindo WWTP: (a) estimated percentage of the total energy consumption related to each process of the tertiary treatment; (b) energy consumption of each process involved in the tertiary treatment; and (c) cost relative to the reagents used in the oxidation and coagulation–flocculation chambers.

The estimation of ozonation energy consumption was performed according to the criteria of Krichevskaya et al. [95], referring to a specific energy consumption of the ozone generator of 7 kWh kg⁻¹ O₃. Consequently, the energy consumed by the ozonation treatment was estimated at 0.054 kWh m⁻³.

In Figure 7, from the energy consumption, the cost per cubic metre of treated water by the c-UF coupled to ozonation process was estimated to be 0.0284 € m⁻³. The highest consumption comes from the c-UF unit, while the self-cleaning system turns out to be the smallest (0.00013 € m⁻³), but significant for the process efficiency based on the innumerable technical advantages mentioned above.

Finally, taking into account the economic costs related to energy and reagents of the conventional tertiary treatment and the c-UF system coupled to an ozonation process, a cost of 0.0325 € m⁻³ was determined for the proposed new system versus the cost of 0.0534 € m⁻³ for the conventional tertiary treatment, which would mean an economic savings of 39.1%. Authors such as Jodar-Abellan et al. [13] estimated a water reclamation cost of 0.06 € m⁻³ for the tertiary treatment in a WWTP in Valencia (Spain), a cost significantly higher than the alternative proposed in this work. In addition, the c-UF system coupled to ozonation allows us to obtain high-quality reclaimed water more than meets the minimum requirements established by the EU 2020/741 regulation and anticipates

future restrictions on water reuse concerning the removal of CECs. This action would foster a circular economy between large cities and the agricultural sector through safe, sustainable and environmentally friendly food production, thus avoiding the discharge of urban wastewater into the water environment.

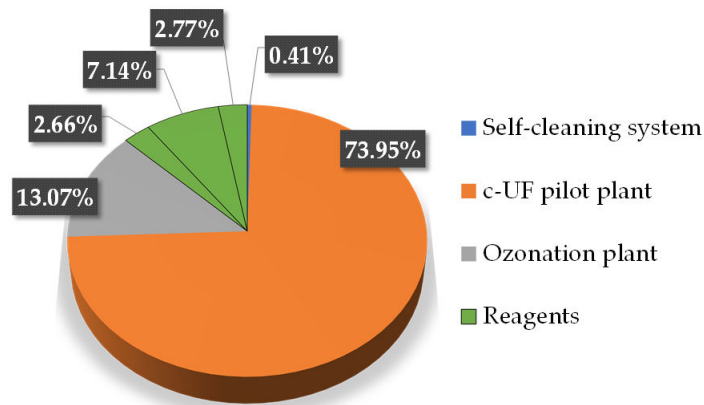


Figure 7. Partial costs (€ m^{-3}) of the proposed c-UF/ozonation treatment: c-UF (0.024), ozonation (0.0042) and reagents (0.00086), expressed as percent of the total cost of 0.0325 € m^{-3} .

4. Conclusions

In this work, a novel continuous ultrafiltration system with self-cleaning capacity coupled to an ozonation process for water reclamation from a WWTP was studied for use in agriculture. The ability of c-UF to retain CECs of frequent appearance and pathogenic microorganisms was evaluated. During c-UF, it was observed that CECs such as amitriptyline (63.9%) and perfluorooctanesulfonamide (48.4%) performed better than others such as ciprofloxacin (16.7%) or sulfamethoxazole (10.2%). These differences in removal yields are associated with changing adsorption mechanisms according to each compound and determinant in the removal of this type of contaminant.

Regarding other physical–chemical parameters, it was observed that the self-cleaning system of the c-UF unit contributed to a reduction in turbidity of 95–96% and suspended solids of 90.1–100%. The incorporation of the self-cleaning system did not result in a significant reduction in the DOC (15–25%) compared to the c-UF unit without it.

The presence of *E. coli* bacteria, total coliforms and toxicity were studied as macroparameters indicative of the microbiological quality of the water. Regardless of whether the self-cleaning system was used in the c-UF unit, both *E. coli* and total coliforms were completely removed in the permeate stream.

Regarding the ozonation process following the c-UF, for treating the reject stream, ozonation was more effective with those CECs containing functional groups, such as amines, phenols and double bonds. All identified CECs were completely removed except for 2-hydroxybenzothiazole and caffeine, with 39.7% and 38.1%, respectively. Regarding the inactivation of pathogenic microorganisms with an ozone dose of 6.4 mg L^{-1} and a contact time of 180 min, the study revealed an absence of bacteria such as *E. coli* and a toxicity less than one. A first-order kinetic model of serial stages was proposed that describes the removal of SS with an error of less than 5%.

The water reclaimed with c-UF technology, followed by ozonation, meets the criteria established in the new European regulation (EU 2020/741) in each and every one of the parameters specified by the regulations.

Finally, taking into account the economic costs related to the energy and reagents of the conventional tertiary treatment system and the c-UF system with a self-cleaning system coupled to an ozonation process, a cost of 0.0325 € m^{-3} was determined for the novel system proposed versus a cost of 0.0534 € m^{-3} for the conventional tertiary treatment system.

Implementing this proposal would contribute to fighting against climate change and compliance with the SDG and Directive 2000/60/EC by addressing the problem of water scarcity, as well as promoting a circular economy between large cities and the agricultural sector. A further step in this research could focus on the effect that these regenerated waters rich in nutrients (nitrogen and phosphorous) could have on the fertilisation of crops.

5. Patents

The c-UF system used in this work has been patented in Spain under patent number ES201431341A.

Author Contributions: Conceptualization, J.I.L. and C.F.; methodology and analyses, J.I.L., C.F. and N.E.; model validation, A.d.L. and N.V.; formal analysis, N.V., A.d.L. and C.F.; investigation, C.F. and A.d.L.; original draft preparation, C.F., J.M.L. and A.d.L.; review and editing, C.F., J.I.L. and J.M.L.; supervised the experimentation, J.I.L. and N.E.; acquired the funding, J.I.L. and N.E. All authors have read and agreed to the published version of the manuscript.

Funding: The authors are grateful to the University of the Basque Country (UPV/EHU) for their financial support of this study through the PPGA20/33 project, and C. Ferreiro's predoctoral PIF grant (PIF16/367).

Institutional Review Board Statement: Not applicable.

Informed Consent Statement: Not applicable.

Acknowledgments: Authors are acknowledge to the Consorcio de Aguas Bilbao Bizkaia for their assistance in the sampling from Galindo's WWTP and Fluytec S.A. for their c-UF unit used for this study.

Conflicts of Interest: The authors declare no conflict of interest.

Abbreviations

σ	Mean standard deviation
η_{O_3}	Efficiency of the ozonation treatment, mg O ₃ mg SOM ⁻¹
BOD ₅	Biochemical oxygen demand, mg O ₂ L ⁻¹
C ₀	Initian concentration of certain pollutant, mg L ⁻¹
C _{exp}	Experimental concentration, mg L ⁻¹
C _{O₃}	Ozone concentration at the reactor inlet, mg L ⁻¹
C _{O₃,out}	Ozone concentration in the gas phase at the outlet of the reactor, mg L ⁻¹
C _{sim}	Simulated concentration obtained from simulating the first-order serial model, mg L ⁻¹
EC ₅₀	Half maximal effective concentration refers to the concentration of pollutant, mg L ⁻¹
F _G	Ozone flow rate, mg min ⁻¹
k	Kinetic oxidation constant, M ⁻¹ s ⁻¹
k ₁	First-order constant referred to the appearance of SOM as a consequence of the dissolution of SS, min ⁻¹
k ₂	First-order constant referred to the degradation of the SOM due to the action of the NOSS, min ⁻¹
N	Number of experimental points
NOSS	Non oxidizable suspended solid, mg L ⁻¹
OSS	Oxidizable suspended solid, mg L ⁻¹
P	Pressure, bar
Q _A	Feed stream, m ³ h ⁻¹
Q _P	Permeate stream, m ³ h ⁻¹
Q _R	Reject stream, m ³ h ⁻¹
SOM	Soluble organic matter, mg L ⁻¹
T	Temperature, °C
TOC	Total organic carbon, mg L ⁻¹
Toxicity	Toxicity of the sample, TU
V	Reactor volume, L
Y	Recovery factor, %

AOP	Advanced Oxidation Process
CEC	Contaminant of emerging concern
CEF	Chemical Enhanced Flushing
CIP	Cleaning In Place
CNT	Carbon nanotube
c-UF	Continuous ultrafiltration
DOC	dissolved organic carbon
EDC	Endocrine disruptors
ESI	electrospray ionization source
G-L	Gas–liquid contact
LC-MS-MS	Liquid chromatography with tandem mass spectrometry equipment
MBR	Membrane bioreactor
MQ	Milli-Q quality water
PAN	Polyacrylonitrile
PES	Polyethersulfone
PPCP	Pharmaceutical and Personal Care Product
PVC	Polyvinylchloride
PVDF	Polyvinylidene fluoride
QqQ	Triple quadrupole
SDI	Silt density index
SPE	Solid-phase extraction
SS	Suspended solids
TU	Toxicity unit
WWTP	Wastewater treatment plant

References

- Kookana, R.S.; Drechsel, P.; Jamwal, P.; Vanderzalm, J. Urbanisation and emerging economies: Issues and potential solutions for water and food security. *Sci. Total Environ.* **2020**, *732*, 139057. [CrossRef]
- Luthy, R.G.; Wolfand, J.M.; Bradshaw, J.L. Urban Water Revolution: Sustainable Water Futures for California Cities. *J. Environ. Eng.* **2020**, *146*, 04020065. [CrossRef]
- Aitken, D.; Rivera, D.; Godoy-Faúndez, A.; Holzapfel, E. Water Scarcity and the Impact of the Mining and Agricultural Sectors in Chile. *Sustainability* **2016**, *8*, 128. [CrossRef]
- Maiolo, M.; Pantusa, D. A proposal for multiple reuse of urban wastewater. *J. Water Reuse Desalin.* **2017**, *8*, 468–478. [CrossRef]
- Chojnacka, K.; Witek-Krowiak, A.; Moustakas, K.; Skrzypczak, D.; Mikula, K.; Loizidou, M. A transition from conventional irrigation to fertigation with reclaimed wastewater: Prospects and challenges. *Renew. Sustain. Energy Rev.* **2020**, *130*, 109959. [CrossRef]
- Visanji, Z.; Sadr, S.M.K.; Johns, M.B.; Savic, D.; Memon, F.A. Optimising wastewater treatment solutions for the removal of contaminants of emerging concern (CECs): A case study for application in India. *J. Hydroinform.* **2019**, *22*, 93–110. [CrossRef]
- Mijangos, L.; Ziarrusta, H.; Ros, O.; Kortazar, L.; Fernández, L.A.; Olivares, M.; Zuloaga, O.; Prieto, A.; Etxebarria, N. Occurrence of emerging pollutants in estuaries of the Basque Country: Analysis of sources and distribution, and assessment of the environmental risk. *Water Res.* **2018**, *147*, 152–163. [CrossRef] [PubMed]
- United States Environmental Protection Agency. Contaminant Candidate List (4-CCL). Available online: <https://www.epa.gov/ccl/contaminant-candidate-list-4-ccl-4-0> (accessed on 9 October 2020).
- Ferreiro, C.; Gómez-Motos, I.; Lombraña, J.I.; De Luis, A.; Villota, N.; Ros, O.; Etxebarria, N. Contaminants of Emerging Concern Removal in an Effluent of Wastewater Treatment Plant under Biological and Continuous Mode Ultrafiltration Treatment. *Sustainability* **2020**, *12*, 725. [CrossRef]
- Chowdhary, P.; Bharagava, R.N.; Mishra, S.; Khan, N. Role of Industries in Water Scarcity and Its Adverse Effects on Environment and Human Health. In *Environmental Concerns and Sustainable Development*; Springer: Singapore, 2019; pp. 235–256. ISBN 9789811358890.
- Jeong, H.; Bhattarai, R.; Adamowski, J.; Yu, D.J. Insights from socio-hydrological modeling to design sustainable wastewater reuse strategies for agriculture at the watershed scale. *Agric. Water Manag.* **2020**, *231*, 105983. [CrossRef]
- Rezaei, N.; Diaz-Elsayed, N.; Mohebbi, S.; Xie, X.; Zhang, Q. A multi-criteria sustainability assessment of water reuse applications: A case study in Lakeland, Florida. *Environ. Sci. Water Res. Technol.* **2018**, *5*, 102–118. [CrossRef]
- Jodar-Abellan, A.; López-Ortiz, M.I.; Melgarejo-Moreno, J. Wastewater Treatment and Water Reuse in Spain. Current Situation and Perspectives. *Water* **2019**, *11*, 1551. [CrossRef]
- European Parliament, Council of the EU. Regulation (EU) 2020/741 of the European Parliament and of the Council of 25 May 2020 on Minimum Requirements for Water Reuse; EU: Luxembourg, 2020; Volume 177, pp. 32–55.
- Tójar-Hurtado, J.-C.; Mena-Rodríguez, E.; Fernández-Jiménez, M.-Á. Spanish Agriculture and Water: Educational Implications of Water Culture and Consumption from the Farmers' Perspective. *Water* **2017**, *9*, 964. [CrossRef]

16. Silva, N.B.; Leonel, L.P.; Tonetti, A.L. UV-LED for Safe Effluent Reuse in Agriculture. *Water Air Soil Pollut.* **2020**, *231*, 1–10. [[CrossRef](#)]
17. Chávez, A.M.; Ribeiro, A.R.; Moreira, N.F.F.; Silva, A.M.T.; Rey, A.; Álvarez, P.M.; Beltrán, F.J. Removal of Organic Micropollutants from a Municipal Wastewater Secondary Effluent by UVA-LED Photocatalytic Ozonation. *Catalysts* **2019**, *9*, 472. [[CrossRef](#)]
18. Compagni, R.D.; Gabrielli, M.; Polesel, F.; Turolla, A.; Trapp, S.; Vezzaro, L.; Antonelli, M. Risk assessment of contaminants of emerging concern in the context of wastewater reuse for irrigation: An integrated modelling approach. *Chemosphere* **2020**, *242*, 125185. [[CrossRef](#)] [[PubMed](#)]
19. Lamba, M.; Ahammad, S.Z. Performance comparison of secondary and tertiary treatment systems for treating antibiotic resistance. *Water Res.* **2017**, *127*, 172–182. [[CrossRef](#)]
20. Benner, J.; Helbling, D.E.; Kohler, H.-P.E.; Wittebol, J.; Kaiser, E.; Prasse, C.; Ternes, T.A.; Albers, C.N.; Amand, J.; Horemans, B.; et al. Is biological treatment a viable alternative for micropollutant removal in drinking water treatment processes? *Water Res.* **2013**, *47*, 5955–5976. [[CrossRef](#)]
21. Bensalah, F.; Iddou, A.; Hentit, H.; Aziz, A.; Shishkin, A. Activated Carbon Design from Sludge to Remove Red Scarlet Nylosan “F3GL” in Aqueous Solution. *Key Eng. Mater.* **2018**, *762*, 87–92. [[CrossRef](#)]
22. Dhangar, K.; Kumar, M. Tricks and tracks in removal of emerging contaminants from the wastewater through hybrid treatment systems: A review. *Sci. Total Environ.* **2020**, *738*, 140320. [[CrossRef](#)]
23. Andriantsiferana, C.; Mohamed, E.F.; Delmas, H. Sequential adsorption-photocatalytic oxidation process for wastewater treatment using a composite material TiO₂/activated carbon. *Environ. Eng. Res.* **2015**, *20*, 181–189. [[CrossRef](#)]
24. Im, D.; Nakada, N.; Kato, Y.; Aoki, M.; Tanaka, H. Pretreatment of ceramic membrane microfiltration in wastewater reuse: A comparison between ozonation and coagulation. *J. Environ. Manag.* **2019**, *251*, 109555. [[CrossRef](#)] [[PubMed](#)]
25. Kim, G.-Y.; Sungkyunkwan University; Kim, M.-G.; Lee, C.-H.; Kim, H.-S.; Kim, J.-H.; Lee, K.-I. A study on mitigation of membrane fouling by ozonation/coagulation in ultrafiltration. *J. Korean Soc. Water Wastewater* **2017**, *31*, 161–168. [[CrossRef](#)]
26. Stackelberg, P.E.; Gibbs, J.; Furlong, E.T.; Meyer, M.T.; Zaugg, S.D.; Lippincott, R.L. Efficiency of conventional drinking water treatment processes in removal of pharmaceuticals and other organic compounds. *Sci. Total Environ.* **2007**, *377*, 255–272. [[CrossRef](#)]
27. Cuartucci, M. Ultrafiltration, a cost-effective solution for treating surface water to potable standard. *Water Pract. Technol.* **2020**, *15*, 426–436. [[CrossRef](#)]
28. Mojiri, A.; Zhou, J.L.; Robinson, B.; Ohashi, A.; Ozaki, N.; Kindaichi, T.; Farraji, H.; Vakili, M. Pesticides in aquatic environments and their removal by adsorption methods. *Chemosphere* **2020**, *253*, 126646. [[CrossRef](#)] [[PubMed](#)]
29. Liu, P.; Zhang, H.; Feng, Y.; Yang, F.; Zhang, J. Removal of trace antibiotics from wastewater: A systematic study of nanofiltration combined with ozone-based advanced oxidation processes. *Chem. Eng. J.* **2014**, *240*, 211–220. [[CrossRef](#)]
30. Rivera-Utrilla, J.; Sánchez-Polo, M.; José, R.-U. Ozonation of 1,3,6-naphthalenetrisulphonic acid catalysed by activated carbon in aqueous phase. *Appl. Catal. B Environ.* **2002**, *39*, 319–329. [[CrossRef](#)]
31. Rodríguez-Narvaez, O.M.; Peralta-Hernandez, J.M.; Goonetilleke, A.; Bandala, E.R. Treatment technologies for emerging contaminants in water: A review. *Chem. Eng. J.* **2017**, *323*, 361–380. [[CrossRef](#)]
32. Chen, H.; Zahraa, O.; Bouchy, M. Inhibition of the adsorption and photocatalytic degradation of an organic contaminant in an aqueous suspension of TiO₂ by inorganic ions. *J. Photochem. Photobiol. A Chem.* **1997**, *108*, 37–44. [[CrossRef](#)]
33. Hagen, K. Removal of particles, bacteria and parasites with ultrafiltration for drinking water treatment. *Desalination* **1998**, *119*, 85–91. [[CrossRef](#)]
34. Acero, J.L.; Benítez, F.J.; Leal, A.I.; Real, F.J.; Teva, F. Membrane filtration technologies applied to municipal secondary effluents for potential reuse. *J. Hazard. Mater.* **2010**, *177*, 390–398. [[CrossRef](#)] [[PubMed](#)]
35. Benítez, F.J.; Real, F.J.; Acero, J.L.; Casas, F. Use of ultrafiltration and nanofiltration processes for the elimination of three selected emerging contaminants: Amitriptyline hydrochloride, methyl salicylate and 2-phenoxyethanol. *Environ. Prot. Eng.* **2017**, *43*, 125–141. [[CrossRef](#)]
36. Dharupaneedi, S.P.; Nataraj, S.K.; Nadagouda, M.; Reddy, K.R.; Shukla, S.S.; Aminabhavi, T.M. Membrane-based separation of potential emerging pollutants. *Sep. Purif. Technol.* **2019**, *210*, 850–866. [[CrossRef](#)]
37. Muhamad, M.S.; Salim, M.R.; Lau, W.J.; Yusop, Z.; Hadibarata, T. The Removal of Bisphenol A in Water Treatment Plant Using Ultrafiltration Membrane System. *Water Air Soil Pollut.* **2016**, *227*, 1–12. [[CrossRef](#)]
38. Sui, Q.; Huang, J.; Deng, S.; Chen, W.; Yu, G. Seasonal Variation in the Occurrence and Removal of Pharmaceuticals and Personal Care Products in Different Biological Wastewater Treatment Processes. *Environ. Sci. Technol.* **2011**, *45*, 3341–3348. [[CrossRef](#)]
39. Carr, D.L.; Morse, A.N.; Zak, J.C.; Anderson, T.A. Biological Degradation of Common Pharmaceuticals and Personal Care Products in Soils with High Water Content. *Water Air Soil Pollut.* **2011**, *217*, 127–134. [[CrossRef](#)]
40. Chen, H.; Zhuang, R.; Yao, J.; Wang, F.; Qian, Y.; Masakorala, K.; Cai, M.; Liu, H. Short-term effect of aniline on soil microbial activity: A combined study by isothermal microcalorimetry, glucose analysis, and enzyme assay techniques. *Environ. Sci. Pollut. Res.* **2013**, *21*, 674–683. [[CrossRef](#)]
41. Lahti, M.; Oikari, A. Microbial Transformation of Pharmaceuticals Naproxen, Bisoprolol, and Diclofenac in Aerobic and Anaerobic Environments. *Arch. Environ. Contam. Toxicol.* **2010**, *61*, 202–210. [[CrossRef](#)]
42. Alresheedi, M.T.; Basu, O.D.; Barbeau, B. Chemical cleaning of ceramic ultrafiltration membranes—Ozone versus conventional cleaning chemicals. *Chemosphere* **2019**, *226*, 668–677. [[CrossRef](#)]

43. Ferreira, C.; Villota, N.; Lombraña, J.I.; Rivero, M.J.; Zúñiga, V.; Rituerto, J.M. Analysis of a Hybrid Suspended-Supported Photocatalytic Reactor for the Treatment of Wastewater Containing Benzothiazole and Aniline. *Water* **2019**, *11*, 337. [CrossRef]
44. Noutsopoulos, C.; Mamais, D.; Mpouras, T.; Kokkinidou, D.; Samaras, V.; Antoniou, K.; Gioldasi, M. The role of activated carbon and disinfection on the removal of endocrine disrupting chemicals and non-steroidal anti-inflammatory drugs from wastewater. *Environ. Technol.* **2014**, *35*, 698–708. [CrossRef] [PubMed]
45. Von Sonntag, C.; Von Gunten, U. *Chemistry of Ozone in Water and Wastewater Treatment: From Basic Principles to Applications*; Iwa Publishing: London, UK, 2012; ISBN 978-1-84339-313-9.
46. De Luis, A.; Lombraña, J.I. pH-Based Strategies for an Efficient Addition of H₂O₂ during Ozonation to Improve the Mineralisation of Two Contaminants with Different Degradation Resistances. *Water, Air, Soil Pollut.* **2018**, *229*, 372. [CrossRef]
47. Gomes, J.; Matos, A.; Gmurek, M.; Quinta-Ferreira, R.M.; Martins, R.C. Ozone and Photocatalytic Processes for Pathogens Removal from Water: A Review. *Catalysts* **2019**, *9*, 46. [CrossRef]
48. Martínez, P.O.; Echevarría, F.G. Equipo de Filtrado Mejorado y Procedimientos de Uso. ES201431341A, 24 March 2016.
49. United States Environmental Protection Agency. Procedures for Collecting Wastewater Samples. Available online: <https://www.epa.gov/quality/procedures-collecting-wastewater-samples> (accessed on 27 November 2020).
50. Black & Veatch Corporation. *White's Handbook of Chlorination and Alternative Disinfectant*, 5th ed.; Wiley: Trenton, NJ, USA, 2010; ISBN 978-0-470-18098-3.
51. Mijangos, L.; Ziarrusta, H.; Olivares, M.; Zuloaga, O.; Möder, M.; Etxebarria, N.; Prieto, A. Simultaneous determination of 41 multiclass organic pollutants in environmental waters by means of polyethersulfone microextraction followed by liquid chromatography–tandem mass spectrometry. *Anal. Bioanal. Chem.* **2017**, *410*, 615–632. [CrossRef]
52. American Public Health Association (APHA); American Water Works Association (AWWA); Water Environment Federation (WEF). *Standard Methods for the Examination of Water and Wastewater*, 21st ed.; APHA; AWWA; WEF: Washington, DC, USA, 2005; ISBN 978-0875530475.
53. Lopera, A.E.-C.; Ruiz, S.G.; Alonso, J.M.Q. Removal of emerging contaminants from wastewater using reverse osmosis for its subsequent reuse: Pilot plant. *J. Water Process. Eng.* **2019**, *29*, 100800. [CrossRef]
54. Stavbar, S.; Hrnčič, M.K.; Premzl, K.; Kolar, M.; Turk, S. Šostar Sub- and super-critical water oxidation of wastewater containing amoxicillin and ciprofloxacin. *J. Supercrit. Fluids* **2017**, *128*, 73–78. [CrossRef]
55. Egea-Corbacho, A.; Ruiz, S.G.; Alonso, J.M.Q. Removal of emerging contaminants from wastewater using nanofiltration for its subsequent reuse: Full-scale pilot plant. *J. Clean. Prod.* **2019**, *214*, 514–523. [CrossRef]
56. Machado, K.C.; Grassi, M.T.; Vidal, C.; Pescara, I.C.; Jardim, W.F.; Fernandes, A.N.; Sodré, F.F.; Almeida, F.V.; Santana, J.S.; Canela, M.C.; et al. A preliminary nationwide survey of the presence of emerging contaminants in drinking and source waters in Brazil. *Sci. Total Environ.* **2016**, *572*, 138–146. [CrossRef] [PubMed]
57. Kang, J.; Price, W.E. Occurrence of phytoestrogens in municipal wastewater and surface waters. *J. Environ. Monit.* **2009**, *11*, 1477–1483. [CrossRef] [PubMed]
58. Gros, M.; Petrovic, M.; Barceló, D. Analysis of Emerging Contaminants of Municipal and Industrial Origin. In *Emerging Contaminants from Industrial and Municipal Waste: Occurrence, Analysis and Effects*; The Handbook of Environmental Chemistry; Barceló, D., Petrovic, M., Eds.; Springer: Berlin/Heidelberg, Germany, 2008; pp. 37–104. ISBN 978-3-540-74795-6.
59. Yu, Q.; Geng, J.; Zong, X.; Zhang, Y.; Xu, K.; Hu, H.; Deng, Y.; Zhao, F.; Ren, H. Occurrence and removal of progestagens in municipal wastewater treatment plants from different regions in China. *Sci. Total Environ.* **2019**, *668*, 1191–1199. [CrossRef]
60. Loos, R.; Carvalho, R.; António, D.C.; Comero, S.; Locoro, G.; Tavazzi, S.; Paracchini, B.; Ghiani, M.; Lettieri, T.; Blaha, L.; et al. EU-wide monitoring survey on emerging polar organic contaminants in wastewater treatment plant effluents. *Water Res.* **2013**, *47*, 6475–6487. [CrossRef]
61. Guedes-Alonso, R.; Montesdeoca-Esponda, S.; Pacheco-Juárez, J.; Sosa-Ferrera, Z.; Santana-Rodríguez, J.J. A Survey of the Presence of Pharmaceutical Residues in Wastewaters. Evaluation of Their Removal using Conventional and Natural Treatment Procedures. *Molecules* **2020**, *25*, 1639. [CrossRef] [PubMed]
62. Das, S.; Ray, N.M.; Wan, J.; Khan, A.; Chakraborty, T.; Ray, M.B. Micropollutants in Wastewater: Fate and Removal Processes. *Phys. Chem. Wastewater Treat. Resour. Recove.* **2017**. [CrossRef]
63. Polesel, F.; Andersen, H.R.; Trapp, S.; Plósz, B.G. Removal of Antibiotics in Biological Wastewater Treatment Systems—A Critical Assessment Using the Activated Sludge Modeling Framework for Xenobiotics (ASM-X). *Environ. Sci. Technol.* **2016**, *50*, 10316–10334. [CrossRef]
64. Fan, G.; Su, Z.; Lin, R.; Lin, X.; Xu, R.; Chen, W. Influence of Membrane Materials and Operational Modes on the Performance of Ultrafiltration Modules for Drinking Water Treatment. *Int. J. Polym. Sci.* **2016**, *2016*, 1–8. [CrossRef]
65. Bourgeois, K.N.; Darby, J.L.; Tchobanoglous, G. Ultrafiltration of wastewater: Effects of particles, mode of operation, and backwash effectiveness. *Water Res.* **2001**, *35*, 77–90. [CrossRef]
66. Chen, Y.; Xu, W.; Zhu, H.; Wei, D.; He, F.; Wang, D.; Du, B.; Wei, Q. Effect of turbidity on micropollutant removal and membrane fouling by MIEX/ultrafiltration hybrid process. *Chemosphere* **2019**, *216*, 488–498. [CrossRef] [PubMed]
67. Xu, W.; Yue, Q.; Gao, B.; Du, B. Impacts of organic coagulant aid on purification performance and membrane fouling of coagulation/ultrafiltration hybrid process with different Al-based coagulants. *Desalination* **2015**, *363*, 126–133. [CrossRef]
68. De Oliveira, A.R.M.; Borges, A.C.; Matos, A.T.; Nascimento, M. Estimation on the Concentration of Suspended Solids from Turbidity in the Water of Two Sub-Basins in the Doce River Basin. *Eng. Agríc.* **2018**, *38*, 751–759. [CrossRef]

69. Kim, S.; Chu, K.H.; Al-Hamadani, Y.A.; Park, C.M.; Jang, M.; Kim, D.-H.; Yu, M.; Heo, J.; Yoon, Y. Removal of contaminants of emerging concern by membranes in water and wastewater: A review. *Chem. Eng. J.* **2018**, *335*, 896–914. [[CrossRef](#)]
70. Yang, M.; Chen, J.; Peng, B.; Yu, Z.; Chu, H.; Zhou, X. Performance and properties of coking nanofiltration concentrate treatment and membrane fouling mitigation by an Fe(II)/persulfate-coagulation-ultrafiltration process. *RSC Adv.* **2019**, *9*, 15277–15287. [[CrossRef](#)]
71. Shaaban, A.M.F.; Hafez, A.I.; Abdel-Fatah, M.A.; Abdel-Monem, N.M.; Mahmoud, M.H. Process engineering optimization of nanofiltration unit for the treatment of textile plant effluent in view of solution diffusion model. *Egypt. J. Pet.* **2016**, *25*, 79–90. [[CrossRef](#)]
72. Gopinath, K.P.; Madhav, N.V.; Krishnan, A.; Malolan, R.; Rangarajan, G. Present applications of titanium dioxide for the photocatalytic removal of pollutants from water: A review. *J. Environ. Manag.* **2020**, *270*, 110906. [[CrossRef](#)]
73. Mwabi, J.K.; Mamba, B.B.; Momba, M.N.B. Removal of Escherichia coli and Faecal Coliforms from Surface Water and Groundwater by Household Water Treatment Devices/Systems: A Sustainable Solution for Improving Water Quality in Rural Communities of the Southern African Development Community Region. *Int. J. Environ. Res. Public Health* **2012**, *9*, 139–170. [[CrossRef](#)] [[PubMed](#)]
74. Guzman-Colis, G.; Thalasso, F.; Marcela Ramirez-Lopez, E.; Rodriguez-Narciso, S.; Lilian Guerrero-Barrera, A.; Avelar-Gonzalez, F. Spatial-Temporal Evaluation of the Water Quality of the San Pedro River. *Rev. Int. Contam. Ambient.* **2011**, *27*, 89–102.
75. Falsanisi, D.; Liberti, L.; Notarnicola, M. Ultrafiltration (UF) Pilot Plant for Municipal Wastewater Reuse in Agriculture: Impact of the Operation Mode on Process Performance. *Water* **2010**, *2*, 872–885. [[CrossRef](#)]
76. Slavik, I.; Jehmlich, A.; Uhl, W. Impact of backwashing procedures on deep bed filtration productivity in drinking water treatment. *Water Res.* **2013**, *47*, 6348–6357. [[CrossRef](#)]
77. Si, X.; Hu, Z.; Huang, S. Combined Process of Ozone Oxidation and Ultrafiltration as an Effective Treatment Technology for the Removal of Endocrine-Disrupting Chemicals. *Appl. Sci.* **2018**, *8*, 1240. [[CrossRef](#)]
78. Beltran, F.J. *Ozone Reaction Kinetics for Water and Wastewater Systems*; CRC Press: Boca Raton, FL, USA, 2003.
79. Valdés, H.; Zaror, C.A.; Jekel, M. Removal of Benzothiazole from Contaminated Waters by Ozonation: The Role of Direct and Indirect Ozone Reactions. *J. Adv. Oxid. Technol.* **2016**, *19*, 338–346. [[CrossRef](#)]
80. Rosal, R.; Rodríguez, A.; Perdígón-Melón, J.A.; Petre, A.; García-Calvo, E.; Gómez, M.J.; Agüera, A.; Fernández-Alba, A.R. Degradation of caffeine and identification of the transformation products generated by ozonation. *Chemosphere* **2009**, *74*, 825–831. [[CrossRef](#)]
81. Kuang, J.; Huang, J.; Wang, B.; Cao, Q.; Deng, S.; Yu, G. Ozonation of trimethoprim in aqueous solution: Identification of reaction products and their toxicity. *Water Res.* **2013**, *47*, 2863–2872. [[CrossRef](#)] [[PubMed](#)]
82. Qu, F.; Wang, H.; He, J.; Fan, G.; Pan, Z.; Tian, J.; Rong, H.; Li, G.; Yu, H. Tertiary treatment of secondary effluent using ultrafiltration for wastewater reuse: Correlating membrane fouling with rejection of effluent organic matter and hydrophobic pharmaceuticals. *Environ. Sci. Water Res. Technol.* **2019**, *5*, 672–683. [[CrossRef](#)]
83. Iakovides, I.; Michael-Kordatou, I.; Moreira, N.; Ribeiro, A.; Fernandes, T.; Pereira, M.; Nunes, O.; Manaia, C.; Silva, A.; Fatta-Kassinos, D. Continuous ozonation of urban wastewater: Removal of antibiotics, antibiotic-resistant Escherichia coli and antibiotic resistance genes and phytotoxicity. *Water Res.* **2019**, *159*, 333–347. [[CrossRef](#)]
84. Ostoich, M.; Serena, F.; Falletti, L.; Fantoni, A. Control of dangerous substances in discharges and microbiological abatement: European framework and a case study of an ozone disinfection system. *Water Sci. Technol.* **2013**, *67*, 1238–1246. [[CrossRef](#)] [[PubMed](#)]
85. Sousa, J.M.; Macedo, G.; Pedrosa, M.; Becerra-Castro, C.; Castro-Silva, S.; Pereira, M.F.R.; Silva, A.M.T.; Nunes, O.C.; Manaia, C.M. Ozonation and UV_{254nm} radiation for the removal of microorganisms and antibiotic resistance genes from urban wastewater. *J. Hazard. Mater.* **2017**, *323*, 434–441. [[CrossRef](#)] [[PubMed](#)]
86. Serajuddin, M.; Chowdhury, A.I.; Haque, M.; Haque, E. Using Turbidity to Determine Total Suspended Solids in an Urban Stream: A Case Study. *Int. J. Eng. Trends Technol.* **2019**, *67*, 83–88. [[CrossRef](#)]
87. Teixeira, L.C.; De Paiva, J.B.D.; Pereira, J.E.D.S.; Lisbôa, R.D.M. Relationship between Turbidity and Suspended Sediment Concentration From a Small Hydrographic Basin in Santa Maria (Rio Grande Do Sul, Brazil). *Int. J. River Basin Manag.* **2016**, *14*, 1–10. [[CrossRef](#)]
88. M. & E. Inc.; Tchobanoglous, G.; Burton, F.; Stensel, H.D. *Wastewater Engineering: Treatment and Reuse*; McGraw-Hill Education: New York, NY, USA, 2002; ISBN 978-0-07-041878-3.
89. Sanchez, M.; Rivero, M.J.; Ortiz, I. Kinetics of dodecylbenzenesulphonate mineralisation by TiO₂ photocatalysis. *Appl. Catal. B Environ.* **2011**, *101*, 515–521. [[CrossRef](#)]
90. Álvarez, P.M.; Pocostales, J.P.; Beltrán, F.J. Granular activated carbon promoted ozonation of a food-processing secondary effluent. *J. Hazard. Mater.* **2011**, *185*, 776–783. [[CrossRef](#)]
91. Ferreiro, C.; Villota, N.; Lombraña, J.; Rivero, M.J. An efficient catalytic process for the treatment of genotoxic aniline wastewater using a new granular activated carbon-supported titanium dioxide composite. *J. Clean. Prod.* **2019**, *228*, 1282–1295. [[CrossRef](#)]
92. Shoushtarian, F.; Negahban-Azar, M. Worldwide Regulations and Guidelines for Agricultural Water Reuse: A Critical Review. *Water* **2020**, *12*, 971. [[CrossRef](#)]
93. Nutt, S.G.; Tran, J.; Vriezen, C.; Fuga, G.; Zaleski, A.; Miot, A.; Pagilla, K.; Lee, M.; Ross, M.; Palmer, T. Addressing BOD₅ Limitations through TOC Correlations—A International Investigation. *Proc. Water Environ. Fed.* **2013**, *2013*, 2567–2577. [[CrossRef](#)]

-
94. *European Union Eurostat Regional Yearbook*, 2018 ed.; Statistical books; Publications Office of the European Union: Luxembourg, 2018; ISBN 978-92-79-87876-3.
 95. Krichevskaya, M.; Klauson, D.; Portjanskaja, E.; Preis, S. The Cost Evaluation of Advanced Oxidation Processes in Laboratory and Pilot-Scale Experiments. *Ozone Sci. Eng.* **2011**, *33*, 211–223. [[CrossRef](#)]

4. Ondorioak eta etorkizuneko aukerak



4.1. Ondorioak

4.1.1. UV/H₂O₂-an oinarritutako prozesuak

UV/H₂O₂ prozesuek 4-klorofenola duten disoluzioak deuseztatzeko nolako eraginkortasuna duten aztertu zen. Hasieran ikusi zenez, beste konposatu fenoliko batzuekin gertatzen zen era berean, klorofenola ere hasierako poluitzailea baino azpiproduktu are toxikoagoetan degrada zitezkeen erreakzioaren lehen etapetan. Azpiproduktu horiek fotolisi zuzenaren beraren ondorioz ager zitezkeen, edo, agian, oxigeno peroxidoaren kontzentrazio baxua erabiltzearen ondorioz. Tarteko produktu toxiko horiek guztiz deuseztatzeko beharri eta poluitzaile-karga bakoitzarekin erabilitako oxidatzaile-dosiari erreparatuz, hauek ondorioztatu ziren:

- Degradazioaren eta toxikotasunaren arteko elkarrekikotasunaren hipotesiaren arabera, oxidazioaren tarteko konposatu nagusiak hainbat *lumpetan* taldekatu ziren toxikotasunaren eta parametro fotolitiko batzuen arabera, hala nola iraungitze-koefizientea eta errendimendu kuantikoa.
- *Lumpetan* oinarritutako eredu zinetiko bat proposatu zen H₂O₂-aren kontzentrazioak azken efluentearen toxikotasunean duen eragina aztertzeko. Proposatutako ereduak balioztatu egin zen simulatutako balioak esperimentalekin alderatu ostean, eta % 5etik beherako desbideratze estandar erlatiboa lortu zen.
- pH-kondizio eta hidrogeno peroxidoaren dosi ezberdinak aztertu ziren, parametro zinetikoak eta fotolitikoak zenbatesteko, eta tratatutako efluentearik toxikotasun txikiagoa eta biodegradagarritasun handiagoa izan zitzan zein kondizio behar ziren ondorioztatzeko.
- 6,0ko pH-arekin eta H₂O₂ (*R*= 200) dosi batekin lortu zen toxikotasunik baxuena (9,95 TU) 120 minutu baino denbora laburragoan. Gainera, degradazio primario osoa (4-klorofenol) lortu zen, % 40ko mineralizazioa eta kolorearen erabateko galera.

4.1.2. Fotofenton sisteman oinarritutako prozesuak

Karbamazepinaren degradazioari aplikatutako Fenton-en fotorreakzioa ebaluatu zen, hainbat eragiketa-kondizioen arabera; besteak beste, pH-a, hidrogeno peroxidoaren kontzentrazioa eta burdinadun katalizatzailearen dosia hartu ziren kontuan. Esperimentuekin egiaztatu ahal izan zen, erabilitako eragiketa-kondizioen arabera, urek uhertasun handia eta kolorea hartzen zutela, oxidazio-tratamenduak irauten zuen bitartean. Hala, tratatutako uren uhertasunaren eta kolorearen arazoak aurkitu ziren, degradazio-bideekin duten harremana ikusi zen eta azpiproduktu nagusiak zehaztu ziren. Honako ondorio hauek lortu ziren:

Uhertasunari dagokionez:

- Esperimentuetan ikusi zen nola eragiten zuten kontrol-aldagaiak (pH-ak, hidrogeno peroxidoak eta katalizatzailearen kontzentrazioak) uhertasunean, karbamazepina-disoluzioen oxidazioan.
- Sortutako degradazio-bitartekariak eragingo lukete uhertasuna, tratamenduan lortutako oxidazio-mailaren arabera.
- 2,0 eta 2,5 pH-en artean, 1 NTU-tik beherako uhertasun minimoa agertu zen, katalizatzaileak ioi ferrosoaren forma zuelako. 3,0tik gorako pH-balioetan, berriz, burdinak egoera oxidatua zuenez (hidroxido ferrikoa esekiduran, batez ere),

uhertasuna handiagoa zen. 2,0 mM-etik gorako H_2O_2 -dosien bidez soilik gutxitu ahal izan zen uhertasuna, 5 NTU-tik gertuko balioetaraino.

- Uhertasun handieneko kondizioak aztertuta, degradazioaren mekanismo orokor bat zehaztu ahal izan zen. Karbamazepina, adibidez, lau degradazio-bidezidor nagusiren bidez oxidatzen zen, bi epoxido buru zirela: (10, 11-epoxi karbamazepina) eta 2,3-epoxi karbamazepina. Bakoitzak beste bi azpibidezidorretara bideratzen zuen prozesua. (2,3-epoxi karbamazepina) epoxidoaren azpibidezidorretako batean 1-(2-azido bentzoiko)-(1H, 3H)-kinazolina-2,4-diona (BaQD) agertu zen, eta, hori Fe^{3+} -arekin konbinatuta, uhertasun handiaren erantzule diren koordinazio-konplexuak sortu ziren.

Koloreari dagokionez:

- Oxidatzailearen eta karbamazepinaren arteko erlazio estekiometrikoaren bidez, erreakzioan lortutako degradazio-bitartekoen izaera zehaztu zitekeen. Hala, hidrogeno peroxidoaren dosi baxuak erabilita ($R < 10$) urak kolorea hartu zuen balio maximo batera iritsi arte, zeina degradazio-azpiproduktuen agerpenarekin erlazionatuta baitzegoen (oxo- eta dioxokarbamazepinak). Kolorea gutxituz joan zen, horiek degradatu eta akridinak eta akridona hidroxilatuak agertu ahala.
- Erlazio estekiometriko altuak erabilita ($R > 25$), kolore-agerpenaren zinetika azkarragoa izan zen, erlazio baxuak erabilita baino, eta, ondorioz, kolore gabeko disoluzioa lortu den.
- Ondorioztatuenez, kolore maximoa eta hondar-kolorea areagotu egiten ziren erabilitako burdin kontzentrazioarekin batera. Kolore maximoaren kasurako, $k_{\text{Fe}} = 0,0075 \text{ AU L mg}^{-1} \text{ Fe}$ batezbesteko erlazioa aurkitu zen, Fe^{3+} -a duten konplexu metalikoak eratzen zirelako. Esekiduran zeuden burdin espezieak ziren hondar-kolore minimoaren arduradunak.

4.1.3. Fotokatalisi heterogeneoa errektore hibridoetan eta FBRan

TiO_2 -a atxikita zeukan fotorreaktore komertzial bat hartu, eta hobetzeko aukera aztertu zen, eraginkortasunez aplikatzeko anilina eta bentzotiazola dituen efluente industrial batean. Ekintza katalitiko indartu egin zen TiO_2 -a esekiduran gehituta, eta, hala, TiO_2 -a atxikita/esekiduran duen sistema hibrido bat eratu zen. Adsortzioaren fenomenoak ikertu zen, eta hainbat eragiketa-kondiziotan egindako ikerketa zinetikoan kontuan hartu izan zen.

Halaber, atal horren barruan, sistema fotokatalitiko eraginkor bat eskala pilotuan ezartzeko aukera aztertu zen, FBR batean MnO_2/GAC katalizatzaile berri bat erabilita, anilina eta bentzotiazola zuten benetako hondakin-urak eraginkortasunez deuseztatzeko. GAC euskarri batetik abiatuta—Hydrodarco[®] 3000 (HD 3000)—material katalitiko berri bat garatu zen sintesi hidrotermala erabilita, eta, ondorioz, GACaren gainazalean MnO_2 -aren fase metalikoaren banaketa egokia lortu zen.

TiO_2 -a atxikita/esekiduran zuen fotorreaktore hibridoa hobetzeari zegokionez, ondorio hauek lortu ziren:

- Anilinak eta bentzotiazolak TiO_2 P25-en gainean jasandako adsortzioak Langmuir-en isoterma jarraitu zion. Adsortzio-orekaren konstanteak ($K_L (T = 20 \text{ }^\circ\text{C})$) 0,138 eta $0,419 \text{ L mg}^{-1}$ izan ziren, hurrenez hurren, anilinarekin eta bentzotiazolarekin kasuatarako. Analisi termodinamikotik ondorioztatu zen anilina eta bentzotiazolarekin TiO_2 -aren gaineko adsortzioa kimisortzio-prozesu baten bidez

gertatzen zela. Prozesu hori ezinbestekoa izan zen degradazioaren zinetika azaltzeko.

- Oxidazio fotokatalitikoan, anilina degradatzeko kondiziorik onenak pH = 12,0-an gertatzen zirela ($k_{app} = 0,327 \text{ h}^{-1}$) zehaztu zen. Bestalde, pH = 2,5 balioan lortu ziren degradazio-errendimendurik baxuenak ($k_{app} = 0,112 \text{ h}^{-1}$), degradazioaren bitartekari gisa sortutako polianilinak eragindako opakutasuna zela eta. Bentzotiazolaren kasuan, oxidazioaren zinetika geldoagoa izan zen, karga negatiboa zuten hainbat azpiproduktu sortu zirelako eta gertaera horrek TiO_2 -aren gaineko kimisortzioa eragotzi zuelako.
- Esekiduran dagoen TiO_2 -aren $100,0 \text{ mg L}^{-1}$ gehitzea izan zen anilina ($k_{app} = 0,408 \text{ h}^{-1}$) edo bentzotiazola ($k_{app} = 0,181 \text{ h}^{-1}$) deuseztatzeko komenigarriena. Esekidura kontzentratuagoak erabiltzeak galarazi egin zion argi ultramoreari errektorearen horman immobilizatutako TiO_2 -ra iristen.
- Aurkitu zenez, pH = 12,0 eta esekiduran dagoen katalizatzailearen $60,0 \text{ mg L}^{-1}$ -ko dosia ziren kondiziorik egokienak bi poluitzaileak batera tratatzeko. Euskarridun katalizatzailea soilik erabili zuen konfigurazioarekin alderatuz gero, kondizio horietan %23 gehiago mineralizatu zen, eta anilina eta bentzotiazolaren % 90 degradatzeko behar den energiaren kostua $2,19 \text{ € m}^{-3}$ -koa izan zen.

FBR errektore batean egindako prozesu fotokatalitikoaren eraginkortasuna hobetu asmoz MnO_2/GAC fotokatalizatzailea prestatzeko moduari dagokionez, hauek ondorioztatu ziren:

- Konposite berritzaile bat lortzeko metodologia bat, MnO_2 -a gehituta eraldatu den ikatz aktibatu pikortsua darabilena (MnO_2/GAC) eta KMnO_4 -disoluzioekin egindako sintesi hidrotermala baliatzen zuenak. Hala lortutako material katalitikoak arrakastaz erabili zen FBR errektore batean, anilina eta bentzotiazola zituen efluente industrial bat tratatzeko.
- Konpositean, $\alpha\text{-MnO}_2$ kristala zegoen, X izpien difrakzioaren bidez ikusi zenez. Bestalde, MnO_2 partikulak bikain sakabanatzen ziren GACaren gainazalean, SEM, HRTEM eta AFM bidez lortutako irudiek erakusten zuten. Gainera, H_2 -arekin egindako kimisortzio-azterketek erakusten zuten, azalera espezifikoak %9,47 handiagoa zen hasierako GACarena baino ($601,2 \text{ m}^2 \text{ g}^{-1}$). Nabarmentzekoa izan zen MnO_2/GAC -3 konposite aldaerarekin energia-banda debekatua lortu zela ($0,95 \text{ eV}$); horri esker, UV-A argiarekin erabiltzeko aukera lortu zen. XPS bidezko analisiaren bidez, MnO_2 -aren oxidazio-egoera jakin ahal izan zen. Datu hori erabakigarria zen konpositearen hiru aldaeren jardura katalitikoak baloratzeko (aldaera bakoitzak MnO_2 kantitate ezberdina zuen). % 3,78 MnO_2 zuen MnO_2/GAC -3 aldaerak (XRF, *X-ray Fluorescence*, bidez kalkulatu zen datu hori) izan zuen portaerarik onena, degradazio primarioari eta mineralizazioari zegokienez.
- Hasierako kontzentrazioa $12,0 \text{ mg L}^{-1}$ zuten ur industrialetan anilina eta bentzotiazola deuseztatzeko kondizio egokienak zehazteko garaian, parametro hauek garrantzitsuak ziren: geometria, partikula-tamaina, fluidoaren gainazaleko abiadura, pH-a eta katalizatzaile-dosia. Hori horrela, 9,0 balioko pH-a eta $0,9 \text{ g L}^{-1}$ -ko dosia erabilita, anilinarekin % 84,7 eta bentzotiazolaren % 67,0 deuseztatu zen, hurrenez hurren. Gainera, % 81,6ko mineralizazioa lortu zen ordubeteko errektorearen ondoren.
- Anilinarekin eta bentzotiazolaren degradazioa modelatzeko pseudolehen ordenako zinetika bat. Kondiziorik onenetan balio hauek lortu ziren: $k_{app,ANI} = 1,75 \text{ h}^{-1}$ eta $k_{app,BTH} = 1,04 \text{ h}^{-1}$. Beste parametro batzuek, hala nola oxidazioaren tarteko egoerak

—AOS (*average oxidation state*) 0,63—, erakutsi zuten tratatutako efluenteak biodegradatzeko kondizio egokiak zituela.

- 6 zikloren ondoren MnO₂/GAC-3 fotokatalizatzaile berritzaileak zuen egonkortasun aparta; tratamenduaren kostu ekonomikoa 0,17 € m⁻³ izango litzateke. Ondorioz, material katalitiko hau gakoa zen deuseztatzeko zailak ziren poluitzaile organikoak zituzten hondakin-ur industrialak tratatzeko teknologia eraginkorra proposatzeko garaian.

4.1.4. Ozonizazio katalitikoa

Teknologia honen aplikazioa aztertzeko, Ad/Ox prozesua eta ikatz aktibatu pikortsua (Kemisorb[®] 530) erabili ziren, erreaktore erdijarraituan eta jarraituan ur fenolikoak tratatzeko. Horretarako, ikatz aktibatua fenol-disoluzioetan zuen adsortzioaren analisia egin behar izan zen, eta aldibereko funtzionamenduak (Ad/Ox) zer abantaila dituen baloratu behar izan zen aurrez, ikatz aktibatua adsortzio-material gisa eta hidroxilo erradikalen sortzaile gisa zituen ezaugarriak era orekatuan aprobeztatu.

Atal honen bigarren zatirako hobetu egin zen erabilitako katalizatzailea. Horretarako, ikatz aktibatu pikortsuan atxikitako TiO₂-a zuen katalizatzaile berritzaile bat sintetizatu zen (TiO₂/GAC), ezaugarri jasangarriak eta ingurumenarekiko egokiak zituena. TiO₂/GAC konpositeak hiru tekniken bidez prestatu ziren (murgiltze bidezko inpregnazioa, teknika hidrotermala eta hauspeatze-teknika), ezaugarri ezberdinak zituzten ikatz aktibatuzko bi euskarritan: Norit[®] GAC 1240 Plus eta Norit[®] ROX 0.8. Lortutako titanio dioxidozko konpositeen jarduera katalitikoa baloratu zen, anilina zuten uretan eta eragiketako kondizio (pH eta ozono-dosi) ezberdinetan probatuta eta lortutako degradazio primarioa eta mineralizazioa aztertuta.

Fenola zuten uren tratamenduan ikatz aktibatu komertzialaren gaineko ozonizazioa egitean, ondorio hauek lortu ziren:

- Adsortzioa eta ozonizazioa ondoren egiterakoan (Ad/Ox prozesua egitean, alegia) hauts-formatuan zegoen ikatz aktibatua nahiz ikatz aktibatu pikortsua erabilia, hobetu egin ziren fenola deuseztatzeko zinetika eta mineralizazio-maila, ozonizazio-prozesu arruntean lortutakoekin alderatuta. Berdin gertatu zen ozono-dosi txikiak aplikatuta ere: fenola deuseztatzeko errendimendua ia % 100ekoa izan zen.
- Erreakzio-eredu zinetiko trifasiko bat (Ad/Ox) definitu behar izan zen G-L transferentziaren etapak eta likidoan (eta katalizatzailearen gainazalean ere) gertatutako adsortzio- eta oxidazio-etapak deskribatzeko eta, horren bidez, karbono aktibatuaren presentzia ozonizazio katalitikoa aztertzeko.
- Freundlich-en adsortzio-parametroekin batera, eredu zinetikoaren adsortzioaren konstante zinetikoa (k_{ads}) oinarrizkoa izan zen adsortzio-ozonizazio prozesuaren ezaugarriak zehazteko. Adsortzio-parametroak eta likidoan eta solidoan oxidazioak zituen konstante zinetikoak (k_{oxL} eta k_{oxS}) ondo konbinatuz gero, egoera egonkorrera iristeko behar zen hasierako trantsizio-etaparen iraupena zehaztu zitekeen.
- Ad/Ox prozesuak ondoz ondoko zikloak izateak ez zuen eraginik izan solidoko oxidazio-konstantean (k_{oxS}), ez mineralizazioari zegokionez, ez degradazio primarioari dagokionez. Likidoko oxidazio-konstanteak (k_{oxL}) zuen balioa, aldiz, txikitu egin zen ikatz aktibatu pikortsuaren gainazala gero eta gehiago estaltzearen ondorioz.

- Sistema jarraitura egokitutako Ad/Ox eredu zinetikoa ondo egokitu zen datu esperimentaletara, eta desbideratze estandar erlatiboa ez zen izan %5 baino handiagoa aztertutako kasu adierazgarri gehienetan. Horrenbestez, katalizatzaile berriak aztertzeko eta ozonizazio katalitikorako ekipamenduan berrikuntzak egiteko prozesuetan, Ad/Ox eredu zinetikoak aukera handiak zituen diagnostikorako eta diseinurako oinarritzko erreminta bat izateko, eskala pilotuan nahiz eskala industrialean.
- Oxidazio-konstanteen balioak ezagututa, jakin zitekeen zer funtzio zuen ikatz aktibatu pikortsuak ozonizazio-prozesuan eta zein interakzio zituen fenolarekin. pH alkalinoetan (pH = 11,0) degradazio eta mineralizazio handiagoa hauteman zen. Likidoko eta solidoko konstante zinetikoak hauek izan ziren, hurrenez hurren: $0,20 \text{ min}^{-1}$ eta $2,1 \times 10^{-3} (\text{mg L}^{-1})(\text{mg g}^{-1} \text{GAC min})^{-1}$. $19,0 \text{ mg L}^{-1}$ -ko balio kritikotik gorako ozono-kontzentrazioa erabili izanak mugatu egin zituen zinetika eta fenolaren adsortzio-gaitasuna, eta, ondorioz, txikitu egin zen mineralizazioaren errendimendua. Presioak edo gas-emariak izan zezakeen eraginari zegokionez, ez zen hobekuntza esanguratsurik ikusi ozonoa gas-fasetik likidora transferitzean.
- pH = 11,0 balioa, $19,0 \text{ mg L}^{-1}$ -ko ozono-kontzentrazioa eta $0,4 \text{ L h}^{-1}$ -ko gas-emaria erabiliz lortu ziren eragiketa-kondiziorik onenak. Kondizio horietan, ikatz aktibatuaren funtzio katalitikoaren eta adsortzio-funtzioaren arteko oreka hauteman zen.

Anilnadun urak eraginkortasunez arazteko TiO_2/GAC konpositeak erabiltzeari dagokionez, hauek ondorioztatu ahal izan ziren:

- TiO_2 -a eta ikatz aktibatua zuten material berriak sintetizatzeko hainbat metodo proposatu ziren, ozonizazio katalitikoko prozesuak sustatzeko. Emaizarik onenak TiO_2/GAC katalizatzaile berri batekin lortu ziren. Hura prestatzeko teknikan, TiO_2 -a hauspeatu zen Norit® GAC 1240 Plus ikatz aktibatu pikortsuaren gainean, TiCl_4 -aren aitzindari ziren disoluzio alkoholodunak erabilita.
- TiO_2 -aren nanokristalen (10 nm) banaketa homogeneoa lortu zen, bai ikatz aktibatuaren kanpoko gainazalean, bai ikatz aktibatuaren poroetan. Konposatuaren kanpoko gainazala % 25 handitu zen; gainera, $985 \text{ m}^2 \text{ g}^{-1}$ -ko BET azalera lortu zen, eta % 9,1eko TiO_2 -karga material katalitikoaren gainean.
- Eragiketa-aldagaiak (pH-a eta ozono-dosia) optimizatu ziren. Balio hauek finkatu ziren, hurrenez hurren: 7,0 eta $5,4 \text{ mg L}^{-1}$ edo $26,8 \text{ mg O}_3/\text{mg TOC}$. Hala, anilina guztiz degradatzen zen 5 minutuan, eta, 45 minutuan, % 80tik gorako mineralizazioa eta kolorea guztiz kentzea lortzen zen, $0,64 \text{ €/kg TOC}$ kostuarekin.
- Eragiketa-aldagai nagusiek G–L materia-transferentzian eta erreazioan zuten eragina, aurretik definitutako Ad/Ox eredu zinetikoa aplikatuta. Ondorioz, Norit® GAC 1240 Plus ikatz aktibatua erabiliz egiten zen oxidazio katalitiko bat zetorren Langmuir-Hinshelwood mekanismoarekin, eta oxidazioaren gehiengoa fase likidoan egiten zen. TiO_2/GAC konpositearen kasuan, berriz, ereduaren zenbatetsitako oxidazio-konstanteak, likidoan nahiz solidoan, bat zetorren Eley-Rideal motako mekanismo eraldatu batekin.
- Likidoan edo solidoan egindako oxidazio-erreakzioen garrantzi erlatiboa, oxidazio-konstante zinetikoak zenbatetsi ondoren. Konstanteak pH-arekin aldatu ziren batez ere. Hau da, pH azidotan erreazioak batez ere likidoan gertatu ziren; pH basikoan, aldiz, oxidazioa berdin gertatu zen solidoan eta likidoan. Ozono-dosi handiak erabiltzeak mugatu egiten zuen TiO_2/GAC katalizatzailearen zinetika eta

adsortzio-gaitasuna. Hori dela eta, ozono-dosi neurtuak erabiltzea gomendatzen zen, GACean jalkitako TiO_2 -aren adsortzioa eta oxidazioa orekatzeko.

- Katalizatzailearen gehiegizko karga erabiltzeak zuen eraginkortasun eza. TiO_2/GAC konposatuaren 5 g L^{-1} -tik gorako kantitateek handitu egin zuten uhertasuna, azido oxamikoa sortzen zuten degradazio-bidezidorrak eragiten zituztelako.
- TiO_2/GAC konpositea sustatzeko eragiketa-kondizio onenak zehaztea: $\text{pH} = 7,0$, $5,4 \text{ mg L}^{-1}$ -ko ozono-dosia eta $3,3 \text{ g L}^{-1}$ -ko katalizatzaile-karga. Hala, % 80,2ko mineralizazioa lortu zen.
- TiO_2/GAC materialak poluitzailea adsorbatzeko gaitasun handiagoa izatea, eta, aldi berean, poluitzaileak ozonoaren eraso jasatera bideratzea. Horrez gain, TiO_2 -a agertzeak leheneratze-efektua ere bazuen, eta, GAC komertzialarekin ez bezala, ez zen galtzen adsortzio-gaitasunik etengabe erabilia ere. Horrenbestez, TiO_2/GAC materiala gakoa zen jasangarritasun-printzipioekin bat egiten duten eraginkortasun handiko ozonizazio-ekipamendu modernoak garatzeko eta diseinatzeko garaian.

4.1.5. Ultrasoinuen bidezko aurretratamenduak ozonizazio-prozesuetan duen eragina

Ultrasoinuekin (US) aurrez tratatuta ozonizazio-prozesua indartzeko aukera aztertu zen, ur-baliabideetan zeuden eta ozonoarekiko erregogorrek ziren substantzia humikoak deuseztatzeko asmoz. Sonikazio-maiztasuna (98 kHz, 300 kHz eta 1 MHz), potentzia (10-40 W) eta lagin-bolumena (150-400 mL) aztertu ziren, aurretratamenduak ondorengo ozonizazio-prozesuan nolako eraginkortasuna zuen ebaluatzeko. Ondorio hauek lortu ziren:

- Ultrasoinuen bidezko aurretratamendua eginda, nabarmen murriztu zen azido humikodun laginen fluoreszentsia-igorpenaren intentsitatea (470 nm-ko banda), aztertutako maiztasun guztietan. Eraitzen arabera, 300 kHz-eko maiztasuna eta 40 W-eko potentzia (400 mL) 30 minutuz aplikatzea zen egokiena.
- $7,4 \text{ mg L}^{-1}$ -ko ozono-kontzentrazioarekin 30 minutuko tratamendua egin zen ultrasoinu-proben kontrasteko erreferentzia gisa, eta karbono organiko totala (TOC, *total organic carbon*) % 36 murriztea lortu zen haren bidez. Halaber, ozonizazioaren ondoren, pisu molekular txikiagoko degradazio-bitartekariak agertu ziren, eta nabarmen gutxitu ziren kolorea (% 85) eta SUVA_{254} (% 70).
- Ultrasoinuen bidezko aurretratamenduarekin ez zen nabarmen hobetu erreferentziako ozonizazio-tratamenduaren errendimendua. Ondorioz, ozonizazioa soilik erabilia lortutako emaitzen antzekoak lortu ziren, mineralizazioari (hondar-TOCa), koloreari eta SUVA_{254} -ri (SUVA, *specific ultraviolet absorbance*) dagokienez.

Ultrasoinuekin aurretratutako laginetan, fluoreszentsia-igorpenean aldaketa esanguratsuak detektatu ziren, mineralizazio-maila berdina lortu arren. Tratutako laginen fluoreszentsia-analisiak xehetasunez aztertuta, ikusi zen adsortzioz deusezta daitezkeen eta biodegradatzeko egokiak ziren substantziak zeudela. Horrek adierazten zuen adsortzio-eragiketekin edo eragiketa biologikoekin osa zitekeela tratamendua.

4.1.6. Ultrairagazketa eta ozonizazio prozesuen integrazioa

Prozesuak integratzeko beste adibide batean, funtzionamenduan zegoen hondakin-uren araztegi (HUA) bateko tratamendu biologikoaren efluenta aztertu zen, eta hari konektatutako ultrairagazketa-instalazio (c-UF) batetik zetorren errefus-korrontea

ozonizazioz tratatzean gertatutakoa aztertu zen. Prozesuen konbinazioari zegokionez, eragiketa bakoitzean 39 poluitzaile berri (CEC) deuseztatzeko aukera ebaluatu zen. CECak deuseztatzean prozesu bakoitzak nola parte hartzen zuen aztertu zen, CEC bakoitzaren biodegradagarritasunari eta ezaugarri fisiko-kimikoei erreparatuz. Halaber, c-UF instalazioak mikroorganismo patogenoak harrapatzeke zuen gaitasuna ebaluatu zen. Ondorio hauek lortu ziren:

- Tratamendu biologikoan CECak deuseztatzeko errendimendua konposatu bakoitzaren degradazio espezifikoaren eta biodegradagarritasunaren mende zegoen. Horren arabera, genisteina, metilparabenoa, progesterona, testosterona, kafeina eta parasetamola deuseztatzeko eraginkortasuna % 99,5etik gorakoa izan zen. Alabaina, irbesartana, karbamazepina, diurona eta fenitoinaren kasuan, batez besteko deuseztatze-tasak ez zuen % 20,0 gainditu.
- Ultrairagazketan, amitriptilina eta perfluorooktanosulfonamida CECak hobeto erauzi ziren (% 63,9 eta % 48,4, hurrenez hurren) ziprofloxazina edo sulfametoxazola baino (% 16,7 eta % 10,2, hurrenez hurren). Aldagarritasun handia ikusi zen erauzketa-errendimenduetan, eta, oro har, % 32 ingurukoa izan zen batezbestekoa. Hautemandako errendimendurik baxuenak kontzentrazio baxuetan eta/edo altuetan agertu ziren. Emaidza horiek azaltzeko, adsortzio-eredu bat proposatu zen. Eredu horretan, adsortzioak eragindako zikintzea deskribatu zen. Adsortzio hori itzulezina zen, eta, aipatu kasuetan, iragazketa-mintzean gertatzen zen.
- Ultrairagazketa-unitateak zuen garbiketa automatikoko sistemari esker, uhertasuna % 95-96 murriztu zen, eta esekiduran zegoen solidoa, berriz, % 90,1-100, baina ez zuen eragin handirik izan DOCak gutxitzen (% 15-25).
- Toxikotasun-probek erakutsi zuten, ultrairagazketak eraginkortasunez murrizten zuen tratamendu biologikotik zetorren efluenteak lehendik zuen toxikotasun urria. *E. coli* eta koliforme totalen presentzia aztertu zen, uraren kalitate mikrobiologikoaren adierazgarri ziren makroparametro gisa. Ultrairagazketa-unitatean garbiketa automatikoko sistema erabili edo ez, guztiz desagertu ziren *E. coli* eta koliforme totalak iragazitako korrontetik.
- Ultrairagazketaren errefusa ozonizazioarekin tratatuta, guztiz deuseztatu ziren identifikatutako CEC guztiak, salbu 2-hidroxibentzotiazola eta kafeina (% 39,7 eta % 38,1, hurrenez hurren).
- Errefus-korrontearen ozonizazio bidez esekiduran zeuden solidoen deuseztatzea deskribatzeko, etapak lehen ordenako seriean zuen eredu zinetiko bat erabili zen, % 5a baino errore baxuagoarekin. Tratutako efluenteak ez zuen *E. coli* edo antzeko bakteriorik, ezta toxikotasunik ere ($TU < 1$).
- Ultrairagazketaren teknologia eta ozonizazioa aplikatu zaien ur leheneratuak Europako zuzentarau berriak (2020/741 EB) ezarritako irizpideak betetzen zituen. Prozesuaren kostu ekonomikoa $0,0325 \text{ € m}^{-3}$ zen, emaitza baliokidea lukeen ohiko tratamendu tertziarioarena ($0,0534 \text{ € m}^{-3}$) baino txikiagoa.

4.2. Etorkizuneko aukerak

Litekeena da datozen hamarkadetan ura izatea baliorik handienetako duen ondasunetako bat, erregai fosilen gainera. Azken horiek merkatu egingo dira teknologia garbiago eta berriztagarriagoetarako trantsizioa dela eta. Hala ere, klima-aldaketaren eta uraren erabilera arduragabearen ondorioz, inbertsio handiak beharko dira populazioak kontsumitzeko behar duen ura edo giza jarduerak kaltetutako ekosistemak berreskuratzeko behar diren urak leheneratzeko.

Bestalde, efluente mota ezberdinei irtenbidea emateko erabili ditugun AOPak (ozonizazio-sistema integratu zaion ultrairagazketa-instalazioak izan ezik) eskala pilotuan ikertu beharko lirateke eskala handitzean sortzen diren arazo komunak tratatu ahal izateko (materia-transferentzia, lagin errealetako beste konposatu batzuekin dauden interferentziak eta abar). Halaber, orain arte AOPak eskala handian ezartzea oztopatu duen beste alderdi bat eragiketaren kostua izan da. Hala ere, akats larria litzateke tratamendu-lerro osoan AOPak bere horretan bakarrik hartzea. Tratamendu-lerro paraleloak ere aztertu beharko lirateke. Hala, AOPek funtzio garrantzitsua izango lukete poluitzaile-karga murrizten, eta, ondoren, beste tratamendu konbentzional batekin konbinatuko litzateke, edo ez, kasu eta helburu jakin bakoitzaren arabera. Horri dagokionez, 3.1 kasuan (UV/H₂O₂ teknologia) hartutako estrategiari jarraitu beharko litzaiotke etorkizuneko ikerketetan.

Energia berriztagarrien erabilera oinarritzkoa da AOPen esparruan. Hala, eguzki-argiaren bidez aktiba daitezkeen AOP fotokimikoen abantaila nabarmena dute, ura tratatzeaz gain energia ekoiztu baitezakete aldi berean. Horrek argi erakusten du MnO₂/GAC eta antzeko materialek erabilerak izan ditzaketela, baita beste oxido batzuekin (TiO₂-arekin) batera ere; halakoei buruzko ikerketak egin dira dagoeneko. Teknika horietan, hauek hobetu beharko lirateke: (i) erdieroaleen banda debekatuko energiaren murrizketa; (ii) eramaileen garraio mota; (iii) materialen kristalinitatea; (iv) gainazaleko eremua; (v) fotokatalizatzailearen egonkortasuna (prestaketa-teknika egokiarekin kontrolatu daiteke azken hori). Hala ere, material berrien garapenari dagokionez, azken hamarkadetan argitaratutako artikuluetan aurkeztu diren teknika guztiek dituzte abantaila eta ahultasun propioak, katalizatzailearen egonkortasunari, eraginkortasunari, ekoizpen-kostuari, egiturei eta errendimenduari dagokienez. Prestaketa-teknika askok ingurumen-karga handiak dakartzate berekin, eta ezin dira maila industrialean aplikatu arrazoi horregatik. Tesi honetan eta antzekoetan garatutako katalizatzaileak izango lirateke, ziurtasun osoz, datozen urteetako AOP berrien gakoak.

Bestalde, eta AOP askotan erabilitako katalizatzaileei dagokienez, materialen zientzian egindako aurrerapenek izugarri lagundu dezakete, propietate interesgarriak dituzten material berriak aurkitzen ari baitira. Horrek erakusten du ingurumenean aplikatzekoak diren AOPen ikerketa modernoak diziplinartekoa izan behar duela, eta zientziaren eta ingeniariaren hainbat arlo esku hartu behar dutela arazoa arrakastaz konpondu ahal izateko.

Beste ekintza-lerro batek bat egiten du prozesuen integrazioaren ideiarekin, ingurumen-arazoak konpontzeko teknologia guztiek izan behar baitute bideragarritasun ekonomikoa. Hala ere, AOPak mintz-teknologiekin behar bezala konbinatuta, adibidez, guztiz bideragarriak izan daitezke. Ozonizazioarekin batera beste operazioetan parte hartzen duten konfigurazioak (3.11 eta 3.12 kasuetan

aurkeztutakoak, adibidez, zeinetan ozonizazioari konektatu zitzaien ultrairagazketa prozesu batek) jasagarriak izan daitezke, ekipamendua behar bezala diseinatuta, prozesua optimizatuta eta eragiketa-kontrol burutsua eginda.

Eranskina



A.1. Biltzar zientifikoetan egindako ekarpenak

- Ferreiro, C.; Villota, N.; Lombraña, J.I.; Rivero, María J. Analysis of the adsorption mechanisms in the TiO₂/UV photocatalysis to degrade benzothiazole and aniline. Poster bidezko komunikazioa. 5th European Conference on Environmental Applications of Advanced Oxidation Processes (EAAOP 5). Praga (Txekiar Errepublika). Hasiera-data: 2017/06/25 – Amaiera-data: 2017/06/29
- Ferreiro, C.; Lombraña, J.I.; Rivero, María J. Ozonización catalítica de benzotiazol en presencia del composite TiO₂/GAC: Efecto de las variables de control y mecanismo de degradación. Poster bidezko komunikazioa. XIII Congreso Español de Tratamiento de Aguas. León (Espainia). Hasiera-data: 2018/06/18 - Amaiera-data: 2018/06/20
- Ferreiro, C.; Condori, O.; Lombraña, J.I.; Villota, N.; Rivero, María J. Contribution of TiO₂/GAC catalytic ozonation to the sustainable treatment of aniline wastewaters from the vulcanization accelerator manufacturing. Poster bidezko komunikazioa. 10th European meeting on Solar Chemistry and Photocatalysis Environmental Applications (SPEA10). Almería (Espainia). Hasiera-data: 2018/06/04 - Amaiera-data: 2018/06/08
- Villota, N.; Ferreiro, C.; Lombraña, J.I.; Rivero, María J. Efecto del reactivo Fenton combinado con luz UV y ondas de ultrasonidos en la oxidación de cafeína. Ahozko komunikazioa. ANQUE-ICCE-CIBIQ 2019. Santander (Espainia). Hasiera-data: 2019/06/19 - Amaiera-data: 2019/06/21
- Ferreiro, C.; Villota, N.; Lombraña, J.I.; Rivero, María J. Análisis de la eficiencia y rutas de degradación a través de un modelo trifásico de ozonización TiO₂/GAC para la eliminación de anilina de aguas residuales. Ahozko komunikazioa. ANQUE-ICCE-CIBIQ 2019. Santander (Espainia). Hasiera-data: 2019/06/19 - Amaiera-data: 2019/06/21
- Ferreiro, C.; Villota, N.; Lombraña, J.I.; Lomas, J.M.; Rivero, María J. Analysis of control parameters in a TiO₂/UV reacting system for wastewater treatment containing benzothiazole and aniline. Ahozko komunikazioa. 15th International Conference on Environmental Science and Technology (CEST2017). Rhodes (Grezia). Hasiera-data: 2017/08/31 - Amaiera-data: 2017/09/02
- Villota, N.; Lomas, J.M.; Lombraña, J.I.; Ferreiro, C. Fenton reagent in combination with UV light and ultrasound waves applied for caffeine oxidation. Ahozko komunikazioa. 16th International Conference on Environmental Science and Technology (CEST2019). Rhodes (Grezia). Hasiera-data: 2019/09/04 - Amaiera-data: 2019/09/07
- Ferreiro, C.; Sardón, L.; Lomas, J.M.; Villota, N. Effect of iron catalyst on caffeine oxidation by sono-Fenton technology. Ahozko komunikazioa. 16th International Conference on Environmental Science and Technology (CEST2019). Rhodes (Grezia). Hasiera-data: 2019/09/04 – Amaiera-data: 2019/09/07
- Sardón, L.; Ferreiro, C.; Camarero, L.M.; Lomas, J.M.; Villota, N. Effect of hydrogen peroxide on caffeine oxidation by sono-Fenton technology. Ahozko komunikazioa. 16th International Conference on Environmental Science and

Technology (CEST2019). Rhodes (Grezia). Hasiera-data: 2019/09/04 - Amaiera-data: 2019/09/07

- Villota, N.; Cruz, A.; Lombraña, J.I.; Ferreiro, C.; Marcé, M.; Esplugas, S. pH Effect on Paracetamol Removal from Aqueous Solutions Using Laboratory and Pilot-Scale Semicontinuous Ozonation Reactors. Poster bidezko komunikazioa. 6th European Conference on Environmental Applications of Advanced Oxidation Processes (EAAOP-6). Portoroz-Portorose (Eslovenia). Hasiera-data: 2019/06/26 - Amaiera-data: 2019/06/30
- Muniozguren P.A.; Ferreiro, C.; Lombraña, J.I.; Lee, J. Influence of ultrasound and ozone for the treatment of humic acids. Ahozko komunikazioa. 4th Iberoamerican Conference on Advanced Oxidation Processes (IV CIPOA). Natal (Brasil). Hasiera-data: 2019/11/18 - Amaiera-data: 2019/10/22
- Ferreiro, C.; Alegre, N.; Villota, N.; Lombraña, J.I.; Rivero, M.J.; Zúñiga, V.; Rituerto, J. M. Aplicación del reactor de lecho fluidizado en la eliminación fotocatalítica de compuestos recalcitrantes mediante composites de MnO₂/GAC. Ahozko komunikazioa. XXVII Congreso Iberoamericano de Catálisis 2020 (CICAT 2020). Puerto Vallarta (Mexiko). Hasiera-data: 2020/10/26 - Amaiera-data: 2020/10/28
- Villota, N.; Ferreiro, C.; Lombraña, J.I.; Camarero, L. M. Oxidation of acetaminophen by ultrasound waves and H₂O₂ combined technology. Ahozko komunikazioa. 14th Mediterranean Congress of Chemical Engineering (MeCCE-14). Bartzelona (Espainia). Hasiera-data: 2020/11/16 - Amaiera-data: 2020/11/20
- Villota, N.; Ferreiro, C.; Lombraña, J.I.; Camarero, L. M. Comparison of caffeine oxidation by Fenton reagent in combination with UV light and ultrasound waves. Ahozko komunikazioa. 14th Mediterranean Congress of Chemical Engineering (MeCCE-14). Bartzelona (Espainia). Hasiera-data: 2020/11/16 - Amaiera-data: 2020/11/20

A.2. Bestelako ekarpenak

- Gómez-Motos, I.; Villota, N.; Ferreiro, C.; Lombraña, J.I. Degradación de contaminantes emergentes mediante ultrafiltración y ozono. Editorial Académica Española. International Book Market Service Ltd. OmniScriptum Publishing Group. Maurizio Errepublika. 2018. ISBN: 978-6202098731. ICEE: 0.299 Q4 (229/258) SPI Scholarly Publisher's Indicators.

A.3. Material osagarria

A.3.1. 1. argitalpenaren material osagarria

Supplementary Information

Kinetic modelling for concentration and toxicity changes during the oxidation of 4-chlorophenol by UV/H₂O₂

Cristian Ferreiro ^{1,*}, Josu Sanz ², Natalia Villota ³, Ana de Luis ⁴ and

José Ignacio Lombraña ¹

¹ Department of Chemical Engineering, Faculty of Science and Technology, University of the Basque Country UPV/EHU, Barrio Sarriena s/n, 48940 Leioa, Spain; ji.lombrana@ehu.eus

² Department of Mathematics and Science Didactics, Faculty of Education, Philosophy and Anthropology of Donostia-San Sebastián, University of the Basque Country UPV/EHU, Barrio Sarriena s/n, 48940 Leioa, Spain; josu.sanz@ehu.eus

³ Department of Chemical and Environmental Engineering, Faculty of Engineering Vitoria-Gasteiz, University of the Basque Country UPV/EHU, Nieves Cano, 12, 01006 Vitoria-Gasteiz, Spain; natalia.villota@ehu.eus

⁴ Department of Chemical and Environmental Engineering, Faculty of Engineering in Bilbao, University of the Basque Country UPV/EHU, Plaza Ingeniero Torres Quevedo, 1, 48013 Bilbao, Spain; ana.deluis@ehu.eus

* Correspondence: cristian.ferreiro@ehu.eus

Table S1. Reported methods of treating industrial wastewater containing 4-chlorophenol.

Advanced oxidation technology	Notes	Reference
Photo-Fenton	In the first stage, a heterogeneous reaction occurs on the surface of iron. In the second stage, a homogeneous reaction (Fenton reaction) is observed. The first stage proceeds through a radical pathway where 4-chlorocatechol is one of the reactants (the hydroxyl radical attacks the substrate). The second stage involves the participation of <i>ortho</i> -parachlorophenolperoxyl radicals and O ₂ .	1
UV/TiO ₂	It has been observed that the increase in the size of the TiO ₂ crystals (effect of the calcination temperature) favours the removal of 4-chlorophenol.	2
UV/ZnO	The dependence of pseudo-zero-order kinetics on the different operational variables for the removal of 4-chlorophenol was investigated. It has been observed that inorganic anions such as Cl ⁻ and SO ₄ ²⁻ , common in water, act as blockers of the active centres. The proposed reaction mechanism involves an <i>o</i> -hydroxylation step that leads to the formation of high amounts of catechol.	3
UV/O ₃ /H ₂ O ₂	Ozone decomposition results in the formation of hydroxyl radicals. The presence of the hydroxyl radicals did not result in an increased rate of oxidation at pH = 9. The values of the pseudo-first-order kinetic constants (4-chlorophenol degradation reaction) estimated in the pH range of 7-12 were not significantly different from each other.	4
UV/TiO ₂ /H ₂ O ₂	Photocatalytic processes carried out with a combination of UV light and H ₂ O ₂ were less efficient (in producing mineralised compounds) than the UV/O ₃ and UV/H ₂ O ₂ processes. A significant effect was not observed.	5
UV/H ₂ O ₂	It has been found that the addition of H ₂ O ₂ increases the photolytic reaction rate by an order of magnitude. The extent of mineralisation of 4-chlorophenol is improved and degradable compounds are produced in large amounts.	6

References

- Zhou, T., Li, Y., Ji, J., Wong, F.-S. & Lu, X. Oxidation of 4-chlorophenol in a heterogeneous zero valent iron/H₂O₂ Fenton-like system: Kinetic, pathway and effect factors. *Separation and Purification Technology* **62**, 551-558 (2008).
- Sharma, S., Mukhopadhyay, M. & Murthy, Z. V. P. Treatment of Chlorophenols from Wastewaters by Advanced Oxidation Processes. *Separation & Purification Reviews* **42**, 263-295 (2013).
- Gaya, U. I., Abdullah, A. H., Zainal, Z. & Hussein, M. Z. Photocatalytic treatment of 4-chlorophenol in aqueous ZnO suspensions: Intermediates, influence of dosage and inorganic anions. *Journal of Hazardous Materials* **168**, 57-63 (2009).
- Pera-Titus, M., García-Molina, V., Baños, M. A., Giménez, J. & Esplugas, S. Degradation of chlorophenols by means of advanced oxidation processes: a general review. *Applied Catalysis B: Environmental* **47**, 219-256 (2004).
- Ruppert, G., Bauer, R. & Heisler, G. UV-O₃, UV-H₂O₂, UV-TiO₂ and the photo-Fenton reaction - comparison of advanced oxidation processes for wastewater treatment. *Chemosphere* **28**, 1447-1454 (1994).

6. Çatalkaya, E. Ç., Bali, U. & Şengül, F. Photochemical degradation and mineralization of 4-chlorophenol. *Environ Sci & Pollut Res* **10**, 113-120 (2003).

A.3.2. 5. argitalpenaren material osagarria

Supplementary Material

Removal of Aniline and Benzothiazole Wastewaters Using an Efficient MnO₂/GAC Catalyst in a Photocatalytic Fluidised Bed Reactor

Cristian Ferreiro ^{1,*}, Natalia Villota ², José Ignacio Lombrana ¹, María J. Rivero ³, Verónica Zúñiga ⁴ and José Miguel Rituerto ⁴

¹ Department of Chemical Engineering, Faculty of Science and Technology, University of the Basque Country UPV/EHU, Barrio Sarriena s/n, 48940 Leioa, Spain; ji.lombrana@ehu.eus

² Department of Chemical and Environmental Engineering, Faculty of Engineering Vitoria-Gasteiz, University of the Basque Country UPV/EHU, Nieves Cano 12, 01006 Vitoria-Gasteiz, Spain; natalia.villota@ehu.eus

³ Department of Chemical and Biomolecular Engineering, University of Cantabria, 39005 Santander, Spain; riveromj@unican.es

⁴ General Química, S.A.U. (Grupo Dynasol), 01213 Lantaron, Spain; veronica.zuniga@repsol.com (V.Z.); jrituertol@repsol.com (J.M.R.)

* Correspondence: cristian.ferreiro@ehu.eus; Tel.: +34-946-012-512

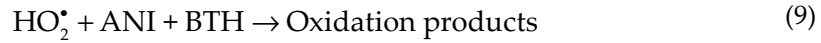
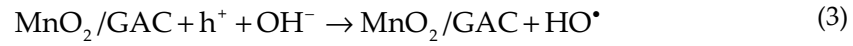
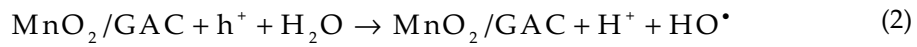
Table S1. Previous studies of photocatalysis using manganese oxides supported on carbonaceous materials.

Catalyst	Operating conditions	Comments	Ref.
α -MnO ₂	[Cat.] = 0.025 g $\tau = 1.655 \times 10^{-3} \text{ mol h}^{-1} \text{ g cat}^{-1}$ T = 25 °C Time = 8 h [% removal] = 100	Up to 100% conversion into acetone using an amorph MnO ₂ photocatalytic system for 2-propanol removal. The α -MnO ₂ phase was more active and regenerable than other manganese oxides.	[1]
α -MnO ₂ /CNT	[Cat.] = 0.4 g L ⁻¹ C ₀ = 20 mg L ⁻¹ T = 25 °C Time = 75 min [% removal] = 24	Compared different crystalline phases of MnO ₂ . Found that α -MnO ₂ particles supported on carbon nanotubes (CNT) improved the surface area of the hybrid structure and had a better performance under visible light.	[2]
MnO ₂ /AC	[Cat.] = 3.0 g L ⁻¹ C ₀ = 60 mg L ⁻¹ T = 25 °C Time = 5 min [% removal] = 98.53	Compared the catalytic activity of MnO ₂ nanoparticles to that of MnO ₂ /AC composites. The composite removed 31.96% more Congo Red (CR) dye than the nanoparticles. The presence of mineral ions led to a higher dye degradation rate.	[3]
GO/MnO ₂	[Cat.] = 0.5 g L ⁻¹ C ₀ = 60 mg L ⁻¹ T = 25 °C Time = 120 min [% removal] = 98	Observed that the catalytic activity during Reactive Black 5 (RB5) removal was higher than that of their starting materials. The presence of graphene oxide with a 20% MnO ₂ content helped to increase the generation of hydroxyl radicals and facilitated their separation from the solution, in contrast to MnO ₂ nanoparticles.	[4]
MnO ₂ /AC	[Cat.] = 0.5 g L ⁻¹ C ₀ = 100 mg L ⁻¹ T = 25 °C Time = 60 min [% removal] = 85	Impregnated an activated carbon with a 20% BMnO ₂ content. Concluded that carbon impregnated with BMnO ₂ showed a higher potential for RB5 degradation.	[5]

Photocatalytic reaction mechanism with MnO₂/GAC composites

The improvement can be attributed to the reaction mechanisms which occur on the surface of the catalyst. The trigger mechanism begins with light absorption ($h\nu$), generating electron-hole ($e^- - h^+$) pairs, which act as reducing and oxidising agents (Eq. 1). During oxidation, water (Eq. 2) or hydroxide ions (OH^-) (Eq. 3) adsorbed on the catalyst generate hydroxyl radicals (HO^\bullet), while oxygen prevents the recombination of electron-hole pairs (Eq. 4). Subsequently, when irradiating a photon of energy equal to or greater than the band gap energy, the excitation of electrons in the conduction band (CB) is produced and it generates an equal number of holes in the valence band (VB) (Eqs. 5– 7). At that point, Eqs. 8–9, the high oxidative species generated are responsible for ANI and BTH oxidation to other degradation by-products.

According to Ameta [6] and Rahmat et al. [7], the equations below describe a plausible mechanism of photocatalysis of an activated carbon material modified with MnO₂ (MnO₂/GAC):



Achieving a high removal efficiency during the photocatalytic process requires [8–10]: i) an adequate diffusion of contaminants from the liquid phase to the surface of the MnO₂ catalyst, ii) a strong adsorption of organic pollutants on the surface of MnO₂, iii) redox reactions at the catalyst surface level, and iv) desorption of oxidation products. Based on these conditions, the reactor could play a key role not only in terms of degradation but also in terms of ANI and BTH mineralisation. Therefore, the application of advanced oxidation processes (AOPs) with suitable reactor technology can reduce catalyst damage whilst increasing reuse [11].

Analytical methods for influent characterization

Nitrite, nitrates, chlorides and phosphates were measured by ion chromatography (IC) using a Dionex Model 2010i Ion Chromatograph (Dionex, Sunnyvale, CA, USA) with a conductivity detector, Model CDM-1 (Dionex, Sunnyvale, CA, USA). Chromatographic separation was achieved using a IonPac-AS4 (250 × 4.0 mm, Dionex, Sunnyvale, CA, USA) column with a IonPac-AG4 guard column (50 × 4.0 mm, Dionex, Sunnyvale, CA, USA). The eluent used consisted in a mixture of 3.5 mM NaHCO₃ and 2.0 mM Na₂CO₃. A sample volume of 50 µL was injected according with the method described by Urasa and Ferede [12].

Quality assurance (QA) and quality control (QC) protocols

The protocols followed for the determination of the different parameters listed in Table 1 were described below. The samples were subjected to drastic conditions to acid hydrolysis (1N HCl), basic hydrolysis (1N NaOH), sunlight and temperature (30 °C). Subsequently, the amount recovered was determined in triplicate after 7 days.

Table S2. Limit of quantification values (LOQ) and limit of detection values (LOD) of different parameters.

Parameter	LOQ	LOD
Aniline (mg L ⁻¹)	0.01	30.0
Benzothiazole (mg L ⁻¹)	0.02	24.0
Nitrite (mg NO ₂ L ⁻¹)	0.0010	50.0
Nitrate (mg NO ₃ L ⁻¹)	0.0015	75.0
Chloride (mg Cl L ⁻¹)	0.003	80.0
Total phosphorus (mg P L ⁻¹)	0.002	32.0
Phosphates (mg PO ₄ L ⁻¹)	0.001	46.0

Table S3. Linearity values of different parameters.

Parameter	Range	Regression equation	R ²
Aniline (mg L ⁻¹)	0.1-20.0	y = 3.780 x + 2.350	0.998
Benzothiazole (mg L ⁻¹)	0.1-20.0	y = 7.033 x + 8.196	0.998
Nitrite (mg NO ₂ L ⁻¹)	0.002-0.1	y = 5.280 x + 3.040	0.993
Nitrate (mg NO ₃ L ⁻¹)	0.002-4.0	y = 2.098 x + 9.636	0.998
Chloride (mg Cl L ⁻¹)	0.01-65.0	y = 2.558 x + 3.146	0.991
Total phosphorus (mg P L ⁻¹)	0.01-0.1	y = 3.973 x + 5.480	0.995
Phosphates (mg PO ₄ L ⁻¹)	0.01-0.3	y = 3.108 x + 2.721	0.998

Table S4. Specificity values of different parameters.

Parameter	Condition	Amount added	Amount recovered	Degradation (%)
Aniline (mg L ⁻¹)	Acidic degradation	12.0	11.7	1.87
	Alkaline degradation	12.0	11.7	2.12
	Solar light	12.0	11.6	3.04
Benzothiazole (mg L ⁻¹)	Acidic degradation	12.0	11.8	1.15
	Alkaline degradation	12.0	11.9	0.71
	Solar light	12.0	11.8	0.98
Nitrite (mg NO ₂ L ⁻¹)	Acidic degradation	0.050	0.049	1.54
	Alkaline degradation	0.050	0.048	2.2
	Solar light	0.050	0.048	2.03
Nitrate (mg NO ₃ L ⁻¹)	Acidic degradation	1.50	1.47	1.64
	Alkaline degradation	1.50	1.44	3.72
	Solar light	1.50	1.48	0.99
Chloride (mg Cl L ⁻¹)	Acidic degradation	30.0	29.3	2.31
	Alkaline degradation	30.0	28.9	3.47
	Solar light	30.0	29.6	1.02
Total phosphorus (mg P L ⁻¹)	Acidic degradation	0.05	0.04	0.8
	Alkaline degradation	0.05	0.04	1.74
	Solar light	0.05	0.05	2.8
Phosphates (mg PO ₄ L ⁻¹)	Acidic degradation	0.100	0.097	2.7
	Alkaline degradation	0.100	0.099	0.85
	Solar light	0.100	0.096	3.87

Table S5. Accuracy values of different parameters.

Parameter	Range	Recovery (Mean ± % RSD)
Aniline (mg L ⁻¹)	0.1-20.0	100.91 ± 0.024
Benzothiazole (mg L ⁻¹)	0.1-20.0	100.24 ± 0.030
Nitrite (mg NO ₂ L ⁻¹)	0.002-0.1	100.14 ± 0.020
Nitrate (mg NO ₃ L ⁻¹)	0.002-4.0	100.08 ± 0.007
Chloride (mg Cl L ⁻¹)	0.01-65.0	100.05 ± 0.026
Total phosphorus (mg P L ⁻¹)	0.01-0.1	100.32 ± 0.013
Phosphates (mg PO ₄ L ⁻¹)	0.01-0.3	100.56 ± 0.011

Table S6. Precision values of different parameters.

Parameter	Concentration	Standard solution		Sample solution		Mean	SD	% RSD
		Intra-day precision	Inter-day precision	Intra-day precision	Inter-day precision			
Aniline (mg L ⁻¹)	12.0	12.020	12.013	12.051	12.042	12.0315	0.0179	0.149
Benzothiazole (mg L ⁻¹)	12.0	12.090	12.047	12.100	12.084	12.08025	0.0231	0.191
Nitrite (mg NO ₂ L ⁻¹)	0.05	0.0510	0.0490	0.0521	0.0514	0.050875	0.0013	2.614
Nitrate (mg NO ₃ L ⁻¹)	1.50	1.5039	1.5010	1.5120	1.5109	1.50695	0.0053	0.354
Chloride (mg Cl L ⁻¹)	30.0	30.017	30.011	30.029	30.024	30.02025	0.0078	0.026
Total phosphorus (mg P L ⁻¹)	0.05	0.059	0.053	0.051	0.055	0.0545	0.0034	6.267
Phosphates (mg PO ₄ L ⁻¹)	0.10	0.1024	0.1031	0.1015	0.1043	0.102825	0.0011	1.148

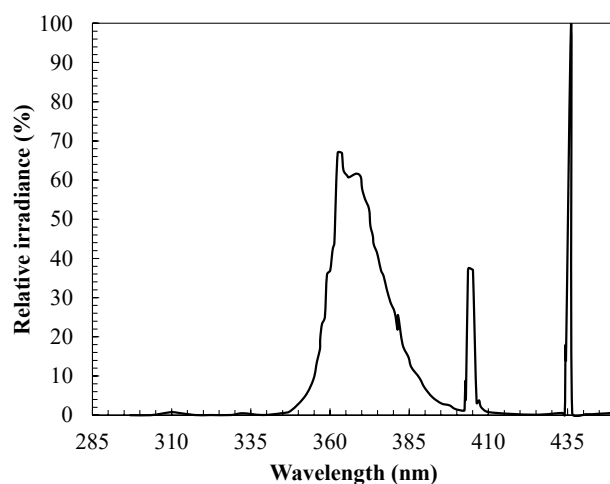
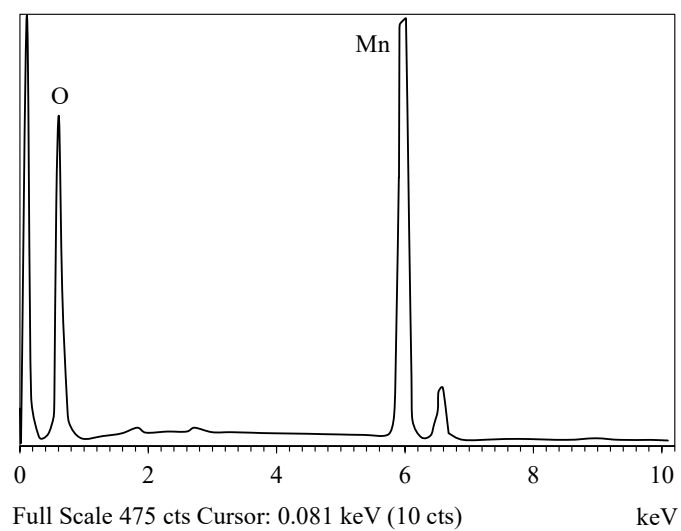
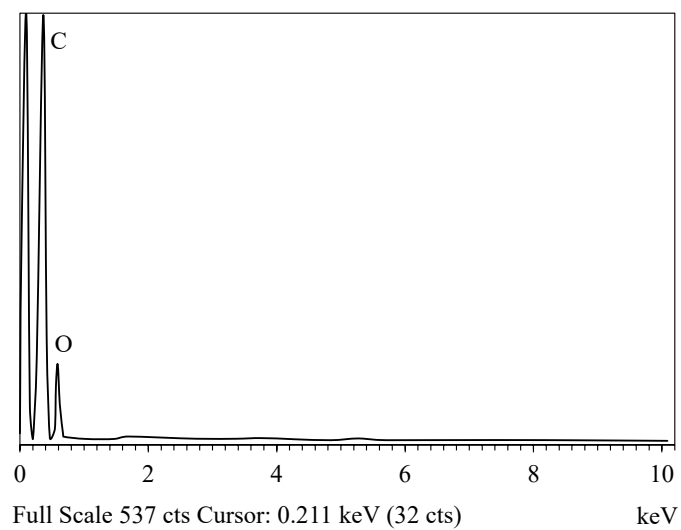


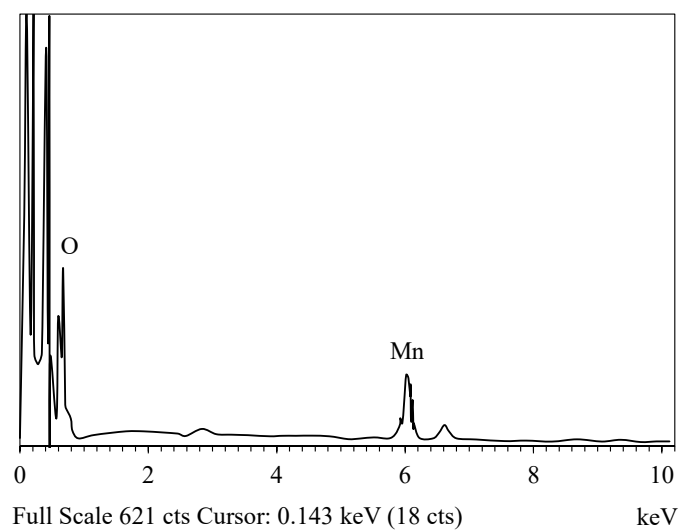
Figure S1. Spectrum of the UV-A lamp used in the experimental equipment.



(a)

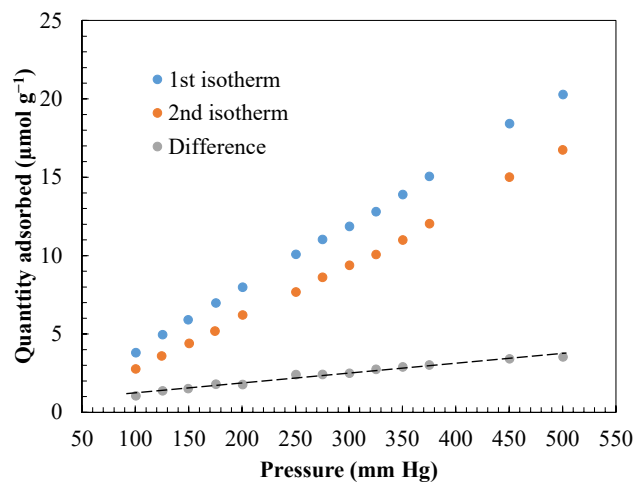


(b)

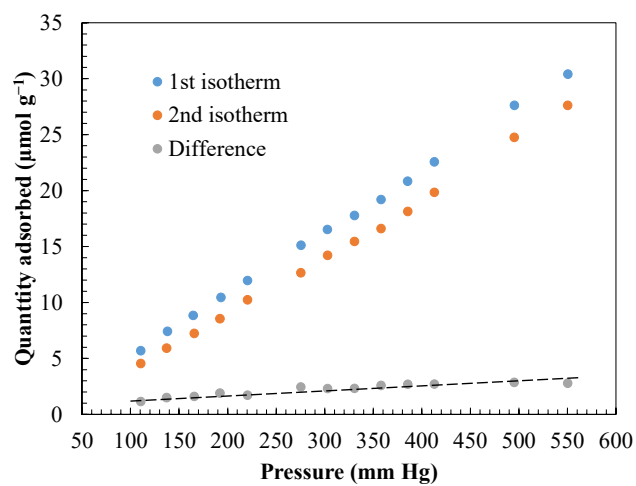


(c)

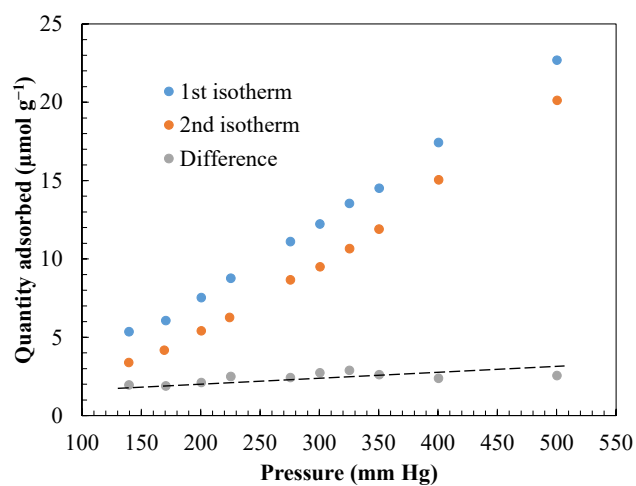
Figure S2. EDX spectra of the materials used in the study: (a) synthesised MnO_2 powder; (b) Commercial activated carbon Hydrodarco[®] 3000; (c) Synthesized MnO_2/GAC -3 composite.



(a)

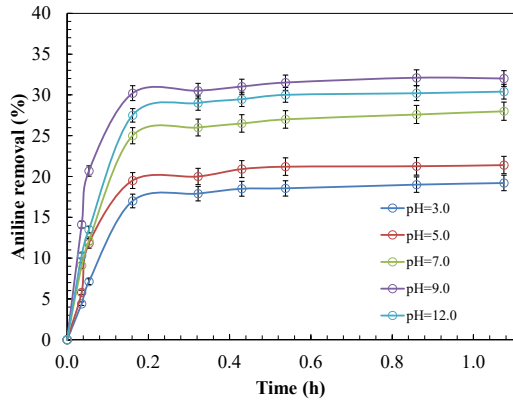


(b)

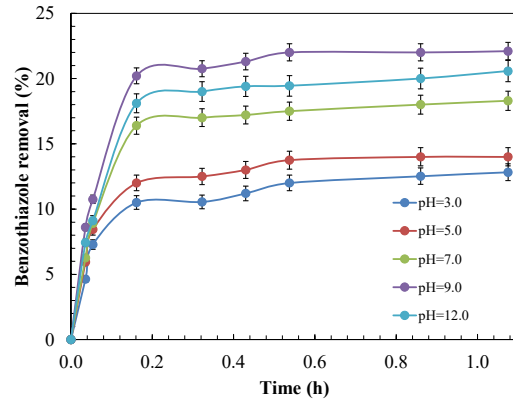


(c)

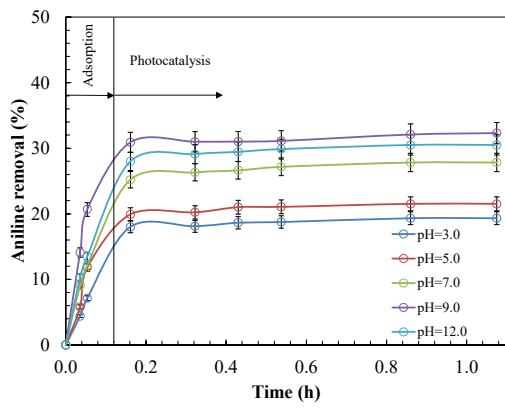
Figure S3. Determination of the H₂ monolayer chemisorbed on the surface of the three MnO₂/GAC composites synthesised in this study: (a) MnO₂/GAC-1; (b) MnO₂/GAC-2; (c) MnO₂/GAC-3.



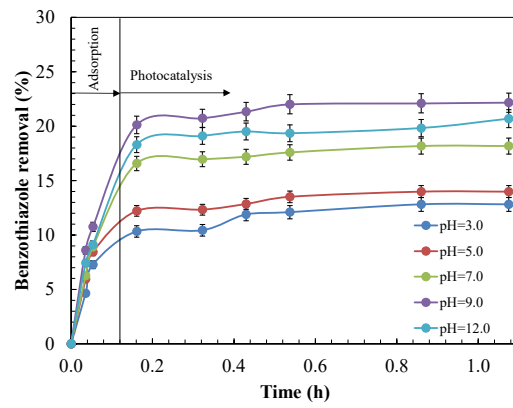
(a)



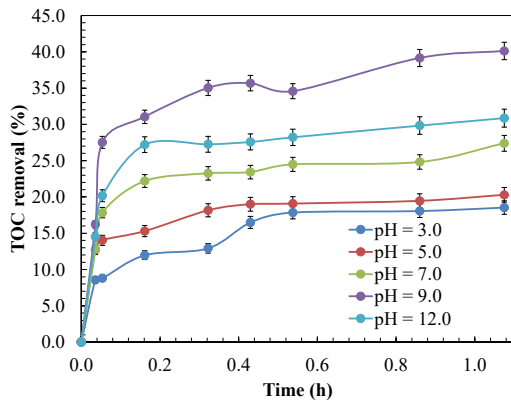
(b)



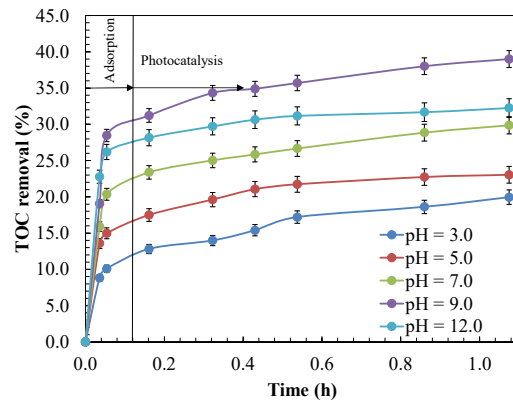
(c)



(d)



(e)



(f)

Figure S4. pH effect on the efficiency of the ANI and BTH removal process using GAC Hydrodarco® 3000 during the adsorption and photocatalysis processes. Evolution of the: (a,b) Adsorption; (c,d) Photocatalysis in primary degradation (e,f) and in mineralisation in the adsorption and photocatalysis processes, respectively. Experimental conditions: $C_0 = 12.0 \text{ mg L}^{-1}$; $m_{\text{CAT}} = 0.9 \text{ g L}^{-1}$; Irradiation dose = 155.8 W m^{-2} ; $T = 26 \text{ }^\circ\text{C}$.

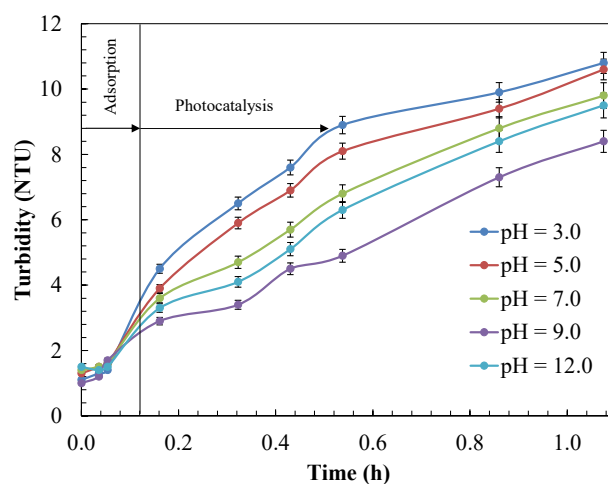


Figure S5. pH effect on turbidity during the photocatalysis of industrial effluents containing ANI and BTH using the GAC Hydrodarco® 3000. Experimental conditions: $C_0 = 12.0 \text{ mg L}^{-1}$; $m_{\text{CAT}} = 0.9 \text{ g L}^{-1}$; Irradiation dose = 155.8 W m^{-2} ; $T = 26 \text{ }^\circ\text{C}$.

References

1. Cao, H.; Suib, S.L. Highly Efficient Heterogeneous Photooxidation of 2-Propanol to Acetone with Amorphous Manganese Oxide Catalysts. *J. Am. Chem. Soc.* **1994**, *116*, 5334–5342, doi:10.1021/ja00091a044.
2. Warsi, M.F.; Bilal, M.; Zulfiqar, S.; Khalid, M.U.; Agboola, P.O.; Shakir, I. Enhanced Visible Light Driven Photocatalytic Activity of MnO_2 Nanomaterials and Their Hybrid Structure with Carbon Nanotubes. *Mater. Res. Express* **2020**, *7*, 105015, doi:10.1088/2053-1591/abbf8d.
3. Khan, I.; Sadiq, M.; Khan, I.; Saeed, K. Manganese Dioxide Nanoparticles/Activated Carbon Composite as Efficient UV and Visible-Light Photocatalyst. *Environ. Sci. Pollut. Res.* **2019**, *26*, 5140–5154, doi:10.1007/s11356-018-4055-y.
4. Saroyan, H.; Kyzas, G.Z.; Deliyanni, E.A. Effective Dye Degradation by Graphene Oxide Supported Manganese Oxide. *Processes* **2019**, *7*, 40, doi:10.3390/pr7010040.
5. Saroyan, H.S.; Arampatzidou, A.; Voutsas, D.; Lazaridis, N.K.; Deliyanni, E.A. Activated Carbon Supported MnO_2 for Catalytic Degradation of Reactive Black 5. *Colloids Surf. A-Physicochem. Eng. Asp.* **2019**, *566*, 166–175, doi:10.1016/j.colsurfa.2019.01.025.
6. Ameta, S. *Advanced Oxidation Processes for Wastewater Treatment: Emerging Green Chemical Technology*; Academic Press, San Diego, CA, USA, **2018**; ISBN 978-0-12-810499-6.
7. Rahmat, M.; Rehman, A.; Rahmat, S.; Bhatti, H.N.; Iqbal, M.; Khan, W.S.; Bajwa, S.Z.; Rahmat, R.; Nazir, A. Highly Efficient Removal of Crystal Violet Dye from Water by MnO_2 Based Nanofibrous Mesh/Photocatalytic Process. *J. Mater. Res. Technol.* **2019**, *8*, 5149–5159, doi:10.1016/j.jmrt.2019.08.038.
8. Tang, N.; Tian, X.; Yang, C.; Pi, Z.; Han, Q. Facile Synthesis of $\alpha\text{-MnO}_2$ Nanorods for High-Performance Alkaline Batteries. *J. Phys. Chem. Solids* **2010**, *71*, 258–262, doi:10.1016/j.jpcs.2009.11.016.
9. Lin, H.; Chen, D.; Liu, H.; Zou, X.; Chen, T. Effect of MnO_2 Crystalline Structure on the Catalytic Oxidation of Formaldehyde. *Aerosol Air Qual. Res.* **2017**, *17*, 1011–1020, doi:10.4209/aaqr.2017.01.0013.
10. Wang, B.; Zhang, H.; Wang, F.; Xiong, X.; Tian, K.; Sun, Y.; Yu, T. Application of Heterogeneous Catalytic Ozonation for Refractory Organics in Wastewater. *Catalysts* **2019**, *9*, 241, doi:10.3390/catal9030241.
11. Farines, V.; Baig, S.; Albet, J.; Molinier, J.; Legay, C. Ozone Transfer from Gas to Water in a Co-Current Upflow Packed Bed Reactor Containing Silica Gel. *Chem. Eng. J.* **2003**, *91*, 67–73, doi:10.1016/S1385-8947(02)00137-7.
12. Urasa, I.T.; Ferede, F. The Determination of Phosphates Using Ion Chromatography: An Evaluation of Influential Factors. *Int. J. Environ. Anal. Chem.* **1986**, *23*, 189–206, doi:10.1080/03067318608076445.

A.3.3. 7. argitalpenaren material osagarria

Supplementary Material

Application of combined adsorption–ozonation process for phenolic wastewater treatment in a continuous fixed-bed reactor

Cristian Ferreiro ^{1,*}, Ana de Luis ², Natalia Villota ³, Jose María Lomas ³, José Ignacio Lombrana ¹ and Luis Miguel Camarero ³

¹ Department of Chemical Engineering, Faculty of Science and Technology, University of the Basque Country UPV/EHU, Barrio Sarriena s/n, 48940 Leioa, Spain; ji.lombrana@ehu.eus

² Department of Chemical and Environmental Engineering, Faculty of Engineering in Bilbao, University of the Basque Country UPV/EHU, Plaza Ingeniero Torres Quevedo, 1, 48013 Bilbao, Spain, ana.deluis@ehu.eus

³ Department of Environmental and Chemical Engineering, Faculty of Engineering of Vitoria-Gasteiz, University of the Basque Country UPV/EHU, 01006 Vitoria-Gasteiz (Spain); natalia.villota@ehu.eus (N.V.); josemaria.lomas@ehu.eus (J.M.L.); luismiguel.camarero@ehu.eus (L.M.C.)

* Correspondence: cristian.ferreiro@ehu.eus; Tel.: +34-946-012-512

1. State of the art

Table S1. Previous studies on the treatment of wastewater through catalytic ozonation processes in the presence of activated carbon.

Pollutant	Operating conditions	Comments	Ref.
Acid blue 9, mordant black 11, reactive blue 19, reactive orange 16	Fixed-bed reactor (100 × 6 cm); $m_{\text{CAT}} = 200 \text{ g}$; $F_G = 30 \text{ g O}_3 \text{ h}^{-1}$; Neutral pH	Complete colour removal and a significant decrease in chemical oxygen demand (COD) were obtained in contrast to ozone treatment alone.	[1]
1,2-dihydroxybenzene	Fixed-bed reactor; $m_{\text{CAT}} = 2 \text{ g}$; $F_G = 6 \text{ mmol O}_3 \text{ min}^{-1}$; pH = 8	Ozonation combined with adsorption on activated carbon was shown effective to remove 1,2-dihydroxybenzene in 60 minutes.	[2]
Chlorophyll <i>a</i>	Fixed-bed reactor; $m_{\text{CAT}} = 2.1 \text{ kg}$; $F_G = 5.0 \text{ g O}_3 \text{ h}^{-1}$; pH = 8.5	Catalytic ozonation with activated carbon was able to remove more than 95% of the chlorophyll <i>a</i> and reduce 76% of the COD in only 30 min.	[3]
Natural organic matter (NOM)	Slurry-type reactor; $m_{\text{CAT}} = 0.5 \text{ g L}^{-1}$; $\text{CO}_{3,\text{G}} = 60 \text{ mg L}^{-1}$; pH = 7 / 9	The efficiency of the O_3/GAC , O_3/OH^- , and $\text{O}_3/\text{H}_2\text{O}_2$ systems for the removal of natural organic matter was compared. The same removal efficiency was obtained.	[4]
Polyphenols	Semibatch reactor; $M_{\text{CAT}} = 0.5 \text{ g L}^{-1}$; $F_G = 0.15 \text{ L O}_3 \text{ min}^{-1}$; pH = 3 – 7	Ozonisation processes alone and combined (O_3/AC) were compared. It was observed that the ozonisation process with activated carbon improved significantly the primary degradation and mineralisation. The consumption of ozone was reduced via the O_3/AC process.	[5]
Carbamazepine and atrazine	Slurry-type reactor; $M_{\text{CAT}} = 0.1 \text{ g L}^{-1}$; $\text{CO}_{3,\text{G}} = 10 \text{ mg L}^{-1}$; pH = 7.3	Powdered activated carbon catalysed ozonation was more efficient for the removal of ozonation-resistant organics pollutants than ozone alone.	[6]

2. Experimental system characterisation

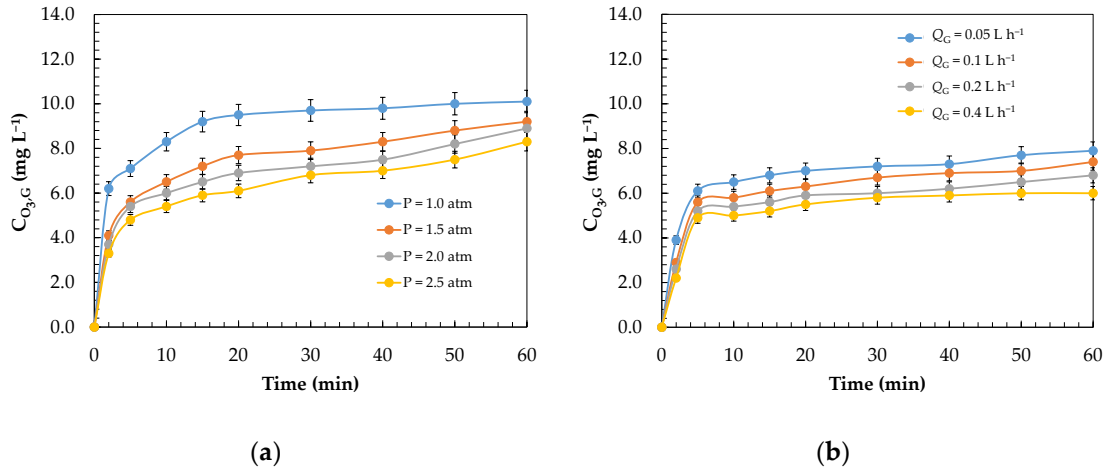


Figure S1. Evolution of ozone concentration at the reactor outlet gas stream. Effect of: (a) Pressure¹; (b) Ozone flow rate². Experimental conditions: ¹ $C_{P_0} = 250.0 \text{ mg L}^{-1}$, $\text{pH} = 11.0$, $C_{O_3,G} = 12.0 \text{ mg L}^{-1}$, $Q_L = 12 \text{ mL min}^{-1}$, $Q_G = 0.05 \text{ L h}^{-1}$, $V = 0.14 \text{ L}$. ² $C_{P_0} = 250.0 \text{ mg L}^{-1}$, $P = 2.5 \text{ atm}$, $\text{pH} = 11.0$; $C_{O_3,G} = 19.0 \text{ mg L}^{-1}$, $Q_L = 12 \text{ mL min}^{-1}$, $V = 0.14 \text{ L}$.

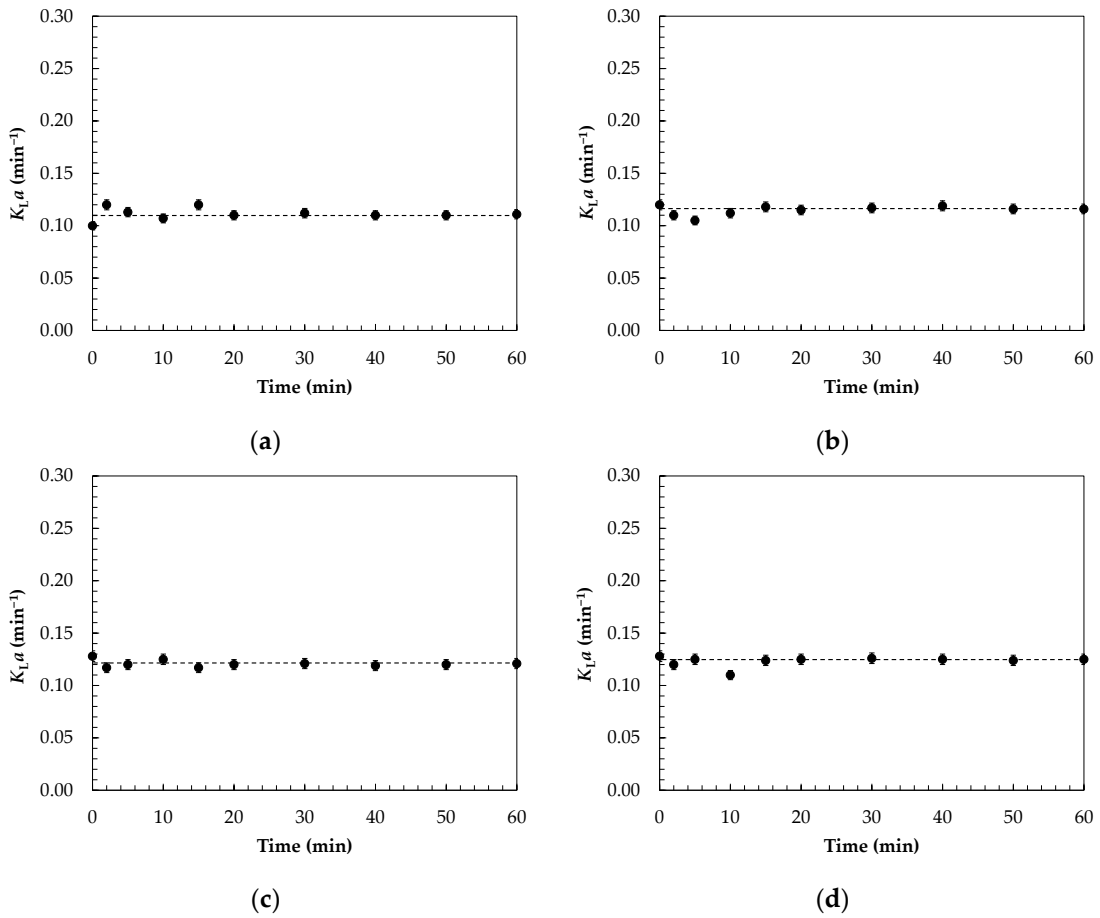


Figure S2. Determination of mass transfer coefficient of the experimental system for various pressures: (a) 1.0 atm; (b) 1.5 atm; (c) 2.0 and (d) 2.5 atm. Experimental conditions: $C_{P_0} = 250.0 \text{ mg L}^{-1}$, $\text{pH} = 11.0$, $C_{O_3,G} = 12.0 \text{ mg L}^{-1}$, $Q_L = 12 \text{ mL min}^{-1}$, $Q_G = 0.05 \text{ L h}^{-1}$, $V = 0.14 \text{ L}$.

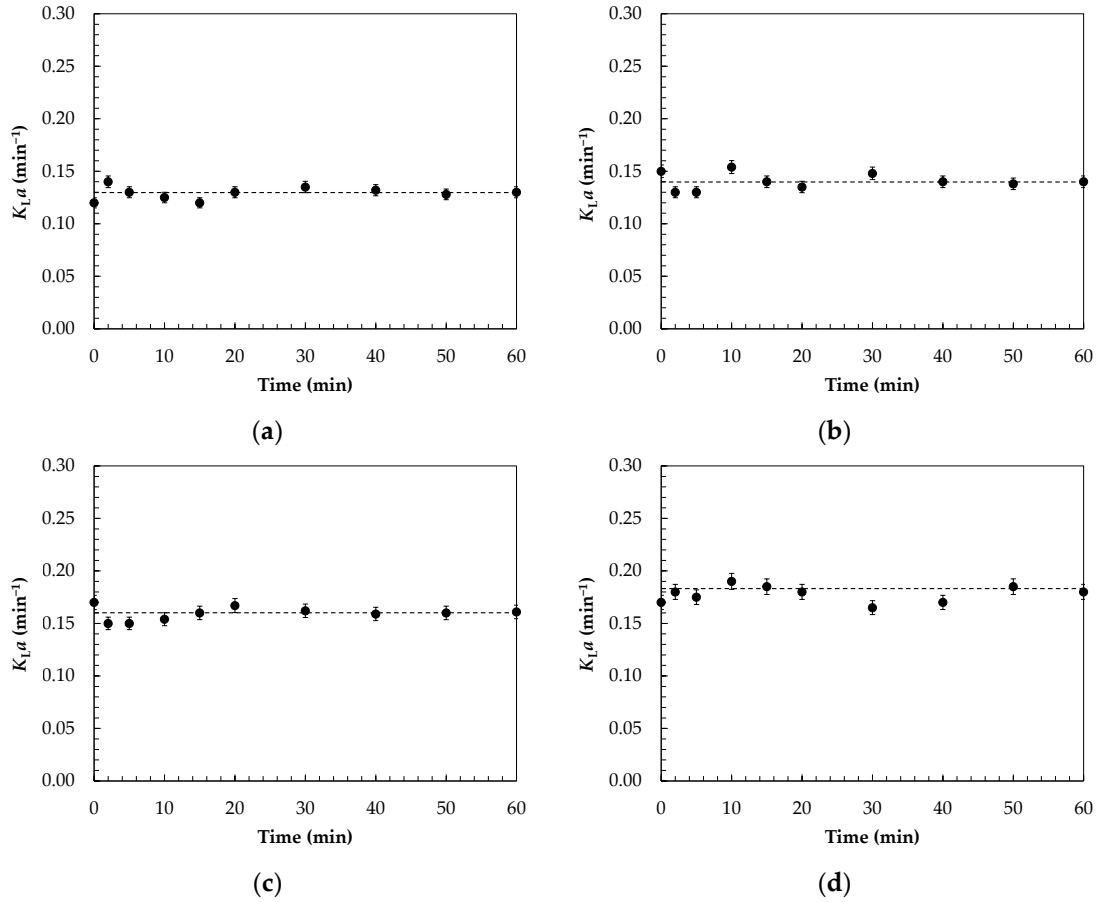


Figure S3. Determination of mass transfer coefficient of the experimental system for various ozone flow rates: (a) 0.05 L h⁻¹; (b) 0.1 L h⁻¹; (c) 0.2 L h⁻¹ and (d) 0.4 L h⁻¹. Experimental conditions: C_{P0} = 250.0 mg L⁻¹; pH = 11.0, P = 2.5 atm; C_{O_{3,G}} = 19.0 mg L⁻¹, Q_L = 12 mL min⁻¹, V = 0.14 L.

3. Hydroxyl radical generation

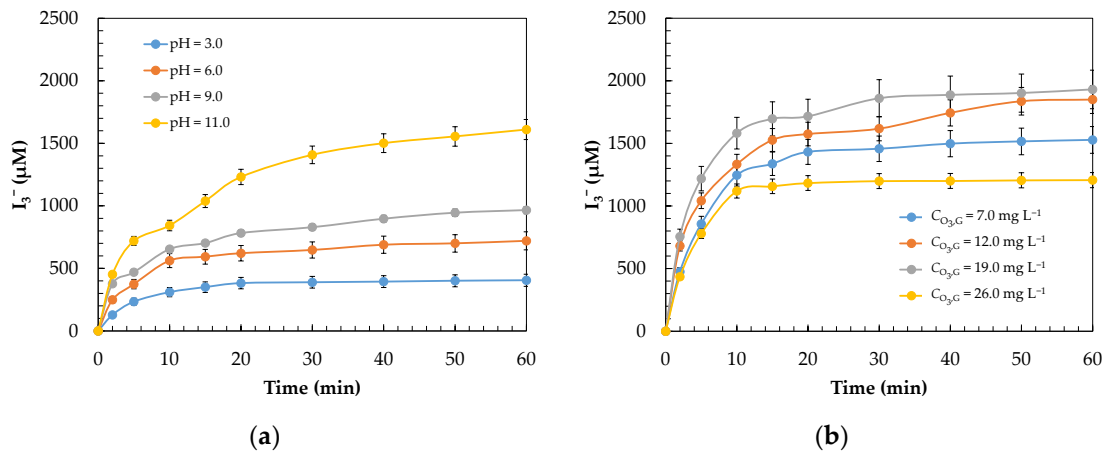


Figure S4. I₃⁻ concentration as a function of time for 0.1 M KI. Effect of: (a) pH¹ and (b) Ozone dose². Experimental conditions: ¹ C_{P0} = 250.0 mg L⁻¹, P = 1.0 atm, C_{O_{3,G}} = 12.0 mg L⁻¹, Q_L = 12 mL min⁻¹, Q_G = 0.05 L h⁻¹, V = 0.14 L. ² C_{P0} = 250.0 mg L⁻¹, P = 2.5 atm, pH = 11.0, Q_L = 12 mL min⁻¹, Q_G = 0.05 L h⁻¹, V = 0.14 L.

4. Oxidation by-products analysis

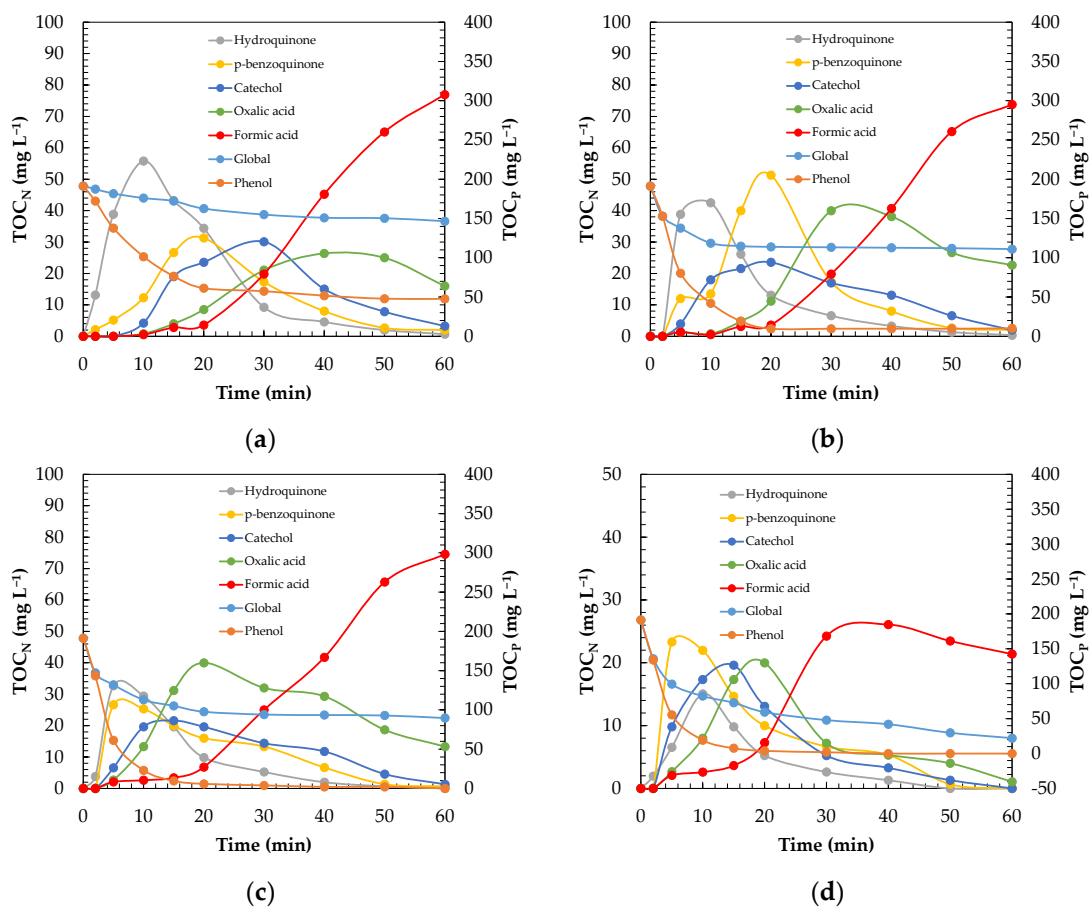


Figure S5. Analysis of the main degradation by-products during catalytic ozonation of phenol. Effect of: (a) pH = 3.0; (b) pH = 6.0; (c) pH = 9.0 and (d) pH = 11.0. Experimental conditions: $C_{P_0} = 250.0 \text{ mg L}^{-1}$, $P = 1.0 \text{ atm}$, $C_{O_3,G} = 12.0 \text{ mg L}^{-1}$, $Q_L = 12 \text{ mL min}^{-1}$, $Q_G = 0.05 \text{ L h}^{-1}$, $V = 0.14 \text{ L}$.

References

1. Lin, S.H.; Lai, C.L. Kinetic Characteristics of Textile Wastewater Ozonation in Fluidized and Fixed Activated Carbon Beds. *Water Research* **2000**, *34*, 763–772, doi:10.1016/S0043-1354(99)00214-6.
2. Zaror, C.; Soto, G.; Valdés, H.; Mansilla, H. Ozonation of 1,2-Dihydroxybenzene in the Presence of Activated Carbon. *Water Science and Technology* **2001**, *44*, 125–130, doi:10.2166/wst.2001.0267.
3. Mousavi, S.M.S.; Dehghanzadeh, R.; Ebrahimi, S.M. Comparative Analysis of Ozonation (O₃) and Activated Carbon Catalyzed Ozonation (ACCO) for Destroying Chlorophyll a and Reducing Dissolved Organic Carbon from a Eutrophic Water Reservoir. *Chemical Engineering Journal* **2017**, *314*, 396–405, doi:10.1016/j.cej.2016.11.159.
4. Sánchez-Polo, M.; Salhi, E.; Rivera-Utrilla, J.; Gunten, U. von Combination of Ozone with Activated Carbon as an Alternative to Conventional Advanced Oxidation Processes. *Ozone: Science & Engineering* **2006**, *28*, 237–245, doi:10.1080/01919510600714170.
5. Giráldez, I.; García-Araya, J.F.; Beltrán, F.J. Activated Carbon Promoted Ozonation of Polyphenol Mixtures in Water: Comparison with Single Ozonation. *Ind. Eng. Chem. Res.* **2007**, *46*, 8241–8247, doi:10.1021/ie0708881.

6. Alameddine, M.; How, Z.T.; Gamal El-Din, M. Advancing the Treatment of Primary Influent and Effluent Wastewater during Wet Weather Flow by Single versus Powdered Activated Carbon-Catalyzed Ozonation for the Removal of Trace Organic Compounds. *Science of The Total Environment* **2021**, 770, 144679, doi:10.1016/j.scitotenv.2020.144679.

A.3.4. 8. argitalpenaren material osagarria

Supporting Information

An efficient catalytic process for the treatment of genotoxic aniline wastewater using a new granular activated carbon-supported titanium dioxide composite

Ferreiro C^{a,*}, Villota N^b, Lombraña JI^a, Rivero Maria J^c.

^a Department of Chemical Engineering, Faculty of Science and Technology, University of the Basque Country UPV/EHU, 48940, Leioa, Spain; ji.lombrana@ehu.eus (J.I.L.)

^b Department of Chemical and Environmental Engineering, Escuela de Ingeniería de Vitoria-Gasteiz, University of the Basque Country UPV/EHU, 01006, Vitoria-Gasteiz, Spain; natalia.villota@ehu.eus (N.V.)

^c Department of Chemical and Biomolecular Engineering, University of Cantabria, 39005 Santander, Spain; riveromj@unican.es (M.J.R.)

* Corresponding author: cristian.ferreiro@ehu.eus (C.F.)

1. Experimental system characterisation

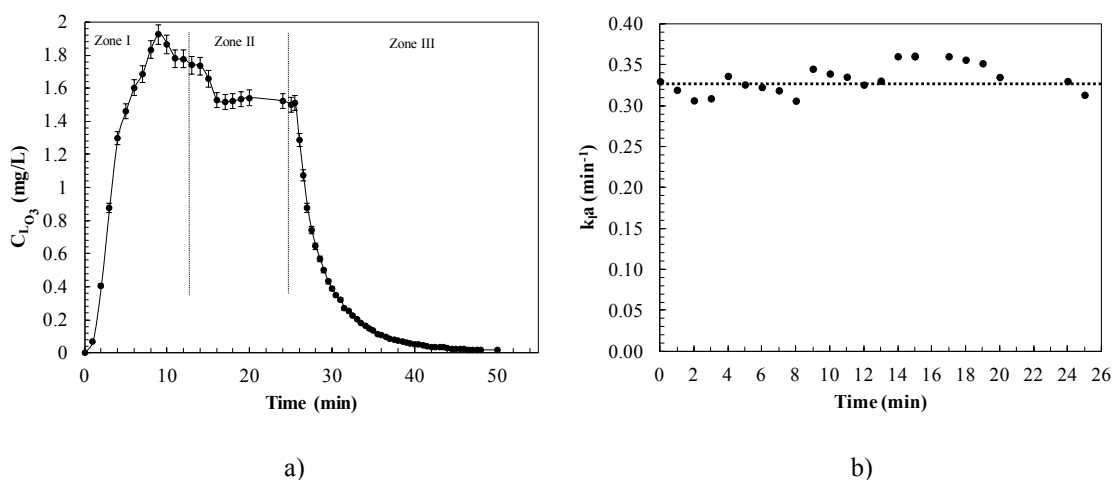


Fig. S1 C_{O_3} values during the ozonation of deionised water (a) and determination of mass transfer coefficient (b) for the experimental system. Experimental conditions: $F_G = 2.5$ g O_3/h ; $C_{GO_3, in} = 5.4$ mg/L; $V_{react} = 1.5$ L; $P = 1$ atm; $T = 18.0$ °C; $pH = 7.0$; stirring = 60 rpm.

2. Ozone effect on aniline degradation

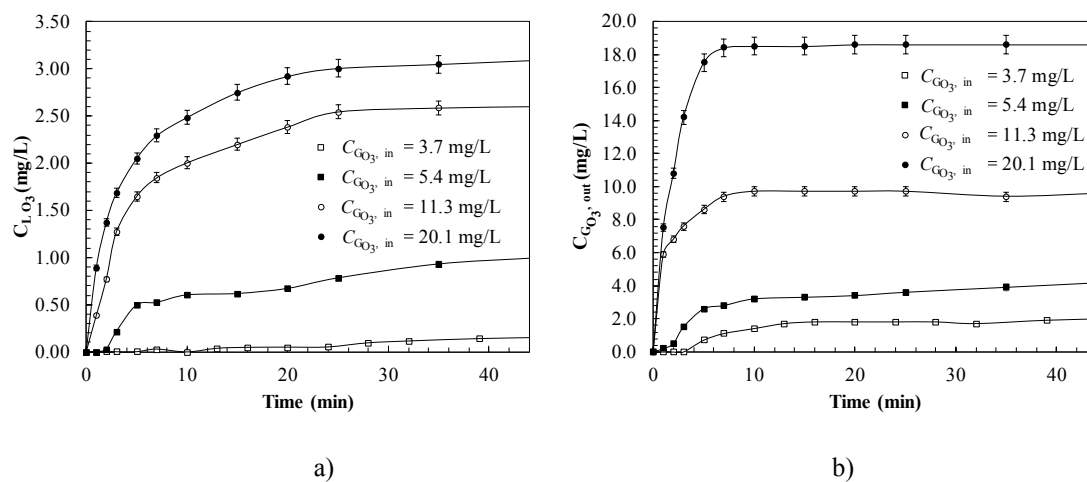


Fig. S2 Evolution of dissolved ozone concentration (a) and ozone concentration at the reactor outlet gas stream (b) during the catalytic ozonation of aniline using TiO_2/GAC composite synthesised by the precipitation method at $C_{GO_3, in} = 3.7; 5.4; 11.3; 20.1$ mg/L doses. Experimental conditions: $F_G = 2.5$ g O_3/h ; $C_0 = 20.0$ mg/L; $T = 18.0$ °C; $P = 1$ atm; $pH = 7.0$; $m_{cat} = 5.0$ g; $V_{react} = 1.5$ L.

A3.5. 9. argitalpenaren material osagarria

Article

Heterogeneous Catalytic Ozonation of Aniline-Contaminated Waters: A Three-Phase Modelling Approach Using TiO₂/GAC

Cristian Ferreiro*, Natalia Villota, José Ignacio Lombrana and María J. Rivero.

Supplementary Materials

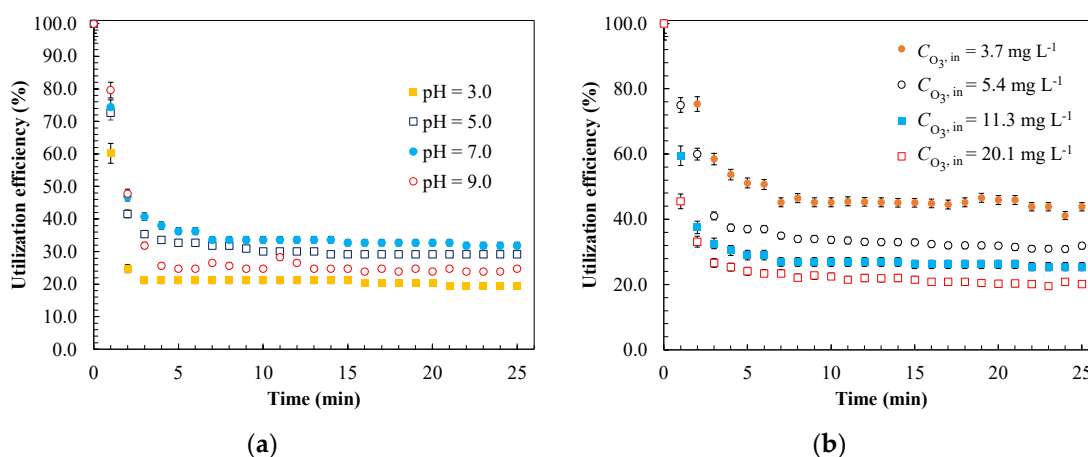


Figure S1. Utilization efficiencies of ozone in a TiO₂/GAC catalytic system at different pHs (a)¹ and inlet ozone concentrations (b)² in the experimental ozonation system. Experimental conditions: $Q_G = 4 \text{ L min}^{-1}$; $M_{CAT} = 3.3 \text{ g L}^{-1}$; $T = 18.0 \text{ }^\circ\text{C}$; $P = 1 \text{ atm}$; $V_{\text{reac}} = 1.5 \text{ L}$; ($Agitation$) = 60 rpm. ¹ $C_{O_3, \text{in}} = 11.3 \text{ mg L}^{-1}$. ² pH = 7.0.

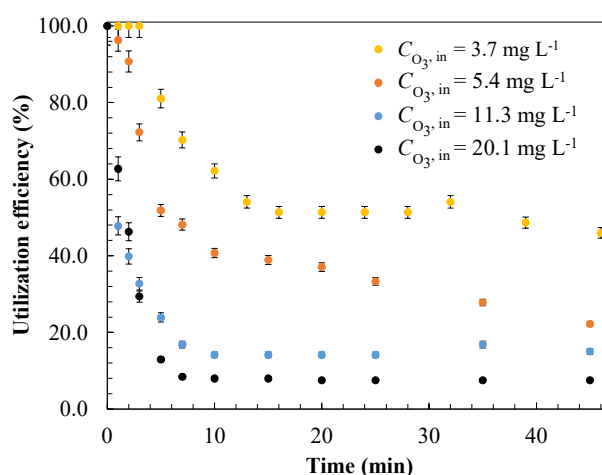


Figure S2. Effect of the ozone dose on the control stage during catalytic ozonation of aniline with the TiO₂/GAC catalyst. Experimental conditions: $Q_G = 4 \text{ L min}^{-1}$; pH = 7.0; $M_{CAT} = 3.3 \text{ g L}^{-1}$; $T = 18.0 \text{ }^\circ\text{C}$; $P = 1 \text{ atm}$; $V_{\text{reac}} = 1.5 \text{ L}$; ($Agitation$) = 60 rpm.

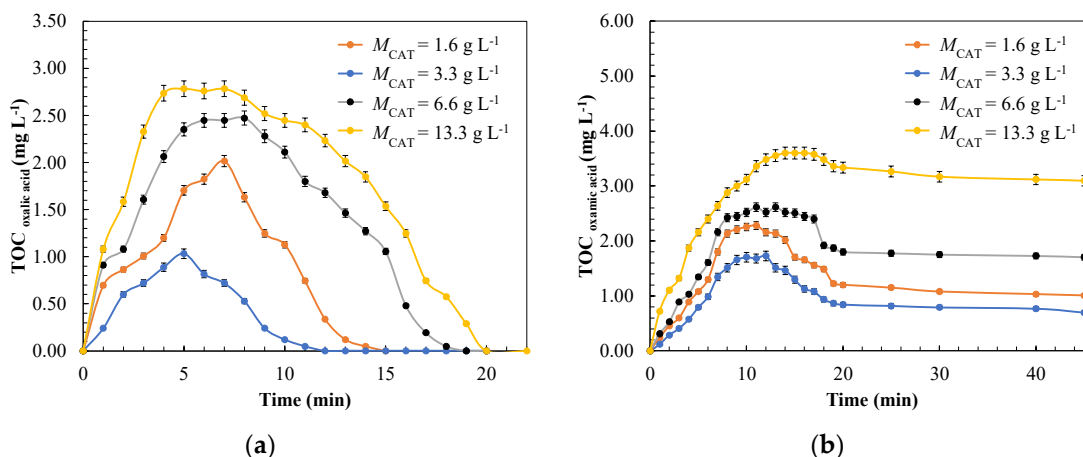


Figure S3. Analysis of some by-products formed during the TiO_2/GAC ozonation of aniline in terms of TOC. Effect of catalyst dosage on the evolution of: (a) oxalic and (b) oxamic acid during ozonation. Experimental conditions: $Q_G = 4 \text{ L min}^{-1}$; $\text{Co}_{3,\text{in}} = 5.4 \text{ mg L}^{-1}$; $\text{pH} = 7.0$; $T = 18.0 \text{ }^\circ\text{C}$; $P = 1 \text{ atm}$; $V_{\text{reac}} = 1.5 \text{ L}$; (*Agitation*) = 60 rpm.

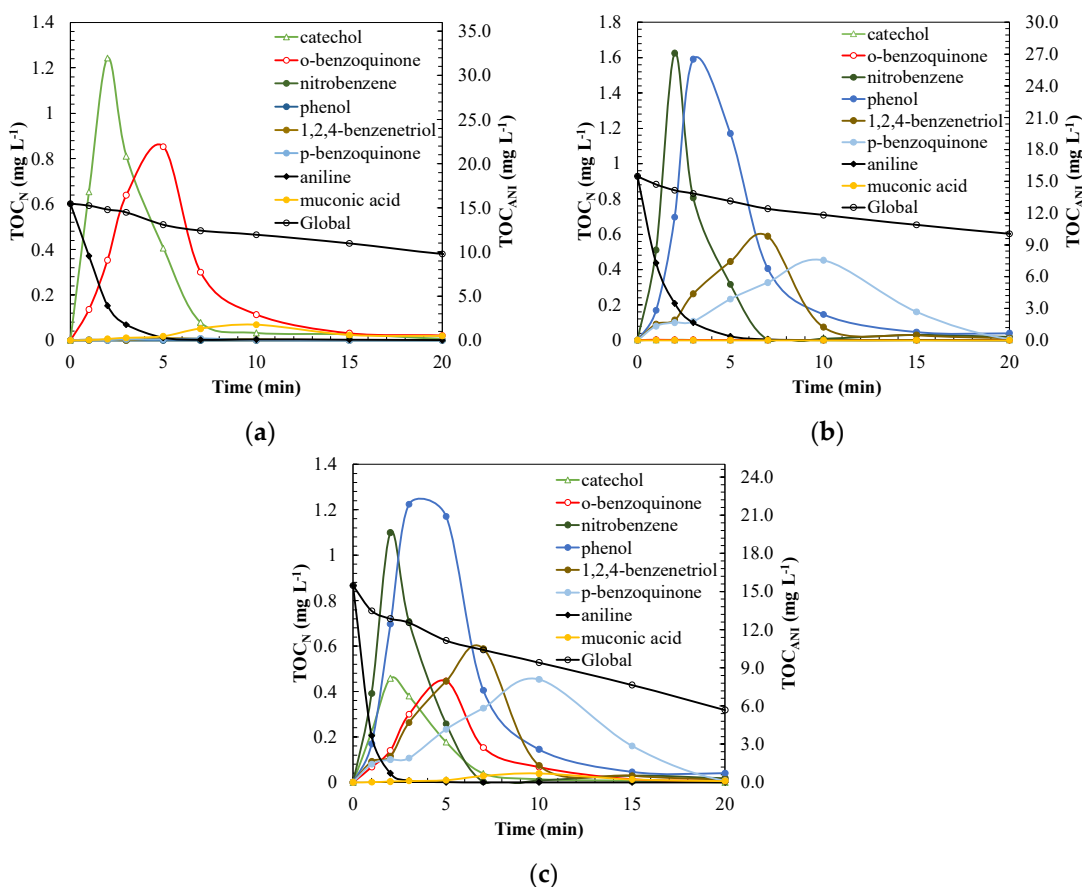


Figure S4. Analysis of the main intermediates in the aniline catalytic ozonation with TiO_2/GAC in terms of TOC, excluding oxalic and oxamic acid in different cases: (a) molecular attack of ozone at $\text{pH} = 3.0$; (b) ozone in excess and dominance of radical attack ($\text{pH} = 7.0$ and ozone dose of 20.1 mg L^{-1}); and (c) most favourable conditions ($\text{pH} = 7.0$, 5.4 mg L^{-1} ozone concentration) or combined molecular radical attack. Experimental conditions: $Q_G = 4 \text{ L min}^{-1}$; $M_{\text{CAT}} = 3.3 \text{ g L}^{-1}$; $T = 18.0 \text{ }^\circ\text{C}$; $P = 1 \text{ atm}$; $V_{\text{reac}} = 1.5 \text{ L}$; (*Agitation*) = 60 rpm.

A.3.6. 10. argitalpenaren material osagarria

Analysis of Ultrasonic Pre-treatment for the Ozonation of Humic Acids

Pello Alfonso-Muniozguren^{1,2}, Cristian Ferreiro², Elodie Richard^{1,3},
Madeleine Bussemaker¹, José Ignacio Lombraña^{2*}, Judy Lee^{1*}

¹*Chemical and Process Engineering, University of Surrey, Guildford, GU27XH, United
Kingdom*

²*Department of Chemical Engineering, Faculty of Science and Technology, University of the
Basque Country UPV/EHU, 48940, Leioa, Spain*

³*Department of Chemistry, IUT Besançon-Vesoul, University of Franche-Comté, 25000
Besançon, France*

*j.y.lee@surrey.ac.uk /*ji.lombrana@ehu.eus

Elemental analysis (CHONS)

The composition of the natural organic matter (NOM) depends on its origin, ranging from low molecular weight hydrophilic acids to macromolecules such as HAs [48]. The particular characteristics of the HAs are important since the choice of the most appropriate treatment may be influenced by those characteristics [49]. Therefore, the properties of the HAs used in the present study are shown in Table S 1 and compared to naturally occurring HAs collected from the Uzquiza swamp (Burgos, Spain) [50, 51].

Table S 1. Characterisation of studied humic acids.

Sample	Elemental composition					Atomic H/C ratio	Atomic O/C ratio	Atomic C/N ratio	pK _a	E ₃ /E ₅
	C (%)	H (%)	O (%)	N (%)	S (%)					
Synthetic HA*	42.91	4.48	26.61	1.32	< 0.2	1.24	0.47	37.93	9.28	6.59
Natural HA**	51.76	5.15	—	1.65	—	1.18	—	36.61	—	—

* Present work

** Vidal (2003)

In general, the synthetic HA used in the present study (50 mg HA/L, equivalent to 21 mg TOC/L) has similar characteristics in terms of elementary composition and atomic ratio to that of real samples. The presence of more nitrogen in natural HA as opposed to synthetic HA indicates that the former has a greater potential to form nitrogenous disinfection by-products such as trichloronitromethanes [52, 53]. On the other hand, considering the H/C ratio of the samples, it should be noted that synthetic HAs (1.24) have greater aliphatic or less aromatic character than natural HAs (1.18). This reduction means that the natural HA is less protonated and consequently the macromolecule is more stable than the synthetic one. Natural HA holds a 51.76% carbon. This is significantly

higher than that of the synthetic sample (42.91%), which shows natural HA has a higher degree of humification.

The E_3/E_5 ratio obtained from synthetic HA (6.59) indicates that the humic substance has a small molecular size of approximately 13 kDa and a weakly developed aromatic nucleus [20]. The pKa of the synthetic HA (9.28) corresponds to a phenolic structure. The value of this parameter significantly influences solubility and by extension, the ultrasound/ O_3 treatment [19, 51].

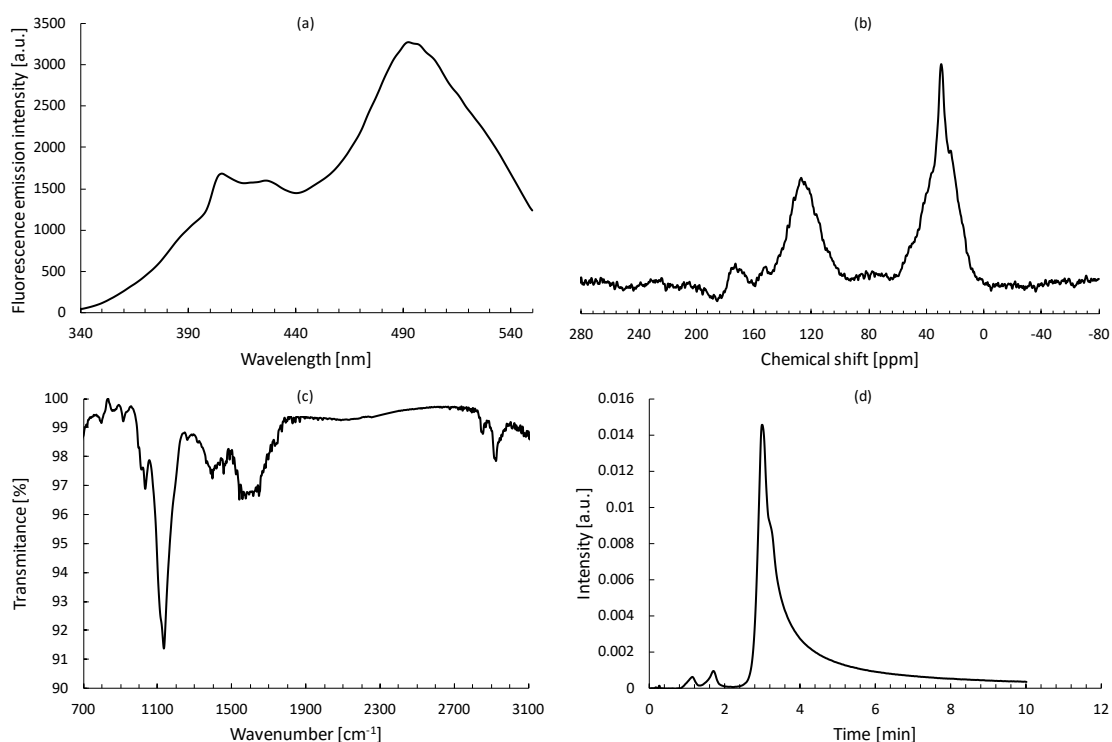


Figure S 1. Humic acids 50 mg/L. (a) Fluorescence; (b) ^{13}C NMR; (c) FTIR; (d) HPSEC.

Fluorescence analysis

Figure S1a shows the fluorescence spectrum of the HAs, where the range of different fluorophore groups are displayed in the emission range from 340 nm to 550 nm. There are two distinct fractions: firstly the region with the highest wavelength (460-550 nm), which corresponds to the humic region and consists of organic matter from natural origin, in which aromatic and hence, more recalcitrant compounds predominate [54, 55]. Then secondly, the region with the lowest wavelength (340-410 nm) which corresponds to protein-like microbial sub-products with a behaviour similar to tryptophan (e.g. naphthalene) and a biodegradable character. This biodegradable nature leads to an easy elimination of this fraction of HA with the treatment proposed in the present study [38, 56].

¹³C NMR spectroscopy analysis

The ¹³C NMR spectrum of the humic compound used in this work is shown in Figure S 1b. Four carbon groups corresponding to the aliphatic region were distinguished with a chemical shift of 0-60 ppm. This is in agreement with what was discussed in the elementary spectroscopic analysis [57]. One peak corresponding to the aromatic region was observed with a chemical displacement of 112-145 ppm, common in substances formed from the condensation of heterocyclic compounds and polymerisation of carbohydrates with proteins [58]. Another peak was measured in the phenolic region with a displacement of 145-163 ppm, being this peak the one with the lowest abundance of the four groups identified. Finally, the region corresponding to carboxylic groups was measured with a displacement of 163-180 ppm [20]. Nothing significant was measured in the spectral region of 180-220 ppm assigned to ketones and aldehydes [55, 59].

FTIR analysis

Figure S1c shows the infrared spectrum of the synthetic HA. From the figure the 2850-2960 cm^{-1} band is characteristic of saturated groups and shows typical values of methyl and methylene groups (C-H tension), the band at 1720 cm^{-1} (corresponding to the C=O vibration tension) and the band at 1405 cm^{-1} (corresponding to flexion outside the O-H plane) [41]. The intensity of the 1720 cm^{-1} band is attributable to the acidic nature of the HA. The band at 1620 cm^{-1} corresponds to aromatic groups or alkenes with C=C tension. The relative intensity of this peak indicates that this HA has a strong aromatic nature (aromatic rings) [55]. The CO tension bands that are assignable to oxygenated groups appear at 1220 cm^{-1} (corresponding to carboxylic acids and phenols), while the band at 1260 cm^{-1} corresponds to aromatic ethers or unsaturated chains [60]. The 1030 and 1095 cm^{-1} bands would refer to aliphatic alcohols and ethers, while the band present at 805 cm^{-1} would be associated to tri- and tetra-substituted aromatic rings [46]. Finally, mention that the intensity of the band at 1540 cm^{-1} would correspond to the presence of amino groups, according to the amount of nitrogen measured by the elementary analysis (1.32%). This would be of great importance due to its potential to form nitrogenous disinfection by-products after chlorination [50].

HPSEC analysis

Four characteristic peaks are distinguished in Figure S1d: biopolymers formed by proteins and polysaccharides with a molecular weight greater than 640 kDa, humic substances with a molecular weight of approximately 20 kDa, and two small peaks with a size of approximately 2 kDa formed by low molecular weight acids and other neutral compounds of low molecular weight [61, 62].

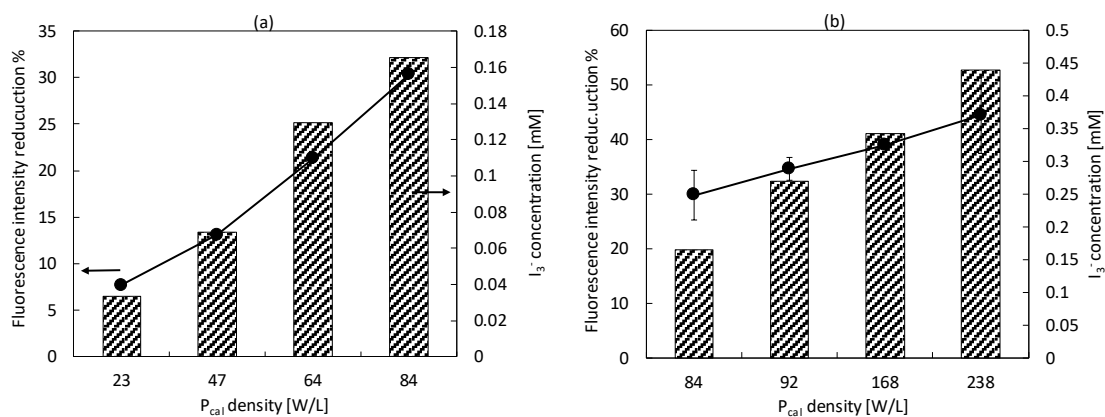


Figure S 2. Fluorescence emission intensity reduction percentage at 470 nm (primary axis) and I_3^- concentration (secondary axis) of 50 mg HA/L at difference calorimetric power densities at 300 kHz for (a) 400 mL sample at applied ultrasonic power of 10, 20, 30 and 40 W (left to right) and for (b) applied ultrasonic power of 40 W with 400, 300, 200 and 150 mL samples (left to right).

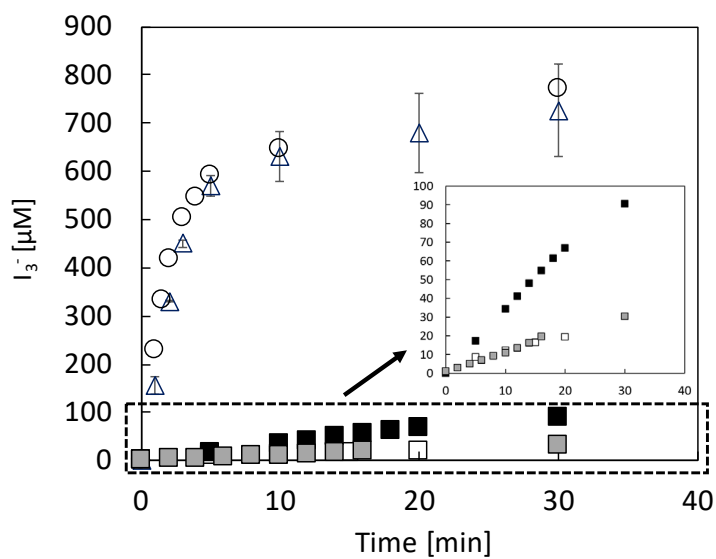


Figure S 3. I_3^- concentration as a function of time. Ultrasound conditions: 40 W at 98 kHz (\square), 300 kHz (\blacksquare), and 1 MHz (\blacksquare). Ozonation : 7.4 mg $\text{O}_3/\text{L}_{\text{gas}}$ (Δ) and 11.3 mg $\text{O}_3/\text{L}_{\text{gas}}$ (\circ). The insert shows the zoomed in plot of the 0-100 μM I_3^- interval. 400 mL sample and 0.1 M KI.

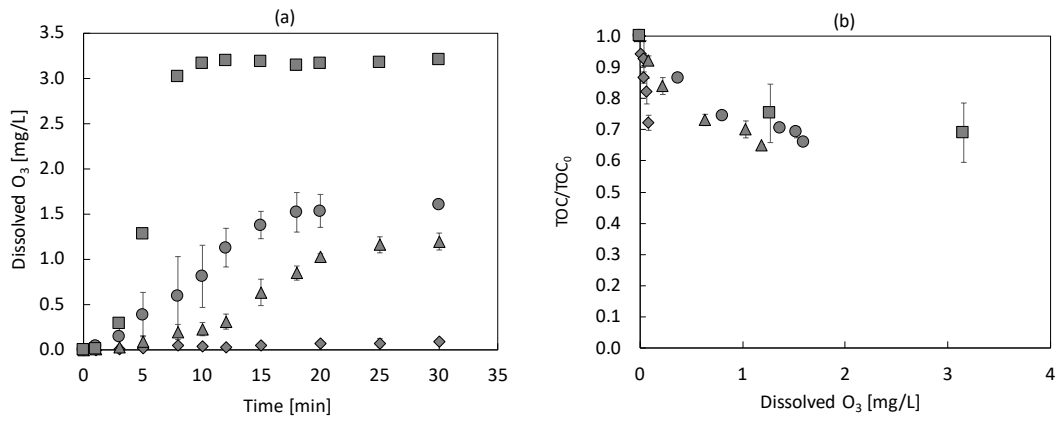


Figure S 4. (a) Dissolved ozone concentration as a function of time and (b) TOC/TOC₀ as a function of dissolved O₃. 5.4 mg O₃/L_{gas} (◆), 7.4 mg O₃/L_{gas} (▲), 11.3 mg O₃/L_{gas} (●), 19.7 mg O₃/L_{gas} (■).

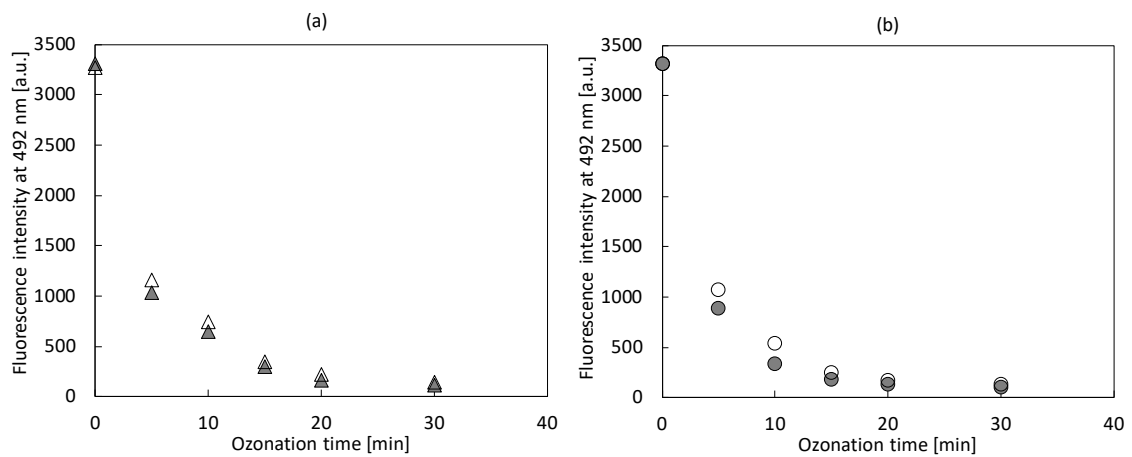


Figure S 5. Fluorescence emission intensity peak at wavelength 492 nm as a function of ozonation time. (a) 7.4 mg O₃/L (▲), ultrasound + 7.4 mg O₃/L (△); (b) 11.3 mg O₃/L (●), ultrasound + 11.3 mg O₃/L (○). 30 min ultrasound pre-treatment at 300 kHz and 40W. 400 mL samples.

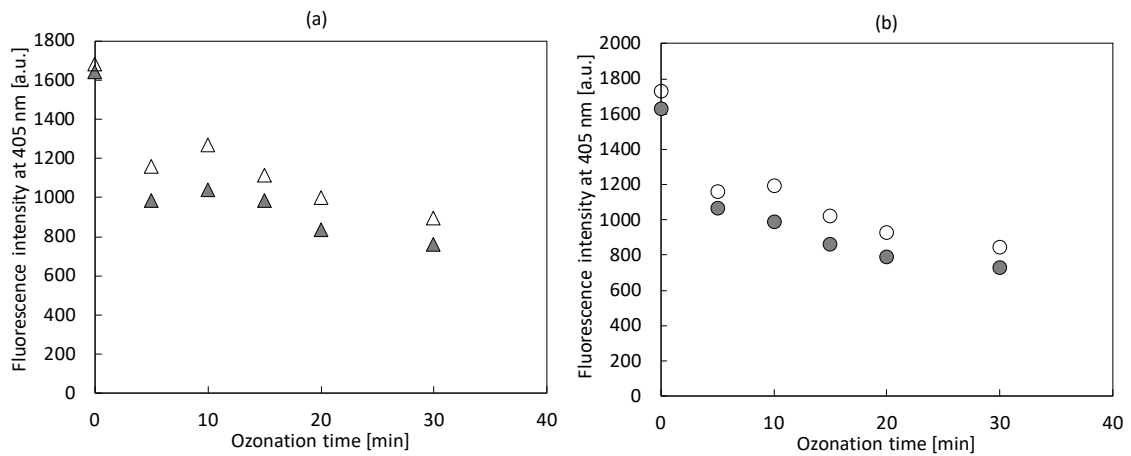


Figure S 6. Fluorescence emission intensity peak at wavelength 405 nm as a function of ozonation time. (a) 7.4 mg O₃/L (▲), ultrasound + O₃ (△); (b) 11.3 mg O₃/L (●), ultrasound + O₃ (○). 30 min ultrasound pre-treatment at 300 kHz and 40W. 400 mL samples.

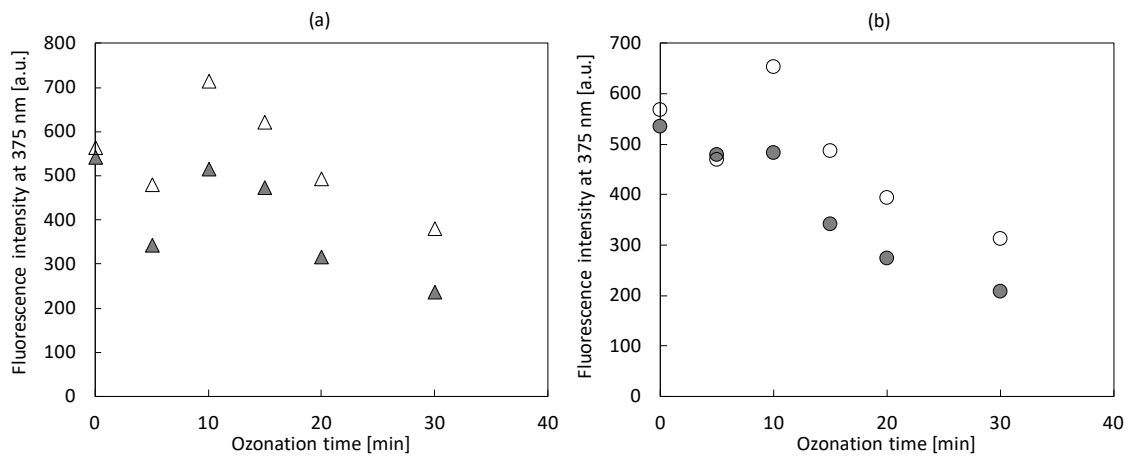


Figure S 7. Fluorescence emission intensity peak at wavelength 375 nm as a function of ozonation time. (a) 7.4 mg O₃/L (▲), ultrasound + O₃ (△); (b) 11.3 mg O₃/L (●), ultrasound + O₃ (○). 30 min ultrasound pre-treatment at 300 kHz and 40W. 400 mL samples.

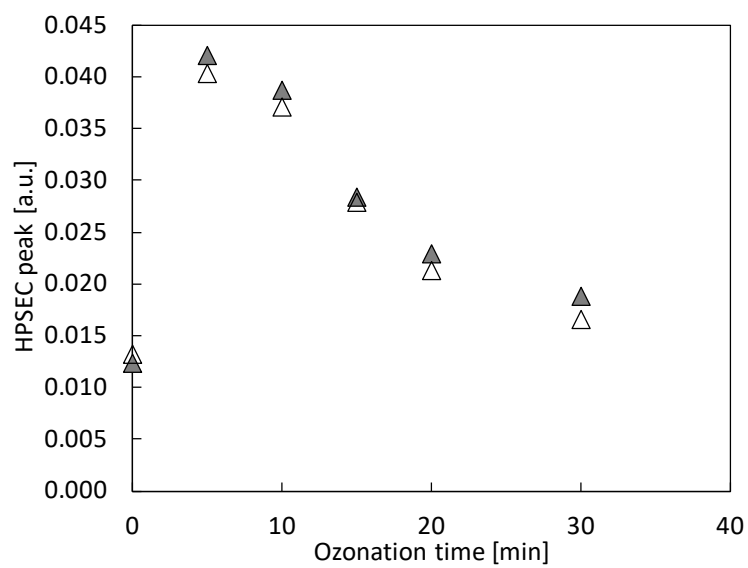


Figure S 8. HPSE peak (at min 3) as a function of O₃ injection time. O₃ alone (\blacktriangle), ultrasound + O₃ (\triangle). O₃ = 7.4 mg O₃/L; 30 min ultrasound pre-treatment at 300 kHz and 40W. 400 mL samples. In Fig. 7 c and d is only shown US+O₃ (\triangle in Fig. S 8), not O₃ alone (\blacktriangle in Fig. S 8).